PTNSS

178(3), 2019

COMBUSTION ENGINES

LDV emissions development work for RDE 4/WLTP and post-Euro 6 and EU Euro 6d certification, testing of hybrid and electric vehicles

BOSMAL

Testing under laboratory conditions on chassis dynamometers in climate controlled test cells

- Euro 6d-compliant emissions testing laboratories for both certification and R&D activities on vehicles with ICE-based, hybrid and fully electric powertrains
- Climate simulation in the range -35˚C to +60˚C
- 4WD and 2WD single-roll 48" chassis dynamometers with slope simulation and motorcycle mounting system
- Bag and dilute emissions measurements (all regulated emissions, NMHC, NO/NO_2)
- Raw emissions measurements (all regulated emissions, NMHC, NO/NO_2) – 2 modal lines with high-accuracy dilution air measurement
- Gravimetric filter (PM) and condensation particle counter (PN) for measuring particulate emissions
- Raw PN, opacimeter, soot sensor and size distribution counter available for R&D activities
- Direct engine speed monitoring
- EGR measurement
- ECU data logging via OBD port
- Power analysers for RCB correction available
- NH_3, N_2O and FTIR analyser available
- Additional devices (thermocouples, analog signals, etc.) supported
- All common driving cycles available; custom cycles can be implemented
- Chassis dyno RDE simulation and CVS-PEMS emissions correlation studies
- Vehicle soaking container, temperature: -40˚C to +40˚C, capacity: 2 SUVs/small vans

Testing under real driving conditions on public roads at various locations (RDE, PEMS)

- Two mobile emissions analysis systems for measurement of emissions (regulated gaseous and PN) and fuel consumption under real driving conditions
- Conforms to all applicable EU legislation; both light-duty (RDE, up to RDE4) and heavy-duty (ISC)
- Flexible systems allowing installation on a wide range of vehicles for both certification and R&D tests
- Equipped with high-accuracy exhaust flow meters, weather stations and GPS units
- THC measurement available in both systems
- Data post-processing, elaboration of results, planning and analysis of test routes, etc.
- PEMS analysis on chassis dyno over any driving cycle

BOSMAL Automotive Research and Development Institute Ltd
Sarni Stok 93, 43-300 Bielsko-Biała, POLAND
phone: +48 33 81 30 539, +48 33 81 30 598
www.bosmal.com.pl, e-mail: sales@bosmal.com.pl

PTNSS Supporting Members
Członkowie wspierający PTNSS

BOSMAL Automotive Research and Development Institute Ltd
Instytut Badań i Rozwoju Motoryzacji BOSMAL Sp. z o.o

Motor Transport Institute
Instytut Transportu Samochodowego

The Institute for Sustainable Technologies
Instytut Technologii Eksploatacji

Institute of Aviation
Instytut Lotnictwa

Automotive Industry Institute
Przemysłowy Instytut Motoryzacji

The Rail Vehicles Institute TABOR
Instytut Pojazdów Szynowych TABOR

Institute of Mechanised Construction and Rock Mining
Instytut Mechanizacji Budownictwa i Górnictwa Skalnego

Industrial Institute of Agricultural Engineering
Przemysłowy Instytut Maszyn Rolniczych

AVL List GmbH

Solaris Bus & Coach S.A.

Air Force Institute of Technology
Instytut Techniczny Wojsk Lotniczych

COMBUSTION ENGINES

A Scientific Magazine

2019, 178(3)

Year LVIII

PL ISSN 2300-9896

Editor:

Polskie Towarzystwo Naukowe Silników Spalinowych
43-300 Bielsko-Biała, Sarni Stok 93 Street, Poland
tel.: +48 33 8130402, fax: +48 33 8125038
E-mail: sekretariat@ptnss.pl
WebSite: http://www.ptnss.pl
Papers available on-line: http://combustion-engines.eu

Editorial:
Institute of Combustion Engines and Transport
Poznan University of Technology
60-965 Poznan, Piotrowo 3 Street
tel.: +48 61 2244505, +48 61 2244502
E-mail: papers@ptnss.pl

Prof. Jerzy Merkisz, DSc., DEng. (Editor-in-chief)
Miłosław Kozak, DSc., DEng. (Editorial Secretary for Science) – papers@ptnss.pl
Prof. Ireneusz Pielecha, DSc., DEng. (Technical Editor)
Joseph Woodburn, MSci (Proofreading Editor)
Wojciech Serdecki, DSc., DEng. (Statistical Editor)
and Associate Editors

Contents

Siadkowska K., Czyż Z. Selecting a material for an aircraft diesel engine block (CE-2019-301) 4
Gis M., Bednarski M., Lasocki J. Determination of pollutant emission of electric vehicle in real traffic conditions in Poland (CE-2019-302) 9
Korczewski Z. Thermal efficiency investigations on the self-ignition test engine fed with marine low sulfur diesel fuels (CE-2019-303)..... 15
Łoza Ł., Wróbel R., Sitnik L. The analysis of vibrations of gasoline and diesel vehicles as a function of their engine sizes (CE-2019-304)..... 20
Sitnik L.J., Zadworny D. Application of the Monte Carlo method in the calculation procedure of the internal combustion engine (CE-2019-305) 24
Stepanenko D., Kneba Z. Thermodynamic modeling of combustion process of the internal combustion engines – an overview (CE-2019-306) 27
Merkisz J., Andrych-Zalewska M., Pielecha J. Analysis of the efficiency of the in-cylinder catalyst to reduce exhaust emissions during the cold start combustion engine (CE-2019-307)..... 38
Hunicz J., Gęca M.S., Kordos P., Rybak A. Effects of combustion timing on pressure rise rates in a residual effected HCCI engine (CE-2019-308) 46
Bogdanowicz A., Kniaziewicz T. Simulation of concentrations harmful compounds from main ship's propulsion engine cooperating with a fixed pitch propeller in dynamic states (CE-2019-309)..... 51
Bebkiewicz K., Chłopek Z., Szczepański K., Laskowska M. Emission of pollutants from motor vehicles in Poland comparing to pollutant emission in the European Union (CE-2019-310)..... 56
Gis W., Pielecha J., Merkisz J., Kruczyński S., Gis M. Determining the route for the purpose light vehicles testing in Real Driving Emissions (RDE) test (CE-2019-311) 61
Matuszewska A., Owczuk M. The influence of non-normative fuel on its operational properties (CE-2019-312) 67
Orliński P., Wojs M.K., Bednarski M., Sikora M. Evaluation of the effect of the addition of bioethanol to gas oil on coking diesel engine injector terminals (CE-2019-313) 71
Andrzejewski M., Pielecha I., Merkisz J., Świechowicz R., Nowak M. Nowoczesne układy napędowe pojazdów szynowych (CE-2019-314) 76
Przybyła G., Rutczyk B., Ziółkowski Ł. Performance of micro CHP unit based on SI engine with quantitative – qualitative load control (CE-2019-315) 82
Bielaczyc P., Klimkiewicz D., Woodburn J., Szczotka A. Exhaust emission testing methods – BOSMAL's legislative and development emission testing laboratories (CE-2019-316) 88
Andrych-Zalewska M., Chłopek Z., Merkisz J., Pielecha J. Exhaust emission from a vehicle engine operating in dynamic states and conditions corresponding to real driving (CE-2019-317)..... 99
Jaworski A., Lejda K., Lubas J., Mądziel M. Comparison of exhaust emission from Euro 3 and Euro 6 motor vehicles fueled with petrol and LPG based on real driving conditions (CE-2019-318) 106
Karpiński P., Pietrykowski K., Grabowski Ł. Turbocharging the aircraft two-stroke diesel engine (CE-2019-319) 112
Swiatek P., Fuc P., Ziolkowski A., Swiatek L., Melwinski P. Tests of a prototype spark-ignited, direct-injection engine powered by JET-A1 fuel (CE-2019-320) 117
Mitianiec W. Study of Atkinson cycle in two-stroke diesel engine with opposed pistons (CE-2019-321) 121
Klyus O., Krause P., Markov V., Skarbek-Żabkin A., Sa B. Evaluation of the suitability of synthetic polymer fuels in self-ignition engines (CE-2019-322) 129
Sitnik L.J. Emissions of e-mobility (CE-2019-323)..... 135
Brzezanski M., Rodak L. Investigation of a new concept of hydrogen supply for a spark ignition engine (CE-2019-324) 140
Gis W., Merkisz J. The development status of electric (BEV) and hydrogen (FCEV) passenger cars park in the world and new research possibilities of these cars in real traffic conditions (CE-2019-325)..... 144
Bebkiewicz K., Chłopek Z., Lasocki J., Szczepański K., Zimakowska-Laskowska M. Inventory of pollutant emission from motor vehicles in Poland using the COPERT 5 software (CE-2019-326) 150
Nowak L., Tutak W. Combustion stability of dual fuel engine powered by diesel-ethanol fuels (CE-2019-327) 155
Gis W., Waśkiewicz J., Menes M. Experts forecasts on the demand for energy carriers in motor vehicle transport in Poland up to year 2035 (CE-2019-328)..... 162
Śliwiński K., Marek W. The use of glycerin as motor fuel (CE-2019-329) 166
Lasocki J., Chłopek Z., Godlewski T. Driving style analysis based on information from the vehicle's OBD system (CE-2019-330)..... 173
Sroka Z.J., Dworaczyński M.K. Assessment of thermodynamic cycle of internal combustion engine in terms of rightsizing (CE-2019-331) 182
Struś M., Poprawski W. Improvement of the compression ignition behaviour and combustion efficiency of the second generation biofuel BIOXDIESEL (CE-2019-332) 187
Skrzek T. Duel fuel compression ignition engine fuelled with homogeneous mixtures of propane and kerosene-based fuel (CE-2019-333) 191
Sokolnicka B., Fuć P., Szymlet N., Siedlecki M., Grzeszczyk R. Harmful exhaust components and particles mass and number emission during the actual drive of a passenger car in accordance with the RDE procedure (CE-2019-334) 198
Kropiwnicki J., Furmanek M. Analysis of the regenerative braking process for the urban traffic conditions (CE-2019-335) 203

Dzida J., Brzeżański M. An analysis of SCR reactor deactivation impact on NO_x emissions from a compression ignition engine (CE-2019-336) 208

Orkisz M., Wygonik P., Kuźniar M., Kalwara M. Comparative analysis of combustion engine and hybrid propulsion unit in aviation application in terms of emission of harmful compounds in the exhausts emitted to the atmosphere (CE-2019-337) 213

Wirkowski P., Markowski J. The influence of operating conditions of the marine gas turbine engine on the level of emission of pollutants contained in the exhaust (CE-2019-338) 218

Brzezanski M., Rodak L. Influence of the method of creating a hydrogen-air mixture on the emission of nitrogen oxides in a spark-ignition engine (CE-2019-339) 224

Gis W., Gis M., Wiśniowski P., Bednarski M. Comparative tests of a passenger car with compression ignition engine on chassis dynamometer during NEDC and WLTC tests and during RDE road test (CE-2019-340) 228

Sroka Z.J., Buczma K. Adaptation of a gas cogeneration system used in power industry to drive inland waterway transport unit (CE-2019-341) 235

Arczewski M. Evaluation of the diesel engine feed by unified battlefield fuel F-34/F-35 mixed with biocomponents (CE-2019-342) 240

Bogdanowicz A., Zadrąg R. Identification of emission indicators harmful compounds for assessment of dynamic state of a marine diesel engine (CE-2019-343) 247

Galant M., Fuć P., Kardach M. Analysis of the ecological effectiveness of passenger transport by jets of various sizes (CE-2019-344) 252

Wolff A. Influence of piston ring profiles and oil temperature distribution on cylinder liner lubrication of a marine two-stroke engine (CE-2019-345) 257

Orkisz M., Wygonik P., Kuźniar M., Kalwara M. Analysis of the possibility of using an engine with a rotating piston as the propulsion of an electric generator in application to a motor glider propulsion (CE-2019-346) 264

Daszkiewicz P., Rymaniak Ł., Kamińska M. Issues of emission evaluation of road-rail vehicles in the aspect of current type approval regulations (CE-2019-347) 269

Pajdowski P., Woodburn J., Bielaczyc P., Puchałka B. Development of RDE test methodology in light of Euro 6d emissions limits (CE-2019-348) 274

Pietras D., Praszkiewicz M., Czarniecki K. Methods of determining the input data of control algorithms for a compression-ignition engine (CE-2019-349) 283

Kozak M. A comparison of thermogravimetric characteristics of fresh and used engine oils (CE-2019-350) 289

Editor
Polish Scientific Society of Combustion Engines
43-300 Bielsko-Biała, Sarni Stok 93 Street, Poland
tel.: +48 33 8130402, fax: +48 33 8125038
E-mail: sekretariat@ptnss.pl
WebSite: http://www.ptnss.pl

Subscriptions
Send subscription requests to the Publisher's address.
Cost of a single issue PLZ30 + VAT.

Preparation for print
ARS NOVA Publishing House
60-782 Poznań, ul. Grunwaldzka 17/10A

Circulation: 650 copies

Printing and binding

Zakład Poligraficzny Moś i Łuczak, sp. j.,
Poznań, ul. Piwna 1

The journal is registered in the Polish technical journals content database – **BAZTECH** www.baztech.icm.edu.pl

The journal is listed in the international database **IC Journal Master List** – **Index Copernicus** www.indexcopernicus.com

Declaration of the original version
The original version of the Combustion Engines journal is the printed version.

Papers published in the
Combustion Engines
quarterly receive 13 points as stated by the Notification of the Minister of Science and Higher Education dated 26 January 2017.

Cover
I – Audi 2.0 TFSI DTM (*fot. www.audi-mediacenter.com*); background (Alberta attraction banff *© Photo by James Wheeler from Pexels*)
IV – R460 Hybrid Turbocharger System (*fot. 034motorsport.com*)

Article citation info:
SIADKOWSKA, K., CZYŻ, Z. Selecting a material for an aircraft diesel engine block. *Combustion Engines*. 2019, **178**(3), 4-8.
DOI: 10.19206/CE-2019-301

Ksenia SIADKOWSKA
Zbigniew CZYŻ

CE-2019-301

Selecting a material for an aircraft diesel engine block

Selecting appropriate materials is presently a complex task as material databases cover tens of thousands of different types of materials. Product designing proceeds in numerous stages and in most of them there are open questions with not only one correct solution but better and worse ones. This paper overviews the Diesel engine body construction materials mentioned in the literature and discusses a certain practical method to select materials for a cylinder head and a Diesel engine block as a prototype. The engine body, depending on its purpose, is most frequently iron or aluminum. If it is important to optimize parts to achieve low weight, aluminum alloys are usually applied, especially in the automotive and aviation industries. In the latter case, weight is even more important so new types of magnesium alloys which are even lighter than aluminum ones are developed and used. However, magnesium alloys are, for example, more flammable and not enough strong so, for safety reasons, this type of material is not used solely in engine bodies.

Key words: *Diesel, engine, aluminum alloys, engine block, prototype*

1. Introduction

The choice of a material for the combustion engine block discussed in this paper is directly related to the designing research on a new type of combustion engine structure done in cooperation with the Construction Office of WSK PZL-KALISZ S.A. The investigated engine is a newly designed two-stroke internal diesel engine. The unit's characteristic feature is three cylinders with three pairs of opposed-pistons (Fig. 1). The engine will generate a power output equal to 100 kW at a crankshaft rotation speed of 3800-4000 rpm with a capacity of about 1.6 l in a diesel cycle. The engine will be equipped with a direct diesel injection system. The progress in this research is described in [4, 5, 11, 16].

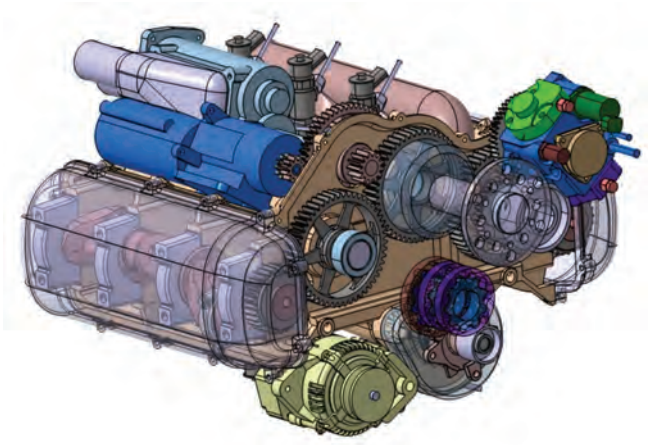

Fig. 1. Visualization of the new construction of the opposed-piston engine

Nowadays, material databases count tens of thousands of different materials so selecting an appropriate structural material is a complex task. Product designing is a multi-step process. Most of these steps face open problems where is no only one correct solution but better and worse ones. The idea of material selection charting introduced in [1] helps in an initial material selection and enables a logical procedure to be used in next stages of such a selection. A type of project (original, adaptive or alternative) already enables a group of desired materials to be initially narrowed down. As far as the original design is expected to be innovative in terms of its materials, an alternative design does not have to be so if its functions are preserved and its modifications involve scale, dimension or a manner to achieve its function. The body of the two-stroke compression-ignition engine can be just classified as an alternative type of design. Cylinder heads and piston engine blocks are usually made of cast iron or aluminum alloys to match their purpose. If it is important to optimize parts for the lowest possible weight, aluminum alloys are usually used, which is typical of the automotive and aviation industries. Actually, in aviation, weight is even more important so new magnesium alloys which are lighter than aluminum alloys are used, however their flammability, lower strength and safety reasons make this material not be used on its own in engine bodies.

World War I and II were heyday periods for the aircraft piston engine. Then, the development of the jet engine hampered their progress for many years. Nowadays, the piston engine is chiefly used in light aircraft: aero clubs, business, cargo, rescue, sport and recreation. Technically, these engines show a pre-war knowledge of theory of operation, design and production technology, especially in comparison with today's automotive drives [14].

According to [14] piston engines constitute the largest weight in every aircraft. Unit weight, or weight per unit of power, used in today's aircraft piston engines is 3–4 times larger than in turbine engines. Individual values of characteristic parameters are: fuel consumption 200–220 g/km/h, power cylinder capacity: 50–60 KM/dm^3, weight: ~0.5 kg/KM. These values relate to spark-ignition engines. Compression-ignition engines due to technological difficulties were not very popular in aviation in the last century and were often used in tanks.

Therefore, this topic is very interesting because light civil aviation is gaining in importance and environmental aspects are crucial here. This is an opportunity to develop aircraft piston engines and apply certain verified automotive solutions because piston engines are constantly improved to satisfy ecological requirements. Currently, compression-ignition engines are increasingly used in the light aviation, e.g. ZOCHE aero-diesel, Wilksch Airmotive,

DeltaHawk Engines, Gemini Diesel, DAIR-100 Diesel Air, Austro Engine AE300 or the conceptual engine by Baker Engineering and Kinetic BEI LLC.

Finding a strong enough type of material to satisfy loads expected in the designed engine is relatively easy. However, finding an optimal solution is not so. It is possible to use alloys which are used, for example, in military applications but their price prevents civil ones. According to [9], a single turbine blade made of a nickel-cobalt alloy known as Inconel is 10 thousand dollars. Piston engines have no blades but have elements that should transfer significant thermal stress.

2. Methodology

A number of material available exceeds capabilities of selection if we resort to analytical capabilities of the human mind only. A kind of software that collects database for specific materials appear to be helpful here. This is an attractive though a very expensive solution, which greatly limits its usefulness [1]. It is worth noting that the approach to the issue of selecting materials presented at least in technical university courses [17] cannot be applied if there is a real need to design elements and select the right material for a designed alternative product. As indicated in [17], selecting materials is an optimization process, so it is necessary to formulate constraints and functions defining material requirements, which means finding the so-called functionality indicator dependent on properties of a material and whose maximization determines an optimal material for a given purpose. This approach is accurate mainly if simple, original products are designed as it enables us to extend an application of new materials.

The functionality indicator is determined from the following algorithm [17]:

- determining the feature to be optimized,
- deriving the equation of the feature to show functional requirements – the function of the objective,
- determining design constraints,
- deriving equations representing design constraints,
- determining free variables,
- substituting free variables calculated from (d) into equation (b),
- grouping the variables into three sets: functional (loads, deflections ...), geometric (size, moments of inertia of sections ...) and material (properties)
- reading the functional indicator.

These are basic guidelines which should be accompanied by other factors like price, ownership of a technology or an ecological impact. In practice, especially if selecting materials for engine components, materials cannot be correctly and effectively selected with no expert knowledge of operations and processes, even if resorting to databases. A simple specification of loads acting on so complex elements that are subjected to variable stress and thermal loads is impossible either. This is verified just after entering material parameters into simulation software, for example parameters that determine mechanical stress or thermal load and after the computation. Accurate calculations are time-consuming, so performing hundreds of repeated calculations for other materials is simply impossible. If load is not known yet, a pre-received material should be adopted. It is, therefore, indispensable to determine what materials could be used for the aircraft piston engine block. Instead of formulating theoretical functionality indicators, time-consuming and complicated to determine loads acting on the product, you can collect information on what materials have been used so far for given elements and choose those that meet requirements set for designed parts, e.g. the engine as it is here. Additional aspects to consider are, of course, availability, price or knowledge and a possibility of an economically justified processing of a given material. This solution should be avoided while designing [1], especially the original product as it hampers development in the field of applied materials. Here, however, we have an adaptive product which is a part of a larger project of a present period of time, fixed-cost, and a necessary level of quality. It seems reasonable here to limit oneself above all to available materials and not search for and test expensive and unreachable ones. It should also be remembered that if you decide on a material not used in a given field yet, you can face new problems such as no accurate material data at given loads, which may lead to significant difficulties and a longer selection period of time, which will also affect quality of calculations. Another important issue is a machining of the material. One can think that companies that professionally manufacture engine components should not find it as a significant problem. The necessity of retooling machines, extending a preparation and completion period of time means high costs and may affect mass production. Mass production companies are hardly interested in unit production, and the need for retooling their technological machines causes a dramatic increase in cost of production. If a prototype project is developed under a research project or by a research center, it becomes another issue affecting a choice of a material. It is necessary to prepare adequate technological facilities to implement production processes.

The first phase of the product life cycle, including manufacturing prototype parts, is very expensive in the whole life-cycle. For example, a unit production of a piston engine with a diameter of a few centimeters in line with a target producing technology amounts to tens of thousands of Polish zlotys. It consists of all production processes that occur during a standard serial production. If there are certain exemptions from a basic technology, this cost can be reduced by up to 80%, however, such a product will probably show poorer strength than its equivalent produced in series. While developing the prototype, some exemptions are necessary chiefly to enable the creation and testing of different versions of parts, and an improvement of the process is postponed in line with the Pareto principle, i.e. 80% of the results come from 20% of outlay and 20% of the results should be covered by 80% of outlay. This principle describes many economics and management phenomena.

In this work, literature analysis is a main tool to select a material for a prototype engine block; however, aircraft engine manufacturer's experience and technological resources are used, too. First, our focus was on the previously used materials for the given element both in the automotive and aviation industries. Then, the development of materials was studied, focusing on selected properties, which accord-

ing to the authors are fundamental, if not decisive here. Also, the authors included availability and data obtained from the material database.

3. Application of aluminum alloys in the production of diesel engine blocks

3.1. Designation

Depending on the source of the article and the time it was written, aluminum alloys have different designation. In order to unify the nomenclature in situations where there is an equivalent in European standards for:

– PN-EN 573 "Aluminum and aluminum alloys – Chemical composition and types of plastically processed products"

or

– PN-EN 1706 "Aluminum and aluminum alloys – Castings – Chemical composition and mechanical properties"

it will be quoted, but due to differences in the content ranges of individual elements for individual alloys, this is not always possible. Then the original nomenclature will be preserved, and possibly the material with the closest composition will be indicated. Below, Table 1 and 2 present exemplary markings of aluminum alloys in standards most frequently used by manufacturers and in scientific publications.

Table 1. Designation of plastic processed aluminum alloys according to selected standards [8]

PN EN 573-3 (numerical)	PN EN 573-3 (chemical)	PN-79/H-82160 (old norm)	ASTM	DIN
2017A	AlCu4MgSi (A)	PA 6	2017	Al-CuMg1

Table 2. Designation of aluminum alloys castings according to selected standards [10]

PN-EN 1706:2001	PN-76/H-88027 (old norm)	ISO 3522/1984	EN 1706:1998
AC-AlSi7Mg	AK7 AlSi7Mg	Al-Si7Mg/Fe/	AC-AlSi7Mg

Aluminum alloys are thermally treated to the state T. The designation together with the description is presented in Table 3. In the context of engine block and cylinder head machining, T6 treatment is the most common.

Table 3. Designation of heat treatment process conditions [6]

Treatment designation	Treatment description
T1	naturally aged after cooling from the increased temperature of the shaping process
T2	cold deformed after cooling from elevated forming temperature and naturally aged
T3	over-saturated, cold deformed and naturally aged
T4	saturated and naturally aged
T5	artificially aged after cooling from an elevated temperature of the shaping process
T6	saturated and artificially aged
T7	saturated and stabilised (obsolete)
T8	over-saturated, cold deformed and artificially aged
T9	over-saturated, artificially aged and cold deformed

3.2. Materials used in the manufacture of diesel engine blocks

In the popular scientific literature, in the context of materials used to manufacture the engine body (depending on the construction this refers to the engine block and cylinder head), most often appear aluminum alloy or wrongly – aluminum, which actually replaced the older and heavier cast iron constructions. However, in the engine design process the information about an unspecified alloy is definitely insufficient, detailed data of a specific material are necessary. Engine manufacturers often do not provide information about the type of alloy used, its properties or the type of treatment used. The "know-how" in cylinder head casting technology is closely guarded and provides an advantage in the market.

The cylinder heads must fulfil two basic material requirements. One of them is resistance to deformation caused by the pressure generated during combustion of the load and assembly loads preventing leaks in the system. The second requirement is resistance to high temperatures to prevent cracks in the cylinder head area between inlet and outlet valves, which are exposed to flame [15].

According to the material base [10], the following alloys can be used for cylinder heads of combustion engines:

– AK52 (AlSi6Cu2),
– AK51 (AlSi5Cu1),
– AK84 (AlSi8Cu4MgMn) (air cooling, Fiat 126p),
– AK53 (AlSi5Cu3Mn).

However, there are situations where producers decide to make their knowledge available to a wider audience. In the paper [13] the tested materials used for the production of cylinder heads are alloys:

– AK51 (AlSi5Cu1)

and

– alloy composed of 8.75% Si, 0.50% Cu, 0.43% Mg, 0.13% Mn, 0.22% Fe, 0.02% Ni, 0.03% Zn, 0.02% Ti, 0.02% Sn, with a composition close to the alloy AK9 (AlSi9Mg) with a content of 8.5-10.5% Si, 0.3% Cu, 0.25–0.4% Mg, 0.25–0.5% Mn.

It is described as a material of the "head of a well-known automotive company". There is also information that the Fiat foundry used an alloy of 6% Si, 2% Cu, 0.3% Mn, i.e. AK52 (4.0-6.0% Si, 1.5-3.5% Cu, 0.3–0.8% Mg, 0.2–0.8 Mn, 0.5 Ni) for the engine block.

According to [15] and [2], A356.0 aluminum alloy (ASTM: 6.5–7.5% Si, 0.2% Cu, 0.25–0.45% Mg, 0.1% Mn) is a widely used material in the production of cylinder heads of internal combustion engines. In the old Polish standard PN-76/H-88027 it is an alloy marked as AK7 (6.0–8.0% Si, 0.2% Cu, 0.25–0.4% Mg, 0.1–0.5 Mn), while in the European standard: AlSi7Mg0.3.

3.3. Overview of research carried out with the application of selected aluminum alloys

This review has focused on the aluminum alloys that are used for CI engine blocks and on the materials considered for such applications. The main conclusions of this work were selected, focusing on the material properties relevant to the critical load conditions of the engine block.

In the paper [2] the influence of T6 type heat treatment of AK7 alloy on thermo-mechanical fatigue and cyclic slow-changing loads was investigated. In experimental studies an improvement in mechanical and slow-changing loads, especially at room temperature, was found. However, the positive effect of heat treatment on thermo-mechanical stability was not so significant anymore and the difference in strength between the alloy with and without heat treatment decreased with the increase in temperature. The authors conclude that heat treatment did not improve thermo-mechanical fatigue properties of the alloy due to over-aging, i.e. softening of the alloy due to exceeding the required temperature or the required artificial aging time, while under isothermal load the strength properties improved significantly.

In the paper [15] the influence of the artificial ageing process on the material samples taken from the cylinder head made of AK7 aluminum alloy and thermally treated with T6 type was investigated. The effects of thermal slow-changing loads and changes in the microstructure during the thermal fatigue test were studied. Under conditions corresponding to the operation of the engine, thermal strength tests of slow-changing loads were carried out in order to describe the nature of elastic, plastic and viscoelastic deformations and thermal fatigue. An important conclusion obtained by the authors of the paper is the fact of improving fatigue life after the application of ageing after heat treatment type T6, but at the same time the strength decreased and the material showed a tendency to deformation. The ageing time also influences the strength properties and enables optimization of fatigue strength.

In the paper [12] the fatigue properties of the alloy marked as ASTM A357.0, heat-treated type T61, composed of 6.5–7.5% Si, 0.2% Cu, 0.4–0.7% Mg, 0.1% Mn, which corresponds to the Polish standard PN-76/H-88027 AK7 alloy (EN: AlSi7Mg0.6), however with a slightly higher magnesium content than A356, were studied. This alloy is used for the production of cylinder heads of diesel engines. The authors pay attention to material defects, such as porosity or oxide coating, which may be the initiators of damage if located on the surface or in the top layer of the cast elements.

The article [12] presents the results of investigations carried out in terms of fatigue strength and micromechanisms of damage on a sample obtained from a new cylinder head taken immediately after leaving the production line. A relationship between the fatigue zone micromechanism and final failure zone and the appearance of fatigue cracks in the area of porosity defect was observed on the surface of the specimen fracture. The main initiator of fatigue crack was the surface porosity in the region of maximum tensile stress. When porosity occurred outside this area, far from the maximum tensile stress, it did not crack the specimen. Other factors such as oxide inclusions, silicon particle size, intermetallic iron molecules did not affect fatigue life due to the predominance of pores previously initiating fractures. This statement is consistent with the results of the paper [3], in which the authors state that porosity is the main factor defining fatigue life of aluminum alloys.

In the paper [7] various aluminum alloys with the following determination were subjected to fatigue tests: AlSi7Mg-T6 (A356), AlSi5Cu3-T7, AlSi5Cu1-T7, AlMg3Si1-T6, AlMg3Si1(Cu)-T6 and AlMg3Si1(Sc,Zr)-T5. The first one is the most commonly used alloy for cylinder heads and is a reference point for the other materials in the context of their use for cylinder heads. Cast aluminum cylinder heads are subjected to increasing thermo-mechanical loading and the space between valve bridge is a critical element. For this reason, the sample geometry was modified (Fig. 2), similar to that of the critical element, and compared to the load model obtained on standardized samples.

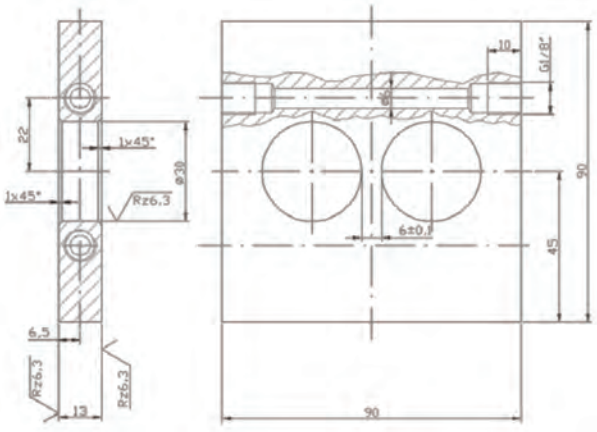

Fig. 2. View of the sample [7]

On the basis of experimental research it has been proposed to build in a numerical ageing model of the alloy in order to improve the model used to determine fatigue life. The cylinder head is exposed to multi-axial loads and varying temperature conditions, but cracks are initiated around the valve seat. The strength of aluminum alloys decreases significantly with increasing temperature. Hardened alloys reduce their strength already at 150–200°C, which also affects the metallurgical properties and microstructure. The local load on the head is in the range of 20–300°C. The anticipation of a decrease in material strength allows the serious consequences of damage to be limited. The lowest coefficient of thermal expansion was obtained for standard alloy A356, regardless of temperature increase. The thermal conductivity of this alloy tested at 50–400°C was also the highest (190 W/(mK)). The mechanical strength of almost all the tested alloys decreases drastically in the range 150–250°C (from about 300–350 MPa to 150–200 MPa), except for the alloy AlMg3Si1(ScZr)-T5, for which the value of permissible stresses remains at the level of 250–300 MPa throughout the temperature range investigated [7].

Despite the fact that the aluminum alloys with the main additives such as silicon and copper (AlSiCu) are characterized by high thermal conductivity, the decrease in strength was not as significant as in the case of the standard alloy A356. The tested aluminum alloys with magnesium and silicon (AlMgSi), despite worse strength and thermal conductivity, were able to withstand up to twice as many thermal-mechanical load cycles to crack than the standard alloy. The studies carried out clearly indicate the influence of aging of the material on tensile strength and stress distribu-

tion associated with a variable temperature field. Determination of the function, which will include thermal load during the heat-resistance tests, will enable a more accurate forecast of the product life under real load conditions. The properties of alloys as a function of time, temperature and the number of fatigue cycles were also determined. An important conclusion from the study is the size of the influence of the ageing temperature on the two tested alloys. In the case of the standard alloy it is high, whereas in the case of AlMg3Si1 (Sc, Zr) – T5 alloy it is low and even imperceptible. The research has also shown higher resistance of AlSiCu alloys to crack initiation in comparison to AlMgSi and AlSiMg alloys. Several numerical simulations for AlSi7Mg and AlSi5Cu3 alloys were carried out and compared with experimental results. Consideration of material aging function in the model turned out to be important especially for the standard alloy, which properties deteriorate drastically in the range of applied thermal loads [7].

4. Conclusions

It was concluded that it is not appropriate to use for the prototype engine block an alloy which is not commercially available. Production of a new alloy in a foundry, only for the purpose of making a prototype engine is not economically justified and, moreover, makes it necessary to determine its material data. It should be mentioned that the aim of the project is the construction of a new engine and therefore testing of new materials exceeds the scope. It is worth mentioning that the information presented in the material databases, i.e. that the physical and mechanical specifications given are only approximations, and the properties of materials may vary significantly depending on the supplier, internal standards, heat treatment, dimensions and other parameters, therefore there is no guarantee of suitability for a specific application.

It is recommended to use the alloy marked AK7 (A356, AlSi7Mg) for the production of the prototype engine block. If the results of simulation studies will indicate the correctness of the selection, and the manufactured element will not show sufficient strength, the cause of the damage should be determined and perhaps another technology of production should be considered, with particular attention on the porosity of the produced element.

Acknowledgements

This work has been realized in the cooperation with The Construction Office of WSK "PZL-KALISZ" S.A." and is part of Grant Agreement No. POIR.01.02.00-00-0002/15 financed by the Polish National Centre for Research and Development.

Bibliography

[1] ASHBY, M.F. Dobór materiałów w projektowaniu inżynierskim, red. Wojciechowski S.M., *WNT*, Warszawa 1998.
[2] AZADI, M., MEHDI M.S. Heat treatment effect on thermomechanical fatigue and low cycle fatigue behaviors of A356.0 aluminum alloy. *Materials&Design*. 2013, **45**, 279-285. DOI:10.1016/j.matdes.2012.08.066.
[3] BUFFIERE, J.Y. et al. Experimental study of porosity and its relation to fatigue mechanisms of model Al-Si7-MgO.3 cast al alloys. *Materials Science and Engineering: A*. 2001, **316**. DOI:10.1016/S0921-5093(01)01225-4.
[4] CZYŻ, Z., SIADKOWSKA, K., SOCHACZEWSKI, R. CFD analysis of charge exchange in an aircraft opposed-piston diesel engine. *MATEC Web of Conferences*. 2019, **252**, 04002. DOI:10.1051/matecconf/201925204002.
[5] GRABOWSKI, Ł., PIETRYKOWSKI, K., KARPIŃSKI, P. Charging process analysis of an opposed-piston two-stroke aircraft diesel engine. *ITM Web of Conferences*. 2017, **15**, 03002. DOI:10.1051/itmconf/20171503002.
[6] Forum Aluminium. Oznaczenia stanów produktów. 2016, http://forumaluminium.pl/pl/forum/6/topic=16.
[7] GRIEB, M.B. et al. Thermomechanical fatigue of cast aluminium alloys for cylinder head applications experimental characterization and life prediction. *Procedia Engineering*. 2010, **2** (1), 1767-1776. DOI:10.1016/j.proeng.2010.03.190.
[8] Investa. Tabela gatunków stopów aluminium. 2017, http://www.investa.pl/oferta/aluminium_poradnik_tabela_gatunkow.html.
[9] KONIECZNY, J. Materiały stosowane w konstrukcjach lotnictwa wojskowego. *Armia*. 2013, **4**, 68-75.
[10] Konsorcjum Biocentrum Ochota. Odlewnicze stopy aluminium wg PN-EN 1706:2001. 2017, http://info.grafen.ippt.pan.pl/bazy/bazy-materialowe/aluminium.html.
[11] MAGRYTA, P., PIETRYKOWSKI, K.,SKIBA, K. FEM simulation research of natural frequency vibration of crankshaft from internal combustion engine, *ITM Web of Conferences*. 2017, **15**, 07004. DOI: 10.1051/itmconf/20171507004.
[12] MATTOS, J.J.I. et al. Fatigue properties and micromechanism of fracture of an AlSiMg0.6 cast alloy used in diesel engine cylinder head. *Procedia Engineering*. 2010, **2**(1), 759-765. DOI:10.1016/j.proeng.2010.03.082.
[13] ORŁOWICZ, W., OPIEKUN, Z. Badania materiałowe odlewów głowic silników. *Solidification of Metals and Alloys*. 1998, **38**, 97-102.
[14] SZCZECIŃSKI, S. Transactions of the Institute of Aviation – Aircraft Powerplant Issues. 2009, **4**(199).
[15] TAKAHASHI, T., KATSUHIKO S. Low cycle thermal fatigue of aluminum alloy cylinder head in consideration of changing metrology microstructure. *Procedia Engineering*. 2010, **2**(1), 767-776, DOI:10.1016/j.proeng.2010.03.083.
[16] TULWIN, T., KARPIŃSKI, P. Analysis of the fuel spray diversity in the opposed-piston engine, *IOP Conf. Series: Journal of Physics: Conf. Series*. 2018, **1101**, 012045 DOI:10.1088/1742-596/1101/1/012045.
[17] WACH, J. Dobór materiałów konstrukcyjnych. 2017, http://fluid.itcmp.pwr.wroc.pl/~jwach/lab/mkie.htm.

Ksenia Siadkowska, MEng. – Faculty of Mechanical Engineering, Lublin University of Technology.
e-mail: *k.siadkowska@pollub.pl*

Zbigniew Czyż, MEng. – Aeronautics Faculty, Polish Air Force University.
e-mail: *z.czyz@law.mil.pl*

Article citation info:
GIS, M., BEDNARSKI, M., LASOCKI, J. Determination of pollutant emission of electric vehicle in real traffic conditions in Poland. *Combustion Engines*. 2019, **178**(3), 9-14. DOI: 10.19206/CE-2019-302

Maciej GIS
Mateusz BEDNARSKI
Jakub LASOCKI

CE-2019-302

Determination of pollutant emission of electric vehicle in real traffic conditions in Poland

Alternative drives have an increasing share in the global, European and Polish market. The city authorities support primarily the development of electromobility. Progress in these issues is also noticeable in Poland.

The increasing number of battery electric vehicles (BEVs) requires increasing energy costs of the country. Therefore, it is necessary to increase energy production. This work estimates how large this energy surplus should be. For this purpose, it was necessary to determine the average energy consumption of an electric vehicle in real traffic conditions, and then to calculate the average energy demand for a selected number of vehicles. Obtained results were related to pollutant emission considered in the well-to-wheel perspective (including generation of electricity).

In the article, the authors also referred to the minimum number of charging stations for electric vehicles on the Trans-European Transport Network (TEN-T) in Poland. This is a necessary condition on which depends the use of BEV vehicles not only on the territory of cities, but also throughout the country.

Key words: *electric vehicle, pollutant emission, RDE, environment, electromobility*

1. Introduction

Electric vehicles are not a novelty in the history of motoring. The first attempts to work on electric vehicles began around 1800. Their popularity was significant until 1900. In later years they were supplanted by vehicles fueled with conventional fuels [13].

The return to electric vehicles is the result of the increasing emission of harmful exhaust gases and the fight to reduce the impact of transport on greenhouse gas emissions.

According to the IEA report, the number of electric vehicles (EV), hydrogen vehicles (FCEV) and plug-in hybrids (PHEV) on global roads in 2017 reached 3.1 million (an increase of 54% y/y). In 2017, more than 1 million electric cars were sold in total (54% more than in 2016), half of which (580 thousand) in China. The second place was taken by the United States with a result of 280,000 pieces [3].

On the roads of the Middle Kingdom, currently there are 1.23 million electric vehicles (40% of the global fleet EV), in Europe 0.82 million, in the US 0.76 million, while in the rest of the world – 0.3 million. In 2018, the largest EV share in the new vehicle market was recorded in Norway (39.2%), Iceland (11.7%) and Sweden (6.3%). China (2.2%), Germany (1.6%), USA (1.2%) and Japan (1.0%) ranked next. [3]

Electric vehicles are now being identified as one of the main pillars of the future motorization. Until 2030, they are to account for around 30-35% of all vehicle sales in the world [5].

2. EV vehicle tests in RDE

2.1. Development of the RDE research route

In order to better determine the real impact of EV vehicles on the environment, it was necessary to determine its real energy consumption in real traffic conditions, according to Real Driving Emissions (RDE) test.

For this purpose, it was necessary to designate a test route that would be representative for the tests and would meet the requirements imposed by the WLTP procedure [14].

Requirements imposed by the legislator are presented in the Table 1.

Determination of the research route (Fig. 1) was dealt with at the Motor Transport Institute. Its development was a priority due to the further possibilities of conducting research [16].

Fig. 1. RDE research route

The designated transit route meets the requirements imposed by the legislator. It complements the WLTP testing procedure. The transit route is representative for Warsaw and allows performing tests in the field of emission tests in accordance with the requirements of the currently applicable WLTP procedure [16].

2.2. The electric vehicle

In order to perform EV vehicle tests in real traffic conditions, one of the popular electric vehicles on the European market was used for this purpose. Its selected technical data are presented in the Table 2. In Fig. 2 the research vehicle is presented.

Table 1. Requirements for the RDE test route [14]

Parametr	Requirements
Outdoor temperature (T_z)	normal range: $0^oC \leq T_z < 30^oC$
	extended bottom range: $-7^oC \leq T_z < 0^oC$
	extended upper range: $30^oC < T_z \leq 35^oC$
The topographical value of conducting the research (h)	normal range: $h \leq 700$ m n.p.m.
	extended range: $700 < h \leq 1300$ m n.p.m.
Assessment of the impact of external weather and road parameters, as well as driving style	total height increase: less than 1200 m/100 km
	relative positive acceleration (RPA): bigger than RPA_{min} (for all driving conditions)
	Coefficient of velocity and acceleration ($v \cdot a_{pos}$): less than $v \cdot a_{pos\ min}$ (for all test conditions)
Thermal condition of the vehicle before the test	cold start of the vehicle: cooling liquid below 70°C, time at least 300 s
	no counting of emissions from a cold start to the RDE test
One time vehicle stop	not longer than 180 s
Operation of exhaust gas treatment systems	single regeneration of the diesel particulate filter may cause the RDE test to be repeated; the occurrence of two regenerations is included in the RDE emission test results
Operation of driving comfort systems	normally used as intended (e.g. operation of the air conditioning system)
Vehicle load	vehicle mass: driver (and passenger) and test equipment; maximum load <90% of the total mass of passengers and the payload of the vehicle
Test requirements	duration 90–120 min
Requirements for the urban part of the test	share 29–44% the length of the entire test
	distance: greater than 16 km
	vehicle speed (v): $v \leq 60$ km/h
	average speed: 15–40 km/h
	staging: 6–30% of the time of the urban part
Requirements for the extra-urban part of the test	share of 23–43% of the total length of the test
	distance: greater than 16 km
	vehicle speed (v): $60 \text{ km/h} < v \leq 90$ km/h
Requirements for the test section of the highway	share of 23–43% of the total length of the test
	distance: greater than 16 km
	vehicle speed (v): $v > 90$ km/h
	driving speed over 100 km/h for at least 5 minutes
	driving speed over 145 km/h for up to 3% of the time

Table 2. Selected technical data of the tested EV vehicle [2]

Parameter	Unit	Value
Length	mm	4140
Width	mm	1800
Hight	mm	1593
Wheelbase	mm	2570
Engine		synchronous with permanent magnets
Power	kW	80.2
Maximum engine rotational speed	rpm	10,500
Range	km	Around 200
Battery type		Lithium-polymer
Number of links	pcs	192
Number of modules	pcs	8
Weight of links	kg	135

Fig. 2. An electric research vehicle

2.3. Measuring equipment

Specialist test equipment was used to test the electric vehicle. The YOKOGAWA WT1806E device (Fig. 3) is a six-channel power analyzer for measuring, among others, power or consumption of energy collected and recovered from batteries and subassemblies of electric and hybrid cars, among others about:

- voltage measurement range 0–1000 V,
- current measurement range: 3 channels 0–5 A, 3 channels 0–50 A,
- basic accuracy not less than 0.05% of reading, +0.05% of the measuring range,
- measurement update frequency (voltage, current, power) of at least 1 ms,
- sampling rate of 2 MS/s, 16-bit converter.

Fig. 3. Research apparatus

2.4. Test results and analysis

The tests carried out on the RDE route allowed to determine the average energy consumption of the vehicle. The tests were repeated several times in order to determine the average of the obtained results.

The results from the electric vehicle tests on the RDE route are shown in Table 3.

Table 3. The average energy consumption of the EV vehicle and the average energy taken from the electricity grid during its charging

1	Unit	Value
Energy consumed during research in RDE	kWh	17.3
Energy collected from the mains while charging	kWh	14.8

On the basis of own tests of an electric vehicle in real traffic conditions, it was possible to examine its average energy consumption and determine how much electricity is needed to charge the batteries after passing the RDE test. Then it was determined with the assumption of daily runs, what would be the energy demand for one vehicle and energy costs related to it (Table 4).

Table 4. Annual energy consumption needed to recharge the batteries of one vehicle and determine the related costs

Parameter	Unit	Value
Daily mileage on business days	km	60
Daily mileage on Sunday and holidays	km	60
Annual mileage on business days	km	15,060
Annual mileage on Sundays and holidays	km	6840
Total mileage	km	21,900
Price 1 kWh for a household (G11 tariff)	zł/kWh	0.55
Annual energy consumption needed to recharge the batteries of one vehicle	kWh	3602
Annual cost of charging one vehicle	zł	1981

3. Impact of EV vehicles on the country's energy demand

Electricity production will increase by about 40% – from 158 TWh in 2010 to 223 TWh in 2050. It will be connected both with the economic development of Poland and with shifting the demand for final energy from fossil fuels towards electricity, resulting from the growing mechanization of industry and services, the spread of electric vehicles (plug-in hybrids) and electrification of water heating and production processes heat in many households so far using coal or gas for this purpose. This will also entail an increase in the demand for power from the current 29 GW to 42 GW after 2040 [17].

The main producer of electricity throughout the forecast period will be coal-fired power plants. The need to satisfy fast growing demand will necessitate investment in new coal capacities already in the current decade, especially that blocks built in the sixties and seventies of the twentieth century will be phased out. As a result of both processes by 2030, electricity production in coal-fired power plants will increase by approx. 20% compared to 2010. At the same time, the demand for electricity will increase by approx. 40%, and lignite resources in existing mines will start to run out. At the same time, opening new deposits of this raw material will be economically unjustified, as long as the price of carbon dioxide emission allowances will grow in line with the assumptions of the reference scenario. The resulting gap between production and demand for electricity will have to be filled by low-emission technologies [17].

The supplement to the coal-fired power plant in the energy system will be primarily renewable sources supported by gas sources operating primarily in the reserve and working in combination with heat production. The reasons for the increase in the relative importance of RES are two. First of all, the avalanche development of solar plants in the world causes a rapid drop in solar energy costs for end users [17].

Taking into account a specific plan to introduce in Poland up to 2020 a million electric cars, this value was assumed to be representative in the calculations. Considering the average energy demand for charging an eclectic vehicle determined in own studies and analyzes, it was possible to determine the energy demand for a million vehicles.

Table 5 shows the energy demand of a million electric vehicles.

Table 5. Energy demand for powering electric vehicles

Parameter	Unit	Value
Annual energy consumption needed to recharge the batteries of one electric vehicle	kWh	3602
Annual energy consumption needed to recharge the batteries of a million electric vehicles	TWh	3.602
An increase in energy demand while powering a million electric vehicles	%	2.2

As it results from the above calculations, a million electric vehicles do not have a significant impact on the overall energy demand of the country. In the current situation, when in 2017 the energy demand of the country amounted to 170 TWh, the increase in demand for a million electric vehicles would amount to 2.2%.

4. Well-to-wheel pollutant emission from EV

It is possible to estimate total emission of air pollutants that can be attributed to EV operation by including the full chain of electricity generation and supply, along with the efficiency of each process considered. Certainly, the result will depend on many factors, i.e. the type of primary energy sources used for electricity generation, technology applied at power station, electricity transmission and distribution losses, efficiency of the vehicle propulsion system, etc. Quantification of pollutant emission for such a wide range is performed in the Well-to-Wheel (WtW) analysis, which takes into account the acquisition of primary energy sources, their processing into energy carriers (electricity or fuel), transport, distribution and final consumption in the vehicle [1]. This approach allows for a comparison of environmental impacts between EV and conventional vehicles with combustion engine.

WtW analysis is divided into two phases [1]:

- WtT (Well-to-Tank), covering the path of the energy carrier up to the place of its storage in the vehicle,
- TtW (Tank-to-Wheel), covering the energy consumption of the vehicle.

In this study, the WtW analysis was performed for the EV described in previous chapters. The aim was to determine total annual emission of: carbon dioxide (CO_2), sulfur dioxide (SO_2), nitrogen oxides (NO_x), carbon monoxide (CO) and particulate matter (TSP) from the EV charged using electricity from power grid in Polish conditions. The scope of the analysis was broken down into the following stages: primary energy sources acquisition and transport, conversion of primary energy sources to electricity at po-

wer station, electricity trade (import and export of the electricity abroad of Poland), electricity supply post-trade, electricity distribution over the power grid, EV charging at low voltage (typical for most users [15]), and conversion of the electricity to mechanical energy in EV (Fig. 4).

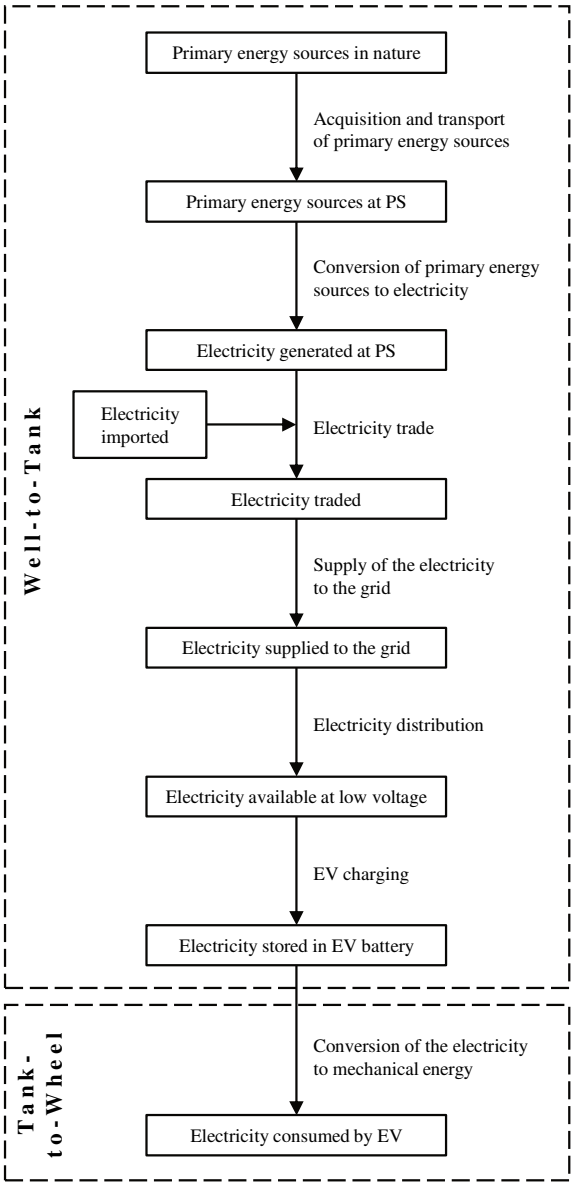

Fig. 4. Stages of the WtW analysis considered in the study; PS – power station

The general research methodology has been adopted from the JEC WTW report version 4a [6, 7]. In the calculations the following assumptions were made:

- EV does not emit air pollutants in the TtW phase,
- renewable primary energy sources do not emit pollutants at the electricity generation stage,
- the data on Polish electricity mix in 2017 (shares of electricity obtained from the combustion of fossil fuels, as well as various renewable energy sources) is derived from the national database on greenhouse gas emissions and other substances, run by KOBiZE (National Centre for Emissions Management) [8],
- emission factors for electricity generation via combustion of fuels are derived from KOBiZE report for 2017 [9],
- emission factors concerning acquisition and transport of primary energy sources to power station are adopted from [11],
- data on electricity traded with other countries was taken from [11].

Table 6 presents the results of calculations of equivalent emission of pollutants for 1 kWh of electricity needed for charging EV at low voltage.

Table 6. Calculated emission factors for electricity needed for charging EV at low voltage in Polish conditions

Pollutant (equivalent)	CO_2	SO_2	NOx	CO	TSP
Unit	g/kWh	mg/kWh	mg/kWh	mg/kWh	mg/kWh
Value	881	825	837	300	50

Taking into account the annual energy demand for one EV in Poland (3602 kWh), annual pollutant emission that can be associated with charging the batteries of EV was calculated. It is presented in Fig. 5.

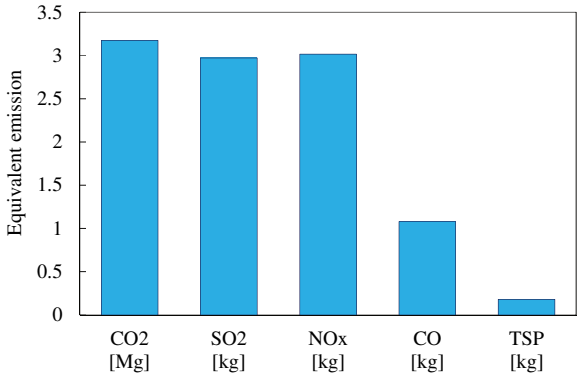

Fig. 5. Annual emission of pollutants associated with charging the batteries of one EV in Polish conditions

Consequently, the total potential emission of pollutants as a result of charging the batteries of one million EVs in Poland can be calculated. The results are given in Table 7.

Table 7. Total potential emission of pollutants associated with charging the batteries of one million EVs in Poland

Pollutant (equivalent)	CO_2	SO_2	NO_x	CO	TSP
Unit	kg	kg	kg	kg	kg
Value	$3.17 \cdot 10^9$	$2.97 \cdot 10^6$	$3.01 \cdot 10^6$	$1.08 \cdot 10^6$	$0.18 \cdot 10^6$

5. Comparison of well-to-wheel pollutant emission from EV and conventional vehicle

In order to better understand and evaluate the results of WtW analysis made for EV (chapter 4), they were compared with the results of WtW analysis for conventional vehicle with an internal combustion engine (ICEV). The ICEV chosen for comparison had similar technical parameters (Table 8) to the EV and was equipped with a compression-ignition engine supplied with diesel oil.

Table 8. Selected technical data of the tested ICEV [2]

Parameter	Unit	Value
Length	mm	4278
Width	mm	1777
Hight	mm	1658
Wheelbase	mm	2555
Engine type		Compression-ignition, 4-cylinder, Common rail
Engine displacement	cm^3	1686
Maximum power	kW @ rpm	96@4000
Maximum torque	Nm @ rpm	300@2000–2500
Gearbox type		Manual

Fuel consumption and pollutant emission concerning the operation of ICEV, i.e. in the TtW phase, were determined in real traffic conditions using exactly the same RDE test route as for the EV (chapter 2). The concentration of exhaust compounds (CO_2, CO, NO_x) and the exhaust gas flow rate were measured using portable exhaust gas analyzer SEMTECH DS from Sensors Inc. The results of road tests are presented in Table 9. Note that the emission of SO_2 and PM was not included in the tests. Instead, SO_2 emission in TtW phase was determined from fuel consumption using emission factor according to the Ecoinvent database [4]. On the other hand, PM emission was excluded from the comparative analysis due to the lack of adequate empirical test results, while its theoretical estimation would be subject to significant uncertainty, taking into account the high impact of engine operating conditions on the emission of this pollutant.

Table 9. Fuel consumption and pollutant emission of ICEV in the TtW phase – results of RDE test

	Fuel consumption	CO_2 emission	SO_2 emission	NO_x emission	CO emission
Unit	dm^3/100 km	g/km	mg/kg	mg/km	mg/km
Value	5.9	157.50	5.02	201.17	148.10

The data from Ecoinvent [4] were also used to calculate the emission of pollutants related to the production, transport and distribution of diesel oil, i.e. in the WtT phase (Table 10). To avoid the impact of additional assumptions on the results of the analysis in the WtT phase, the standard approach from Ecoinvent was adopted. It is adequate to European conditions.

Table 10. Pollutant emission associated with the production, transport and distribution of diesel oil in European conditions – the WtT phase

Pollutant	CO_2	SO_2	NO_x	CO
Unit	g/kg	g/kg	g/kg	g/kg
Value	491.89	4.390	1.797	0.148

Finally, a total emission of pollutants was obtained, combining the TtW and WtT phases. The results for ICEV were compared with the results for EV (Fig. 6).

Analyzing the results of WtW shown in Fig. 6, it is clear that EV has lower overall environmental load than ICEV when considering both the use of the vehicle and the production of fuel or electricity. It is worth emphasizing that this result was obtained for Polish conditions, where the majority of electricity is generated by burning hard and brown coal. In countries with a higher share of renewable energy in the electricity mix, e.g. Norway, the difference between WtW pollutant emission for EV and ICEV would be even greater.

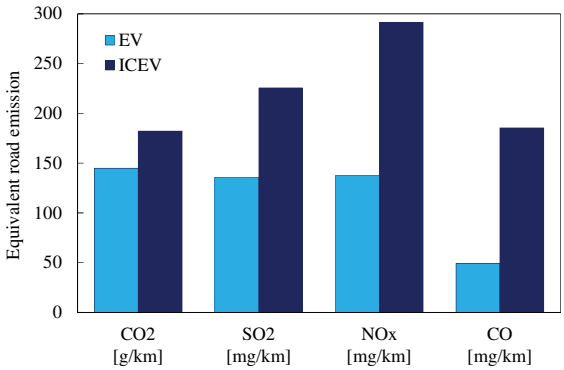

Fig. 6. Comparison of WtW emission for EV and ICEV

6. Number of EV vehicle charging stations on the TEN-T road network and its impact on the environment

The Trans-European Transport Network (TEN-T) is an instrument for the coordination and ensuring coherence and complementarity of infrastructure investments [10].

As a result of the revision of the TEN-T guidelines completed in 2013, a new agreement has been established on the territory of the EU Member States. This system includes a core network that underpins the development of the transport network on which EU activities are to focus, in particular on cross-border sections, missing links, multimodal connections and major bottlenecks, and a comprehensive network ensuring the availability and connectivity of all Union regions [10].

The trans-European TEN-T transport network includes [10]:

– road, rail, air, sea and river routes constituting the most important connections from the point of view of the development of the European Union,
– point elements of infrastructure in the form of sea, air, inland and road-rail terminals.

Taking into account such variables as the location and infrastructure of given road sections, the number of fast charging points for electric vehicles was determined. Their minimum amount is 60 points. With such infrastructure, it will be possible to use electric vehicles on roads belonging to transport routes

TEN-T and constituting road sections that will be heavily loaded in the perspective of 2020, without worrying about the lack of space for charging vehicles. Assuming that 3.602 TWh of energy and the efficiency of chargers placed next to the TEN-T network is 95% needed to supply one million vehicles [12], annual real energy demand will amount to 3.752 TWh.

7. Conclusions

Electric cars are considered the future of motoring. They are becoming more and more popular. In addition, there are a number of benefits related to the operation or subsidies for their purchase.

EV vehicles in daily use require the vehicle to be charged. As a result, the energy demand of the country increases. As it results from the calculations presented in the article, the increase in the demand for electricity for a million EV vehicles, only amounts to 2.2%. On the scale of national energy demand, this is not much.

The article also presents the total potential emission of pollutants associated with charging batteries of one million electric vehicles in Poland – WtW (Well-to-Wheel). Calculations show that the emission equivalent is: for CO_2 – $3.17 \cdot 10^9$ kg, SO_2 – $2.97 \cdot 10^6$ kg, NO_x – $3.01 \cdot 10^6$ kg, CO – $1.08 \cdot 10^6$ kg, TSP – $0.18 \cdot 10^6$ kg. WtW pollutant emission for electric vehicle was compared with WtW emission for conventional vehicle, equipped with compression-ignition engine. It was found that electric vehicle has lower overall emission of pollutants than conventional vehicle when considering vehicle operation and the production of fuel or electricity.

After calculations of the emission related to the charging of an electric vehicle, the article focuses on determining the minimum number of EV vehicle charging stations on the TEN-T road network. It turns out that 60 charging points located on the main transit routes in Poland are sufficient to efficiently use EV vehicles.

Nomenclature

CO	carbon monoxide
CO_2	carbon dioxide
EV	electric vehicle
KOBiZE	Krajowy Ośrodek Bilansowania i Zarządzania Emisjami
NO_x	nitrogen oxides
RDE	real driving emissions
SO_2	sulfur dioxide
TEN-T	Trans-European Transport Network
TSP	Total Suspended Particles
WLTP	Worldwide harmonised Light duty vehicle Test Procedure

Bibliography

[1] CHŁOPEK, Z., LASOCKI, J. Comprehensive evaluation of the environmental hazard caused by the operation of automotive vehicles. *The Archives of Automotive Engineering – Archiwum Motoryzacji*. 2011, **54**(4), 19-36.

[2] http://kia.com

[3] http://www.elektro.info.pl/aktualnosc/id8599,iea-liczba-pojazdow-elektrycznych-na-swiecie-przekroczyla-3-mln-sztuk

[4] https://www.ecoinvent.org/

[5] https://wysokienapiecie.pl/13819-stacje-ladowania-powstaja-przy-trasach-i-w-miastach/

[6] JEC (JRC-Eucar-Concawe). Tank-To-Wheels Report Version 4a – Well-to Wheels Analysis of Future Automotive Fuels and Powertrains in the European Context. Available at: https://ec.europa.eu/jrc/en/jec

[7] JEC (JRC-Eucar-Concawe). Well-To-Wheels Report Version 4.a: Well-to Wheels Analysis of Future Automotive Fuels and Powertrains in the European Context. 2014. Available at: https://ec.europa.eu/jrc/en/jec

[8] KOBiZE. The national database on greenhouse gas emissions and other substances. Available at: krajowa-baza.kobize.pl/

[9] KOBiZE. Wskaźniki emisyjności CO_2, SO_2, NO_x, CO i pyłu całkowitego dla energii elektrycznej na podstawie informacji zawartych w Krajowej bazie o emisjach gazów cieplarnianych i innych substancji za 2017 rok, 2018.

[10] mib.gov.pl.

[11] MORO, A., LONZA, L. Electricity carbon intensity in European Member States: Impacts on GHG emissions of electric vehicles. *Transportation Research Part D: Transport and Environment*. 2018, **64**, 5-14. DOI: 10.1016/j.trd.2017.07.012

[12] CZYŻ, P., CICHOWSKI, A. Przegląd systemów ładowania elektrycznych osobowych pojazdów i koncepcja dwukierunkowej ładowarki pokładowej. Zeszyty Naukowe Wydziału Elektrotechniki i Automatyki Politechniki Gdańskiej. 2017, **57**.

[13] RAJASHEKARA K. Present status and future trends in electric vehicle propulsion technologies. *IEEE Power&Energy Society*. 2013.

[14] Rozporządzenie Wykonawcze Komisji (UE) 2018/1002 z dnia 16 lipca 2018 r. zmieniające rozporządzenie wykonawcze (UE) 2017/1153 w celu wyjaśnienia i uproszczenia procedury korelacji oraz dostosowania jej do zmian w rozporządzeniu (UE) 2017/1151.

[15] UN ECE. Regulation 101, Rev.3. United Nation Economic Commission for Europe. 2013. Available at: http://www.unece.org/ trans/main/wp29/wp29regs101-120.html.

[16] Wdrożenie procedury dotyczącej przejazdu dla realizacji badań emisji zanieczyszczeń spalin (RDE). Praca statutowa 06/18/ITS/008. Instytut Transportu Samochodowego.

[17] Wnioski z analiz prognostycznych na potrzeby Polityki energetycznej Polski do 2050 roku. Załącznik 2 do Polityki energetycznej Polski do 2050 roku. Ministerstwo Gospodarki. Warszawa 2015.

Maciej Gis, DEng. – Environment Protection Centre in Motor Transport Institute.
e-mail: *maciej.gis@its.waw.pl*

Mateusz Bednarski, MEng. – Faculty of Automotive and Construction Machinery Engineering, Warsaw University of Technology.
e-mail: *mateusz.bednarski@pw.edu.pl*

Jakub Lasocki, DEng. – Faculty of Automotive and Construction Machinery Engineering, Warsaw University of Technology.
e-mail: *jakub.lasocki@pw.edu.pl*

Article citation info:
KORCZEWSKI, Z. Thermal efficiency investigations on the self-ignition test engine fed with marine low sulfur diesel fuels. *Combustion Engines*. 2019, **178**(3), 15-19. DOI: 10.19206/CE-2019-303

Zbigniew KORCZEWSKI

CE-2019-303

Thermal efficiency investigations on the self-ignition test engine fed with marine low sulfur diesel fuels

Within the article an issues of implementing the new kinds of marine diesel fuels into ships' operation was described taking into account restrictions on the permissible sulphur content introduced by the International Maritime Organization. This is a new situation for ship owners and fuel producers, which forces the necessity to carry out laboratory research tests on especially adapted engine stands. How to elaborate the method enabling quality assessment of the self-ignition engine performance, considered in three categories: energy, emission and reliability, represents the key issue of the organization of such research. In the field of energy research, it is necessary to know the thermal efficiency of the engine as the basic comparative parameter applied in diagnostic analyzes and syntheses of sequentially tested marine diesel fuels. This type of scientific research has been worked out for two years in the Department of Marine and Land Power Plants of the Gdańsk University of Technology, as a part of the statutory activities conducted in cooperation with the Regional Fund for Environmental Protection in Gdansk and the LOTOS Group oil company.

This article presents the algorithm and results of thermal efficiency calculations of the Farymann Diesel D10 test engine in the conditions of feeding with various low-sulfur marine diesel fuels: distillation and residual fuels. This parameters stands for one of ten diagnostic measures of the ranking of energy and emission quality of newly manufactured marine diesel fuels being built at the Department.

Key words: *marine diesel fuels, engine tests, Sankey diagram, thermal efficiency*

1. Introduction

In accordance with the IMO (International Maritime Organization) decision, the permissible sulfur content in marine diesel fuels is drastically reduced starting with 1 January 2020, from the current maximum of 3.5% to 0.5% per unit masses, for vessels operating in all international waters, except for the previously designated Sulfur Emission Control Area (SECA)[1] [1, 3]. At the same time, it is still possible to use high-sulfur marine diesel fuels, provided that the ship is equipped with an exhaust desulfurization system, operating in a closed system, which will guarantee reduction of sulfur oxides emission in exhaust gases of marine engines to the level 6 g/kWh[2] [1, 2].

Observing a development of new technologies allowing the reduction of sulfur content in marine diesel fuels or the reduction of the content of sulfur oxides in engines' exhaust gases, it can be concluded that they are primarily focused on the maximum reduction of production costs, which will determine their further applicability. When comparing the prices of low- and high-sulfur marine diesel fuels, it turns out that having applied traditional technologies, a difference in the purchase price of 1 tons can reach even 300 dollars, which at the daily consumption of 20–30 tons gives savings up to 10,000 dollars [6].

In the long term, eg. annual perspective, this is up to 3 million dollars (taking into account necessary downtimes in the ship's usage). Then, it is worth considering retrofitting a ship's power plant with the exhausts desulfurization system, Such investment should pay back after 2–3 years of the ship's usage. For this reason, more and more shipowners decide to take such a step, as long as the technical conditions allow it.

On the other hand, intensive technological works are being undertaken by refine-ries to lower the production costs of low-sulfur marine diesel fuels, so-called modified fuels. This type of works additionally require conducting engine tests, aimed at assessing the energy, emission and reliability effects of their application. For obvious reasons, preliminary tests should be carried out in laboratory conditions, on specially adapted and metered engine test beds, according to the methodology that allows formulation of the unambiguous assessment of their suitability for feeding real objects, i.e. full-size marine Diesel engines.

This type of research works has been conducted for two years in the Department of Marine and Land Power Plants of the Faculty of Ocean Engineering and Ship Technology at the Gdańsk University of Technology [4]. One of the key issues of this methodology is the assessment of the energy quality of the tested marine diesel fuels, which is based on the thermal efficiency of the laboratory engine. Its construction should be maximally simplified, preferably single-cylinder, which guarantees high accuracy of calculations of the transformed energy streams [4, 7, 8].

2. Thermal efficiency of the SI engine

In order to determine the calculation formula for the thermal efficiency of a single-cylinder Diesel engine, it is necessary to develop a simplified energy balance of the working process realised in its cylinder section (Fig. 1).

Within the considerations, it was assumed that the energy balance equation will be determined for the cylinder section of the engine bounded by the system boundary, which stands for the inner surface of the cylinder and there is no accumulation of the internal energy of the working medium in the cylinder (its accumulation is negligibly small). Therefore, the balance equation for the processes taking place inside the cylinder section has the same form for the steady and unsteady processes:

$$\dot{H}^{*}_{exch} + P_i + \dot{Q}_{cs} - \dot{H}^{*}_{air} - \dot{Q}_{fuel} = 0 \qquad (1)$$

where: $\dot{H}^{*}_{exch}$ – enthalpy flux of the exhaust discharged from the cylinder, P_i – indicated power of the engine, $\dot{Q}_{cs}$ –

[1] In these zones, from January 1, 2015, the sulfur content in the fuel may not exceed 0.1% per mass unit.
[2] The investment costs of such an installation amount to EUR 4–5 million.

heat flux transmitted by the thermodynamic medium in the cylinder section to its walls, $\dot{H}^*_{air}$ – enthalpy flux of the air feeding the cylinder section, $\dot{Q}_{fuel}$ – heat flux brought to the engine with the fuel feeding the cylinder section.

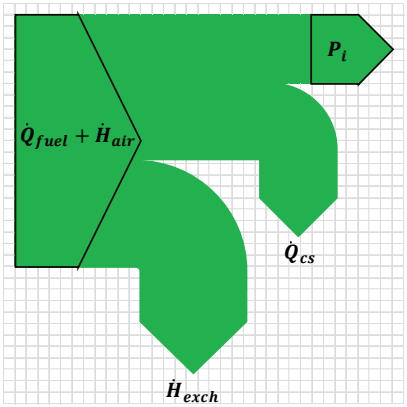

Fig. 1. Hypothetical flow diagram of energy flow in the cylinder section of a single-cylinder Diesel engine

Thermal efficiency represents the basic parameter of a Diesel engine characterizing the efficiency of its work in terms of thermal-flow approach, in steady states, i.e. when the average values of its effective torque, rotational speed and thermal state are unchanged over time. For these operating conditions, the average values of energy flows: input and output from the cylinder section also remain unchanged. In the simplest approach, thermal efficiency η_{th}, constitutes a ratio of the indicated power P_i to the energy flow brought to the engine with the feeding fuel $\dot{Q}_{fuel}$ and air $\dot{H}^*_{air}$ during one operation cycle:

$$\eta_{th} = \frac{P_i}{\dot{Q}_{fuel} + \dot{H}^*_{airpow}} \tag{2}$$

In the next steps of calculation, the following are determined:

A heat flux brought to the engine along with the fuel feeding the cylinder section:

$$\dot{Q}_{fuel} = \dot{m}_{fuel} \cdot \left(\xi_{cc} \cdot LCV + h_{fuel} - h_{fuelCC}\right) \tag{3}$$

where: $\dot{m}_{fuel}$ – a mass stream of the fuel feeding the cylinder section, determined by the weight method, from the amount of fuel m_{fuel} burnt in the engine at a given time, ξ_{cc} – a heat release coefficient in the combustion chamber, taking into account the losses of the heat brought with the fuel as a consequence of the incomplete combustion, dissociation of the exhaust gases and heat's penetration to the cylinder walls (it is estimated that ξ_{cc} takes values from 0.80 to 0.95, depending on the construction and dimensions of the combustion chamber and the value of the excess-air ratio), LCV – lower calorific value of the fuel, $h_{fuel} = c_{pfuel}(t_{fuel}) \cdot t_{fuel}$ – specific enthalpy of the fuel at the given temperature t_{fuel}, $h_{fuelCC} = c_{pfuel}(t_{CC}) \cdot t_{CC}$ – specific enthalpy of the fuel brought to the combustion chamber (CC) at the temperature inside the CC – t_{CC} (heat lost to warm the fuel to the temperature inside the combustion chamber).

In the first approximation (especially for distillation fuels, not requiring preheating before delivery to the engine's combustion chamber), the influence of the fuel enthalpy and heat release coefficient in the combustion chamber may be neglected, assuming, in a simplified form, that the heat flux brought to the engine with the fuel equals the flux of the fuel's chemical energy:

$$\dot{Q}_{fuel} = \dot{m}_{fuel} \cdot LCV \tag{4}$$

The enthalpy flux of the air feeding the cylinder section may be determined from the following relationship:

$$\dot{H}^*_{air} = \dot{m}_{air} \cdot c_{pair}(t^*_{air}) \cdot t^*_{air} \tag{5}$$

Due to small alterations of the air temperature at the intake of the naturally aspirated test engine, it might be assumed that the specific heat at constant pressure of the air c_{pair} is constant. In turn, the air mass stream $\dot{m}_{air}$ in equation (5) may be determined by using the mutual relations between the mass stream of the feeding fuel $\dot{m}_{fuel}$ and the mass stream of the air flowing into the working space of the cylinder section $\dot{m}_{air}$, which are determined with the excess-air-ratio λ:

$$\lambda = \frac{\dot{m}_{air}}{\dot{m}_{fuel} \cdot L_o} \tag{5}$$

where: L_0 – theoretical (minimum) air requirement for burning 1kg of fuel (constant for the given fuel type).

Hence, the mass stream of the feeding air is determined from the dependence, as follows:

$$\dot{m}_{air} = \lambda \cdot \dot{m}_{fuel} \cdot L_o \tag{6}$$

The theoretical air requirement for burning 1 kg of fuel with a known chemical composition expressed by mass contents of carbon C, hydrogen H, sulfur S and oxygen O is determined from the equation derived from the stoichiometric relations for total and complete combustion reactions (there is neither fuel nor oxygen in the exhaust) [7, 8]. After appropriate transformations, it takes the form in which L_0 is expressed in kg of air per kg of fuel:

$$L_o = \frac{1}{0{,}232} \cdot \left(\frac{8}{3}C + 8H + S\text{-}O\right) \ \frac{\text{kg air}}{\text{kg fuel}} \tag{7}$$

The above equations show that in order to calculate a thermal efficiency of the test engine, the measuring system should be designed in such a way to make possible determining: the engine's indicated power, the excess-air-ratio, temperatures of the feeding air and fuel as well as the fuel consumption in the adjusted, representative steady load condition. It is also necessary to know the basic chemical composition of the fuel and its calorific value [1].

3. Measurement results and their analysis

In order to investigate the effectiveness of the proposed method for determining a thermal efficiency of the test SI engine, experimental research was carried out on the Farymann Diesel engine of D10 type fed with six different marine diesel fuels. No adjustments were made to the engine injection system while introducing a new type of the fuel.

In the first stage of the research, the elementary chemical composition and lower calorific value of the tested fuels were determined – Table 1.

In the next stage of the research, the measurements of engine control parameters were carried out in accordance with the developed methodology – Fig. 2 [4]. As can be easily noticed from the presented scheme of recording and processing the measurement signals, in the engine tests of a new type of marine fuels, highly specialized measuring equipment was applied – stationary as well as portable, which allows precise observation of the engine's working and associated (residual) processes in steady and unsteady (transient) states.

In order to determine a thermal efficiency of the test engine, the following parameters were registered, simultaneously:

- rotational speed (angular position in ^{o}CSR) of the engine's crankshaft – n (measurement accuracy ±0.1%, sampling period – 0.5 ms),
- indicated pressure – p_c (measurement accuracy ±3%, sampling period – 15 μs, every 1^{o}CSR),
- fuel consumption – m_{fuel} (measurement accuracy ±0.2%, sampling period – 12.5 ms),
- fuel temperature – t_{fuel} (measurement accuracy ±2%, sampling period – 93.75 ms),
- consumption (by evaporation) of the cooling water – m_w (measurement accuracy ±0.2%, sampling period – 12.5 ms),
- cooling water temperature – t_w (measurement accuracy ±2%, sampling period – 93.75 ms),
- lubricating oil temperature – t_{ol} (accuracy of ±2%, sampling period – 93.75 ms),
- exhaust temperature – t_{exch} (measurement accuracy ±1%, sampling period – 0.1 ms),
- load current of the generator (armature) – I_{arm} (measurement accuracy ±1.5%, sampling period – 0.1 ms),
- voltage at the terminals of generator's armature – U_{arm} (measurement accuracy ±1.5%, sampling period – 0.1 ms),
- excess-air-ratio – λ (measurement accuracy ±1.0%, sampling period – 2 s),
- temperature of the test engine's external surfaces (thermogram) – t_M (measurement accuracy ±1.5%, sampling period – 0.1 ms),
- vibration acceleration (with SV80 converter) a_v (measurement accuracy ±0.1%, sampling period – 20 μs).

Table. 1. Basic physicochemical properties and chemical composition of the tested marine diesel fuels: distillation (PD) and residual (PP)

PARAMETER	PD1	PP2	PP3	PP4	PD5	PP6
Cetane number(dist.) / CCAI (Calculated Carbon Aromaticity Index) (resid.)	57,2	747	755	750	51	791
Density in w 15°C, kg/m^3	827,1	884,5	872,7	878,7	820	885
Kinematic viscosity in 40°C (dist.) / 50°C (resid.), mm^2/s	2,99	308	77,83	165,30	2,37	16,48
Flashpoint temperature in a closed cup in °C	61,5	270	88	107	56	102
The content of carbon [%m/m]	86,26	86,10	86,14	86,12	86,63	86,54
The content of hydrogen [%m/m]	11,10	11,90	11,72	11,80	11,20	11,75
The content of nitrogen [%m/m]	0,05	0,02	0,027	0,02	0,04	0,02
The content of sulfur [%m/m]	0,09	0,01	0,028	0,01	0,0008	0,10
Lower Calorific Value [MJ/kg]	43,23	43,08	43,04	43,20	42,70	42,44

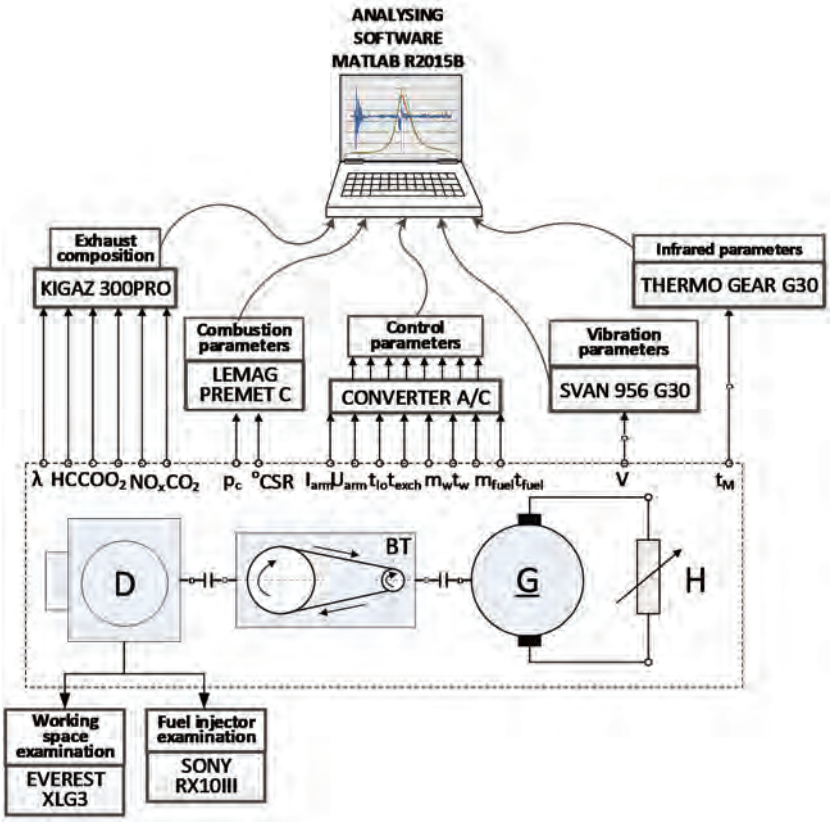

Fig. 2. Schematic diagram of the research test bed with measurement signal conditioning and recording system: D – single-cylinder Farymann Diesel D10 engine; BT – belt transmission (multiplier: transmission ratio i=0,426); G – direct current generator; H – heating system

Energy profiles' investigations of the laboratory engine fed with various types of marine diesel fuels may be carried out after reaching the determined thermal state of its structural design. It means that the cooling system "keeps up" with the receiving heat streams from the elements of the piston-cylinder group, which directly take off the heat released in the fuel combustion process worked out in the combustion chamber. The greater the temperature difference between the working medium and the walls limiting the combustion chamber, the greater the energy flow released as a result of fuel combustion is lost for warming the engine's construction elements. For this reason, before measuring the parameters of the working process, the engine should be wormed up, leading it to the state of thermal stabilization, in which the values of structural clearances and lubricating oil viscosities will be nominal. It is necessary to avoid then engine's long-term unloaded operation, at low rotational speeds, because in such conditions, the process of fuel atomisation and combustion occurs, in this case – incomplete, favouring a deposit formation in the engine's working spaces and in the exhaust passages as well as an increase in emissions of harmful and toxic chemical compounds in the engine's exhaust (especially carbon monoxide).

Within the experimental research program, whose main aim is to perform comparative analysis of the tested marine diesel fuels in terms of their energy quality, a registration of the control parameters is carried out in three/four measurement sequences (if the performed on-line preliminary analysis of the engine control parameters' measurement uncertainty, in particular, fuel consumption, does not indicate the presence of gross errors, the number of measurement sequences is limited to three), in one, always the same (reference) state of the determined engine load. Before each measurement sequence, which lasts exactly 20 minutes, the amounts of fuel and cooling water are made up to the established initial levels in the tanks. By this way, the influence of external disturbances (fixed thermal, flow, dynamic state of the engine, etc.) was minimized. Furthermore, an effectiveness of the observations of the engine functioning increases (the smallest parametrical anomalies are captured), as well as high repeatability of the recorded measurement results is achieved. Their mathematical processing is carried out according to the computational algorithm presented in the second point of the article. Final results of thermal efficiency calculations of the test engine are summarized in Table 2.

However, their graphical interpretation, in the form of an extended Sankey diagram, made for the whole propulsion unit fed with one of the tested fuels, is presented in Fig. 3 [4]. It includes, in addition to the heat flux emitted by the engine's hull to the surrounding $\dot{Q}_{sur}$, and the heat flux through the water in the water in the tank $\dot{Q}_w$, also the mechanical losses in the propulsion unit P_m, the engine's effective power Pe, which is equal to the generator's propulsion power P_{GP} and a stream of the residual heat $\dot{Q}_r$, which stands for energy losses not included in the balance (e.g. a fluxes of acoustic and mechanical vibration energy from the thermal-flow and mechanical system of the entire propulsion unit: engine-multiplier-generator).

Table 2. Calculated values of the engine's thermal efficiency characterizing the energy quality of the tested marine diesel fuels

Marine diesel fuel	PD1	PP2	PP3	PP4	PD5	PP6	Range
η_{th} [%]	58.75	58.58	59.06	58.80	61.79	60.07	3.31

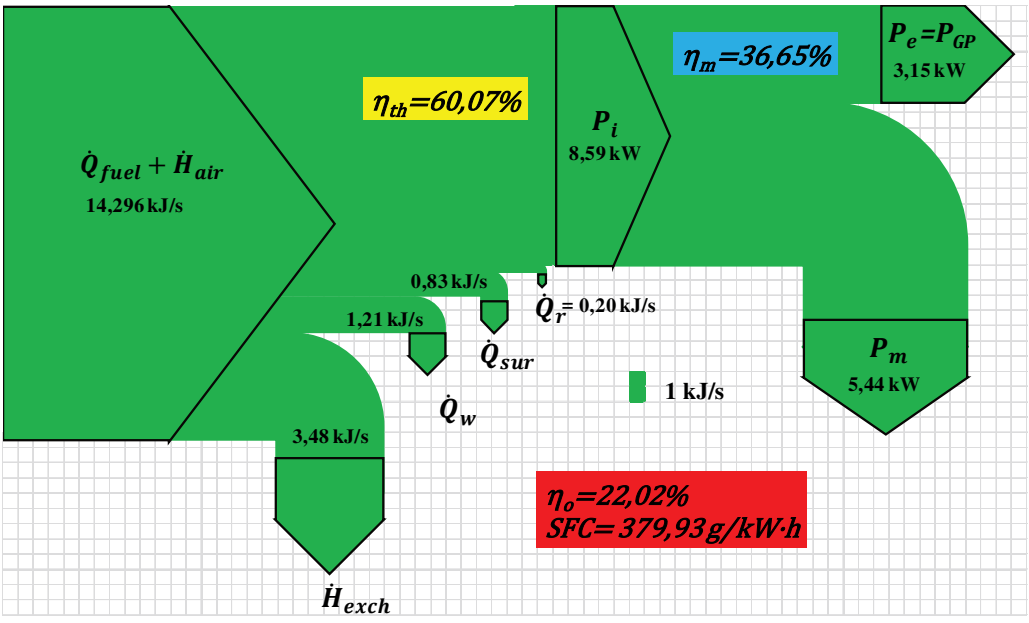

Fig. 3. A stream graph of the energy flow within the Farymann Diesel D10 engine propulsion unit fed with low-sulfur marine diesel fuel PP6

4. Remarks and final conclusions

The following general conclusions can be formulated on the basis of the results obtained:

- The proposed configuration of the measurement signals and processing system of the single-cylinder test engine makes it possible to determine its thermal efficiency, as the basic indicator of the energy quality assessment of newly implemented, modified marine diesel fuels;
- The fuel type alteration has a significant impact on a thermal efficiency of the engine. The value of its range for six tested marine fuels was 3.21%, which indicates a significant diagnostic sensitivity of this parameter.
- A higher calorific value of the fuel feed does not translate directly to the increased thermal efficiency of the engine.
- An impact of various marine diesel fuels on the energy state of the test engine, in the sense of its performance and efficiency, is a complex phenomenon. For this reason, it is necessary to significantly expand the set of diagnostic parameters, which are able, after appropriate normalisation, fulfill the role of a stimulant, destimulant and nominate, determining the energy quality assessment of the considered marine fuels. This will enable a construction of the ranking, in which they will be adjusted in the order from "the best" to " the worst" one according to the determined values of the synthetic (aggregate) variable [4, 5].

Bibliography

[1] KORCZEWSKI, Z. et al. The method of assessing ecological, energy and reliability effects of the application of modified marine diesel fuels for feeding self-ignition engines in real operation conditions. Research project co-financed by the Regional Fund for Environmental Protection in Gdansk. No. RX-10/ 2017. Final Report. *Gdańsk University of Technology* 2019.

[2] KUKUŁA, K. Badania operacyjne w przykładach i zadaniach. *PWN*. Warszawa 2007.

[3] ROZMARYNOWSKA, M. Nowe przepisy IMO odnośnie do zawartości siarki w paliwie statkowym w regionie SECA i związane z tym koszty dla armatorów. *Prace Wydziału Nawigacyjnego Akademii Morskiej w Gdyni*. 2013, **28**.

[4] WOODYARD, D. Pounder's marine diesel engines and gas turbines. 8th edition. *Elsevier*. United Kingdom 2004.

[5] WIŚNIEWSKI, S. Termodynamika techniczna. *WNT*. Warszawa 2005.

[6] Emission Standards, International: IMO Marine Engine Regulations.

[7] Report of the Marine Environment Protection Committee, IMO MEPC 70th session, October 2016.

[8] Emissions of sulfur oxides and nitrogen oxides. Service of the Ministry of Maritime Economy and Inland Navigation. www.gov.pl/web/gospodarkamorska/emisje-tlenkow-siarki-i-tlenkow-azotu (access 12.02.2019)

Prof. Zbigniew Korczewski, DSc., DEng. – Faculty of Ocean Engineering and Ship Technology, Gdańsk University of Technology.
e-mail: *zbikorcz@pg.edu.pl*

Article citation info:
ŁOZA, Ł., WRÓBEL, R., SITNIK, L. The analysis of vibrations of gasoline and diesel vehicles as a function of their engine sizes. *Combustion Engines*. 2019, **178**(3), 20-23. DOI: 10.19206/CE-2019-304

Łukasz ŁOZA
Radosław WRÓBEL
Lech SITNIK

CE-2019-304

The analysis of vibrations of gasoline and diesel vehicles as a function of their engine sizes

This paper presents a study of vibrations appearing in a vehicle in the process of its operation. The authors describe the primary source of the vibrations and their propagation in the entire structure. The observations were performed on the passenger cars with various gasoline and diesel engines. The aim was to examine the level of damping factor in the different locations in the car, precisely specified for the purpose of this studies. The secondary goal was to develop an effective method of obtaining and analyzing signals generated during the engine operation. The chosen instrument was Laser Doppler Vibrometer (LDV), which is used as the non-intrusive measurement utensil to detect velocity variations in designated places. The signals are gathered and collected as group of sinusoidal characteristics in the time domain. In order to achieve specific information about every component of the original signal, the authors apply Fast Fourier Transform (FFT) as the analyzing method. It allows to distinct the basic sinusoidal characteristics in the frequency domain through the spectral analysis. Based on the results, the authors are able to distinguish the dominant modes from the complex signal and indicate their impact on the car.

Key words: *vehicle, vibration, engine, Fourier, vibrometer*

1. Introduction

The non-invasive diagnostic are always the most preferable measurement methods in order to recognize current condition of the examined object, especially when there is no access to multiple, similar items and it is not allowed to damage the integrity of one's parts. Considering these requirements, it is always a challenge to perform valid and detailed measurements. Taking this into account, the certain collection of prerequisites has to be fulfilled:

– understanding the theoretical basics of the measurements,
– proper interpretation of the results,
– consideration of the outside disturbances.

One of the information we can obtain from various objects is mechanical vibration. It is a phenomenon where kinetic energy is converted into potential energy and vice versa until the causing force ceases [1]. The complexity of measurements depends on numbers of degrees of freedom (DOF). In this particular case, the engine as well as the entire car structure has a huge number of the DOF. In order to simplify the calculations, the whole system is represented by deformable constraints, material particles and rigid bodies, depending on the size of the object. The standard approach is to assume the system as continuous, where the number of the DOF is determined. It allows to use integral equations for this calculations, instead of differential ones for discretization [2].

The purpose of this research was to verify the generation of the vibrations and its dependence on the engine size, type of fuel and optional supercharging.

2. Measurements

2.1. Investigated objects

The tests were performed on the three, new Fiat Bravo Model 198 cars: 54A, 54G and 54W with respectively engines: gasoline 1.4BZ 90CV CD, gasoline supercharged 1.4BZ 120CV CD and diesel supercharged 1.6 105CV CD. The engines were mounted crosswise. Their supports function as a structural connection between drive unit and the car body. Each support has a mount with rubber to minimalize the transmission of the driving vibrations generated by the engine and spread into the entire structure [3].

Table 1. Engines specification [4]

	Engine type		
	1.4BZ 90CV CD	1.4BZ 120CV CD	1.6 105CV CD
Engine capacity [cm3]	1368	1368	1598
Power [HP]	90	120	105
Engine mounting	Front crosswise	Front crosswise	Front crosswise
Number of cylinders	4	4	4
Number of valves per cylinder	4	4	4
Type of camshaft	OHC	OHC	DOHC

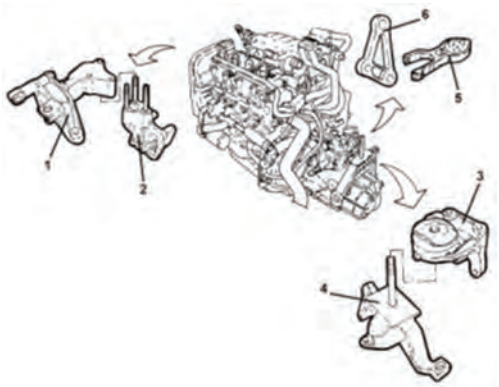

Fig. 1. Elements for mounting examined object (1 – flexible connector on timing gear side, 2 – rigid support on timing gear side, 3 – flexible connector on gearbox side, 4 – rigid support on gearbox side, 5 – reaction rod on differential gear side, 6 – rod fixing support on differential mechanism side) [3]

2.2. Measurement system

One of the non-invasive measurement method is laser vibrometry. In this research the system was based on Laser Doppler Vibrometer (LDV). It utilizes the Doppler effect, which is the change of length of the wave in relation to an observer who is moving relatively to the source. The laser head is both transmitting and receiving device. The laser beam comes out and returns to the head after reflection from the surface. This method allows to obtain velocity and relative displacement of moving objects [2].

The measuring system consists of a Polytec PSV I 400 head, a OFV 5000 controller and a PSV W 400 supervision and acquisition device [5, 6].

During the measurements the cars were standing on their wheels. The crankshafts were rotated to the speed of 2000 min.$^{-1}$ in neutral gear. The test rig was positioned to measure the vertical-vector of the vibrations. Additional mirror was set to direct the laser beam (Fig. 2).

The authors selected two measurements points (Fig. 3, 4) on the unsprung mass to verify the difference of the detected vibrations.

Fig. 2. Test rig (1 – laser head, 2 – mirror, 3 – measurement point on the engine mount)

Fig. 3. Measurement point on the engine mount

Fig. 4. Measurement point on the door handle

3. Results

The measurements are presented in the diagrams below. The vibrations were registered as the time courses of velocities and spectra in the frequency domain after Fast Fourier Transform [7]. The waveforms were recorded for the 2 seconds and with the 2048 Hz sampling frequency. This time period was chosen as adequate to recognize the characteristic of stationary/non-stationary type of signal. At the same time, with such sampling frequency, it allowed to receive large amount of measurement samples as sufficient to perform the FFT.

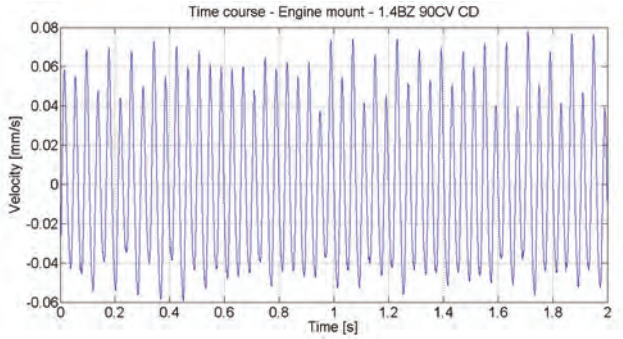

Fig. 5. Time course of the engine mount measurement point on the 1.4BZ 90CV CD engine

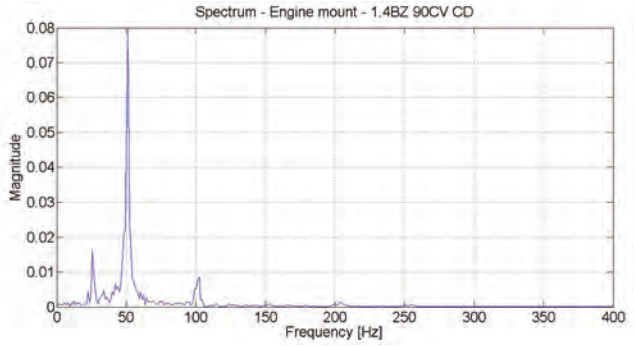

Fig. 6. Frequency spectrum of the engine mount measurement point on the 1.4BZ 90CV CD engine

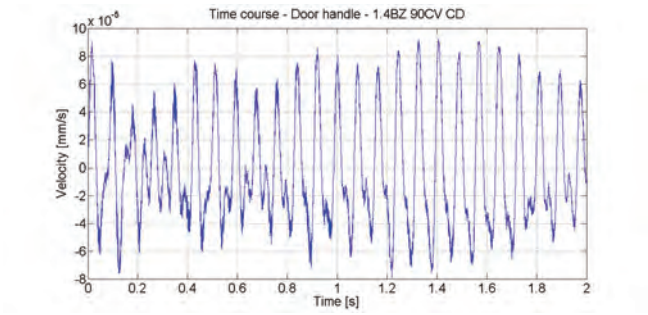

Fig. 7. Time course of the door handle point on the 1.4BZ 90CV CD

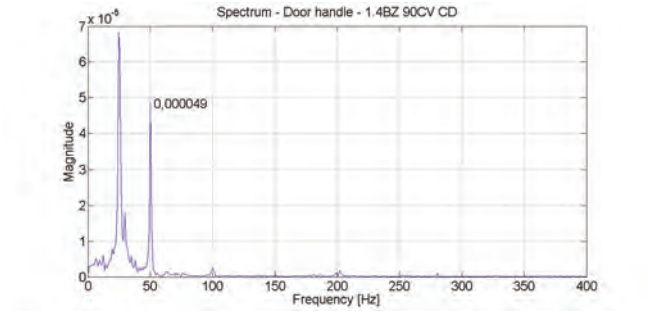

Fig. 8. Spectrum of the door handle point on the 1.4BZ 90CV CD

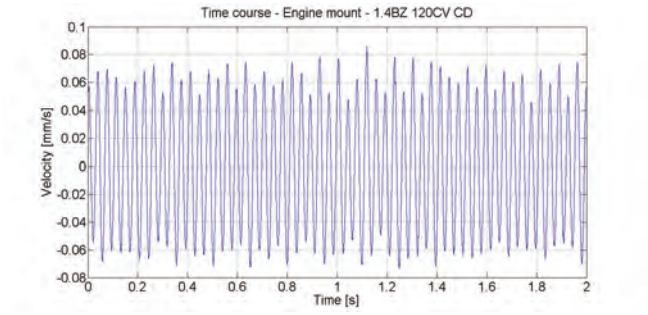

Fig. 9. Time course of the engine mount point on the 1.4BZ 120CV CD

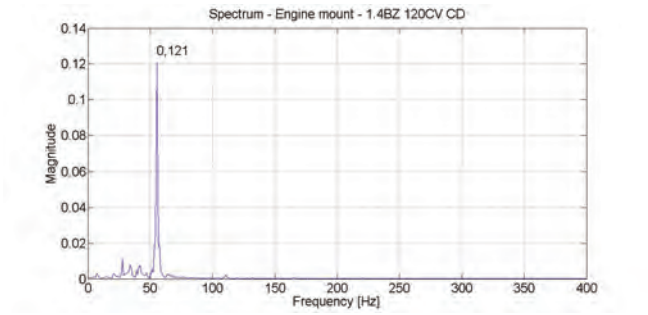

Fig. 10. Spectrum of the engine mount point on the 1.4BZ 120CV CD

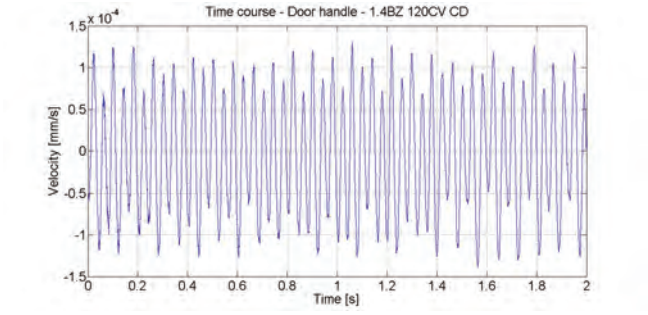

Fig. 11. Time course of the door handle point on the 1.4BZ 120CV CD

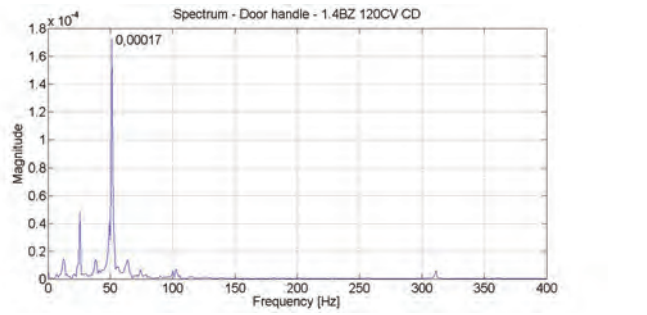

Fig. 12. Spectrum of the door handle point on the 1.4BZ 120CV CD

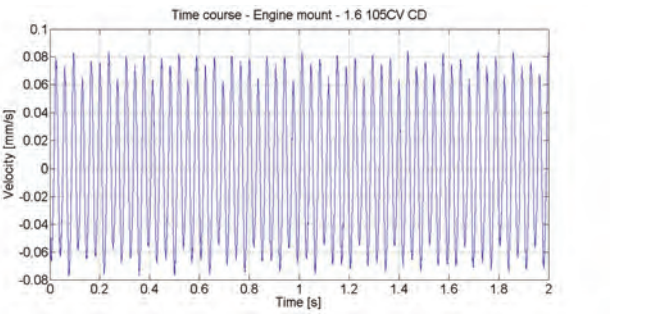

Fig. 13. Time course of the engine mount point on the 1.6 105CV CD

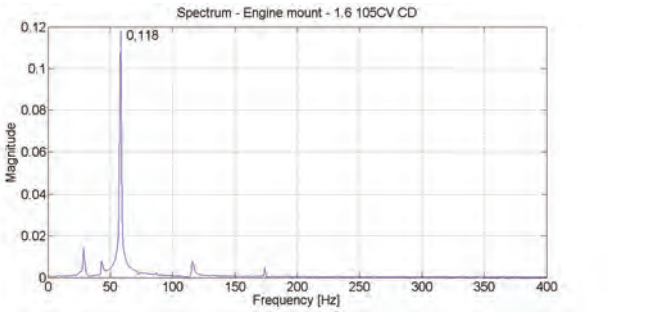

Fig. 14. Spectrum of the engine mount point on the 1.6 105CV CD

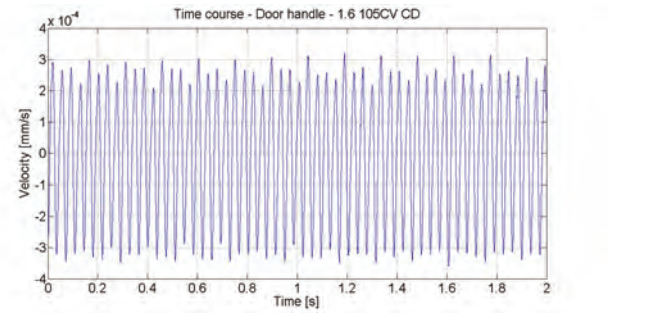

Fig. 15. Time course of the door handle point on the 1.6 105CV CD

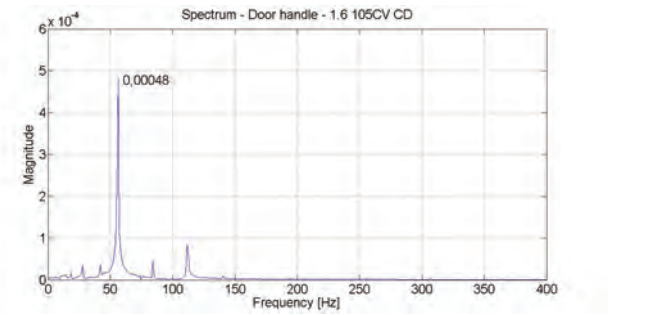

Fig. 16. Spectrum of the door handle point on the 1.6 105CV CD

Table 2. Vibration velocities and magnitudes

		V_{max} [mm/s]	V_{av} [mm/s]	Magnitude
Engine mount	1.4BZ 90CV CD	0.077	0.000087	0.08
	1.4BZ 120CV CD	0.086	0.000084	0.121
	1.6 105CV CD	0.084	–0.00023	0.118
Door handle	1.4BZ 90CV CD	0.000092	–0.000000047	0.000049
	1.4BZ 120CV CD	0.00014	–0.0000034	0.00017
	1.6 105CV CD	0.00036	–0.0000023	0.00048

Based on the results, the authors were able to distinguish the damping ability of the vibrations transfer in the structure of the cars. The Fast Fourier Transform displayed the spectrum with the harmonic frequencies in every measurement run. The maximal values of those harmonics were most significant in the recorded signals. Comparing spectra after measurements in the first and second point, the authors could calculate the created for this purpose damping coefficient, which indicates what the efficiency of the damping parts was.

The coefficient was calculated as follows:

$$c = \frac{\text{magnitude value from first measured point}}{\text{magnitude value from second measured point}} \quad (1)$$

Table 3. Damping coefficient

Engine	c
1.4BZ 90CV CD	1633
1.4BZ 120CV CD	712
1.6 105CV CD	246

4. Conclusions

The vibrations as signals generated by the engine have stationary characteristic. This allows to perform Fast Fourier Transform and obtain harmonic spectrum.

The tendency of the maximum velocities increases with the engines with higher capacities and equipped with supercharger. Simultaneously, the tendency of the average velocities decreases.

In the gasoline engine, the damping phenomenon is lower in the car with more powerful engine with supercharger. The least damped vehicle structure is supercharged Diesel engine with the highest engine capacity.

The supercharger increases overall vibration level propagated in the entire structure of unsprung mass.

The damping of the mounting system is highly effective.

The spectra present that the highest frequency magnitude occur in the low range, similarly in every case and independently of the size and type of engine.

Based on the results, the authors would like to continue the research of such subject in broader range.

It would be intentional to focus on higher number of vehicle of different brands, engine sizes, body types, mileage and production year.

Acknowledgements

Research financed from Wroclaw University of Science and Technology statutory funds no. 0401/003/18.

Nomenclature

LDV	laser doppler vibrometer
FFT	Fast Fourier Transform
DOF	degrees of freedom
OHC	overhead camsahft
DOHC	double overhead camshaft
HP	horse power

Bibliography

[1] DE SILVA, C. Vibrations fundamentals and practice. *CRC Press*. NY 2000.
[2] GIERGIEL, J. Mechanical vibrations (in Polish). *University Scientific-Educational Publishers*. Cracow 2000.
[3] KAŹMIERCZAK, A., WRÓBEL, R. Detection of infection unit defects in diesel engine through analysis of vibrations. *Journal of KONES*. 2007.
[4] FIAT Technical materials, www.fiat.com
[5] www.vibrometry.co.kr/PSV-400.pdf
[6] www.polytec.com/fileadmin/d/Vibrometrie/OM_DS_OFV-5000_E_42346.pdf
[7] BRIGHAM, E. Fast Fourier Transform and its applications. *Pearson*. 1988.

Łukasz Łoza, MEng. – Faculty of Mechanical Engineering, Wroclaw University of Science and Technology.
e-mail: *lukasz.loza@pwr.edu.pl*

Radosław Wróbel, DSc., DEng.– Faculty of Mechanical Engineering, Wroclaw University of Science and Technology.
e-mail: *radoslaw.wrobel@pwr.edu.pl*

Prof. Lech Sitnik, DSc., DEng. – Faculty of Mechanical Engineering, Wroclaw University of Science and Technology.
e-mail: *lech.sitnik@pwr.edu.pl*

Article citation info:
SITNIK, L.J., ZADWORNY, D. Application of the Monte Carlo method in the calculation procedure of the internal combustion engine. *Combustion Engines*. 2019, **178**(3), 24-26. DOI: 10.19206/CE-2019-305

Lech J. SITNIK
Dominik ZADWORNY

CE-2019-305

Application of the Monte Carlo method in the calculation procedure of the internal combustion engine

The aim of the work is to check the possibility of applying the Monte Carlo method to the calculation procedure of internal combustion engines. This has been accomplished by modifying existing algorithms in such a way that the variables responsible for the main parameters of the engine are selected in a random manner using Solver written in Microsoft Excel. It turns out that this method can actually be implied, however, it has some limitations related to the high complexity of calculations.

Key words: *internal combustion engine, Monte Carlo method, compression ignition engine, calculations*

1. Introduction

The Monte Carlo method is one of the most popular methods of process modeling, mainly due to the ease of its application and the speed of obtaining results. Its areas of application include, among others, such areas as mass service systems, quality control and reliability, physics, chemistry, or even the real estate market. Among the above, mechanics and issues related to internal combustion engines are very rare, and it is a pity.

The Monte Carlo technique is a way to make a mathematical model of too complex processes, that is, the description of which would take too much time, or is simply impossible, due to the nature of the problem. The basis for this technique is the random selection of certain quantities that are responsible for the course of a given process. The accuracy of the results obtained depends on the number of attempts (but not always) and the quality of the pseudo-random number generator used, of course assuming that the draw takes place in accordance with a known distribution. Exploring the secrets of the mentioned method is very important in times of dynamic development, because it can enable us to "draw" a motor or another device with given parameters in just a few moments.

It would seem that we are slowly entering the era of electric vehicles, and internal combustion engines will lose their popularity in the coming years, but in reality there are a few issues with switching to fully electric means of transport. First of which is that a significant part of the world does not have infrastructure in the form of charging stations, and the amount of electricity produced is far from being needed to supply a huge amount of electric means of transport. Another difficulty is that the batteries weigh quite a lot these days and for example manufacturing a lorry that would have sufficient range would be neither possible nor profitable given the amount of batteries that would have to be used. All comes down to the energy equation, adding weight to any given vehicle makes it use more energy to move, and so far electric cars weigh undeniably more that their petrol powered counterparts. This leads to the issue of growing popularity of hybrid vehicles. In this case, the combustion engine usually works at a constant speed and load, and the energy it produces is used to charge the batteries, which power the electric motors, the main source of the drive. Such a scenario is perfect for the Monte Carlo method since it significantly simplifies calculations because the full range of rotational speeds and loads is not taken into account.

2. Implementation of work

2.1. Calculation procedure

The work is based largely on a computational program, written using Microsoft Excel, for compression ignition engines. The algorithms are relatively new, while the ranges of variable values have already been several or a dozen years old at the time of writing the program, so you can say that today they are not fully current data. For this reason, in the further part of the work, the impact of the change in the scope of these coefficients was checked.

Each of the sheets refers to a separate engine work phase, or related issues. The program consists of over 90 sheets, starting from pressures and temperatures in the processes of suction, compression, combustion and exhaust, going through the main geometric parameters, such as piston stroke and its diameter, all kinds of stresses and moments, to all the necessary details such as the dimensions of the crank head and foot or the entire geometry of the crankshaft. In this work, all attention is focused on the first few sheets of the program, and its goal is to generate an engine that consumes as much air as possible while taking the least fuel.

2.2. Modification of the program

To successfully prepare the program for the implementation of the Monte Carlo method, the first part of the program was imported to a single sheet, where it is easier to organize and modify all data. Then, after writing correctly functioning calculation algorithms, it was necessary to group and describe all variables, constants and results of calculations occurring in the tested part of the file. The result is a division into three groups (Tables 1–3).

A) Variables

This group includes all coefficients that will be randomly drawn by the generator, their values are chosen randomly, and the only condition is that they fit into particular ranges for each variable. In the initial phase of writing and modifying the program, there were fears that the compartments in which the above-mentioned coefficients lie are outdated, because they were determined several years ago. In order to check the above theory, each of the ranges of values was extended by about 10 to 25 percent, which un-

fortunately did not affect the final result in any way. This means that the problem is more complex and you should check all possible configurations of changes, that is, change the ranges of one, several or each of the above coefficients, in all possible ways. Unfortunately, in a program such as Microsoft Excel, using only Solver would be too time-consuming, and it is not known whether the results obtained would be satisfactory.

Table 1.Variables and ranges of their values

Variables			
Symbol	Name	Range	Unit
η_v	Fill factor	0.7 - 0.9	
ε	Compression degree	13 - 26	
ΔT	The temperature increase of the charge flowing into the cylinder, caused by hot walls	10 - 25	K
p_r	Exhaust gas pressure	0.105 - 0.12	MPa
T_r	The temperature of the residual fumes	600 - 1000	K
m_s	Exponent of polystyrene comp[ression	1.27 - 1.38	
W_u	The caloryfic value of fuel	36 - 44	MJ/kg
ξ	Coefficient of heat utilization	0.7 - 0.9	
$\chi_{śr}$	Adiabatic exponent	1.27 - 1.29	
m_r	Expansion exponent	1.18 - 1.3	
ν	theoretical volume of the stroke, suction and outlet loops	0.92 - 0.97	
η_m	Mechanical efficiency of the engine	0.7 - 0.9	

B) Constants

In this category, all constants taking part in the calculation process are included. The coefficient of excess air is in fact a variable value, however, it depends on the degree of pressure increase, so it can not be a random number, therefore some simplification was applied and the values closest to the average were selected.

Table 2. Constants and their values

Constans			
Symbol	Name	Value	Unit
p_0	Ambient pressure	0.10	MPa
T_0	Ambient temperature		K
λ	Coefficient of excess air	1.40	
M_o	The theoretical ambient of air needed to burn of 1kg of fuel	14.41	kg
α'	The degree of pressure increase	1.90	

C) Results

The last group contains all the values resulting from the random matching of variables in interaction with constants, this group defines to us whether the Monte Carlo method makes sense, because on the basis of these results we can determine if output values are achievable using today's technology.

Table 3. The results of subsequent actions on constants and variables

Results		
Symbol	Name	Unit
p_1	Pressure of the end of charging	MPa
T_1	The temperature of the end of charging	K
p_2	Pressure of the end of compression	MPa
T_2	The temperatuure of the end of compression	K
v_0	The specific volume of the ambient air	m^3
V_k	The volume of the compresssion chamber	m^3
p_{max}	Maximum of combustion pressure	MPa
β	Volume growth factor	
v_4	Gas volume at the theortical end of combustion	m^3
p_5	Pressure at the end of expansion	MPa
ε_r	Degree of expansion	
$p_i =$	Theoretical average of the induiicated pressure	MPa
p_i	Average indicated pressure	MPa
p_i	Average usefull pressure	MPa
Vs	**The stroke volume needed to burn of 1 kg of fuel**	**m^3**

2.3. Solver

Having already divided and grouped data, it is possible to move on to the most important element of the created program, namely the Solver add-in available in Excel. Thanks to this application, a subroutine has been written which will select random coefficients from the variable category based on a given result. In this case, the result is Vs, i.e. the stroke volume needed to burn 1 kg of fuel. This number should be as high as possible, because the goal is to use as much air and as little fuel as possible. In the Solver addition, the final cell has been selected and given a certain value (in this case it is Vs = maximum, marked in red, Fig. 1). Then all the restrictions are added (marked in yellow, Fig. 1), these are the ranges in which the variables contain. After determining the boundary conditions, the entire algorithm is being completed for all intermediate results, i.e. the remaining elements from the third group, because the final result depends on them, and they depend on the variables. The last step is to choose the solving method (marked in green, Fig. 1), Due to the high complexity of the problem, the evolutionary method was chosen.

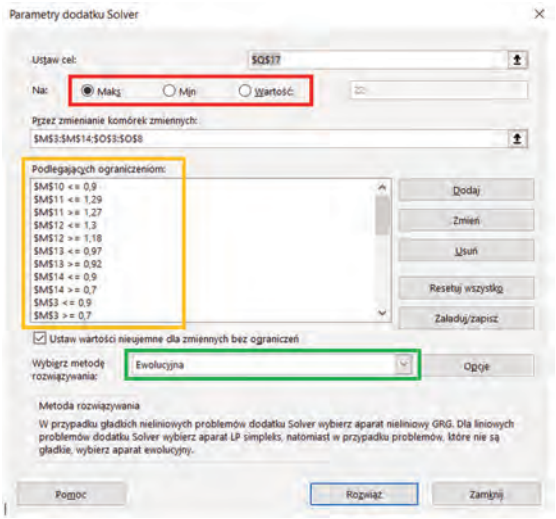

Fig. 1. View of the Solver add-in (print screen in polish)

2.4. An example of implementing the Monte Carlo method

After saving all algorithms and checking the operation of the program together with Solver, an exemplary application of the Monte Carlo method was developed. First step was finding the scope from the minimum to maximum value of Vs. Having found it, a certain value was chosen as the target, it was of course within the range from minimum to maximum, for example 0.023 m^3. Further calculations were carried out, and Table 4. presents the coefficients obtained. Of course, finding a certain Vs is just one of the many possibilities of Solver, the operator of the program chooses which values will be drawn, and thus what the operation of the additive will be based on. The goal may be any element from the Results column, or even a different, more advanced indicator, however it will require extending the application with a further series of data. Another important factor is that the ranges in which coefficients are included are outdated, this means they should be updated before developing the program any further. Unfortunately

this was not possible using Solver, because random changes in scopes would not provide valuable results, the issue of the ranges should be considered individually from scratch. However, the main purpose is to show the possibilities of applying the Monte Carlo method, accuracy of the results is in this case a secondary matter. The more expanded the program, the larger the area of application can be covered, it is possible to write a program that will "draw" the entire engine, including the geometry.

Table 4. Values of the variables and results for Vs = 0.023 m^3

Variables		Constants		Results	
η_v	0.70	p_0	0.10	p_1	0.08
ε	18.29	T_0	298.00	T_1	325.58
ΔT	10.55	λ	1.40	p_2	4.11
p_r	0.12	M_t	14.41	T_2	974.20
T_r	768.75	α	1.90	v_0	0.86
m_s	1.38	l	1.00	v_k	1.43
W_u	38.90			p_{max}	7.81
ξ	0.77			β	1.23
$\chi_{śr}$	1.28			v_4	1.75
m_r	1.19			p_5	0.31
ν	0.93			ε_r	14.93
η_m	0.77			$\dot{P}$ =	0.85
				p_i	0.75
				p_i	0.58
				Vs	24.65

Having a certain value of Vs and all other coefficients, last thing left to do to get the outline of the indicator graph is to determine the basic parameters defining the engine, such as engine power, number of cylinders, rotational speed or fuel consumption. Of course, also these values can be freely modified, depending on the needs. After setting these parameters, the result of the calculation was generated in the form of the main points of the indicator chart, referring to the maximum and minimum pressures, volumes and temperatures in the engine's work cycle. Based on them, it is possible to predict the course of these parameters and draw a graph showing the way this engine works.

Table 5. Results of the calculation, main points of the indicator chart

Variable	cm^3	Variable	Mpa	Variable	K	$^{\circ}C$
V1=	830.97	P1=	0.08	T1=	322.01	48.86
V2=	32.50	P2=	5.07	T2=	801.51	528.36
V3=	32.50	P3=	9.64	T3=	1521.75	1248.60
V4=	46.02	P4=	9.64	T4=	2154.78	1881.63
V5=	830.97	P5=	0.25	T5=	947.12	673.97
V6=	830.97	P6=	0.11			
V7=	32.50	P7=	0.11			

The above illustration shows the 7 most important values of volume and pressures and 5 temperatures. For volume, they are the maximum cylinder volume at the end of charging and expansion (V_1, V_6, V_7), then at the end of compression (V_2, V_3, V_7), and the volume at the theoretical end of combustion (V_4). On the other hand, the pressures are distinguished as the end of charging pressure (p_1), during compression (p_2), the maximum combustion pressure (p_3, p_4), expansion (p_5) and exhaust gas pressure (p_6, p_7).

Temperatures in turn result from increases in volume as well as pressures and the shape of the compression and expansion curves. The first one is the temperature at the end of charging (T_1), then the compression (T_2). T_3 is the result of multiplying the previous one (T_2) by the degree of pressure increase (α), T_4 in turn is equal to T_3 times the volume increase factor. The last of the temperatures (T_5) also includes the exponent of the expansion, which determines how much a drop in temperature after the combustion process is achieved.

3. Conclusions

The main purpose of the work was to check the possibility of applying the Monte Carlo method to the calculation of internal combustion engines, in this case the self-ignition engine. From the above, it can be seen that this method is possible and, moreover, relatively easy to apply.

Although the results obtained are not sufficient to design the entire engine, including geometry, they help determine what should be guided in the design and construction process. It was also found that the Monte Carlo technique has an incredibly wide range of applications and should be consistently implemented in more and more fields of science. A huge plus of this method, despite the low accuracy of results, is that in a very short time we get some results that shape the view of the rest of the problem. It is much easier to carry out further research knowing what it is aiming for and having already this initial "piece of success".

Returning to the engines, if the decision was made to design the motor based on the known method, the focus should be on maximizing the program, taking into account forces and stresses, as well as the entire geometry. Of course, not all variables can be simply set on the level drawn, most of them depend on many other factors that should be known first. Only when we know how to influence such values as exhaust gas pressure or the exponent of pressure polystyrene and many others, we will find out whether it is worth striving for those determined on the basis of a draw, or perhaps it would be better to sometimes use a classic calculation model. After finding the golden mean, between the Monte Carlo method and the analytical approach, we get a calculation program for internal combustion engines, combining satisfactory speed of calculation and sufficient accuracy of results.

Bibliography

[1] JANICKA, A., KOLANEK, C., WALKOWIAK, W. Applied Thermodynamics – internal combustion engine Laboratory.

[2] Owen Art. Monte Carlo Methods. 2002.

[3] SITNIK L. Program obliczeniowy silnika spalinowego o zapłonie samoczynnym, Wrocław 2007.

Prof. Lech J. Sitnik, DSc., DEng. – Faculty of Mechanical Engineering, Wroclaw University of Science and Technology.
e-mail: *lech.sitnik@pwr.edu.pl*

Dominik Zadworny, Eng. – Faculty of Mechanical Engineering, Wrocław University of Science and Technology.
e-mail: *ddominik.zet@gmail.com*

Article citation info:
STEPANENKO, D., KNEBA, Z. Thermodynamic modeling of combustion process of the internal combustion engines – an overview. *Combustion Engines*. 2019, **178**(3), 27-37. DOI: 10.19206/CE-2019-306

Denys STEPANENKO
Zbigniew KNEBA

CE-2019-306

Thermodynamic modeling of combustion process of the internal combustion engines – an overview

The mathematical description of combustion process in the internal combustion engines is a very difficult task, due to the variety of phenomena that occurring in the engine from the moment when the fuel-air mixture ignites up to the moment when intake and exhaust valves beginning open. Modeling of the combustion process plays an important role in the engine simulation, which allows to predict in-cylinder pressure during the combustion, engine performance and environmental impact with high accuracy. The toxic emissions, which appears as a result of fuels combustion, are one of the main environmental problem and as a result the air pollutant regulations are increasingly stringent, what makes the investigation of the combustion process to be a relevant task.

Key words: *thermodynamic combustion model, internal combustion engine, convective heat transfer coefficient, Wiebe burning law, single-zone model, two-zone model, heat transfer submodel*

1. Introduction

The combustion process in the internal combustion engines is a chemical reaction between the fuel and oxidant, with the emission of heat and light. Explosive combustion in a closed volume is one of the most complex and complicated phenomena that are modeled mathematically. The aim of the combustion process modeling is to determine operational parameters and the impact from the engine to the environment.

Increasing of the stringent regulations [6–8] that are aimed to lowering toxic emissions during the ICE combustion process with simultaneously maintaining the high efficiency of engine operation conditions and lowering the fuel consumption, provides to continuous investments, related with the engine development.

Computer modeling and simulation are important tools that are used for obtaining optimal engine designs and allowing significantly reduce time and cost constraint, that are needed for making modifications in existing and/or creating new design solutions of ICE. The existing computational methods and computer programs that are most commonly used for modeling processes that are occurring inside ICE can be divided into two main categories: thermodynamic models (the whole cylinder is considered as one cell. For this cell applies the mass, the energy and the state balance equations) and Computational Fluid Dynamic (CFD) models (engine elements are divided into a high number (hundreds of thousands) of three-dimensional cells and for each of them solved the systems of energy, mass, momentum and state balance equations. This model provides three-dimensional modeling of gas flow and fuel injection into cylinder and/or engine manifold, turbulent mixing of fuel with air, evaporation of fuel-air mixture, ignition and combustion processes. However, this leads to a higher computational time and requires a lot of computing power from the computers). CFD models are most commonly used when the detailed analysis of phenomena that is occurring inside the cylinder during combustion is needed.

Thermodynamic combustion models (TCM) cannot provide analysis with same prediction as CFD. However, TCM are able to predict the combustion process under various engine operating conditions with the required level of accuracy, which is confirmed by many researchers (examples are given in the section below). Based on the number of zones into which the cylinder volume can be divided, thermodynamic models can be classified into three subgroups: single-zone model, two-zone model and multi-zone model.

The choice of the calculation method (CFD or TCM) is based on the main aim of modeling and simulation. However, the thermodynamic models are more attractive, due to lower computational complications and time needed for the calculating of the combustion process. In the case of complex mathematical models, most often used a combination of TCM and CFD methods, for examples the firms which are leaders in calculating engine parameters such, as RICARDO WAVE [24] and AVL BOOST [1] provide the ability to simulate a TCM with combination of CFD model (used to describe the gas flow in three dimensions inside the intake and exhaust manifolds [5, 11, 12]). Due to the fact, that the 3D mesh is limited to specific elements of the intake and/or exhaust manifolds, this allows to minimize the unavoidable increases of the time consuming during the calculation of the engine operating parameters associated with using of CFD models.

This paper discusses the selected issues that are most often described when a single-zone or a two-zone thermodynamic combustion model is using.

Multi-zone thermodynamic models in this paper are presented only as a brief overview, because the overview of this models requires individual paper to

describe all features and properties. This models are quite accurately described in [3, 10, 16, 30].

2. Thermodynamic model

In the TCM the internal combustion engine is represented as an open thermodynamic system (single-zone model) or a combination of several thermodynamic systems (two- or multi- zone model).

The fast pressure equalization speed in the relatively small volume (engine cylinder) expect that the pressure inside the cylinder depends on time (τ) or crankshaft angle (φ) (Eq. 1) and does not depend on x, y, z coordinates [16], therefore, the thermodynamic model is considered as a zero-dimensional model

$$\varphi = \omega \cdot \tau \tag{1}$$

According to the assumptions above, it can be concluded that TCM – is used for energy analysis of the combustion process in the entire volume of the ICE cylinder and solves the issues in which can be assumed that the gas parameters are independent of coordinates and depend only on the time (or crankshaft angle), also the usage of TCM allows to analyze toxic emission during the combustion process.

In terms of CFD, the TCM represent the entire cylinder as one cell for which are applied the equations of mass, energy and state balance.

Thermodynamic models are used to solve two main issues:

1. Direct issue. Determination of the pressure change inside the cylinder as a function of the crankshaft angle p(φ), based on the previously defined amount of energy released during the combustion of the fuel charge $Q_x(\varphi)$ and heat transfer through the walls $Q_w(\varphi)$.

2. Reverse issue. Determination the amount of heat energy generated during the combustion of the fuel charge $Q_x(\varphi)$, based on the previously defined pressure inside the cylinder p(φ), which obtained from experimental data or from the computer simulation. Also needed to define heat transfer through the walls $Q_w(\varphi)$, if only one pressure is defined than can be determined only amount of total heat dQ, according to Eq. 2

$$dQ = dQ_x - dQ_w \tag{2}$$

In order to create TCM, must be solved three equations which are depending on the TCM type.

General equations:

1. The first law of thermodynamics used to describe the processes occurring in the combustion chamber consists in the fact that the change of internal energy in the cylinder is equal to the sum of the work of the piston, the amount of heat and enthalpy in- or out-flowing gas (Eq. 3).

The first law of thermodynamics for the ICE can be defined as

$$dU = d(u \cdot m) = dQ - dW + dH \tag{3}$$

2. The ideal gas law

$$pV = mRT \tag{4}$$

3. Mass conservation law

$$dm = \sum dm_i \tag{5}$$

2.1. TCM basic assumptions

Regardless to the model type, the basic assumptions are the same (differences in model assumptions presented in the relevant parts of this paper):

a) The thermodynamic parameters and composition of the working medium at any moments are homogeneous and stoichiometric and changing only with the crankshaft angle or time.

b) The initial temperature conditions are calculated by means of the perfect gas equation based on the measured pressure, mass of the mixture that is entered into the combustion chamber and the volume of the combustion chamber. The mass of air is measured by using a MAP (manifold absolute pressure) or MAF (mass air flow) sensor, the mass of the fuel is calculated by using a measured air-fuel ratio

$$AFR = \frac{m_{air}}{m_{fuel}} = \frac{n_{air} \cdot MW_{air}}{n_{fuel} \cdot MW_{fuel}} \tag{6}$$

c) Blow-by mass (m_{BB}) of the air to fuel mixture is so small compared to the other masses that are taken into account in the mass conservation law calculation. In the simplest TCM the air to fuel mixture losses by leakage in the piston rings and valves does not taken into account. Of course, depending on the model requirements, the blow-by mass could be taken into account (Eq. 31 and Eq. 32).

d) The heat transfer area is limited by the cylinder head, the top surface of the piston and the cylinder wall.

3. Thermodynamic submodels

3.1. Thermodynamic properties

To estimate the thermodynamic properties of the gas (variations of specific heat, enthalpy and entropy with temperature) in the cylinder as a function of temperature can be calculated by the well known linear or polynomial Eq. 7, Eq. 8 and Eq. 9, based on the polynomial tables of JANAF.

Instantaneous gas properties are calculated by the simultaneous numerical integration of differential equations

$$Cp_i(T) = R\left(a_1 + a_2 T + a_3 T^2 + a_4 T^3 + a_5 T^4\right) \quad [9] \tag{7}$$

$$hp_i(T) = R\left(a_1 + a_2\frac{T}{2} + a_3\frac{T^2}{3} + a_4\frac{T^3}{4} + a_5\frac{T^4}{5} + \frac{a_6}{T}\right) \quad [9] \ (8)$$

$$S(T) = R\left(a_1 \cdot \ln T + a_2 T + a_3\frac{T^2}{2} + a_4\frac{T^3}{3} + a_5\frac{T^4}{4} + a_7\right) \quad [9] \ (9)$$

3.2. The cylinder volume submodel

The total cylinder volume (V(φ)) is the sum of the volumes of the combustion chamber (V_c) and the cylinder volume (V_s), and depends on the instantaneous position of the piston. The Eq. 10 is based on the kinematic and kinetic of crankshaft as shown in Fig. 1, and can be written as

$$V(\varphi) = V_c + V_s(\varphi) \quad (10)$$

The combustion chamber volume

$$V_c = \frac{V_s}{\varepsilon - 1} \quad (11)$$

The instantaneous volume of the cylinder can be calculated on a per-anglestep basis using the following equation

$$V(\varphi) = V_c + \frac{\pi B^2}{4}\left(l + r - r\cdot\cos(\varphi) + \sqrt{(l - r\cdot\sin(\varphi))^2}\right) \quad [24] \ (12)$$

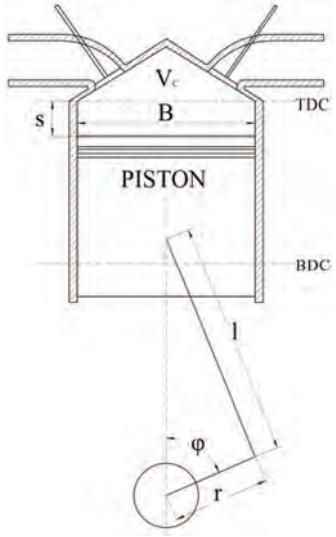

Fig. 1. Schematics of crank mechanism

The piston position is calculated using a standard crank/slider calculation as shown below. As default 0 deg refers to the piston position at top dead centre

$$S_p = \left(l + r - r\cdot\cos(\varphi) + \sqrt{(l - r\cdot\sin(\varphi))^2}\right) \quad [24] \ (13)$$

Cylinder volume change ($V_s(\varphi)$) in the differential form, can be written as

$$\frac{dV}{d\varphi} = \frac{\pi B^2}{4}\left(r\cdot\sin(\varphi) + \frac{r^2\cdot\sin(\varphi)\cdot\cos(\varphi)}{\sqrt{l^2 - r^2\cdot\sin(\varphi)}}\right) \quad [17] \ (14)$$

3.3. Heat transfer submodel

One of the most important submodels of TCM is a heat transfer, this submodel predict a heat transfer from a closed volume (cylinder) to the walls representing as a cylinder head, cylinder liner, top surface of the piston and valve head areas located in the combustion chamber. There are three different types of heat transfer: diffusion, convection and radiation. In this work, only the convective heat transfer was described.

Basically, the heat transfer calculation does not require high computing power. To calculate the amount of heat transferred to the walls, used the Newton-Richman law, that can be written, as

$$dQ_w = \alpha_w A_w (T - T_w)dt \quad [9, 17] \ (15)$$

According to Eq. 15 the heat transfer depends on time, in order to obtain connection with TCM, the Eq. 15 must be dependence on the crankshaft angle. The simplest conversion between time (t) and crankshaft angle (φ), can be written as

$$dt = \frac{d\varphi}{6n} \quad [16] \ (16)$$

where: t – is expressed in (s), n – is expressed in (rpm), φ – is expressed in (deg).

The most important parameter of the heat transfer submodel is the heat transfer coefficient (α_w).

There are many semi-empirical equations used to predict heat transfer coefficient, the most popular equations in the point of view of the prediction accuracy are Woschni's, Hohenberg's and Annand's equations.

a) Woschni heat transfer coefficient

The Woschni's correlation is well-known and widely used for calculation the heat transfer coefficient in both SI and Diesel engines and is given by Eq. 17. While the other correlations consider the gas velocity to be constant during the engine cycle, the Woschni's correlations provides the most detailed approach in the estimation of convective heat transfer and takes into account the gas velocity increases in the cylinder during the combustion, but the usage of this correlation without calibration often does not allow to calculate the instant heat transfer coefficient with required accuracy

$$\alpha_w = 130\frac{p^{0,8} w^{0,8}}{T^{0,52} B^{0,2}} \quad [9, 15] \ (17)$$

The value of the in-cylinder gas velocity depending on the working period of engine and can be calculated from the Eq. 18 and Eq. 19.

During the gas exchange and compression period

$$w = 2{,}28 \cdot C_m \quad [9, 15] \ (18)$$

During the combustion period

$$w = 2{,}28 \cdot C_m + 3{,}34 \cdot 10^{-3} \cdot \frac{V_c T}{pV} \cdot (p - p_c) \quad \text{[9, 15] (19)}$$

Mean piston speed (C_m), given by

$$C_m = \frac{S_p \cdot n}{30} \quad \text{[15] (20)}$$

where: n – is expressed in [rpm].

Woschni's heat transfer coefficient included the pressure difference between fired and motored operation ($p - p_c$) in the characteristic velocity to account for the effect of the combustion on the heat transfer [4].

b) Hohenberg heat transfer coefficient

According to Hohenberg, Woschni's correlation underestimates the heat transfer coefficient during compression and overestimates it during combustion. In addition, he stressed its difficulty of use [9]. Based on Woschni's work, Hohenberg proposed the correlation given by Eq. 21

$$\alpha_w = 130 \cdot p^{0.8} \cdot T^{-0.4} \cdot V^{-0.06} \cdot (C_m + 1.4)^{0.8} \quad \text{[4, 9] (21)}$$

c) Annand heat transfer coefficient

Unlike the previous two that were created for Diesel engines and afterwards, adapted for the SI ones, Annand's correlation originated from tests with SI engines [9]. The heat transfer coefficient is evaluated as shown in Eq. 22. Annand's correlations consider the gas velocity to be constant during the engine cycle equal to mean piston speed (C_m)

$$\alpha_w = c \frac{k_g}{D} \cdot Re^{0,7} + 4{,}3 \cdot 10^{-9} \cdot \left(\frac{T^4 - T_w^4}{T - T_w} \right) \quad \text{[9] (22)}$$

where: c – Annand's correlations parameter for a two-stroke engine often equal to 0.26 and for four-stroke engine equal to 0.49.

The second term of Eq. 22 accounts the radiation influence, which most often is neglected for SI engines [9].

3.4. Combustion submodel

The combustion duration is described by the amount of energy that released due to the combustion of the charge (Q_x) and can be written, as

$$\frac{dQ_x}{d\varphi} = Q_t \cdot \frac{dx_b}{d\varphi} \quad (23)$$

Total thermal energy of the fuel released during the combustion process (Q_t), given by

$$Q_t = m_{fuel} \cdot LHV_f \quad \text{[17, 21, 29] (24)}$$

The Wiebe function is widely used to estimate the rate of burned fuel mass in thermodynamic calculations, and allows the independent input of function shape parameters (m) and of burn duration, and represented by relation above

$$x_b = 1 - \exp\left(-\alpha \cdot \left(\frac{\varphi - \varphi_0}{\Delta\varphi} \right)^{b+1} \right) \quad \text{[16, 29] (25)}$$

Wiebe equation parameter α, determining the quality of combustion, and can be written, as

$$\alpha = \ln(1 - x^*) = -6{,}908 \quad \text{[16] (26)}$$

where: $x^* = 0.999$ – value of burned fraction at the end of combustion.

In the differential form Wiebe equation, can be written as

$$\frac{dx_b}{d\varphi} = \alpha \cdot \frac{b+1}{\Delta\varphi} \cdot \left(\frac{\varphi - \varphi_0}{\Delta\varphi} \right)^b \cdot (1 - x_b) \quad \text{[17] (27)}$$

The semi-empirical Wiebe function is characterrized by the simplicity of description and universality. In the presence of experimental data it is always possible to estimate the appropriate values of the Wiebe function parameters (Eq. 25), which allows to, provide simulation of the combustion process with required accuracy.

4. Single-zone model

It is a simplest TCM, that is used the basic TCM assumptions described in subchapter 2.1. In single zone models, cylinder charge is assumed to be uniform and the cylinder volume regarded as a single-zone. A single-zone model is often used if there is a need for a fast and preliminary analysis of the engine performance. However, single-zone considerations are associated with averaging temperature inside the cylinder during the combustion duration, which reduces the accuracy of the toxic emissions calculation.

This disadvantage can be eliminated by using a two-zone or multi-zone model that allows, to predict engine toxicity more accurately.

According to the assumptions of the single-zone model and the thermal balance presented on the Fig. 2, a system of three equations for this model in the differential form can be writing, as

$$\frac{d(m \cdot u)}{d\varphi} = \frac{dQ_x}{d\varphi} - \sum \frac{dQ_w}{d\varphi} - p\frac{dV}{d\varphi} + h_{in}\frac{dm_{in}}{d\varphi} - h_{out}\frac{dm_{out}}{d\varphi} \quad (28)$$

$$p\frac{dV}{d\varphi} + \frac{dp}{d\varphi}V = mR\frac{dT}{d\varphi} + m\frac{dR}{d\varphi}T + \frac{dm}{d\varphi}RT \quad (29)$$

$$\frac{dm}{d\varphi} = \frac{dm_{in}}{d\varphi} + \frac{dm_{out}}{d\varphi} \quad (30)$$

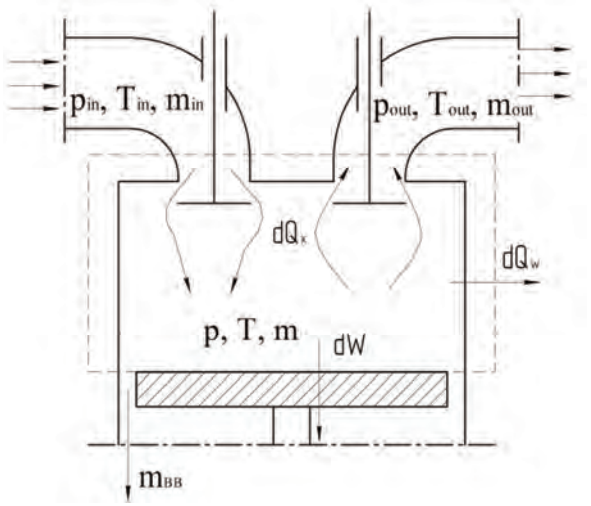

Fig. 2. Thermal balance of the single-zone model

The combustion process take place when the intake and exhaust valves are closed (closed cycle without gas exchanges), so assumed that the mass inflow equals zero (m_{in} = 0), and out flowing mass equals zero (m_{out} = 0), then Eq. 28, can be written as follows

$$\frac{d(m \cdot u)}{d\varphi} = \frac{dQ_x}{d\varphi} - \sum \frac{dQ_w}{d\varphi} - p\frac{dV}{d\varphi} \tag{31}$$

If a higher accuracy in the calculation of the combustion model is needed, then blow-by mass takes into account, and then the energy balance equation, can be presented by the following equation

$$\frac{d(m \cdot u)}{d\varphi} = \frac{dQ_x}{d\varphi} - \sum \frac{dQ_w}{d\varphi} - p\frac{dV}{d\varphi} - h_{BB}\frac{dm_{BB}}{d\varphi} \quad [1] \ (32)$$

To calculate the value of the instantaneous internal energy, it is needed to determine all components in the right side in the energy conservation equation (Eq. 3). To simplify the TCM calculations, used the submodels described in the third chapter of this paper.

4.1. Research carried out using the single-zone model

The author [32] investigate the combustion process of an SI engine fuelled with methane and methane-hydrogen blend. The studies were aimed to estimate the prediction accuracy of the combustion process modeling with single and double forms of Wiebe function. The results confirmed that the usage of the double Wiebe function increases the calculating accuracy. However, the difference between experimental pressure curves and simulated ones, estimated at about 3%, which is caused by temperature averaging. The author [2] in order to predict the in-cylinder pressure for the diesel engine fueled by diesel and biodiesel implemented a single-zone combustion model and used the triple-Wiebe function to describe the heat release process. The simulation results are presented in Fig. 3. However, similar to the previous author, the average temperature caused differences in pressure curves, estimated at 2.5%. Similar results are obtained by the authors [20, 21, 25, 27] and others.

Unlike to the previous authors, the studies of the author [13] were aimed to sensitivity analysis of the Wiebe function coefficients to the various engine loads. Moreover, method of confirming the number of combustion phases and method of estimating start angle of combustion were proposed by the authors [13].

In summary, it can be concluded that the average temperature in the cylinder does not have a significant influence over the engine performance prediction. According to the author [28] the ten percent of heat transfer prediction error leads to the order of one per cent performance prediction error [18]. A single-zone models, allows to predict the heat release rate with high accuracy. However, there are differences between experimental pressure curves and simulated ones caused by temperature averaging which is presented in Fig. 4.

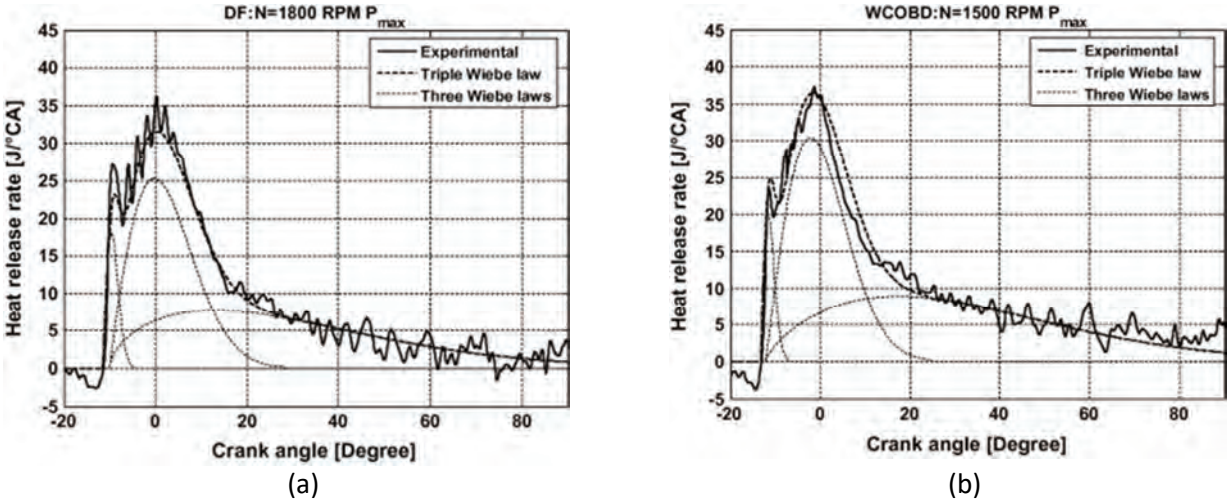

Fig. 3. HRR of the CI engine fueled with diesel (a) and biodiesel (b) [2]

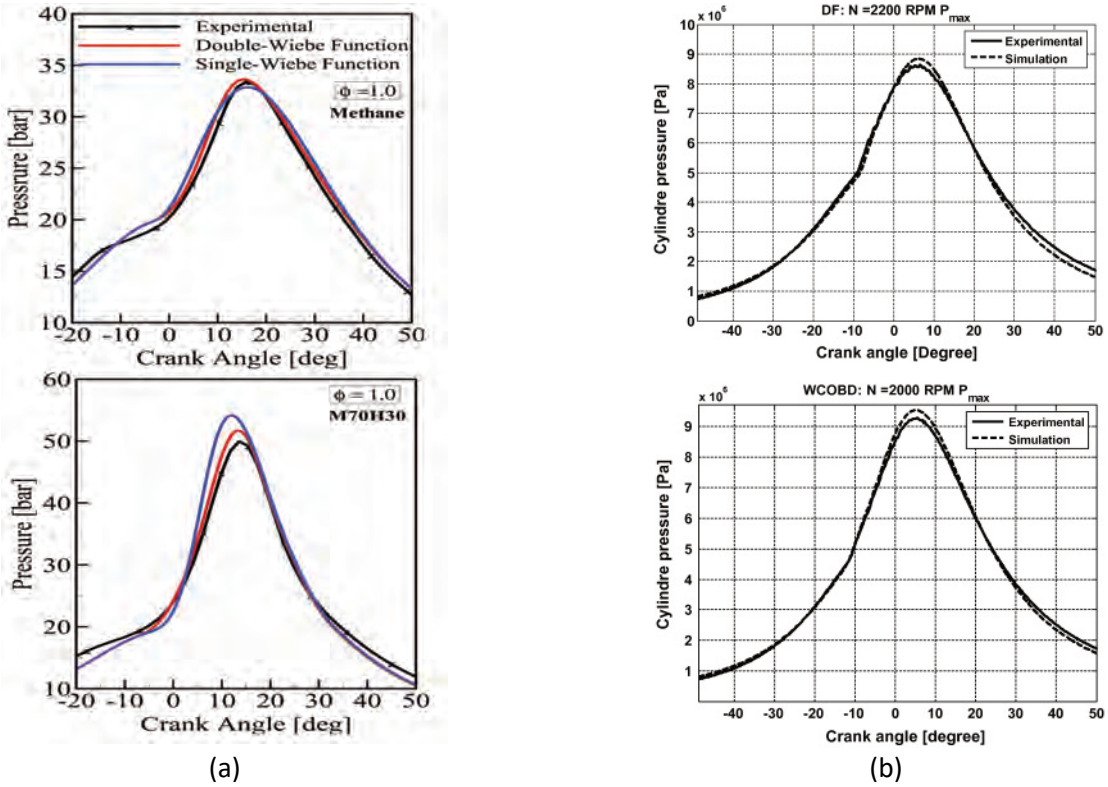

Fig. 4. Comparison of pressure development in single zone model (a) [32] and (b) [2]

5. Two-zone model

The two-zone combustion model is an extension of the single-zone model, which is due to its additional assumptions, gives more accurate prediction of the engine performance and toxic emission calculations.

Additional assumptions of the two-zone model:

a) The basis of the two-zone model, is the division of the cylinder volume (V) (Eq. 33) and the mass of the working fluid (m) inside the cylinder (Eq. 34) into two zones (the unburned zone (m_u and V_u) and burned zone (m_b and V_b)) by a thin zone of the combustion reaction (flame front), The division of the combustion chamber is shown on Fig. 5.

$$V = V_u + V_b \tag{33}$$

$$m = m_{fuel} + m_{air} = m_u + m_b \tag{34}$$

b) The pressure inside the cylinder is uniform at any moment.

c) Each zone has its own temperature, which is uniform in its own zone. There is no heat exchange between zones.

d) Working fluid that fills the cylinder is homogeneous and contains air, fuel vapor and residual gases.

e) Each zone has its own heat transfer coefficient and contact area (with cylinder walls, cylinder head, top surface of the piston). The calculations of the contact area based on the instantaneous value of the burned mass.

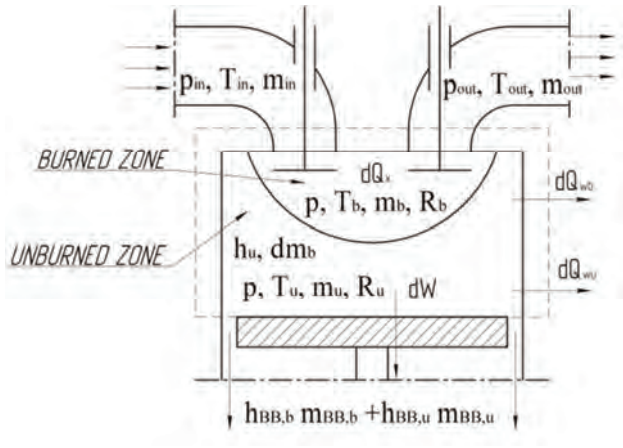

Fig. 5. Thermal balance of the two-zone model

Due to the division of the cylinder chamber into two zones, equation of energy conservation for each zone, can be written as follows:

Burned zone

$$\frac{d(m_b \cdot u_b)}{d\varphi} = -p\frac{dV_b}{d\varphi} + \frac{dQ_x}{d\varphi} - \sum\frac{dQ_{wb}}{d\varphi} + h_u\frac{dm_b}{d\varphi} - h_{BB,b}\frac{dm_{BB,b}}{d\varphi}$$

[1, 14] (35)

Unburned zone

$$\frac{d(m_u u_u)}{d\varphi} = -p\frac{dV_u}{d\varphi} - \sum\frac{dQ_{wu}}{d\varphi} - h_u\frac{dm_b}{d\varphi} - h_{BB,u}\frac{dm_{BB,u}}{d\varphi}$$

[1, 14] (36)

In the equation above the $h_u \frac{dm_b}{d\varphi}$ – includes the enthalpy flow from the unburned zone to the burned as a result of the conversion of the fresh load to the combustion products.

The ideal gas law

$$p = \frac{1}{V} \cdot \left(m_b \cdot R_b \cdot T_b + m_u \cdot R_u \cdot T_u \right) \qquad [1] \ (37)$$

Mass conservation law

$$\frac{dm}{d\varphi} = \frac{dm_{in}}{d\varphi} + \frac{dm_{out}}{d\varphi} + \frac{dm_{BB}}{d\varphi} = \frac{dm_b}{d\varphi} + \frac{dm_u}{d\varphi} + \frac{dm_{BB}}{d\varphi} \qquad (38)$$

5.1. Research carried out using the two-zone model

Due to the fact that the combustion chamber is divided into two zones, it gives a more accurate prediction of the temperature inside the cylinder. Therefore, many publications devoted to a two-zone modeling of the combustion process, except the similar issues that are also solved by single-zone modeling (presented in the [18, 26, 29, 31] and others), aimed to additional issues:

1. Analysis of the influence of the various engine operation conditions (load, rotational speed, EGR rate and others) on the emissivity and combustion characteristics. The studies of the authors [14] were aimed to predicting the effect of ethanol–gasoline (E0, E5, E10, E20, E30 and E50) fuel blends on the performance and emission characteristics of SI engine. The studies of the authors [23] were aimed to investigate and analyze the impact of the EGR rate and engine loads, on the combustion and emissions characteristics of the diesel engine by two-zone modeling.

2. Analysis the impact of different heat transfer correlations (Eq. 17, Eq. 21, Eq. 22 and others (not presented in this paper)) on the heat transfer submodel prediction and results of combustion modeling. This type of analysis was carried out by the authors [9], for study they used SI engine fueled with wet ethanol. Results showed that Hohenberg's correlation (Eq. 21) together with Wiebe function, gives the most accurate results, in the prediction of the in-cylinder pressure and heat flux through the cylinder walls (Fig. 6). A similar study was carried out on the SI engine fueled with natural gas by the authors [19]. The results shown that the Hohenberg's or Eichelberg's correlation together with Wiebe's function gives the good calculation result.

It can be concluded that, the two-zone model compared to a single-zone model allows to, additionally assess emission characteristics and analyze the heat transfer submodel, which leads to a better simulation results.

6. Multi-zone model

If it is needed to create the TCM with highest accuracy and lower time-consumption (compared to CFD models), more often used multi-zone models. They are an extension of the single- and two- zone models and uses the basic assumptions of single- and two-zone models.

Additional assumptions of the multi-zone model:

a) The cylinder volume is divided into a predetermined number of zones (there are different ways for division some examples presented in Fig. 7 [3] and Fig. 8 [10]). The simulation results are presented in Fig. 9.

b) The pressure in each zones are the same and equal to the pressure in the cylinder.

6.1. Baratt's multi-zone divided example

The author [3] create a multi-zone model to analyzing the combustion process and toxic emission of a SI engine fueled with CNG.

The combustion chamber volume is divided into an unburned gas zone (V_u) and a burned gas region (V_b), which has been split into six 'zones' (shown in Fig.7). The numbers in the picture show each of the burned zones. In real simulations, a burned zone is generated each 5° crank angle, and thus 15–20 burned zones (the exact number depends upon the combustion duration) are generally generated at the end of combustion (EOC) [3].

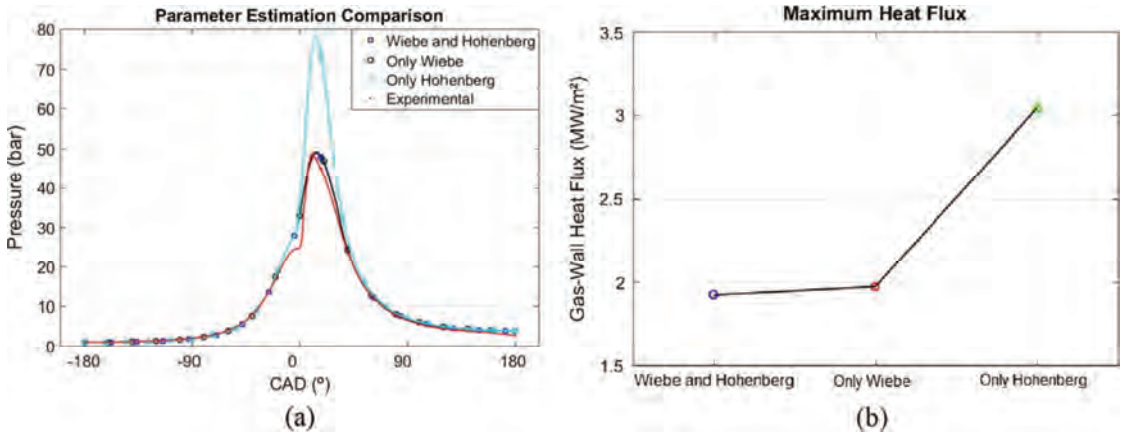

Fig. 6. Three cases estimation comparison using Hohenberg's correlation for (a) the in-cylinder pressure and (b) the maximum heat flux [9]

The following Eq. 39 is obtained by constraining the sum of the volumes of the unburned region (V_u) and of the burned zones ($V_{b,i}$, where subscript (i) ranges from 1 to n) in order to be equal to the instantaneous cylinder volume (V) [3]

$$dV = dV_u + \sum_{i=1}^{n} dV_{b,i} \qquad [3]\ (39)$$

The mass conservation law, applied to the cylinder content, yields

$$dm = d\left(m_{fuel} + m_{air} + m_r\right) = dm_u + dm_{b,n} \qquad [3]\ (40)$$

The energy conservation equation for the unburned zone and for each burned zone i, can be written, as

$$-q_u A_u dt + V_u dp = m_u dh_u \qquad [3]\ (41)$$

$$-q_{b,i} A_{b,i} dt + V_{b,i} dp = m_{b,i} dh_{b,i} \qquad [3]\ (42)$$

The ideal gas law, is given by relation

$$pV = m_u R_u T_u + \sum_{i=1}^{n} m_{b,i} R_{b,i} T_{b,i} \qquad [3]\ (43)$$

The equations of this multi-zone TCM are the same as for the two-zone model, difficulties in the equations and calculating are associated only with the increased number of zones, also in this multi-zone model is necessary to take into account heat transfer between zones.

6.2. Fathi multi-zone divided example

The author [10] proposed to divided combustion chamber into 13 zones, shown in Fig. 8. There is no mass transfer between zones, and the inter-zonal interactions is confined to the heat transfer between neighbouring zones and the work done due to the zonal volume changes [10].

The first law of thermodynamics for each zone in a system with a constant mass is expressed by the equation

$$\frac{dU_z}{dt} = -p\frac{dV_z}{dt} + \frac{dQ_z}{dt} \qquad [10]\ (44)$$

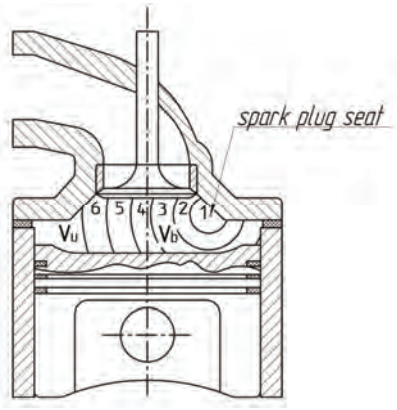

Fig. 7. Multi-zone division by Baratt [3]

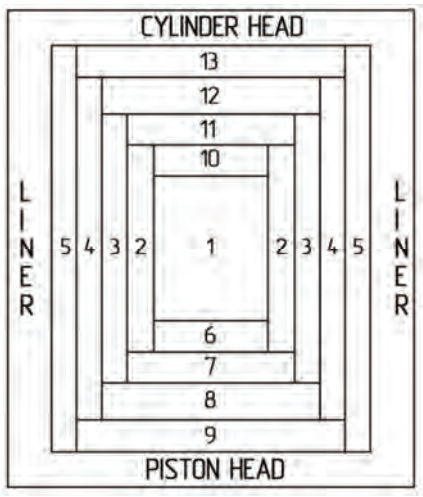

Fig. 8. Zonal configuration for multi-zone modeling [10]

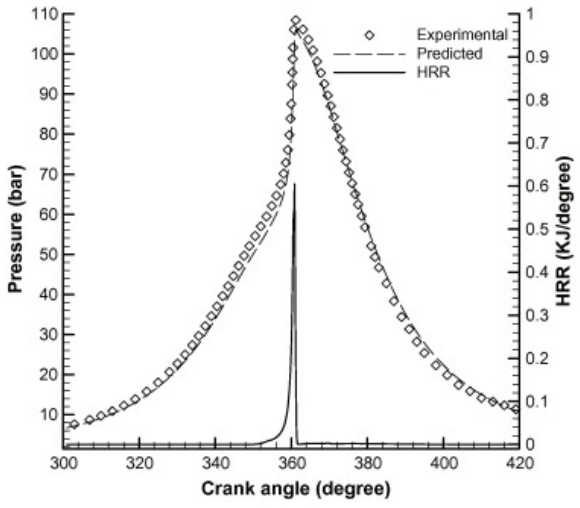

(a)

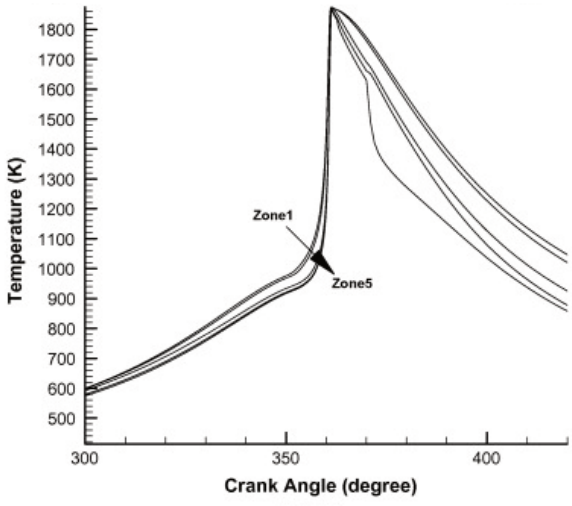

(b)

Fig. 9. In-cylinder pressure and temperature [22]

Since all zones have a uniform pressure, total in-cylinder mass during multi-zone modeling is constant, mass of each zone remains constant, and the combustion chamber volume is the sum of all zones volumes, the first ordinary differential equations for the multi-zone model can be derived [10], as

$$\frac{dp}{dt} = -\frac{1}{V^2}\cdot\frac{dV}{dt}\sum_{z=1}^{n} m_z R_z T_z + \frac{1}{V}\cdot\sum_{z=1}^{n}\left(m_z T_z \frac{dR_z}{dt} + m_z R_z \frac{dT_z}{dt}\right) \text{[10] (45)}$$

Mass conservation equation for multi-zone model is determined as follows

$$\frac{dm_{z,i}}{dt} = V_z M_i \omega^*_{z,i} \quad \text{[10] (46)}$$

Eq. 46 according to the author [10] is solved by using the Cantera chemical kinetics solver.

6.3. Simulation results

The multi-zone model allows to analysis in-cylinder temperature of different zones, which gives a positive effect on the simulation accuracy (Fig. 9).

7. Conclusions

All TCM overviewed in this paper are based on the differential equations of energy conservation, state and mass. All parameters of these equations, depends on the crankshaft angle or time. Therefore, this models are called zero-dimensional. TCM division is based on the number of zones inside the cylinder. The choosing of the calculation method based on the main aim and required computational accuracy of the model. However, for a numerical description of the combustion process and analysis of the impact of various engine parameters (load, rotational speed, EGR rate, etc.) on the combustion process and emission characteristics of ICE, the two-zone model is most commonly used, because it allows to predict the engine operational parameters with the required level of accuracy.

Based on the analysis of the references presented in this paper, it could be concluded that it cannot be definitely determine which correlation of the convective heat transfer coefficient gives the better results. In some cases, the heat transfer correlation gives more accurate results in other cases they cause more calculation errors. Therefore, the convective heat transfer correlation must be selected separately for each specific case.

Modeling of the combustion process by using the Wiebe's function allows to, calibrate the shape parameters and burn duration. The ability to change several parameters in one equation allows to fit them to the experimental data with the smallest errors.

Nomenclature

α	Wiebe equation parameter that determining the quality of combustion
α_w	convective heat transfer coefficient
a_1–a_7	JANAF polynomial coefficients
A_w	heat exchange area
b	semi empirical Wiebe equation parameter (the Wiebe's function shape parameter)
B	cylinder bore
BDC	bottom dead center
c	Annand's correlations parameter
C_m	mean piston speed
c_p	specific heat
CFD	computational fluid dynamic
dt	calculation step by time
H	change of enthalpy in- or out-flowing gas
h_{in}, h_{out}	specific enthalpy of in- or out-flowing gas
h_p	specific enthalpy
ICE	internal combustion engine
l	connecting rod length
LHV_f	lower heating value of fuel
k_g	thermal conductivity coefficient
m	total mass of the charge in the cylinder (air + fuel)
m_{air}	mass of air
m_{BB}	blow-by mass
m_b	mass of charge in-cylinder burned zone
m_{fuel}	mass of fuel
m_r	mass of residual gas
m_u	mass of charge in-cylinder unburned zone
MW_{air}	molecular weight of air
MW_{fuel}	molecular weight of fuel
n	crankshaft rotation speed
n_{air}	number of moles of air
n_{fuel}	number of moles of fuel
p	in-cylinder pressure
p_c	in cylinder pressure during motor operation
Q	total amount of in-cylinder heat
Q_w	wall heat loss
Q_x	heat of combustion
Q_t	total thermal energy of the fuel (released during the combustion process)
q_uA_u, $q_{b,i}A_{b,i}$	moduli of the global heat transfer from the considered zone (u or i) to the adjacent zones and to the combustion chamber walls [3]
R	universal gas constant
r	crank radius (half the stroke)
s	entropy
S_p	instantaneous piston position
SI	spark-ignition
T	in-cylinder temperature

T_w	cylinder wall temperature
TDC	top dead center
TCM	thermodynamic combustion model
U	internal energy
u	specific internal energy
V	in-cylinder volume
V_b	in-cylinder burned zone volume
V_u	in-cylinder unburned zone volume
V_c	combustion chamber volume
W	the work on the piston
w	in cylinder gas velocity
x_b	burned mass fraction
x*	amount of burned fraction at the end of combustion
φ	crankshaft angle
τ	time
ω	crankshaft angular speed
ω^*	consumption/production rate of species during combustion [10]
ε	engine compression ratio
φ	crankshaft angle
φ_0	crankshaft angle of combustion start
$\Delta\varphi$	combustion duration

Bibliography

[1] AVL. AVL-Boost Software Combustion Models, User Man., 2015.

[2] AWAD, S., VARUVEL, E.G., LOUBAR, K., TAZEROUT, M. Single zone combustion modeling of biodiesel from wastes in diesel engine. *Fuel.* 2013, **106**, 558-568.

[3] BARATTA, M., FERRARI, A., ZHANG, Q. Multi-zone thermodynamic modeling of combustion and emission formation in CNG engines using detailed chemical kinetics. *Fuel.* 2018, **231**, 396-403.

[4] BROEKAERT, S., DE CUYPER, T., DE PAEPE, M., VERHELST, S. Evaluation of empirical heat transfer models for HCCI combustion in a CFR engine. *Appl. Energy.* 2017, **205**, 1141-1150.

[5] CLAYWELL, M. Coupled WAVE coupled WAVE-VECTIS simulation of an intake simulation of an intake restricted engine.

[6] CRIPPA, M., GRANIER, C. Forty years of improvements in European air quality: regional policy-industry interactions with global impacts. *Atmos. Chem. Phys.* 2016. **16**(6), 3825-3841.

[7] BIELACZYC, P., WOODBURN, J. Current directions in LD powertrain technology in response to stringent exhaust emissions and fuel efficiency requirements. 2016, **166**(3), 62-75.

[8] European Parliament, Council of the European Union. Regulation (EC) No 715/2007 of the European Parliament and of the Council of 20 June 2007 on type approval of motor vehicles with respect to emissions from light passenger and commercial vehicles (Euro 5 and Euro 6) and on access to vehicle repair and mai. *Off. J. Eur. Union*. 2007, **L171**, 1-16.

[9] FAGUNDEZ, J.L.S., SARI, R.L., MARTINS, M.E.S., SALAU, N.P.G. Comparative analysis of different heat transfer correlations in a two-zone combustion model applied on a SI engine fueled with wet ethanol. *Appl. Therm. Eng*. 2017, **115**, 22-32.

[10] FATHI, M., SOMERS, B. Stand-alone single- and multi-zone modeling of direct injection homogeneous charge compression ignition (DI-HCCI) combustion engines. *Appl. Therm. Eng*. 2017, **125**, 1181-1190.

[11] GRABOWSKI, Ł., PIETRYKOWSKI, K., WENDEKER, M. *AVL simulation tools practical applications*. 2017. 2012.

[12] GUIZZETTI, M., ITALIA, F.A.P. Combined WAVE-VECTIS simulation of an intake manifold of V6 PFI gasoline engine. 1-15.

[13] HU, S., WANG, H., YANG, C., WANG, Y. Burnt fraction sensitivity analysis and 0-D modelling of common rail diesel engine using Wiebe function. *Appl. Therm. Eng*. 2017, **115**, 170-177.

[14] ILIEV, S.P. Developing of a 1-D combustion model and study of engine characteristics using ethanol- gasoline blends. *Proc. World Congr. Eng*. 2014, **II**, 1-6.

[15] KABANOV, O. Choosing of calculation method for heat transfer process in gas engine with spark ignition. 2012, 96-102.

[16] KAVTARADZE, R.Z. IC engines theory. Book for universities. *N.E. Bauman*, Moscow 2008.

[17] KÉROMNÈS, A. Internal combustion engine modeling. 2017.

[18] LOGANATHAN, S., LEENUS, J.M., NAGALINGAM, B., PRABHU, L. Heat release rate and performance simulation of DME fuelled diesel engine using oxygenate correction factor and load correction factor in double Wiebe function. *Energy*. 2018, **150**, 77-91.

[19] LOUNICI, M.S., LOUBAR, K., BALISTROU, M., TAZEROUT, M. Investigation on heat transfer evaluation for a more efficient two-zone combustion model in the case of natural gas SI engines. *Appl. Therm. Eng*. 2011, **31**(2-3), 319-328.

[20] MAROTEAUX, F., SAAD, C. Diesel engine combustion modeling for hardware in the loop applications: effects of ignition delay time model. *Energy*. 2013, **57**, 641-652.

[21] MAROTEAUX, F., SAAD, C., AUBERTIN, F. Development and validation of double and single Wiebe function for multi-injection mode Diesel engine combustion modelling for hardware-in-the-loop applications. *Energy Convers. Manag*. 2015, **105**, 630-641.

[22] NOBAKHT, A.Y., KHOSHBAKHI, S.R., RAHIMI, A. A parametric study on natural gas fueled HCCI combustion engine using a multi-zone combustion model. *Fuel.* 2011, **90**(4), 1508-1514.

[23] RAKOPOULOS, C.D., RAKOPOULOS, D.C., MAVROPOULOS, G.C., KOSMADAKIS, G.M. Investigating the EGR rate and temperature impact on diesel engine combustion and emissions under various injection timings and loads by comprehensive two-zone modeling. *Energy*. 2018, **157**, 990-1014.

[24] Ricardo. "Ricardo software WAVE," User Man., 2016.

[25] SHAHBAKHTI, M., KOCH, C.R. Thermo-kinetic combustion modeling of an HCCI engine to analyze ignition timing for control applications. *Spring Tech. Meet. Combust. Institute/Canadian Sect.* 2007, 1-7.

[26] SONG, R., SCHOCK, H. A control-oriented model of turbulent jet ignition combustion in a rapid compression machine. *Proc. Inst. Mech. Eng. Part D J. Automob. Eng.* 2017, **231**(10), 1315-1325.

[27] SORUSBAY, C., SOYHAN, H.S. Double-Wiebe function: an approach for single-zone HCCI engine modeling. *Appl. Therm. Eng*. 2007, **28**(11-12), 1284-1290.

[28] STONE, R. Introduction to internal combustion engines. **3**. *Springer* 1999.
[29] SUN, Y., WANG, H., YANG, C., WANG, Y. Development and validation of a marine sequential turbocharging diesel engine combustion model based on double Wiebe function and partial least squares method. *Energy Convers. Manag.* 2017, **151**, 481-495.
[30] VERHELST, S., SHEPPARD, C.G.W. Multi-zone thermodynamic modelling of spark-ignition engine combustion – an overview. *Energy Convers. Manag.* 2009, **50**(5), 1326-1335.
[31] YANG, X., ZHU, G.G. A control-oriented hybrid combustion model of a homogeneous charge compression ignition capable spark ignition engine. *Proc. Inst. Mech. Eng. Part D J. Automob. Eng*. 2012, **226**(10), 1380-1395.
[32] YILDIZ, M., ALBAYRAK ÇEPER, B. Zero-dimensional single zone engine modeling of an SI engine fuelled with methane and methane-hydrogen blend using single and double Wiebe function: a comparative study. *Int. J. Hydrogen Energy.* 2017, **42**(40), 25756-25765.

Denys Stepanenko, MEng. – Faculty of Mechanical Engineering, Gdansk University of Technology.
e-mail: *denstepa@student.pg.edu.pl*

Zbigniew Kneba, DSc., DEng. – Faculty of Mechanical Engineering, Gdansk University of Technology.
e-mail: *zkneba@pg.edu.pl*

Article citation info:
MERKISZ, J., ANDRYCH-ZALEWSKA, M., PIELECHA, J. Analysis of the efficiency of the in-cylinder catalyst to reduce exhaust emissions during the cold start combustion engine. *Combustion Engines*. 2019, **178**(3), 38-45. DOI: 10.19206/CE-2019-307

Jerzy MERKISZ
Monika ANDRYCH-ZALEWSKA
Jacek PIELECHA

CE-2019-307

Analysis of the efficiency of the in-cylinder catalyst to reduce exhaust emissions during the cold start combustion engine

The article concerns the use of an in-cylinder catalyst that allows reducing the exhaust emissions during diesel engine operation. This is an additional method of exhaust emission reduction – however, the active component is placed inside the combustion chamber – hence much closest to the combustion process. This allows reducing the emissions at the very source (catalyst applied on the glow plugs). Such solutions are necessary because the reduction of exhaust emissions from vehicles is a key aspect of reducing the negative impact of transport on the environment.

Key words: *exhaust emission, in-cylinder catalyst, diesel engine*

Introduction

Due to the way passenger cars are used, especially during urban driving, they are characterized by low mileage between individual starts, so they often experience ignition in a cold state and operate in underheated engine conditions [6]. According to Scandinavian research [8], in Sweden, 2.7 billion cold engine starts in Sweden are made in passenger cars, and in Finland – 2.6 billion. Cold engine-starts cause about 90% of the total hydrocarbon and carbon monoxide emissions and 50–70% of oxides emissions from passenger cars in the Nordic countries, thus they are a significant contributor of harmful substances emissions from automotive sources.

Because the amount of time the engine spends operating in cold conditions is significant, more and more attention is brought to the problems caused by cold engine operation. When operating at low loads and idling the engine thermal condition is unstable and the reactions occurring inside and outside the cylinder (in the exhaust system) are somewhat disturbed. Additionally, fuel combustion in these conditions is partial and incomplete. Due to how passenger cars are used, mainly for urban driving, there is little distance covered between individual starts (Fig. 1), so they are often started from the cold engine state and operate in unfavorable engine conditions.

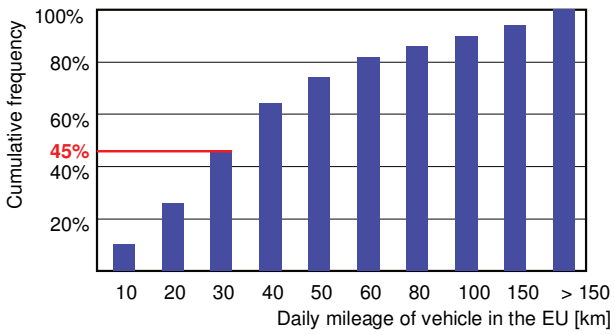

Fig. 1. Mileage of European passenger cars [14]

Figure 1 shows that 45% of routes travelled are shorter than 30 km, so the engine is cold and the catalytic converter does not fully operate, especially when stationary – therefore it is possible to use various solutions to reduce this phenomenon [1]. In order to eliminate harmful exhaust emissions, it is pivotal to equip every vehicle with an exhaust aftertreatment system for flue gas whose composition, temperature and flow rates are constantly changed during operation. The catalytic reactors used in the automotive industry are expected to reduce harmful components of exhaust gases as well as to have high durability [10, 24]. A very important factor is controlling the parameters of exhaust gases, in particular their changes in the engine exhaust system [11, 23]. The technology of exhaust aftertreatment systems is being continuously developed due to the ever lower emission limits. There are many solutions of exhaust aftertreatment systems, and their effectiveness often depends on the mutual relations and cooperation of individual system components (Fig. 2).

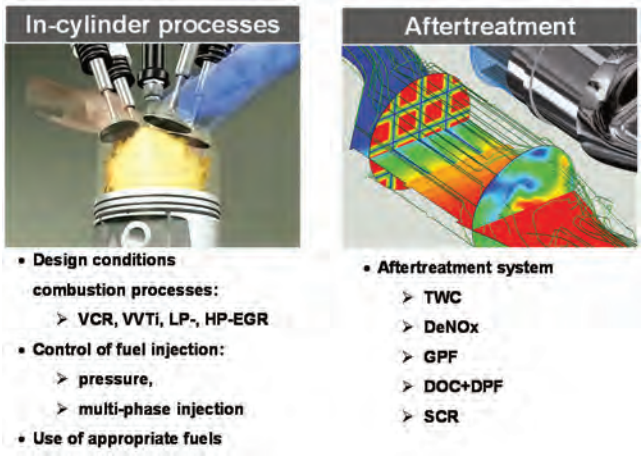

Fig. 2. Methods for reducing exhaust emissions; VCR (Variable Compression Ratio), VVTi (Variable Valve Timing with intelligence), ERG (Exhaust Gas Recirculation) of (LP – low pressure, HP – high pressure), TWC (Three Way Catalyst), Decrease NO_x – systems for reducing the NO_x emissions, GPF (Gasoline Particle Filter), DOC (Diesel Oxidation Catalyst), SCR (Selective Catalytic Reduction)

Overall, toxicity is determined by local processes in the combustion chamber, which take place in dynamic conditions, occurring for a short duration (on the order of milli-

seconds or shorter). Therefore, it is reasonable to introduce additional agents to improve the atomization, evaporation, diffusion of fuel vapors and their mixing with air, as well as for the oxidation of fuel, for example, the use of catalysts within the combustion chamber or immediately after the flue gas leave the chamber.

The use of a catalyst inside the combustion chamber can cause problems regarding the location, i.e. the choice of the surfaces and elements to be covered with catalytic materials. A separate problem arises as the issue of durability of the catalytic coatings used.

1. Feasibility of in-cylinder catalysts use

The need to reduce exhaust emissions from internal combustion engines has led to the introduction of multifunctional catalytic reactors used in both spark and compression ignition engines. However, there are problems associated with the use of catalytic converters, including the efficiency of carbon monoxide and hydrocarbons oxidation is only high when the engine is powered by a stoichiometric mixture, on top of that the reactor needs to reach its operating temperature (*light-off*). Obtaining the proper operating temperature of the catalytic converter is achieved primarily through its placement in the exhaust system. Thus, a concept was born to place the catalyst in the combustion chamber itself.

Research on ecological issues in internal combustion engines and the beneficial effects of internal catalyst, placed in the cylinder, on engine performance and exhaust emission were investigated as early as in the mid-twentieth century. The use of the catalytic coating in the cylinder were mainly aimed at reducing the smoke opacity in Diesel engines by reducing the ignition delay [7, 16, 21, 26]. Other advantages were the subject of research in which the internal catalyst (covering the outlet valve with platinum) resulted in the reduction of carbon monoxide and hydrocarbon emissions in the Diesel engine powered by methanol [15] and diesel fuel [27, 28]. The issue of nitrogen oxides reduction using an in-cylinder catalyst is based on using a platinum catalyst [22], but due to the high costs of such a solution, it was postulated that it could be replaced with molybdenum compounds [25].

The results of research on in-cylinder catalysts were also published in articles [5, 9, 12, 13, 17, 18, 20], which have shown a positive effect that a catalytic layer on some elements of the combustion chamber has on reducing the concentration of carbon monoxide and hydrocarbons, which unfortunately depends on the properties of the catalyst used and the operating conditions of the internal combustion engine. Such tests were carried out only in stable conditions of engine operation, whereas in this article an attempt was made to determine the ecological benefits of using an in-cylinder catalyst mainly in the dynamic operating conditions of the compression ignition internal combustion engine as well as in real operation.

2. Aim and scope of research

Increasingly more emphasis is placed on reducing the negative environmental impact of combustion engine vehicles, both from the legal institutions of individual countries as well as international organizations and associations. This drives the search for ever more advanced technical solutions for the internal combustion engine that will limit this negative impact and meet the current exhaust emission limits [2–4, 19]. Among these activities, the most important ones are those that have a direct impact on the improvement of combustion and the reduction of the toxic exhaust components formation while still in the engine's combustion chamber. The distinguishing feature of this article is that it focuses mostly on conducting tests in the operating conditions corresponding to the engine cold start.

The formulation of the research aim lead to the following assumptions as part of the scope of research:

- the catalyst is applied on an easily replaceable element – glow plug (test object),
- the material of the catalyst is platinum – it reduces the concentration of carbon monoxide and hydrocarbons and to a small extent allows for a reduction of solid particles in the Diesel engine,
- internal catalyst – platinum works mainly during start-up and heating of the engine, that is why the tests will be carried out before the catalytic reactor (DOC),
- tests were performed comparatively: glow plug without a catalyst cover and covered with a catalyst (modified),
- additionally an analysis of the glow plug heating time and its influence on the exhaust emission was carried out,
- a Diesel engine with the Euro 4 emission category, the most frequently occurring in the European Union (1.3 JTD, MultiJet), was selected for the tests.

3. Research methodology

3.1. Prototype components

The subject of research and analysis were glow plugs with the following parameters (Fig. 3):

- catalog number: 0250203002,
- trade abbreviation (HKB): GLP016,
- material number (KSN), marketing number: 16,
- connection type: PIN,
- mounting depth: 28 mm,
- threaded fitting 1: M8 × 1.0,
- length: 120 mm,
- control voltage: 11 V,
- tilting angle forming the cone: 93°.

A new solution used in this research was the implementation of prototype glow plugs, with a 34 mm long heating section (4 mm longer compared to previous solutions – Fig. 4).

Fig. 3. Standard glow plugs (heating section length – 30 mm)

Fig. 4. Prototype glow plugs with an extended heating section length (34 mm)

The new prototype glow plugs were longer by 4 mm, which resulted in a 50% increased active surface area of the internal catalyst. The heating section was made of stainless steel (sheet) type INOX (18Cr9Ni), with a thickness of 0.05 mm. Such a metal sheet is used for making catalytic reactors with a metal carrier. This made it possible to eliminate the ceramic layer that was applied to a standard plug with a catalytic coating having a heating section length of 30 mm. The lack of a ceramic layer made it possible to reduce the thermal insulation, and as a result the heating of the glow plugs was faster leading to a higher catalytic layer operating temperature.

3.2. Test object

A compression ignition combustion engine was used for the research (as well as equipped in the passenger car used for the tests, with a mileage of 92,000 km, where the engine met the Euro 4 emission standard). The test object was a supercharged engine with a 1.3 dm^3 displacement, with the designation 1.3 JTD (MultiJet) and Euro 4 emission class – the test stand is shown in Fig. 5.

Fig. 5. The test engine mounted on the dynamometer along with the engine control unit

The exhaust aftertreatment system is typical for Diesel direct injection engines, i.e. a two-way catalytic converter (a particulate filter was not required in vehicles of this emission category). The choice of such a research object was dictated by the fact that more than 50% of cars in the European Union are equipped with such engines. At the same time, the Euro 4 emission standard was in force from January 1, 2006 to 2010, and the average age of cars imported to Poland is 11.5 years (of which 42% are with diesel engines). Therefore, the Diesel engine is the most representative engine in Europe and for Poland. Another reason is that it is an engine where the emission of carbon monoxide and hydrocarbons can be reduced easily – by simply replacing the glow plug.

3.3. Measuring equipment

The Semtech DS analyzer manufactured by Sensors was used to measure the concentration of harmful compounds in the exhaust gas. It allowed measurement of harmful compounds concentration including - carbon monoxide, hydrocarbons, nitrogen oxides and carbon dioxide. The analyzer processing unit received data directly from the engine diagnostic system. The analyzer consists of the measurement modules:

– FID (*Flame Ionization Detector*) used to determine the total hydrocarbon concentration in exhaust gases,
– NDUV (*Non-Dispersive Ultraviolet*), designed to measure the concentration of nitrogen oxide and nitrogen dioxide,
– NIDR (*Non-Dispersive Infrared*) infrared radiation, designed to measure the concentration of carbon monoxide and carbon dioxide,
– electrochemical for determining the oxygen content in the exhaust gas.

The TSI 3090 EPSS™ analyzer (Engine Exhaust Particle Sizer™ Spectrometer) was used to study the particle size distribution of particulate matter. It enabled the measurement of a discrete range of particle diameters (in the range from 5.6 nm to 560 nm) emitted in the exhaust gases based on their different velocity. Due to the device's data acquisition frequency of up to 10 Hz, the analyzer can be used for the study of particulate emissions in transient engine states. The diagram of the setup of presented devices is shown in Fig. 6.

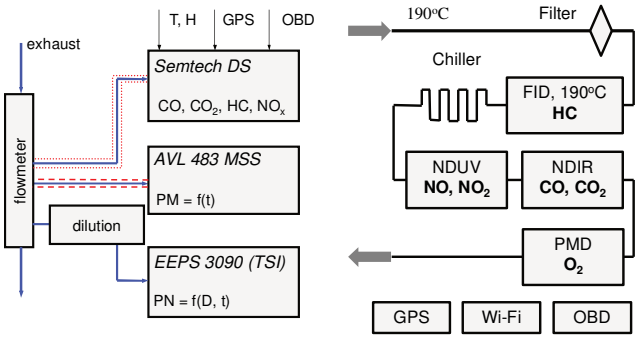

Fig. 6. Setup diagram of the measurement system used for testing the exhaust emission of gaseous and particulate compounds; T – ambient temperature, H – air humidity

4. Measurement results

Considering the ecological benefits of the research capabilities specified in the articles [2], another modification of catalytic-coated glow plugs was proposed. The proposal concerned the elongation of glow plugs, in such a way that the heating section coated with the catalyst protrudes as much as possible into the combustion chamber, and at the same time to maximally increase the area of its active reaction surface with combustion gases. Therefore, a longer

glow plug (by about 4 mm, the total length of the prototype plug was 34 mm long) was compared with a standard plug (with a heating section length of 30 mm) and a catalytic-coated plug (with the heating section length of also 30 mm). The tests were carried out in cold engine start conditions, and the measurement of exhaust emissions was performed upwind from the catalytic converter.

The tests were performed for the same exhaust components as for the previous research points. In the case of carbon monoxide concentration, in the whole measurement duration of 1200 s, the smallest value was observed for the prototype glow plugs; just after engine start-up the concentration was 4000 ppm and it was 20% lower than in the case of the shorter catalyst coated plug. Similar results were observed for the carbon monoxide emission intensity (constant exhaust gas mass flow). It should be noted that after about 600 s no significant differences are observed in both concentration and intensity of carbon monoxide emissions, regardless of the type of glow plugs and the length of the heating section of the catalyst coated glow plugs. As a result, carbon monoxide emissions in the range of 8–10 g were obtained during this study (Fig. 7).

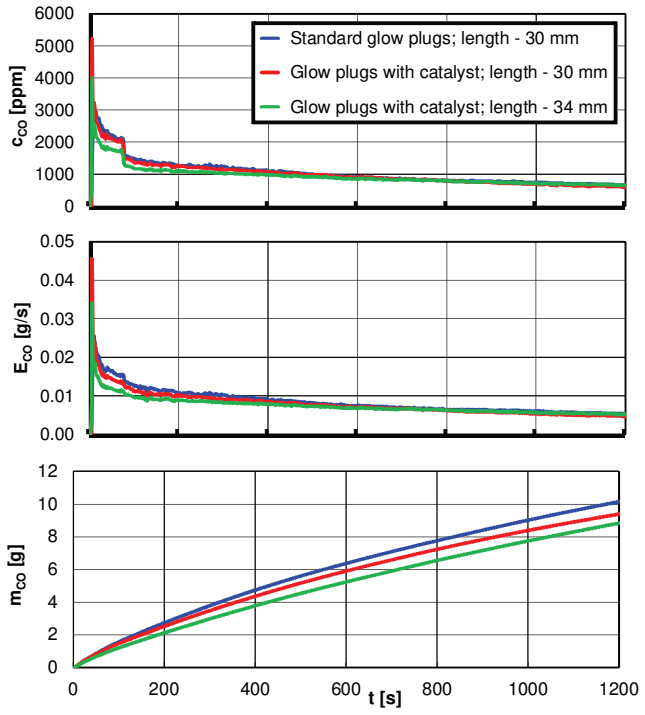

Fig. 7. Concentration, emission and emission intensity of carbon monoxide during tests of the Diesel engine depending on the type of glow plugs and the length of glow plugs coated with catalyst

A similar situation occurred in the case of hydrocarbon concentration analysis. The highest increase in concentration (over 600 ppm) was observed for the standard plugs, while similar values (around 600 ppm) were obtained during the study using catalyst coated plugs with a length of 30 mm. For prototype plugs, this value was around 500 ppm. After a period of approximately 100 s, the concentration was observed to stabilize at the level of 250–300 ppm along with a further slow reduction of concentration to the level of 150 ppm at the end of the measurement test. The intensity of hydrocarbon emission had a very similar characteristic to the hydrocarbon concentration results, and the final value was similar for all cases and was about 0.0005 g/s. The hydrocarbon emission values, depending on the type of glow plugs and the length of the catalytic-coated glow plugs, ranged from 0.9–1.1 g (Fig. 8).

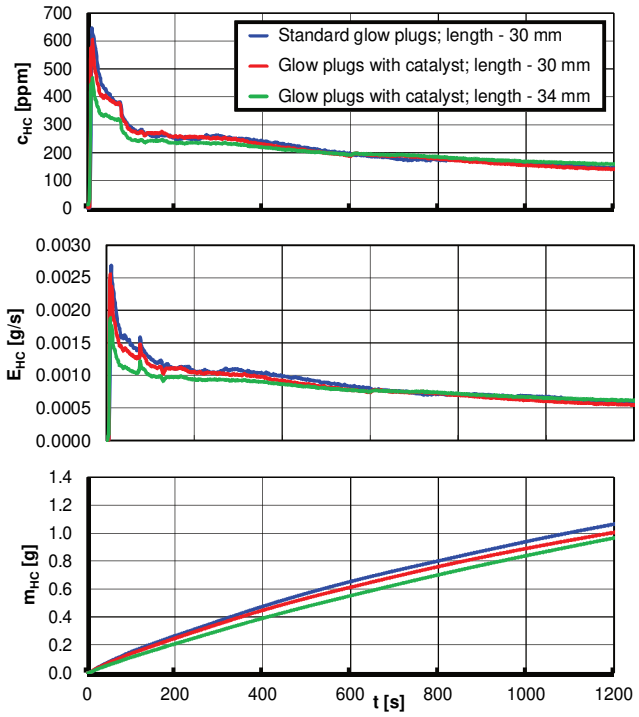

Fig. 8. Hydrocarbons emission, emission intensity, and concentration in Diesel engine tests depending on the type of glow plugs and the length of glow plugs section coated with the catalyst

A different character of the observed results was found in the case of nitrogen oxides concentration analysis. The smallest increase in concentration (about 120 ppm), but the largest eventual value, was observed in the case of the prototype glow plugs. The concentration of nitrogen oxides in the first period after the engine start was 50–70 ppm (lower values were observed for standard plugs). A similar situation was in the case of the nitrogen oxide emission intensity analysis - the largest values were typically observed for the prototype plugs. After a period of approximately 100 s, a rapid increase in the emission intensity of nitrogen oxides to the value of about 0.0005–0.001 g/s was observed, caused by the change of engine settings (consistent operation of the engine controller independent of the type of glow plugs used). Obtained nitrogen oxides emission values for the three considered cases of the glow plug types and length of the catalytic-coated section were in the range of 0.9–1.1 g (Fig. 9).

Particle number analysis does not provide easily differentiated test results. All concentration measurement results are very similar in character and values to each other. The final particle number values allow a proper assessment of the environmental benefits of the glow plugs used. The number of particles in the entire measurement test for different types of glow plugs ranged between $4–5.5 \cdot 10^{11}$ (Fig. 10).

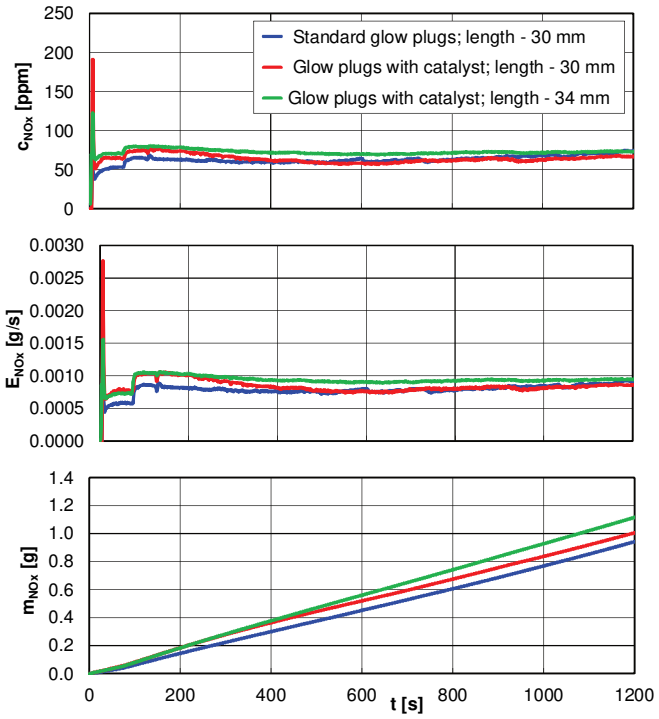

Fig. 9. Nitrogen oxides emission, emission intensity, and concentration in Diesel engine tests depending on the type of glow plugs and the length of glow plugs section coated with the catalyst

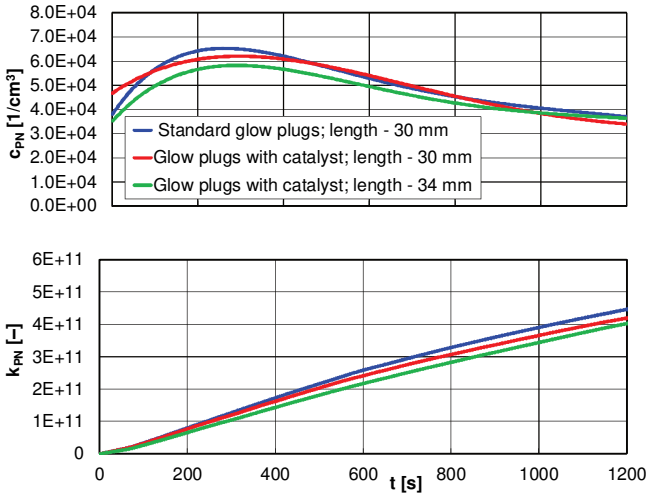

Fig. 10. The numerical concentration and the particle number in Diesel engine tests depending on the type of glow plugs and the length of glow plugs section coated with the catalyst

The smallest differences in the analyzed results were observed in carbon dioxide emission for different glow plugs with different catalyst coated section lengths. The lowest level of repeatability occurred only in the first 200 s after the engine start, while the later measurements of the concentration and emission intensity values were the same. Carbon dioxide emissions also changed only in the range of 270–300 g depending on the type of glow plugs and the catalyst coated section length (Fig. 11).

5. Measurement uncertainty analysis

Most of the discussion regarding the variability and inaccuracy of data when testing the concentration (or emission) of exhaust emissions from internal combustion engines concerns measurement uncertainty treated in a holistic way. The most important factors affecting the measurement uncertainty of exhaust emissions in these models were the uncertainties related to the vehicle engine and the ambient conditions. However, comparing the changes that have occurred in the regulations regarding the permitted limit values of individual exhaust components, it should be noted that the limits have been reduced several fold, which also resulted in a significant exhaust emissions concentration reduction and absolute results in grams per cycle (given cycle measurement). The exhaust gas analyzer is also of great importance when performing measurements within the test framework. Most importantly its measuring range, repeatability of measurements as well as the accuracy of measuring the concentration of individual compounds in the background (in the ambient air).

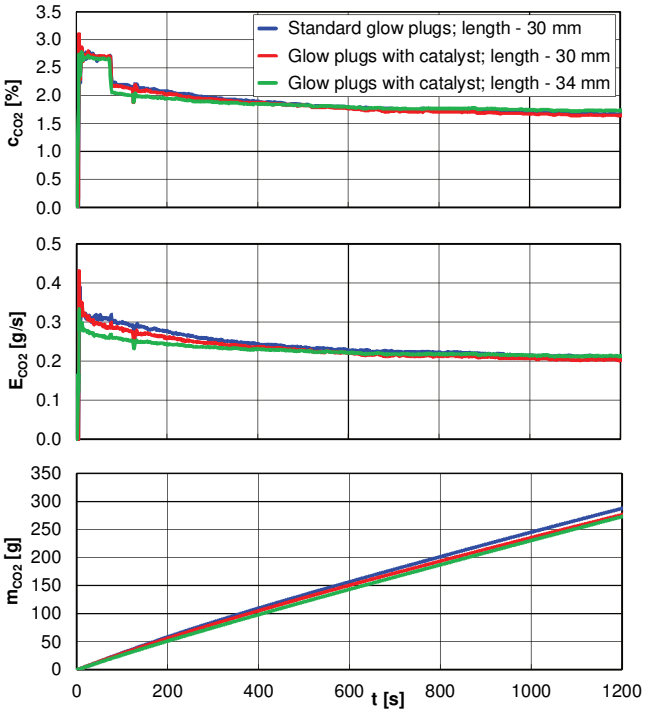

Fig. 11. Carbon dioxide emission, emission intensity, and concentration in Diesel engine tests depending on the type of glow plugs and the length of glow plugs section coated with the catalyst

The following analysis presents a method for determining the emission measurements separation between the standard and catalytic coated glow plugs. In other words, the analysis concerns a situation in which the obtained results can be treated as different, i.e. their average values at the appropriate level of significance are different. To prove this, 20 measurements of emissions of selected exhaust compounds were performed during cold engine start for standard and catalyst coated plugs (to make the article more concise, an example result of carbon monoxide emission was shown). The measurements were taken upwind from the catalytic converter to eliminate the additional effect of exhaust aftertreatment devices.

Considering the results of measurements of carbon monoxide emission (standard glow plugs), the variability range of this compound was (9.8 g, 10.4 g], and the highest

frequency of results (6 measurements out of 20) was the range (10 g, 10.1 g] (Fig. 12a). The approximation of the discrete probability density with normal distribution with expected value estimation and variance is shown in Fig. 12b. For the results of carbon monoxide emission tests (modified glow plugs), a similar characteristic of obtained results was found (Fig. 13a). The results variability range was from 9.1 g to 9.7 g, and the most results (8 data points) were in the range (9.4 g, 9.5 g]. The probability density graph was similar to the graph from Fig. 12b, and was also consistent with the graph of the normal distribution (Fig. 13b).

In order to establish that the average values of carbon monoxide emissions for standard and catalyst coated plugs are different, the hypothesis that the expected values of the average results obtained are the same was verified (at the significance level of 0.05). The hypotheses in the form H_0: $m_{CO\ std\ avg} = m_{CO\ cat\ avg}$, H_1: $m_{CO\ std\ avg} \neq m_{CO\ cat\ avg}$ were verified using the statistics:

$$t_u = \frac{m_{CO\ std\ avg} - m_{CO\ cat\ avg}}{\sqrt{\frac{n_{std}S^2_{CO\ std} + n_{cat}S^2_{CO\ cat}}{n_{std} + n_{cat} - 2}\left(\frac{1}{n_{std}} + \frac{1}{n_{cat}}\right)}} \quad (1)$$

where: $m_{CO\ std\ avg} = 10.08$ g, $m_{CO\ cat\ avg} = 9.41$ g, $n_{std} = 20$, $n_{cat} = 20$, $S_{CO\ std} = 0.1236$ g, $S_{CO\ cat} = 0.1221$ g.

Which results in:

$$t_u = \frac{10.08 - 19.41}{\sqrt{\frac{20\times0.1236^2 + 20\times0.1221^2}{20 + 20 - 2}\left(\frac{1}{20} + \frac{1}{20}\right)}} = 16.9 \quad (2)$$

From the t-Student's distribution tables for the significance level $\alpha = 0.05$ and $n_1 + n_2 - 2 = 38$ degrees of freedom, the critical value was $t_{u,crit} = 2.024$. Because the test result value for average values of carbon monoxide emission is determined by the inequality $|t_u| = 16.9 > t_{u,crit}$, the hypothesis H_0 should be rejected, so the average carbon monoxide emission values for measurements using standard and catalytic coated plugs are different. Figure 14 also shows that the intervals determined by average carbon monoxide emission values and two-fold standard deviation do not overlap. It is a confirmation that the obtained average values of carbon monoxide emissions using the standard and modified glow plugs are different (at the significance level of 0.05).

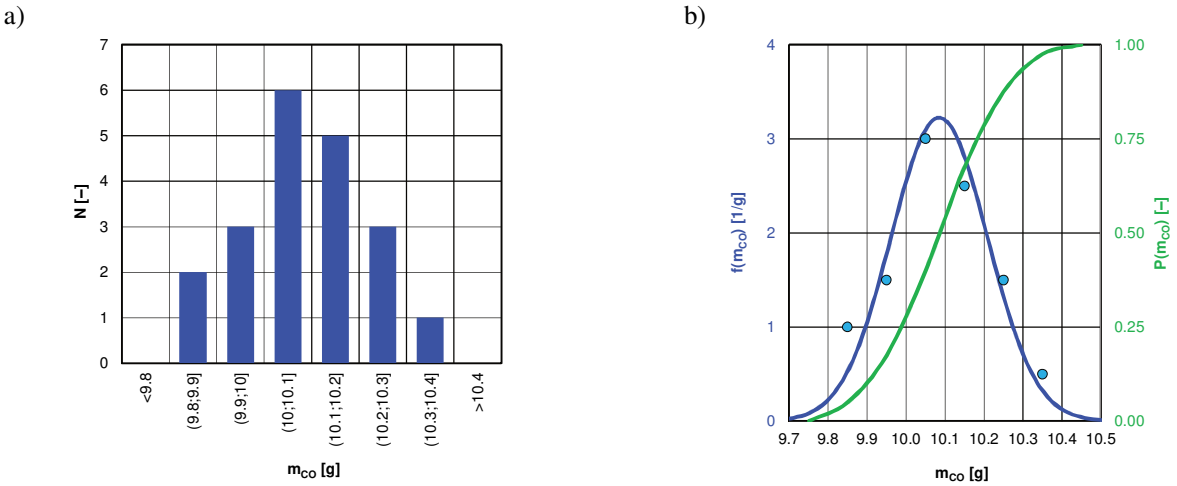

Fig. 12. Carbon monoxide emission histogram (standard plugs) in value ranges (a), approximated probability density and its cumulative distribution function (b)

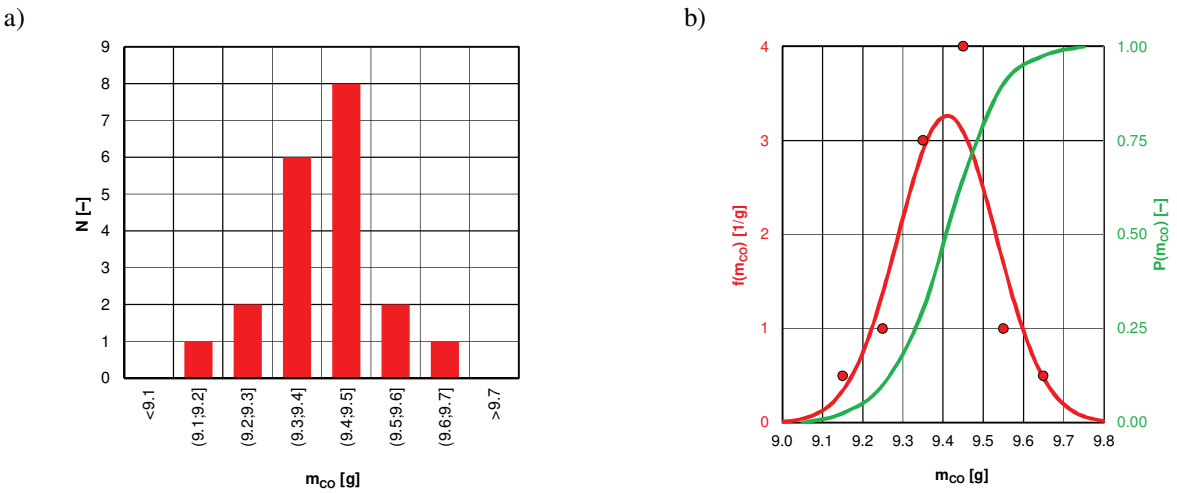

Fig. 13. Carbon monoxide emission histogram (catalyst-coated plugs) in the value ranges (a), approximated probability density and its cumulative distribution function (b)

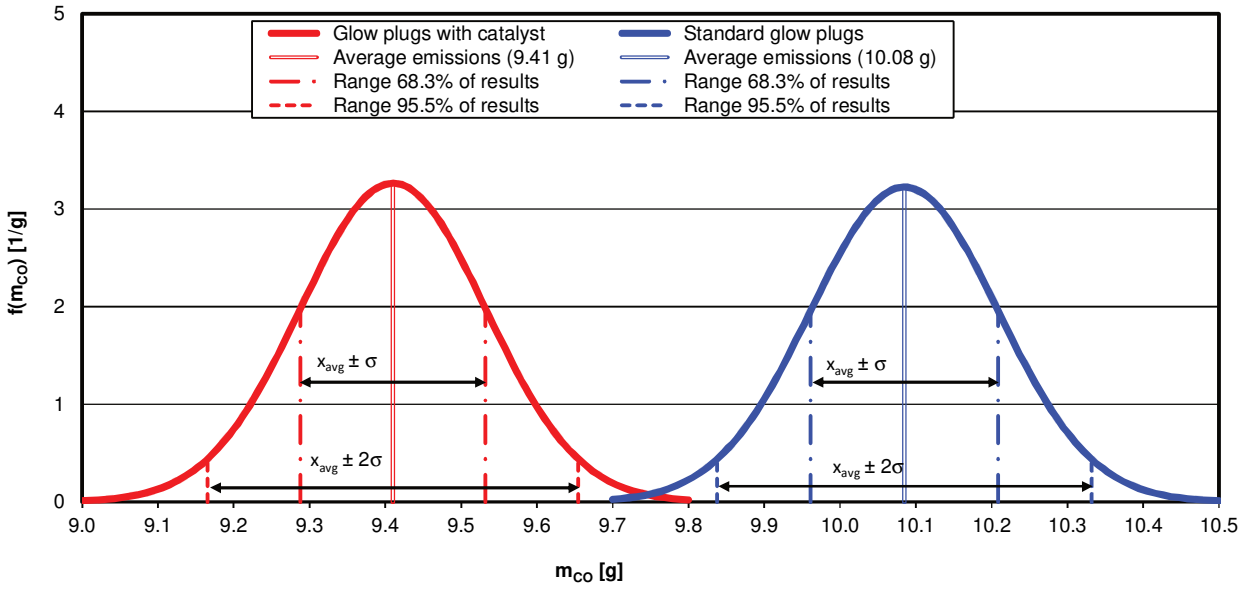

Fig. 14. Probability density for two values of expected carbon monoxide emissions for standard and catalyst coated glow plug tests

6. Conclusions

The following results are only comparative for plugs with a catalytic coating 30 mm long and 34 mm long (prototype). Studies on the influence of the length of catalyst coated glow plugs during cold engine start on the exhaust emission values, resulted in the following conclusions:

a) carbon monoxide emission (Fig. 15a):
   – catalyst coated candles, heating section 30 mm: 9.4 g,
   – catalyst coated candles, heating section 34 mm: 8.8 g,
b) hydrocarbons emission (Fig. 15b):
   – catalyst coated candles, heating section 30 mm: 1.01 g,
   – catalyst coated candles, heating section 34 mm: 0.97 g,
c) nitrogen oxides emission (Fig. 15c):
   – catalyst coated candles, heating section 30 mm: 1.01 g,
   – catalyst coated candles, heating section 34 mm: 1.12 g,
d) carbon dioxide emission (Fig. 15d):
   – catalyst coated candles, heating section 30 mm: 277 g,
   – catalyst coated candles, heating section 34 mm: 273 g,
e) particle number emission (Fig. 15e):
   – catalyst coated candles, heating section 30 mm: $4.2 \cdot 10^{11}$,
   – catalyst coated candles, heating section 34 mm: $4.0 \cdot 10^{11}$.

During comparative tests of engine exhaust emissions with catalyst coated glow plugs with various lengths of heating elements for the Diesel engine cold start, the following results were obtained (values given relative to the emission values for a catalyst coated glow plug with a heating element length of 30 mm):

– a relative reduction in carbon monoxide emissions by 12.9%,
– a relative reduction of hydrocarbon emissions by 9.3%,
– a relative increase in emissions of nitrogen oxides by 14.3%,
– a relative decrease in the particle number by 9.8%,
– a relative reduction of carbon dioxide emissions by 5.1%.

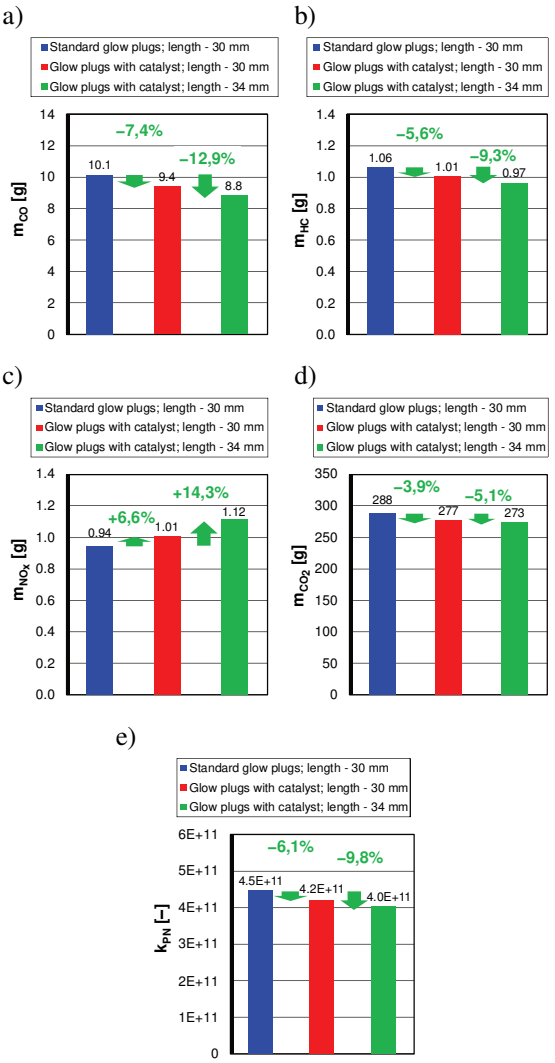

Fig. 15. Emissions comparison of carbon monoxide, hydrocarbons, nitrogen oxides, carbon dioxide and the particle number depending on the type and length of glow plugs

Bibliography

[1] AHLERS, S., BRÜCK, R., CARTUS, T., STOCK, H. Procedure and design of exhaust systems to fulfill all emission limits during real driving conditions: In Use Conformity, *39th International Vienna Motor Symposium.* Vienna 2018.

[2] ANDRYCH-ZALEWSKA, M. Improving the environmental performance of the internal combustion engine by the use of in-cylinder catalyst. *Combustion Engines*. 2017, **1**.

[3] ANDRYCH-ZALEWSKA, M. The possibilities and development of in-cylinder catalytic coating. *Journal of KONES*. 2017, **3**.

[4] ANDRYCH-ZALEWSKA, M. Wpływ katalizatora wewnętrznego na emisję spalin w stanach pracy silnika o zapłonie samoczynnym odpowiadających jego użytkowaniu trakcyjnemu, *Rozprawa doktorska*. Poznań 2018.

[5] ANDRYCH-ZALEWSKA, M., WALKOWIAK, W., KOLANEK, C. Heat release in spark ignition engine with internal catalyst. *Journal of KONES*. 2015, **4**.

[6] BIELACZYC, P., MERKISZ, J., PIELECHA, J. Stan cieplny silnika spalinowego a emisja związków szkodliwych. *Wyd. Politechniki Poznańskiej*, Poznań 2001.

[7] BRADSTREET, S. Flame sprayed catalyst coatings. *The Clay Products News and Ceramic Record.* 1961, **24**.

[8] BURK, P., HOCHMUTH, J., ANDERSON, D., et al. Cold start hydrocarbon emissions control. *Automotive Engineering*. 1995, **10**.

[9] HU, Z., LADOMMATOS, N. Reduction of unburnt hydrocarbon emissions from spark ignition engines using in-cylinder catalysts. *Journal of Automobile Engineering*. 1996, **210**.

[10] KENECHT, W. Diesel engine development in view of reduced emission standards, *Energy*, 2008, **33**.

[11] KOZAK, M., MERKISZ, J., BIELACZYC, P. Wpływ właściwości paliwa na emisję szkodliwych składników spalin przez samochód osobowy napędzany silnikiem o zapłonie samoczynnym. *Silniki spalinowe.* 2005, **1**.

[12] MELLO, J., BEZAIRE, D., SRIRAMULU, S., WEBER, R. Performance and economics of catalytic glow plugs and shields in direct injection natural gas engines for the next generation natural gas vehicle program. Final report. *National Renewable Energy Laboratory*, NREL/SR-540-34286, 2003.

[13] MERKISZ, J., PIELECHA, J. Możliwości obniżenia emisji cząstek stałych w silnikach ZS poprzez zastosowanie katalizatora. *IV Sympozjum EKODIESEL'98*. Warszawa 1998.

[14] MERKISZ, J., PIELECHA, J., RADZIMIRSKI, S. New trends in emission control in the European Union. *Springer Tracts on Transportation and Traffic*. 2014, **4**.

[15] MITCHELL, W., LITZINGER, T., LEE, W. Effects of in-cylinder catalysts on combustion and emissions of a D.I. diesel engine fuelled on neat methanol. *SAE Technical Paper* 920688, 1992.

[16] NAVALIHINA, M., ROMANOVSKY, B., TOPCHIEVA, K. Investigation of acidic properties of zeolite by high temperature poisoning technique, *Catalysis and Kinetic*. 1971, **12**.

[17] NEDUNCHEZCHIAN, N., DHANDAPANI, S. Effects of in-cylinder catalytic coating on the performance of a two-stroke spark ignition engine. *Indian Journal of Engineering & Materials Sciences*. 2001, **8**.

[18] NORMAND, B., FERVEL, V., CODDET, C., NIKITINE, V. Tribological properties of plasma sprayed alumina–titania coatings: role and control of the microstructure. *Surface and Coatings Technology*. 2000, **123**.

[19] PIELECHA, J. Identyfikacja parametrów cząstek stałych z silników spalinowych. Rozprawa habilitacyjna. *Wyd. Politechniki Poznańskiej*, Poznań 2012.

[20] REKSA, M., ANDRYCH-ZALEWSKA, M., MIHAYLOV, V. The impact analysis of hydroxide mixture addition on the combustion process in the diesel engine. *MTM Machines, Technologies, Materials*. 2014, **2**.

[21] SAMAHOV, A., ZAIDMAN, M., CHIZHIK, M. Change of activity of catalysts during exploitation. Novosibirsk: *Science, Siberia branch* 1976.

[22] SAMSONOV, G. Catalytic properties of refractory compounds and principles of creation of refractory materials with preassigned properties. Principles of Choice of Catalysts for Heterogeneous. *Catalysis*. 1966, **11**.

[23] SITNIK, L., ANDRYCH-ZALEWSKA, M. Statistics of indicated pressure in combustion engine. *Scientific Conference on Automotive Vehicles and Combustion Engines*, KONMOT 2016.

[24] SITNIK, L., ANDRYCH-ZALEWSKA, M., HALLER, P., WŁOSTOWSKI, R. Badania emisji gazowego silnika o zapłonie iskrowym w aspekcie parametrów sterowania. *Raporty Wydziału Mechanicznego Politechniki Wrocławskiej*. 2015, **137**.

[25] USOV, U., SKVORZOVA, E., KLUSHNIKOVA, G. Dehydrogenating methylhexane on chromia-alumina and molybdena-alumina catalysts. *Neftekhimiya.* 1963, **3**.

[26] VASILEV, I., GAVRILINKO, P., ZVONOV, V. Method of definition of catalytic activity of combustion chamber surface of IC engine. *USSR Author Certificate* 1312206, 1987.

[27] WINKLER, M., PARKER, D. The role of diesel ceramic coatings in reducing automotive emissions and improving combustion efficiency. *SAE Technical Paper* 930158, 1993.

[28] WONG, V., BAUER, W., KAMO, R. et al. Assessment of thermal barrier coatings for IC engines. *SAE Technical Paper* 950980, 1995.

Prof. Jerzy Merkisz, DSc., DEng. – Faculty of Transport Engineering, Poznan University of Technology.
e-mail: *jerzy.merkisz@put.poznan.pl*

Monika Andrych-Zalewska, DEng. – Faculty of Mechanical Engineering, Wrocław University of Technology.
e-mail: *monika.andrych@pwr.edu.pl*

Prof. Jacek Pielecha, DSc., DEng. – Faculty of Transport Engineering, Poznan University of Technology.
e-mail: *jacek.pielecha@put.poznan.pl*

Article citation info:
HUNICZ, J., GĘCA, M.S., KORDOS, P., RYBAK, A. Effects of combustion timing on pressure rise rates in a residual effected HCCI engine. *Combustion Engines*. 2019, **178**(3), 46-50. DOI: 10.19206/CE-2019-308

Jacek HUNICZ
Michał GĘCA
Paweł KORDOS
Arkadiusz RYBAK

CE-2019-308

Effects of combustion timing on pressure rise rates in a residual effected HCCI engine

Realization of a low temperature combustion concept in homogeneous charge compression ignition (HCCI) engines is a cutting-edge technology that offers clean combustion in parallel with high thermal efficiency. Low combustion temperature prevents from NO_x formation whereas homogeneous mixture assures smokeless exhaust. However, achieving the production feasibility by HCCI technology is hampered by high pressure rise rates and the resulting combustion noise at a high load operation. This paper explores combustion timing parameters that are capable of maintaining permissible levels of pressure rise rates under a high load regime. On the basis of experimental data collected at a high load HCCI operation, pressure rise level was correlated with combustion duration. Furthermore, combustion duration has been found to scale with in-cylinder volume, for which 50% of mass fraction burned appeared. The results showed quantitatively limitations of engine load, pointing out on required combustion timings to achieve acceptable combustion harshness depending on engine load.

Key words: *HCCI, boost, pressure rise rate*

1. Introduction

Reciprocating combustion engines are responsible for one third of global CO_2 emissions, and moreover pose a high risk due to the presence of toxic components in the exhaust. Nitrogen oxides and particulate matters (PM) are the most dangerous exhaust components. Furthermore these compounds are very difficult to remove from the exhaust using catalytic converters or various types of filters. However, homogeneous charge compression ignition (HCCI) combustion engine allows for realization of the combustion process so that the formation of these components will be minimized. HCCI combustion can be achieved via internal exhaust gas recirculation with the use of so-called negative valve overlap (NVO). This technique consists of trapping exhaust gases from the previous cycle in the cylinder. As a result of compression of the exhaust, air and fuel mixture, oxidation reactions occur simultaneously in the entire volume and at low temperature, which prevents from the formation of nitrogen oxides. At the same time, due to a homogeneous mixture, formation of particulate matters is radically diminished.

Despite of the indisputable advantages of this innovative combustion technique, HCCI combustion systems are still in the research phase. One of the issues to be solved is high pressure rise rate (PRR) inside the cylinder resulting from the volumetric nature of combustion. This form of combustion harshness limits high engine loads. For high PRR pressure pulsations in the combustion chamber are generated, which lead to an increase in noise emitted by the engine and an increase in loads acting on the crankshaft system [15]. The waves, which are generated by the significant PRR, produce a similar effect to knocking combustion [14]. During combustion in a spark ignition engine, the flame is gradually spreading in the combustion chamber. Pressure is also increasing gradually. In the HCCI engine, there is sudden combustion of the entire mixture in the cylinder. This results in a high rates of heat release and high PRRs in the cylinder. PRR reduction can be realized by means of two major methods: increasing fuel dilution and reducing the combustion reaction rates, or combustion retarding via mixture stratification [10].

Dec and Yang [2] applied boost to HCCI engine and heating-up of the intake air for increasing internal energy of the in-cylinder fluid. In addition, the engine was equipped with direct fuel injection into the cylinder. They reached the engine load of 0.88 MPa in indicated mean effective pressure) IMEP at boost pressure of 0.18 MPa and without neither external EGR nor internal EGR. Further increase in the intake pressure caused exceeding the combustion harshness limit.

Kulzer et al. [9] applied single fuel injection during the NVO period and boost pressure of up to 0.3 MPa. The authors noted that an increase of the in-cylinder charge dilution by air provides a substantial, simultaneous reduction of PRR and the NO_x emission. However, at high boost pressures the compressor energy demand could consume the advantage of higher thermal efficiency of the HCCI working process [8].

Canakci [1] and Yap et al. [17] applied relatively low boost of up to 0.14 MPa to gasoline port injected engines. It was observed that boosting enabled a substantial reduction of the NO_x emission, while excessive PRR was noted. Scaringe et al. [11] also reported an increase in PRR at higher boost pressures. They noted that the high load limit under PRR constant cannot be extended by the alternating method of fuel dilution i.e. EGR rate versus air-excess ratio. Wildman et al. [16] reasoned that boost cannot improve the engine output, because high load limit of HCCI engine is constrained by PRR rather than fresh air aspiration limitations.

Dec et al. [3] applied the direct fuel injection and the port fuel injection in order to create partially fuel stratification. It has been observed that increasing the fuel split ratio was capable of PRR reduction. However, this method was effective only for highly boosted engine operation. Turkcan et al. [13] in their research applied solely direct fuel injec-

tion and split injection technique in the HCCI engine. In the first stage 4/5 of fuel was injected early during the intake phase to create a premixed charge. Whereas the remaining 1/5 fuel dose was introduced directly during the compression stroke. The authors observed that the retarded secondary injection timings caused a reduction in PRR.

Hunicz et al. [7] investigated the effects of various injection strategies and different fuel dose divisions under variable boost pressure. The authors noted that stratification is an effective measure to reduce both the PRR and NO_x emissions. Nevertheless, as in the case of the abovementioned experimental studies, the results showed a trade-off between the NO_x and CO/HC/PM emissions. Recent work by Hunicz and Mikulski [4] has shown that PRR can be effectively controlled via variation in mass of fuel injected during the NVO period for reforming. This technique enabled effective control of fuel reactivity [5] and also provided the substantial thermal effects [6].

Present paper further explores limitations of HCCI engine operation that come from combustion timing parameters. On the basis of large number of experimental data this study indicated required combustion timing indexes to achieve acceptable PRR levels depending on engine load.

2. Experimental test stand and research conditions

The experiments were performed on single-cylinder research engine reinstalled in new laboratories at Lublin University of Technology (Fig. 1). The combustion system that enabled HCCI operation comprised bowl-shaped combustion chamber located in the cylinder head and a side-mounted swirl-type, single-stream, electromagnetic gasoline injector. Supercharging was provided by an externally driven compressor with air temperature conditioning system. Furthermore, a hydraulic variable valve actuation system enabled an independent adjustment of intake and exhaust valve opening phases and lifts. During the research the valvetrain was set to achieve NVO and thus enabled HCCI combustion. The detail data of the test engine, along with the valvetrain settings that were used in the present research are shown in Table 1.

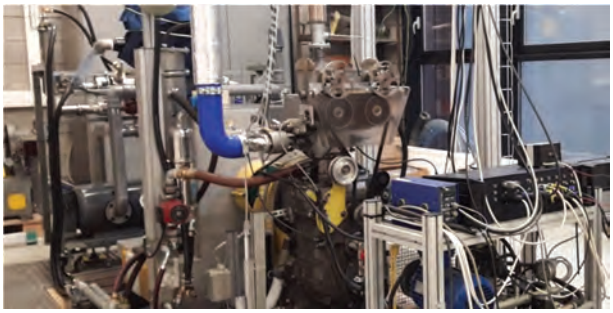

Fig. 1. Experimental test stand

The research engine was coupled to a direct current dynamometer with automatic speed control. The system automation also included a thermal air mass flow meter, a fuel balance and a set of pressure and temperature transducers for monitoring of all media conditions. The excess air ratio (λ) was measured with the use of LSU 4.2 Bosch lambda probe and ETAS lambda meter.

Combustion thermodynamic analysis was performed using AVL BOOST software, where measured in-cylinder pressure was used as input data. To provide this signal a GH12D miniature pressure transducer from AVL was installed directly in the engine head and connected via charge amplifier to the test bench acquisition system. The PC-based high speed pressure recording system was triggered by an optical encoder with resolution of 3600 pulses per crankshaft revolution and acquired signals from 100 cycles.

Table 1. Research engine parameters

Parameter	Unit	Value
Displaced volume	cm^3	498.5
Bore	mm	84
Stroke	mm	90
Compression ratio	-	11.7
No of valves	-	2
Intake valve opening location	°CA aTDC	80
Intake valve opening duration	°CA aTDC	130
Intake valve lift	mm	3.6
Exhaust valve opening location	°CA aTDC	520
Exhaust valve opening duration	°CA aTDC	119
Exhaust valve lift	mm	2.9

The engine was fueled with pump-grade gasoline with 95 research octane number. All experiments were performed at a single rotational speed of 1500 rev./min. The experimental matrix comprised boost pressure sweeps from naturally aspirated conditions to approximately 0.15 MPa intake pressure. Intake temperature was kept constant at 30°C, whereas engine cooling liquid temperature was maintained at 90°C. The boost pressure sweeps were repeated for various injection schemes that provided different degrees of fuel reactivity (achieved via NVO injection) and different degrees of stratification (achieved via late fuel injection). Additionally, three overall fuel quantities were applied providing net IMEPs at levels of 0.42 MPa, 0.58 MPa, and 0.71 MPa. During the research nearly 100 engine operating points were investigated in terms of thermodynamic analysis. Combustion timing parameters were derived from cumulative heat release curves. Pressure rise rate was calculated as a ratio of pressure differences between 95% mass fraction burned (MFB) and 5% MFB, and the 5%–95% MFB angular duration.

3. Results

Figure 2 shows a series of in-cylinder pressure traces for moderate IMEP and variable intake pressure. It can be noted that increase of boost pressure advances autoignition. However, PRRs apparently stabilize. To provide more details Fig. 3 shows heat release rate (HRR) curves for the same set of data. It can be noted that for the examined boost sweep the peak HRR was more than doubled in parallel with substantial auto ignition advance. Namely, an increase in the boost pressure by 0.03 MPa resulted in an increase in HRR from 40 to 100 J/°CA. In addition, location of the maximum HRR was advanced by 15°CA. It

indicates that timing of maximum reaction rate and combustion duration are correlated in a way that at small volumes reaction rate is higher.

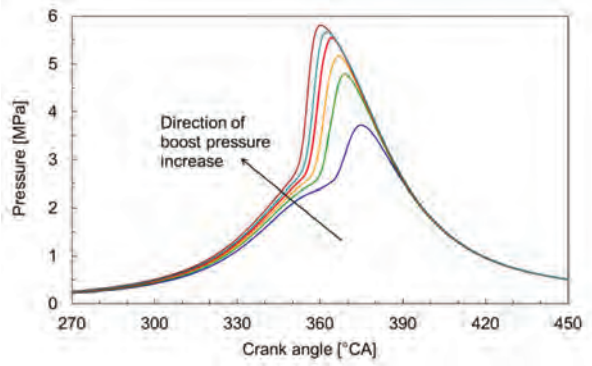

Fig. 2. In-cylinder pressure at IMEP ≈ 0.58 MPa for boost pressure between 0.11 MPa and 0.14 MPa

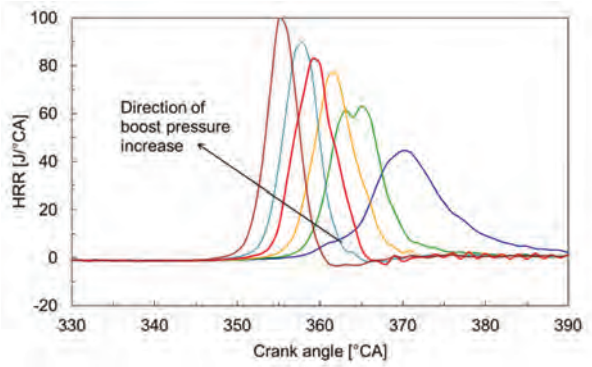

Fig. 3. Heat release rates at IMEP ≈ 0.58 MPa for boost pressure between 0.11 MPa and 0.14 MPa

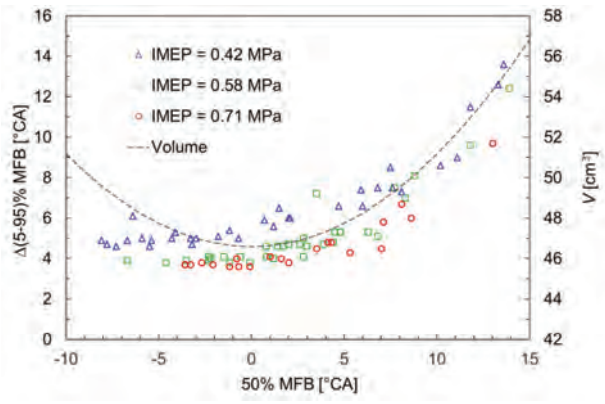

Fig. 4. Combustion duration expressed as period between 5% and 95% MFB as a function of location of 50% MFB for all investigated conditions. Dotted line shows in-cylinder volume

The correlation between combustion duration and combustion timing parameters for all investigated conditions are provided in Fig. 4. Additionally, Fig. 4 includes scaled in-cylinder volume curve, showing that combustion duration correlates with a volume, however only if the center of combustion takes place after TDC. Thus, the larger combustion chamber volume for retarded combustion, the lower reaction rate. Additionally, it was noted by Sjöberg et al. [12] that retarding the combustion phasing reduces the HRR by amplifying the benefit of the naturally occurring thermal stratification. It can also be observed from Fig. 4 that increase in fueling increases combustion rates.

The in-cylinder pressure change resulting from combustion theoretically can be calculated using the first law of thermodynamics

$$\Delta p = \frac{1}{V}\left[\Delta Q(\gamma - 1) - \gamma \cdot p \cdot \Delta V\right], \tag{1}$$

where: V is a volume of the cylinder, ΔQ is a gross heat release rate and γ is a ratio of specific heats. PRR in HCCI engine can be expressed with relatively high accuracy even if the Eq. 1 is simplified. Namely, heat transfer can be ignored as well as volumetric expansion term can be neglected, because combustion is quick, thus takes place at almost constant volume. Considering the above, the pressure rise rate can be estimated by the following formula:

$$\mathrm{PRR} \approx \frac{(\gamma - 1)\cdot Q}{V \cdot \Delta(5-95)\%\,\mathrm{MFB}}, \tag{2}$$

where Q is the amount of chemical energy provided with the fuel. In-cylinder volume in Eq. 2 can be considered constant and its value at 50% MFB point can be used.

As can be noted from Eq. 2 the combustion duration is a leading factor affecting PRR. Figure 5 shows the dependence of PRR on combustion duration. It can be noted that PRR increase progressively with increasing reaction rates for all investigated conditions. Obviously, it can be observed that the increase in the load causes the increase in PRR. However the effect of the amount of chemical energy would be diminished by the trade-off between 50% MFB location and reaction rate, as shown in Fig. 4.

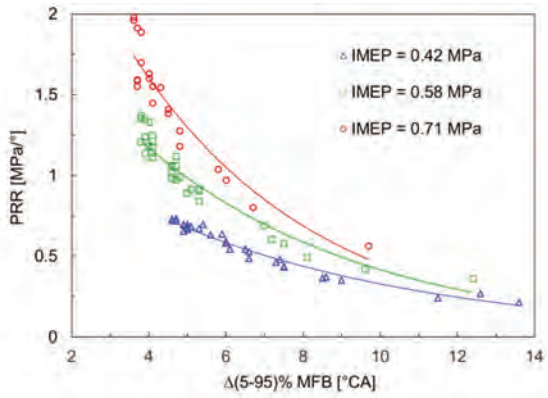

Fig. 5. Pressure rise rates as a function of combustion duration for all investigated conditions

It should be noted that for HCCI combustion, the rate of pressure increase should not exceed the range 0.5–0.7 MPa/°CA [17]. Increase of the PRR beyond this limit causes the engine knock. For the highest applied load it is hardly possible to meet the harshness limit, what requires advanced control strategies to increase the reaction rate, i.e. optimized valve timings and reduction of boost pressure. However, it was shown in [4] that this strategy increases NO_x emissions. For IMEP = 0.41 MPa the limit can be easily met, allowing to optimize combustion in terms of emissions and efficiency. For average investigated load of

IMEP = 0.58 MPa, achieving acceptable PRR requires extension of combustion duration to 7–8°CA.

Moreover in order to consider volume factor, Fig. 6 shows PRRs as functions of the inverse of combustion duration and a volume at 50% MFB for all investigated conditions. It can be noted that the measurement points are arranged linearly, depending on the IMEP. Some scattering of the points can result from variable thermal efficiency, that requires different fuel's energy to achieve given IMEP.

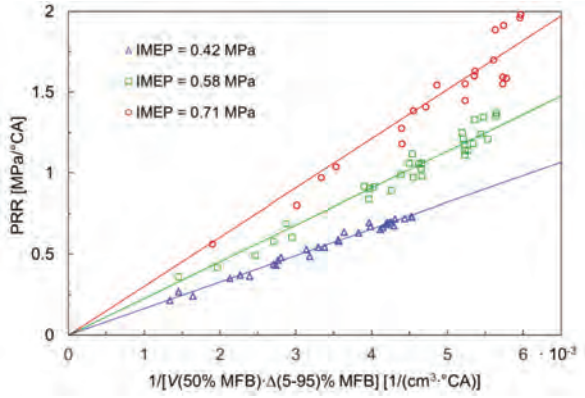

Fig. 6. Pressure rise rates as a function of the inverse of combustion duration and volume at 50% MFB for all investigated conditions

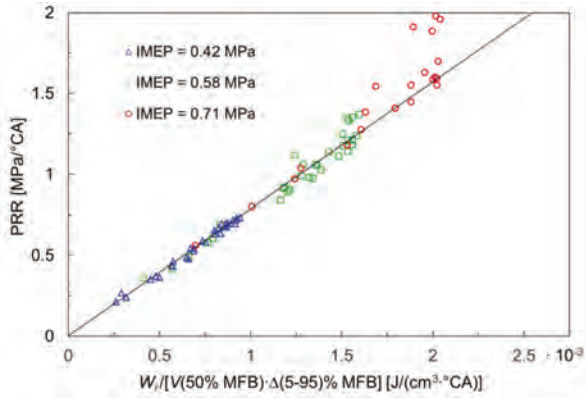

Fig. 7. Pressure rise rates as a function of the indicated work divided by combustion duration and volume at 50% MFB for all investigated conditions

The result of the regression with a full set of variables, including indicated work (W_i) is shown in Fig. 7. Such a presentation of the data shows the boundary combustion timing parameters required to achieve acceptable PRR level. For the highest engine load there is some number of operating points above the trend line. It can be attributed to an increase of specific heats ratio, because EGR decreases at high amounts of fuel and heavy boost.

4. Conclusions

This paper explored combustion timing parameters that are capable of maintaining permissible levels of pressure rise rates under high load regime of HCCI engine. The experimental matrix included various valvetrain settings, direct fuel injection strategies and boost pressures. The results led the authors to draw the following conclusions:

1. Combustion duration has been found to scale with in-cylinder volume, for which 50% of mass fraction burned appeared. This correlation occurs only if the 50% mass fraction burned of combustion takes place after TDC. It indicates that these two measures to reduce PRR work simultaneously.
2. Increase of fueling reduces reaction time that further contributes to increase PRRs at high engine load regime.
3. For investigated conditions the range of attainable combinations of 50% MFB and combustion durations were the same for all three quantities of fuel. Moreover these combustion timing parameters appear to be a boundary of HCCI operation.
4. Among investigated conditions, only case of IMEP = 0.41 MPa provided acceptable combustion harshness over a wide range of control parameters, enabling combustion optimization in terms of emissions and thermal efficiency. For IMEP = 0.58 MPa only few cases laid below the threshold of 0.7 MPa/°CA.
5. The results clearly indicate that high load HCCI operation limits result almost solely from fuel quantity. Utilization of other measures to reduce PRR can widen operating range in much lesser extent.
6. Further investigations into widening HCCI operation mode towards high loads should be focused on reduction of reaction rates via higher fuel dilution and wider spread of mixture reactivity control by variations of NVO fuel injection.

Acknowledgements

This work was funded by the National Science Centre of Poland, under the grant No. 2015/17/B/ST8/03279. The authors wish to thank AVL List GmbH for making simulation software available within a framework of AVL University Partnership Program.

Nomenclature

CA	crank angle
EGR	exhaust gas recirculation
HC	hydrocarbons
HCCI	homogeneous charge compression ignition
HRR	heat release rate
IMEP	indicated mean effective pressure
MFB	mass fraction burned
NO_x	nitrogen oxides
NVO	negative valve overlap
p	pressure
PM	particulate matter
PRR	pressure rise rates
Q	energy
TDC	top dead center
V	volume
W_i	indicated work
γ	ratio of specific heats

Bibliography

[1] CANAKCI, M. Combustion characteristics of a DI-HCCI gasoline engine running at different boost pressure. *Fuel*. 2012, **96**, 546-555. DOI:10.1016/j.fuel.2012.01.042.

[2] DEC, J.E., YANG, Y. Boosted HCCI for high power without engine knock and with ultra-low NO_x emissions – using conventional gasoline. *SAE International Journal of Engines*. 2010, **3**, 750-767. DOI:10.4271/2010-01-1086.

[3] DEC, J.E., YANG, Y., DRONNIOU, N. Boosted HCCI – controlling pressure-rise rates for performance improvements using partial fuel stratification with conventional gasoline. *SAE International Journal of Engines*. 2011, **4**(1), 1169-1189. DOI:10.4271/2011-01-0897.

[4] HUNICZ, J., MIKULSKI, M. Application of variable valve actuation strategies and direct gasoline injection schemes to reduce combustion harshness and emissions of boosted HCCI engine. *Journal of Engineering for Gas Turbines and Power*. 2019, **141**(7). DOI:10.1115/1.4043418.

[5] HUNICZ, J. An experimental study into the chemical effects of direct gasoline injection into retained residuals in a homogeneous charge compression ignition engine. *International Journal of Engine Research*. 2016, **17**(10), 1031-1044. DOI:10.1177/1468087416636492.

[6] HUNICZ, J., MIKULSKI, M. Investigation of the thermal effects of fuel injection into retained residuals in HCCI engine. *Applied Energy*. 2018, **228**, 1966-1984, DOI:10.1016/j.apenergy.2018.07.075.

[7] HUNICZ, J., TMAR, A., KRZACZEK, P. Effects of mixture stratification on combustion and emissions of boosted controlled auto-ignition engines. *Energies*. 2017, **10**(12), 2172. DOI:10.3390/en10122172.

[8] HYVÖNEN, J., HARALDSSON, G., JOHANSSON, B. Supercharging HCCI to extend the operating range in a multi-cylinder VCR-HCCI engine. *SAE Technical Paper* 2003-01-3214. 2003. DOI:10.4271/2003-01-3214.

[9] KULZER, A., NIER, T., KARRELMEYER, R. A thermodynamic study on boosted HCCI: Experimental results. *SAE Technical Paper* 2011-01-0905. 2011. DOI:10.4271/2011-01-0905.

[10] KWON, O.S., JEONG, D.W., LIM, O.T., LIDA, N. The research about thermal stratification effect on pressure rise rate in supercharged HCCI engine based on numerical analysis. *SAE Technical Paper* 2009-32-0141. 2009.

[11] SCARINGE, R.J., WILDMAN, C., CHENG, W.K. On the high load Limit of boosted gasoline HCCI engine operating in NVO mode. *SAE International Journal of Engines*. 2010, **3**, 35-44. DOI:10.4271/2010-01-0162.

[12] SJÖBERG, M., DEC, J.E., CERNANSKY, N.P. The potential of thermal stratification and combustion retard for reducing pressure-rise rates in HCCI engines, based on multi-zone modeling and experiments. *SAE Technical Paper* 2005-01-0113. 2005. DOI:10.4271/2005-01-0113.

[13] TURKCAN, A., OZSEZEN, A.N., CANAKCI, M. et. al. An experimental and modeling study to investigate effects of two-stage direct injection variations on HCCI combustion. *Combustion Science and Technology*. 2015, **187**(4), 642-658. DOI:10.1080/00102202.2014.960562.

[14] VRESSNER, A. et al. Pressure oscillations during rapid HCCI combustion. *SAE Technical Paper* 2003-01-3217. 2003. DOI:10.4271/2003-01-3217.

[15] WESTBROOK, C.K. et al. The autoignition chemistry of paraffinic fuels and pro-knock and anti-knock additives: a detailed chemical kinetic study. *SAE Technical Paper* 912314. 1991. DOI:10.4271/912314.

[16] WILDMAN, C., SCARINGE, R.J., CHENG, W.K. On the maximum pressure rise rate in boosted HCCI operation. *SAE Technical Paper* 2009-01-2727. 2009. DOI:10.4271/2009-01-2727.

[17] YAP, D., WYSZYNSKI, M.L., MEGARITIS, A., XU, H. Applying boosting to gasoline HCCI operation with residual gas trapping. *SAE Technical Paper* 2005-01-2121. 2005. DOI:10.4271/2005-01-2121.

Jacek Hunicz, DSc., DEng. – Faculty of Mechanical Engineering, Lublin University of Technology.
e-mail: *j.hunicz@pollub.pl*

Paweł Kordos, DEng. – Faculty of Mechanical Engineering, Lublin University of Technology.
e-mail: *p.kordos@pollub.pl*

Michał Gęca, MEng. – Faculty of Mechanical Engineering, Lublin University of Technology.
e-mail: *michal.geca@pollub.pl*

Arkadiusz Rybak, MEng. – Faculty of Mechanical Engineering, Lublin University of Technology.
e-mail: *a.rybak@pollub.pl*

Article citation info:
BOGDANOWICZ, A., KNIAZIEWICZ, T. Simulation of concentrations harmful compounds from main ship's propulsion engine cooperating with a fixed pitch propeller in dynamic states. *Combustion Engines*. 2019, **178**(3), 51-55. DOI: 10.19206/CE-2019-309

Artur BOGDANOWICZ
Tomasz KNIAZIEWICZ

CE-2019-309

Simulation of concentrations harmful compounds from main ship's propulsion engine cooperating with a fixed pitch propeller in dynamic states

The article presents a mathematical model of a marine propulsion system and a computer program based on the LabVIEW environment. For a purpose of model construction, a ship's hull resistance was identified and an approximation equations of the Wageningen institute for ship propellers were used. The ship's motion equations were used to build the propulsion system model. On the basis of conducted tests of Sulzer 6AL20 / 24 marine engine, a map of concentrations harmful compounds was created in various load state and transferred to a computer program.

Key words: *simulation, modelling, emission, marine diesel engine*

1. Introduction

In real operating conditions of vessels, almost always on a propulsion system and a ship's hull affect external extortion, which directly or indirectly cause smaller or larger changes in operation of a propulsion system. We distinguish here the extortion from a ship's crew and determined by weather conditions and a change of sail area.

The first type of extortion includes changes:

- a speed of vessel,
- a sail direction by overriding an engine,
- a propeller pitch,
- a position of a rudder blade.

As result of these interactions are a change of an engine load, and connected with it, a crankshaft speed, a propeller force and a ship's speed. Most of these extortions take place on a roadstead and in port areas close to human agglomerations. As a result of a dynamic load shift, there is a change in a emission of harmful compounds into the atmosphere, which on a scale of ship's movement in a port area has a significant impact on residents and human agglomerations in coastal regions.

In addition to seagoing vessels, which leave a port area and head towards an open sea, we distinguish special units in a form of tugs, dredgers, pilot vessels, fishing vessels, trawlers or other boats whose power plants operate in dynamic load states. The work of these vessels takes place even around the clock. Tugboats assist in mooring and unmooring merchant ship, or dredgers carrying out work deepening port areas using this day in the evening, where traffic in a port is limited.

The first part of the article presents ship's operation modes in port regions. Criteria for particular modes of operation of ships sailing in this area have been defined. The concept of land supply is also presented as one of the ways to reduce the emission of harmful compounds into the atmosphere by ships. The concept of "On-shore Power Supply" (OPS) has also been defined as one of the ways to reduce the emission of harmful compounds into the atmosphere by ships.

The second part of the article presents the model of a drive system, which has been implemented in the Labview graphical programming environment [2].

2. Dynamic states of work in port areas

Emission of harmful compounds depends mainly on a load of a propulsion system. The power demand is related to manoeuvring a vessel. For sea-going vessels, there is a direct relationship between a power generated by a propulsion system and a ship's speed. For special units such as tugs, dredgers, ferries, whose main mode of operation are manoeuvres (e.g. acceleration, deceleration, mooring work, circulations, etc.), the relationship between power and ship's speed is not the same. As other modes of work in port areas, we can distinguish a berth at a wharf and the mode of using a land supply so-called "On-shore Power Supply" (OPS).

The speed and position of a vessel depends mainly on the operating mode of a ship. Criteria for individual work modes are presented in table no. 1. The Automatic Identification System (AIS) system is an especially useful tool when determining the speed of a ship, which provides automatic data exchange, which helps to avoid collisions between vessels and identifies a ship for shore-based traffic surveillance systems Vessel Traffic Service (VTS).

Table 1. Criteria defining ship operation modes [4]

Operating mode	Criterion
Manoeuvring	A ship carries out manoeuvres for mooring / unmooring.
Hotelling	A ship stands at a wharf to rebuild a readiness for the voyage.
Cruise	A ship on a way.
OPS	Ship's operating mode, which aims to reduce the emission of harmful compounds into the atmosphere.

Figure 1 presents sample data of ship's traffic in Swedish city – Göteborg. At an entrance or exit of a port it is necessary to perform manoeuvres by ships. Therefore, in port areas, regions are defined, which are applied to port maps as a manoeuvring region e.g. in a form of turning basins. In these areas it is assumed that ships reduce their speed, accelerate or slow down. In contrast to ships standing at a wharf and using power generators, from ships carrying out loading or unloading operations with a exception of their own power supply, the concept of "On-shore Power Supply" (OPS) has been introduced.

The "On-shore Power Supply" is a region where a ship can completely shut off all its marine engines. OPS is also known as:

– Coldironing system.
– Alternative Maritime Power (AMP).
– Shoreside electricity.
– Shore power.

The main goal of OPS is to reduce the emission of toxic compounds (mainly greenhouse gases – GHG) in the port areas. In addition, thanks to this, it can provide energy savings and economic benefits for ship owners.

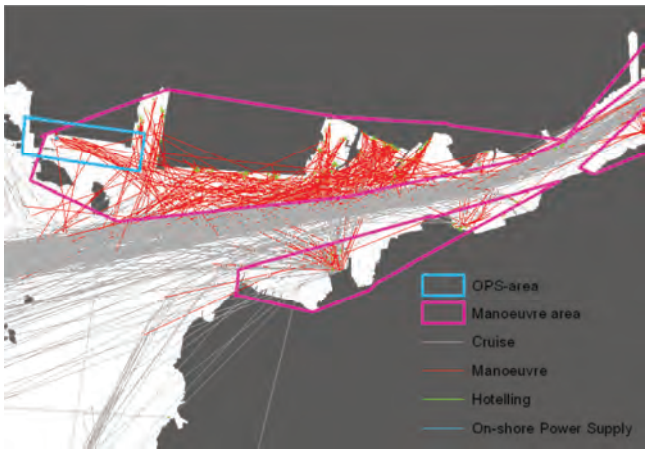

Fig. 1. Ship mode of operation in Swedish city – Göteborg [4]

3. Research facility

In the process of modelling the propulsion system, data obtained as a result of empirical research on a SULZER laboratory type 6AL20/24 engine were used [6]. The engine is a linear, non-reversible, water-cooled, 4-stroke diesel engine with direct fuel injection, turbocharging and charge air cooling (Fig. 2). Technical data of the engine are shown in table no. 2.

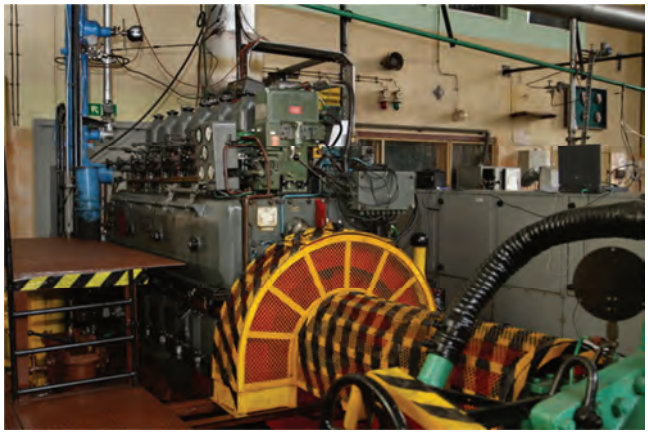

Fig. 2. Laboratory engine SULZER 6AL20/24 [8]

The main purpose of the work [6] was to prepare universal characteristics unit emissions of toxic compounds. An exemplary characteristic is shown in Fig. 3. In the plot of creating the characteristics, tests of concentrations of harmful compounds were carried out using the HEXIBA MEXA – 9130D exhaust gas analyser. The obtained data has been filtered out from disturbances and from measuring errors. Values of average concentrations of harmful compounds emitted were obtained using the formula:

$$A_{SA} = \frac{1}{l_i}\sum_{i=1}^{l_i} A_i \quad (1)$$

where: A_{SA} – arithmetic average, A_i – result of a measurement, l_i – number of measurements.

Table 2. Technical data of Sulzer 6AL20/24 engine [6]

The number of cylinders	i = 6
Nominal power	P_{nom} = 420 kW
Nominal speed	n_{nom} = 750 min^{-1}
Idle speed	n_{BL} = 350 min^{-1}
The diameter of the cylinder	D = 200 mm
Piston stroke	S = 240 mm
Compression	ε = 12.7
Engine stroke volume	V_{ss} = 45.2 dm^3
Average speed of the piston	$c_{śr} = 6\,\frac{m}{s}$
Cylinders work order	1–4–2–6–3–5
Maximum combustion pressure	p_{max} = 10.5–11.0 MPa
Fuel injection pressure	p_w = 24.5 MPa
Individual fuel consumption	$g_e = 212\,\frac{g}{kW \cdot h}$
Number of valves per cylinder	z = 4
Type of start-up	pneumatic, compressed air

Based on the characteristics (Fig. 3), an emission map was prepared, and used in the simulation of ship's propulsion model (Fig. 4).

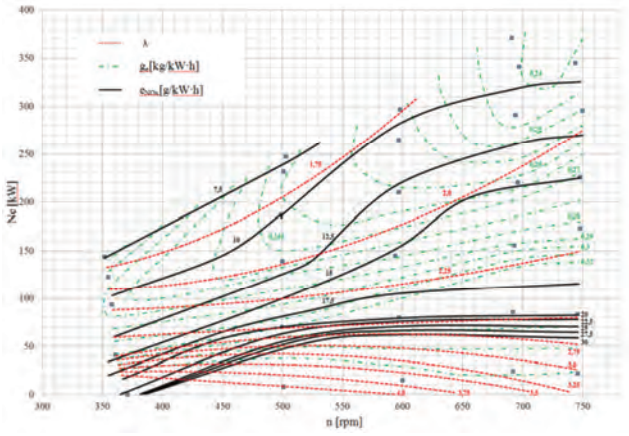

Fig. 3. Universal characteristics of the unit emission of NOx[8]

4. Ship's propulsion model

The mathematical relationship between the individual model blocks is illustrated in Fig. 5. This is a one-dimensional model. It is based on two basic integrating blocks (A and B blocks). These blocks in the simulation model convert data from nodes to the unit's progressive velocity and rotational speed of the drive system. The linear velocity of a ship is calculated by integrating a difference between a propeller thrust forces and total resistance of a hull in simulating time. It is made by block B.

Using the second principle of Newton's dynamics, obtained [7]:

$$\frac{d(D \cdot v)}{dt} = (T - R) \quad (2)$$

where: D – displacement of a ship [kg], v – speed of a ship [m/s], T – propeller thrust [N], R – total hull resistance [N].

After integration on both sides, equations (1) were obtained:

$$v = \int \frac{1}{D}(T - R)\,dt + v_0 \tag{3}$$

where: v_0 – initial speed of the ship [m/s].

The calculated linear velocity stays in the loop and returns to the block calculating the resistance of a hull. Block A calculates the rotational speed of a drive shaft. After reusing the second Newton's dynamics principle [7]:

$$\frac{d(2\cdot\pi\cdot I\cdot n)}{dt} = (M - Q) \tag{4}$$

where: I – moment of inertia [kg·m^2], n – rotation speed [1/s], M – engine torque [N·m], Q – propeller torque [N·m].

Integrating the equation (3) on both sides:

$$n = \int \frac{1}{2\cdot\pi\cdot I}(M - Q)\,dt + n_0 \tag{5}$$

where: n_0 – initial rotation speed [1/s].

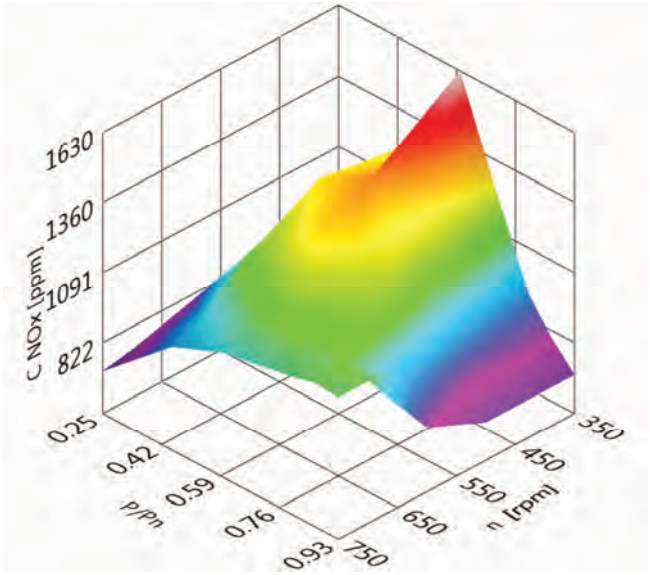

Fig. 4. Concentration NO_x map

The dependencies 2 and 4 were used as the basis for modelling in the programmatic environment. Figure 6 presents a program based on the Labview environment. In addition, cooperative subprograms have been developed whose mutual relations are necessary to carry out dynamic simulations and they are: hull ("Hull"), gear ("Gear"), ship engine ("Engine") and propeller ("Prop"). As an engine speed controller, the Proportional-Integral-Derivative controller (PID) has been selected, which with appropriate settings of the gain coefficients like proportional (K_p), differentiating (K_d), integral (K_i) is to simulate the ship's governor. It is possible to set (reference) the rotational speed of a propulsion system, which the PID controller used to maintain. The governor controls an engine via a fuel rack (modifying the fuel dose supplied to engine cylinders), making an appropriate correction ensuring constant engine speed, which was also used in the model. The result of calculations made with the help of an "Engine" subprogram is a torque, which then goes to a gear subprogram ("Gear"). Due to the set transmission ratio (in this case 1:2), the torque value increases at a expense of a marine engine. The results obtained in the simulation form the basis for calculations in the block propeller "Prop", while the value of the gear's torque returns to the sum node. As a result of the "Prop" subprogram calculation, receives the propeller torque (goes to the sum node) and the thrust force of the propeller (goes to the next summation node calculating the difference with the total resistance of the hull). In the subprogram "Hull" the total resistance of a hull is calculated depending on speed of a ship [3]:

$$R = \sum_i R_{(i)} = R_F + R_{VP} + R_W + R_D \tag{6}$$

where: R_F – friction resistance [N], R_{VP} – shape resistance [N], R_W – wave resistance [N], R_d – remaining resistance [N].

The propeller computational algorithm uses the approximations of a propeller B-series with a fixed pitch from the Wageningen research institute. The derived Wageningen polynomials determine a propeller torque and thrust coefficients depending on the blade number, propeller pitch, diameter, expanded area and advance coefficient, also taking into account the Reynolds number [1].

$$K_T = f_T\left(J, \frac{P}{D_p}, \frac{A_E}{A_0}, Z, R_e, \frac{t}{c}\right) \tag{7}$$

$$K_Q = f_Q\left(J, \frac{P}{D_p}, \frac{A_E}{A_0}, Z, R_e, \frac{t}{c}\right) \tag{8}$$

where: J – advance coefficient, P – propeller pitch, D_p – propeller diameter, A_E – expanded area, A_0 – disc area, Z – blade number, R_e – Reynolds number, t/c – blade thickness coefficient.

Figures 9–10 presents results of simulation of concentrations of harmful compounds for the SULZER marine engine type 6AL20/2, which has been implemented in a simulated propulsion system with a fixed pitch screw.

Technical data of the ship used in the simulation were adopted as follows:

- displacement – 300 t,
- total length – 35 m,
- breadth – 8 m,
- draught – 3 m,
- propeller diameter – 1.5 m,
- blade number – 4,
- P/D coefficient – 1.4,
- propeller expanded area – 1.8 m^2.

Simulation of concentrations of harmful compounds was carried out during the acceleration of the ship from 0 to 7 knots.

4. Summary

The simulation model of the marine propulsion system presented in the article is the basis for the development of a model of emission of harmful compounds in dynamic change of load. It is based on emission maps that are necessary to simulate concentrations of harmful compounds. Further development of the program will include a more detailed refinement of the model using neural networks and

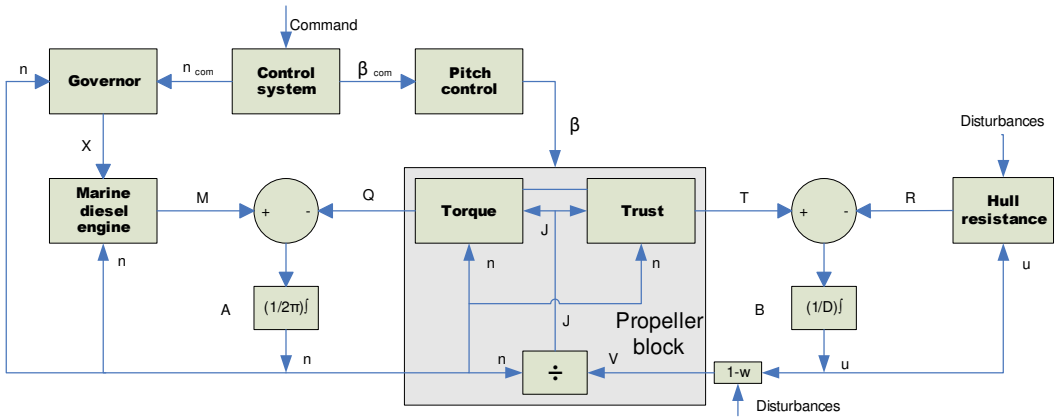

Fig. 5. Block diagram of a ship's propulsion system [6]

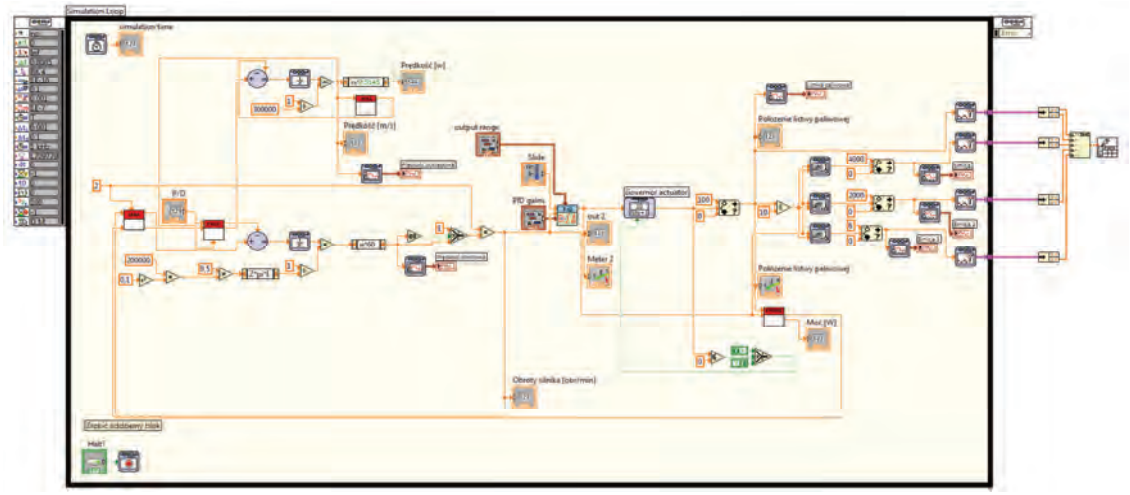

Fig. 6. Simulation model of a ship's propulsion in the Labview environment

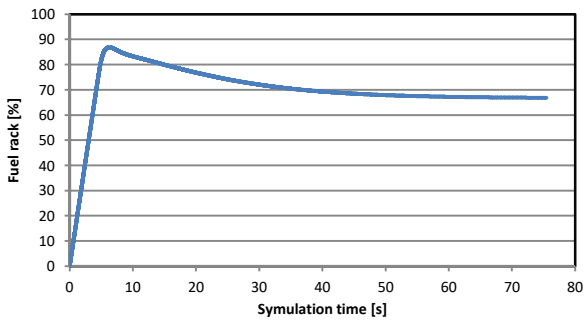

Fig. 7. Position of fuel rack during simulation

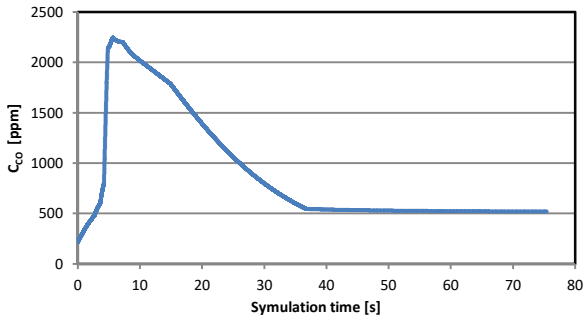

Fig. 8. Concentration of carbon monoxide during simulation

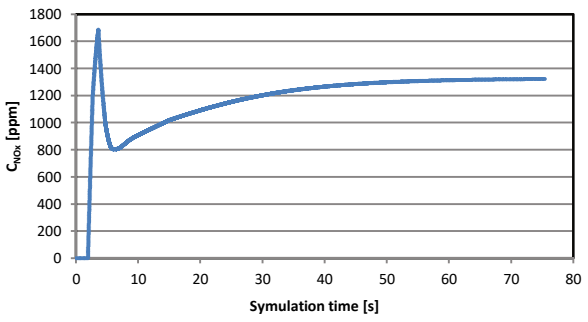

Fig. 9. Concentration of nitrogen oxides during simulation

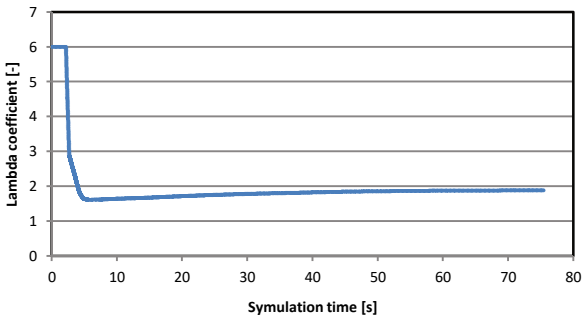

Fig. 10. Lambda coefficient during simulation

weather modules in the form of changing weather conditions (wind strength) and sea states. It would also be advisable to evaluate its adherence based on a comparison of the experimental results of a laboratory engine and an engine in a marine propulsion system of a real marine vessel operated in sea conditions during a dynamic change of load due to port maneuvers or maneuvers closely related to the purpose of a ship, for example, a salvage ship putting an anchorage for diving work.

Bibliography

[1] CARLTON, J. Marine Propellers and Propulsion. *MPG Books Ltd.*

[2] CHRUŚCIEL, M. Labview w praktyce. *Wydawnictwo BTC*. Legionowo 2008.

[3] KNIAZIEWICZ, T. Modelowanie procesów emisji spalin okrętowych tłokowych silników spalinowych napędu głównego w rzeczywistych warunkach eksploatacji. *Zeszyty naukowe AMW*. Gdynia 2013.

[4] MARIN, Sea shipping emission 2014. Final report. Bilthoven Netherlands 2016.

[5] MERKISZ, J., PIASECZNY, L., KNIAZIEWICZ, T. Zagadnienia emisji spalin silników okrętowych. *Wydawnictwo Politechniki Poznańskiej*. Poznań 2016.

[6] PIASECZNY, L. Metody wyznaczania statycznych i dynamicznych charakterystyk emisji związków toksycznych z silników spalinowych statków morskich. *Sprawozdanie z projektu badawczego N509 572 839*. AMW Gdynia 2013.

[7] SCHULTEN, P. The interaction between diesel engines, ship and propellers during . manoeuvring. *DUP science is an imprint of Delft University Press*. Delft 2005.

[8] WOJNOWSKI, W. Okrętowe siłownie spalinowe. *AMW* Gdynia 1998.

Tomasz Kniaziewicz, DSc., DEng. – Faculty of Mechanical and Electrical Engineering, Polish Naval Academy.
e-mail: *t.kniaziewicz@amw.gdynia.pl*

Artur Bogdanowicz, MEng. – Faculty of Mechanical and Electrical Engineering, Polish Naval Academy.
e-mail: *a.bogdanowicz@amw.gdynia.pl*

Article citation info:
BEBKIEWICZ, K., CHŁOPEK, Z., SZCZEPAŃSKI, K., LASKOWSKA, M. Emission of pollutants from motor vehicles in Poland comparing to pollutant emission in the European Union. *Combustion Engines*. 2019, **178**(3), 56-60. DOI: 10.19206/CE-2019-310

Katarzyna BEBKIEWICZ
Zdzisław CHŁOPEK
Krystian SZCZEPAŃSKI
Magdalena ZIMAKOWSKA-LASKOWSKA

CE-2019-310

Emission of pollutants from motor vehicles in Poland comparing to pollutant emission in the European Union

The inventory results of pollutant emission from motor vehicles in Poland comparing to the emission of pollutants in the European Union have been presented in the paper. The analysis is based on the official results of the pollution inventory reported to the European Union. Emission of the following substances was considered for the years 1990–2016 for Poland and the European Union from all civilization and road transport activities: carbon monoxide, non-methan volatile organic compounds, nitrogen oxides and particulate matter consisting of fractions: total suspended particles, PM10 and PM2.5. It was observed that the share of pollutant emission from road transport in Poland is smaller than for the entire European Union. This is especially evident in the case of particulate matter and nitrogen oxides. As a result of the analysis of the emission inventory in the European Union, it was confirmed that the share of motorisation in the emission of pollutants harmful to human health is significantly smaller in Poland than in the entire European Union. Therefore, conducting a detailed analysis of specific distance emission of pollutants from a statistical vehicle as well as extending research on greenhouse gas emission from motor vehicles is recommended.

Key words: *inventory of pollutant emission, motor vehicles*

1. Introduction

Since 1990 the emission of pollutants from sectors of civilization activity which is harmful to the health of living organisms have been regularly inventoried in the European Union and in most other European countries [3–8, 10, 12, 13]. Also other countries prepare an inventory of pollutant emission, including the United States of America, Canada and Asia [1, 2, 11]. While reports on the inventory of pollutant emission from anthropogenic sources are published, relatively few results of analyzes are issued. This is also due to the fact that until present day the methodology for the inventory of pollutant emission from particular sectors of civilization activity has not been strictly unified, even in such structures as the European Union. The structure of pollutant emission estimation is relatively precisely unified, *inter alia* due to the characteristics of emission sources [5, 8–10], but there is still a large freedom in adopting emission characteristics [9]. Also, the intensity of civilization activity is relatively unclear, e.g. the annual mileage of motor vehicles in elementary categories [4–7]. Despite these reservations, data presented in published reports on anthropogenic pollution emission are official and as such they may be used in analyzes.

In this paper the share of pollutant emission from the road transport sector in Poland and the European Union over the period 1990–2016 [8, 10] has been analyzed.

Substances estimated in official reports in the European Union are listed below [8, 10]:

- carbon monoxide – CO,
- non-methane volatile organic compounds – NMVOC,
- nitrogen oxides reduced to nitrogen dioxide – NO_x,
- ammonia – NH_3,
- total suspended particles – TSP,
- particulate matter PM10,
- particulate matter PM2.5,
- black carbon – BC,
- sulphur oxides reduced to sulphur dioxide – SO_2,
- priority heavy metals: lead – Pb, cadmium – Cd and mercury – Hg,
- additional heavy metals: arsenic – As, chromium – Cr, copper – Cu, nickel – Ni, selenium – Se and zinc – Zn,
- persistent organic pollutants – POPs.

This article presents the results of the analysis for the following substances: carbon monoxide, non-methane volatile organic compounds, nitrogen oxides and particulate matter dimensional fractions: total suspended particles, PM10 and PM2.5.

Not all substances, analyzed in this work, are in official reports issued in the European Union. The limitation applies to particulate matter PM10 and PM2.5. Not all Member States had performed inventories of these substances before 1999, *inter alia* Austria, Belgium and Germany [8, 10].

The COPERT 5 software was used for the inventory of pollutant emission in Poland for the years 1990–2016. The following categories of motor vehicles are included in the inventory of pollutant emission from road transport [4–10]:

1. Passenger cars:
   - gasoline passenger cars with spark ignition engine,
   - liquefied petroleum gas passenger cars with spark ignition engine,
   - passenger cars with compression ignition engine,
   - hybrid passenger cars.
2. Light commercial vehicles (light duty vehicles):
   - light commercial vehicles with spark ignition engine,
   - light commercial vehicles with compression ignition engine.
3. Heavy duty trucks:
   - heavy duty trucks – rigid (heavy duty container trucks),
   - heavy duty trucks – articulated (tractor units, ballast tractors).
4. Urban buses.

5. Coaches.
6. Motorcycles.
7. Mopeds.

The methodology for determining the emission of total pollution from motor vehicles is compatible with [9]. The methodology for the selection of parameters for the COPERT software is described in [4–7]. The methodology for determining emission of pollutants from sectors other than road transport is compatible with [7–10].

2. Results of the inventory of the analyzed pollutant emission in the European Union and Poland

Figures 1–6 present the annual emission of pollutants from all sectors of civilization activity and from the road transport sector in the European Union: total – EU-T and from motor vehicles – EU-RT, and annual emission of pollutants in Poland: total – PL-T and motor vehicles – – PL-RT in 1990–2016.

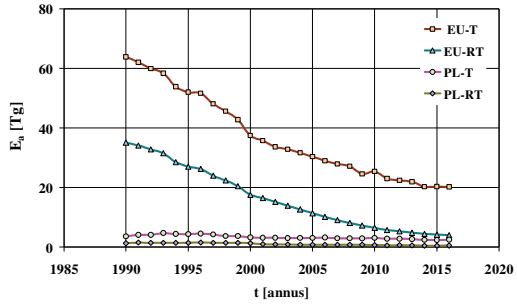

Fig. 1. Annual emission of carbon monoxide: total in the European Union – EU-T, from motor vehicles in the European Union – EU-RT, total in Poland – PL-T, from motor vehicles in Poland – PL-RT in years 1990–2016

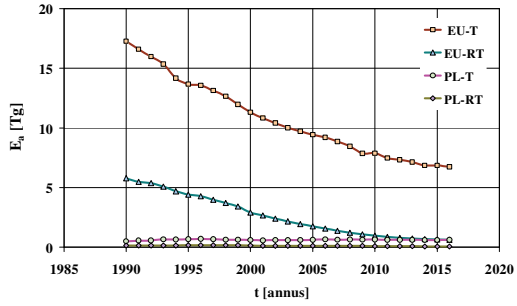

Fig. 2. Annual emission of non-methane volatile organic compounds: total in the European Union – EU-T, from motor vehicles in the European Union – EU-RT, total in Poland – PL-T, from motor vehicles in Poland – PL-RT in years 1990–2016

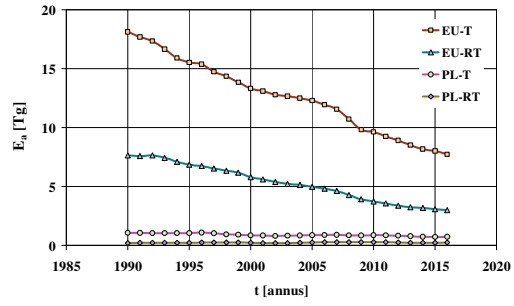

Fig. 3. Annual emission of nitrogen oxides: total in the European Union – EU-T, from motor vehicles in the European Union – EU-RT, total in Poland – PL-T, from motor vehicles in Poland – PL-RT in years 1990–2016

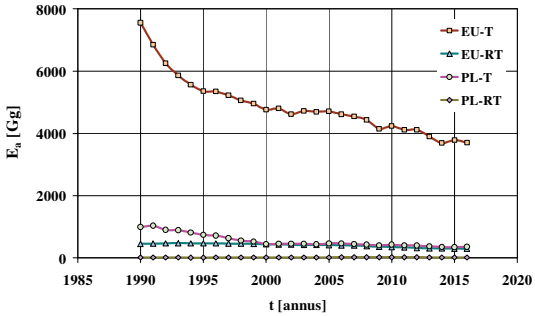

Fig. 4. Annual emission of total suspended particles: total in the European Union – EU-T, from motor vehicles in the European Union – EU-RT, total in Poland – PL-T, from motor vehicles in Poland – PL-RT in years 1990–2016

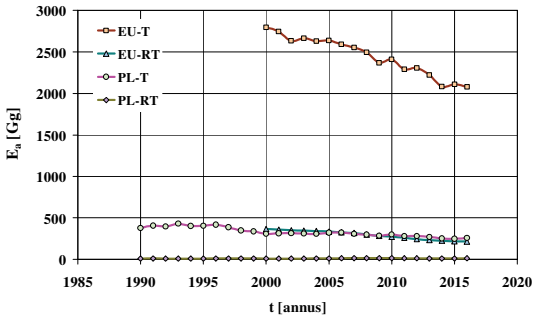

Fig. 5. Annual emission of particulate matter PM10: total in the European Union – EU-T, from motor vehicles in the European Union – EU-RT, total in Poland – PL-T, from motor vehicles in Poland – PL-RT in years 1990–2016

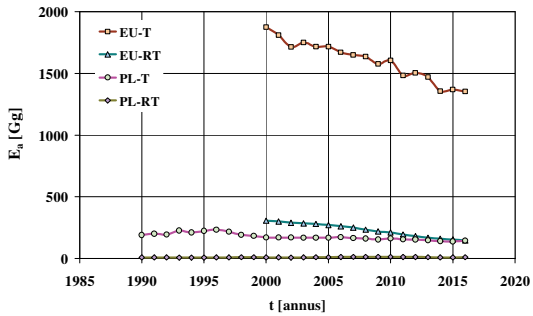

Fig. 6. Annual emission of particulate matter PM2.5: total in the European Union – EU-T, from motor vehicles in the European Union – – EU-RT, total in Poland – PL-T, from motor vehicles in Poland – – PL-RT in years 1990–2016

3. Results of the analysis of pollutant emission inventories in the European Union and in Poland

Figures 7–12 show the share of annual emission in Poland from all sectors of civilization activity and from the road transport sector comparing to the annual emission in the European Union for pollutants: for total emission – T and for emission from motor vehicles – RT in the years 1990–2016.

The average share of annual emission of pollutants in Poland comparing to the annual emission in the European Union is:

– for all sectors of civilization activity – 0.094: from 0.062 – for non-methane volatile organic compounds to 0.120 – for particular matter PM10,
– for road transport – 0.051: from 0.032 – for particular matter to 0.076 – for carbon monoxide.

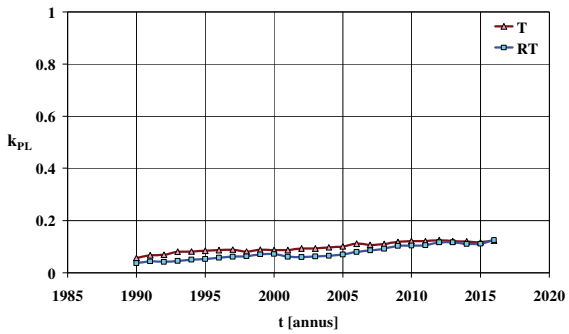

Fig. 7. Share of annual emission in Poland comparing to the annual emission in the European Union for carbon monoxide: for total emission – T and for emission from motor vehicles – RT in years 1990–2016

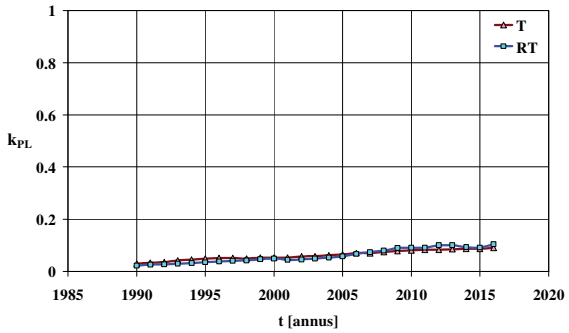

Fig. 8. Share of annual emission in Poland comparing to the annual emission in the European Union for non-methane volatile organic compounds: for total emission – T and for emission from motor vehicles – RT in years 1990–2016

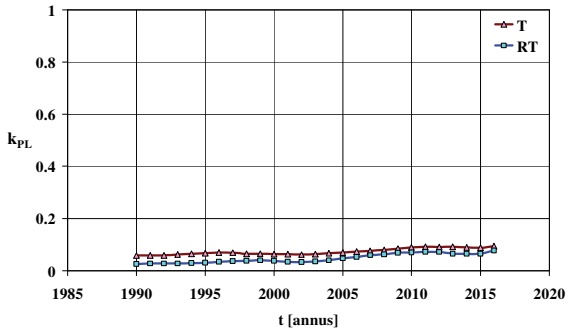

Fig. 9. Share of annual emission in Poland comparing to the annual emission in the European Union for nitrogen oxides: for total emission – T and for emission from motor vehicles – RT in years 1990–2016

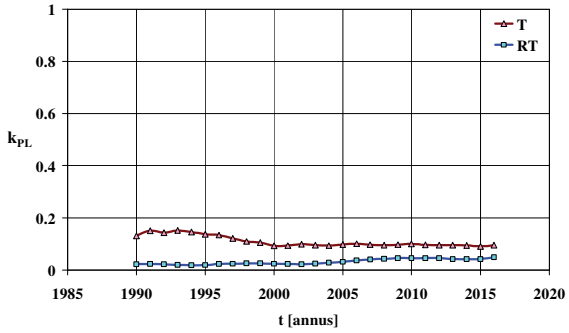

Fig. 10. Share of annual emission in Poland comparing to the annual emission in the European Union for total suspended particles: for total emission – T and for emission from motor vehicles – RT in years 1990–2016

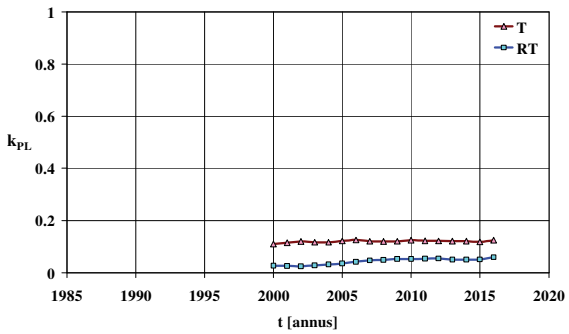

Fig. 11. Share of annual emission in Poland comparing to the annual emission in the European Union for particulate matter PM10: for total emission – T and for emission from motor vehicles – RT in years 1990–2016

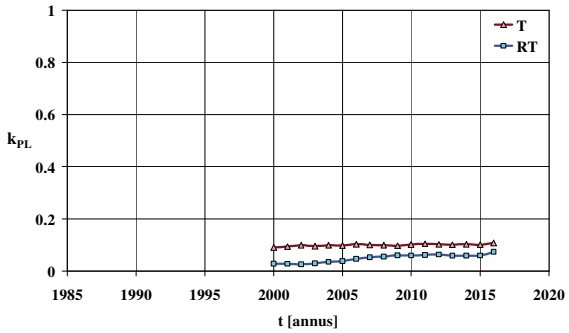

Fig. 12. Share of annual emission in Poland comparing to the annual emission in the European Union for particulate matter PM2.5: for total emission – T and for emission from motor vehicles – RT in years 1990–2016

Figures 13–18 show the share of annual emission from motor vehicles in relation to total annual emission: in Poland – PL and in the European Union – EU in 1990–2016.

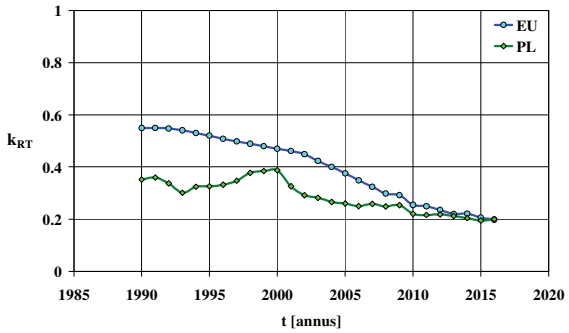

Fig. 13. Share of annual emission from motor vehicles comparing to the total annual emission for carbon monoxide: in Poland – PL and in the European Union – EU in years 1990–2016

The average share of annual emission of pollutants from motor vehicles in relation to the total annual emission is:

– for the European Union – 0.228: from 0.087 – for particular matter to 0.414 – for nitrogen oxides,
– for Poland – 0.141 – from 0.026: for particular matter to 0.286 – for carbon monoxide.

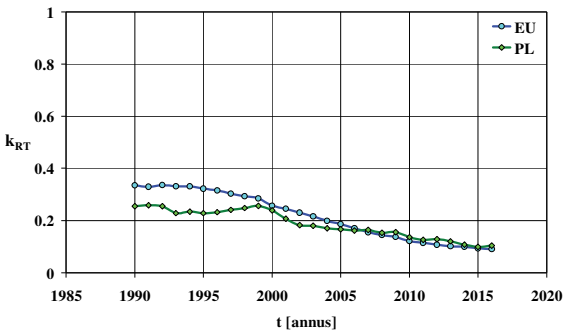

Fig. 14. Share of annual emission from motor vehicles in relation to the total annual emission for non-methane volatile organic compounds: in Poland – PL and in the European Union – EU in years 1990–2016

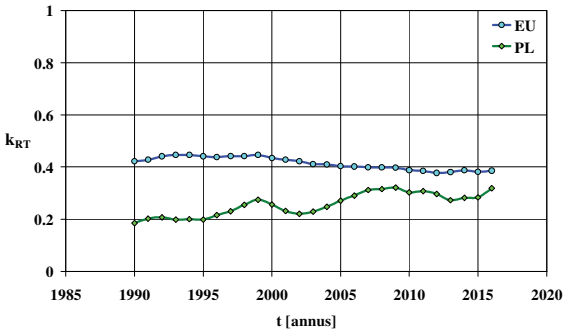

Fig. 15. Share of annual emission from motor vehicles comparing to the total annual emission for nitrogen oxides: in Poland – PL and in the European Union – EU in years 1990–2016

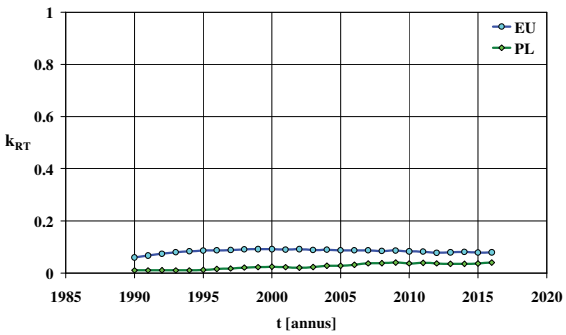

Fig. 16. Share of annual emission from motor vehicles comparing to the total annual emission for total suspended particles: in Poland – PL and in the European Union – EU in years 1990–2016

In the case of carbon monoxide and non-methane volatile organic compounds, there is a noticeable tendency of reducing the share of annual emission from motor vehicles in comparison to the annual emission from all sectors of civilization activity.

4. Recapitulation

Inventory of pollutants emission from anthropogenic sources is an effective method of assessing the environmental threat posed by particular sectors of civilization activity. A requirement to maintain the objectivity of this assessment is development of a coherent method of estimating pollutant emission from particular sectors of civilization activity. Unfortunately, despite many attempts to standardize the methodology of estimating the total emission of pollutants by individual countries, the full coherence of methods applied by Member States of the European Union requires further development [8, 10].

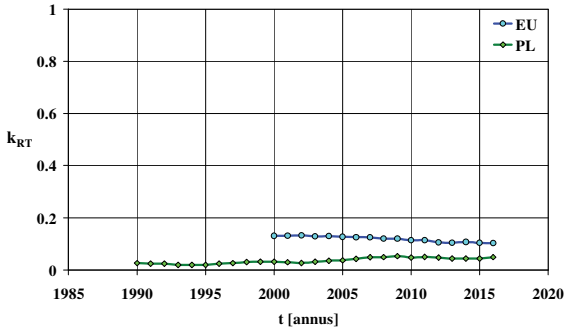

Fig. 17. Share of annual emission from motor vehicles comparing to the total annual emission for particulate matter PM10: in Poland – PL and in the European Union – EU in years 1990–2016

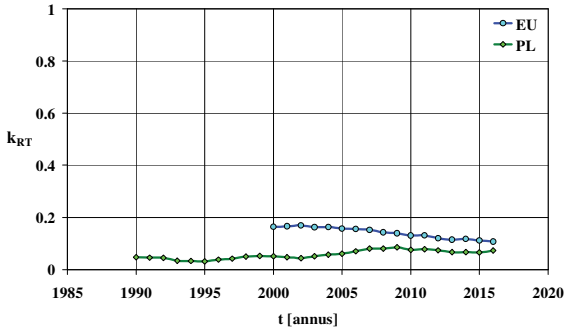

Fig. 18. Share of annual emission from motor vehicles comparing to the total annual emission for particulate matter PM2.5: in Poland – PL and in the European Union – EU in years 1990–2016

Based on the study results presented above, the following conclusions can be drawn:

1. The share of annual emission of pollutants in Poland in comparison to the annual emission in the European Union is lower for road transport than for all sectors of civilization activity. This positive trend concerns mainly particular matters – all particle size fractions.
2. The share of annual emission of pollutants from motor vehicles compared to the total annual emission is lower for Poland than for the European Union. Therefore the actions undertaken in Poland to reduce pollutant emission from motor vehicles are considered as effective, the more that the dynamic development of the Polish automotive industry is not accompanied by a noticeable increase in the analyzed share.

Nomenclature

As	arsenic	Cd	cadmium
BC	black carbon	CO	carbon monoxide

Cr	chrome	PM exhaust	particular matter from exhaust system
Cu	copper	PM10	particular matter PM10
E_a	annual emission	PM2.5	particular matter PM2.5
Hg	mercury	POPs	persistent organic pollutants
k_{PL}	share	RT	road transport
k_{RT}	share	Se	selenium
NFR	nomenclature for reporting	SO_2	sulphur oxides
NH_3	ammonia	t	time
Ni	nickel	T	total
NMVOC	non-methane volatile organic compounds	TSP	total suspended particles
NO_x	nitrogen oxides	Zn	zinc
Pb	lead		

Bibliography

[1] 1990–2016 Air pollutant emission inventory report. Environment and Climate Change Canada. 2018.

[2] 2014 National Emissions Inventory, version 2 Technical Support Document. U.S. Environmental Protection Agency Office of Air Quality Planning and Standards Air Quality Assessment Division Emissions Inventory and Analysis Group Research Triangle Park, North Carolina. 2018.

[3] Air Pollutant Inventories for England, Scotland, Wales, and Northern Ireland: 1990–2016. Ricardo Energy & Environment for the Department for Environment, Food & Rural Affairs, The Scottish Government, The Welsh Government and The Northern Ireland Department for Agriculture, Environment and Rural Affairs. 2018.

[4] BEBKIEWICZ, K., CHŁOPEK, Z., SZCZEPAŃSKI, K., ZIMAKOWSKA-LASKOWSKA, M. Assessment of results of pollutant emission inventory of the road transport sector in Poland in 2000–2015. *The Archives of Automotive Engineering – Archiwum Motoryzacji*. 2017, **78**(4), 5-25.

[5] BEBKIEWICZ, K., CHŁOPEK, Z., SZCZEPAŃSKI, K., ZIMAKOWSKA-LASKOWSKA, M. Issues of modeling the total pollutant emission from vehicles. *Proceedings of the Institute of Vehicles*. 2017, **1**(110), 103-118.

[6] BEBKIEWICZ, K., CHŁOPEK, Z., SZCZEPAŃSKI, K., ZIMAKOWSKA-LASKOWSKA, M. Results of air emission inventory from road transport in Poland in 2014. *Proceedings of the Institute of Vehicles*. 2017, **1**(110), 77-88.

[7] CHŁOPEK, Z., DĘBSKI, B., SZCZEPAŃSKI, K. Theory and practice of inventory pollutant emission from civilization related sources: share of the emission harmful to health from road transport. *The Archives of Automotive Engineering – Archiwum Motoryzacji*. 2018, **79**(1), 5-22.

[8] EEA Report No 6/2018. European Union emission inventory report 1990–2016 under the UNECE Convention on Long-range Transboundary Air Pollution (LRTAP). Luxembourg: Publications Office of the European Union. 2018.

[9] EMEP/EEA air pollutant emission inventory guidebook – 2016. European Environment Agency.

[10] https://gispub.epa.gov/neireport/2014 (2019-02-10).

[11] LI, M. et. al. Anthropogenic emission inventories in China: A review. *National Science Review*. 2017, **4**(6), 834-866.

[12] Poland's Informative Inventory Report 2018. Submission under the UN ECE Convention on Long-range Transboundary Air Pollution and the Directive (EU) 2016/2284 Warszawa. National Centre for Emission Management (KOBiZE) at the Institute of Environmental Protection – National Research Institute. February 2018.

[13] UK Emission Mapping Methodology A report of the National Atmospheric Emission Inventory 2016. Ricardo Energy & Environment for Department for Business, Energy and Industrial Strategy; Department for Environment, Food and Rural Affairs; The Scottish Government; Welsh Government; Department of Agriculture, Environment and Rural Affairs for Northern Ireland. 2018.

Katarzyna Bebkiewicz, MEng. – Institute of Environmental Protection – National Research Institute in Warsaw.
e-mail: *katarzyna.bebkiewicz@kobize.pl*

Krystian Szczepański, DSc., DEng. – Director of the Institute of Environmental Protection – National Research Institute in Warsaw.
e-mail: *krystian.szczepanski@ios.edu.pl*

Prof. Zdzisław Chłopek, DSc., DEng. – Professor in the Institute of Environmental Protection – National Research Institute in Warsaw.
e-mail: *zdzislaw.chlopek@kobize.pl*

Magdalena Zimakowska-Laskowska, DSc., DEng. – Institute of Environmental Protection – National Research Institute in Warsaw.
e-mail: *magdalena.zimakowska-laskowska@kobize.pl*

Article citation info:
GIS, W., PIELECHA, J., MERKISZ, J. et al. Determining the route for the purpose light vehicles testing in Real Driving Emissions (RDE) test. *Combustion Engines*. 2019, **178**(3), 61-66. DOI: 10.19206/CE-2019-311

Wojciech GIS
Jacek PIELECHA
Jerzy MERKISZ
Stanisław KRUCZYŃSKI
Maciej GIS

CE-2019-311

Determining the route for the purpose light vehicles testing in Real Driving Emissions (RDE) test

In the regulations concerning approval of light vehicles starting from September 2019 it will be necessary to conduct exhaust emissions tests both on a chassis dynamometer and for real driving emissions. It is a legislative requirement set forth in EU regulations for the purpose of the RDE (Real Driving Emissions) procedure.

To decide on the RDE route for the purpose of the LV exhaust emissions tests many requirements must be fulfilled, regarding for example external temperature and the topographic height of the tests, driving style (driving dynamic parameters), trip duration, length of respective test sections (urban, rural, motorway, etc.). The works on outlining RDE routes are continued across the country in various research centres. Specifying the RDE route for test purposes, i.e. works in which the authors of this article are actively involved, has become a major challenge for future approval surveys concerning the assessment of hazardous emissions from light vehicles and for development studies focusing on – for example – the consumption of energy in electric and hybrid vehicles.

The test route has been chosen to ensure that the test is performed on a continual basis. Data were recorded on a constant basis with the minimum duration of the test achieved. The test involved light vehicles and PEMS device for measuring the exhaust emissions, vehicle's speed, completed route, etc. The device was installed in such manner as to ensure that its impact on the exhaust emissions from the tested vehicle and on the device's operation is the least.

The vehicle load was consistent with the requirements of the standard and included the aforesaid measurement device, the driver and the operator of PEMS. The tests were carried out on working days. The streets and roads used for the tests were hard-surfaced. Measurements were performed in accordance with the requirements of RDE packages (Package 1–4), i.e. taking into account – among others – the engine cold start.

The article discusses the method of outlining the test route fulfilling the specific requirements for RDE testing. Chosen results of exhaust emissions from a passenger car with a spark-ignition engine along the defined RDE test route have been provided.

The tests discussed in the article are introductory in the area of RDE tests and provide an introduction into further studies of exhaust emissions and energy consumption in real driving conditions in conventional vehicles and vehicles with alternative engines, e.g. hybrid and electric vehicles.

Key words: *RDE, vehicle, transport, passenger cars, test, ecology, homologation*

1. Introduction

The approval process of light vehicles in the European Union comprises a procedure for the measurement of real driving emissions generated by those vehicles. In accordance with the requirements (Commission Regulation (EU) no. 582/2011, Commission Regulation (EU) no. 2018/932) for all new approvals the emissions of CO, THC, NMHC, CH_4, NO_x is measured in RDE, which cannot exceed 1.5 times the maximum Euro VI limit [1–4].

The parameters of road tests cannot be any parameters. It is necessary to select adequately the test route. The route must include driving in urban, rural and motorway areas. It is only one of the many requirements that must be met. The scope of those requirements is presented in Table 1.

2. Moving Averaging Window method for exhaust emissions

The Moving Averaging Window method provides an insight on the real-driving emissions (RDE) occurring during the test at a given scale. The test is divided in subsections (windows) and the subsequent statistical treatment aims at identifying which windows are suitable to assess the vehicle RDE performance.

The "normality" of the windows is conducted by comparing their CO_2 distance-specific emissions with a reference curve. The test is complete when the test includes a sufficient number of normal windows, covering different speed areas (urban, rural, motorway). It consists of the following steps:

– calculation of emissions by sub-sets or "windows,
– identification of normal windows,
– verification of test completeness and normality,
– calculation of emissions using the normal windows,
– specifying dynamic trip parameters.

The instantaneous emissions must be integrated using a Moving Averaging Window method, based on the reference CO_2 mass (Fig. 2). The principle of the calculation is as follows: the mass emissions are not calculated for the complete data set, but for sub-sets of the complete data set, the length of these sub-sets being determined so as to match the CO_2 mass emitted by the vehicle over the reference laboratory cycle (WLTC). The moving average calculations are conducted with a time increment corresponding to the data sampling frequency (usually 1 Hz). These sub-sets used to average the emissions data are referred to as "averaging windows". The calculation described in the present point may be run from the last point (backwards) or from the first point (forward).

Table 1. Specific requirements regarding RDE tests [1–4]

Parameter	Requirements
Ambient temperature (T_z)	– normal range: $0^oC \le T_z < 30^oC$
	– lower extended range: $-7^oC \le T_z < 0^oC$
	– upper extended range: $30^oC < T_z \le 35^oC$
Topographic height of test areas (h)	– normal range: $h \le 700$ m a.s.l.
	– extended range: $700 < h \le 1300$ m a.s.l.
Impact of external weather and road parameters and the driving style	– accumulated height increase: less than 1200 m/100 km
	– (RPA): greater than RPA_{min} (in all driving conditions)
	– product of acceleration and speed ($v \cdot a_{pos}$): less than $v \cdot a_{pos\ min}$ (in all driving conditions)
Thermal condition of the vehicle prior to tests	– cold start: coolant less than 70^oC, time of at least 300 s
	– emission upon cold start not included in RDE test
Single vehicle downtime	– no more than 180 s
Exhaust after-treatment system's operation	– single regeneration of PM filter can result in RDE test repetition; two regenerations are included in the results of exhaust emissions in RDE test
Driving comfort system operation	– used normally according to purpose (e.g. air-conditioning system)
Vehicle load	– weight of vehicle: driver (and passenger) and test equipment; max. load < 90% of the sum of weight of passengers and vehicle's usable mass
Test requirement	– duration 90–120 min
Requirements for the urban test part	– 29–44% of the entire test length
	– distance more than 16 km
	– speed (v): $v \le 60$ km/h
	– average speed: 15–40 km/h
	– break: 6–30% of the total urban time
Requirements for the rural part	– 23–43% of the entire test length
	– distance: greater than16 km
	– vehicle's speed (v): $60 \text{ km/h} < v \le 90$ km/h
Requirements for the motorway part	– 23–43% of the entire test length
	– distance: greater than16 km
	– vehicle's speed (v): $v > 90$ km/h
	– driving speed of more than 100 km/h for at least 5 min
	– driving speed of more than 145 km/h for at least 3% of the time

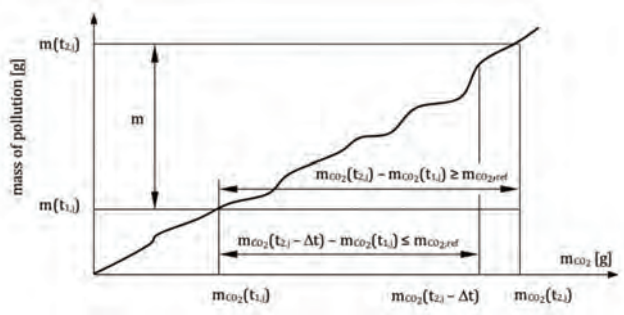

Fig. 2. Definition of CO_2 mass based averaging windows [1–4]

Duration of i-window average ($t_{2,j} - t_{1,j}$) is determined according to the following formula (Fig. 2):

$$m_{CO_2}(t_{2,j}) - m_{CO_2}(t_{1,j}) \ge m_{CO_2,ref} \quad (1)$$

where: $m_{CO_2}(t_{i,j})$ – is the CO_2 mass measured between the test start and time ($t_{i,j}$), [g]; $m_{CO_2,ref}$ – is the half of the CO_2 mass [g] emitted by the vehicle over the WLTP cycle (type I test, including cold start); $t_{2,j}$ – shall be selected such as:

$$m_{CO_2}(t_{2,j} - \Delta t) - m_{CO_2}(t_{l,j}) < m_{CO_2,ref} \le m_{CO_2}(t_{2,j}) - m_{CO_2}(t_{1,j}) \quad (2)$$

where Δt is the data sampling period (1 s or less).

The reference points P_1, P_2 and P_3 (Fig. 3) required to define the curve shall be established as follows:

- P_1: v_{P1} = 19 km/h (average speed of the 1 Low Speed phase of the WLTP cycle),
- $b_{CO_2,P1}$ – on-road emission of CO_2 [g/km] of 1 Low Speed phase of the WLTC phase increased by 20%,
- P_2: v_{P2} = 56.6 km/h (average speed of the 3 High Speed phase of the WLTP cycle),
- $b_{CO_2,P2}$ – on-road emission of CO_2 [g/km] of 3 Low Speed phase of the WLTC phase increased by 10%,
- P_3: v_{P3} = 92.3 km/h (average speed of the 4 Extra High Speed phase of the WLTP cycle),
- $b_{CO_2,P3}$ = on-road emission of CO_2 [g/km] of 4 Low Speed phase of the WLTC phase increased by 5%.

The CO_2 emissions are calculated as a function of the average speed using two linear sections (P_1, P_2) and (P_2, P_3).

The section (P_2, P_3) is limited to 145 km/h on the vehicle speed axis.

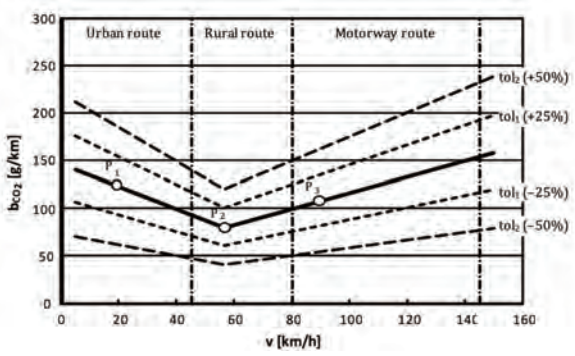

Fig. 3. Vehicle CO_2 characteristic curve

Urban windows are characterized by average vehicle ground speeds smaller than 45 km/h, rural windows are characterized by average vehicle ground speeds greater than or equal to 45 km/h and smaller than 80 km/h, motorway windows are characterized by average vehicle ground speeds greater than or equal to 80 km/h and smaller than 145 km/h. The primary tolerance and the secondary tolerance of the vehicle CO_2 characteristic curve are respectively $tol_1 = 25\%$ and $tol_2 = 50\%$. The test shall be complete when it comprises at least 15% of urban, rural and motorway windows, out of the total number of windows. The test shall be normal when at least 50% of the urban, rural and motorway windows are within the primary tolerance defined for the characteristic curve. If the specified minimum requirement of 50% is not met, the upper positive tolerance tol_1 may be increased by steps of 1% until the 50% of normal windows target is reached. When using this mechanism, tol_1 shall never exceed 30%.

Having ascertained that the test is complete, the weighing factor for each window shall be determined in the following tolerance ranges:

- if the window falls within the 1st degree tolerance, i.e.:

$$b_{CO_2}\left(1-\frac{tol_1}{100}\right) \le b_{CO_2,i} \le b_{CO_2}\left(1+\frac{tol_1}{100}\right) \quad (3)$$

the weighing factor *shall be equal 1.*

- if the window falls within the tolerance range from +25% to +50%, i.e.:

$$b_{CO_2}\left(1+\frac{tol_1}{100}\right) \le b_{CO_2,i} \le b_{CO_2}\left(1+\frac{tol_2}{100}\right) \quad (4)$$

its weighing factor shall be determined with the following formula:

$$w = k_{11}\, h + k_{12} \quad (5)$$

where: $k_{11} = \frac{1}{tol_1 - tol_2}$, a $k_{12} = \frac{tol_2}{tol_2 - tol_1}$,

– if the window falls within the tolerance range from –50% to –25%, i.e.:

$$b_{CO_2}\left(1-\frac{tol_2}{100}\right) \le b_{CO_2,i} \le b_{CO_2}\left(1-\frac{tol_1}{100}\right) \quad (6)$$

its weighing factor shall be determined with the following formula:

$$w = k_{21}\, h + k_{22} \quad (7)$$

where: $k_{21} = \frac{1}{tol_2 - tol_1}$, a $k_{22} = \frac{tol_2}{tol_2 - tol_1}$,

– if the window falls below tolerance range –50% or above +50%, i.e.:

$$b_{CO_2,i} \le b_{CO_2}\left(1-\frac{tol_2}{100}\right) \text{ or } b_{CO_2,i} \ge b_{CO_2}\left(1+\frac{tol_2}{100}\right) \quad (8)$$

its weighing factor is w = 0.

The value of h for every window is determined based on the following formula:

$$h = 100\left(\frac{b_{CO_2,i} - b_{CO_2}}{b_{CO_2}}\right) \quad (9)$$

After the weighing factor for every window is determined, it is marked on the chart where every weighing factor (w) is marked on the y axis, tolerance percentage (h) on x axis (Fig. 4).

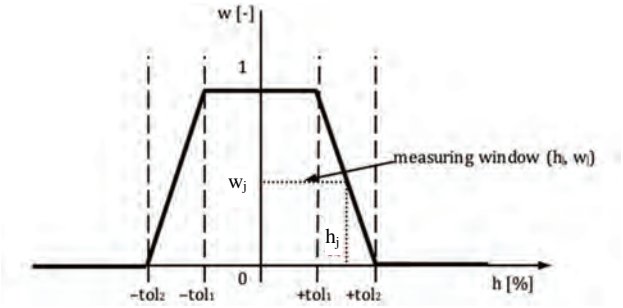

Fig. 4. Averaging window weighing function [1–4]

After all those steps are performed, the CO_2 on-road emissions for every window are illustrated on the characteristic curve chart (Fig. 5).

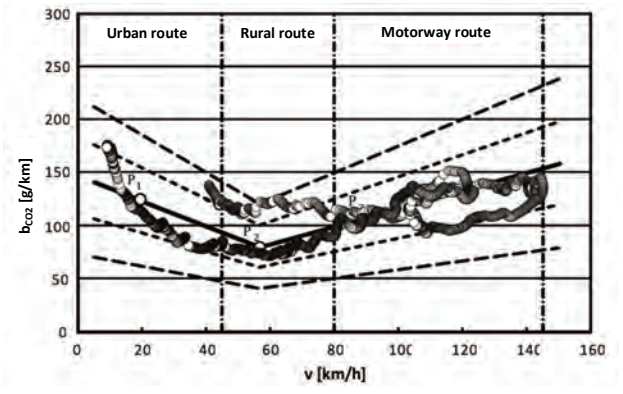

Fig. 5. Vehicle CO_2 characteristic curve with CO_2 emissions in respective windows, during on-road tests [1–4]

Next the severity indices shall be calculated separately for the urban (m), rural (p) and motorway (a) categories by summarising windows for a particular category (h_k) and dividing by the total number (N), e.g. for the urban category:

$$u = \frac{\sum h_k}{N},\ k = m, p, a \tag{10}$$

and the complete trip:

$$u = \frac{f_m h_m + f_p h_p + f_a h_a}{f_m + f_p + f_a} \tag{11}$$

where: $f_m = 0.34$, $f_p = 0.33$, a $f_a = 0.33$.

In the end the distance-specific emissions in [mg/km] are calculated for the complete trip each gaseous pollutant in the following way:

$$b_j = 1000 \cdot \frac{f_m b_{j,m} + f_p b_{j,p} + f_a b_{j,a}}{f_m + f_p + f_a} \tag{12}$$

and for the on-road emission of particulate matter:

$$b_{PN} = \frac{f_m b_{PN,m} + f_p b_{PN,p} + f_a b_{PN,a}}{f_m + f_p + f_a} \tag{13}$$

To determine dynamic trip parameters the following must be determined: value of 95 centile of the product of driving speed and positive acceleration greater than 0.1 m/s^2 (expressed in m^2/s^3) and relative positive acceleration (expressed in m/s^2) for urban, rural and motorway shares.

The value of the 95th centile of the product $(v \cdot a_+)$ – formulated as $(v \cdot a_+)_{k\_[95]}$ – is determined in the following manner: value of products $(v \cdot a_+)_{i,k}$ in every test part (k – urban, rural and motorway share) is categorised in a growing order for all data sets of $a_{i,k} \geq 0.1$ m/s^2 (number of data sets must be greater than 150) and the total number of windows N_k is determined.

In the next step the centile values are allocated to the product $(v \cdot a_+)_{i,k}$ in the following manner: the lowest value of the product $(v \cdot a_+)$ has centile of $1/N_k$, the second lowest – $2/N_k$, the third lowest – $3/N_k$, and the highest value – $N_k/N_k = 100\%$. Value $(v \cdot a_+)_{k\_[95]}$ stands for $(v \cdot a_+)_{i,k}$, for which $j/N_k = 95\%$ (j – successive value of product of speed and positive acceleration). If $j/N_k = 95\%$ cannot be achieved, then $(v \cdot a_+)_{k\_[95]}$ is determined based on line interpolation of successive samples j and (j + 1), for which $j/N_k < 95\%$ and $(j + 1)/N_k > 95\%$.

The validity of the trip is verified for every urban, rural and motorway share. If the value of $(v \cdot a_+)_{k\_[95]}$ meets the equation for every test step (Fig. 6a):

$$(v \cdot a_+)_{k\_[95]} < 0{,}136 \cdot \bar{v}_k + 14{,}4 \quad \text{for } \bar{v}_k \leq 74{,}6 \text{ km/h} \tag{15}$$

$$(v \cdot a_+)_{k\_[95]} < 0{,}0742 \cdot \bar{v}_k + 18{,}966 \text{ for } \bar{v}_k > 74{,}6 \text{ km/h} \tag{16}$$

the trip is valid.

RPA – relative positive acceleration for every step of the test is determined based on the following formula:

$$RPA_k = \frac{\sum_{j=1}^{N_k} \Delta t \cdot (v \cdot a_+)_{j,k}}{\sum_{j=1}^{L} d_{i,k}} \tag{14}$$

where: RPA_k – relative positive acceleration for urban, rural and motorway shares, m/s^2, Δt – data sampling period (1 s), N_k – number of windows for urban, rural, and motorway shares with positive acceleration, L – total number of windows for urban, rural, and motorway shares.

If RPA_k value meets the equation for every test step – Eq. (14):

$$RPA > -0{,}0016 \cdot \bar{v}_k + 0{,}1755 \quad \text{for } \bar{v}_k \leq 94{,}05 \text{ km/h} \tag{15}$$

$$RPA > 0{,}025 \quad \text{for } \bar{v}_k > 94{,}05 \text{ km/h} \tag{16}$$

the trip is valid.

3. Determing the test route

Several driving trips were performed in order to outline the test route. Three test vehicles were used to perform the trips. Technical data of those vehicles are presented in Table 2 below.

Table 2. Parameters of vehicles used to delineate RDE route

	Vehicle I	Vehicle II	Vehicle III
Production year	2017	2008	2017
Engine displacement	1598 cm^3	1798 cm^3	1502 cm^3
Drive unit power	100 kW	92 kW	105 kW
Type of fuel	Diesel oil	Petrol	Petrol
Vehicle category	M1	M1	M1
Vehicle mass	1375 kg	1340 kg	1690 kg

After every attempt to outline the trip route, an analysis of the resulting data was performed, based on which it was determined whether its requirements were met. PEMS-Semtech DS measuring equipment – among others – was used for this purpose [5–7]. Table 3 and Table 4 presents parameters of the test trips.

Having fulfilled requirements for a route, a series of measurements was carried out to verify the accuracy of the obtained results. The outlined test route is shown in Fig. 6 below.

Fig. 6. Test route

Table 3. RDE test parameters – test example (unfulfilled test)

Test accuracy			
Test parameter	Result	Requirement	Correctness
Urban route [km]	27.78	> 16	Correct
Rural route [km]	20.76	> 16	Correct
Motorway route [km]	14.49	> 16	Incorrect
Overall route [km]	63.04	> 48	Correct
Urban share [%]	44.07	29–44	Incorrect
Rural share [%]	32.94	33 ±10	Correct
Motorway share [%]	22.99	33 ±10	Incorrect
Average speed in urban route [km/h]	31.80	15–40	Correct
Share of downtime in urban route [%]	16.18	6–30	Correct
Trip time above 100 km/h [min]	7.13	> 5	Correct
Max. driving speed [km/h]	126.00	< 160	Correct
Trip time above 145 km/h	0.00	< 3	Correct
Duration of trip [min]	77.97	90–120	Incorrect
Dynamic test conditions			
Urban: number of data $a > 0.1$ m/s^2	956	> 150	Correct
Rural: number of data $a > 0.1$ m/s^2	272	> 150	Correct
Motorway: number of data $a > 0.1$ m/s^2	140	> 150	Incorrect
Urban: average speed [km/h]	31.80		
Rural: average speed [km/h]	70.26		
Motorway: average speed [km/h]	111.24		
Urban: 95th centile $V.a_{pos}$ [m^2/s^3]	12.27	< 18.765	Correct
Rural: 95th centile $V.a_{pos}$ [m^2/s^3]	16.42	< 23.995	Correct
Motorway: 95th centile $V.a_{pos}$ [m^2/s^3]	15.43	< 27.220	Correct
Urban: RPA [m/s^2]	0.14	> 0.125	Correct
Rural: RPA [m/s^2]	0.06	> 0.063	Correct
Motorway: RPA [m/s^2]	0.06	> 0.025	Correct

Table 4. RDE test parameters – test example (fulfilled test)

Test accuracy			
Test parameter	Result	Requirement	Correctness
Urban route [km]	32.51	> 16	Correct
Rural route [km]	28.42	> 16	Correct
Motorway route [km]	29.21	> 16	Correct
Overall route [km]	90.14	> 48	Correct
Urban share [%]	36.06	29–44	Correct
Rural share [%]	31.53	33 ±10	Correct
Motorway share [%]	32.41	33 ±10	Correct
Average speed in urban route [km/h]	33.29	15–40	Correct
Share of downtime in urban route [%]	13.54	6–30	Correct
Trip time above 100 km/h [min]	14.57	> 5	Correct
Max. driving speed [km/h]	128.00	< 160	Correct
Trip time above 145 km/h	0.00	< 3	Correct
Duration of trip [min]	97.95	90–120	Correct
Dynamic test conditions			
Urban: number of data $a > 0.1$ m/s^2	1039	> 150	Correct
Rural: number of data $a > 0.1$ m/s^2	393	> 150	Correct
Motorway: number of data $a > 0.1$ m/s^2	309	> 150	Correct
Urban: average speed [km/h]	33.29		
Rural: average speed [km/h]	71.54		
Motorway: average speed [km/h]	112.84		
Urban: 95th centile $v.a_{pos}$ [m^2/s^3]	13.92	< 18.968	Correct
Rural: 95th centile $v.a_{pos}$ [m^2/s^3]	18.36	< 24.170	Correct
Motorway: 95th centile $v.a_{pos}$ [m^2/s^3]	18.60	< 27.338	Correct
Urban: RPA [m/s^2]	0.14	> 0.122	Correct
Rural: RPA [m/s^2]	0.07	> 0.061	Correct
Motorway: RPA [m/s^2]	0.08	> 0.025	Correct

The specified test route fulfils the requirements imposed by the legislator. It supplements the WLTC test procedure. The test route is characteristic for Warsaw and allows for conducting studies on emissions consistent with the requirements of the prevailing WLTC procedure.

4. Summary

Further RDE tests along the outlined route shall be performed to compare the results obtained from the Averaging Window Method and from other methods of determining exhaust emissions in on-road tests, i.e. the method using all measurement data and power binning method.

Nomenclature

BEV	Battery Electric Vehicle
EV	Electric Vehicle
FCEV	Fuel Cell Electric Vehicle
NEDC	New European Driving Cycle
RDE	Real Driving Emissions
WLTP	Worldwide harmonised Light Duty Vehicle Test Procedure

Bibliography

[1] Commission Regulation (EU) 2016/427 of 10 March 2016 amending Regulation (EC) No 692/2008 as regards emissions from light passenger and commercial vehicles (Euro 6).

[2] Commission Regulation (EU) 2016/646 of 20 April 2016 amending Regulation (EC) No 692/2008 as regards emissions from light passenger and commercial vehicles (Euro 6)

[3] Commission Regulation (EU) 2017/1154 of 7 June 2017 amending Regulation (EU) 2017/1151 supplementing Regulation (EC) No 715/2007 of the European Parliament and of the Council on type-approval of motor vehicles with respect to emissions from light passenger and commercial vehicles (Euro 5 and Euro 6) and on access to vehicle repair and maintenance information, amending Directive 2007/46/EC

of the European Parliament and of the Council, Commission Regulation (EC) No 692/2008 and Commission Regulation (EU) No 1230/2012 and repealing Regulation (EC) No 692/2008 and Directive 2007/46/EC of the European Parliament and of the Council as regards real-driving emissions from light passenger and commercial vehicles (Euro 6)

[4] Commission Regulation (EU) 2018/1832 of 5 November 2018 amending Directive 2007/46/EC of the European Parliament and of the Council, Commission Regulation (EC) No 692/2008 and Commission Regulation (EU) 2017/1151 for the purpose of improving the emission type approval tests and procedures for light passenger and commercial vehicles, including those for in-service conformity and real-driving emissions and introducing devices for monitoring the consumption of fuel and electric energy

[5] MERKISZ, J., PIELECHA, J. Selected remarks about RDE test. *Combustion Engines*. 2016, **166**(3), 54-61.

[6] MERKISZ, J., PIELECHA, J., JASIŃSKI, R. Remarks about real driving emissions tests for passenger cars. *Archives of Transport*. 2016, **39**(3), 51-63.

[7] Product Guide, AVL Gas PEMS, AVL List GmbH, Graz 2012.

Wojciech Gis, DSc., DEng. – Professor in Motor Transport Institute.
e-mail: *wojciech.gis@its.waw.pl*

Prof. Jerzy Merkisz, DSc., DEng. – Faculty of Transport Engineering, Poznan University of Technology.
e-mail: *jerzy.merkisz@put.poznan.pl*

Prof. Jacek Pielecha, DSc., DEng. – Faculty of Transport Engineering, Poznan University of Technology.
e-mail: *jacek.pielecha@put.poznan.pl*

Prof. Stanisław Kruczyński, DSc., DEng. – Environment Protection Centre, Motor Transport Institute.
e-mail: *stanislaw.kruczynski@its.waw.pl*

Maciej Gis, DEng. – Environment Protection Centre, Motor Transport Institute.
e-mail: *maciej.gis@its.waw.pl*

Article citation info:
MATUSZEWSKA, A., OWCZUK, M. The influence of non-normative fuel on its operational properties. *Combustion Engines*. 2019, **178**(3), 67-70. DOI: 10.19206/CE-2019-310

Anna MATUSZEWSKA
Marlena OWCZUK

CE-2019-312

The influence of non-normative fuel on its operational properties

Fuels that do not meet the requirements of quality standards cannot be used to power vehicle engines. The work involved physicochemical analyses of non-normative fuel and its effect on the operational properties of the powered vehicle. The research fuels were two gasolines, characterized by a reduced resistance to oxidation processes due to their long-term storage. The results were compared to the properties of conventional fuels that met all normative requirements. The studies have shown that the fuel slightly deviating from the standard parameters does not noticeably affect the useful properties of the vehicle.

Key words: *non-normative fuels, long term storage, fuel aging, gasoline*

1. Introduction

All UE countries are obligated to keep 90-day intervention stocks of crude oil as well as liquid fuels and 30-day intervention stocks of natural gas. In Poland, these requirements are regulated by the act from 2007 year on crude oil reserves, petroleum products and natural gas [1]. The increasing demand for gasoline and diesel oil causes that the strategic reserves of fuels also should increase. The fuels intended for storage and to later use of them in vehicles need to meet requirements regulated by the act on the system of monitoring and controlling the quality of fuels [2]. The quality requirements for gasoline are specified in the EN 228 standard and for diesel oil in the EN 590 one. The specifications for fuels are more and more restrictive, so the retention of their quality during long-term storage is problematic. During storage process the properties of fuels deteriorate as a results of changes occurring in their chemical structure. The changes are caused by different factors as: chemical composition, atmospheric conditions, presence of inhibitors or activators of oxidation reactions and type of the storage tank. The presence of oxygen and free radicals lead to autoxidation, polymerization and condensation of fuels compounds. As a result of these processes the gums are formed and the stability of fuels is decreased [6, 8, 9]. It is difficult to specify universal mechanism of oxidation of petroleum products and in the literature we can find many theories concern this process [4]. The reason of such situation is – among others – complex and different chemical structure and sensitivity to degradation processes of the fuels. Moreover, addition of biocomponents to the fuels (FAME to diesel and bioethanol to gasoline) accelerates oxidation and caused that these mechanism are different and more complex [3, 5, 7]. In order to minimize adverse phenomena during fuel storage, various types of additives are added at the stage of its production. The additives improve – among others – chemical stability, resistance to corrosion and growth of microorganisms as well as low temperature properties of fuels.

Fuels that do not meet all quality requirements must not be used to power vehicle engines. Under the current regulations, such fuels should be disposed as hazardous waste. For this reason, in the literature, there is no research on the impact of aged fuel after long-term storage on behavior of the vehicle. The authors of this paper conducted research to determine the influence of non-normative fuel on operational properties of the vehicle.

2. The research object and methods

Authors investigated the influence of non-normative fuel on the operational properties of vehicles. The tests were carried out at the Automotive Industry Institute (PIMOT) in Warsaw. The research materials were two fuels:

– 95 octane gasoline, containing up to 5% (v/v) bioethanol (denoted as Pb 95),
– 98 octane gasoline, without bioethanol, containing about 12.6% (v/v) ETBE (denoted as Pb 98).

The physicochemical properties of tested gasolines according to the EN ISO 228 standard were performed before operational tests. The tests were carried out in the PIMOT Analytical Laboratory. Both gasolines did not meet the requirements for the existent gum content of fuel, as shown in Table 1. In terms of other fuel parameters, the tested gasolines met the requirements of the EN ISO 228 standard.

Table 1. Parameters that were not met by tested gasolines

Parameter	Fuel	Test result	Standard requirements
The existent gum content [mg/100 ml]	Pb 95	22	max 5
	Pb 98	20	

Operational tests were conducted in the PIMOT Vehicle Research Laboratory and in the PIMOT Vehicle Control Station. The following parameters were tested:

– fuel consumption and effective power of the engine, on the Schenk Komeg EMDY 48 chassis dynamometer,
– exhaust emissions from vehicle engine (CO, CO_2, HC, NO_x) at idle speed and at speed above idle, using the Capelec CAP 3201-4GAZ flue gas analyser,
– dynamic acceleration of the vehicle in the following speed ranges: (0–100) km/h, (60–100) km/h on the third gear and (80–120) km/h on the fourth gear, using the RaceLogic device.

The tests were carried out for two years, on two selected vehicles, with spark ignition engines and with similar technical parameters, presented in Table 2.

The obtained test results were compared with the results for the reference fuel, which was a commercial gasoline that met the requirements of the EN 228 standard. Addi-

tionally, to check the influence of non-normative fuel on the lubricating oil properties, the samples of engine oil were tested during operational tests.

Table 2. Technical data for tested vehicles

Parameter	Vehicle 1	Vehicle 2
Brand	Skoda	Skoda
Model	Octavia	Octavia
Body styles	Sedan	Sedan
Year of production	2005	2005
Type of fuel	Gasoline	Gasoline
Mileage [km]	301 887	279 897
Engine capacity [cm^3]	1781	1781
Nominal power of engine [kW]	110	110
Top speed [km/h]	217	217

Physical and chemical tests of the oil were carried out in the PIMOT Analytical Laboratory. The samples of lubricating oil were collected periodically during each engine oil change. The lubricating oil was changed after changing the test fuel. Changes in the properties of the oil were compared with the parameters of fresh oil and oil obtained after the reference fuel operational test. During operational tests the fully synthetic commercial engine 5W-40 class oil was used to lubricate the engines of both tested vehicles. The tested parameters of oil samples and used test methods are presented in Table 3.

Table 3. The tested parameters of oil samples and used test methods

Parameter	Method
Kinematic viscosity at temperature 100˚C	EN ISO 3104
Kinematic viscosity at temperature 40˚C	EN ISO 3104
Contamination content	Own method
Fuel content	PN/C-04083
Carbon residue – Micro method	EN ISO 10370
Flash point – Pensky-Martens closed cup method	EN ISO 2719

3. Research results

Table 4 presents the average results of the concentration of particular components of the exhaust gases, obtained from the vehicle 1, while in Table 5 from the test of vehicle 2.

Table 4. Average concentration of the exhaust gases components from vehicle 1

No.	Type of fuel	Number of kilometers	CO [% v/v]	CO_2 [% v/v]	HC [ppm v/v]	NO_x [ppm v/v]	λ
0	Reference	15 569	0.09	15.4	49.5	20.0	1.035
1	PB 95	16 969	0.23	15.0	84.5	58.0	1.085
2	PB 95	19 545	0.05	15.2	41.5	21.0	1.032
3	PB 95	23 993	0.15	14.9	68.0	42.5	1.023
4	PB 95	26 012	0.01	15.7	47.0	10.5	1.011
5	PB 95	27 204	0.13	15.6	65.0	63.0	0.998
6	PB 95	30 040	0.11	15.6	39.5	72.5	1.002
7	PB 95	31 420	0.02	15.8	37.0	10.0	1.007
8	PB 98	33 953	0.17	15.3	94.5	82.5	0.999
9	PB 98	36 186	0.02	15.5	42.5	22.0	1.009
10	PB 98	44 454	0.04	15.9	29.0	32.5	1.005
11	PB 98	46 744	0.10	15.7	59.5	12.5	1.005
12	PB 98	48 703	0.05	14.6	46.0	33.0	1.000
13	PB 98	51 919	0.13	15.7	26.5	68.0	1.000

The test results presented in Tables 4 and 5 indicated that there was no correlation between the concentration of exhaust components and the type of fuel used. Average concentrations of exhaust components were within following limits:

- CO: (0.05–0.23)% v/v for vehicle 1 and (0.05–0.59)% v/v for vehicle 2,
- HC: (26.5–94.5) ppm for vehicle 1 and (10.0–90.5) ppm for vehicle 2,
- NO_x: (10.0–82.5) ppm for vehicle 1 and (13.0–76.5) ppm for vehicle 2.

Values of concentrations of exhaust gases components, recorded during supplying the engine with non-normative fuels, were within wide limits. Results of emission for the reference fuel also were within these limits. It has to be borne in mind, that the analyses for the reference fuel were carried out only once (prior to the commencement of operational tests). According to the Authors, it is likely that in the next test for reference fuel, the concentration of exhaust gases components would also be different (as in the case of non-normative fuels).

Table 5. Average concentration of the exhaust gases components from vehicle 2

No.	Type of fuel	Number of kilometers	CO [% v/v]	CO_2 [% v/v]	HC [ppm v/v]	NO_x [ppm v/v]	λ
0	Reference	14 884	0.32	14.7	39.0	31.0	1.060
1	PB 95	16 111	0.06	15.5	24.5	40.0	1.030
2	PB 95	16 796	0.08	15.6	20.0	22.5	1.060
3	PB 95	17 907	0.37	14.2	28.5	76.5	1.035
4	PB 95	19 011	0.29	13.7	36.5	53.0	1.024
5	PB 95	19 831	0.59	13.9	18.5	13.0	1.060
6	PB 95	22 060	0.12	15.6	10.0	15.0	1.007
7	PB 95	23 785	0.10	15.5	17.0	23.5	1.015
8	PB 95	27 993	0.08	15.5	46.5	13.5	1.008
9	PB 95	33 207	0.32	14.7	15.0	70.0	1.008
10	PB 98	36 118	0.17	15.3	47.0	16.0	1.028
11	PB 98	40 625	0.09	15.6	52.0	28.0	1.013
12	PB 98	44 613	0.12	15.7	13.0	29.5	1.010
13	PB 98	50 697	0.05	15.7	90.5	28.0	1.010

Data in Tables 4 and 5 also indicate differences in gas concentration values for the same fuel (reference or non-normative) for different vehicles and for different measurement periods. These differences may be the result of many factors, including e.g.:

- age of the vehicle (over fourteen years old),
- setting of engine control parameters,
- variable climatic periods of tests conducting (different conditions of vehicle operation depending on the season),
- accuracy and sensitivity of used measuring device,
- measurement methods (location of the measuring probe),
- different chemical composition of fuels, which could have translated into the different course of the combustion process of fuels.

During the operational tests, the vehicles acceleration time also was measured. The average results of these mea-

surements are presented on Fig. 1. On the base of research results concerning the vehicles acceleration time it has been stated that there is no significant influence of non-normative fuels on that parameter. The vehicle acceleration times for both vehicles supplied with non-normative fuels were similar, for three different speed ranges and throughout the research period, to these measured for vehicles fuelled with reference fuels.

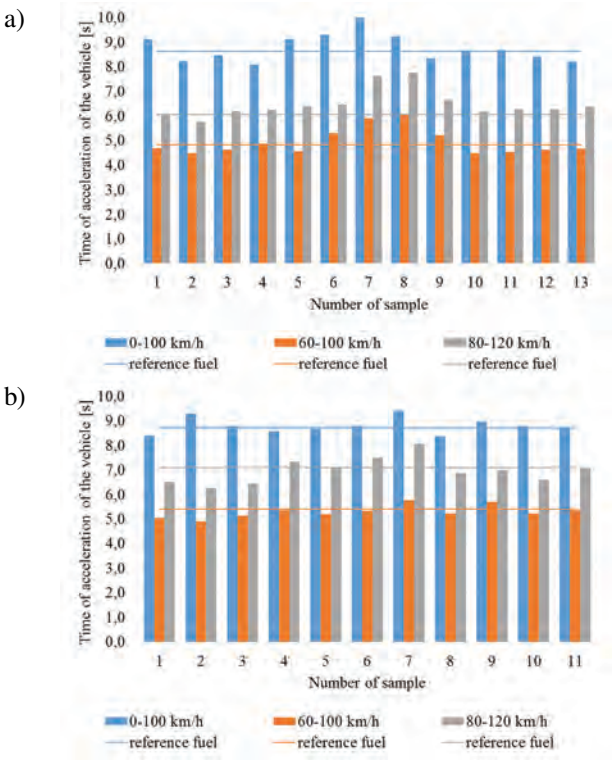

Fig. 1. Average acceleration time of vehicles for: a) vehicle 1, b) vehicle 2

Research results of physicochemical properties of engine oil samples collected during operational test are presented in Tables 6 and 7. Based on the obtained results, it was found that no significant changes in all tested parameters of lubricating oil occurred during operational tests of non-normative fuels in comparison to the reference fuels. Observed changes are typical for used lubricating oil. The samples of engine oil from both vehicles had lower viscosity and ignition temperature value, especially of in case of vehicle 2, what was caused by presence of fuel entered the lubrication system. The content of contamination presented in all oil samples remained low and was at similar level like in fresh oil.

In comparison with fresh engine oil, we observed slight decrease in carbon residue value for all samples of oils after driving tests. This parameter describes the tendency of lubricating oil to form carbonaceous deposits under degradation conditions. The ability to form carbon residue is related to the chemical composition of the oil, especially to the presence of unsaturated, macromolecular chemical compounds. Slight deterioration of this parameter means that used during tests lubricating oil retains its protective properties for a long time and aging processes of oil occurring slow.

Table 6. Physicochemical properties of engine oil samples collected during operational test of vehicle 1

Parameter	Fresh oil	Sample		
Type of fuel	–	Reference	PB 95	PB 98
V100 [mm^2/s]	13.50	12.12	12.40	12.16
V40 [mm^2/s]	84.02	77.86	82.13	78.16
Contamination content [%, m/m]	< 0.005	< 0.005	< 0.005	< 0.005
Carbon residue [%, m/m]	1.14	1.68	1.68	1.82
Fuel content [%, v/v]	0	2.4	2.0	1.8
Flash point [°C]	240	193	230	240

Table 7. Physicochemical properties of engine oil samples collected during operational test of vehicle 2

Parameter	Fresh oil	Sample		
Type of fuel	–	Reference	PB 95	PB 98
V100 [mm^2/s]	13.50	13.22	13.07	12.55
V40 [mm^2/s]	84.02	83.70	80.92	78.41
Contamination content [%, m/m]	< 0.005	< 0.005	< 0.005	0.005
Carbon residue [%, m/m]	1.14	1.86	1.86	1.74
Fuel content [%, v/v]	0	1.6	1.4	1.4
Flash point [°C]	240	222	236	232

4. Conclusions

During two-year operational tests, vehicles fuelled with aged fuels has travelled an average of approximately 51,000 km. During operational tests on a selected group of vehicles, no negative impact of the tested non-normative gasolines on the operational properties of vehicles was found. There were no observed:

- faults,
- problems connected with starting the engine,
- excessive smoke during start-up or heating up of engine,
- deterioration of the acceleration dynamics of tested vehicles
- deterioration of physicochemical properties of engine oil and its losses during operational test.

Performed tests have shown that fuel, which slightly deviates from the normative requirements, does not noticeably affect the useful properties of the vehicle.

Nomenclature

CO	carbon monoxide
CO_2	carbon dioxide
EN	European Norm International
ETBE	ethyl tert-butyl ether
FAME	fatty acid methyl esters
HC	hydrocarbons (equivalent of hexane C_6H_{14})
ISO	Organization for Standardization
NO_X	nitrogen oxides
ON	diesel oil
ON BIO	diesel oil with FAME
Pb 95	unleaded 95 octane gasoline
Pb 98	unleaded 98 octane gasoline

Bibliography

[1] Act of 16 February 2007 on stocks of crude oil, petroleum products and natural gas, the principles of proceeding in circumstances of a threat to the fuel security of the State and disruption on the petroleum market. Journal of Laws No. 52 item 343, with later changes.

[2] Act of 25 August 2006 on fuel quality monitoring and control system. Journal of Laws No. 169 item 1200, with later changes.

[3] CHRISTENSEN, E., MCCORMICK, R.L. Long-term storage stability of biodiesel and biodiesel blends. *Fuel Processing Technology*. 2014, **128**, 339-348. DOI: 10.1016/j.fuproc.2014.07.045.

[4] OWCZUK, M., KOŁODZIEJCZYK, K. Liquid fuel ageing processes in long-term storage conditions. Chapter in: Storage Stability of Fuels (edited by Biernat K.). InTech. 2015, 101-129. DOI: 10.5772/59799.

[5] PEREIRA, C.C., PASA, V.M.D. Effect of alcohol and copper content on the stability of automotive gasoline. *Energy Fuels*. 2005, **19**, 426-432. DOI: 10.1021/ef049849h.

[6] RITA, C.C., PEREIRA, VÂNYA, M.D., PASA. Effect of mono-olefins and diolefins on the stability of automotive gasoline. *Fuel*. 2006, **85**, 1860-1865, DOI: 10.1016/j.fuel.2006.01.022.

[7] SALUJA, R.K., KUMAR, V., SHAM, R. Stability of biodiesel – a review. *Renewable and Sustainable Energy Reviews*. 2016, **62**, 166-181. DOI: 10.1016/j.rser.2016.05.001.

[8] XIONG, Y., SU, P., ZHOU, J., QI, S. Research on the rate prediction model of diesel oxidation in storage. *Chemical Engineering Transactions*. 2016, **51**, 115-120, DOI: 10.3303/CET1651020.

[9] ZANIER, A. Thermal-oxidative stability of motor gasolines by pressure d.s.c. *Fuel*. 1998, **77**, 865-870, DOI: 10.1016/S0016-2361(97)00265-2.

Anna Matuszewska, DEng. – Department of Fuel and Bioeconomy, Automotive Industry Institute.
e-mail: *a.matuszewska@pimot.eu*

Marlena Owczuk, DEng. – Department of Fuel and Bioeconomy, Automotive Industry Institute.
e-mail: *m.owczuk@pimot.eu*

Article citation info:
ORLIŃSKI, P., WOJS, M.K., BEDNARSKI, M., SIKORA, M. Evaluation of the effect of the addition of bioethanol to gas oil on coking diesel engine injector terminals. *Combustion Engines*. 2019, **178**(3), 71-75. DOI: 10.19206/CE-2019-313

Piotr ORLIŃSKI
Marcin K. WOJS
Mateusz BEDNARSKI
Mieczysław SIKORA

CE-2019-313

Evaluation of the effect of the addition of bioethanol to gas oil on coking diesel engine injector terminals

The article presents the results of empirical research and their analysis regarding the impact of diesel oil and diesel oil mixture with bioethanol on coking the test injector nozzles of the XUD9 engine from PSA. The research included three fuel deals: diesel fuel as the base fuel and diesel oil mix with ONE10 bioethanol (10% bioethanol plus diesel oil (V/V)), ONE20 (20% bioethanol plus diesel oil (V/V)). They were conducted on the basis of CEC PF-023 developed by CEC (Coordinating European Council). Each of the above-mentioned fuels was tested using a new set of injectors. The propensity of the fuel for coking the injector tips was expressed as a percentage reduction in the air flow through the nozzles of each injector for the given sheer increments. The test result was the average percentage of airflow reduction for all nozzles at 0.1 mm spike increments and was measured according to ISO 4010 "Diesel engines. Calibrating nozzle, delay pintle type". The test results for individual atomizers of the above-mentioned test engine in the area of sediment formation from flowing fuel shown a lower tendency to coke the injectors using diesel fuel-bioethanol in comparison to the use of pure diesel oil. Based on the CEC PF-023 test, it can be noticed that the level of contamination of the tested injectors for ONE10 fuel is about 3% lower, and for ONE20 fuel is about 4% lower than the level of pollution for diesel fuel.

Keywords: *injection coking, combustion, fuel plant, environmental protection, engine diagnostics*

1. Introduction

More and more stringent emission standards force the automotive industry to conduct research and seek technical solutions to ensure the least possible harmful effect of vehicles on the natural environment [6, 8, 17, 18].

For manufacturers of internal combustion engines, the main goal is to reduce noise, fuel consumption and emissions of toxic exhaust components – mainly from compression-ignition engines. One solution may be to supply combustion engines with fossil fuels with the addition of biofuel, which may be bioethanol [4]. The preparation of such a mixture and its application may reduce the emission of selected components of toxic fumes to the atmosphere [3, 16]. The great advantage of this type of fuels is also their availability. Mainly due to the fact that parts of such a fuel mixture are produced from renewable sources, which are subject of regeneration [2, 7, 14, 21]. One of the areas of research on bioethanol is its impact on the formation of the IDID (Internal Diesel Injector Deposit).

The internal injector deposition (IDID) phenomenon reduces the dynamics of internal injector working parts or their complete blocking. It may causes damage to important components of the engine's fuel supply system [5, 9, 11, 13].

Therefore, a test for coking injectors is very important in the preliminary processes of fuels intended for later commercial use. Thanks to it, we are able to determine the capping of nozzle tips that can cause problems with starting the engine, an uneven operation of the engine, uncontrolled changes in power and torque of the engine, and even its unexpected stop. As a consequence, it has an impact on the durability of the engine's fuel supply system and its operational parameters, such as the amount of fuel consumption or the level of emissions of selected toxic components of exhaust gases into the atmosphere [12, 15, 20].

2. Research purpose

The aim of the research is to analyze and evaluate the coking of the ends of injectors a self-ignition engine powered with liquid fuels of alternative vegetable origin. Empirical studies were carried out for diesel oil (ON) and a mixture of this fuel with bioethanol: ONE10 (10% bioethanol plus diesel) and ONE20 (20% bioethanol plus diesel). The tests were carried out on a test bench equipped with the XUD9A test engine used for this type of research by many research centres. The tests included assessing the degree of coking of atomizers in accordance with the CEC PF-023 procedure.

3. Physicochemical properties of fuels

For proper operation of the combustion engine, fuel with strictly defined physical and chemical properties is needed. Power systems have properties and constraints related to their construction and control, which are adapted to the appropriate physicochemical properties used in fuel engines [1, 10, 19].

For empirical studies, diesel oil (ON) and bioethanol (E) were used as a component of the mixture. Table 1 presents the physicochemical properties of the basic fuels used in the tests.

Table 1. Basic physicochemical properties of engine fuels used in tests

Parameter	Unit	Diesel fuel	Bioethanol
Cetane number	–	51.2	10
Heat value	MJ/kg	42.4	27.3
Density at 15°C	g/cm^3	0.836	0,795
Kinematic viscosity	mm^2/s	2.92	0.93
Surface tension	N/m	3,63·10^{-2}	–
Flash-point	°C	13	–
Cloud point	°C	–16	–
The temperature of blocking the cold filter	°C	–34	–

Table 1cont.

Parameter	Unit	Diesel fuel	Bioethanol
Average elementary composition	%		
C		87.3	52.2
H		12.7	13.7
O		0	34.1
Sulfur content S	mg/kg	8	–
Water content	mg/kg	43.5	–
Solid impurities content	mg/kg	4	–
Coke residue in a 10% distillation residue	%(m/m)	0.02	–
Research on the corrosive effect on copper plates		1	–

In addition to diesel fuel, a test mix of this fuel with dehydrated bioethanol with the following composition was also used:

- ONE10 – 89% ON + 0.4% Rokanol O3 + 0.6% Rokok L3S + 10% Bioethanol (E-diesel),
- ONE20 – 78% ON + 1% Rokanol O3 + 1% Rokanol L3S + 20% Bioethanol (E-diesel).

The examined physicochemical properties of the above-mentioned mixtures are presented in Table 2.

Table 2. Selected physicochemical properties of mixtures

Parameter	Unit	Value	
		ONE10	ONE20
Flash-point (open crucible)	ºC	34	32
Cloud point	ºC	< +23	< +23
Density at 15 ºC	kg/m^3	832.5	828.2
Kinematic viscosity at 40 ºC	mm^2/s	2.43	2.27

Blends of diesel oil with bioethanol: ONE10 (10% bio-ethanol plus diesel) and ONE20 (20% bio-ethanol plus diesel) can be, due to their physicochemical properties, substitute fuels for diesel.

4. Research stand and test method

The research stand included:

- XUD9A research engine,
- Schenck W400 electromagnetic brake with a controller enabling constant engine speed,
- Electronic servomotor for setting the injection pump,
- Air consumption measurement system consisting of a laminar flow meter type E 7035 and a pressure difference meter type MK1,
- Standard systems for measuring speed, torque, fuel consumption, oil and coolant temperature, and other devices that meet the requirements of PN-88/S-02005,
- Device for determining injector opening pressure from L. Hartridge Ltd,
- Device for measuring atomizer throughput in accordance with ISO 4010.

The empirical studies of coking of injectors were carried out on a test stand at the Vehicles Institute, Warsaw University of Technology, which is shown in Fig. 1. The sediment formation was evaluated on the basis of CEC PF-023 tests using a new set of injectors for each fuel tested.

The scope of the measurements included the assessment of the degree of coking of the nozzles in accordance with the CEC PF-023 procedure, based on the examination of the propensity to contaminate fuel atomizers. LUCAS RDNO 6887 D 03 CFR type sprayers were used for testing. The tests were carried out in accordance with the above-mentioned standard and in the following order:

- measurement of the throughput of brand new sprays in accordance with ISO 4010,
- setting the injector opening pressure in accordance with the requirements of the CEC PF-023 procedure and mounting them on the engine,
- performing a ten-hour test sample in accordance with the CEC PF-023 procedure,
- capacity measurement of disassembled and contaminated atomizers in accordance with ISO 4010.

Fig. 1. The test stand equipped with XUD9A engine [12]

The propensity of fuel for cooking the injector tips is expressed as a percentage reduction in the air flow through the nozzles of each of the 4 injectors for a given needle lift value.

The test result is the mean value of the percentage air-flow reduction for all 4 nozzles at a needle lift of 0.1 mm.

5. Research results

The tendency of fuels to form sediments is determined by measuring the air flow through the nozzles before and after the test. The result is expressed as the average percentage decrease in air flow through the nozzles. The results of flow rate tests through nozzles are presented in Tables 3–11 and graphically in Figures 2–7.

Table 3. Results of spray flow rate measurements before the test – ON

uplift [mm]	nozzle 1 [cm^3/min]	nozzle 2 [cm^3/min]	nozzle 3 [cm^3/min]	nozzle 4 [cm^3/min]
0.05	201	200	217	225
0.1	250	248	248	258
0.2	255	283	267	283
0.3	303	367	312	317
0.4	417	500	443	432
0.5	800	850	817	867

Table 4. Results of spray flow rate measurements after the test – ON

uplift [mm]	nozzle 1 [cm^3/min]	nozzle 2 [cm^3/min]	nozzle 3 [cm^3/min]	nozzle 4 [cm^3/min]
0.05	93	90	120	110
0.1	133	125	128	130
0.2	147	142	175	173
0.3	183	200	212	223
0.4	283	282	287	375
0.5	567	647	533	763

Table 5. Calculation results – ON

uplift [mm]	R1 [cm^3/min]	R2 [cm^3/min]	R3 [cm^3/min]	R4 [cm^3/min]	average [%]
0.05	53.6%	55.2%	44.6%	51.1%	51.1%
0.1	46.7%	49.5%	48.3%	49.7%	**48.5%**
0.2	42.5%	50.0%	34.4%	38.8%	41.4%
0.3	39.6%	45.5%	32.1%	29.5%	36.6%
0.4	32.0%	43.7%	35.4%	13.1%	31.0%
0.5	29.2%	23.8%	34.7%	11.9%	24.9%

Table 6. Results of spray flow rate measurements before the test – ONE10

uplift [mm]	nozzle1 [cm^3/min]	nozzle2 [cm^3/min]	nozzle 3 [cm^3/min]	nozzle 4 [cm^3/min]
0.05	165	198	215	223
0.1	251	252	249	251
0.2	253	281	264	281
0.3	301	363	309	314
0.4	413	496	439	428
0.5	799	812	819	859

Table 7. Results of spray flow rate measurements after the test – ONE10

uplift [mm]	nozzle 1 [cm^3/min]	nozzle 2 [cm^3/min]	nozzle 3 [cm^3/min]	nozzle 4 [cm^3/min]
0.05	84	90	115	108
0.1	137	134	132	136
0.2	148	145	177	175
0.3	185	202	214	226
0.4	286	277	320	339
0.5	584	599	642	689

Table 8. Calculation results – ONE10

uplift [mm]	R1 [cm^3/min]	R2 [cm^3/min]	R3 [cm^3/min]	R4 [cm^3/min]	average [%]
0.05	49.1%	54.8%	46.4%	51.6%	50.5%
0.1	45.5%	46.8%	47.0%	45.7%	**46.3%**
0.2	41.4%	48.3%	33.1%	37.7%	40.1%
0.3	38.4%	44.4%	30.8%	28.1%	35.4%
0.4	30.7%	44.0%	27.2%	20.8%	30.7%
0.5	26.9%	26.2%	21.7%	19.8%	23.6%

Table 9. Results of spray flow rate measurements before the test – ONE20

uplift [mm]	nozzle 1 [cm^3/min]	nozzle 2 [cm^3/min]	nozzle 3 [cm^3/min]	nozzle 4 [cm^3/min]
0.05	201	200	217	225
0.1	250	248	248	258
0.2	255	283	267	283
0.3	303	367	312	317
0.4	417	500	443	432
0.5	800	850	817	867

Table 10. Results of spray flow rate measurements after the test – ONE20

uplift [mm]	nozzle 1 [cm^3/min]	nozzle 2 [cm^3/min]	nozzle 3 [cm^3/min]	nozzle 4 [cm^3/min]
0.05	100	92	120	110
0.1	140	135	135	143
0.2	156	150	175	173
0.3	198	205	212	223
0.4	293	301	287	375
0.5	645	647	634	663

Table 11. Calculation results – ONE20

uplift [mm]	R1 [cm^3/min]	R2 [cm^3/min]	R3 [cm^3/min]	R4 [cm^3/min]	average [%]
0.05	50.2%	54.0%	44.6%	51.1%	50.0%
0.1	44.0%	45.5%	45.6%	44.6%	**44.9%**
0.2	38.8%	47.1%	34.4%	38.8%	39.8%
0.3	34.7%	44.1%	32.1%	29.5%	35.1%
0.4	29.7%	39.8%	35.4%	13.1%	29.5%
0.5	19.4%	23.8%	22.4%	23.5%	22.3%

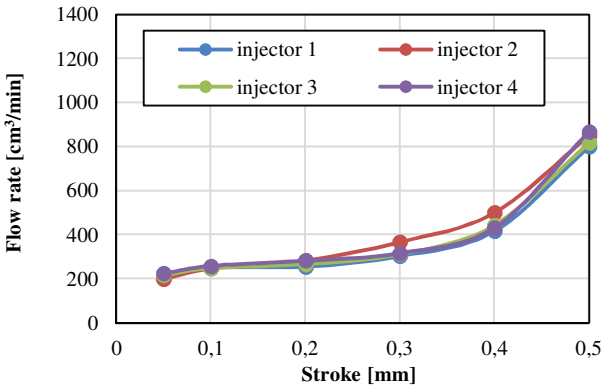

Fig. 2. The flow rate through nozzles before the test for ON fuel

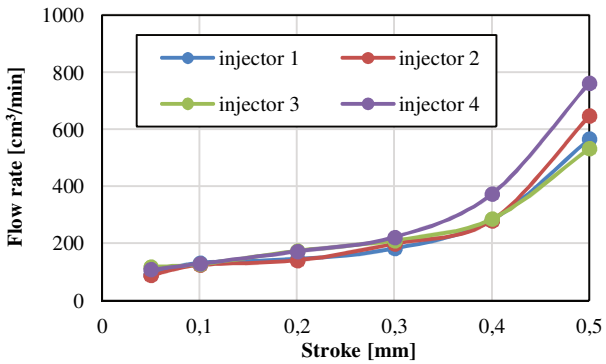

Fig. 3.The flow rate through nozzles after the test for ON fuel

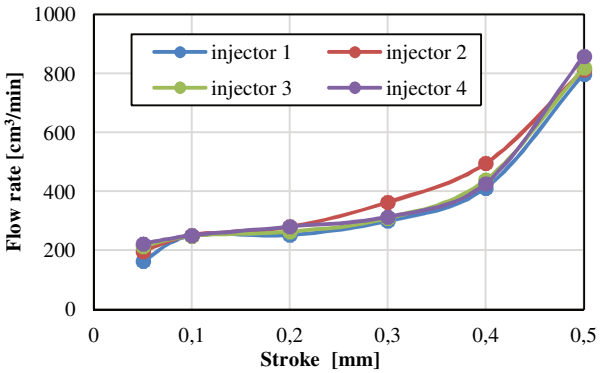

Fig. 4.The flow rate through nozzles before the test for ONE10 fuel

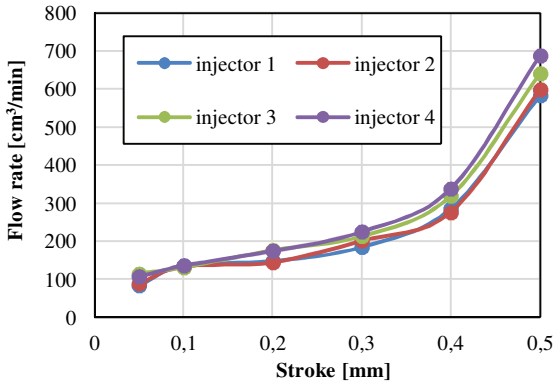

Fig. 5.The flow rate through nozzles after the test for ONE10 fuel

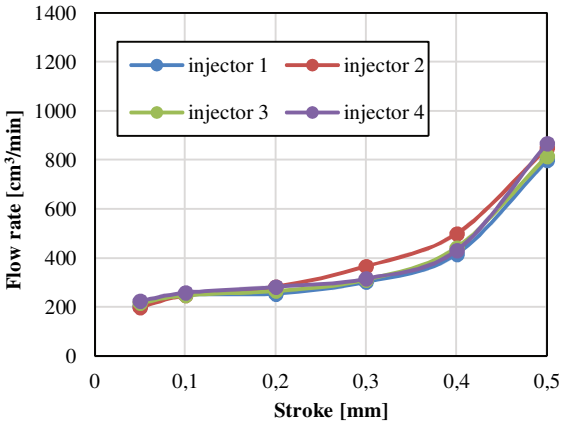

Fig. 6. The flow rate through nozzles before the test for ONE20 fuel

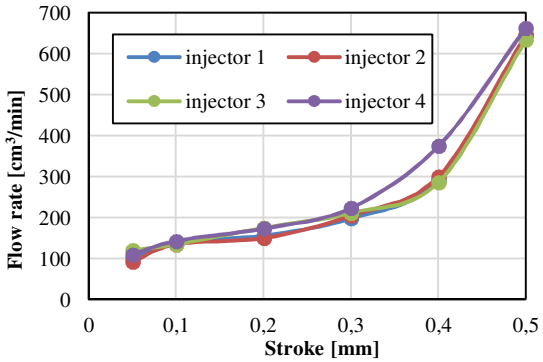

Fig. 7. The flow rate through nozzles after the test for ONE20 fuel

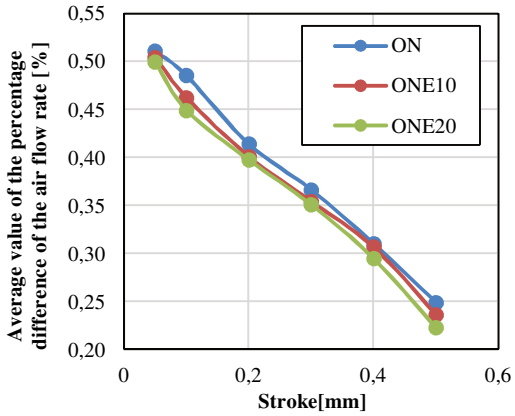

Fig. 8. The average value of the difference in the air flow rate through injectors obtained in the CEC test PF-023 while covering the test engine with three fuels

5. Conclusions

The tests showed a lower tendency to coke the injectors using diesel fuel-bioethanol in comparison to the use of pure diesel oil.

Based on the CEC PF-023 test, it can be noticed that the level of contamination of the tested injectors (at a heel of 0.1 mm) for ONE10 fuel is about 3% lower than the level of diesel injector contamination.

The level of injector coking for ONE20 fuel is about 4% lower than the level of pollution for diesel fuel.

Lower susceptibility to coking the injectors using a mixture of bioethanol and diesel oil compared to the diesel oil itself gives the possibility of reducing deposits at the ends of the injectors.

Surface coking at the tip of the needle tip - the sprayer and nozzle openings reduce or block the flow of fuel through the injector and change the spraying quality and microstructure of the sprayed stream. In addition, the contamination of the injector tip reduces the distance of the diffusion flame to the injector causing heat exchange between the deposits and deposits created in the sprayer, not with the spray of fuel creating a rich fuel-air mixture, which causes a slower combustion process and increased particulate matter emission.

In summary, sediments have a negative impact on the operation of injectors in CI engines. The problem is important from the point of view of their durability and reliability because their components have small dimensions, low mass and are manufactured with high accuracy using very advanced techniques. In contrast, the tolerance of performance of individual cooperating elements has a direct impact on the time and size of injection doses. All this indicates that the tendency to injectors coking is a considerable problem, which can be partially eliminated with the addition of bioethanol to diesel oil.

Nomenclature

ON	diesel oil
ONE10	10% bioethanol + diesel
ONE20	20% bioethanol + diesel
E	bioethanol
R1	injector 1
R2	injector 2
R3	injector 3
R4	injector 4
IDID	Internal Diesel Injector Deposit

Bibliography

[1] BEDNARSKI, M., SAMOILENKO, D., ORLIŃSKI, P., SIKORA M. Evaluation of the diesel engine parameters after regeneration of its fuel delivery system. *Transp. Means – Proc. Int. Conf.* 2017, **2**, 547-553.

[2] DHARMA, S., ONG, H.C., MASJUKI, H.H. et al. An overview of engine durability and compatibility using biodiesel–bioethanol–diesel blends in compression-ignition engines. *Energy Convers. Manag.* 2016, **128**, 66-81.

[3] HERREROS, J.M., SCHROER, K., SUKJIT, E., TSOLAKIS, A. Extending the environmental benefits of ethanol–diesel blends through DGE incorporation. *Appl. Energy*. 2015, **146**, 335-343.

[4] KHAN, Z., DWIVEDI, A.K. Fermentation of biomass for production of ethanol: a review. *Univers. J. Environ. Res. Technol.* 2013, **3**, 1-13.

[5] KIM, Y., SONG, H. Effects of injector design parameter on nozzle coking in diesel engines. J. *ILASS-Korea*. 2012, **17**, 140-145.

[6] KRUCZYŃSKI, S., GIS, W., ORLIŃSKI, P., SIKORA, M. Influence of the use of ethanol fuel on selected parameters of the gasoline engine. *IOP Conf. Ser. Mater. Sci. Eng.* 2018, **421**, 042041.

[7] KUSZEWSKI, H. Experimental investigation of the effect of ambient gas temperature on the autoignition properties of ethanol–diesel fuel blends. Fuel. 2018, **214**, 26-38.

[8] LASOCKI, J., BEDNARSKI, M., SIKORA, M. Simulation of ammonia combustion in dual-fuel compression-ignition engine. *IOP Conf. Ser. Earth Environ. Sci*. 2019, **214**, 012081.

[9] LEE, C.-W., REITZ, R.D., KURTZ, E. The impact of engine design constraints on diesel combustion system size scaling. 2010, *SAE Technical Paper* 2010-01-0180.

[10] MAZURUK, P., WOJS, M., ORLIŃSKI, P., SIKORA, M. Detection of damage to the power supply system of diesel engine under field conditions. *Combustion Engines*. 2017, **56**, 159-163.

[11] MONTANARO, A., ALLOCCA, L. Impact of the nozzle coking on spray formation for diesel injectors. 2013, *SAE Technical Paper* 2013-01-2546.

[12] ORLIŃSKI, P., WOJS, M., MAZURUK, P., KRUCZYŃSKI, P. Influence of biodiesel on injection nozzle coking. *Combustion Engines*. 2015, **162**(3), 599-607.

[13] RISBERG, P.A., ADLERCREUTZ, L., GÓMEZ AGUILERA, M. et al. Development of a heavy duty nozzle coking test. 2013, *SAE Technical Paper* 2013-01-2674.

[14] SAKTHIVEL, P., SUBRAMANIAN, K.A., MATHAI, R., Indian scenario of ethanol fuel and its utilization in automotive transportation sector. *Resour. Conserv. Recycl*. 2018, **132**, 102-120.

[15] SCHUCKERT, S., WACHTMEISTER, G. Characteristics of control piston motion and pressure inside of a common rail diesel injector. *Proc. ILASS–Europe 2017. 28th Conf. Liq. At. Spray Syst.*, Valencia 2017.

[16] SHAHIR, S.A., MASJUKI, H.H., KALAM, M.A. et al. Performance and emission assessment of diesel–biodiesel–ethanol/bioethanol blend as a fuel in diesel engines: A review. *Renew. Sustain. Energy Rev*. 2015, **48**, 62-78.

[17] SIKORA, M., BEDNARSKI, M., LASOCKI, J. et al. Ammonia as a fuel for spark-ignition engines. *Zesz. Nauk. Inst. Pojazdów/Politech. Warsz.* 2017, **5**(114).

[18] SIKORA, M., ORLIŃSKI, P., BEDNARSKI, M., WOJS, M. Evaluation of the heat release rate in the combustion chamber of the self-ignition engine powered by sunflower methyl esters. *Proc. Inst. Veh*. 2018, **1**(115)/201, 27-34.

[19] STANIK, W., JAKÓBIEC, J., WĄDRZYK, M. Design factors affecting the formation of the air-fuel mixture and the process of combustion in compression ignition engines. *Combustion Engines*. 2013, **154**(3), 40-50.

[20] STANIK, W., MAZANEK, A., JAKÓBIEC, J. Badania oleju napędowego zawierającego 7%(v/v) FAME i dodatek cetanowy w zakresie oceny użytkowej i czystości wtryskiwaczy czopikowych. *Combustion Engines*. 2015, **54**(3), 933-943.

[21] SUHAIMI, H., ADAM, A., MRWAN, A.G. et al. Analysis of combustion characteristics, engine performances and emissions of long-chain alcohol-diesel fuel blends. *Fuel*. 2018, **220**, 682-691.

Piotr Orliński, DSc., DEng. – Faculty of Automotive and Construction Machinery Engineering, Warsaw University of Technology.
e-mail: *piotr.orlinski@pw.edu.pl*

Mateusz Bednarski, MEng. – Faculty of Automotive and Construction Machinery Engineering, Warsaw University of Technology.
e-mail: *mateusz.bednarski@pw.edu.pl*

Marcin K. Wojs, DEng. – Faculty of Automotive and Construction Machinery Engineering, Warsaw University of Technology.
e-mail: *marcin.wojs@pw.edu.pl*

Mieczysław Sikora, MEng. – Faculty of Automotive and Construction Machinery Engineering, Warsaw University of Technology.
e-mail: *mieczyslaw.sikora@pw.edu.pl*

Article citation info:
ANDRZEJEWSKI, M., PIELECHA, I., MERKISZ, J. et al. Nowoczesne układy napędowe pojazdów szynowych. *Combustion Engines.* 2019, **178**(3), 76-81. DOI: 10.19206/CE-2019-314

Maciej ANDRZEJEWSKI
Ireneusz PIELECHA
Jerzy MERKISZ
Robert ŚWIECHOWICZ
Mateusz NOWAK

CE-2019-314

Modern drive systems of rail vehicles

Rail vehicles are one of the sources of environmental pollution in the transport sector. Therefore, it is necessary to equip these vehicles with modern drive systems. This article concerns the issues of contemporary and future-oriented solutions of drive systems used in rail vehicles. The article analyzes energy storage possibilities including: electrochemical, mechanical and hydraulic accumulators. The conducted analyzes have taken into account the importance of how frequently they charge up, which dictates their possible applications. Characteristics of hybrid drive systems were presented, with particular emphasis on parallel systems of: hydrostatic, flywheels and electrochemical batteries. The analysis of energy flow control strategies in hybrid drive systems of railway vehicles has been made. In the summary, a solution was chosen that resulted in high conversion efficiency of the energy extracted from the vehicle's wheels.

Keywords: *rail vehicles, combustion engines, hybrid drive systems*

1. Introduction

In recent years, the share of CO_2 emissions from the transport sector has been steadily increasing (Fig. 1). This share of CO_2 emissions has increased from 22.7% in 2010 to 23.4% in 2013 [24]. In 2013, carbon dioxide emissions from rail transport reached 3.5%, while it accounted for 8% of the world's passenger and freight volume. The railway sector in 2013 also accounted for just 2% of the total energy consumed in the transport sector. Rail vehicles were fueled with petroleum products in 57% of cases, and in 36.4% of cases with electricity.

In 2013, six regions and countries (EU28, USA, Russia, China, India, Japan) accounted for 78% of total CO_2 emissions in the rail sector, of which one quarter were emitted by China.

Coal consumption by the rail sector drastically decreased in 1990-2013. In the same period, electricity consumption in rail transport increased from 17.2% to 36.4%.

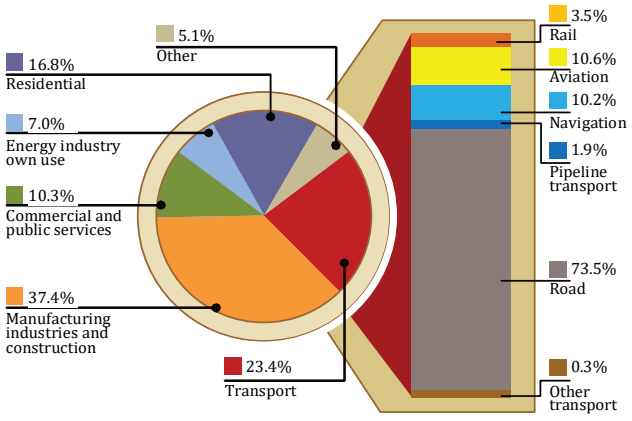

Fig. 1. Carbon dioxide emission as a result of fossil fuel combustion in various industry and transport sectors [24]

The share of electrified railway lines increased by 163% in the span between 1975-2013 at the global level. China and Korea increased their share by 325% and 343% respectively between 1990-2013.

In 2013, the specific energy consumption in passenger rail transport reached 138 kJ/km, whereas this volume in rail freight transport amounted to 129 kJ/tkm. The energy consumption in this transport sector in the years 1975-2013 decreased by 63% and 48% respectively for passenger and freight transport. Individual emissions of carbon dioxide in the railway sector show a similar improvement rate: they were reduced by 60% in passenger transport and by 38% in freight transport in the years 1975-2013.

2. Energy storage systems in rail transport vehicles

The constant pursuit of reducing emissions from transport means has lead to restrictions also being applied to rail vehicles. The introduction of subsequent exhaust emission limits in relation to rail traction vehicles means that the currently applicable EU legal acts include Stage III B and Stage V limits. The latter limit is in force for new vehicle approvals from this year onwards [7, 20]. Despite the trend where the share of drives relying on combustion engines in the total number of rail vehicles continues to decrease, there is a tendency to replace the conventional combustion systems with hybrid systems [5, 15]. Meinert et al. [16] proposed the use of energy storage systems (ESS) in rail vehicles, such as: hydrostatic systems, batteries, flywheels and double-layer capacitors (DLC). The energy management strategy is focused on reducing fuel consumption and minimizing the toxic exhaust emissions. In paper [16] the authors stated that the use of additional energy storage technologies is not enough to eliminate exhaust after-treatment systems from engines that are to comply with Stage III B standards. This is the result of testing the exhaust emissions of rail vehicle engines according to the ISO 8178. Which is done under specific engine load conditions, e.g. at the point of maximum load, in which additional circuits (electric or other) do not properly fulfill their task.

Ghaviha et al. [9] divided energy storage systems into stationary systems (SESS – stationary) and systems inside railway vehicles (OESS – On-board). The authors also point to the use of currently ultra-capacitors, batteries and flywheels in rail vehicles in both SEES and OESS systems.

The system that has been in use the longest is the flywheel (used in Japan since 1970) [9].

Research conducted by Rupp et al. [21] indicate the possibilities of using flywheels to reduce the energy consumption by 9 to 31% (depending on the traffic conditions of light rail vehicles).

Energy storage methods in means of transport have been presented in Fig. 2. Possibilities of using energy storage systems in the context of vehicle power, energy and discharging time were presented in Fig. 3.

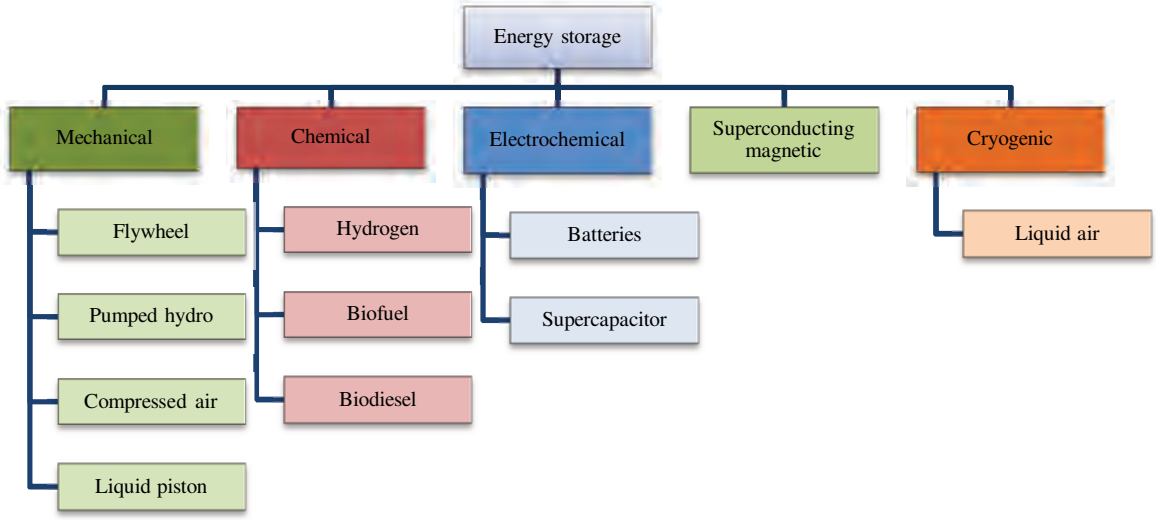

Fig. 2. Energy storage systems classification tree [2]

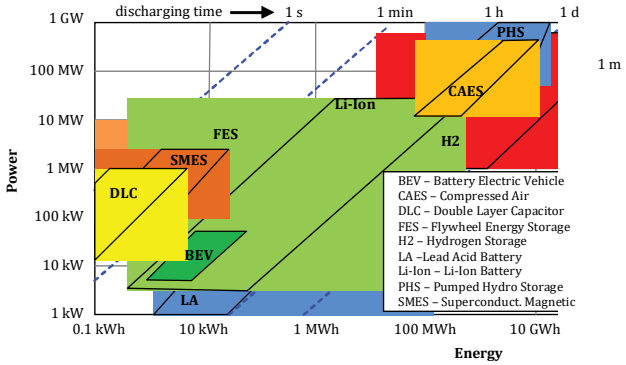

Fig. 3. Comparison of power, energy and discharging time of typical energy storage systems [10]

3. Railway vehicle hybrid drive systems constructions

3.1. Introduction

Hybrid drive systems used in rail vehicles may be equipped with:

a) hydrostatic systems (hydraulic),
b) flywheels,
c) lithium-ion batteries

and others.

Hydraulic drive systems include hydraulic motors/pumps whose power is greater than 4 kW/kg, and with efficiency of over 93%. In addition, the power density of hydraulic accumulators is about 10 times greater than that of electrochemical batteries and is about 5 kW/kg. Unfortunately, the energy density is about 15 times lower with respect to Li-Ion batteries – 4–11 kJ/kg [22].

Comparison of power and energy indicators for different batteries reveals the different parameters of these batteries. Electrochemical systems (both NiMH and Li-Ion batteries) have a much higher energy density than power densities (Fig. 4). Therefore, their use in rail vehicles significantly increases the vehicle range.

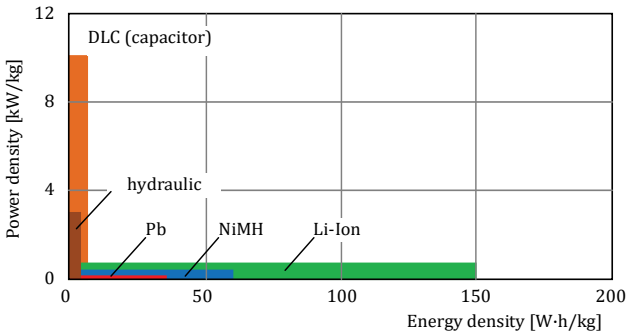

Fig. 4. Comparison of power and energy density of available batteries [11]

The use of hydraulic or ultra-capacitor systems does not provide similar energy density values. However, the high power density of the ultracapacitors allows them to be used in heavy vehicles. High power density energy storage systems allow them to be quickly charged, and this results in them being more effective when used in conditions of frequent stops.

It is possible to categorize the following hybrid drive solutions (based on compression-ignition diesel engines):

a) hybrid parallel hydrostatic drive (hydraulic),
b) hybrid parallel drive with a flywheel (mechanical),
c) hybrid parallel drive with an ultra-capacitor system,
d) diesel-electric (battery) hybrid drive system,
e) diesel-electric (battery and ultracapacitors) hybrid drive system.

3.2. Hydrostatic systems

Hybrid parallel hydrostatic drive (hydraulic) is presented in Fig. 5. The coupling (gear) is mounted between the electric motor (MG) and the main transmission. It is a system in which the combustion engine is connected in parallel with the hydraulic system.

A different construction is presented in Fig. 6. It also contains a parallel connection of the hydraulic drive with the internal combustion engine, the generator and the electric motor connected in series. In this solution, the combustion engine is used only to drive the current generator (reference G in Fig. 5). In the mechanical transmission, the torque values are added up from the hydraulic system and from the electric motor system (MG).

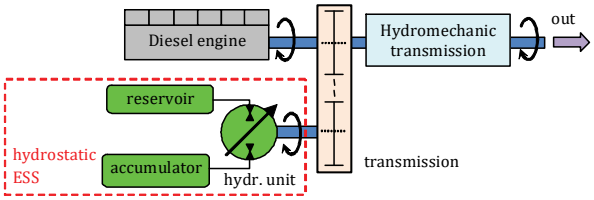

Fig. 5. A parallel hybrid drive of an internal combustion engine with a hydromechanical transmission and a hydrostatic system [17]

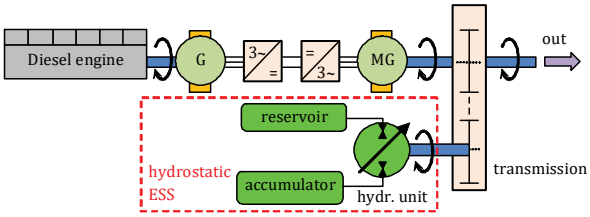

Fig. 6. A parallel hybrid drive of a hydrostatic system and a serial connection of a combustion engine with a generator and an electric motor [17]

The layout shown in Fig. 5 is currently implemented, among others by Bosch-Rexroth [4] and Plasser & Theurer (Fig. 7).

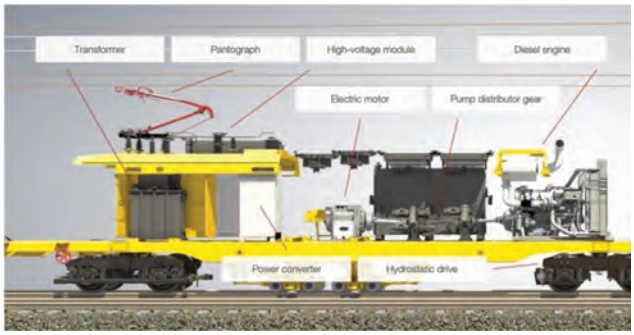

Fig. 7. The hybrid drive of a rail vehicle with a hydrostatic system (09-4X Dynamic Tamping Express E3 and the BDS 2000 E3 - Plasser & Theurer) [25]

Hydraulic motors have not only higher efficiency than electric motors, but in addition – they generate similar torque values – they have much smaller dimensions (Fig. 8). Such conditions allow these systems to be used even in passenger cars as well as placing the hydraulic motors at the wheels of the vehicle (or on the wheels themselves).

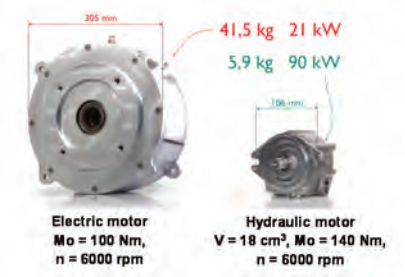

Fig. 8. Technical parameters comparison of electric and hydraulic motors [1]

3.3. Hybrid systems with flywheels in rail vehicles

Another solution for hybrid systems in rail vehicles is the use of flywheels (Fig. 9). The main parameters of flywheels used in rail vehicles include:

a) rotational speed in the range of 25,000–30,000 rpm,
b) the value of available energy from the range of 6 kWh to 12 kWh, of which about 75% can be used (no work generated at low rotational speeds),
c) energy density of approximately 2 kWh/m^3,
d) average charging and discharging time (flywheels are placed between ultracapacitors and electrochemical batteries),
e) efficiency of about 90%.

An example of a solution for parallel hybrid drive with a combustion engine and flywheel is shown in Fig. 9. The flywheel in this solution serves as the drive system of the current generator in a serial connection with an electric motor. In such a system, recovery of flywheel energy requires two-way operation of both electrical machines (MG – Fig. 9).

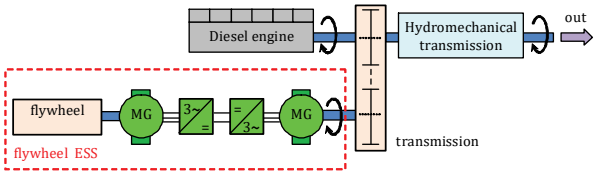

Fig. 9. A parallel hybrid drive with an internal combustion engine and a flywheel connected in series with a generator and an electric motor [17]

The use of an internal combustion engine in a hybrid drive as a current generator and flywheel also for electric current production is shown in Fig. 10. It is a parallel connection of an internal combustion engine (operating in a drive system with a power generator and electric motor connected in series) and a flywheel connected to a power generator. The output drive for the wheels is generated only by an electric motor. The lack of a flywheel system would allow the system to be classified as a series hybrid drive system.

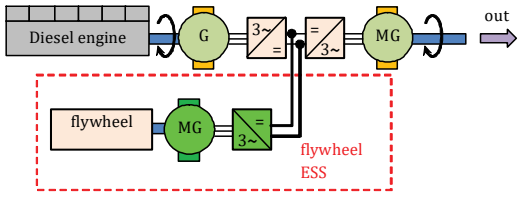

Fig. 10. Parallel hybrid drive with an internal combustion engine (DE) and a flywheel system working in series with an electric motor [17]

An example of the application of this technology in rail vehicles is shown in Fig. 11. The flywheel presented is the result of a project in cooperation between Ricardo Artemis Intelligent Power and Bombardier. The project concerns the reduction of energy consumption by about 10% using high-speed flywheels as sources of kinetic energy storage.

Fig. 11. The flywheel and its components with 220 kJ TorqStor from Ricardo [6]

3.4. Hybrid systems with electrochemical batteries

Electrochemical energy sources are the most widespread energy storage systems. Their high energy density makes it possible to obtain a higher vehicle range than with the use of other energy storage systems: mechanical or hydraulic.

A typical parallel hybrid drive system of an internal combustion engine and an electrochemical battery is shown in Fig. 12. The use of AC motors requires constant voltage converters (from battery) to alternating voltage (higher efficiency values of such motors, especially in the low speed range). In such a system (so-called mild hybrid) one electric machine with reversible operation is used.

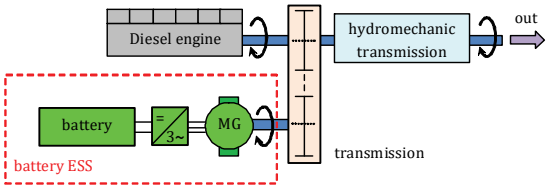

Fig. 12. A hybrid parallel drive of an internal combustion engine (DM) with a hydromechanical transmission, a battery system and an electric motor [14, 17]

The use of an electrochemical battery instead of a flywheel (as in Fig. 10) results in a similar configuration of the parallel hybrid drive with the combination of an internal combustion engine (operated in series with an electric motor) with an electrochemical battery system (Fig. 13).

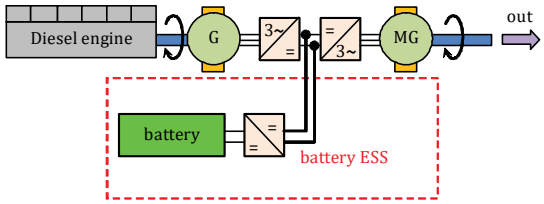

Fig. 13. A parallel hybrid drive of an internal combustion engine (DE) with a system of batteries operating in series with an electric motor in a drive system [17]

The use of electrochemical batteries allows using a configuration, which will provide a high value of power or high value of energy stored. High power density ensures a modular design, while high energy density – appropriate range of the rail vehicle. Examples of such Hitachi battery solutions are shown in Table 1.

Table. 1. Battery configurations in applications for hybrid drive of rail vehicles [18]

Description	High power density	High Energy density
$P = \eta(1-\eta)\frac{U^2}{R}$ $P = \frac{U^2}{4R}$	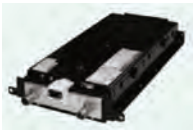	
Model	MA2a	CH75-6
Configuration	48 cells (series)	6 cells (series)
Voltage/ capacity	173 V; 5.5 Ah	22.2 V; 75 Ah
Energy density	46 Wh/dm^3 (100%)	102 Wh/dm^3 (221%)
Power density	865 W/kg (346%)	250 W/kg (100%)
Applications	• Compromise between power and capacity • Fast charging during regenerative braking	• High energy density → compact dimensions • A slight drop in efficiency at lower temperature

4. Energy flow control strategies

The diesel-electric hybrid drive is characterized by cyclic recharges and discharges of the battery. The nominal battery charge (SOC) is approximately 50% (Fig. 14). The use of Ni-MH batteries means that their charge/discharge level is not too high – it is in the range of 40–60%. The use of Li-Ion batteries allows for much higher threshold values: up to 80% SOC when charging and down to about 20% when discharged. If the typical range for a battery is 25–75% SOC, this means that the capacity of the battery used must be twice as large as the intended capacity. For this reason, the use of ultracapacitors may increase the usability of electrochemical energy storage sources.

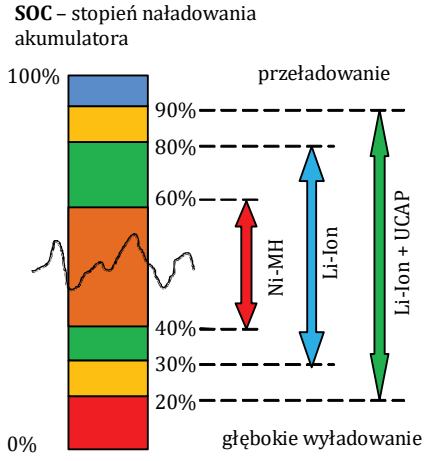

Fig. 14. Conditions for charging and discharging typical battery systems in hybrid drive systems [12, 19]

The specificity of rail vehicles operation and the hybrid drive systems used in them forces specific types of cooperation between the drive sources. An example of a typical rail vehicle operating speed curve is shown in Fig. 15a. It shows that the initial driving fragment is made using only the electric drive. In such conditions, the system discharges the batteries from the maximum level (about 60%) – zone D (Fig. 15b). Achieving and maintaining a specific speed

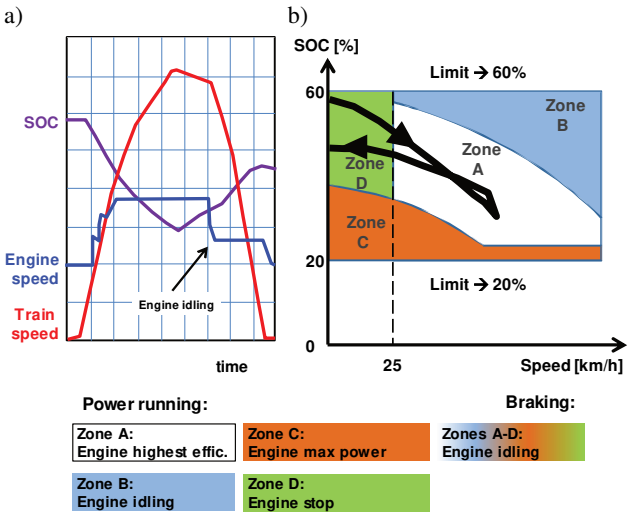

Fig. 15. Example of a hybrid drive system control: a) route, b) hybrid control zones, taking into account the battery charge level [8]

results in a constant rotational speed of the internal combustion engine and further discharge of the batteries (parallel drive). The internal combustion engine operating conditions correspond to its high efficiency. Due to the considerable kinetic energy of such a composition, it is possible to limit the power of the internal combustion engine and to let it idle (Fig. 15a – engine idling, zone A – Fig. 15b). The speed reduction is achieved using regenerative braking, which results in the recovery of the kinetic energy of the vehicle and increasing the level of charge of the batteries. Drive operation characteristics (line in Fig. 15b) moves from zone A to zone D.

Similar research is currently being conducted, and concerns the limitation of SOC changes applied to rail vehicles lithium-ion battery [23].

5. Conclusions

The use of hybrid drive systems in rail vehicles can result in a significant reduction of toxic exhaust emissions and a reduction in fuel consumption. Similarly to other vehicle categories, the use of this drive type allows pushing the engine operating points on the internal combustion engine characteristics towards higher overall efficiency. In the case of rail vehicles, the biggest benefit of using a hybrid drive is limiting the combustion unit idle operation time, where the share of idling for shunting rail vehicles ranges from 50 to 70% [3, 13]. By eliminating the idling operation of the combustion engine, significant economic benefits are obtained. Kałuża [13] assessed that in the case of the SM31 locomotive, the daily reduction of diesel oil consumption, resulting only from the limitation of the time the internal combustion engine spend idling and without load, may amount to approx. 160–168 dm^3.

As it was mentioned in this paper, the type of hybrid drive, and along with it the energy storage technology it uses, should be selected on an individual basis depending on the purpose and nature of the work performed by the rail vehicle. At the stage of selecting the aforementioned solutions, it is important to assess the drive energy demand. With long-term demand for electricity, the best solution should be choosing electrochemical batteries, which are also available in different configurations, focused on higher power density or higher energy density. In that case, the engine more often work in the field of highest efficiency, even during battery charging. That way help to improve the range of the vehicle. In turn, frequent stops and starts (such as in shunting work) makes high power, fast charging and discharging the more favorable features for a drive system, thus ultra-capacitors and flywheels become the better solution to use.

Nomenclature

DLC	double-layer capacitor
ESS	energy storage system
G	generator
Li-Ion	lithium-ion battery
MG	motor/generator
Mo	torque
n	engine/motor speed
Ni-MH	nickel metal hydride battery
OESS	on-board energy storage system
Pb	lead-acid battery
SESS	stationary energy storage system
SOC	state of charge
UCAP	ultracapacitor
V	volume

Bibliography

[1] ACHTEN, P. The Hydrid a hydraulic hybrid transmission. Seminar für Fahrzeugtechnik – Institut für Fahrzeugtechnik und Mobile Arbeitsmaschinen, 12 November 2009.

[2] ANEKE, M., WANG, M. Energy storage technologies and real life applications – A state of the art review. *Applied Energy*. 2016, **179**, 350-377. DOI: 10.1016/j.apenergy.2016.06.097

[3] BABEŁ, M. Zwiększenie efektywności pracy lokomotyw spalinowych SM31 w eksploatacji. *Technika Transportu Szynowego*. 2012, **1-2**, 41-44.

[4] BASELEY, S., EHRET, C., GREIF, E., KLIFFKEN, M. Hydraulic hybrid systems for commercial vehicles. *SAE Technical Paper*. 2007, 2007-01-4150. DOI: 10.4271/2007-01-4150

[5] COUSINEAU, R. Development of a hybrid switcher locomotive the Railpower Green Goat. *IEEE Instrumentation & Measurement Magazine*. 2006, **9**(1), 25-29. DOI: 10.1109/MIM.2006.1634954
[6] DDFlyTrain flywheel hybrid technology to deliver around 10% fuel savings, rapid ROI. www.greencarcongress.com/2015/06/20150617-ddflytrain.html
[7] Directive 2004/26/EC of the European Parliament and of the Council of 21 April 2004 amending Directive 97/68/EC on the approximation of the laws of the Member States relating to measures against the emission of gaseous and particulate pollutants from internal combustion engines to be installed in non-road mobile machinery. data.europa.eu/eli/dir/2004/26/oj.
[8] FUJII, T., TERAYA, N., OSAWA, M. Development of an NE train. *JR EAST Technical Review*. 2004, **4**, 62-70.
[9] GHAVIHA, N., CAMPILLO, J., BOHLIN, M., DAHLQUIST, E. Review of application of energy storage devices in railway transportation. *Energy Procedia*. 2017, **105**, 4561-4568. DOI:10.1016/ j.egypro.2017.03.980
[10] GUNEY, M.S., TEPE, Y. Classification and assessment of energy storage systems. *Renewable and Sustainable Energy Reviews*. 2017, **75**, 1187-1197, DOI: 10.1016/j.rser.2016.11.102
[11] HORIBA, T., MAESHIMA, T., MATSUMURA, T. et al. Applications of high power density lithium ion batteries. *Journal of Power Sources*. 2005, **146**(1-2), 107-110. DOI:10.1016/j.jpowsour.2005.03.205
[12] Hybrid Locomotive, SustRail, Grant Agreement n: 265740 FP7.
[13] KAŁUŻA, A. Lokomotywa manewrowa sześcioosiowa SM31. Przetwarzanie danych z dwóch obserwowanych rejonów pracy. Warianty modernizacji źródeł energii układu napędowego. *Logistyka*. 2014, **6**, 5124-5137.
[14] KINI, G. Energy management systems, 2011, *InTech*. www.intechopen.com/books/energy-management-systems/management-of-locomotive-tractiveenergy-resources
[15] MAYET, C., POUGET, J., BOUSCAYROL, A., LHOMME, W. Influence of an energy storage system on the energy consumption of a diesel-electric locomotive. *IEEE Transactions on Vehicular Technology*. 2014, **63**(3), 1032-1040. DOI: 10.1109/TVT.2013.2284634
[16] MEINERT, M., MELZER, M., KAMBUROW, C. et al. Benefits of hybridisation of diesel driven rail vehicles: Energy management strategies and life-cycle costs appraisal. *Applied Energy*. 2015, **157**, 897-904. DOI: 10.1016/j.apenergy.2015.05.051
[17] MEINERT, M., PRENLELOUP, P., SCHMID, S., PALACIN, R. Energy storage technologies and hybrid architectures for specific diesel-driven rail duty cycles: Design and system integration aspects. Applied Energy. 2015, 157, 619-629. DOI: 10.1016/j.apenergy.2015.05.015
[18] NAGAURA Y., OISHI R., SHIMADA M., KANEKO T. Battery-powered Drive Systems: Latest Technologies and Outlook. *Hitachi Review*. 2017, **66**(2), 138-144.
[19] NELSON, R.F. Power requirements for batteries in hybrid electric vehicles. *Journal of Power Sources*. 2000, **91**(1), 2-26. DOI: 10.1016/S0378-7753(00)00483-3
[20] Regulation (EU) 2016/1628 of the European Parliament and of the Council of 14 September 2016 on requirements relating to gaseous and particulate pollutant emission limits and type-approval for internal combustion engines for non-road mobile machinery, amending Regulations (EU) No 1024/2012 and (EU) No 167/2013, and amending and repealing Directive 97/68/EC. http://data.europa.eu/eli/reg/2016/1628/oj.
[21] RUPP, A., BAIER, H., MERTINY, P., SECANELL M. Analysis of a flywheel energy storage system for light rail transit, *Energy*. 2016, **107**, 625-638. DOI: 10.1016/j.energy.2016.04.051
[22] RYDBERG, K.-E. Energy efficient hydraulic hybrid drives. *The 11th Scandinavian International Conference on Fluid Power – SICFP'09*, June 2-4, 2009, Linköping, Sweden.
[23] TAKAKUSAKI, A., SONODA, H., KOUNO, Y. Development of the optimal charge and discharge control method for diesel hybrid trains under high operational load. *JR EAST Technical Review*. 2017, **37**, 55-60.
[24] The IEA-UIC Railway handbook on energy consumption & CO_2 emissions 2016 Edition, www.uic.org/IMG/pdf/iea-uic_railway_handbook_2016.pdf
[25] The next step – the hybrid machine. Environmental protection & sustainability, https://www.plassertheurer.com

Maciej Andrzejewski, DEng. – Łukasiewicz Research Network – Rail Vehicles Institute "TABOR" in Poznan.
e-mail: *m.andrzejewski@tabor.com.pl*

Prof. Jerzy Merkisz, DSc., DEng. – Faculty of Transport Engineering, Poznan University of Technology.
e-mail: *jerzy.merkisz@put.poznan.pl*

Prof. Ireneusz Pielecha, DSc., DEng. – Faculty of Transport Engineering, Poznan University of Technology.
e-mail: *ireneusz.pielecha@put.poznan.pl*

Mateusz Nowak, DEng. – Łukasiewicz Research Network – Rail Vehicles Institute "TABOR" in Poznan.
e-mail: *m.nowak@tabor.com.pl*

Robert Świechowicz, MSc. – Faculty of Transport Engineering, Poznan University of Technology.
e-mail: *robswiech@wp.pl*

Article citation info:
PRZYBYŁA, G., RUTCZYK, B., ZIÓŁKOWSKI, Ł. Performance of micro CHP unit based on SI engine with quantitative-qualitative load control. *Combustion Engines*. 2019, **178**(3), 82-87. DOI: 10.19206/CE-2019-315

Grzegorz PRZYBYŁA
Bartłomiej RUTCZYK
Łukasz ZIÓŁKOWSKI

CE-2019-315

Performance of micro CHP unit based on SI engine with quantitative-qualitative load control

The paper presents data resulting by the preliminary experimental tests performed on a micro CHP (combined heat and power) 7 kWel unit. The engine load has been controlled by throttle position (quantitatively) or/and the value of air excess ratio (qualitatively) QQLC. By this way the engine efficiency can be improved in the range of partial loads by reducing the exergy losses during the inlet stroke. During the tests engine has been powered with LPG fuel. The engine performance together with environmental impact has been studied in this paper. Used method shows that despite the reduction of the load from 5.6 kW to 4.7 kW while burning the lean mixture, the efficiency of electricity generation increased slightly. The efficiency grew by approx. 1.41 percentage point comparing with the results obtained for almost constant load but obtained by burning the lean mixture (λ = 1.3), followed by increased throttling and combustion of the stoichiometric mixture.

Key words: *CHP, SI engine, LPG, natural gas, emission, electrical efficiency*

1. Introduction

In the first decade of the 21st century, there was a marked increase in electricity consumption in Poland. In the years 2000-2010 it amounted to less than 18%, which was an increase of over 21 TWh compared to the value recorded in 2000. Over the next eight years, i.e. in the years 2010-2018, there was a further increase and significantly higher than in the first decade because by less than 27% in relation to 2010. Recent data indicate that in 2018 electricity consumption in Poland amounted to 171 GWh [1–3].

The growing demand for electricity in our country will most likely grow dynamically in the coming years. The previously indicated clear upward trend observed in recent decades can be considered as a proof of that statement. In addition, an increase in electricity consumption in the near future will be caused by the growing appearance of electric and plug-in hybrid vehicles on the market [4, 5].

With regard to these data, it may be beneficial to use local low power cogeneration systems. Microcogeneration (mCHP – micro Combined Heat and Power) can be realized based on an internal combustion engine powered by natural gas or LPG. In view of the Directive 2004/8/EC, microgeneration concerns combined generation of electricity with a maximum electrical power of less than 50 kWe. The implementation of mCHP systems can significantly contribute to the propagation of low-emission heat and electricity generation in our country. With this, a new concept of electricity generation appears with the participation of the so-called prosumers.

2. The research object and methods

Low power cogeneration systems powered by combustion engines can be used in residential buildings, rural buildings, public facilities, hospitals, and in particular in buildings where there is a long-term, preferably all-year round demand for heat. The use of micro-cogeneration is justified wherever it can meet the needs of one or more consumers for whom the connection to a centralized heating grid would not be economically feasible.

When using reciprocating engines in mCHP systems, both diesel and spark ignition engines can be utilized. Where, it should be noted, diesel engines can be used in a dual fuel configuration, that is with the main fuel being a gas, and the combustion being initiated by a pilot dose of liquid fuel. Currently, natural gas is the most suitable fuel for feeding CHP systems, mainly due to its wide availability. In the case of hindered availability of natural gas, mCHP systems are usually powered with LPG or liquid fuel. At the same time, the liquid fuel feed is most often used for self-ignition engines.

Due to their properties, most gaseous fuels are suitable for correctly feeding internal combustion, piston engines. This is due, among other things, to their good ability to form homogeneous mixtures, which is important from the point of view of the implementation of the correct combustion process in the spark ignition engine. In addition, gaseous fuels are usually characterized by wide flammability limits. Another advantage is the fact that usually gas fuels have a higher value of the hydrogen to carbon ratio relative to liquid fuels, which leads to a reduction in CO_2 emissions. Table 1 presents selected parameters of natural gas type GZ50, propane and butane.

Table 1. Properties of natural gas and propane and butane [6]

Fuel	Composition (by volume)	MN –	LHV MJ/m^3	e_{dv} MJ/m^3	FL (eq. ratio) lower/ upper
Natural Gas	CH_4 = 98.5% CO_2 = 0.1% N_2 = 1% other: C_2H_6, C_3H_8, C_4H_{10}	90	35.3	2.91	0.49/1.66
Propane	C_3H_8	35	91	2.19	0.49/2.5
Butane	C_4H_{10}	10	118.6	2.24	0.57/3.06

As can be shown from the data in Table 1 there is a significant difference in the methane number for both fuels. One of the parameters, the value of which directly affects the energy efficiency of the engine is the compression ratio. Energy efficiency increases with an increasing compression ratio. Theoretically, fuels with a higher methane number should ensure that the engine achieves higher energy efficiency. The higher value of the methane number allows to

burn the fuel with a higher compression ratio compared to fuels with a lower methane number. It should be noted, however, that the high methane value does not guarantee proper operation of the engine with high efficiency. Different fuels are characterized by different ranges of flammability limits, burning speed, minimum ignition energy. Taking into account the mentioned values, there may be, for example, a problem with the proper combustion of lean mixtures in an internal combustion engine. Combustion of lean mixtures in internal combustion engines brings measurable benefits in the form of reduction of nitrogen oxide NO_x emissions and an increase of the energy efficiency of the engine.

3. The research object and methods

The paper presents the results of test of a micro CHP system composed of a spark ignition engine, an asynchronous generator and heat exchangers. The micro-CHP system is being created as a result of the implementation of a scientific and research project in cooperation with the Silesian University of Technology and Budexpert sp. z o.o. Ultimately, the proposed system is to meet the energy needs of a single-family home, maintaining high annual average of the efficiency of electricity generation. The system can be assembled in various configurations, eg instead of an asynchronous machine, a synchronous machine is to be used. In this configuration, there will be a possibility of a connection with the power grid or isolated working only for the needs of the facility in which the system was installed. In Figure 1, a prototype cogeneration system with additional components is presented.

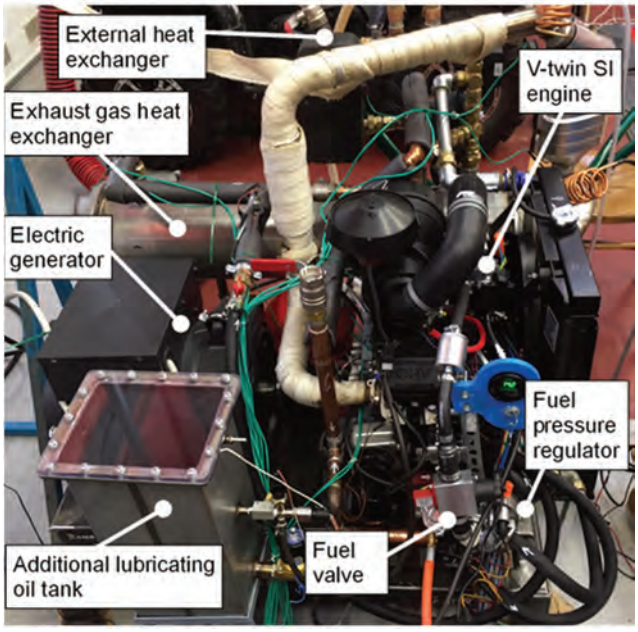

Fig. 1. The prototype cogeneration system

In residential buildings, the demand for heat is dependent on seasonal changes. For this reason, in order to fully use the potential of a co-generator it is necessary to use heat accumulators with a high heat capacity. Due to this, the internal combustion engine can start periodically and work with high efficiency, ensuring high energy efficiency of the entire cogeneration system. The installation of the heat accumulator however brings additional initial investment costs which, at the high price of low-power cogeneration systems available on the market, becomes economically unjustified.

One of the possible ways to increase the efficiency of the internal combustion engine during its operation at partial loads is to limit the loss of exergy in the inlet channel of the engine. This can be achieved by using a larger throttle opening while maintaining a certain dose of fuel to generate the required torque. This regulation leads to the formation of a lean ($l >> 1$) mixture powering the combustion engine. Depending on the properties of the fuel used, the limit value of stable operation of the internal combustion engine (flammability limit of the mixture) will vary.

The research on the prototype cogeneration unit was carried out while fuelling the engine with LPG. During the testing, the combustion engine was driving an asynchronous generator. To provide an electrical load, the system had been connected to the power grid. The heat generated by the system was transferred to a radiator with a variable cooling capacity. The electric power of the cogeneration system was modulated by changing the throttle position and thus influencing (indirectly by increasing the torque of the internal combustion engine) the change of the rotational speed of the asynchronous generator. The tests were carried out for a variable value of ignition advance angle and two different mixture compositions. Tests were carried out for three different loads of the internal combustion engine during the combustion of a stoichiometric mixture. In addition, tests were conducted for one of the three mentioned loads of the internal combustion engine while burning a lean mixture ($\lambda = 1.3$).

During the testing, the electric power was measured by the Fluke Norma 5000 power analyzer. In turn, the mass stream of fuel consumed by the engine was measured using a Sartorius weight. Also, the composition of dry exhaust gases at the outlet of the combustion engine was measured using the Capelec CAP 3000 flue gas analyzer. The temperature at selected points in the system was measured using k-type thermocouples.

4. Research results

On the basis of the conducted research, the energy parameters and emission factors were compared in the range of variable control parameters of the internal combustion engine. Figure 2 shows the influence of ignition advance angle on the value of electric power generated in the cogeneration system. For the stoichiometric mixture, the influence of throttling caused by the change of the throttle position is also visible. Combustion of a lean mixture with an air excess ratio $\lambda = 1.3$ allows obtaining a similar value of electric power as with a stoichiometric mixture with the position of the throttle causing 15 kPa of pressure drop. When burning a lean mixture, the pressure drop is lower and amounts to 9 kPa. At the same time achieving a comparable value of electric power requires a higher value of the ignition advance angle. The research on the combustion of lean mixtures had been limited to a single series due to high fluctuations in the electric current in the output circuit of the electrical machine. These fluctuations were caused by

the excessive variability of the torque of the internal combustion engine due to the low value of the moment of inertia of the standard flywheel.

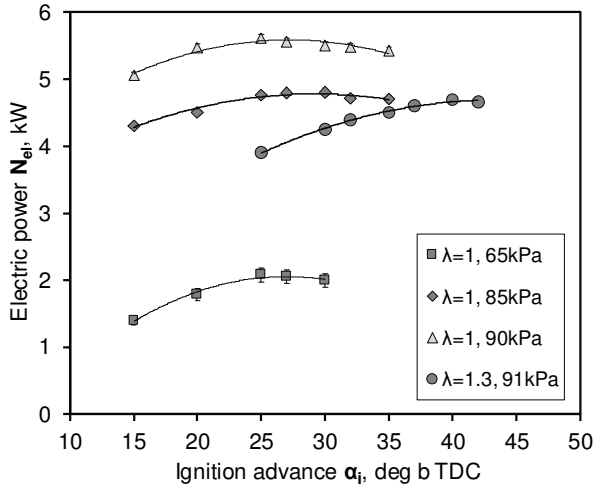

Fig. 2. Electric output power vs ignition timing, throttle position and mixture composition

Figure 3 presents the resultant values of the efficiency of electricity generation in the examined system. For the measurement series made during stoichiometric mixture combustion, the effect of the loss of exergy in the inlet channel on the level of efficiency obtained is clearly visible. For the electric power of just under 2.1 kW, the thermal efficiency of electricity generation is 16%. While for an electrical power of 5.6 kW efficiency reaches 25.6%.

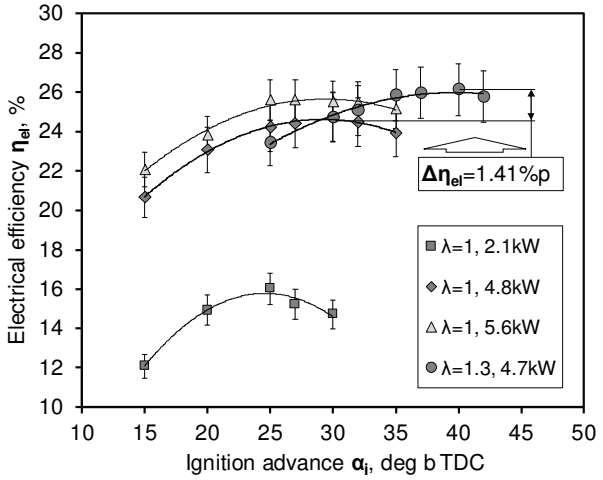

Fig. 3. Electrical efficiency vs ignition timing, throttle position and mixture composition

Figure 3 also shows the effect of using a quality-quantity regulation to limit the power output of the generator. Instead of throttling during the combustion of the stoichiometric mixture (λ = 1, 4.8 kW), almost the same engine output can be obtained by depleting the mixture (λ = 1.3, 4.7 kW) with a greater throttle opening. This treatment enables an efficiency increase of 1.41 percentage points.

Figures 4 to 10 show the specific emission and concentration of toxic exhaust substances. The concentration of individual components of the exhaust gas has been recalculated for to reference conditions corresponding to a 5% molar proportion of oxygen in dry exhaust gases. The given values have been determined for the composition of the exhaust gases measured directly at the engine outlet. The equipment used allowed to measure carbon monoxide, hydrocarbons (in terms of hexane) and nitrous oxide. NO_x emission factors were calculated taking into account the NO_2 molar mass.

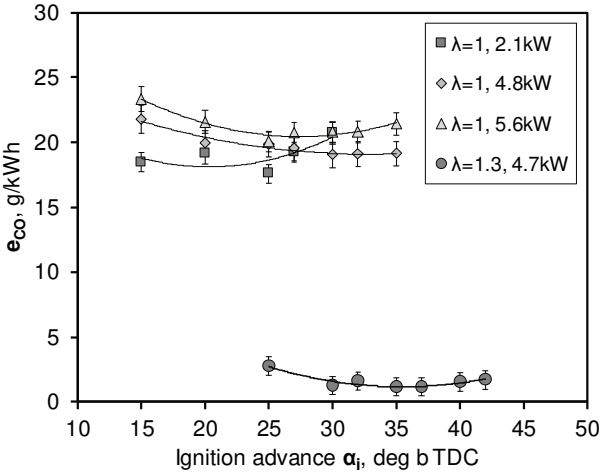

Fig. 4. Specific emission of CO vs ignition timing, throttle position and mixture composition

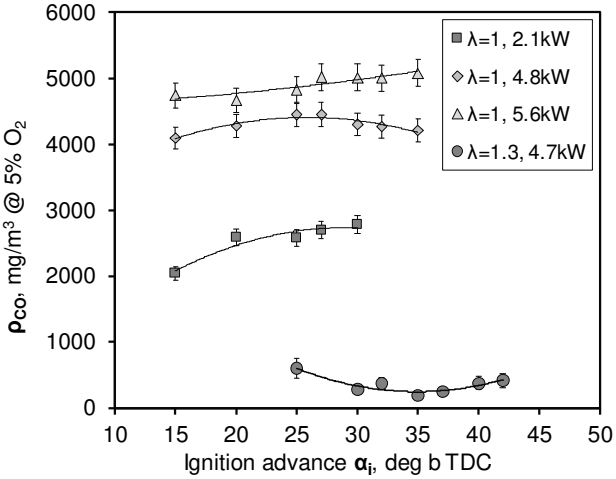

Fig. 5. CO concentration adjusted to 5% of O_2 in dry exhaust vs ignition timing, throttle position and mixture composition

The highest level of carbon monoxide exhaust pollution is recorded for higher values of the cogeneration system load. The composition of the mixture is also significant. During the combustion of the lean mixture, the lowest values of carbon monoxide emission were obtained. The situation is similar in the case of hydrocarbon emissions. The reason may be the fact that the fuel-air mixture was prepared in a mixer whose geometry and location is still being optimized. Hence, likely the lean mix was better prepared due to the higher oxygen content in the fresh load. In addition, the lean combustion process took place at the engine load level, which ensures good thermal conditions for the combustion process.

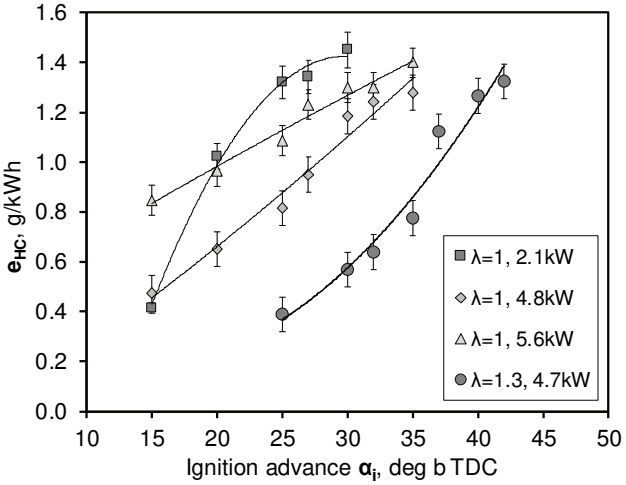

Fig. 6. Specific emission of HC vs ignition timing, throttle position and mixture composition

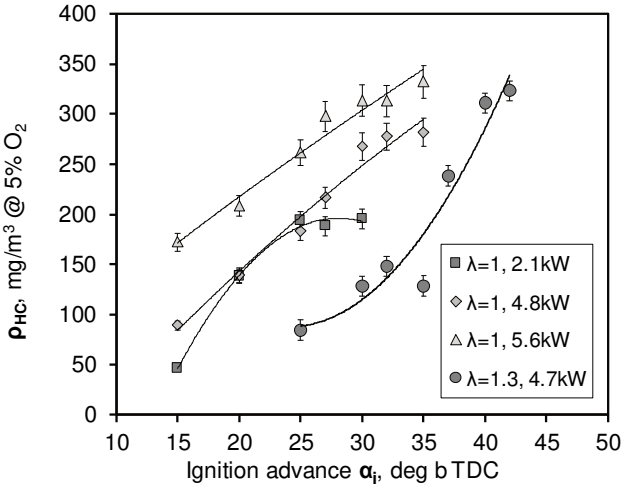

Fig. 7. HC concentration adjusted to 5% of O_2 in dry exhaust vs ignition timing, throttle position and mixture composition

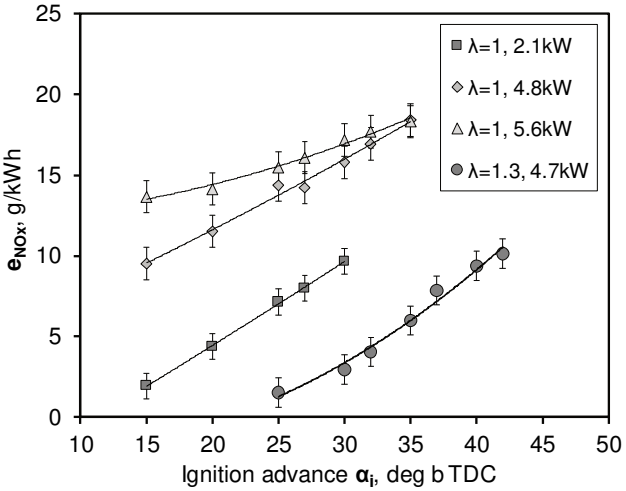

Fig. 8. Specific emission of NO_x vs ignition timing, throttle position and mixture composition

The amount of nitrogen oxides emission in a spark ignition engine is closely related to the instantaneous charge temperature in the engine cylinder. The higher the value of the ignition advance angle, the higher the average temperature during the combustion process (for a specific composition of the combustible mixture). Therefore, Figures 7 and 8 show an increase in NO_x emissions in proportion to the increase in ignition timing. A higher engine load (proportional to the load of the electricity generation) results in a higher value of heat generated in the cylinder. This, in turn, affects the increase of the charge temperature (for a predetermined value of the ignition advance angle). For this reason, it is evident that during the combustion of the stoichiometric mixture, the higher load of the internal combustion engine is associated with a higher emission of nitrogen oxides.

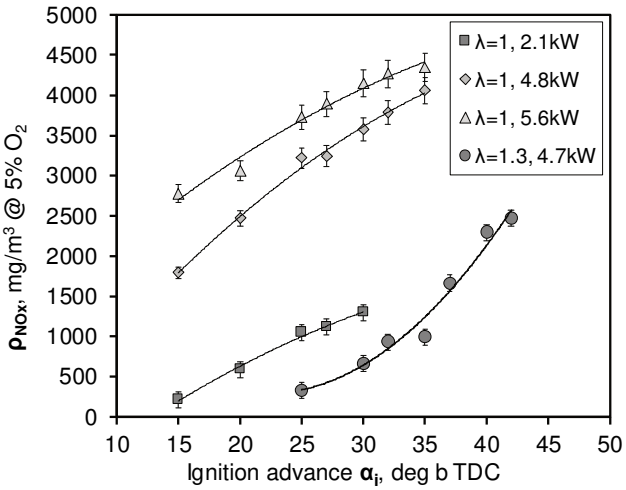

Fig. 9. NO_x concentration adjusted to 5% of O_2 in dry exhaust vs ignition timing, throttle position and mixture composition

Figures 10 and 11 present the results of the flue gas temperature trend measured at the outlet of the cylinder No. 1 and the cylinder No. 2 respectively. The visible temperature drop together with the increasing value of the ignition advance angle results from the course of the charge expansion. The earlier ignition leads to a higher value of the maximum pressure being reached in the engine cylinder and its location being closer to the TDC during the load expansion [7].

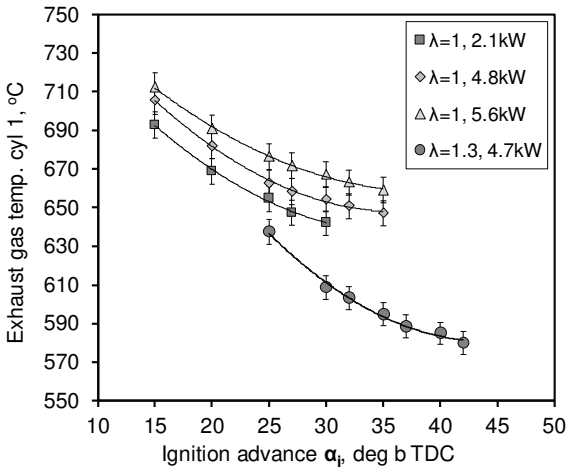

Fig. 10. Exhaust gas temperature measured on cylinder 1 outlet vs ignition timing, throttle position and mixture composition

Variable thermal conditions during expansion significantly affect the emptying rate of the exhaust cylinder. The decreasing pressure value in the final draining phase and the amount of charge determine the temperature value in the exhaust channel. The temperature values measured in both cylinders differ slightly.

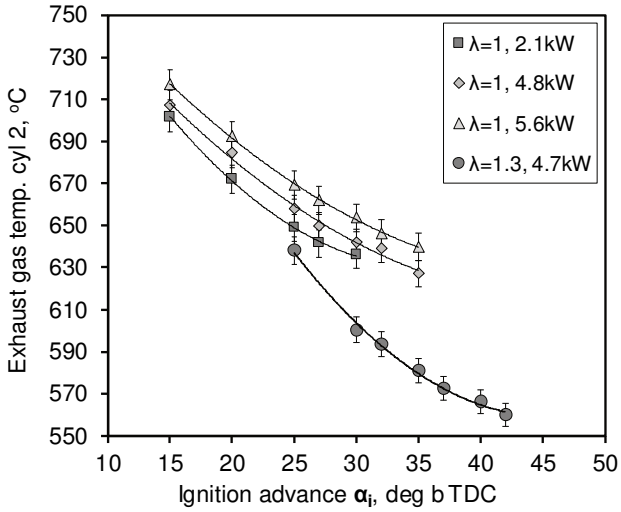

Fig. 11. Exhaust gas temperature measured on cylinder 2 outlet vs ignition timing, throttle position and mixture composition

Taking into account the quantitative and qualitative regulation, it can be noticed that the temperature of the exhaust gases is lower by approx. 50 K by comparing the results for the stoichiometric and lean mixture. This is in the conditions in which, the maximum power of the system during the combustion of the stoichiometric mixture was 4.8 kW, and when burning a lean mixture it stood at 4.7 kW.

5. Conclusions

The preliminary tests of the prototype microcogeneration system lead to the formulation of the following conclusions:

1. The application of the mixed regulation method, ie the combination of quantitative and qualitative regulation, gives the opportunity to increase the efficiency of electricity generation during the operation of the system with a partial load. Despite the reduction of the load from 5.6 kW to 4.7 kW while burning the lean mixture, the efficiency of electricity generation increased slightly. The efficiency grew by approx. 1.41 percentage point comparing with the results obtained for almost constant load but obtained by burning the lean mixture (λ = 1.3), followed by increased throttling and combustion of the stoichiometric mixture.
2. Combustion of lean mixtures results in greater unevenness of the engine's running, relative to the combustion of a stoichiometric mixture. Increasing the control range of the lean mixture requires the use of a flywheel with a greater moment of inertia. Its value must be selected so as to ensure stable operation of the electrical generator.
3. The use of a three-way catalytic converter will allow to reduce harmful emissions such as CO, HC and NO_x. However, its correct operation will be ensured only during the combustion of stoichiometric mixtures. When combusting lean mixtures, the catalytic converter will only allow for oxidation reactions. For this reason, it is important to optimize the ignition advance angle, which on the one hand will allow to achieve a satisfactory level of energy efficiency during the combustion of lean mixtures, and on the other hand will not result in exceeding the NO_x emission limit, limited by legislation.
4. Variation of the exhaust gas temperature depending on the control parameters of the internal combustion engine (ignition timing, excess air ratio) requires a proper management of the heat collection system. This will be implemented using the master cogenerator control system.

Nomenclature

CO	carbon monoxide	MN	methane number
HC	hydrocarbons	LHV	lower heating value
NO_x	nitrogen oxides	e_{dv}	calorific value of air fuel mixture

Acknowledgement

This work was supported by the project: „Prace badawczo-rozwojowe ukierunkowane na opracowanie mikrokogeneratora o mocy elektrycznej poniżej 40kW wraz z nowatorskim systemem sterowania silnikiem spalinowym i możliwością zasilania gazem ziemnym lub LPG w celu wykorzystania potencjału innowacyjnego i stworzenia trwałej przewagi konkurencyjnej" implemented as part of the Regional Operational Program of the Silesian Region for the years 2014-2020 (European Regional Development Fund).

Bibliography

[1] ROLLERT, K.E. The underlying factors in the uptake of electricity demand response: The case of Poland. *Utilities Policy*. 2018, **54**, 11-21.

[2] https://www.cire.pl/item,149871,1,0,0,0,0,0,zuzycie-energii-elektrycznej-w-polsce-rosnie.html (access 07.03.2019).

[3] GAWLIK, L., SZURLEJ, A., WYRWA, A. The impact of the long-term EU target for renewables on the structure of electricity production in Poland. *Energy*. 2015, **92**(2), 172-178.

[4] DARZI, M., JOHNSON, D., ULISHNEY, C., OLIVER, D. Gaseous fuels variation effects on first and second law analyses of a small direct injection engine for micro-CHP systems. *Energy Conversion and Management*. 2019, **184**, 609-625.

[5] SPOLETINI, E. Economic analysis and technical issues of low temperature PCM thermal storage combi. *Energy Procedia*. Vol. 2016, **101**, 1151-1158.

[6] PRZYBYLA, G., POSTRZEDNIK. S., ZMUDKA, Z. The impact of air-fuel mixture composition on SI engine performance during natural gas and producer gas combustion. *Scientific conference on automotive vehicles and combustion engines* (KONMOT 2016), *IOP Conference Series-Materials Science and Engineering*. 2016, **148**. Article Number: UNSP 012082.

[7] NADALETI, W.C., PRZYBYLA, G. Emissions and performance of a spark-ignition gas engine generator operating with hydrogen-rich syngas, methane and biogas blends for application in southern Brazilian rice industries. Energy. 2018, **154**, 38-51.

Grzegorz Przybyła, DEng. – Institute of Thermal Technology, Silesian University of Technology.
e-mail: *gprzybyla@polsl.pl*

Łukasz Ziółkowski, MEng. – Institute of Thermal Technology, Silesian University of Technology.
e-mail: *lziolkowski@polsl.pl*

Bartłomiej Rutczyk, MEng. – Institute of Thermal Technology, Silesian University of Technology.
e-mail: *brutczyk@polsl.pl*

Article citation info:
BIELACZYC, P., KLIMKIEWICZ, D., WOODBURN, J., SZCZOTKA, A. Exhaust emission testing methods – BOSMAL's legislative and development emission testing laboratories. *Combustion Engines*. 2019, **178**(3), 88-98. DOI: 10.19206/CE-2019-316

Piotr BIELACZYC
Dariusz KLIMKIEWICZ
Joseph WOODBURN
Andrzej SZCZOTKA

CE-2019-316

Exhaust emission testing methods – BOSMAL's legislative and development emission testing laboratories

The latest legislation regarding the reduction of harmful exhaust emissions, greenhouse gases and fuel consumption determines not only maximum permissible emissions factors, but also emissions testing methods and laboratory design and additionally leads to the development of new research methods. BOSMAL has risen to meet these challenges by investing in an updated, state-of-the-art emissions testing laboratory, housed within a climate chamber and in parallel investing in a completely new laboratory designed with incoming and future legislative requirements in mind. This paper presents BOSMAL's improved M1/N1 vehicular emissions and fuel consumption laboratory in a climatic chamber and BOSMAL's standard chamber for the testing of vehicles in accordance with European Union, US and Japanese standards. The specifications, capabilities and design features of the sampling, analysis and development research possibilities and climate simulation systems are presented and discussed in relation to the increasing drive for cleaner, light duty road vehicles (including hybrids and electric vehicles). The recently-renovated laboratory with extended standard temperature range and the laboratory with climatic chamber are described in the context of the newest European Union legislation on the emission in the range of Euro 6d testing requirements. The laboratories permit BOSMAL's engineers to compete in the international automotive arena in the development of new, more ecologically friendly and increasingly fuel efficient vehicles.

Key words: *emission testing, emission test methods, climatic simulation, Euro 6, WLTP*

1. Introduction

Vehicular transport is one of the biggest sources of harmful emissions and major changes in engine and vehicle design have been observed in recent years in response to emissions reduction legislation [1, 2] (in the EU: the introduction of the Worldwide harmonized Light vehicles Test Procedures (WLTP) over the years 2018/2019, and the scheduled introduction of Euro 6d in 2020/2022). An additional factor is widespread pressure for the reduction of greenhouse gases, mostly by reduction of CO_2 emissions. One of the major challenges for humanity is to fight global warming by reducing greenhouse gas emission (particularly CO_2 but CH_4 and N_2O as well) to the atmosphere, by 45 per cent by 2020 and 60 per cent by 2050 [3]. As mentioned, road transport is currently one of the largest single sources of CO_2 emissions in the EU [4] and the group of 20 largest economies (G20) accounted for 81% of global CO_2 emissions overworld [5]. The introduced changes in the legislation regarding type approval of new vehicles and the first vehicles registered determine new requirements in the test methodology in the emissions laboratories based on the WLTC cycles as a part of the Worldwide harmonized Light vehicles Test Procedures (WLTP in ECE Global Technical Regulation No. 15) which will decrease the divergence between laboratory test and real world emissions [6]. The European Union has introduced the new WLTC cycle, which ensures development of vehicle testing based on real-world driving data.

The legislation of other countries (with the motivation of reduction global CO_2 emissions) leads them to use the World-Harmonized Light-Duty Vehicles Test Procedure as well. The China 6 Standard will be mandatory from 2023 and is generally based on the Euro 6 regulation. In Japan the WLTP has been established in law from 2018 as the official procedure of emission testing, while the Indian government introduced the FAME policy (Faster Adoption & Manufacturing of (Hybrid &) Electric Vehicle) to boost and support hybrid and electrical vehicles' position on the market [7].

The fleet target for CO_2 emission in Europe in 2020 of 95 g/km and 68–78 g/km in 2025 (proposal) [8] leads to the inevitability of implementation of new technologies and high accuracy of measurements and vehicle testing. In order to meet the new requirements of legislation and changes in the methodology of emissions testing on the chassis dynamometers at BOSMAL AR&DI Ltd. [9], the company's emissions laboratories are constantly improved and updated to meet the requirements of current and incoming regulations. Based on the demanding requirements of the test procedures (WLTP) and the limits enforced over the new driving cycle (WLTC), vehicle manufacturers should introduce many new solutions and new systems for management of aftertreatment systems. This forces the acquisition of as many data as possible and the use advanced measurement techniques during vehicle testing in the emission laboratory. Modern emissions testing laboratories like BOSMAL's should be ready for incoming new measurement requirements – and must, in parallel, educate personnel, young engineers to be ready to fulfil the special customer requirements via high quality services and extensive knowledge. In 2017, the Emissions Laboratory No. 1 was equipped with a modern AVL emission system and together with the existing Emissions Laboratory No. 2 equipped with the Horiba emission system and the climate chamber, fully meets the current challenges posed by legislative requirements and development testing. Both BOSMAL's laboratories have an Accreditation for homologation testing and meets requirements of the PN-EN ISO/IEC 17025:2005 standard (No. AB 128 – full scope of accreditation of the testing laboratory is available to download [9]). The laboratories provide

the opportunity to meet future requirements for low-emission testing of vehicles fuelled with conventional fuels, alternative fuels [10] and testing hybrid and electric vehicles.

This paper presents the research possibilities of BOSMAL's emission laboratories in the scope of tests compliant with corresponding regulations and procedures as well as in developmental testing of vehicles of categories M and N.

2. Characteristics of the emissions laboratories

BOSMAL's emissions testing laboratories are advanced, ambient (Emission Laboratory No. 1) and climate-controlled (Emission Laboratory No. 2) facilities for performing emissions, fuel consumption and performance tests over a range of driving cycles and a broad range of ambient conditions. Exhaust emissions testing itself is carried out with the aid of sampling bags (legislative tests), diluted and raw modal analysis (development tests) for use with CI, SI and hybrid vehicles. These facilities permit the execution of a wide range of legislative and development emissions tests, including:

- CVS bag diluted emissions testing to international standards [11, 12],
- CO_2 emissions and fuel consumption measurement according to EU standards [13, 14],
- gravimetric and numerical quantification of particulate matter emission according to [15, 16],
- measurement of battery current balance according to [11],
- measurement of compounds which are unregulated in the EU, such as N_2O, NH_3 using additional analyzers,
- measurement of soot and particulate matter from raw exhaust gases using additional devices,
- checks of vehicles according to Conformity of Production (COP) requirements [11, 12],
- maximum power measurement on the wheels of vehicle [14],
- electric consumption energy and electric vehicles range [11, 12].

A schematic diagram of both laboratories and vehicle soak areas are presented in Fig. 1. In the next part of this paper, the wide range of possibilities of emission tests in BOSMAL's laboratories in the range of legislated and unlegislated emission tests are presented.

2.1. Legislative emissions measurement

As mentioned previously, BOSMAL's laboratories permit the execution of legislative emissions tests according to existing international and global regulations such as [2, 17, 18]. These types of emission tests should fulfill restrictive requirements which are described in the regulations and therefore demand that the laboratories are equipped with suitable measurement devices of high accuracy.

Ambient conditions for exhaust emissions tests

The base or heart of the laboratories are their ambient and climatic chambers within which emissions, fuel consumption and performance measurements are performed. In the Emission laboratory No. 1 activities can be carried out in the temperature range +14°C to +28°C (Fig. 2). The chambers are equipped with temperature and humidity control systems, which facilitate the maintenance of the desired temperature and humidity levels. The software in Laboratory No. 1 (ambient chamber) (Fig. 3) permits the following during emission tests:

- temperature control within the range +14°C to +28°C,
- control accuracy (temperature tolerance): ±2.0°C,
- control over the humidity value during emissions tests: from 5.5 to 12.2 grams of water per kilogram of dry air for temperatures within the range +14°C to +28°C,
- variation in humidity level: ≤ 5%.

In Emission Laboratory No. 2 (Fig. 4), all activities can be performed at temperatures ranging from –35°C to +60°C. Such a temperature range far exceeds current legislative requirements; the 95°C temperature range capability is a response to the current and future requirements of engine and vehicle development projects, cold start ability at low temperatures, etc., and oil, fuel and catalyst manufacturers' testing demands.

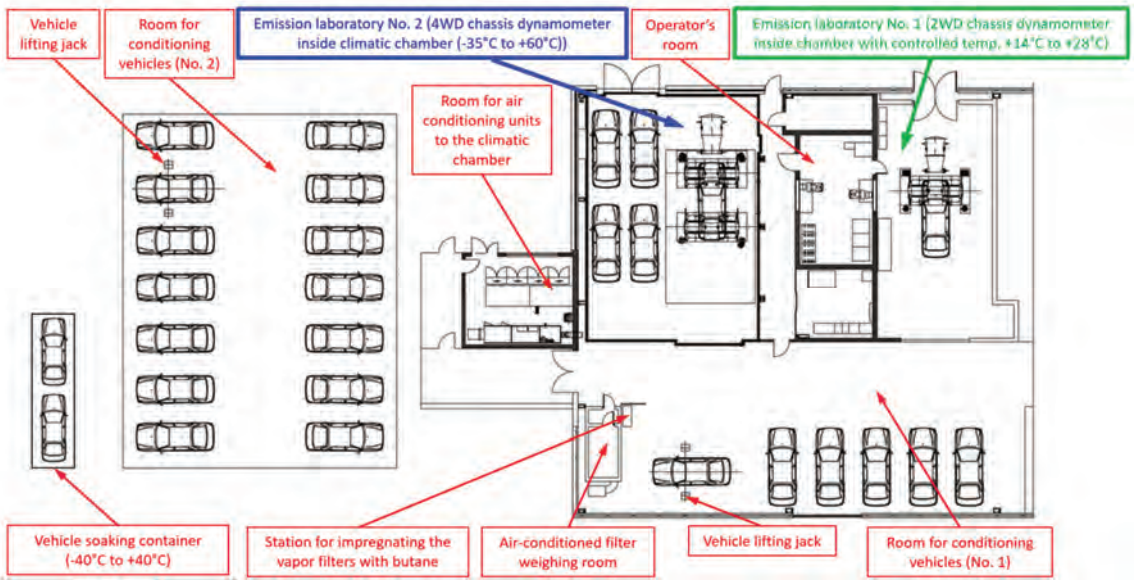

Fig. 1. Technical drawing of BOSMAL's Emission Testing Laboratories No. 1 (green description) and No. 2 (blue description) and heat soak areas

Fig. 2. Internal view of the ambient chamber of Emission Laboratory No. 1, showing the single roller chassis dynamometer and the windspeed fan in front

Fig. 3. Air conditioning control system in Laboratory No. 1

During operation of the climatic chamber, (including during the execution of emission and vehicle performance tests), the chamber permits:

- temperature control over the range –35°C to +60°C,
- control accuracy (temperature tolerance): ±1.0°C (under static conditions, with zero heat load); ±1.2°C (during emissions tests); ±2°C (during performance tests),
- variation in humidity level: ≤ 5%,
- temperature gradient (with the chamber empty): 0.5°C per minute during warm-up and cool-down phases,
- control over the humidity value during emissions tests: from 5.5 to 15.0 grams of water per kilogram of dry air at temperatures ranging from +20°C to +35°C.

The climatic chamber's control software permits the execution of user-defined automated programs, so that stabilization of the temperature in the chamber can be achieved well before any testing begins (Fig. 5).

The climatic chamber's roof features standard lamps to provide even illumination throughout the chamber, but may be upgraded to include high-power solar lamps in the future, as required for the EPA's supplemental air conditioning test cycle ('SFTP-SC03'), performed at a temperature of +35°C with a solar flux of 850 ±45 W/m^2 [19, 20].

In addition to fulfilling US testing requirements, such an upgrade would also extend the laboratory's capabilities in terms of reproduction and simulation of real driving emissions tests, including worst-case scenarios.

A simple comparison of the ambient conditions in both BOSMAL's laboratories is presented in Table 1.

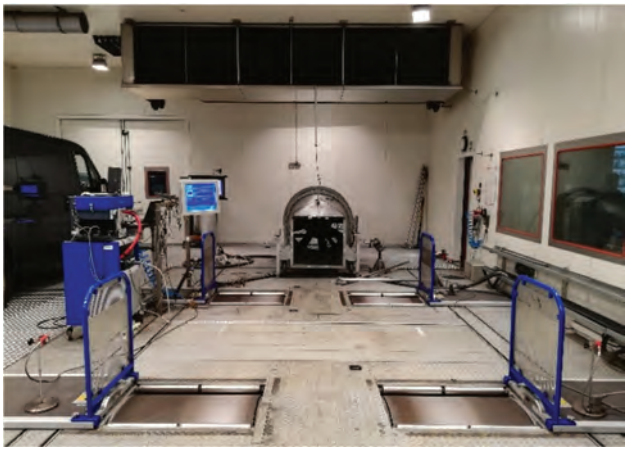

Fig. 4. Internal view of the climatic chamber of Emission Laboratory No. 2, showing the double rollers chassis dynamometer and the windspeed fan in front

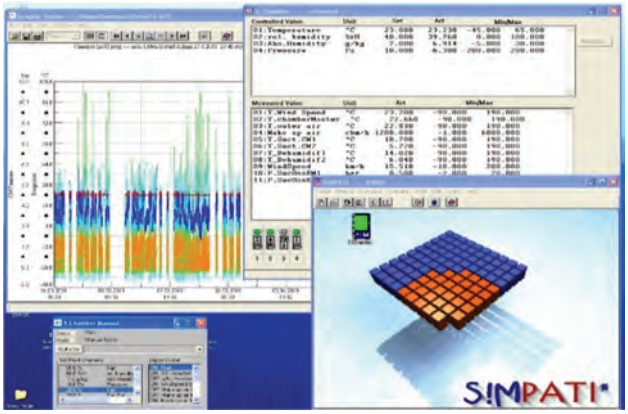

Fig. 5. Simpati climatic chamber control software in Laboratory No. 2

Table 1. Specification of the ambient conditions regulation inside the BOSMAL's Emission Laboratories

Parameter	Unit	EmiLab.1	EmiLab.2
Temp. control range	°C	+14/+28	–35/+60
Control accuracy during emission test (tolerance)	°C	±2.0	±1.2
Humidity during emission test	gH_2O/kg dry air	5.5–12.2	5.5–15.0
Variation in humidity level	%	≤ 5	≤ 5

Aside from the possibility of thermal conditioning ('soaking') of vehicles inside the climatic chamber of Emission Laboratory No. 2, in the direct vicinity of both laboratories are located two soak areas and a soak container with key parameters as described in Table 2.

Table 2. Specification of BOSMAL's soak areas

Parameter	Soak Area 1	Soak Area 2	Soaking Container	EmiLab2
Vehicle capacity – large car/small van	6 pcs.	14 pcs.	2 pcs.	7–8 pcs.
Temperature range	+20°C +30°C	+20°C +28°C	–40°C +40°C	–35°C +60°C
Battery charging	Yes	Yes	No	Yes

Chassis dynamometers

The laboratory chassis dynamometers (AVL Zoellner 48" compact) are mounted in the ambient and climatic chamber floors (see Fig. 2 and Fig. 4). Fully integrated in the laboratory management system (AVL iGEM and HORIBA VETS), they are controlled by software which includes functions not only for emissions testing according to international test cycles (EU cycles: WLTC, RTS95 (used for RDE development work), NEDC, WMTC; US cycles: FTP-75, HWFET, US06; Japanese cycles: JC08), but also for obtaining engine power measurements under both static and dynamic conditions and can be capable of simulating various non-legislative driving cycles used for R&D purposes. In order to carry out cycle-based emissions tests, the laboratories feature a single roller chassis dynamometer in Emission Laboratory No. 1 (2WD) and a twin axle single roller chassis dynamometer in Emission Laboratory No. 2 (4WD), both made by AVL of Austria, with the specification presented in Table 3.

Table 3. Specification of the chassis dynamometers

Parameter	Unit	EmiLab.1	EmiLab.2
Number of axles	pcs.	1	2
Number of rollers	pcs.	2	4
Roller diameter	mm	1219.2	1219.2
Distance between inner roller edges	mm	914	914
Axle base	mm	–	2 000–4 600
Nominal power	kW	153	153
Peak power	kW	258	258
Maximum velocity	km/h	200	250
Simulated mass 2WD	kg	454–5448	454–5448
Simulated mass 4WD	kg	–	800–5448
Motorcycle sim. mass	kg	–	150–454

The AVL-Zoellner 48" compact chassis dynamometer systems in BOSMAL's laboratories for exhaust emissions analysis is designed for testing 2 axled motor vehicles with either front, rear and all-wheel drive and with axle loads of up to 2000 kg. The design of these chassis dynamometers are based on the US EPA C100081T1 specification and the AAIM/EPA/CARB acceptance procedure, Regulation GTR 15, Regulations EC (No. 715/2007, 692/2008 and 595/2009), EPA 40 CFR 1066, TRIAS 31-J042(3)-01 and TRIAS 99-006-01. These test systems are designed with the AC power engines positioned between the rollers. The wind-speed fans are positioned in front on the chassis dynamometer to simulate speed-proportional air flow at speeds 0–150 km/h (Fig. 2 and Fig. 4). The chassis dynamometer in the Emission Laboratory No. 2 includes the functional extension to test motorcycles (Fig. 6), mopeds and scooters with the inertia simulation range from 150 kg to 454 kg.

Emissions testing systems

The laboratories feature emissions analysis suites from the Austrian firm AVL in Emission Laboratory No. 1 and the Japanese firm Horiba in Emission Laboratory No. 2. The AVL emissions system in Laboratory No. 1 consists of a CVS i60 sampling system, together with a dilution tunnel (Fig. 7), a set of AMA i60 SII D1 LE exhaust analyzers and an AVL iGEM management system (Fig. 8).

Fig. 6. View of a motorcycle positioned on the chassis dynamometer in Emission Laboratory No. 2

Fig. 7. AVL's dilution tunnel in Emission Laboratory No. 1

Fig. 8. AVL iGEM emission system management in Emission Laboratory No. 1

The Horiba emissions system in Laboratory No. 2 consists of a CVS-CFV sampling system, together with a dilution tunnel (Fig. 9), a set of MEXA 7400 HRTLE exhaust analyzers and a VETS7000NT management system (Fig. 10).

Fig. 9. HORIBA's dilution tunnel in Emission Laboratory No. 2

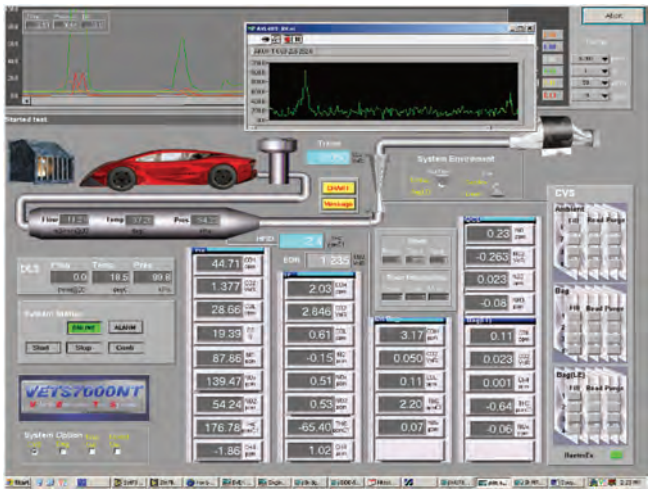

Fig. 10. HORIBA VETS emission system management in Emission Laboratory No. 2

Sample bags of both emissions systems for the sampling of ambient and exhaust gases are housed in a heated, insulated units maintained at 35°C to prevent condensation. The dilution tunnels are connected to installations for filtering diluted exhaust gas through particulate matter filters, which are weighed before and after testing to quantify emission of PM from any vehicle type. The AVL iGEM control software and the HoribaVETS7000NT control software maintain the analyzers and their various activities during testing and analysis of bag emissions, such as calibration, purging, etc. Both systems automate the signals sent to the driver's aids, and include options for testing over all the test cycles previously mentioned, as well as any other cycle added to the system via the implementation of new programs. Additionally, the software monitors the laboratories' environmental parameters (temperature, pressure, humidity) as well as ambient concentrations of HC, CH_4, CO, and O_2 within the chamber to ensure that each test is safe, reliable, repeatable and thoroughly documented.

The climatic chamber for PM stabilization and weighting

European emission legislation (and others) also require increased accuracy of particulate sample filter weighing, as well as specially equipped climatic rooms in which to install the microbalance for filter weighing. The climatic chamber for stabilization and weighing of PM membrane filters for use in emission tests has been described previously [19], and is shown in Fig. 11. The temperature inside the chamber is maintained within the range +20°C to +30°C (with a tolerance of ±2°C), and the humidity is maintained within the range 35%–55% (with a tolerance ±6%), throughout the prescribed stabilization and weighing periods for the PM membrane filter.

REESS charge balance measurement

The measurement of RCB in all phases of WLTC is required for all batteries installed on the vehicles (all low voltage and high voltage batteries) [11, 15]. The electricity balance (ΔE_{REESS}) is equivalent to the value of current at the end of the cycle compared to the beginning of the cycle, multiplied by the nominal battery voltage (e.g. 12 V) to give a final value for the change in electrical power. The REESS charge balance measurement for WLTP testing can have an influence on the final fuel consumption results and a legislative exhaust emissions laboratory must be equipped with measurement devices capable of providing this functionality. The current measurement on the electrical and hybrid vehicles during all type of emission test and preconditioning cycles as well. In BOSMAL's emissions systems, those requirements are fulfilled by using a Hioki Power PW3390 Analyzer and suitable current measurement probes (Fig. 12) in the Horiba VETS emission system and standalone current probes directly connected to the AVL iGEM system (Fig. 12, Table 4). The current measurement is integrated over time at minimum frequency of 20 Hz yielding the measured value of current, expressed in ampere-hours Ah [21]. The Hioki Power Analyzer PW 3390 has four current channels and four voltage channels, which provide to possibilities to measure all four current and voltage signals at the same time.

Fig. 11. The balance, filter conditioning racks and filter cartridges in the climate controlled weighing chamber

Fig. 12. Hioki Power Analyzer PW3390 with the current probe using as a set (Horiba system) or as a standalone device (AVL iGEM system)

2.2. Emissions measurement for development purposes (non-legislative measurements)

BOSMAL has over 45 years' experience and wide possibilities of development emission measurement with diluted and undiluted modal analysis of exhaust gas. BOSMAL's laboratories have the possibilities to carried the engine

('Pre-Cat') and tailpipe ('Post-Cat') development undiluted measurement and diluted modal analysis from the dilution tunnel on a second-by-second basis (for use with CI, SI and Hybrid vehicles). These facilities permit the execution of a wide range of development emissions tests, including:

Table 4. Specification of the Hioki 3390 Power Analyzer and the current probes CT6843 and CT6844

Parameter	Unit	Hioki 3390
Voltage range (7 ranges)	V	15–1500
Current range	A	0.1–20 kA
Frequency range	Hz	0.5–20
Current channels	–	4
Voltage channels	–	4
Parameter	**Unit**	**Current probe CT6843**
Rated current	A	200
Operating temperature	°C	–40 to +85
Maximum frequency	kHz	500
Parameter	**Unit**	**Current probe CT6844**
Rated current	A	500
Operating temperature	°C	–40 to +85
Maximum frequency	kHz	200

- modal analysis of diluted and raw exhaust gases,
- modal analysis of raw exhaust sampled from two locations (nominally pre-cat & post-cat, but the sampling locations are flexible),
- measurement and archival of temperatures from up to eight thermocouples mounted at different locations on the vehicle and on the exhaust line at 10 Hz,
- measurement of the air-fuel ratio and calculation of λ and the EGR percentage,
- catalytic converter efficiency testing (and determination of light-off time) for elimination of THC, CH_4, NMHC, CO, NO, NO_2 and NO_x,
- measurement of unregulated compounds such as N_2O, NH_3 using additional analyzers,
- measurement of modal (raw, undiluted exhaust gas) PN using an additional particulate counter with advanced, optional hardware for sampling under high temperature and pressure conditions,
- unregulated soot measurement of undiluted exhaust gas,
- opacity N [%] or absorption coefficient k [m^{-1}] measurement of undiluted exhaust gas.

The mentioned measurements are described below, with the examples of devices used in BOSMAL's laboratories.

Views of the prefilters of the raw exhaust gas sampling lines for emissions measurements using the AVL emission system and Horiba OVNs (raw exhaust gas sampling lines of Horiba emission systems) are presented below (Fig. 13 and Fig. 14). The analyzers used in both emission system with the ranges of gases are presented in Table 5 and Table 6.

Fig. 13. The prefilters of tailpipe modal measurement of AVL iGEM emission system

Fig. 14. The Horiba OVNs of tailpipe modal measurement of Horiba emission system

Table 5. Component detection ranges of the Horiba MEXA exhaust gas analysis system

MEXA 7400 HTRLE + MEXA 7500 DEGR Modal Emission Analysis System								
Line			Low Emission	Diluted	PreCat	PostCat	EGR	Tracer CO_2
Component (detection principle)			Range	Range	Range	Range	Range	Range
CO (L)	(NDIR)	[ppm]	0 - 500	0 - 1 000	0 - 5 000	0 - 5 000	-	-
CO (H)	(NDIR)	[%]	-	0 - 10	0 - 10	0 - 5 000	-	-
CO_2	(NDIR)	[%]	0 - 20	0 - 20	0 - 20	0 - 20	0 - 20	0 - 20
O_2	(MPA)	[%]	-	-	0 - 25	-	-	-
NO_x	(CLD)	[ppm]	0 - 100	0 - 1 000	0 - 6 000	0 - 6 000	-	-
NO	(CLD)	[ppm]	-	-	0 - 6 000	0 - 6 000	-	-
THC	(FID)	[ppmC1]	0 - 50	0 - 3 000	0 - 37 000	0 - 37 000	-	-
THC	(HFID)	[ppmC1]	-	0 - 3 000	-	-	-	-
CH_4	(GC-FID)	[ppmC1]	0 - 400	-	0 - 20 000	0 - 20 000	-	-
THC / CH_4	(HFID)	[ppmC1]	-	-	0 - 37 000 (THC) 0 - 20 000 (CH_4)	0 - 37 000 (THC) 0 - 20 000 (CH_4)	-	-

Table 6. Component detection ranges of the AVL AMA exhaust gas analysis system

AVL AMA i60 Modal Emission Analysis System						
Line			Diluted	PreCat	PostCat	Tracer CO_2
Component (detection principle)			Range	Range	Range	Range
CO (L)	(NDIR)	[ppm]	0 - 5 000	0 - 1 000	0 - 1 000	-
CO (H)	(NDIR)	[%]	0 - 0.5	0 - 10	0 - 10	-
CO_2	(NDIR)	[%]	0 - 20	0 - 20	0 - 20	0 - 20
O_2	(PMD)	[ppm]	-	0 - 250 000	0 - 250 000	-
NO_x / NO	(CLD)	[ppm]	0 - 1 000	0 - 6 000	0 - 6 000	-
THC	(FID)	[ppmC1]	0 - 3 000	0 - 37 000	0 - 10 000	-
CH_4	(FID) (NMHC Cutter)	[ppmC1]	0 - 400	0 - 20 000	0 - 3 000	-

The raw modal results calculation is based on the Tracer CO_2 method in the Horiba emission system as a stand-alone line. In the AVL emission systems, the Tracer CO_2 method is used, and the second possibility in AVL emission system is the measurement of highly dynamic gas flows. The AVL emission system was built to include the AVL FLOWSONIX™ Air measurement unit (Fig. 15). The ultrasonic transit time measurement principle combined with specifically developed AVL ultrasonic sensors is capable of measuring highly dynamic bidirectional air flows with a data rate of up to 1 kHz [22]. The working range of air flow measurement is 0–2600 kg/h. The ultrasonic sensor is more precise in comparison to the CO_2 Tracer method during the emission testing of vehicle with partially or fully hybridized powertrains (including mild hybrids and the simplest variants: micro hybrids with Stop & Start systems).

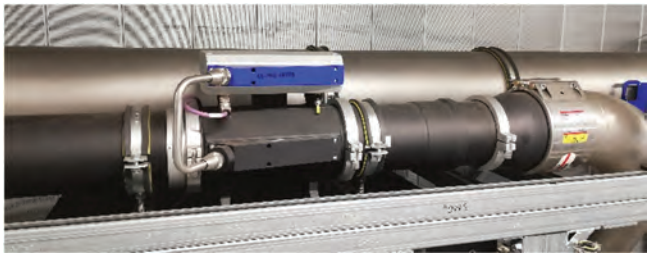

Fig. 15. The AVL FLOWSONIX™ unit mounted on the dilution tunnel in Emission Laboratory No. 1

Dedicated RNC measurement devices

Emissions of reactive nitrogen compounds (RNCs) such as nitric oxide (NO), nitrogen dioxide (NO_2), and ammonia (NH_3) have a real impact on air quality in city centres and urban agglomerations. Unregulated compound of exhaust emission gas like NH_3 contributes to the formation of secondary particulate aerosols, an important air pollutant of impacts on human health [24]. In BOSMAL's laboratories online modal measurements are provided by two types of RNC/NH_3 analysers: MEXA 1400QL-NX (Fig. 16) measuring all RNCs, produced by the Japanese firm HORIBA and AMA i60 LDD measuring NH_3 only (Fig. 16) produced by the Austrian firm AVL. The specifications of both devices are presented in Table 7. The MEXA-1400QL-NX is an analyser for direct measurement of all four RNCs: NO, NO_2, N_2O, NH_3 simultaneously in exhaust gas in real-time, sampled at the tailpipe or closer to the vehicle's aftertreatment or even in the CVS system as well. The measuring principle of MEXA-1400QL-NX based on the IR spectroscopy method.

Table 7. Specification of the HORIBA MEXA-1400QL-NX and AVL AMA i60 LDD

Parameter	HORIBA MEXA-1400QL-NX	AVL AMA i60 LDD
Measuring principle	Quantum Cascade Laser infrared spectroscopy	Fourier-Transform InfraRed (Laser Diode Detector)
Min. NH_3 range	0–50 ppm	0–100 ppm
Max. NH_3 range	0–2 000 ppm	0–5 000 ppm
Sample gas condition	113°C	190°C
Permissible Ambient Temperature	Stable within the range of 5°C to 35°C	+5°C up to +40°C, optional air condition on request
Response time $T_{10\text{-}90}$ for NH_3	Within 2.5 s (by switching N_2 to NH_3, at 50 ppm range)	≤ 1.5 sec (depending on the flow)

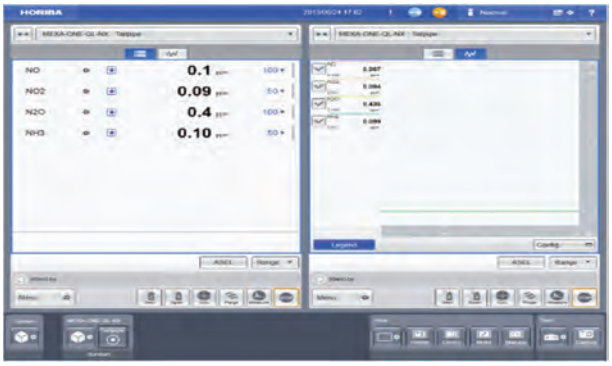

Fig. 16. View of software of HORIBA MEXA-1400QL-NX stand-alone analyzer of NH_3 in the emission laboratory

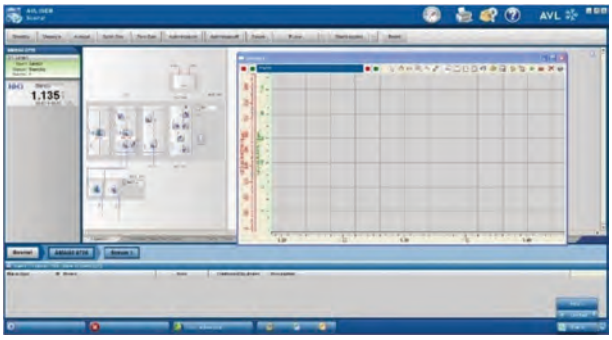

Fig. 17. View of software of AVL AMA i60 LDD stand-alone analyzer of NH_3 in the emission laboratory

Soot measurement

All combustion engines, but especially compression ignition and spark ignition engines with direct injection (DISI) produce unhealthy particles (soot) which are one of dangerous pollutants emitted by combustion engines and which have been regulated in various ways since the 1980s [25, 26]. In development testing on the chassis dyno, BOSMAL can carry out undiluted soot measurements performed using AVL Opacimeter AVL439 (Fig. 18) and Micro Soot Sensor AVL483 (Fig. 19) devices as tailpipe and engine out measurements. In the case of engine out measurements a special conditioning unit controlled by AVL483 (high pressure optional unit) is required, which provide the possibility to perform development testing of engines in the range of pressure relative to ambient pressure from 0 mbar to +3000 mbar. The exhaust gas temperature could increase up to 800°C in comparison to tailpipe measurement, where the temperature is normally limited to 600°C.

Fig. 18. AVL439 Opacimeter with high pressure optional unit (below)

Fig. 19. View of AVL483 Micro Soot Sensor unit

Particle number counter

Measurement of particle number (PN) in the range of direct undiluted exhaust was introduced in BOSMAL's laboratories in 2010. The AVL APC features a wide measuring range (CPC count ≤ 10 000 particles/cm^3) for various engine-aftertreatment combinations, so that repeatable results can be obtained for CI and DISI vehicles with engine out sampling and tailpipe sampling by using a high pressure and temperature solution (Fig. 21). This specification provides to use concentration reduction (known as 'PCRF' in this context) in the range of 2 000–20 000 compared to 100–3 000 for tunnel measurement (the legislative method). The main difference of the principle of both options' functionality is the possibility to increase the PND1 dilution level and updated software is required for this purpose. While the main purpose of these systems is legislative measurements, the systems also archive second-by-second data of raw PN emissions from undiluted exhaust gases, so that comparisons with the second-by-second data of PN emissions from the legislative tunnel measurement could be presented. Such a comparison between diluted and undiluted measurement possibilities is presented in Table 8.

Fig.20. Advance high pressure and temperature option for undiluted emissions measurement of APC AVL device

Table 8. Comparison of diluted and undiluted PN measurement

Parameter	Diluted (CERTIFICATION)	Undiluted option (ADVANCE)
Measuring range	0 … 30,000 p/cm³	0 … 30,000 p/cm³ up to 50,000 p/cm³
Field of application	Diluted measurement (CVS), partial flow dilution (PFDS)	Diluted measurement (CVS), partial flow dilution (PFDS), raw exhaust measurement
Total Dilution	100–3 000	2 000–20 000
Exhaust temperature	≤ 200°C	≤ 600°C Up to 1000°C
Exhaust pressure	± 200 mbar	± 200 mbar Up to 2000 mbar

TSI EEPS size distribution spectrometer

The current debate in the EU on the application of the particle measurement size below 23 nm (down to 10 nm) [16, 24] creates the requirement to measure and test the emission of particle number in the range below the current lower limit. This can be achieved via the Engine Exhaust Particle Sizer (EEPS™) 3090 spectrometer device, which measures the size distribution of engine exhaust particle emissions from 5.6 to 560 nm with the fastest time resolution available (10 Hz). Users can visualize and study the dynamic behaviour of particle emissions that occur during

transient test cycles, during the first few seconds following a cold start, or during regeneration of a particle trap or diesel particulate filter (DPF). For development purposes, it is possible to analyse the particle size distribution as an function of particle size (Fig. 21). The sampling line is heated up to 80°C, 120°C or 150°C and the gases are diluted in the Rotating Disk Thermodiluter which is especially suited for sampling, diluting, and conditioning exhaust particles in based on two nominal dilution ranges: 1st range from 15:1 to 300:1 and 2nd range from 150:1 to 3 000:1. A view of the thermodiluter mounted at the tailpipe sampling point is presented in Fig. 22.

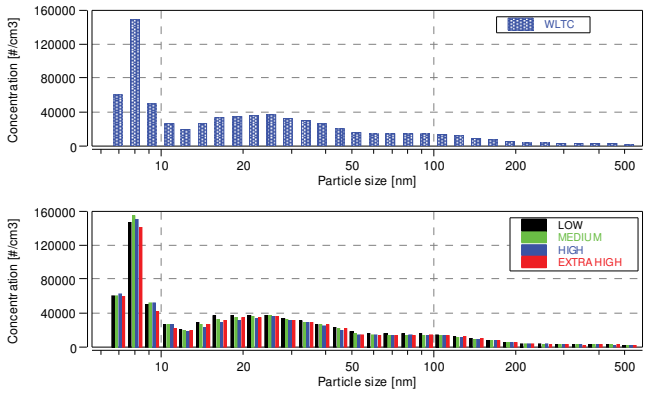

Fig. 21. An example of the particle size distribution over the WLTC

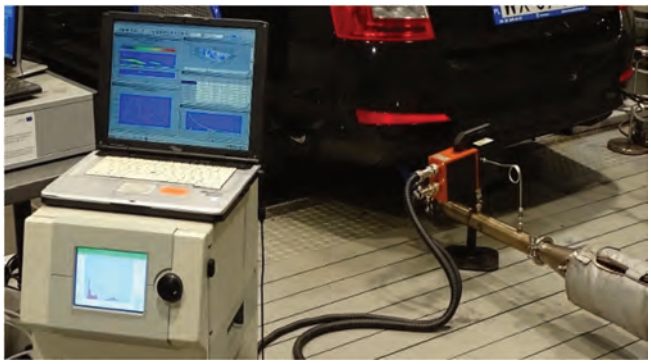

Fig. 22. The EEPS spectrometer and the Rotating Disk Thermodiluter with the heated sampling line mounted on the tailpipe during an emission test

3. RDE testing

New requirements for type approval testing [11, 15] include real driving emissions (RDE) tests as well. RDE tests require the measurement of exhaust emissions outside the laboratory using portable emissions measurement systems (PEMS), but for R&D purposes, such devices can also be used in the laboratory on a chassis dynamometer instead of on the road. As such, PEMS systems can be understood to be components of a modern exhaust emissions laboratory. BOSMAL's laboratories are equipped with an AVL M.O.V.E. GAS PEMS and PN PEMS system and a HORIBA OBS-ONE PEMS system. Both systems and their use for legislative and development testing will be presented during the 8th International Congress on Combustion Engines in Cracow, Poland, on 17–18 June, 2019 and a description and detailed technical discussion will be published in this journal with the title *Development of RDE test methodology in light of Euro 6d emissions requirements (Author: Dr Piotr Pajdowski, Co-authors: Joseph Woodburn, Piotr Bielaczyc, Bartosz Puchałka)*. Overall views of both PEMS systems are presented in Fig. 23 and Fig. 24.

4. Summary

The introduction of new, ever more stringent emissions standards, such as Euro 6d [11, 15, 17, 26], the planned Euro 7 standard, globally-harmonized test procedures (the WLTP) and even local emissions limits (city/local authority vehicle circulation restrictions) [27] necessitate continuous financial and intellectual investment in emissions testing systems, technical know-how and thorough knowledge of test procedures and the interpretation of results.

Fig. 23. M.O.V. E. GAS PEMS and M.O.V.E. PN PEMS mounted on a passenger car for an RDE test

Fig. 24. OBS-ONE HORIBA mounted inside a passenger car for an RDE test

BOSMAL Automotive R&D Institute (Bielsko-Biala, Poland) is one of the largest research centers in Europe specializing in research on engines and automotive components as well as complete cars. BOSMAL cooperates with many leading vehicle and engine manufacturers to explore and launch new models of vehicles (gasoline, Diesel, CNG, LNG, hybrid – and increasingly electric) that meet increasingly stringent emission standards and assists in the development of new engine designs, reducing vehicular fuel consumption and the introduction of alternative powertrains and fuels. The two state-of-the-art laboratories described in this paper permit BOSMAL to compete in the international

automotive arena in the testing and fulfilling of new requirements, more complex measurement techniques used in automotive emissions research. The laboratories have already been put to use in a range of projects representing the cutting-edge tests required by the industry, including a wide range of exhaust emissions analysis, performance tests, fuel consumption tests, engine oils and fuel assessments, after-treatment systems research and cold start drivability/ emissions testing at various test cell temperatures. The performance of the new facilities have been highly satisfactory for BOSMAL and its customers alike. In addition to changes to testing hardware and its control software, test methods must be continually evaluated and developed, in concert with the demands of relevant legislation and private customers' expectations and test specifications. Possession of an accreditation No. AB 128 (Fig. 25) for type approval in the range of exhaust emissions and fuel consumption testing mean BOSMAL has a place among the most professional and advanced laboratories of this type in Europe. The BOSMAL AR&DI Ltd. is a private and independent company which are offering wide range of accredited testing, service, design and production for all Customers which want to perform specialized works witch high professional quality.

Fig. 25. BOSMAL's accreditation certificate for testing laboratory AB 128 with confirmation of the PN-EN ISO/IEC 17025:2005 standard

Nomenclature

CARB	California Air Resources Board
CI	Compression ignition
CNG	Compressed natural gas
CVS	Constant volume sampling
DISI	Direct injection spark ignition
DPF	Diesel particulate filter
EPA	Environmental Protection Agency
EU	European Union
FTIR	Fourier-transform infrared spectroscopy
GHG	Greenhouse gas emissions
IR	Infrared spectroscopy
nm	nanometer
PEMS	Portable Emission Measurement System
PM	Particulate mass
PN	Particle number
PNC	Particle number counter
ppm	Parts per million
RCB	REESS charge balance
RDE	Real Driving Emissions
REESS	Rechargeable electric energy storage system
RNC	Reactive Nitrogen Compound
SCR	Selective Catalytic Reduction
SFTP	Supplemental Federal Test Procedure
SI	Spark ignition
VETS	Vehicle Emissions Testing System (Horiba trademark)
WLTC	Worldwide harmonized light-duty cycle
WLTP	Worldwide harmonized light-duty test procedures

Bibliography

[1] BIELACZYC, P. Global development of emissions reduction strategies from light duty vehicles, 2nd International Conference on the Sustainable Energy and Environmental Development, *IOP Conf. Series: Earth and Environmental Science*. 2019, **214**, 012139. DOI: 10.1088/1755-1315/214/1/012139.

[2] BIELACZYC, P., WOODBURN, J. Trends in Automotive Emission Legislation: *Impact on LD Engine Development, Fuels, Lubricants and Test Methods: a Global View, with a Focus on WLTP and RDE Regulations, Emission Control Science and Technology*. 2019, **5**, 86-98. DOI: 10.1007/s40825-019-0112-3.

[3] European Commission, Communication from the Commission to the European Parlament, the Council, the European Parliament and Social Committee and the Committee of the Regions, Commission Work Programme 2019, Strasbourg, 23.10.2018, COM(2018) 800 final.

[4] Transport & Environment (T&E), CO_2 Emissions from cars: the facts, April 2018.

[5] OLIVIER, J.G.J., SCHURE, K.M., PETERS, J.A.H.W. Trends in global CO_2 and total greenhouse gas emissions: 2017 Report, Netherlands Environmental Assessment Agency. *The Hague*, 2017, PBL publication number: 2674.

[6] European Environment Agency (EEA), Average CO2 emissions from newly registered motor vehicles. 11 Jun 2018.

[7] Continental, Worldwide Emission Standards and Related Regulations, Passenger Cars / Light and Medium Duty Vehicles, September 2017.

[8] International Council on Clean Transportation Europe (ICCT), European Vehicle Market Statistics, Pocketbook 2017/18.

[9] https://www.bosmal.eu/676-scope_of_accreditation_of_the_testing_laboratory_no._ab_128_02.08.2018_en

[10] BIELACZYC, P., SZCZOTKA, A., WOODBURN, J. Carbon dioxide emissions and fuel consumption from passenger cars tested over the NEDC and WLTC – an overview and experimental results from market representative vehicles, 2nd International Conference on the Sustainable Energy and Environmental Development. *IOP Conf. Series: Earth and Environmental Science*. 2019, **214**, 012136. DOI: 10.1088/1755-1315/214/1/012136.

[11] Commission Regulation (EU) 2017/1151 of 1 June 2017 supplementing Regulation (EC) No 715/2007 of the European Parliament and of the Council on type-approval of motor vehicles with respect to emissions from light passenger and commercial vehicles (Euro 5 and Euro 6) and on access to

vehicle repair and maintenance information, amending Directive 2007/46/EC of the European Parliament and of the Council, Commission Regulation (EC) No 692/2008 and Commission Regulation (EU) No 1230/2012 and repealing Commission Regulation (EC) No 692/2008. Official Journal of the European Union, L 175, 1-643, 7.7.2017.

[12] Commission Regulation (EC) No 692/2008 of 18 July 2008 implementing and amending Regulation (EC) No 715/2007 of the European Parliament and of the Council on type-approval of motor vehicles with respect to emissions from light passenger and commercial vehicles (Euro 5 and Euro 6) and on access to vehicle repair and maintenance information. Official Journal of the European Union, L199, 1-136, 28.7.2008.

[13] Regulation No 101 of the Economic Commission for Europe of the United Nations (UN/ECE)—Uniform provisions concerning the approval of passenger cars powered by an internal combustion engine only, or powered by a hybrid electric power train with regard to the measurement of the emission of carbon dioxide and fuel consumption and/or the measurement of electric energy consumption and electric range, and of categories M1and N1vehicles powered by an electric power train only with regard to the measurement of electric energy consumption and electric range. Supplement 7 to the original version of the Regulation—Date of entry into force: 18 June 2007.

[14] Regulation No 115 of the Economic Commission for Europe of the United Nations (UN/ECE) Uniform provisions concerning the approval of: I. specific LPG (liquefied petroleum gases) retrofit systems to be installed in motor vehicles for the use of LPG in their propulsion system; II. specific CNG (compressed natural gas) retrofit systems to be installed in motor vehicles for the use of CNG in their propulsion system, Supplement 6 to the original version of the Regulation – Date of entry into force: 10 June 2014.

[15] Global technical regulation No. 15, Global technical regulation on Worldwide harmonized Light vehicles Test Procedures (WLTP), Amendment 3, Established in the Global Registry on 15 November 2017.

[16] GIECHASKIEL, B., LAHDE, T., SUAREZ-BERTOA, R. et al. Particle number measurements in the European legislation and future JRC activities. *Combustion Engines*. 2018, **174**(3), 3-16. DOI: 10.19206/CE-2018-301.

[17] BIELACZYC, P., WOODBURN, J., GANDYK, M. Trends in automotive emissions, fuels, lubricants, legislation and test methods – a global view, with a focus on the EU & US – Summary of the 5th International Exhaust Emissions Symposium (IEES). *Combustion Engines*. 2016, **166**(3), 76-82. DOI: 10.19206/CE-2016-342.

[18] United States Electronic Code of Federal Regulations, Title 40, Part 86.161, 86.161-00. Air conditioning environmental test facility ambient requirements. www.law.cornell.edu/cfr/text/40/86.161-00.

[19] BIELACZYC, P., SZCZOTKA, A., PAJDOWSKI, P., WOODBURN, J. Development of vehicle exhaust emission testing methods – BOSMAL's new emission testing laboratory. *Combustion Engines*. 2011, **144**(1), 3-12.

[20] United States Electronic Code of Federal Regulations, Title 40, Part 1066, 1066.835. Exhaust emission test procedure for SC03 emissions: www.law.cornell.edu/cfr/text/40/1066.835.

[21] www.hioki.com/en/products/detail/?product_key=6413

[22] www.avl.com/-/avl-flowsonix-air

[23] JAWORSKI, P. et al. SCR systems for NO_x reduction in heavy and light duty vehicles. *Combustion Engines*. 2016, **164**(1), 32-36.

[24] GIECHASKIEL, B., SCHIEFER, E., SCHINDLER, W. et al. Overview of soot emission measurements instrumentation: from smoke and filter mass to particle number European Commission. 2013-01-0138, TSAE-13AP-0138. DOI: 10.4271/2013-01-0138.

[25] GIECHASKIEL, B., LAHDE, T., CLAIROTTE, M. et al. Post Euro 6/VI activities focusing on particle number, Expert Panel Discussion EU/China Emissions Regulations, SAE WCX, 2019. DOI: 10.13140/RG.2.2.26039.37286.

[26] Delphi Technologies launches 26th worldwide emissions standards book. 2018/2019, Apr 26, 2018, www.delphi.com/newsroom/press-release/delphi-technologies-launches-26th-worldwide-emissions-standards-book.

[27] BIELACZYC, P. Particulate number (PN) & gaseous emissions in the EU automotive emissions context. Expert Panel Discussion EU/China Emissions Regulations. SAE WCX, 2019.

Piotr Bielaczyc, DEng. – Engine Research Department, BOSMAL Automotive Research and Development Institute Ltd in Bielsko-Biała.
e-mail: *piotr.bielaczyc@bosmal.com.pl*

Dariusz Klimkiewicz, DEng. – Exhaust Emission Laboratory, BOSMAL Automotive Research and Development Institute Ltd in Bielsko-Biała.
e-mail: *dariusz.klimkiewicz@bosmal.com.pl*

Joseph Woodburn, MSci – Exhaust Emission Laboratory, BOSMAL Automotive Research and Development Institute Ltd in Bielsko-Biała.
e-mail: *joseph.woodburn@bosmal.com.pl*

Andrzej Szczotka, DEng. – Exhaust Emission Laboratory, BOSMAL Automotive Research and Development Institute Ltd in Bielsko-Biała.
e-mail: *andrzej.szczotka@bosmal.com.pl*

Article citation info:
ANDRYCH-ZALEWSKA, M., CHŁOPEK, Z., MERKISZ, J., PIELECHA, J. Exhaust emission from a vehicle engine operating in dynamic states and conditions corresponding to real driving. *Combustion Engines*. 2019, **178**(3), 99-105. DOI: 10.19206/CE-2019-317

Monika ANDRYCH-ZALEWSKA
Zdzisław CHŁOPEK
Jerzy MERKISZ
Jacek PIELECHA

CE-2019-317

Exhaust emission from a vehicle engine operating in dynamic states and conditions corresponding to real driving

The article presents the exhaust emission results from a diesel engine in dynamic states of engine operation in the driving tests: NEDC (New European Driving Cycle) and Malta test, developed at the Poznan University of Technology. The NEDC and Malta tests were carried out as simulations on the engine test bench mimicking the driving tests conditions. The test results of the emission of carbon monoxide, hydrocarbons and nitrogen oxides obtained in each of the tests were presented. The dynamic states have been classified depending on the time derivative value of the torque and engine rotational speed. Both the positive and negative as well as zero time derivative values of torque and rotational speed were considered. Therefore, overall six types of dynamic states were analyzed. A high sensitivity of exhaust emission to various types of dynamic states was found. The exhaust emission sensitivity to dynamic states in the Malta test was found to be higher than for the NEDC test, although these tests have similar properties (average rotational speed and average torque). This is due to the fact that the NEDC test is created on the basis of the similarity of zero-dimensional characteristics of the car's speed characteristic, whereas the Malta test was designed in accordance with the principle of faithful representation in the time domain of the NEDC speed curve.

Keywords: *combustion engines, exhaust emissions, dynamic states*

1. Introduction

The functional properties of internal combustion engines depend on the operating states of the engines, which means also on the occurrence of dynamic states of operation [3–8]. As operating states of internal combustion engines, one can consider – in thermally stabilized conditions – the quantities characterizing the engine operation. Therefore, the engine operating conditions that were considered for analysis included: rotational speed and torque, characterizing the engine load [6].

The exhaust emissions [3, 4, 6–8] are particularly important among the properties of internal combustion engines. While the influence of static states of engines' operation on exhaust emission is possible to evaluate unambiguously as a result of empirical research, the diversity of types of dynamic states prevents such unambiguity of test results [6]. Therefore, the exhaust emission testing taking into account dynamic states is usually carried out in dynamic tests adopted as standards. As a result of such tests, averaged value results are obtained, characterizing the total effect of these states, both dynamic and static, on the exhaust emission. Such tests are carried out in type approval procedures. It is much more difficult to try to assess specific types of dynamic states on the operating properties of internal combustion engines. The results obtained this way [3, 4, 6–8] are, however, difficult to generalize.

In this work, attempts have been made to test the emission of pollutants from the compression-ignition engine in dynamic states in tests: NEDC (New European Driving Cycle) [9] and the Malta test [1, 2], developed at Poznan University of Technology to simulate the NEDC test in accordance with the similarity criterion of zero dimensional characteristics of the vehicle speed characteristic.

2. Test object and measuring equipment

The test object was a Fiat 1.3 JTD (MultiJet) engine. It was a 4-cylinder compression-ignition engine with turbocharging with displacement of 1.3 dm^3, and having a Euro 4 emission class.

Engine dynamometer tests were carried out at the AVL Dynoroad 120 kW that enabled testing in dynamic conditions. The dynamometer software enables simulation of the operating states of an internal combustion engine corresponding to the engine operation in the conditions of vehicle movement. As a result, it was possible to test the engine on the test bench simulating real vehicle operating conditions for a Fiat Idea passenger car, in the NEDC and Malta tests.

The exhaust gas analysis was performed with the Semtech DS analyzer. The analyzer meets the ISO 1065 requirements in the field of exhaust emissions testing with PEMS systems. The Semtech DS analyzer is equipped with the following measuring modules:

- FID (*Flame Ionization Detector*) for determining hydrocarbon concentration,
- NDUV type analyzer (*Non-Dispersive Ultraviolet*) to measure the concentration of nitric oxide and dioxide,
- NIDR (*Non-Dispersive Infrared*) type analyzer to measure carbon monoxide and carbon dioxide concentration,
- electrochemical analyzer for oxygen concentration determination.

In addition to measuring the concentration of exhaust components, the Semtech DS analyzer also allows the measurement of the exhaust gases mass flow.

Measurement values in dynamic conditions were recorded at a frequency of 10 Hz.

The test object and measuring apparatus are described in detail in [1, 2].

3. Test results

Figures 1 and 2 show the rotational speed characteristic in the NEDC and Malta tests, and in Figures 3 and 4 the relative torque characteristic in these tests.

The relative torque for a specific engine speed is defined as the torque ratio for this speed and the maximum torque for the same speed:

$$M_{er}(n) = \frac{M_e(n)}{M_{e\,max}(n)} \tag{1}$$

where: $M_e(n)$ – torque at engine speed n, $M_{e\,max}(n)$ – maximum torque at engine speed n, n – engine speed.

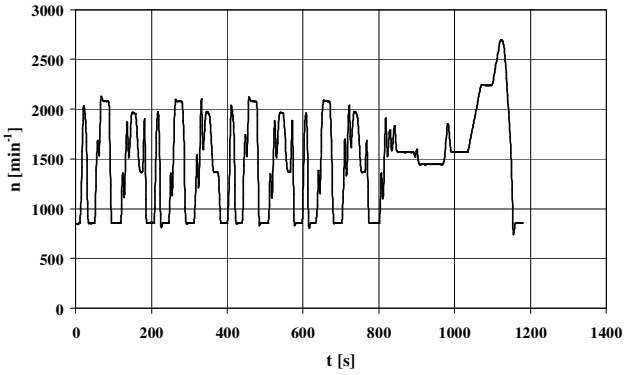

Fig. 1. Engine speed characteristic for the NEDC test

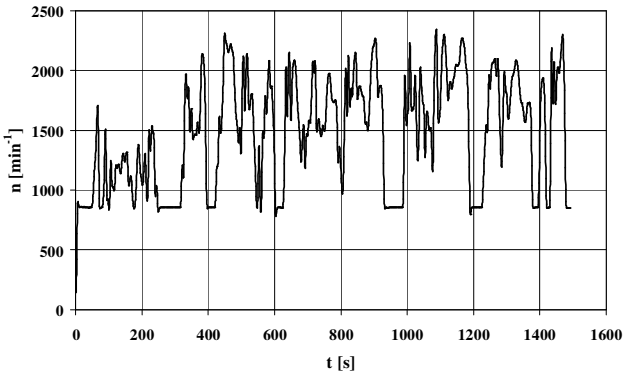

Fig. 2. Engine speed characteristic for the Malta test

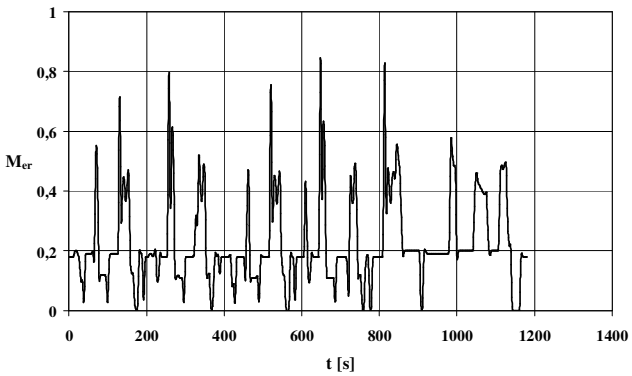

Fig. 3. Relative torque characteristic for the NEDC test

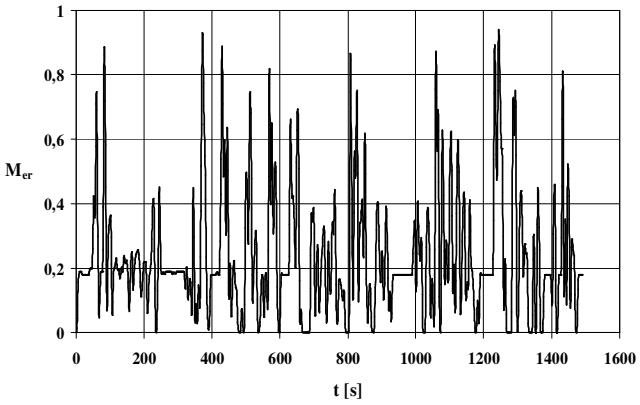

Fig. 4. Relative torque characteristic for the Malta test

The average values of rotational speed and relative torque are similar for both tests – Fig. 5 and 6, while the differences occur in the case of the variation coefficient (Fig. 7 and 8) – the relative coefficient of variation of the torque for the Malta test is noticeably greater (relative difference of around 0.3) – Fig. 8.

Figures 9–14 show the exhaust emission intensity characteristics of carbon monoxide, hydrocarbons and nitrogen oxides in the NEDC and Malta tests.

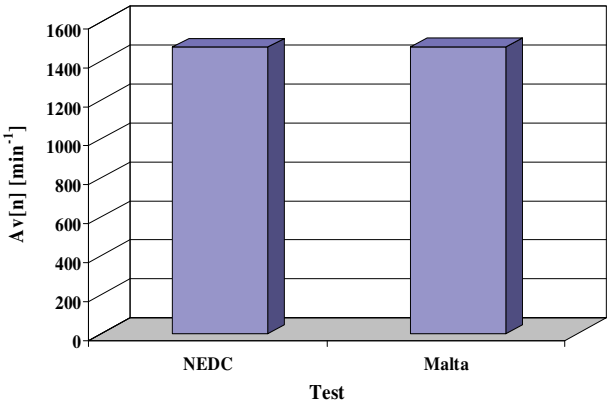

Fig. 5. Average engine speed value in the NEDC and Malta tests

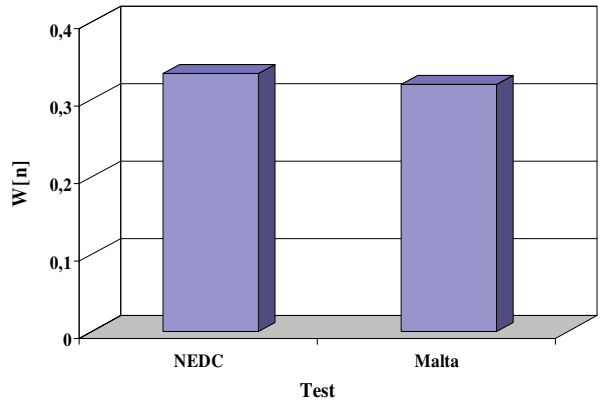

Fig. 6. Rotational speed coefficient of variation in NEDC and Malta tests

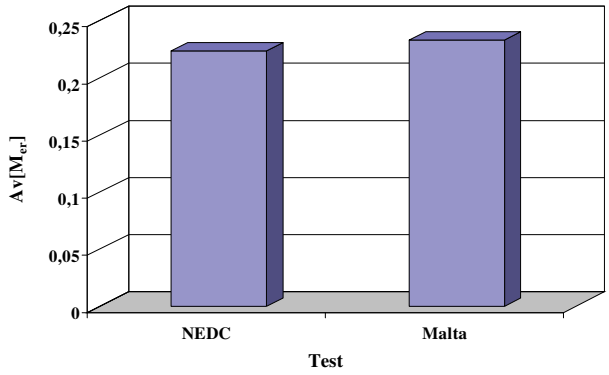

Fig. 7. Mean relative torque value in the NEDC and Malta tests

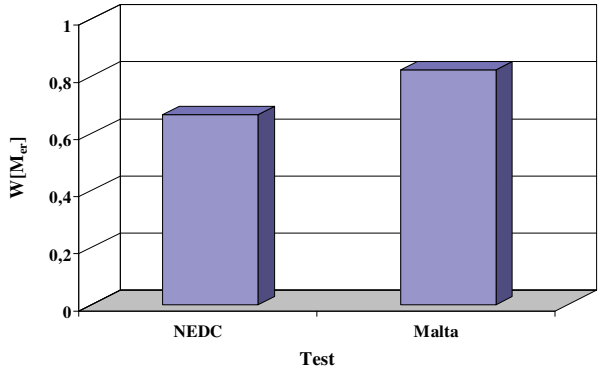

Fig. 8. The relative torque variation coefficient in the NEDC and Malta tests

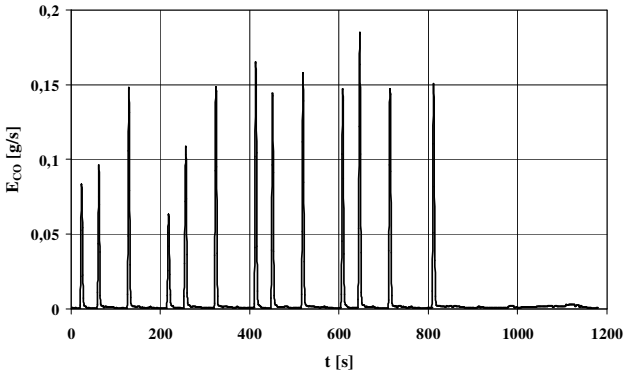

Fig. 9. The emission intensity of carbon monoxide in the NEDC test

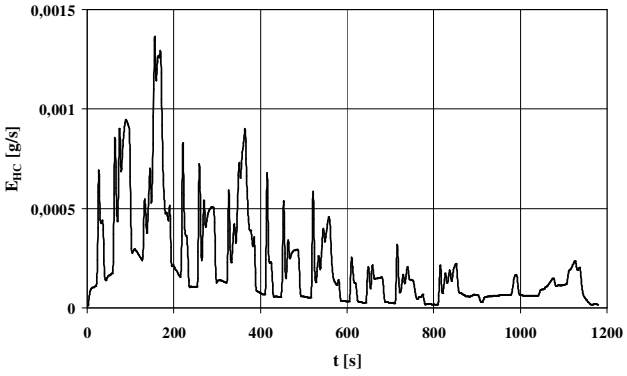

Fig. 10. The emission intensity of hydrocarbons in the NEDC test

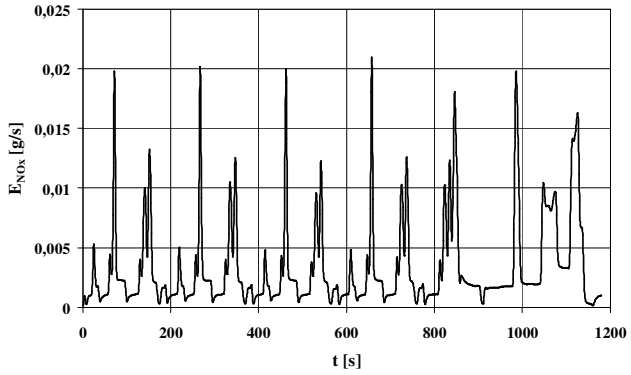

Fig. 11. The emission intensity of nitrogen oxides in the NEDC test

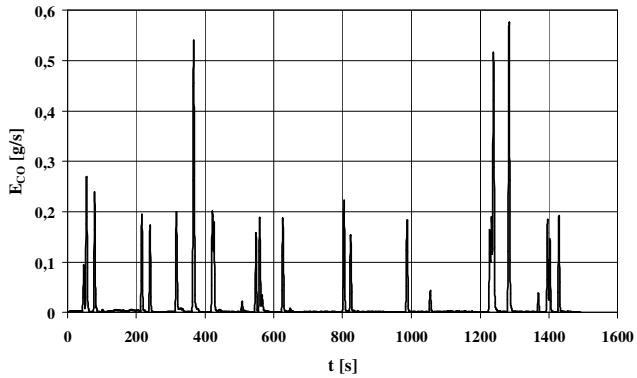

Fig. 12. The emission intensity of carbon monoxide in the Malta test

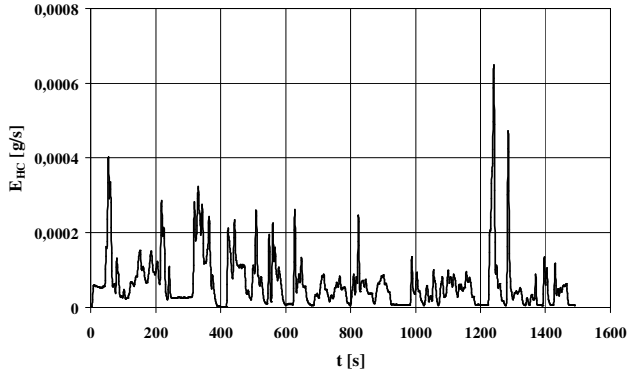

Fig. 13. The emission intensity of hydrocarbons in the Malta test

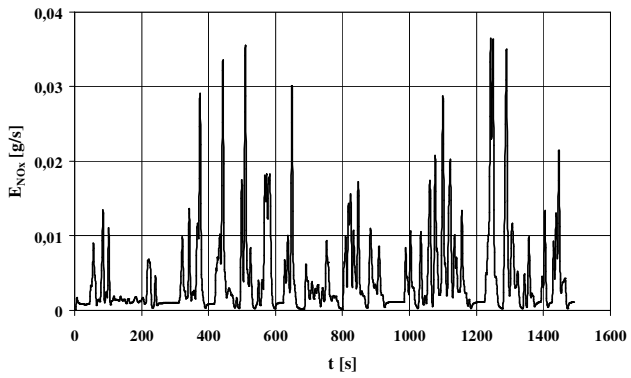

Fig. 14. The emission intensity of nitrogen oxides in the Malta test

4. Test results analysis

The following defined conditions are accepted as basic dynamic states of the engine operation:

$\frac{dn}{dt} < 0$	$\frac{dn}{dt} = 0$	$\frac{dn}{dt} > 0$
$\frac{dM_e}{dt} < 0$	$\frac{dM_e}{dt} = 0$	$\frac{dM_e}{dt} < 0$

(2)

In addition, dynamic states related to both rotational speed and relative torque can be considered:

$\frac{dn}{dt} < 0 \wedge \frac{dM_e}{dt} < 0$	$\frac{dn}{dt} < 0 \wedge \frac{dM_e}{dt} = 0$	$\frac{dn}{dt} < 0 \wedge \frac{dM_e}{dt} > 0$
$\frac{dn}{dt} = 0 \wedge \frac{dM_e}{dt} < 0$	$\frac{dn}{dt} = 0 \wedge \frac{dM_e}{dt} = 0$	$\frac{dn}{dt} = 0 \wedge \frac{dM_e}{dt} > 0$
$\frac{dn}{dt} < 0 \wedge \frac{dM_e}{dt} < 0$	$\frac{dn}{dt} < 0 \wedge \frac{dM_e}{dt} = 0$	$\frac{dn}{dt} < 0 \wedge \frac{dM_e}{dt} > 0$

(3)

The time derivative constancy condition was taken with an accuracy of ± 0.02 of the derivative range with respect to time. Figures 15–20 show the average value of exhaust emission intensity in the NEDC test and in states corresponding to the negative, zero and positive speed derivative relative to time values and in the states corresponding to the negative, zero and positive time derivative values of the relative torque.

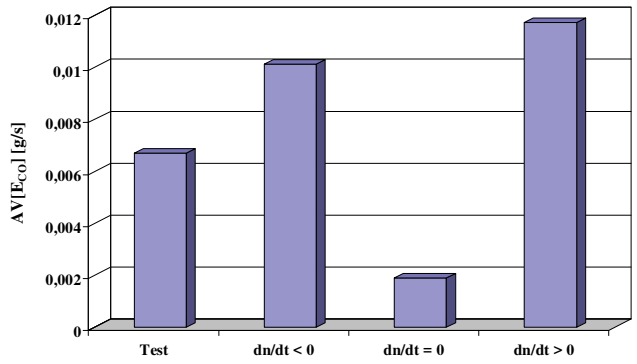

Fig. 15. The average value of the carbon monoxide emission in the NEDC test and in the states corresponding to the negative, zero and positive time derivative values of the engine speed

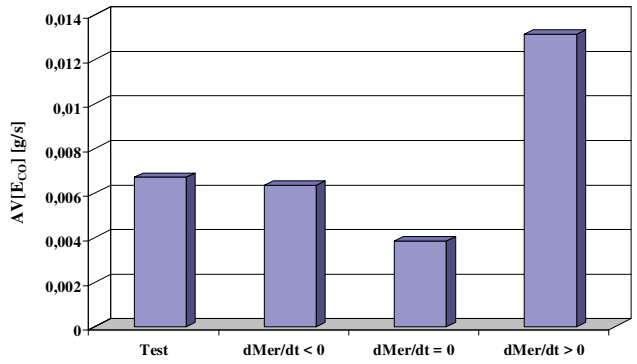

Fig. 16. The average value of the carbon monoxide emission in the NEDC test and in the states corresponding to the negative, zero and positive time derivative values of the engine torque

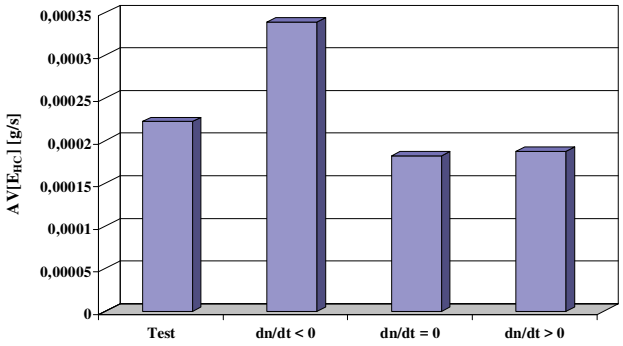

Fig. 17. The average value of the hydrocarbons emission in the NEDC test and in the states corresponding to the negative, zero and positive time derivative values of the engine speed

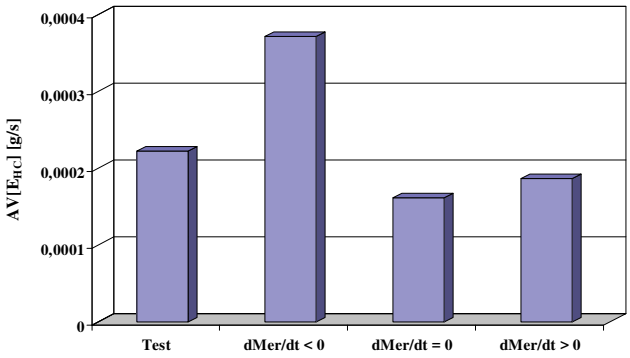

Fig. 18. The average value of the hydrocarbons emission in the NEDC test and in the states corresponding to the negative, zero and positive time derivative values of the engine torque

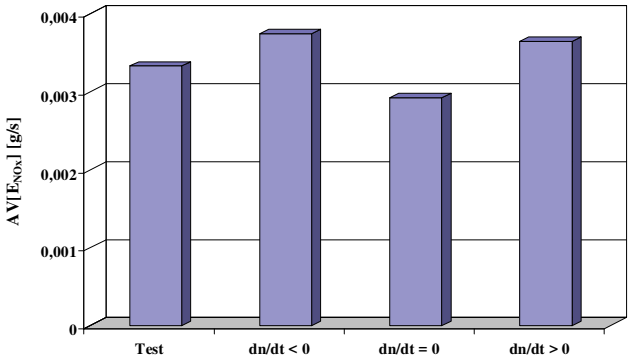

Fig. 19. The average value of the nitrogen oxides emission in the NEDC test and in the states corresponding to the negative, zero and positive time derivative values of the engine speed

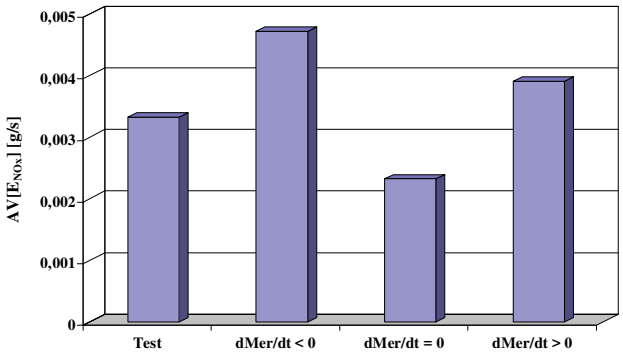

Fig. 20. The average value of the nitrogen oxides emission in the NEDC test and in the states corresponding to the negative, zero and positive time derivative values of the engine torque

Figures 21–26 show the average value of the exhaust emission intensity in the Malta test and in states corresponding to the negative, zero and positive time derivative values of the engine speed and in the states corresponding to the negative, zero and positive time derivative values of the relative torque.

Figures 27–32 present a comparison of the mean exhaust emission intensity in the test and in states corresponding to the negative, zero and positive values of the engine speed derivative with respect to time – for the NEDC and Malta tests.

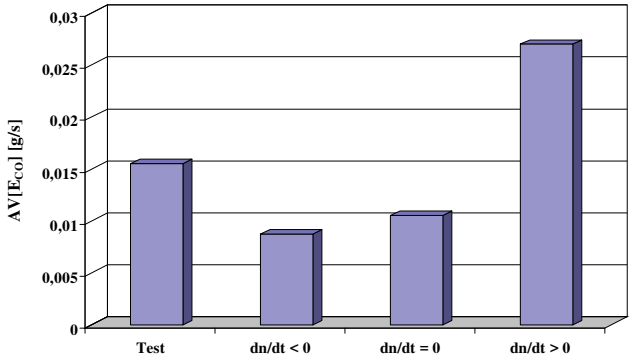

Fig. 21. Mean value of the carbon monoxide exhaust emission in the Malta test and in the states corresponding to the negative, zero and positive values of the engine speed derivative with respect to time

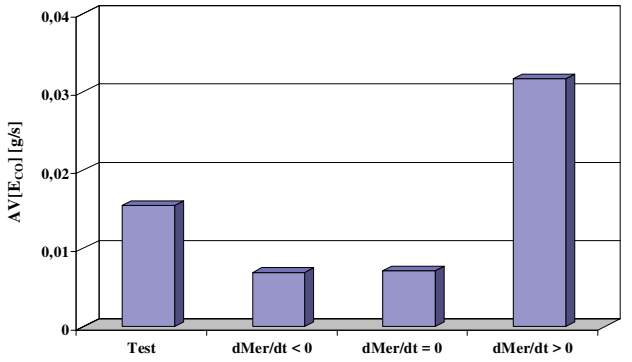

Fig. 22. Mean value of the carbon monoxide exhaust emission in the Malta test and in the states corresponding to the negative, zero and positive values of the engine torque derivative with respect to time

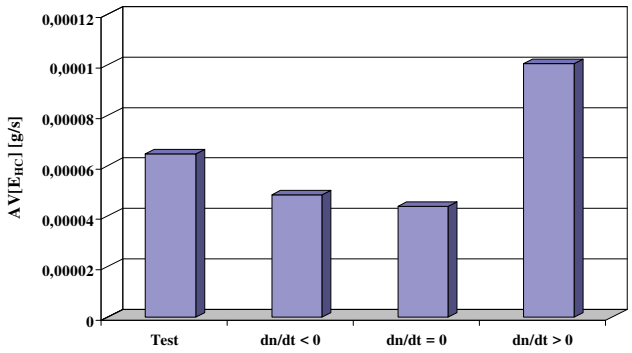

Fig. 23. Mean value of the hydrocarbons exhaust emission in the Malta test and in the states corresponding to the negative, zero and positive values of the engine speed derivative with respect to time

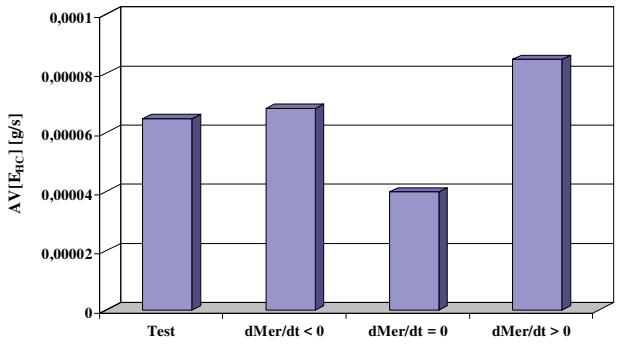

Fig. 24. Mean value of the hydrocarbons exhaust emission in the Malta test and in the states corresponding to the negative, zero and positive values of the engine torque derivative with respect to time

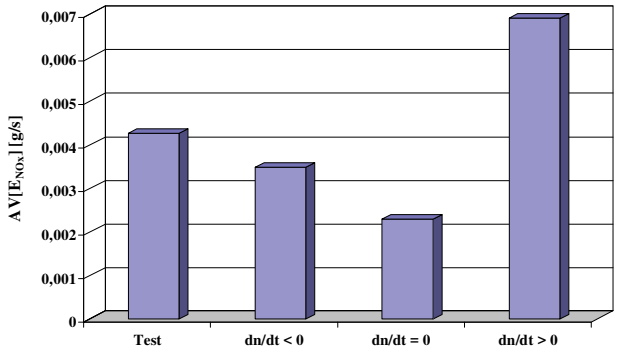

Fig. 25. Mean value of the nitrogen oxides exhaust emission in the Malta test and in the states corresponding to the negative, zero and positive values of the engine speed derivative with respect to time

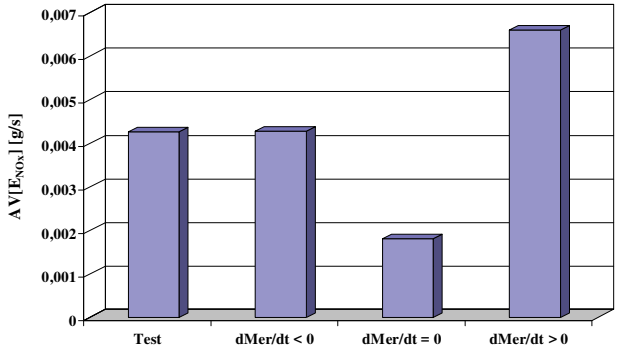

Fig. 26. Mean value of the nitrogen oxides exhaust emission in the Malta test and in the states corresponding to the negative, zero and positive values of the engine torque derivative with respect to time

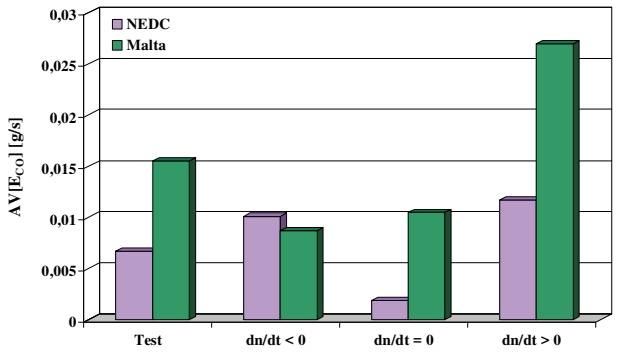

Fig. 27. Comparison of the mean carbon monoxide emission value in the test and in the states corresponding to the negative, zero and positive values of the engine speed derivative with respect to time – for the NEDC and Malta tests

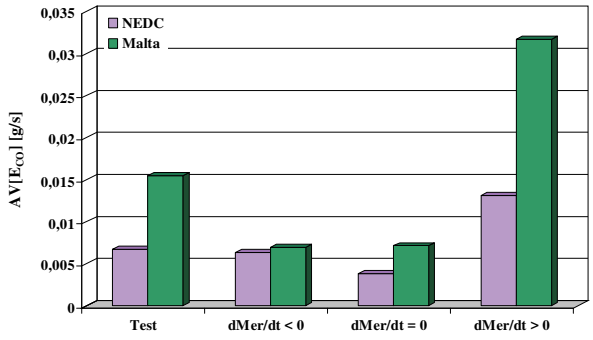

Fig. 28. Comparison of the mean carbon monoxide emission value in the test and in the states corresponding to the negative, zero and positive values of the engine torque derivative with respect to time – for the NEDC and Malta tests

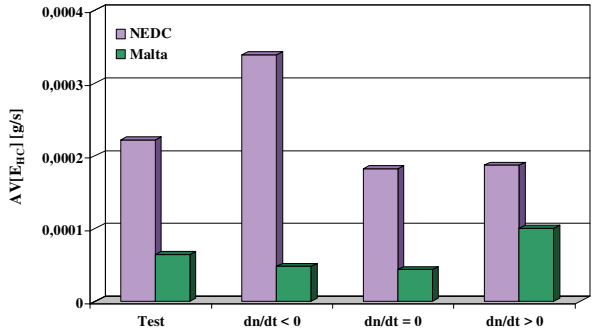

Fig. 29. Comparison of the mean hydrocarbons emission value in the test and in the states corresponding to the negative, zero and positive values of the engine speed derivative with respect to time – for the NEDC and Malta tests

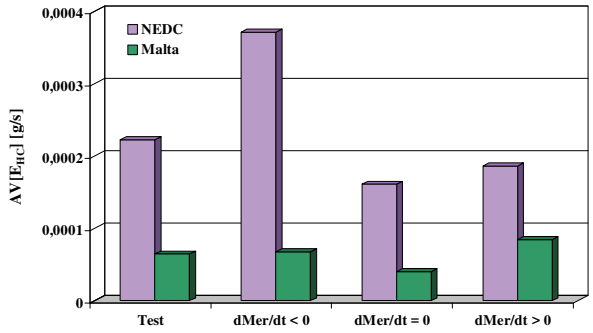

Fig. 30. Comparison of the mean hydrocarbons emission value in the test and in the states corresponding to the negative, zero and positive values of the engine torque derivative with respect to time – for the NEDC and Malta tests

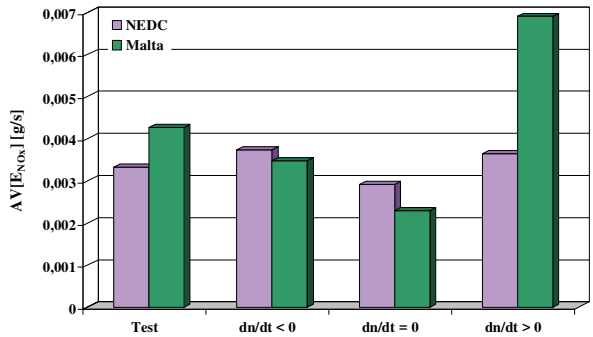

Fig. 31. Comparison of the mean nitrogen oxides emission value in the test and in the states corresponding to the negative, zero and positive values of the engine speed derivative with respect to time – for the NEDC and Malta tests

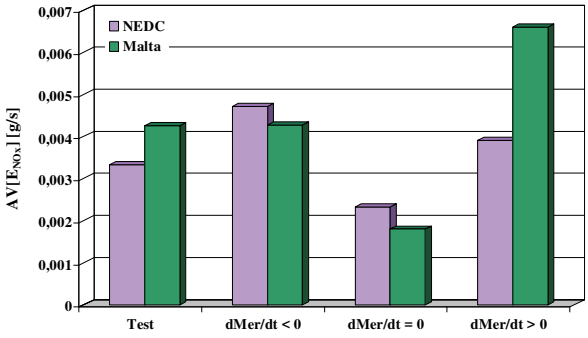

Fig. 32. Comparison of the mean nitrogen oxides emission value in the test and in the states corresponding to the negative, zero and positive values of the engine torque derivative with respect to time – for the NEDC and Malta tests

The sensitivity of exhaust emission values to dynamic states was assessed based on the coefficient of variation of the average exhaust emission intensity value in individual elementary dynamic states – table and fig. 33 and 34.

Table 1. Coefficient of variation of the average exhaust emission intensity value in individual elementary dynamic states

	Test			
Component		CO	HC	NO_x
Dynamic state category				
dn/dt	NEDC	0.666	0.377	0.130
dM_{er}/dt		0.619	0.480	0.334
dn/dt	Malta	0.655	0.490	0.567
dM_{er}/dt		0.933	0.353	0.568

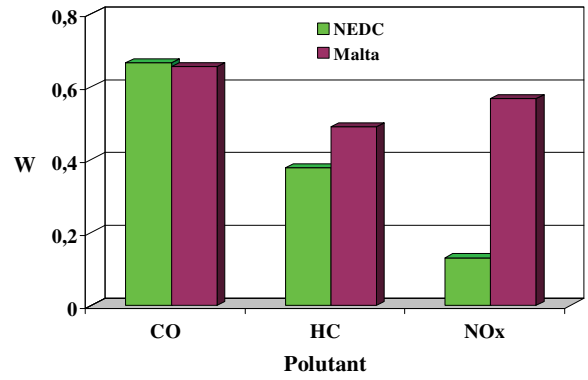

Fig. 33. The coefficient of variation of the average emission intensity value in individual elementary states of dynamic rotational speed variation

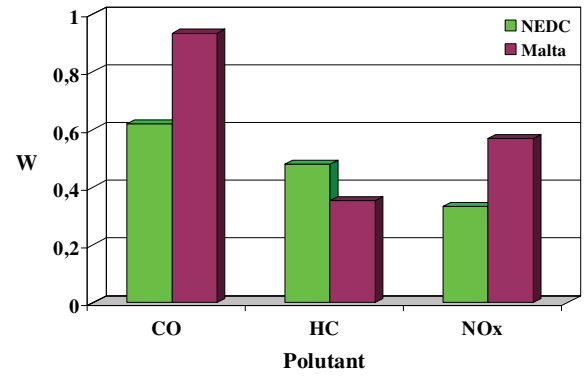

Fig. 34. The coefficient of variation of the average emission intensity value in individual elementary states of dynamic engine torque variation

In general, the exhaust emission sensitivity to dynamic states for torque changes is higher than for changes in rotational speed. The sensitivity of exhaust emissions to dynamic states for the Malta test was also higher. This is mainly due to the fact that the Malta test is created in accordance with the principle of faithful simulation of car speed characteristic in time and the NEDC test in accordance with the principle of similarity of zero-dimensional characteristics of the speed characteristics. Therefore, the Malta test is characterized by stronger dynamic properties.

The highest sensitivity to dynamic states was found for the mean value of carbon monoxide emission in the Malta test and for torque changes, while the smallest – for the average nitrogen oxide emission intensity in the NEDC test and for rotational speed changes.

More detailed results of the analysis can be carried out for the engine operating conditions related to both rotational speed and relative torque, but such analyzes exceed the volumetric capabilities of this work.

5. Conclusions

The article compared exhaust emission in dynamic states in two tests with similar properties: the NEDC test and a Malta test, simulating the NEDC test in road traffic based on the similarities in the average vehicle speed. Dynamic states corresponding to: decreasing, constant and increasing value of engine speed and torque were considered. The following conclusions can be drawn from the research results:

1. Sensitivity of exhaust emission to dynamic states, differentiated due to the type of dynamic states, the test and the measured substance was found.
2. Generally, the exhaust emission sensitivity to dynamic states is greater for changes in torque than for changes in rotational speed.
3. Overall, the exhaust emissions sensitivity to dynamic states is higher for the Malta test than for the NEDC test.
4. The highest sensitivity to dynamic states was found for the mean emission intensity value of carbon monoxide in the Malta test and for changes in torque.
5. The smallest sensitivity to dynamic states was found for the mean emission intensity value of nitrogen oxides in the NEDC test and for engine speed changes.
6. The purposefulness of analyzing the exhaust emission sensitivity for complex dynamic states, including the combination of engine speed and torque variations, was assessed.

Bibliography

[1] ANDRYCH-ZALEWSKA, M., CHŁOPEK, Z., MERKISZ, J., PIELECHA, J. Evaluation of the test drive cycle conditions impact on exhaust emissions from an internal combustion engine. *Combustion Engines*. 2018, **175**(4), 3-9.

[2] ANDRYCH-ZALEWSKA, M. Wpływ katalizatora wewnętrznego na emisję spalin w stanach pracy silnika o zapłonie samoczynnym odpowiadających jego użytkowaniu trakcyjnemu. *Rozprawa doktorska*. Poznań 2018.

[3] ARREGLE, J., BERMUDEZ, V., SERRANO, JR., FUENTES, E. Procedure for engine transient cycle emissions testing in real time. *Experimental Thermal and Fluid Science*. 2006, **30**(5), 485-496.

[4] CHŁOPEK, Z., BIEDRZYCKI, J., LASOCKI, J., WÓJCIK, P. Assessment of the impact of dynamic states of an internal combustion engine on its operational properties. *Eksploatacja i Niezawodnosc – Maintenance and Reliability*. 2015, **17**(1), 35-41.

[5] CHŁOPEK, Z. Synthesis of driving cycles in accordance with the criterion of similarity of frequency characteristics. *Eksploatacja i Niezawodnosc – Maintenance and Reliability*. 2016, **18**(4), 572-577.

[6] CHŁOPEK, Z. Some remarks on engine testing in dynamic states. *Combustion Engines*. 2010, **4**(143), 60-72.

[7] MERKISZ, J., GIS, W. Exhaust emission from vehicles under real conditions. *Proceedings of the Ninth Asia–Pacific International Symposium on Combustion and Energy Utilization*. APISCEU, Beijing 2008.

[8] MERKISZ, J., LIJEWSKI, P., FUĆ, P., WEYMANN, S. Exhaust emission tests from non-road vehicles conducted with the use of PEMS analyzers. *Eksploatacja i Niezawodnosc – Maintenance and Reliability*. 2013, **15**(4), 364-368.

[9] Worldwide emission standards, Passenger cars and light duty vehicles. Delphi. Innovation for the real world. 2016/2017.

Monika Andrych-Zalewska, DEng. – Faculty of Mechanical Engineering at Wrocław University of Technology.
e-mail: *monika.andrych@pwr.edu.pl*

Prof. Jerzy Merkisz, DSc., DEng. – Faculty of Transport Engineering, Poznan University of Technology.
e-mail: *jerzy.merkisz@put.poznan.pl*

Prof. Zdzisław Chłopek, DSc., DEng. – Faculty of Automotive and Construction Machinery Engineering, Warsaw University of Technology.
e-mail: *zdzislaw.chlopek@pw.edu.pl*

Prof. Jacek Pielecha, DSc., DEng. – Faculty of Transport Engineering, Poznan University of Technology.
e-mail: *jacek.pielecha@put.poznan.pl*

Article citation info:
JAWORSKI, A., LEJDA, K., LUBAS, J., MĄDZIEL, M. Comparison of exhaust emission from Euro 3 and Euro 6 motor vehicles fueled with petrol and LPG based on real driving conditions. *Combustion Engines*. 2019, **178**(3), 106-111. DOI: 10.19206/CE-2019-318

Artur JAWORSKI
Kazimierz LEJDA
Janusz LUBAS
Maksymilian MĄDZIEL

CE-2019-318

Comparison of exhaust emission from Euro 3 and Euro 6 motor vehicles fueled with petrol and LPG based on real driving conditions

Constantly increasing requirements regarding emission limits for harmful exhaust components force vehicle manufacturers to improve the construction of vehicle engines as well as exhaust gas cleaning systems. In addition to modifications in the field of technology of motor vehicles themselves, it is also important to study the impact of alternatives to petrol or diesel fuels. One of the most popular fossil fuel is liquid petroleum gas. In the paper, the results of comparative studies on the emission of harmful exhaust components of vehicles meeting the Euro 3 and Euro 6 standards in the field of petrol and LPG fuel use are presented. Emission measurement was performed using a portable emission measurement system from Horiba OBS-2200 under real traffic conditions. The presented results show the differences between the tested vehicles and the fuels used.

Key words: *emission, PEMS, fuel, LPG, RDE*

1. Introduction

In recent years, due to the constantly growing requirements regarding the emission policy, which must be met by car manufacturers, there has been a dynamic development of the construction of internal combustion engines as well as catalytic systems [3]. The main legislative objectives of the European Union concern the reduction of harmful effects on the surrounding environment, both on human health and climate change. The automotive sector is the main source of a different variety of air pollutants, eg hydrocarbons, nitrogen oxides, carbon monoxide, particulate matter as well as greenhouse gases, which include primarily carbon dioxide [2, 4–6, 8].

One of the alternative renewable fuels that have lower emissions of toxic compounds is LPG. LPG is acquired as a naturally occurring product of the natural gas extraction process or as an automatic result of the oil refining production process. LPG meets all four key objectives set by the EU in its guidelines for trans-European energy networks [7]. LPG is petroleum derived colourless gas, consists of propane or butane or from mixtures of both. In everyday usage different mixtures are used depending on the climatic nature of every region [11]. This gas is also characterized by a low price, which makes its popularity grows as an alternative to petrol and diesel.

The aim of the study was to determine the emission value of harmful exhaust components (CO_2, THC, NO_x, CO) for vehicles meeting the Euro 3 and Euro 6 standards in the scope of petrol and LPG fueling. The emission measurement was made by using a portable emission measurement system for the selected route, which included the urban, rural and motorway part.

2. The methodology of the study

The road selected for testing, including the urban, rural and motorway part, is shown in Fig. 1. The route was 40 km long, while the rides were made in June 2018.

The PEMS Horiba OBS-2200 system was used to measure road emissions, the specifications of which are presented in Table 1. PEMS can be installed in the boot of the tested vehicle, while the measuring sensors with a flow meter are connected to the outlet pipe [12]. The exhaust gas pipe must be heated to 190°C to avoid condensation of hydrocarbons. In addition, ambient temperature and humidity sensors, as well as a GPS transmitter, are connected to the system [3]. In order to get a full picture of the impact of the engine operation on the generated emission, the OBDII interface [5, 13, 14] can be connected to the ECU of the vehicle. The RDE test was started by comparing the measurement from the PEMS system with the AMA i60 stationary exhaust gas analysis system. Initial tests were carried out on a chassis dynamometer built in a climate chamber on a passenger car. The test results showed that differences in the emission values of pollutants measured using the PEMS and AMAi60 systems, were within the permissible deviations. Therefore, further measurements of emissions in real traffic conditions can be considered as correct.

Fig, 1. Map with the selected stretch of road test

Table. 1. Selected technical parameters of the PEMS Horiba OBS-2200 system

Parameter	Measurement method	Accuracy
The concentration of exhaust components:		
CO	NDIR – non-dispersive (infrared), range 0–10%	±2.5%
CO_2	NDIR – non-dispersive (infrared), range 0–10%	±2.5%
THC	FID – flame ionization, range 0–10000 ppm	±2.5%
NO_x	CLD – chemiluminescence, range from 0–100 to 0–3000 ppm	±2.5%
Sampling frequency	0.1 Hz	
The heating time of the analyzers	Up to 1 hour	-
Gas flow	Mass flow rate	In the range of ±1.5% of full scale or within ±2.5% of readings

Vehicles used for road emission tests are shown in Fig. 2. The vehicle fulfilling the Euro 3 standard is characterized by a 1991 cm^3 engine, it has manual transmissions, an MPI power system and a TWC catalytic system, while a vehicle meeting the Euro 6 standard has an 1149 cm^3 engine, while the other described parameters are the same as the predecessor, both vehicles are fueled with petrol as well as LPG. On the day of testing, the Euro 3 car had a mileage of 260,000 km, while the Euro 6 was 42,000 km.

Fig. 2. Cars used for road tests with installed PEMS: a) Euro 3, b) Euro 6

3. The road tests results

All 4 tests lasted for a similar time and amounted to around 2500 s, only the travel time for a Euro 3 vehicle fueled with gasoline in the charts is 3000 s, because for illustrative purposes, emissions during cold-start mode were not excluded. The graphs of specific distance emission at the end of the work for all tested harmful exhaust components are already for the engine warmed up. Fig. 3–6 shows the emission intensity of CO_2 for the tested vehicles fueled with petrol and LPG.

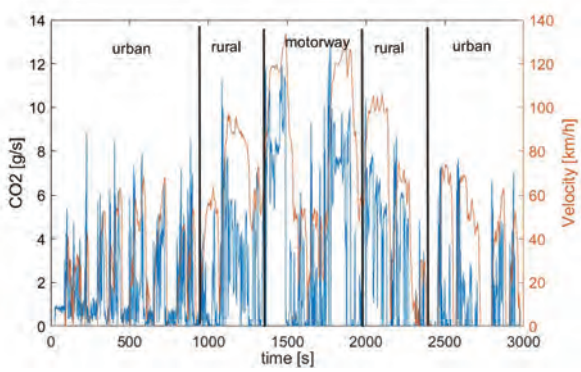

Fig, 3. Emission intensity of CO_2 for Euro 3 petrol fuelled vehicle

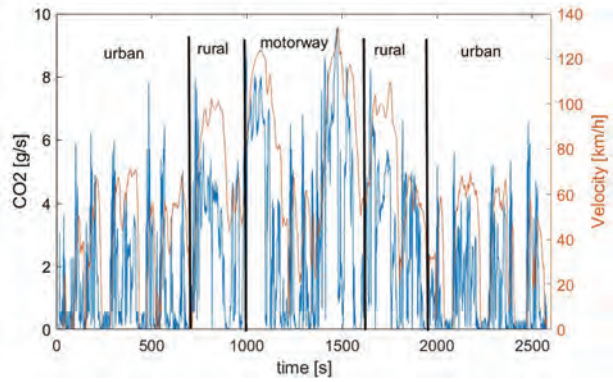

Fig, 4. Emission intensity of CO_2 for Euro 3 LPG fuelled vehicle

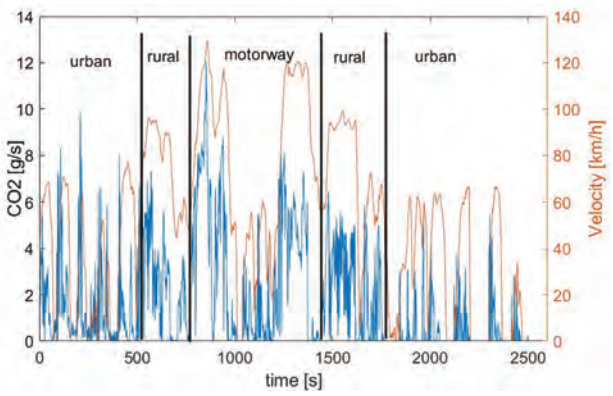

Fig, 5. Emission intensity of CO_2 for Euro 6 petrol fuelled vehicle

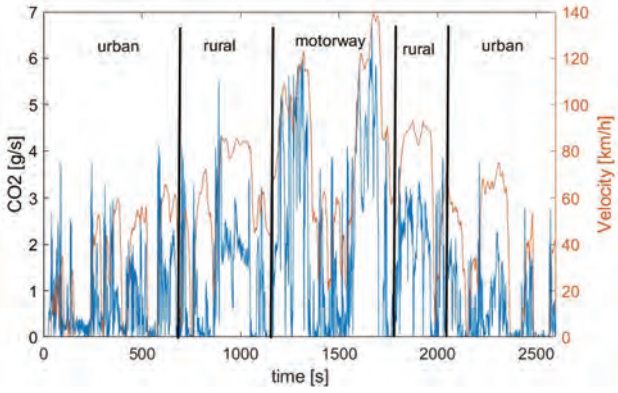

Fig, 6. Emission intensity of CO_2 for Euro 6 LPG fuelled vehicle

Based on Fig. 3–6, it is visible that:

- in relation to Fig. 3, which also has data regarding the cold-start (first 250 s), it can be noticed that the CO_2 emission intensity and its increase as a result of the engine's operating temperature is not so significant compared to other exhaust components, e.g. THC, NO_x,
- the highest CO_2 emission intensity occurs while vehicle speed increase and sudden acceleration,
- the highest CO_2 emission intensity values for all researched cases are for the motorway section, this is related to high speeds on such sections of roads,
- CO_2 emissions intensity for tested LPG-powered vehicles are lower compared to petrol: for Euro 3 vehicle approx. 15%, and for Euro 6 approx. 18%.

Figures 7–10 show the emission of THC for both vehicles tested, fueled with LPG and petrol. As in the previous case, the graph for a petrol-powered Euro 3 vehicle also contains data on the engine's heating phase. Based on the THC emission graphs, it can be observed that:

- the largest part of THC emissions is related to the cold-start of the engine and it accounts for about 66% of the total emissions for the whole ride,
- for the Euro 3 vehicle fueled with LPG, the highest increase in THC emissions occurs for the urban part, while the subsequent parts are characterized by a similarly steady upward trend in emissions,
- for the Euro 6 vehicle fueled both by petrol and LPG, the largest increase in THC emissions occurs for the motorway part and it is the majority of the emission generated during the travel along the test route,
- THC emission for both the Euro 6 and Euro 3 vehicles is lower for LPG than for petrol.

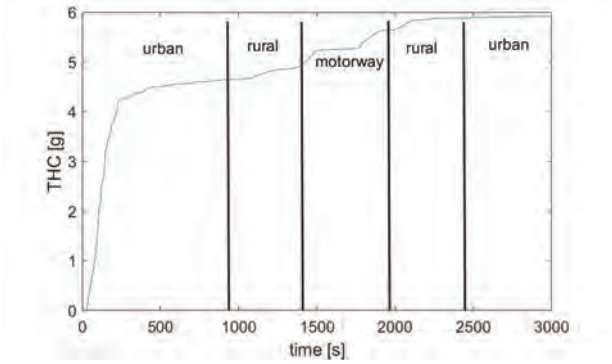

Fig, 7. Emission of THC for Euro 3 petrol fuelled vehicle

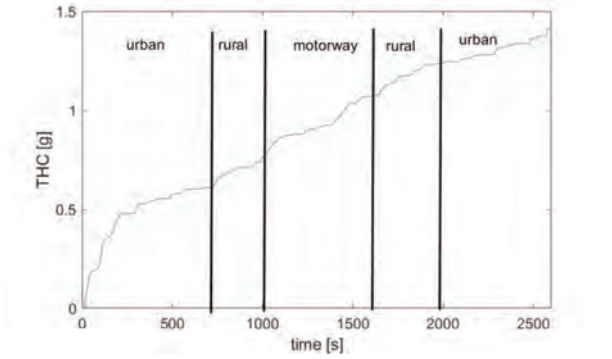

Fig, 8. Emission of THC for Euro 3 LPG fuelled vehicle

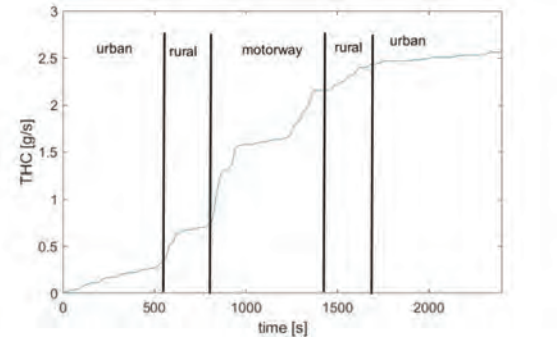

Fig, 9. Emission of THC for Euro 6 petrol fuelled vehicle

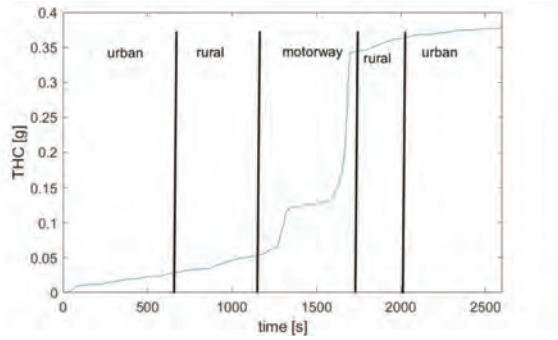

Fig, 10. Emission of THC for Euro 6 LPG fuelled vehicle

Graphs of NO_x emissions intensity as a function of acceleration and velocity are presented in Fig. 11–14.

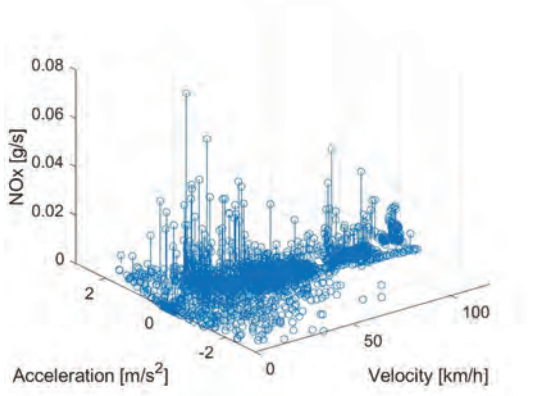

Fig, 11. Correlation between NO_x emission intensity and velocity and acceleration of Euro 3 petrol fuelled vehicle

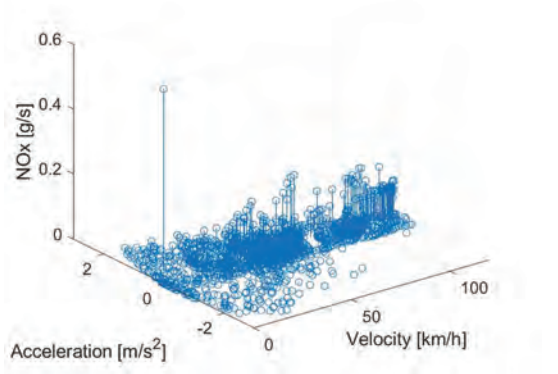

Fig, 12. Correlation between NO_x emission intensity and velocity and acceleration of Euro 3 LPG fuelled vehicle

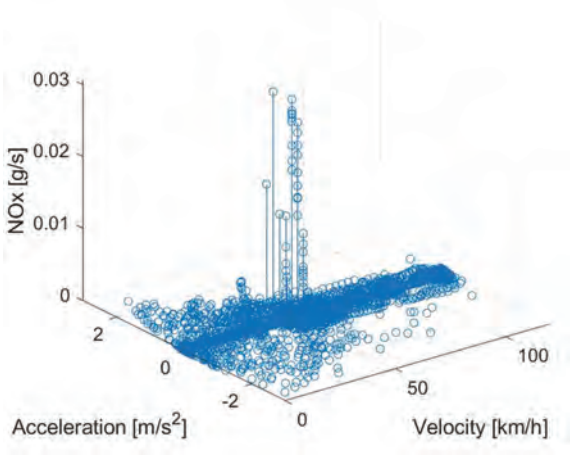

Fig, 13. Correlation between NO_x emission intensity and velocity and acceleration of Euro 6 petrol fuelled vehicle

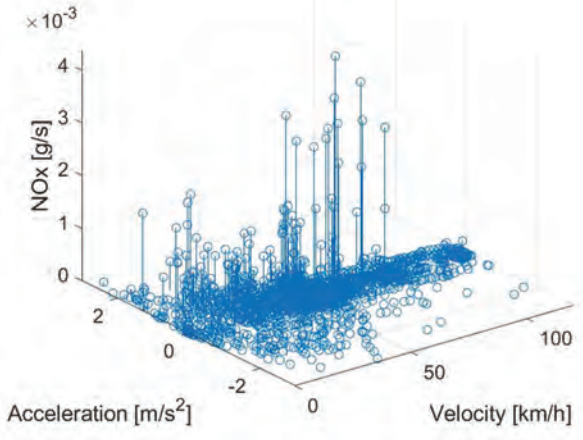

Fig, 14. Correlation between NO_x emission intensity and velocity and acceleration of Euro 6 LPG fuelled vehicle

Based on the NO_x emission intensity graphs shown in Figs 11–14, it can be seen, that:

- the largest NO_x emission intensity for petrol fueled Euro 3 vehicle occurs in the low speed range and temporarily during acceleration of speeds higher than 80 km/h, while for LPG higher NO_x emissions intensity occur for speeds higher than 50 km/h during acceleration of the vehicle,
- for the Euro 6 vehicle, the NO_x emission intensity for petrol shows only temporary higher values at speeds of around 50 km/h, while in the range of other speeds/ accelerations it is relatively low; for LPG, higher NO_x emission intensity values occur in a wider range of speed and acceleration of the vehicle.

Figs 15–18 presents specific distance emission for harmful emission components. The results for NO_x, CO and THC were compiled to emission limits valid for a given vehicle emission standard.

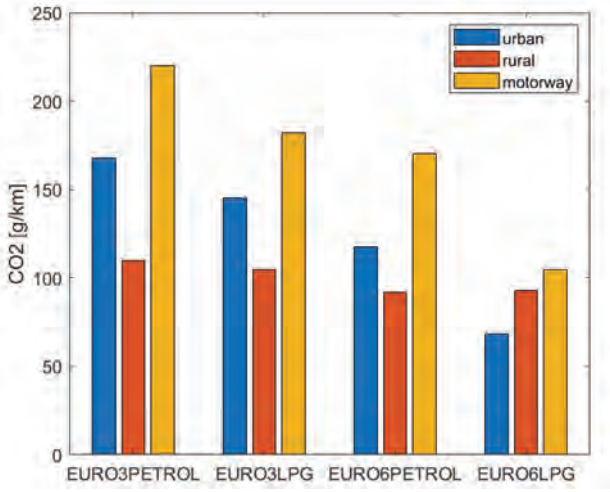

Fig, 15. Specific distance emission of CO_2 for selected parts of road tests

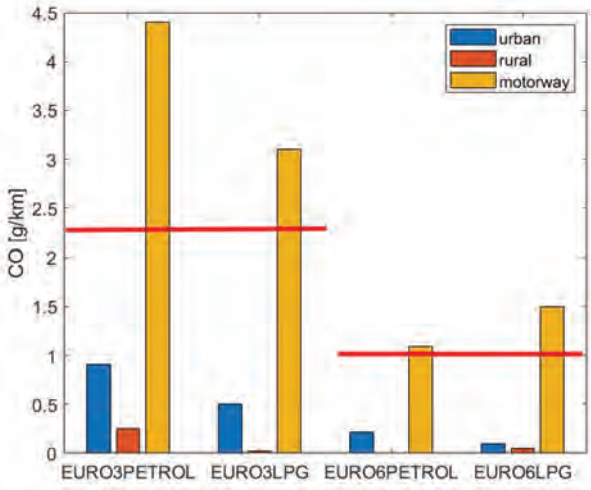

Fig, 16. Specific distance emission of CO for selected parts of road tests (red line is emission limit)

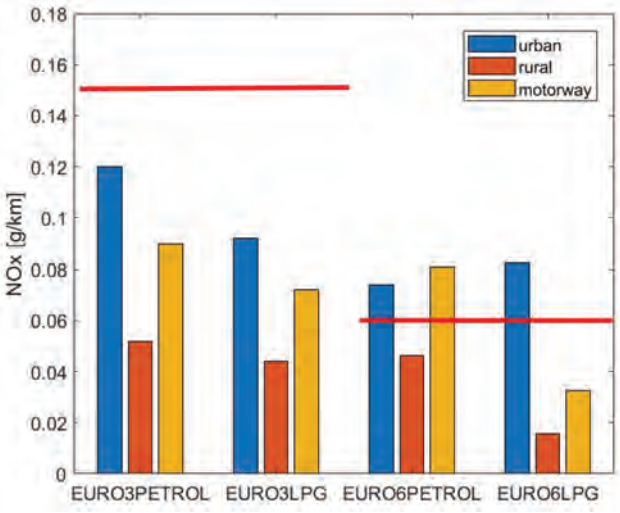

Fig, 17. Specific distance emission of NO_x for selected parts of road tests (red line is emission limit)

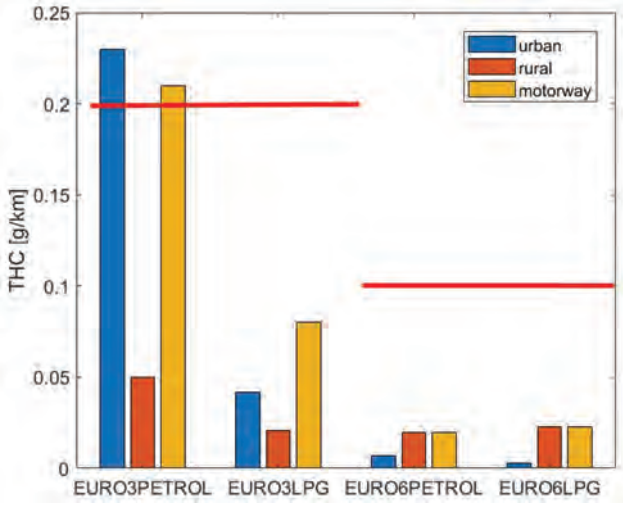

Fig, 18. Specific distance emission of THC for selected parts of road tests (red line is emission limit)

Analyzing the data contained in Fig. 15-18, it can be noted that:

- for all trips the highest CO_2 emission values occurred for the motorway section, this is related to the highest fuel consumption by the tested vehicles at high speed,
- exceeding the Euro 3 and Euro 6 standards limits occurred for CO in the area of passage through the motorway section, the remaining parts of the route and specific distance emissions emitted on them are relatively low,
- exceeding the Euro standard limits for NO_x occurred for the Euro 6 vehicle in the following parts of the test: for petrol – urban, motorway, and for LPG – urban,
- THC specific distance emission reaches the highest values for the Euro 3 vehicle in the petrol range, exceeding the limits for this road test takes place in the urban and motorway part.

4. Conclusions

The results of comparative emission tests for vehicles complying with the Euro 3 and Euro 6 standards fuelled by petrol and LPG presented in the work indicate:

- lower CO_2 specific distance emissions for the Euro 6 vehicle compared to Euro 3 for all road parts, for petrol for the urban part by approx. 25%, rural for approx. 22%, motorway approx. 26%, and for LPG for part of the city about 47%, rural about 20% and motorway about 42%,
- much lower CO specific distance emission of the Euro 6 vehicle in relation to Euro 3, mainly in the aspect of motorway section, which is approximately 4 times smaller for petrol, and 2 times for LPG,
- lower NO_x specific distance emission for the Euro 6 vehicle compared to Euro 3, mainly in the aspect of rural and motorway parts for LPG fueling,
- several times lower THC specific distance emission for both petrol and LPG, for Euro 6 vehicle in relation to Euro 3.

In most cases, the parts of the test within one type of vehicle show the advantage of LPG in relation to petrol in terms of emission of harmful exhaust components.

The presented comparative results of the tested vehicles are indicative and cannot be taken unequivocally, as both vehicles have different mass as well as the used drive unit and the catalytic system. Valuable results can be those within one vehicle in the range of comparison of petrol to LPG.

Certainly, the emission data provided depends also on the driver's driving style and prevailing traffic conditions, which may lead to certain limitations and inaccuracies, but it is important to conduct this type of research because it is crucial to know the amount of emission taking place in the real driving. In fact, every road test is unique. These data are valuable especially in the aspect of learning about the real road emissions, as well as provide the possibility of later use for the development of various types of emission models of fumes pollution [1, 9, 10].

Based on the emission results it can be said, that the LPG represents a good fuel alternative for petrol and therefore it must be taken into consideration in the future of large-scale personal transport.

Nomenclature

LPG	liquefied petroleum gas
CO_2	carbon dioxide
THC	total hydrocarbon
NO_x	nitrogen oxides
CO	carbon monoxide
RDE	real driving emission
PEMS	portable emission measurement system
MPI	multi point injection

Bibliography

[1] AL ALAMI, Y.R. Application of traffic emission models to the estimation of local pollutant hotspots in South Kensington. *1st Civil and Environmental Engineering Student Conference Energy*. 2012, **11**, Imperial College London.

[2] BIELACZYC, P., MERKISZ, J., PIELECHA, J., WOODBURN, J. A Comparison of gaseous emissions from a hybrid vehicle and a non-hybrid vehicle under real driving conditions. *SAE Technical Paper*. 2018.

[3] JAWORSKI, A., LEJDA, K., MĄDZIEL, M., USTRZYCKI, A. Assessment of the emission of harmful car exhaust components in real traffic conditions. *IOP Conf. Series: Materials Science and Engineering*. 2018, **421**, 042031.

[4] JAWORSKI, A., KUSZEWSKI, H., USTRZYCKI, A. et al. Analysis of the repeatability of exhaust pollutants emission research for cold and hot starts under controlled driving cycle conditions. *Environmental Science and Pollution Research*. 2018, **25**, 17862-17877.

[5] LIGTERINK, N.E. On-road determination of average Dutch driving behaviour for vehicle emissions. *TNO Report 2016 R 10188*. 2016.
[6] MERKISZ, J., RYMANIAK, Ł. The assessment of vehicle exhaust emissions referred to CO_2 based on the investigations of city buses under actual conditions of operation. *Maintenance and Reliability*. 2017, **19**(4).
[7] PAPADOPOULOS, G., KERAMYDAS, C., NTZIACHRISTOS, L. et al. Emission factors for a taxi fleet operating on liquefied petroleum gas (LPG) as a function of speed and road slope. *Front. Mech. Eng*. 2018, **41**.
[8] QUEROL, X., VIANA, M., ALASTUEY, A. et al. Source origin of trace elements in PM from regional background, urban and industrial sites of Spain. *Atmos. Environ.* 2007, **41**.
[9] REXEIS, M., HAUSBERGER, S. Trend of vehicle emission levels until 2020 – prognosis based on current vehicle measurements and future emission legislation. *Atmos. Environ*. 2009, **43**.
[10] SMIT, R., MCBROOM, J. Development of a new high-resolution traffic emissions and fuel consumption model. *Road Transp. Res*. 2009, **18**(4).
[11] TASTIC, T., POGOREVC, P., BRAJLIH, T. Gasoline and LPG exhaust emissions comparison. *Advances in Production Engineering & Management*. 2011, **6**.
[12] VARELLA, R., FARIA, M., MENDOZA-VILLAFUERTE, P. et al. Assessing the influence of boundary conditions, driving behavior and data analysis methods on real driving CO_2 and NO_x emissions. *Science of the Total Environment*. 2019, **658**.
[13] VLACHOS, T. et al. The Euro 6 Real-Driving Emissions (RDE) procedure for light-duty vehicles. Effectiveness and practical aspects. *37th International Vienna Motor Symposium*. 2016.
[14] WEISS, M. et al. On-road emissions of light-duty vehicles in Europe. *Environ. Sci. Technol*. 2011, **45**.

Artur Jaworski, DEng. – Faculty of Mechanical Engineering and Aeronautics, Rzeszów University of Technology.
e-mail: *ajaworsk@prz.edu.pl*

Maksymilian Madziel, MSc. – Faculty of Mechanical Engineering and Aeronautics, Rzeszów University of Technology.
e-mail: *mmadziel@prz.edu.pl*

Prof. Kazimierz Lejda, DSc., DEng. – Faculty of Mechanical Engineering and Aeronautics, Rzeszów University of Technology.
e-mail: *klejda@prz.edu.pl*

Janusz Lubas, DSc., DEng. – Faculty of Mechanical Engineering and Aeronautics, Rzeszów University of Technology.
e-mail: *lubasj@prz.edu.pl*

Article citation info:
KARPIŃSKI, P., PIETRYKOWSKI, K., GRABOWSKI, Ł. Turbocharging the aircraft two-stroke diesel engine. *Combustion Engines*. 2019, **178**(3), 112-116. DOI: 10.19206/CE-2019-319

Paweł KARPIŃSKI
Konrad PIETRYKOWSKI
Łukasz GRABOWSKI

CE-2019-319

Turbocharging the aircraft two-stroke diesel engine

The power and efficiency of a two-stroke engine strongly depends on the efficiency of the scavenging process which consists in removing the rest of the exhaust gases from the cylinder and filling it with a fresh charge. The quality of the charge exchange process is significantly influenced by the construction of the intake system. The paper presents a zero-dimensional model of the aircraft two-stroke opposed-piston diesel engine with two variants of the intake system: with a mechanical compressor and a turbocharger connected in series with a mechanical compressor. Simulation studies of the developed cases were carried out in the AVL BOOST software. For the defined engine operating points, its performance was compared for different designs of the intake system. It was confirmed that the use of a turbocharger with a mechanical compressor extends the range of operating at high altitudes.

Key words: *aircraft engine, two-stroke engine, diesel engine, turbocharger, supercharger*

1. Introduction

Two-stroke opposed piston engines (OP2S) have a simpler design, better balance and competitive performance when compared to four-stroke inline engines [1]. The paper [2] presents thermodynamic benefits of the construction of two-stroke engines with opposed pistons. In recent years, numerous research works have been carried out on such engines that differ in the construction of the crank-piston system, e.g. the works [3] and [4] analyzed injection and scavenging processes in OP2S engines.

In two-stroke opposed piston engines, an external device as a mechanical compressor or turbocharger is necessary to carry out the load exchange process. It is also possible to use a combination of these devices. Such a solution is presented in the paper [5] where the blower operates under low load and low speed conditions, while the turbocharger is the main device to exchange a charge. The work [6] discusses the investigations on the influence of selected blower and turbocharger configurations on the performance of a two-stroke diesel engine. The system of two turbochargers in a series system was also analyzed. The analysis of a similar configuration and the general turbocharging analysis of the automotive two-stroke engine were presented in the paper [7]. Research was also carried out on a supercharged two-stroke SI engine with uniflow scavenging under high altitude conditions [8]. In the paper [9], the performance of the turbocharged two-stroke diesel engine was analyzed, focusing on thermal efficiency, load and specific fuel consumption.

As flight altitude increases, volumetric efficiency and thus engine power decreases. An additional turbocharger in the aircraft engine enables the required power to be maintained in high altitude flight as well as a momentary increase in power during take-off and climbing. The benefits of turbocharging a two-stroke diesel engine are presented in the paper [10].

A quick, effective and low-cost method of testing engine's operating parameters are tests using mathematical models. This approach is discussed in the work [11] where a zero-dimensional engine model is presented and the influence of variable compression ratio on engine performance is examined.

The paper analyzes how a turbocharger in a two-stroke opposed piston aircraft diesel engine influences this engine performance at four defined operating points. The created engine model enabled us to compare the selected operating parameters with these calculated for the engine variant equipped only with the mechanical compressor.

2. Engine model

The research object was a three-cylinder two-stroke opposed piston aircraft diesel engine at the design stage. The basic engine parameters are shown in Table 1.

Table 1. Basic technical parameters of the tested engine

Maximum power	100 kW
Engine speed	4200 rpm
Number of cylinders	3
Bore	65.5 mm
Stroke	72 mm
Compression ratio	22:1
Scavenging	Uniflow

In order to perform simulation tests in the AVL BOOST software, a zero-dimensional model of the tested engine in two variants was developed (Fig. 1): with a mechanical compressor (Fig. 2) and a turbine connected in series with a smaller mechanical compressor (Fig. 3). Both variants have an air intercooler at the end of the inlet duct. The Vibe model was adopted as a combustion model and the Woschni model as a heat exchange model.

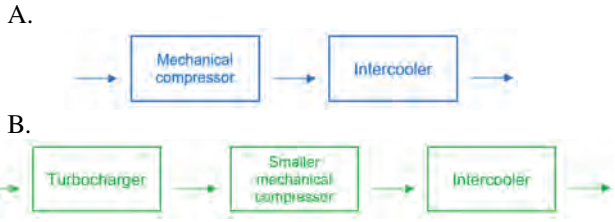

Fig. 1. Analyzed variants of the intake system

In variant A, the Eaton TVS R900 compressor operating map developed by the manufacturer was implemented in the model. The map is defining the efficiency and power

consumed by the device as a function of the compression ratio and mass flow of air.

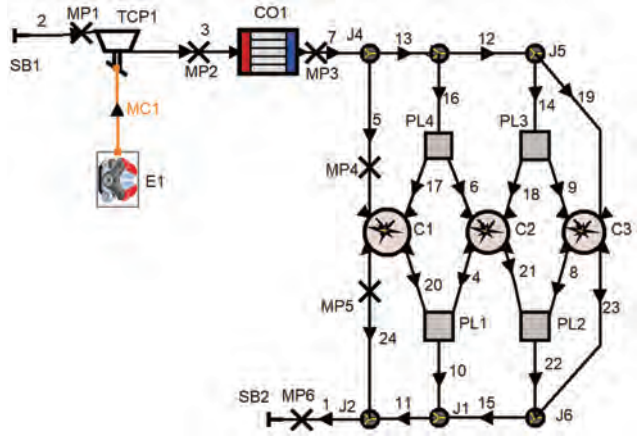

Fig. 2. Model of the engine with the Eaton TVS R900 mechanical compressor

Variant B implemented the Garrett GT-2560R turbocharger maps which presented compressor efficiency as a function of compression and mass air flow as well as mass flow through the turbine as a function of the compression ratio. In the series connection, a smaller Eaton TVS R410 mechanical compressor was used whose operating map was introduced into the model.

Additional calculations were performed for the variant with a changed order of devices, i.e. turbocharger–mechanical compressor–intercooler. This case was rejected after the initial calculations. The Eaton TVS R410 compressor did not provide stable operation in subsequent computational cycles. The obtained power for a cruising power point at an altitude of 4600 m was 62 kW and was 11 kW lower than the reference value for this case.

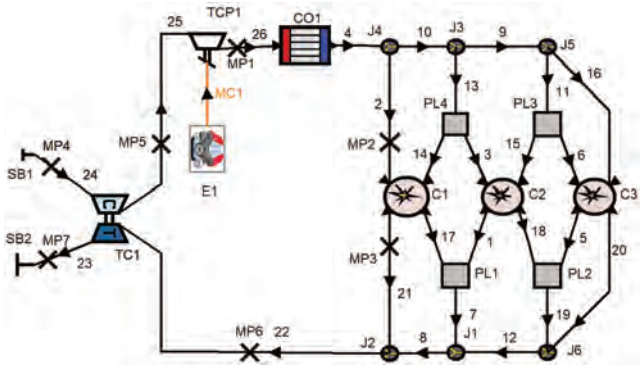

Fig. 3. Model of the engine with the Garrett GT-2560R turbocharger connected in series with the Eaton TVS R410 mechanical compressor

The so-called offset, i.e. a phase shift between the engine crankshafts, was defined in the model. This shift allows improving the scavenging process in a two-stroke engine with uniflow scavenging. The offset was implemented by changing the characteristics of the inlet and outlet windows in the cylinder settings. In the considered case, the crankshaft on the side of the outlet windows is ahead of the crankshaft on the side of the intake windows by 14°.

The calculations were carried out for four defined operating points: take-off power, continuous maximum power, cruising power at 0 m and cruising power at 4600 m (15000 ft). The operating points were characterized by engine speed, air-to-fuel ratio (AFR) and start of combustion angle (SoC). The set-ups of operating points for the first and second variants are shown in Tables 2 and 3, respectively.

Table 2. Defined operating points for the variant with the Eaton TVS R900 mechanical compressor

Operating point	Power [kW]	Engine speed [rpm]	AFR [–]	SoC [°]	H [m]
Take-off power	100	4200	22	+3.5°	0
Maximum continuous power	86	4000	24	–2.5°	0
Cruising power, H = 0 m	73	3800	27	0°	0
Cruising power, H = 4600 m	73	3800	22	–3.5°	4600

Table 3. Defined operating points for the variant with the Garrett GT-2560R turbocharger and the Eaton TVS R410 mechanical compressor

Operating point	Power [kW]	Engine speed [rpm]	AFR [–]	SoC [°]	H [m]	WV [%]
Take-off power	100	4200	22	+2.5°	0	0.53
Maximum continuous power	86	4000	24	–0.5°	0	0.53
Cruising power, H = 0 m	73	3800	27	–1.0°	0	0.57
Cruising power, H = 4600 m	73	3800	22	–2.0°	4600	0.76

The additional parameter for the variant with a turbocharger was the wastegate valve opening coefficient (WV). This parameter controls the power generated by the engine. The SoC angle value for each case was changed so that the maximum cylinder pressure did not exceed 13 MPa. The adopted value results from the design assumptions and strength limits for the tested engine.

3. Results and discussion

The simulation calculations enabled us to obtain the values of selected engine operation parameters for the two variants. These values i.e. the specific fuel consumption, the compressor power, the effective pressure and the pressure in the intake manifold before the cylinders were compared with each other.

For the case of a cruising power at an altitude of 4600 m for the variant with the Eaton TVS R900 compressor, the engine generated the power of 59 kW so the assumed power value of 73 kW was not obtained. For the case with a turbocharger, the defined power was obtained by closing the by-pass valve.

Figure 4 shows the specific fuel consumption for the considered operating points for the analyzed cases. For the variant with a turbocharger, fuel consumption was reduced by up to 12%. For continuous power, specific fuel consumption decreased from 248.3 g/kWh to 217.4 g/kWh. For a cruising power at an altitude of 4600 m, a slight increase in specific fuel consumption up to 223 g/kWh was recorded.

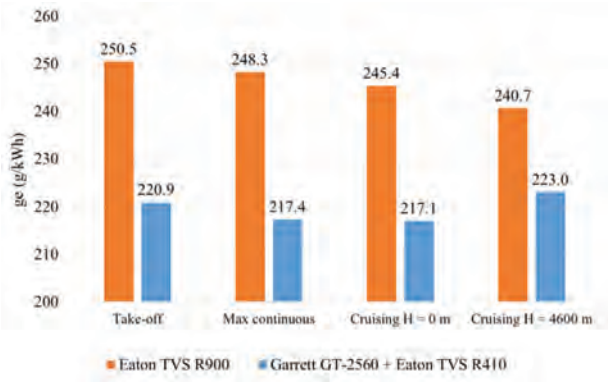

Fig. 4. Comparison of the specific fuel consumption for two analyzed variants

The power consumed by the compressor for the considered cases is shown in Fig. 5. For the case with the Eaton TVS R900 compressor, the power consumed by the compressor decreased with the decreasing power generated by the engine. For the variant with a turbocharger, the consumed power was reduced by more than half for the take-off power operating point and the continuous maximum power point. For cruising power at 4600 m, this value decreased by 32%.

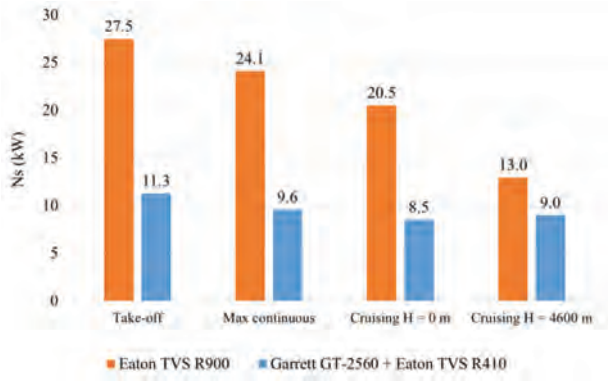

Fig. 5. Comparison of the compressor power for two analyzed variants

The value of the average effective pressure for the variant with the turbocharger was lower by 10–12% than for the variant with the mechanical compressor only. However, for both cases, the same power was obtained due to the fact that the turbocharger improved the filling of the cylinder with fresh air. In the case of the variant with the turbocharger, the increase in altitude did not cause a drop in the effective pressure. A summary of the effective pressure values for the studied cases was shown in Fig. 6.

Intake manifold pressure (Fig. 7) for the variant with a mechanical compressor only was higher by about 40% compared to the variant with the turbocharger. For the case of cruising power at an altitude of 4600 m, the pressure for the variant with the turbocharger was 138 kPa and was 20% higher compared to the variant with the Eaton TVS R900 compressor.

Figure 8 shows a map of the Eaton TVS R900 mechanical compressor with operating points. All points are within the efficiency range of 62-67%. The highest efficiency was obtained for the cruising power at H = 0 m. As the height increases, the operating point shifts to the left towards the smaller mass flow on the map and for the height H = 4600 m, the efficiency is equal to 62%.

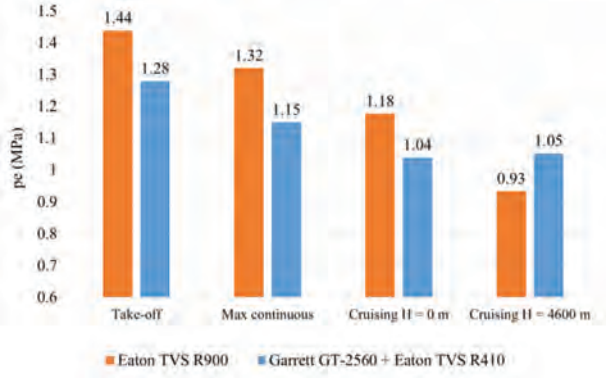

Fig. 6. Comparison of the effective pressure for two analyzed variants

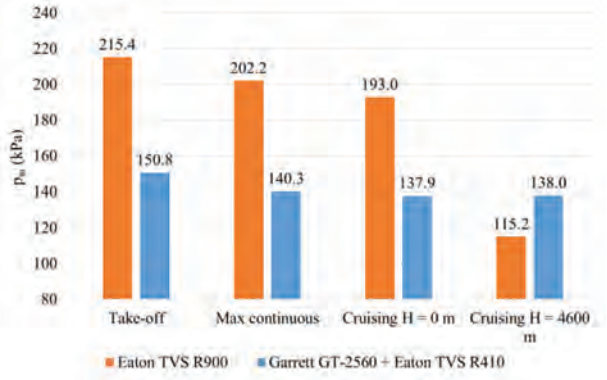

Fig. 7. Comparison of inlet manifold pressure for two analyzed variants

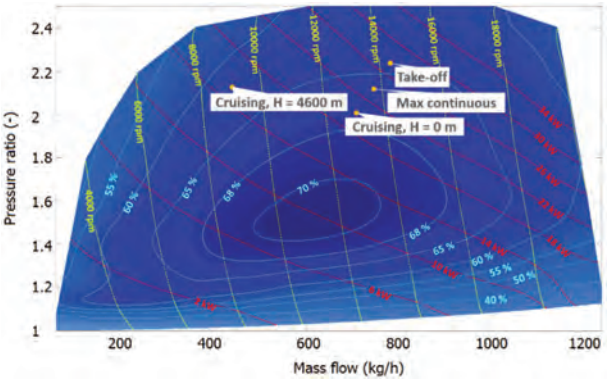

Fig. 8. Eaton TVS R900 compressor map with calculated operating points [12]

The determined operating points for the Eaton TVS R410 compressor are shown in Fig. 9. The efficiency achieved varied in the range of 65-66%. The highest efficiency equal to 66% was obtained for the cruising power point at H = 4600 m. For the cruising power at H = 0 m, the efficiency was equal to 65%. As the height increases, the operating points move on the map upwards through the area with the highest efficiency of the compressor.

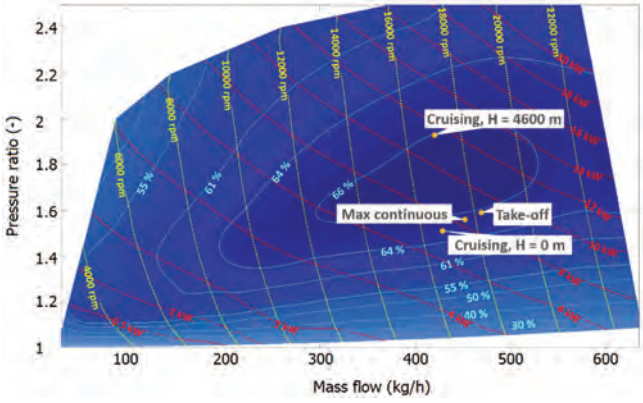

Fig. 9. Eaton TVS R410 compressor map with calculated operating points [13]

The map of the Garrett GT-2560R turbocharger is shown in Fig. 10. The three points: take-off power, maximum continuous power and cruising power at H = 0 m are below the 55% efficiency. With the increase of the height, the operating point is moved upwards on the map, achieving its efficiency about 70% for the cruising power at H = 4600 m.

4. Conclusions

The paper presents the results of research on the model of two-stroke opposed piston aircraft diesel engine. The research investigated the impact of a turbocharger with a mechanical compressor on engine performance. The results obtained for this case were compared to the results for an engine equipped with a mechanical compressor only.

Engine performance was significantly improved by means of a turbocharger with a smaller mechanical compressor. The specific fuel consumption decreased by 12%, the power consumed by the compressor for the maximum continuous power dropped by 14 kW, and the range of engine operation at high altitude increased. In the case of an R900 compressor, it was impossible to achieve the assumed value of a cruising power of 73 kW at 4600 m. By the application of the turbocharger, the defined power was obtained and the intake manifold pressure at high altitudes remained constant compared to the cruising power at H = 0 m.

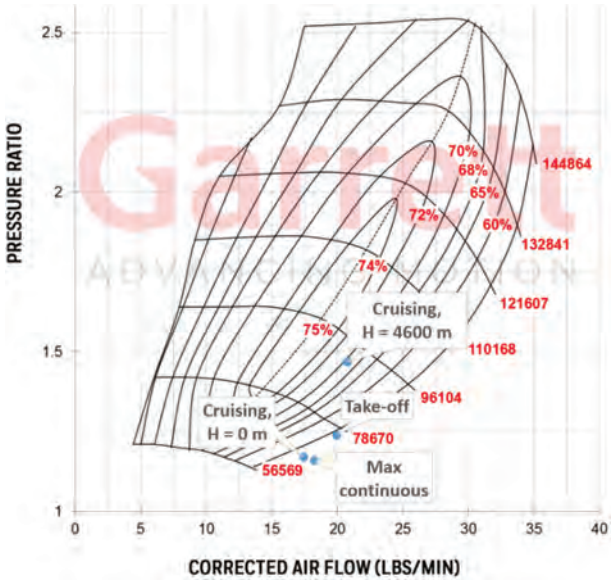

Fig. 10. Garrett GT-2560R turbocharger map with calculated operating points [14]

A turbocharger–mechanical compressor layout, besides improving engine performance, is capable of improving aircraft safety. If one of the devices fails, the other is able to provide fresh air supply to cylinders so it is possible to obtain some power to keep engine and key auxiliary devices temporarily operating.

Acknowledgements

This work has been performed in the cooperation with The Construction Office of WSK "PZL-KALISZ" S.A." and is part of Grant Agreement No. POIR.01.02.00-00-0002/15 financed by the Polish National Centre for Research and Development.

Nomenclature

AFR	air to fuel ratio	SoC	start of combustion
SI	spark ignition	WV	wastegate valve opening coefficient

Bibliography

[1] PIRAULT, J.P., FLINT, M. Opposed piston engines: evolution, use, and future applications. *SAE International*. 2010.

[2] HEROLD, R.E., WAHL, M.H., REGNER, G. et al. Thermodynamic benefits of opposed-piston two-stroke engines. *SAE Technical Paper*. 2011, 2011-01-2216. DOI:10.4271/2011-01-2216

[3] ZHANG, L., SU, T., ZHANG, Y. et al. Numerical investigation of the effects of split injection strategies on combustion and emission in an opposed-piston, opposed-cylinder (OPOC) two-stroke diesel engine. *Energies*. 2017, **10**(5), 684. DOI:10.3390/en10050684

[4] LIU, Y., ZHANG, F., ZHAO, Z. et al. The effects of pressure difference on opposed piston two stroke diesel engine scavenging process. *Energy Procedia*. 2017, **142**, 1172-1178. DOI:10.1016/j.egypro.2017.12.374

[5] BLAIR, G.P. Design and simulation of two-stroke engines. *Society of Automotive Engineers*. 1996.

[6] TIMONEY, S.G. High pressure turbocharging of two-stroke engines. *SAE Transactions*, 1969, 2401-2412. DOI:10.4271/690747

[7] TRYHORN, D.W. Turbocharging the automotive two-stroke cycle engine. *Proceedings of the Institution of Mechanical Engineers*. 1965, **180**(14), 75-84. DOI:10.1243/PIME_CONF_1965_180_387_02

[8] LAND, M.L., CARAMEROS, A. Turbocharged two-stroke-cycle gas engines. *Journal of Engineering for Power*. 1965, **87**(4), 421-438. DOI:10.1115/1.3678291

[9] GUNES, U., UST, Y., KARAKURT, A.S. Performance analysis of turbocharged 2-stroke diesel engine.

[10] FINDLAY, A., HARKER, N., DEN BRAVEN, K.R. Brake specific fuel consumption and power advantages for a turbo-

charged two-stroke direct-injected engine. *International Mechanical Engineering Congress and Exposition*.2008, 269-279. DOI:10.1115/IMECE2008-68371

[11] ALQAHTANI, A., WYSZYNSKI, M.L., MAZURO, P., XU, H. Evaluation of the effect of variable compression ratios performance on opposed piston 2-stroke engine. *Combustion Engines*. 2017, **171**(4), 97-106.

[12] Eaton TVS R900 supercharger specification https://www.eaton.com/us/en-us/catalog/engine-solutions/tvs-r900.specifications.html

[13] Eaton TVS R410 supercharger specification, https://www.eaton.com/us/en-us/catalog/engine-solutions/tvs-r410.specifications.html

[14] Garrett GT-2560R turbocharger specification, https://www.garrettmotion.com/racing-and-performance/performance-catalog/turbo/gt2560r/

Paweł Karpiński, MEng. – Faculty of Mechanical Engineering, Lublin University of Technology.
e-mail: *pawel.karpinski@pollub.edu.pl*

Konrad Pietrykowski, DEng. – Faculty of Mechanical Engineering, Lublin University of Technology.
e-mail: *k.pietrykowski@pollub.pl*

Grabowski Łukasz, DEng. – Faculty of Mechanical Engineering, the Lublin University of Technology.
e-mail: *l.grabowski@pollub.pl*

Article citation info:
SWIATEK, P., FUC, P., ZIOLKOWSKI, A. et al. Tests of a prototype spark-ignited, direct-injection engine powered by JET-A1 fuel. *Combustion Engines*. 2019, **178**(3), 117-120. DOI: 10.19206/CE-2019-320

Piotr SWIATEK
Pawel FUC
Andrzej ZIOLKOWSKI
Lech SWIATEK
Pawel MELWINSKI

CE-2019-320

Tests of a prototype spark-ignited, direct-injection engine powered by JET-A1 fuel

The article presents a part of the work done in a research and development project being made by SWIATEK Lech Swiatek company. It describes the comparison of different fuels used in piston engines with JET-A1 turbine engine fuel. Next, the proposed combustion process of JET-A1 fuel and a prototype one-cylinder engine are described. In details, a special cylinder head and direct injection programmable computer are presented. In the next part, a designed and built test stand is described. Finally, the results and conclusions are presented. The designed test stand enabled to perform assumed tests. The innovative JET-A1 combustion process was possible to perform and the power and torque were higher in 1900-3000 rpm range than with the gasoline fuel. The designed GDI programmable injection computer enabled to fully control the injection and ignition parameters.

Key words: *alternative fuel, test engine, piston aircraft engines, jet-a1*

1. Introduction

The work was carried out as part of a research and development project in the National Centre for Research and Development "INNOLOT" program titled "Development of an innovative aviation engine fueled with JET-A1 fuel". The project fits into environmentally friendly transport solutions.

The aim of the project is to develop the conditions of the combustion process in a JET-A1 fueled piston engine, used for aviation turbine engines. As part of the project, two prototypes of piston engines with different parameters will be developed, intended for use in ultralight and light aircraft. These engines will have a reduced emissivity compared to currently used aircraft piston engines.

One of the stages of the project are tests made on engine models. As part of this stage, a prototype 1-cylinder research engine was developed and made together with a water-brake station and the possibility of feeding two types of fuels. The research was carried out on the test stand, and the results are presented in this article.

2. JET-A1 Fuel characteristics

Table 1 shows the comparison of properties of different liquid fuels. The JET A-1 fuel is intended for the propulsion of turbine aircraft engines. Diesel and gasoline are used in combustion engines of various motor vehicles. AVGAS 100L is a gasoline designed for spark-ignition reciprocating piston engines. Each of these fuels must comply with separate normative requirements, therefore it is impossible to accurately compare them taking into account the standards. For this reason, on the basis of literature, some values have been averaged and rounded to the extent enabling the comparison of selected fuels and are presented in Table 1. Additionally, the results of laboratory tests of JET-A1 fuels from 3 producers are presented.

The JET A-1 fuel is a kerosene fraction in which there are lighter hydrocarbons than in diesel. The ASTM standard does not specify the cetane number of this fuel because it is not an important parameter for turbine engines. According to the available data, it has an octane number 8 and a cetane number of 50. It can be used for spark ignition engines with a low compression ratio or for compression-ignition engines with low ignition delay and extended combustion time compared to diesel [2]. When using fuel for reciprocating engines, it may be necessary to use additives that increase the cetane number. In addition, JET-A1 has a lower viscosity and significantly lower lubricity. For this

Table 1. Comparison of properties of selected liquid fuels (* – results of tests of JET-A1 fuels from 3 manufacturers) [3,6]

Parameter	Unit	Fuel			
		JET-A1	Diesel oil Ekodiesel ULTRA	Gasoline	AVGAS 100LL
Density in temp. 15°C	kg/m^3	795–808* 775–840	820–845	720–755	690–790
Calorific value	MJ/kg	43.1–43.3* 42.8	42.0–44.0	44.0	min. 43.5
Octane number	MON	8.0		95.0–98.0	min. 99.6
Cetane number	–	50.0	min. 51.0	–	5.0
Crystallization temperature, max.	°C	from –65.0 to –50.5* –47.0	–	approx. –40.0	–58.0
Ignition temperature	°C	41.5–44.5* 38	56	–40	< 0
CO_2 emission	kg CO_2/ kg fuel	3.4	–	3.3	3.3
Sulfur content	mg/kg	50–1780* max. 3000.0	max. 10.0	max. 10.0	Max. 500.0

reason, it was decided to use subassemblies of the direct gasoline injection system and thus the fuel without lubricating properties. In relation to diesel fuel, the advantage of JET-A1 fuel is the low temperature of crystallization, reaching a maximum of −47°C. The sulfur content can be over 300 times higher than in the case of diesel or motor gasoline. The ignition temperature is about 20 degrees lower than diesel.

The emission of carbon dioxide during the combustion process is similar for all fuels. Current research shows that the use of JET-A1 fuel in a compression-ignition engine produces higher emissions of carbon monoxide (CO), smoke and a decrease in NO_x emissions [5].

3. JET-A1 combustion process concept

Currently, aviation Diesel engines with a high compression ratio are also manufactured in the world [4]. They can be also powered by JET-A1 fuel and find application in light aircraft with MTOW between 450 and 5670 kg. In addition, several small engine designs for drone propulsion are being developed. They are characterized by different solutions of the combustion process: these are engines operating in a two- or four-stroke cycle, with spark or self-ignition, with reciprocating or rotary pistons. Special processes for preparing the mixture are also implemented, for example with the use of compressed air for mixture preparation [1]. Because of their limited TBO time and low power, these engines can not be used for ultra-light and light planes propulsion.

In the research project, the process of JET-A1 fuel combustion in a spark-ignition engine with a low compression ratio was selected. This process results in lower loads of the components of the crankshaft system in relation to high-pressure Diesel engines, which enables that the engine elements can be lighter. Due to differences in fuels, it was necessary to check the process on a model test engine.

Assumptions related to the combustion process:

1. The operating pressure of GDI gasoline injection systems is max. 150–200 bar, so it was assumed that considering the viscosity of the lower JET A-1 fuel than diesel fuel, the fuel atomization will be sufficient. In older generations of mechanical injection systems of diesel engines, installations were working properly on diesel fuel pressures not much higher than 100 bar.
2. Distributing the injection dose into two parts (Fig. 1): one during the inlet stroke the second in the area of the start of the working stroke will be able to burn the JET A-1 fuel with the danger of burning detonation. The designed controller enables the adjustment of both the size of both doses and their angular position.

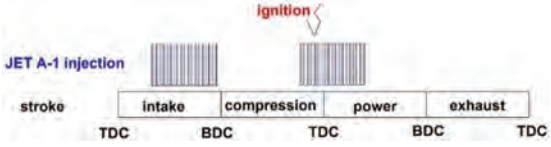

Fig. 1. Distribution of doses of JET A-1 fuel injection

4. Description of the prototype research engine

A prototype 1-cylinder test engine "SB-01" was built. The basic construction for the test engine was a four-stroke, overhead-valve engine with a boxer cylinder system – VW 1600B. Its displacement was 1583 cm^3 and the maximum power was 32 kW. It uses a carbureted fuel supply system and air-cooling. Table 2 shows a comparison of the parameters of both basic and prototype engine.

As part of engine modification, three cylinders were dismantled and blinded. On the free rod-journals of the crankshaft, there were masses installed for balancing the engine. The working cylinder had a bigger bore and piston with 94 mm diameter. New flywheel with increased weight was made and mounted.

Table 2. Technical data of the basic and prototype engine

Parameter	Value	
Engine type	VW 1600 B	SB-01
Displacement [cm^3]	1584	478
Cylinder layout	boxer	–
Cylinder numer	4	1
Bore [mm]	85.5	94
Stroke [mm]	69	
Compression ratio	7.5	9.5
Maximum power [kW]	32 at 4000 rpm	–
Maximum torque [N·m]	106 at 2200 rpm	–
Cooling system	Air-cooled	Crankcase and cylinder air-cooled, cylinder head liquid-cooled
Injection system	Carbourated	Direct injection
Ignition	Single, mechanically controlled	Single, electronically controled

A cylinder head consisting of three parts was made for the engine, which enables easy change of the shape of the combustion chamber and the position of injectors and sparkplugs (Fig. 2). Due to the need for long-term tests, liquid cooling was used in the head. In the lower part (1) there are side walls of the combustion chamber, part of the water jacket and the injector seat (2). The middle part (3) contains the chamber roof, intake (5) and exhaust (6) channels, valve system, the second part of the water jacket with the inlet (7) and the spark plug socket (8). In the upper part (9) the valve rocker system is situated.

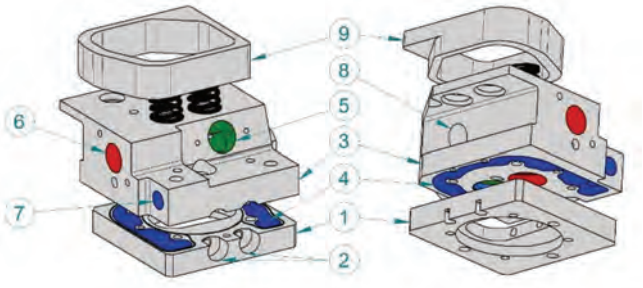

Fig. 2. Prototype cylinder head: 1 – lower part with combustion chamber and water jacket, 2 – injector seats, 3 – middle part, 4 – water jacket, 5 – intake channel, 6 – exhaust channel, 7 – cooling system inlet, 8 – spark plug socket, 9 – upper part

The JET-A1 fuel system used in the SB-01 engine uses elements of the direct gas injection system GDI: the Bosch high-pressure pump 04E127026E and the single Bosch injector 04E133036A**.** A programmable computer devel-

oped for the needs of the project was used to control the injection and ignition process (Fig. 3). During engine operation, the following input data were collected: crankshaft and camshaft positions, intake air temperature, throttle position, oxygen content in the exhaust gasses and pressure in the fuel system. Based on these parameters, the computer controlled the opening time and the injector opening point according to the programmed injection maps. In addition, it was possible to divide the injection dose into two phases. The ignition point was also controlled using separate maps.

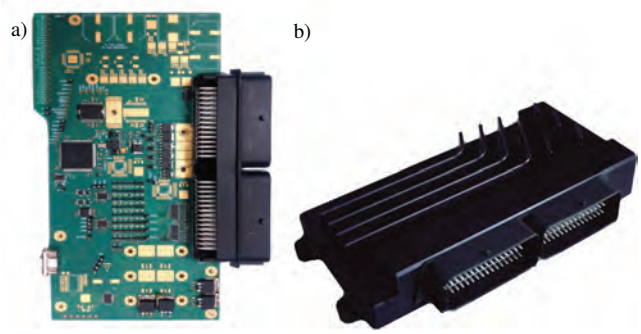

Fig. 3. Programmable computer of the direct injection system GDI a) view of the upper layer of the computer board, b) computer casing

5. Description of the test stand

To carry out comparative tests on the combustion of gasoline and JET-A1 fuel in the assumed process, the test stand marked SBB was designed and constructed (Figs 4 and 5). The tested motor (1) was connected by a clutch to the water brake HW200 (4). The engine speed was read using the encoder (4). The torque was measured on the brake by means of a strain gauge (6). The stand was equipped with two fuel tanks (7) with the possibility of changing the power source for the engine fuel system. The stand enables the measurement of the motor characteristics (power and torque in relation to revolutions) and work under load.

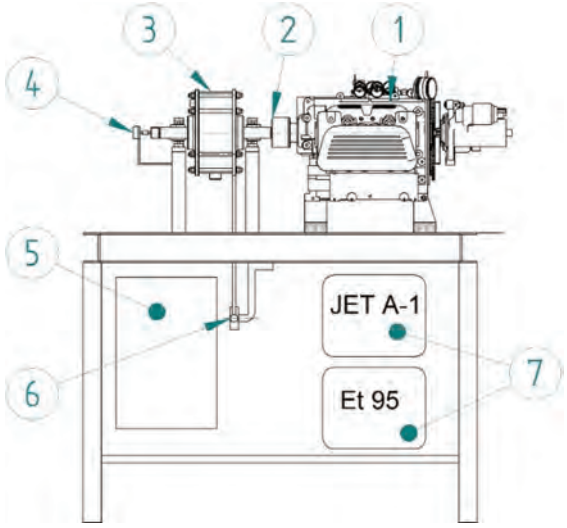

Fig. 4. SBB test stand scheme: 1 – prototype 1-cylinder engine, 2 – clutch, 3 – water brake HW 200, 4 – encoder, 5 – measuring box, 6 – strain gauge, 7 – fuel tanks

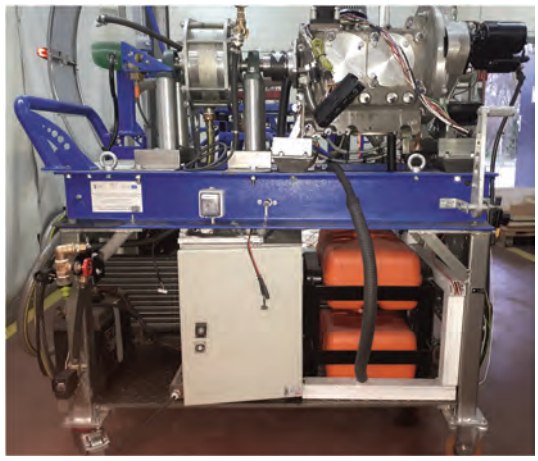

Fig. 5. SBB test stand

6. Results

The tests were carried out in two stages. In the first stage, the engine was powered with EuroSuper 98 gasoline. Engine startup tests and work tests were carried out in the range from 1000 to 3600 rpm. The engine characteristics were obtained with gasoline.

In the second stage, the engine was powered by JET-A1 fuel. Initially, during the increase of the load, there was knocking combustion. In order to eliminate it, the fuel dose was divided into two phases, injected in the intake and compression cycle. Thanks to these changes, the maximum power and engine load were achieved. As a result of the tests, the engine characteristics were obtained (Fig. 6).

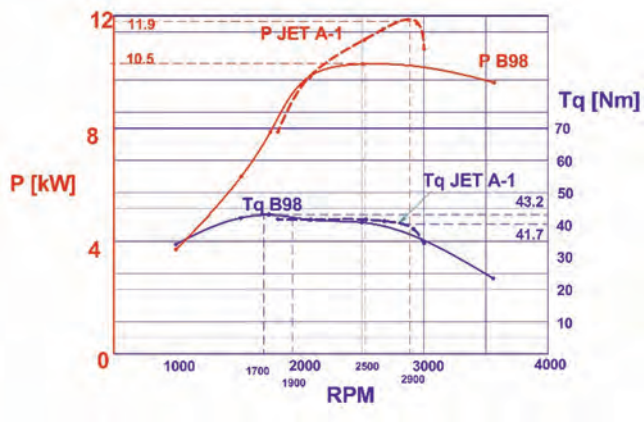

Fig. 6. Comparison of characteristics of a prototype engine powered by JET-A1 fuel and EuroSuper 98 petrol

The engine powered with gasoline obtained a low-speed characteristic with a 10.5 kW maximum power at 2500 rpm and a 43.2 Nm maximum torque at 1700 rpm.

The engine running on JET A-1 fuel obtained a very flat torque curve with a 41.7 Nm maximum at 1900 rpm and falling down above 3000 rpm. In the range 1900–3000 rpm, the torque developed by the engine working on the JET A-1 is higher than when working on gasoline. The engine worked evenly under full load one hour and there was no knocking phenomenon. Combustion was softer and quieter than on gasoline.

7. Conclusions

As part of the research, the following conclusions were formulated:

– The designed and constructed test stand made it possible to carry out the assumed tests and verify the combustion process assumptions.
– The assumed innovative process of JET-A1 fuel combustion in the engine with low compression ratio and spark ignition is possible and is very efficient – in the range 1900–3000 rpm the torque and power are higher than on gasoline.
– Designed direct injection computer enables full control of the combustion process in the test engine and the obtained results prove the assumptions related to the JET A-1 fuel injection and ignition system.

The direction of further work should include examination of other injector settings and optimization of injection parameters in order to increase the obtained power. It will also be necessary to carry out tests on a 4-cylinder engine equipped with a different intake system.

Acknowledgements

The authors are pleased to acknowledge the financial support from the National Centre of Research and Development in the framework of Innolot contract POIR/01.02.00-00-0015/1510 for the work presented in this paper.

Nomenclature

ASTM	American Society of Testing and Materials
BDC	bottom dead center
GDI	gasoline direct ignition
MON	motor octane number
MTOW	maximum takeoff weight
TBO	time between overhaul
TDC	top dead center

Bibliography

[1] DUTCZAK, J. Heavy fuel engines. *Combustion Engines*. 2015, **154**(4), 34-46.
[2] LUFT, S. Podstawy budowy silników. Wyd. 2, *WKiŁ*, Warszawa 2006.
[3] PAGOWSKI, Z. Lotnicze paliwa i oleje. *Prace Instytutu Lotnictwa*. 2009, **4**(199), 117-127.
[4] PAGOWSKI, Z. Pozytywne skutki zastosowania silników Diesla w lotnictwie. *Prace Instytutu Lotnictwa*. 2016.
[5] SOLMAZA, HAMIT, et al. Investigation of the effects of civil aviation fuel Jet A1 blends on diesel engine performance and emission characteristics. *Indian Journal of Engineering and Materials Sciences*. 2014, **21**(2), 200-206.
[6] Fuel producers data.

Piotr Swiatek, DEng. – SWIATEK Lech Swiatek.
e-mail: *swiatek.piotr@gmail.com*

Lech Swiatek, MSc. – SWIATEK Lech Swiatek.
e-mail: *lech@swiatek.com.pl*

Pawel Fuc, DSc., DEng. – Faculty of Transport Engineering, Poznan University of Technology.
e-mail: *pawel.fuc@put.poznan.pl*

Pawel Melwinski, Eng. – SWIATEK Lech Swiatek.
e-mail: *pmelwinski@gmail.com*

Andrzej Ziolkowski, DEng. – Faculty of Transport Engineering, Poznan University of Technology.
e-mail: *andrzej.j.ziolkowski@put.poznan.pl*

Article citation info:
MITIANIEC, W. Study of Atkinson cycle in two-stroke diesel engine with opposed pistons. *Combustion Engines*. 2019, **178**(3), 121-128. DOI: 10.19206/CE-2019-321

Wladyslaw MITIANIEC

CE-2019-321

Study of Atkinson cycle in two-stroke diesel engine with opposed pistons

The paper presents possibilities of change working parameters of two-stroke diesel engine with opposed pistons. Obtaining of higher engine efficiency is realized by applying of Atkinson cycle. Modification of scavenging process by changing pistons' position connecting with two crankshafts enables asymmetrical scavenge timing. Decreasing of shorter time of closing exhaust ports before compression process and longer expansion process give higher engine work and with high charging ratio increases engine power. These types of engines are recently recommended for power plant stations. The paper includes full analysis of engine work with scavenge and combustion processes for different timing phases based on geometry of the CI Leyland L60 engine by using of CFD modelling and own 0D model. Simulation tests indicate a high scavenge efficiency, good penetration of injected fuel and fast combustion process. The work contains figures of pressure, temperature traces and emission of main chemical species in exhaust gases with comparison of engine works for different timing phases. Atkinson cycle in two-cycle work of engine and full combustion process enables to achieve high total efficiency. The study is an input for realization of such processes in a future of power plant engines with different fuelling systems.

Key words: *transport, two-stroke opposite piston engine, Atkinson cycle, scavenging, timing phases*

1. Introduction

Two-stroke opposed piston engines (called from here as "2sOPE") have been and are among the more important ones used in power engineering, on ships, military and industrial equipment because their simplicity, high power density, compactness and lower weights. They do not need of a cylinder head. For this reason, the thermal losses are lower than in hour-stroke engines. Two piston crowns form a combustion chamber often as a shape of distorted spherical chamber. The diesel engines of this type are equipped with fuel injectors placed radially on the circumference of the cylinder. One of the problems is transfer of the drive from two independent crankshafts, usually by a set of gears. One of the pistons controls opening of inlet ports called also as transfer ports and the other controls the exhaust ports. The air is delivered by one pipe or many pipes to transfer chamber surrounding the transfer ports usually on the whole cylinder circumference forcing the air to rotate in the cylinder. On the other hands the exhaust gases leave the cylinder by opening of the exhaust port controlled by the edge of the second piston.

The classical two-stroke engine has symmetrical timing of phases for gas exchange and for that reason the engine loses a lot of mass of charge and sometimes also the fuel. In order to stop such phenomenon, the 2sOPE enables applying of asymmetric opening of the exhaust ports relative to the transfer ports thanks to a different location of the two crankshafts.

Currently, there is a large interest in the use of big CI engines for production of electricity including the 2sOPE due to a significant power factor. An increase of the engine power and decrease of fuel consumption and exhaust gas emission in such engines is possible by applying of the Atkinson solution. The purpose of the work was to obtain information on the impact of changing the ports opening phases of the engine on the operating parameters.

2. Atkinson solution in IC engines

The increase of engine power can be realized by getting more internal work. In 1882 English engineer James Atkinson patented his combustion engine, which enabled a small compression work and larger expansion work in comparison to Otto engine. One of his patents is shown in Fig. 1. However, this solution is realized recently particularly in many hybrid engines [9]. For almost constant rotational speed of the crankshaft the engines give larger torque. Sendyka and Sochan [11] presented the application of Atkinson cycle in a motorcycle 4-stroke SI engine.

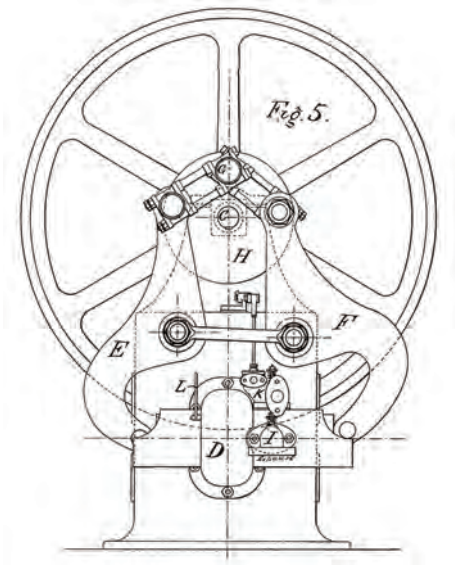

Fig. 1. Patent drawing of the Atkinson "Differential Engine", 1882 [7]

In a classical two-stroke engine realization of Atkinson cycle is almost not possible, but in the past, there were produced many industrial, military and marine two-stroke engines with opposed pistons, which the Atkinson cycle has been applied. One of the most known engines is the 6-cylinder engine Leyland L60 applied by the British army in tanks for very long time. The diagram of the one-cylinder section of this engine is shown in Fig. 2. The other solution of 2sOPE is Rolls Royce K60 with phase shift of two crankshafts enabling asymmetric scavenge process. In two-stroke engines with charging of the fresh air during scavenge process a large amount of the air is escaping to the exhaust ports because a large pressure difference. In four-

stroke engine such situation does not take place. Now the 2sOPE have their renaissance and are generally applied in local energetic plants and other commercial applications [10]. Their advantages were recently described by industry and scientific engineers e.g. from Achates Power [5, 6], how to increase their power and efficiency.

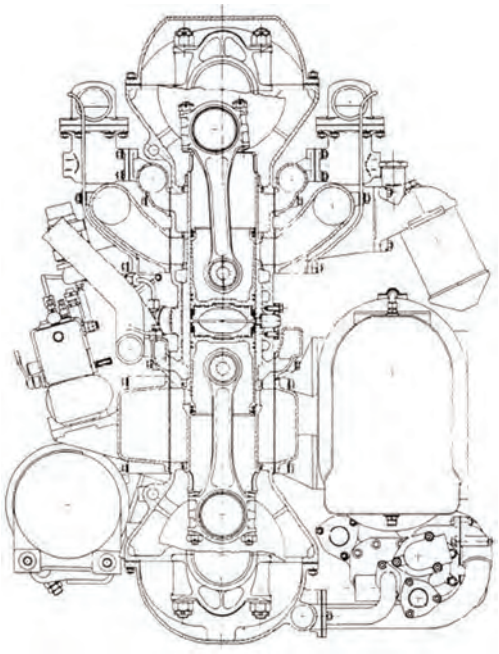

Fig. 2. Leyland L60 two-stroke opposed piston engine

3. Modification of timing system in two-stroke opposite piston engine

Two pistons connected with two separate crankshafts allow to change the exhaust port opening phase relative to the transfer port. The crank of the piston, which reveals and close the exhaust port (called as "exhaust piston") can be moved a certain angle relative to the crank of the other piston (called as "transfer piston"). In the classical two stroke engine, only symmetric phases are realized as shown in Fig. 3. The angle α_w denotes opening of the exhaust port from TDC and angles $\alpha_1 = \alpha_2$ are the delay angles of the transfer port opening.

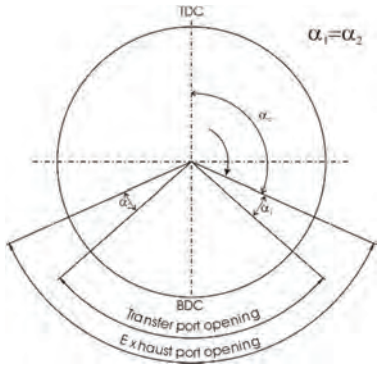

Fig. 3. Symmetric phase timing in two-stroke engine

The Atkinson cycle can be realized by changing of α_1 of a certain angle $\Delta\alpha$, then also the angle α_2 changes by a value $\Delta\alpha$. In this paper it was assumed that the reference crank is the crank of the "transfer port". Later opening of the exhaust port is shown in Fig. 4 and for this case after closing of the transfer port the exhaust port is opened for a longer time. On the other hands the expansion process lasts longer than for symmetric timing. In four stroke engines working at Atkinson cycle this case is mostly applied due to greater efficiency. The question is whether this is also valid for two-stroke opposite piston engine.

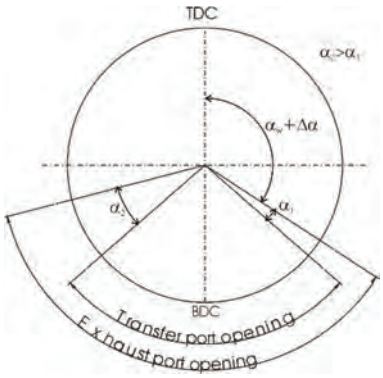

Fig. 4. Asymmetric phase timing in 2sOPE (delay of exhaust ports opening)

Earlier opening of the exhaust port relative to the symmetric timing causes also earlier closing of this port. The timing of such case is shown in Fig. 5, where the angle α_1 is bigger than α_2. Earlier opening of the exhaust port shortens the expansion process and prolongs the compression process. In four stroke engines working with Atkinson cycle causes lower engine efficiency.

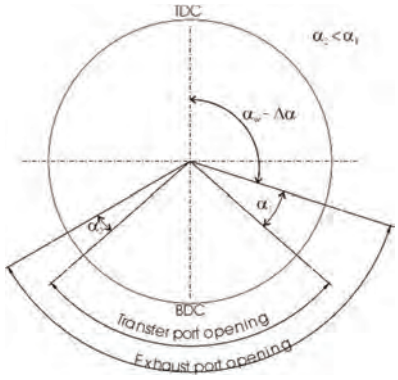

Fig. 5. Asymmetric phase timing in 2sOPE (earlier opening of exhaust ports)

Theoretical cycle of diesel engine assumes that whole dose of fuel is burned at constant pressure. But the work of real diesel engines can be presented according to the Sabathe's cycle, where a part of fuel is burned also at isochoric process. The modified Atkinson cycle for two-stroke opposed diesel engine is presented in Fig. 6 with asymmetric opening (p. 1) and closing (p. 5) of exhaust ports.

Compression of the charge takes place after CE in point 1 and expansion of exhaust gases finishes at point 5, but also after opening of the exhaust ports the gas pressure is still high and does the work. The outflow process (5–6) is almost linear and it reflects the real process.

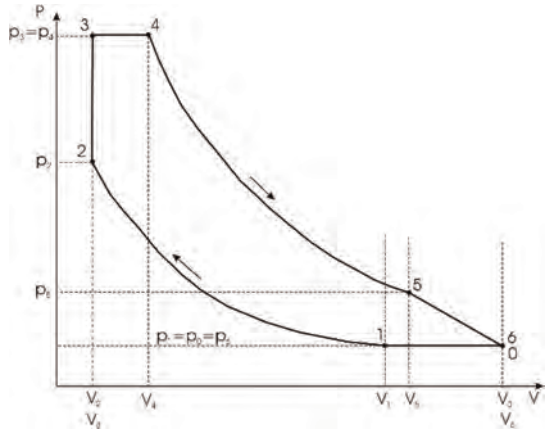

Fig. 6. Modified theoretical Atkinson work cycle in 2sOPE

4. Mathematical model of Atkinson work cycle in diesel two-stroke opposed piston engine

Wide mathematical description of Atkinson cycle for 4-stroke engines gave Ebrahimi [2] in aspect of λ, fuel mass flow rate and residual gases. In the model of 2sOPE it was assumed that the stroke towards TDC takes place from –180° to 0° according to crank rotation of the piston A and the stroke to BDC takes place from 0° to 180°. The simple theoretical model of an engine working cycle does not take into account the processes of fuel injection and evaporation and also combustion process. For that reason only the energy contained in fuel is considered in the model. Realization of the Atkinson cycle takes place when the angle position of the crank, which controls the exhaust piston B is different in relation to the position to the crank of the piston A, which controls the transfer ports of a certain angle $\Delta\alpha$.

$$\alpha_B = \alpha_A + \Delta\alpha \tag{1}$$

So, movements of both pistons h_A and h_B from TDC is calculated from the below equations:

$$h_A = r_A\left(1+\frac{\delta_A}{4}-\cos\alpha_A-\frac{\delta_A}{4}\cos\left(2\alpha_A\right)\right) \tag{2}$$

$$h_B = r_B\left(1+\frac{\delta_B}{4}-\cos\alpha_B-\frac{\delta_B}{4}\cos\left(2\alpha_B\right)\right) \tag{3}$$

where r_A, r_B are the cranks and $\delta_A = r_A/l_A$ and $\delta_B = r_B/l_B$, l_A and l_B are connecting rod lengths. Cylinder volume for each crank position α of the piston A is calculated as follows:

$$V = V_k + F\left(h_A + h_B\right) \tag{4}$$

where F is the piston area. Minimal volume of the combustion chamber V_k is defined on the known value of compression ratio ε and strokes of both pistons S_A and S_B:

$$V_k = \frac{F\left(S_A+S_B\right)}{\varepsilon-1} \tag{5}$$

Maximal cylinder volume at point 0 amounts:

$$V_0 = V_6 = V_k + FS_A + Fh_A\left(\pi+\Delta\alpha\right) \tag{6}$$

Volumes at points 1 and 5 are calculated on the base of knowing values of exhaust port opening angle α_w at symmetrical phases. Crank angles of the piston A when exhaust ports are closed and opened are defined by the below formulas:

$$\alpha_{B1} = -\alpha_w + \Delta\alpha \tag{7}$$

$$\alpha_{B5} = \alpha_w + \Delta\alpha \tag{8}$$

Knowing these values one can calculates the cylinder volumes at points 1 and 5:

$$V_1 = Fr_B\left(1+\frac{\delta_B}{4}-\cos\alpha_{B1}-\frac{\delta_B}{4}\cos\left(2\alpha_{B1}\right)\right) \tag{9}$$

$$V_5 = Fr_B\left(1+\frac{\delta_B}{4}-\cos\alpha_{B5}-\frac{\delta_B}{4}\cos\left(2\alpha_{B5}\right)\right) \tag{10}$$

At Atkinson cycle for diesel engine a part of the injected fuel is burned at constant volume V_2 equal to the minimal cylinder volume V_k:

$$V_2 = V_3 = V_k \tag{11}$$

Compression process takes place from point 1 to point 2 and pressure at point 2 at assumption of adiabatic process with heat ratio coefficient m has value:

$$p_2 = p_1\left(\frac{V_1}{V_2}\right)^m \tag{12}$$

and temperature reaches value:

$$T_2 = T_1\left(\frac{V_1}{V_2}\right)^{m-1} \tag{13}$$

Mass of the injected fuel m_f is calculated based on knowledge of mass of the charge in point 1 (p_1, T_1 are assumed, R – individual gas constant for the air is known) and assumed value of the excess air ratio λ:

$$m_f = \frac{m_1}{\lambda\left(\frac{A}{F}\right)_s} \tag{14}$$

where $\left(A/F\right)_s$ is a ratio of air (A) to fuel (F) for an applied liquid or gaseous fuel. The temperature at point 3 is calculated on the base of internal energy balance during isochoric process:

$$\left(m_1+km_f\right)c_v\Big|_0^{T_3}T_3 = m_1c_v\Big|_0^{T_2}T_2 + km_fW_d \tag{15}$$

where k is a part of fuel consumed during combustion process (value is assumed or determined during experimental tests). The temperature T_3 is obtained from the following equation by several iteration processes determining each time the heat at constant volume c_v appropriate for previously calculated temperature T_3, because $c_v = f(T)$:

$$T_3 = \frac{m_1c_v\Big|_0^{T_2}T_2 + km_fW_d}{\left(m_1+km_f\right)c_v\Big|_0^{T_3}} \tag{16}$$

Pressure at point 3 is the same as at point 4 and is obtained from the general equation of the gas state:

$$p_3 = \frac{(m_1 + km_f)RT_3}{V_2} = p_4 \tag{17}$$

For isobaric process (3–4) the specific heat at constant pressure c_p and individual gas constant R are defined by the following dependencies:

$$c_p = c_v + R \qquad R = \frac{MR}{M} \tag{18}$$

Temperature in point 4 is calculated from energy balance assuming that whole dose of fuel is burned at point 4. Similarly to the isochoric process the temperature T_4 is obtained by several iteration processes determining each time the heat at constant pressure c_p appropriate for previously calculated temperature T_4, because $c_p = f(T)$:

$$T_4 = \frac{(m_1 + km_f)c_p\Big|_0^{T_3} T_3 + (1-k)m_f W_d}{(m_1 + m_f)c_p\Big|_0^{T_4}} \tag{19}$$

One can determine the cylinder volume at point 4 from the gas state equation:

$$V_4 = \frac{(m_1 + m_f)RT_4}{p_4} \tag{20}$$

Pressure and temperature of the final point of expansion process (opening of exhaust ports) is determined from the following dependencies:

$$p_5 = p_4\left(\frac{V_4}{V_5}\right)^m \qquad T_5 = T_4\left(\frac{V_4}{V_5}\right)^{m-1} \tag{21}$$

In theoretical Atkinson cycle one assumes the equal values of pressure p_6, p_1 and p_0. Absolute work of each process is defined by change of pressure and volume and for the compression process 1–2 the work has the following form:

$$L_{1-2} = \int_1^2 pdV \tag{22}$$

Positive work from point 3 to point 6 is determined by the expression:

$$L^+ = p_3(V_4 - V_3) + \frac{p_4V_4}{m-1}\left[1 - \left(\frac{V_4}{V_5}\right)^{m-1}\right] + \frac{p_5 + p_6}{2}(V_6 - V_5) \tag{23}$$

The cylinder pressure course during exhaust port opening in the real two-stroke engines takes place as shown in Fig. 6 (linear drop in pressure). Negative work is obtained from the following expression:

$$L^- = p_0(V_1 - V_0) + \frac{p_1V_1}{m-1}\left[1 - \left(\frac{V_1}{V_2}\right)^{m-1}\right] \tag{24}$$

So total work of Atkinson two-stroke opposed piston engine is a sum of these works. The presented mathematical model is actual also for each type of two-stroke engine. The difference is only the researcher's decision of fuel dose division defined by coefficient k.

5. Determination of Atkinson cycle parameters

Geometric parameters of CI 2sOPE Leyland L60 as a starting point were adopted. The engine data is shown in Table 1. They do not present real values Leyland L60 engine.

Table 1. Engine specification

Rotational speed, rpm	1500
Bore, mm	117.6
Stroke cylinder A, mm	146
Stroke cylinder B, mm	146
Connecting rod length of cylinder A, mm	260
Connecting rod length of cylinder B, mm	260
Compression ratio	20
Transfer ports opening, deg	100
Exhaust ports opening, deg	140

The purpose of the calculations was to determine the trend of changes in operating parameters depending on the change of the timing phases of the exhaust ports in relation to the transfer ports. The real two-stroke heavy duty engine has a chamber of certain volume surrounding the cylinder around the transfer ports named here as "transfer chamber". The similar space exists for the exhaust ports named here as "outflow chamber". The flow model is shown in Fig. 7, where unsteady gas flow inside pipes and through the ports was taken into account (change of pressure waves). The 8 transfer and 8 exhaust ports were assumed for 0D model and CFD model.

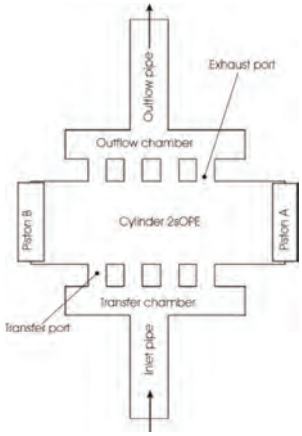

Fig. 7. Calculation model of 2sOPE

Based on the presented mathematical model, geometric data of the engine and assumption of adiabatic processes for perfect gas, thermodynamic parameters of the Atkinson cycle were determined. Calculations were done in the computer program worked out by the author, which enables achieving many other engine parameters. Pressure, temperature and volumes for the points shown in Fig. 6 are presented in Table 2. The minus delay of exhaust port close denotes earlier opening and closing of the exhaust ports in comparison to the symmetric phases. The presented results were obtained at assumption of initial pressure at point 0 and 1 equal 1.013 bar and temperature 293 K (without charging).

Table 2. Thermodynamic parameters of theoretical Atkinson cycle of two-stroke engine with opposed pistons

delay	V_1	V_2	V_4	V_5	p_2	p_3	p_5	T_1	T_2	T_3	T_4	T_5
deg	l	l	l	l	bar	bar	bar	K	K	K	K	K
–15	2.652	0.167	0.284	2.302	48.6	126.5	6.7	293.0	885.6	2255.6	3659.4	1583.9
–10	2.602	0.167	0.284	2.368	47.4	123.6	6.4	293.0	879.0	2246.3	3651.1	1563.7
–5	2.549	0.167	0.285	2.431	46.0	120.5	5.9	293.0	871.7	2236.3	3642.1	1544.7
0	2.492	0.167	0.285	2.492	44.6	117.2	5.6	293.0	863.9	2225.4	3632.5	1526.9
5	2.431	0.167	0.286	2.549	43.1	113.8	5.3	293.0	855.4	2213.8	3622.1	1510.3
10	2.368	0.167	0.287	2.602	41.5	110.2	5.0	293.0	846.4	2201.4	3611.0	1494.8
15	2.302	0.167	0.288	2.652	39.9	106.5	4.7	293.0	836.9	2188.3	3599.4	1480.4

It was assumed, that only 0.3 of dose fuel was burned at isochoric process (k = 0.3). Also, the whole charge was stoichiometric (λ = 1), which in diesel engine has higher value above 1.2. Earlier closing of the exhaust ports influences on higher pressure and temperature in point 2 and also a little bit on these parameters in point 4. In the Otto cycle total work is defined by difference between expansion work and compression work. Modelling of the Atkinson cycle enables calculation of the absolute work of the individual thermodynamic processes in dependence on variation of the delay of closing of exhaust ports. These dependencies are presented in Fig. 8. Higher compression work (negative) $L_{1\text{-}2}$ is done for earlier closing of exhaust ports (–15 deg) in comparison to later opening of these ports, but expansion work (positive) is higher for earlier closing of exhaust ports. The work $L_{3\text{-}4}$ is also higher for this case than for later value of EC.

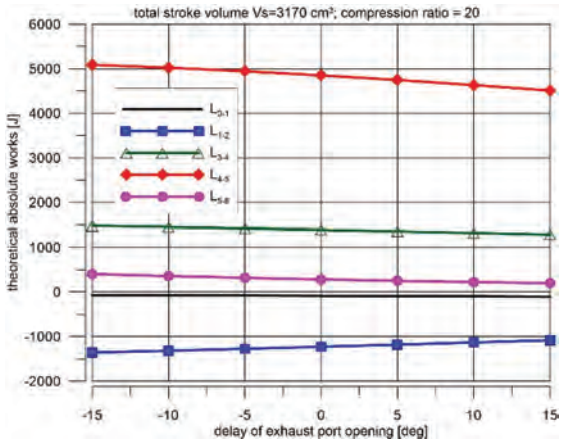

Fig. 8. Theoretical absolute works done during individual thermodynamic processes in a function of delay of opening of exhaust ports

The total theoretical work done by CI according to Atkinson's cycle is a sum of individual works and variation of this work is shown in Fig. 9. There is a significant difference of the total work for delays at 15 deg –15 deg (about 12%). Calculations indicate that for two-stroke engines differently than in four-stroke engines decreasing of the compression process reduces the engine work for the same mass of injected fuel (λ = const). There is almost linear decrease in value of total work with later closing of the exhaust ports.

This phenomenon shows that in the Atkinson cycle shorter compression CA and longer time of expansion process applied in modern 4-stroke engine cannot be used in 2sOPEs. Rather it should be applied the timing with earlier closing of the exhaust ports.

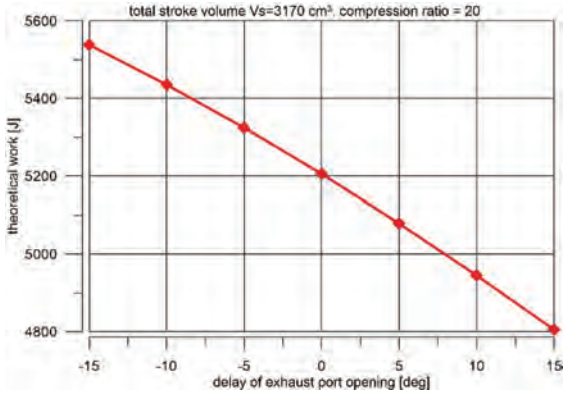

Fig. 9. Theoretical total work done by 2sOPE in a function of delay of opening of exhaust ports

6. CFD modelling of engine work

For the accurate checking of engine thermodynamic parameters, the better is simulation of the work process with CFD program. For that reason, the mesh of such engine was created in pre-processor in KIVA3V [1] with 65840 full hexagonal cells (Fig. 10). The cylinder model contains 8 transfer ports and 8 exhausts port with a certain angle to the cylinder surface, which causes a big swirl of the air in the cylinder during scavenge process. Original KIVA3V program enables calculations of thermodynamic state of the charge during scavenge, combustion and expansion process of two-stroke opposed piston engine.

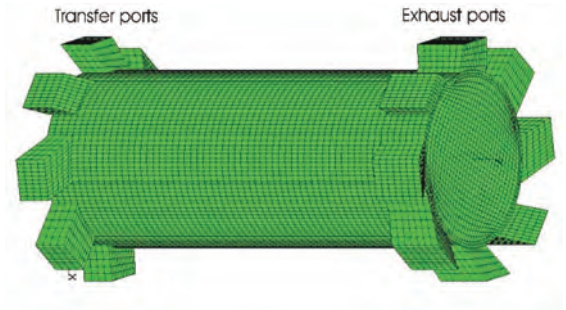

Fig. 10. Mesh of model of Leyland L60 engine

The engine model with the same geometry as shown in Table 1 was analysed at 7 different delay angles of closing of exhaust ports (–15, –10, –5, 0, 0.5, 10 and 15 deg) at constant engine rotational speed 1500 rpm. Turbulence

model κ–ε was applied. Total mass 0.18 g of fuel was delivered by 4 injectors located at a half of cylinder height for one working cycle. Diesel oil was injected 8 deg CA BTDC when temperature of the charge was sufficient for self-ignition. Fuel injection in two-stroke engines is fully described by author in the book [8]. High swirl ratio caused the peripheral motion of the fuel and quick combustion process. Calculation were conducted at assumption of mechanical charging with absolute pressure equal 1.8 bar at the surface inlet of each transfer port. A fresh air with has temperature of 320 K. Heat transfer to the cylinder and piston walls was considered by using Woschni formulas given by Heywood [6].

The CFD engine working model, in contrast to the theoretical model, takes into account fuel injection, evaporation of fuel droplets and combustion process based on chemical reactions basing on Arrhenius formulas. The results of calculations done for different cases of angle delay of closing of the exhaust ports are presented in the charts shown below. High increase of pressure causes a loud work and big forces acting on the whole crank system. Figure 11 presents cylinder pressure courses at three cases (–15, 0 and 15 deg) of CE angles. For earlier closing of the exhaust port the faster increase of pressure during compression process takes place because almost whole delivered fresh air stays in the cylinder. In this case the mixture ignition occurs later and for that reason maximum pressure is lower than for the rest cases. The combustion process is extended on the expansion process. The highest pressure was achieved at symmetrical phases as in classical two-stroke engines. In this case the fuel burns completely in a very short time.

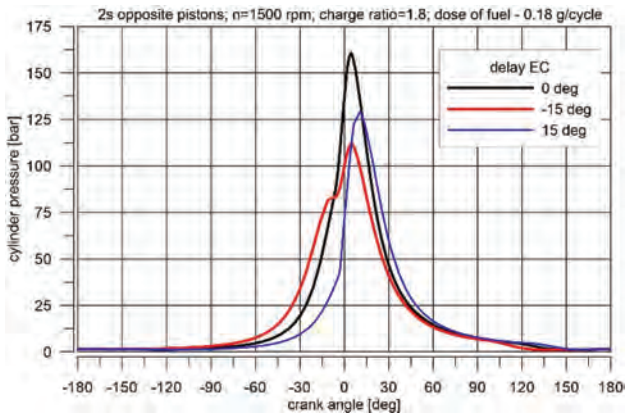

Fig. 11. Cylinder pressure variation in 2sOPE for different delays of exhaust ports closing (EC) in function of crank angle

Variation of mean temperature in the cylinder for three cases is shown in Fig. 12. Starting point of combustion process for delays –15 and 0 deg of exhaust ports closing amounts 1050 K and is higher than for the case of 15 deg of the delay. Highest temperature takes place at this case 15 deg EC delay and also the highest increment of temperature during combustion process is observed despite the same fuel dose for all cases 0.18 g/cycle.

Pressure traces in dependence on volume change (p–V) are shown in Fig. 13 for analysis of engine work. The case with highest pressure does not give highest work. The decision about changing the closing phase of the exhaust ports influences on the engine power. The symmetrical timing phases cause high value of maximal pressure, but it is lower during expansion process. The engine is evaluated in terms of indicated mean effective pressure (imep). Despite of low value of maximal cylinder pressure for the case with delay of –15 deg EC the engine shows higher imep than for the cases with later closing of exhaust ports by the piston (Fig. 14). The difference of imep amounts 1 bar, which is above 10% of maximal value at –10 deg EC of delay.

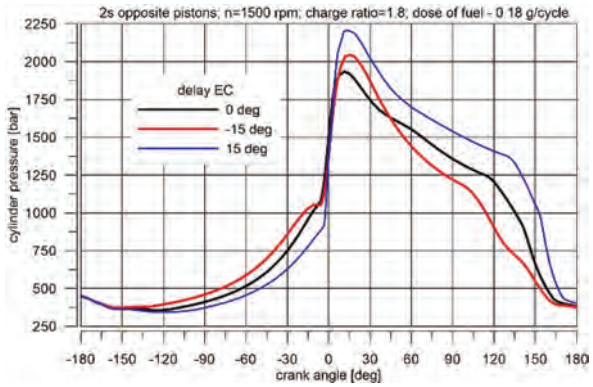

Fig. 12. Temperature course in cylinder for different delays of exhaust port closing

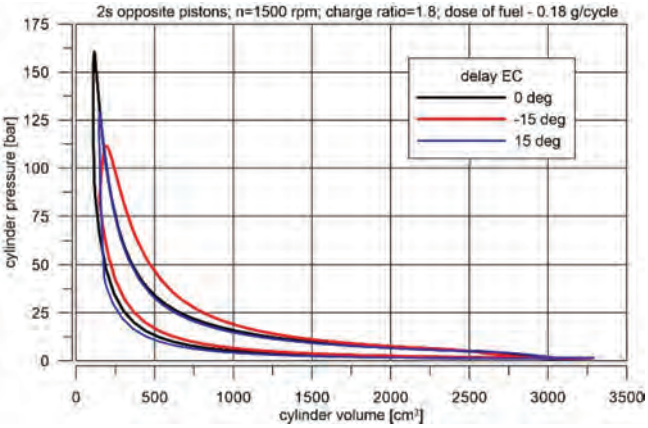

Fig. 13. P-V diagram for different delay of exhaust ports closing (EC)

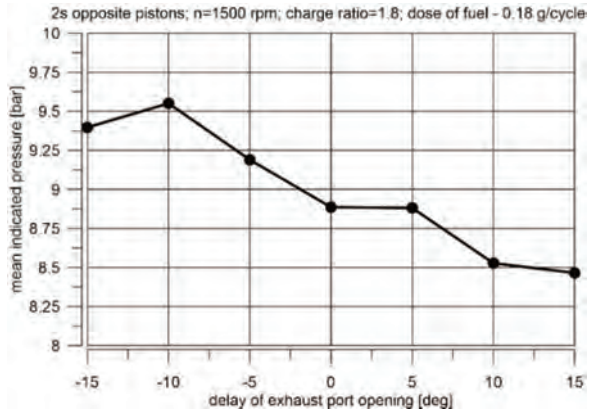

Fig. 14. Variation of mean indicated pressure in dependence of delay of exhaust port close

Total efficiency of the engine is determined by specific fuel consumption (bsfc) and fuel caloric value. Variation of total efficiency of analysed engines is similar as variation of

imep (Fig. 15). For the low dose of fuel, the engine achieves highest efficiency at –10 deg CE of delay of 40%. Delay of closing of outflow ports causes a significant decrease of total efficiency.

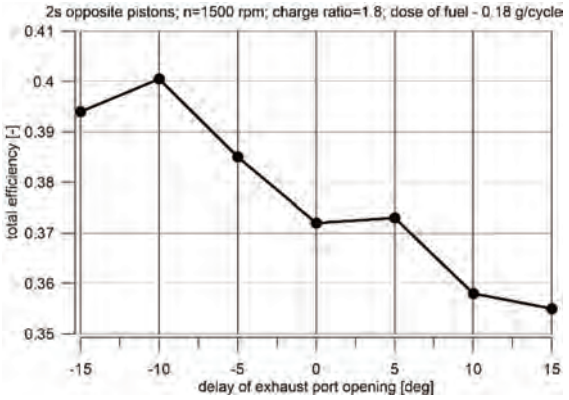

Fig. 15. Variation of engine total efficiency in dependence of delay of exhaust port close

For the same amount of the injected fuel the air excess ratio depends on volumetric efficiency. So, if the excess air ratio increases, it means that the cylinder before combustion process contains a large amount of the fresh air. Figure 15 presents variation of the excess air ratio in dependence of EC delay. For earlier closing of the exhaust ports more air remains in the cylinder. This dependence is almost linear.

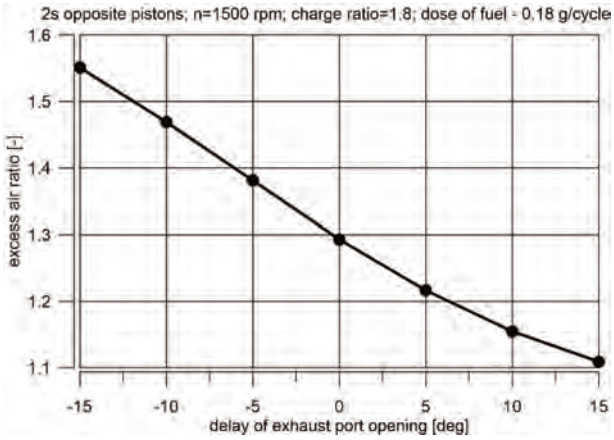

Fig. 16. Air excess ratio (λ) as function of delay exhaust port opening

Compression ignition engines emit pollutants, mainly soot in a form of particulate matters (PM) and a lot of nitrogen oxides (NO_x). Amount of NO_x depends on combustion temperature and for the case with 15 deg EC of delay, where maximal mean temperature achieves value 2250 K, the engine emits most of NO_x. The most important product among NO_x compounds is nitric oxide (NO) and variation of NO mass ratio in the combustion chamber is shown in Fig, 17. Earlier closing of outflow ports causes lower emission of NO_x, but a small amount of hydrocarbons (below 50 ppm) is seen in exhaust gases.

Program CFD enabled achieving more detailed information about scavenge process, spreading of injected fuel, evaporation of fuel droplets, forming of chemical species during combustion process and their distribution inside the cylinder. But these phenomena will be the subject of another dissertation.

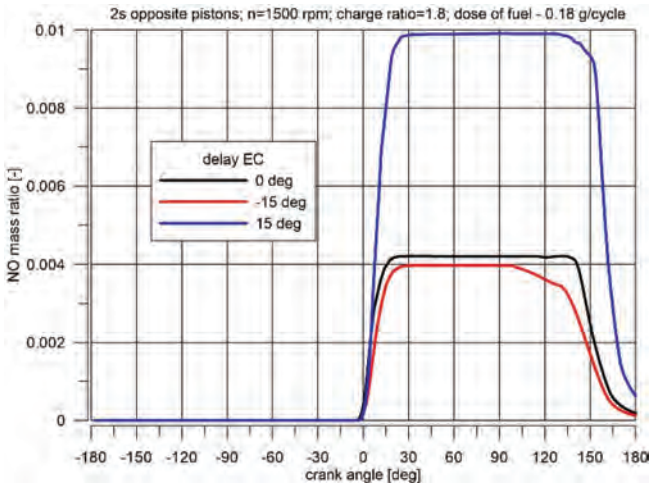

Fig. 17. Variation of NO mass ratio in cylinder of 2sOPE with different delay of exhaust port closure

7. Discussion of results

Recently modification of engine work by the Atkinson cycle is done for many types of engines especially for hybrid vehicles. Typical Atkinson modification by later closing of exhaust and inlet valves in four-stroke engines enables shorter compression period and longer expansion period, which causes less absolute work of compression process and greater expansion work. But in four-stroke engines there is only a small escape of the fresh air during closing of the inlet valves. But it is not true for two-stroke engines especially supercharged engines. Later closing of exhaust port causes an escape of a large amount of the fresh air. For this reason, earlier closing of the exhaust ports just after closing of the transfer ports causes the capture of a larger amount of the fresh air, particularly for charged engine. Then more fuel can be injected in order to achieve more engine power.

Both simulation tests using 0D and CFD programs have shown the need for reverse action than in 4-stroke engine. Earlier opening of the exhaust ports and thus its early closure causes more power, higher total efficiency and also lower emission of NOx. The works done in Achates Power, Inc [4, 5] also confirm such dependences for their production engines. Earlier opening of exhaust ports in 2sOPE causes faster escaping of exhaust gases under higher pressure and the scavenge process is more effective particularly in the supercharged engine. The work presents the theoretical Atkinson cycle for 2sOPE with certain modification of the cycle at outflow with mathematical model. The model is more realistic than it was presented till now.

8. Conclusions

The presented study of the engine's work induces to draw some conclusions and guidelines for potential engine designers and researchers. The study is an input for realization of such processes in a future of power plant engines with different fuelling systems.

1. The paper presents a new theoretical cycle of 2sOPE with Atkinson modification and its mathematical model.

Such model is useful for analysis of thermodynamic parameters at assumption of different settings of openings the engine ports by change the angular cranks settings.
2. Two-stroke opposed piston diesel engines enables to apply an asymmetric timing of exhaust ports phases, which allows to reduce the loss of the fresh charge during scavenge process.
3. Such engine causes a strong swirl of the charge during scavenge process, which influences on a good penetration of the injected fuel and enable better combustion process.
4. Applying of Diesel/Atkinson cycle in the two-stroke OPE by earlier closing of the exhaust ports increases working parameters (imep, total efficiency and volumetric efficiency). Much more fresh air stays in the cylinder after and therefore much more fuel can be delivered by the injector, which enable to achieve more power.
5. Despite shorter expansion time the expansion work of this engine is bigger at earlier exhaust port opening than at later opening.
6. The combustion process in the diesel-Atkinson 2sOPE lasts longer at constant pressure but at lower value of pressure, which is important for durability of whole crank system.
7. 2sOPE with earlier opening of exhaust ports enable decreasing of NO_x due to lower combustion temperature.
8. Inversely than in the four-stroke engine, for more work, the outlet ports must be opened earlier.

Nomenclature

2sOPE	two-stroke opposed piston engine
CE	closing of exhaust port
TDC	top dead centre
BDC	bottom dead centre
imep	indicated mean effective pressure
bsfc	brutto specific fuel consumption
PM	particulate matters
CFD	computational fluid dynamics
CI	compression ignition engine

Bibliography

[1] AMSDEN, A.A. et al. KIVA: a comprehensive model for 2-D and 3-D engine simulations. *SAE Paper 850554.* 1985.
[2] EBRAHIMI, R. Thermodynamic modeling of an Atkinson cycle with respect to relative air-fuel ratio, fuel mass flow rate and residual gases. *Acta Physica Polonica A.* 2013, **124**. DOI:10.12693/APhysPolA.124.29
[3] FLINT, M., PIRAULT, J.P. Opposed piston engines: evolution, use, and future applications. *SAE International.* Warrendale. 2009.
[4] FOSTER, D., HEROLD, R., LEMKE, J. et al. Thermodynamic benefits of opposed-piston two-stroke engines. *SAE Technical Paper 2011-01-2216.* 2011, DOI:10.4271/2011-01-2216
[5] FROMM, L., HEROLD, R., KOSZEWNIK, J., REGNER, G. Modernizing the opposed-piston engine for more efficient military ground vehicle application. *2012 NDIA Ground Vehicle Systems Engineering and Technology Symposium.* Michigan, August 14-16, 2012.
[6] HEYWOOD, J. Internal Combustion Engine Fundamentals. *McGraw-Hill.* New York, 1988.
[7] http://en.wikipedia.org/wiki/Atkinson_cycle
[8] MITIANIEC, W. Fundamentals of fuel injection and emission in two-stroke engines. *Nova Science Publisher.* New York 2018.
[9] NOBUKI, K., KIYOSHI, N., TOSHIHIRO, K. Development of new 1.8-l engine for hybrid vehicles. *SAE Technical Paper 2009-01-1061.* 2009.
[10] REGNER, G. et al. Modernizing the opposed piston two-stroke diesel engine for more efficient commercial vehicle applications. *Achates Power, Inc.* San Diego 2012.
[11] SENDYKA, B., SOCHAN, A. Increase of the total efficiency using the Atkinson cycle in the spark ignition engine. *Journal of KONES Powertrain and Transport.* 2009, **16**(2).

Wladyslaw Mitianiec, DSc., DEng. – Faculty of Mechanical Engineering, Cracow University of Technology.
e-mail: wmitanie@usk.pk.edu.pl

Article citation info:
KLYUS, O., KRAUSE, P., MARKOV, V. et al. Evaluation of the suitability of synthetic polymer fuels in self-ignition engines. *Combustion Engines*. 2019, **178**(3), 129-134. DOI: 10.19206/CE-2019-322

Oleh KLYUS
Paweł KRAUSE
Vladimir MARKOV
Anna SKARBEK-ŻABKIN
Bowen SA

CE-2019-322

Evaluation of the suitability of synthetic polymer fuels in self-ignition engines

The article presents a method for determining the quality of spraying a mixture of oil and synthetic fuels obtained from the processing of polymer materials. Laboratory tests of physical parameters of such a mixture were carried out, which made it possible to determine the limit values for the volume fraction of synthetic fuels. The method of determining the suitability of this type of fuel takes into account the criterion numbers Re and Oh, which include physical parameters such as viscosity, density, and surface tension. The experimental part concerning the distribution of droplets of injected fuel and determination of Sauter Mean Diameter using laser diffraction confirmed the usefulness of the developed method for the assessment of the possibility of using a mixture of petroleum-based and synthetic fuels in self-ignition engines.

Key words: *synthetic polymer fuels, Sauter mean diameter, diesel engines*

1. Introduction

The national environmental policy and international commitments of Poland should ensure sustainable development and usage of resources that would meet the needs of present and future generations. One of the greatest challenges of our time is the progressive depletion of conventional fuels (oil and gas). Another, but also very important, topic is the growing amount of municipal waste of which the largest amount is waste of polymer materials. The management of this type of waste is an increasing issue threatening the ecosystem. 75% of plastic waste is landfilled or "ends" directly in the environment, including 8 million tons a year in the seas and oceans. Even in the European Union, where the most rigorous regulations apply, less than 32% is recycled while the remaining waste is incinerated, stored or exported. Cities and towns around the world need processes to stop the plastic waste stream from being directed to garbage dumps and incinerators. The combustion process is very capital intensive and is one of the most expensive methods of producing energy and eliminating waste. Compared to the recycling process, the incineration of plastics generates almost three times more greenhouse gas emissions and recovers only 20% of the energy contained in polymeric materials [28].

Considering the polymer materials' types and methods of their use, there is no single and simple solution to all the problems related to the waste management. However, one possible direction of the use is a chemical recycling which is associated with the production of liquid alternative fuels. It should be emphasized that, according to the Directive 2014/94/EU of 22nd October 2014 on the deployment of alternative fuels infrastructure, "alternative fuels" means fuels or power sources which serve, at least partly, as a substitute for fossil oil sources in the energy supply to transport and which have the potential to contribute to its decarbonization and enhance the environmental performance of the transport sector. They include, inter alia electricity, hydrogen, biofuels, synthetic and paraffinic fuels, natural gas [6].

Up-to-day, scientific and research works on alternative fuels has focused on the use of biofuels based on oil plants. During almost all Congresses and Scientific Conferences in Poland and abroad (CIMAC, KONMOT, PTNSS, KONSPAL, KONES, OMiU, and others) there was presented and discussed the information on the use of rapeseed or sunflower oil methyl esters and other plant oils. However, there has been no presentation or debate on the research results referring to the usage of synthetic fuels generated from municipal waste or their mixture with petroleum-based fuels. No comprehensive assessment of their use in self-ignition engines has also been presented. And hence, this paper covers the topic mentioned above.

2. Conversion of plastic waste to liquid fuel – technologies

The history of waste polymers processing into fuel fractions in Poland dates back to the end of the 20th century. Technologies originate from carbochemistry covering a detailed analysis of the chemical processing of fossil coal by gasification and liquefaction [24].

Coal liquefaction process was applied during the Second World War to produce synthetic gasoline [24]. In the formal sense, coal is a cross-linked polymer with a complex structure and poor quality. Transferring the processes from coal processing to plastic waste treatment is relatively simple. However, technical problems may be encountered as result of a highly diverse chemical structure of this group of waste. The thermoplastic properties of same are responsible for problems in technological processes at higher temperatures [3, 18].

The technologies are intended to recover energy from waste materials, including non-biodegradable, such as biomass, municipal solid waste, agricultural waste and high-energy-density materials (rubber and polymers). Polymeric materials are non-biodegradable polymers that contain carbon, hydrogen and other elements (chlorine, nitrogen, etc.) [15, 17, 28].

The methodologies for polymer waste processing into liquid fuels include:

– Pyrolysis – the main factor causing the polymers' decomposition is the temperature which usual range is from 523 K to 773 K. The main assumption for the process is the total absence of oxygen. If the oxygen is present, the reactants' oxida-

tion would occur and it would become a semi-burning or burning process. What is also important in this particular part is that the pyrolysis process does not involve reaction with catalysts, but often it is carried out in the presence of water. In order to ensure that the pyrolysis process is run correctly, a low pressure, not exceeding 0.2 MPa, is a prerequisite. The hydrocarbon pyrolysis process may be described by the following simplified chemical equation [22]:

$$C_xH_yO_z + \text{thermal energy} + CO_2 + H_2O = CO + CH_4 + C_2H_6 + CH_2O + \ldots + C_mH_n + C_{-q}$$

Among the pyrolysis products, the liquid phase is the major one (its share equals ca. 60% regardless of the pyrolysis temperature). As the temperature rises, the amount of solid phase decreases in favour of the gas phase [16]:

– Catalytic cracking – the factor leading to the degradation of polymer macromolecules is a suitable catalyst. The course of the catalytic cracking process is similar to the pyrolysis one. As a result of pyrolysis, products of lower molecular weight are obtained (as in catalytic cracking). However, they consist of a whole range of saturated and unsaturated organic compounds, and the process requires a higher temperature. Due to the catalyst, the temperature of the cracking process may be lowered, as well as a much more favourable composition of products may be obtained.

– Catalytic depolymerization – in the catalytic depolymerisation technology (KDV), the key parts are the friction turbine and the catalyst composition. The hydrocarbon molecules of the input material are broken down by the catalyst in the oil suspension cycle at a temperature of 553–615 K. The generated diesel vapor is separated in the distillation column. The main advantages of the KDV process include low process temperature (about 553 K), the high processing efficiency of 80%, high energy efficiency (only about 10% of the fuel produced in it is consumed for own use), low amount of waste and contamination emitted to the environment;

– Thermolysis supported by hydrogenation and izomerization – plastic waste is provided to the reactor where the cracking process takes place. Reactive distillation occurs and sufficiently long-chain hydrocarbons are obtained. Vapors from the reactor are provided directly to the non-pressurized hydrogenation reactor, followed by isomerization. Hydrogenation and izomerization are the second stage of the entire process, which distinguishes it from other such technologies. The process is carried out in a synthesis gas atmosphere, i.e. a mixture of carbon monoxide and hydrogen.

For the purpose of further studies, the authors have decided to apply a conversion technology such as the catalytic depolymerization of synthetic fuel generated from municipal waste. The decision has been made based on the fact that the process is currently the most popularized and the implementation cost is relatively low.

3. Analysis of processes in a combustion chamber of self-ignition engines

A feasibility assessment regarding the use of synthetic fuels or their mixture with petroleum-based fuels in self-ignition engines requires a detailed analysis of the processes occurring in the combustion chamber of these engines. The thermodynamic analysis of the engine's thermal cycle shows that the efficiency of using heat during combustion in a given engine is determined by its location in time [23]. It would be the most optimal from this point of view to combust the entire amount of fuel at a constant volume of the combustion chamber when the piston is at the top dead centre (TDC). However, then the rate of heat evolution would become excessively large causing the impact loads on the crank mechanism and acoustic symptoms in the form of excessive loudness [25]. Therefore, the process of heat release is extended and it covers a specific rotation angle of the crankshaft near TDC. The conditions of efficient heat release and its application, obtaining reduced dynamic loads of the crank mechanism along with the silent-running at the possible lowest level are opposed and any technical solution to this matter shall constitute a compromise [11]. An additional factor hindering this compromise is the content of the exhaust gas, which shall meet certain requirements. Experience shows that satisfactory results for a given engine, both in terms of the crank mechanism loads, engine noise level, exhaust gas composition and cost efficiency of its operation, are extremely difficult to obtain, and the optimal solution may be usually applied only when the course of heat evolution is strictly-defined. Consequently, the entire process shall not be spontaneous, uncontrollable. Therefore, the most important matter related to the self-ignition engine operation is such combustion management that the physical and chemical effects of this process corresponded to the various requirements for engine use [2, 21].

The abovementioned physical and chemical processes may be presented by the following stages – fuel pumping, atomizing, fuel break down into droplets and their evaporation, combustible mixture formation, ignition delay, combustion and heat release.

In the processes prior to the self-ignition, a certain amount of the chemical compounds of fuel and oxygen molecules was found to be torn apart [7]. While the self-ignition process itself takes place in the gas phase. Therefore, in the process of fuel self-ignition, it is essential that fuel evaporates and is mixed with air in the proper proportions. The second condition is met automatically since in the fuel jet area there is a variable concentration of fuel vapours, from a very poor mixture (on the stream periphery) to a very rich one (in the stream core). In order to evaporate the fuel, a certain amount of thermal energy is required. In the self-ignition process, it is significant to transfer the energy from the heated air to atomized fuel droplets. By adopting the appropriate simplification, one may assume that this process takes place under fixed conditions. Therefore, in order to describe the process, the heat transfer equation may be applied in the form of the Newton equation [4, 27]:

$$\tau = Q_n / (t_C - t_f) F \tag{1}$$

where: Q_n – heat necessary to evaporate an amount of fuel that is essential to generate a mixture with air for ignition [J], t_C – average air temperature in ignition delay period [°C], t_f – injected fuel temperature [°C], α – heat transfer coefficient [W/m^{2}K], F – atomized fuel surface [m^2], τ – ignition delay period.

The Q_n value is subject to a fuel type. If the fuel contains a large amount of paraffin fractions, the value of Q_n is low,

while for fuel with a large number of aromatic hydrocarbons, the value of Q_n is higher. The explanation may be that aromatic hydrocarbon particles have greater durability of interatomic connections [1]. When analyzing t_C and t_{pal}, one may note that they are subject to the engine structural parameters (e.g. compression ratio), ambient parameters and in this case, the comparison of various fuel types may be omitted. This also refers to the heat transfer coefficient. However, F shall be analyzed in detail. This is due to the fact that the atomized fuel stream consists of concentrated smallest drops, and their number and diameter directly affect the parameter F, which sequentially has an impact on the processes of evaporation and mixing of fuel vapors with air.

As the main criterion for the liquid atomization process quality, the droplet diameter in the atomized jet is given [5, 7]. As the defined dose of fuel is atomized, its surface area is enlarged and thus the amount of absorbed heat, due to which fuel vaporizes, increases. Simultaneously, the droplet diameter affects the jet macrostructure i.e. the atomization angle and the spray tip penetration as well as the parameters impacting the accuracy of mixing with air, optionally for gathering fuel droplets on the cylinder walls or the piston bottom. The conclusion is that the droplet diameter in the spray is a compromise between the largest possible fuel surface (the shortest droplet diameter) and the spray range in the combustion chamber. The differences between requirements for individual engines may result, among others, from working process management (combustion chamber structure). Unlike chambers with direct injection, in divided or vortex combustion chambers, droplet diameters may be larger and the length of spray may be shorter due to the intense and dynamic mixing process with air.

The quality of fuel atomization process is evaluated on the basis of its accuracy (droplet diameter) and homogeneity (number of droplets of the same diameter), using the average droplet diameter. They have been established as conventional values and they describe a set of homogeneous droplets as a substitute of the actual set (atomization spectrum). Depending on the methodology and the calculation method, the average droplets' diameter may determine such values as number, diameter, area, and volume of droplets. The adoption of an average diameter is subject to the field of application of the atomized liquid and although it does not provide any information on the droplet set itself, it is considered as the most demonstrative quantity for assessing the quality.

Regardless of how the working process in the engine is organized and managed, the following processes take place in the combustion chamber: droplets' vaporization, heat transfer, and exchange, fuel combustion. Therefore, for the quality assessment purpose, the Sauter mean diameter (D_{32} or SMD) is implemented. It is also the relation of the droplet volume to its surface in the actual and theoretical spray.

In the literature, regarding the subject of research [8, 13, 14, 26] there are formulas available that allow calculating D_{32}. They differ in the number of considered physical parameters, constant values, and exponents. In general, these relationships may be presented as follows:

$$SMD = f(\mu, \rho, \sigma, \Delta P, k) \tag{2}$$

where: μ, ρ, σ – dynamic viscosity, density and surface tension of fuel, ΔP – the pressure difference between the pressure of injected fuel and the medium pressure to which it is injected, k – includes structural parameters of the atomizer. It should be highlighted that the majority of the above parameters are physical fuel parameters that are indirectly or directly included in the Reynolds number, Laplace number, Ohnesorge number [12, 19].

The literature analysis indicates that the stream breakdown mechanism may be presented in four stages [14] – viscous flow, transient flow, turbulent flow, and specific atomization. The mechanism has been illustrated by the Ohnesorge diagram where the abovementioned stages are presented. Summing up, the assessment of the suitability of synthetic fuels for self-ignition engines, as an additional feature, may answer the question whether the physical parameters of the fuel or a mixture of this fuel with diesel meet the conditions specified in the Ohnesorge diagram as the specific atomization.

4. Laboratory tests of physical parameters and quality of fuel mixture atomization process

The first stage of tests was performed at the Centre for Fuel and Hydraulic Fluids Testing and Environmental Protection of the Maritime University of Szczecin and at the engine laboratory of the Motor Transport Institute of Warsaw. During that stage, the physical and chemical parameters of the synthetic fuel were determined as well as its mixtures with diesel fuel.

The synthetic fuel equaled to 3, 5, 7, 20% (by volume) to petroleum-based fuel and 100% of synthetic fuel. It was noted that the value of 7% synthetic fuel additive is the threshold for the minimum ignition temperature (according to PN-EN590), lower values of the volume of synthetic fuel additives meet the standard requirements (Fig. 1). However, other physical parameters for both 100% synthetic fuels and mixtures with petroleum diesel meet the requirements imposed by PN-EN590 (Table 1).

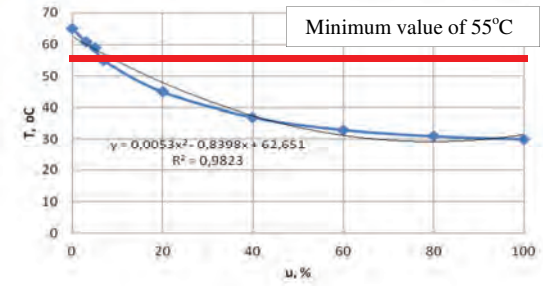

Fig. 1. Relationship between content of synthetic fuel in the fuel mixture (*u*) and flash point [20]

The second stage included the laboratory tests the aim of which was to determine the quality of the atomized fuels. The volume of synthetic fuels in the mixture was limited to 7% due to the ignition temperature of the mixture. As a result of the high accuracy of the outcomes and relatively simple operation of the device used for the research, the laser diffraction method has been selected [10, 12, 25]. This method is based on the measurement of the scattering of the He-Ne laser beam. The Spraytec device of Malvern has been used

for that task (Fig. 2a) with 30 receiver's detectors. They detect scattered light on the stream particles and convert it into an electrical signal. For the laboratory tests purpose, D1LMK148/1 atomizer has been used. The selection of this type of atomizer was driven by the fact that it has three atomization holes. Due to that one of the stream maybe straightforwardly directed into the laser area. Two remaining jets may be directed to properly set traps (Fig. 2b).

Table 1. Physical parameters of selected fuels

		Acc. To PN-EN 590+A1:2011	Results ON+7%PP
		ON "standard"	
Kinematic viscosity at 40ºC, mm^2/s	Min. Max.	2.00 4.50	2.6
Density at 15ºC, kg/m^3	Min. Max.	820.00 845.00	830
Cetane number	Min.	51.0	57
Flash point ºC	Min.	55	55
Surface tension J/m^2		26,08	26,40
Remains after high temperature carbonization, MCR at 10% residue, % mass	Max	0.30	0.08
Lubricity, wear scar diameter (wsd 1.4) at 60 ºC, µm	Max	460	355

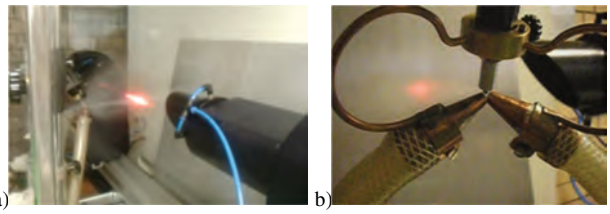

a) b)

Fig. 2. Laboratory stand for testing the quality of fuel atomization (a) and D1LMK148/1 atomizer (b)

In the case of an atomized fuel stream consisting of a large number of drops of various diameters, the measurement of their size distribution is hampered by multiple scattering. Therefore, the Spraytec software uses a multiple scattering algorithm which includes background factors (electronic, optical) and light scattering components [9]. Moreover, the Spraytec software computes the particle size distribution in aerosols by comparing the measured scattering spectrum with an optical model. The main result of the measurements is the calculation of the mean droplet diameter (Sauter mean diameter). Figure 3 presents the examples of droplet diameters for a mixture of petroleum-based fuel with the addition of 7% synthetic fuel. Whereas, Figure 4 demonstrates the results of laboratory tests showing the relation between the Sauter mean diameter and the fuel mixture.

The SMD values, calculated as per the above, have been compared with the values computed based on the formulas presented in the scientific literature [2] including the physical parameters of fuel mixtures (Table 1). The most similar nature of these relations was obtained when the Elkobt equation had been applied (Fig. 4).

The difference between the results obtained experimentally and the values calculated using Elkotb equation may be corrected by the following polynomial relation:

$$f(x) = 0.475x^2 - 1.431x - 6.765 \qquad (3)$$

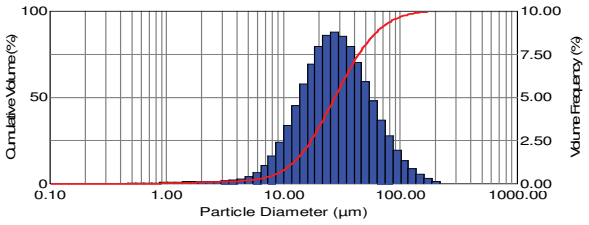

Fig. 3. Atomization spectrum and total distribution of diesel droplets with the addition of 7% synthetic fuel

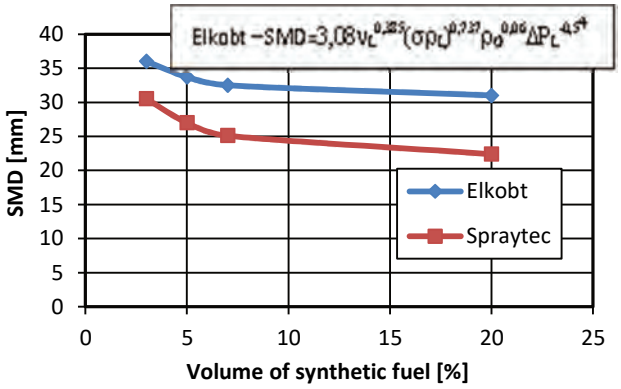

Fig. 4. SMD values calculated using Elkotb equation compared to SMD values obtained by Spraytec

In the above relations, the correlation coefficient R^2 equals to 0.9713 (x – determines the volume fraction of synthetic fuel in a mixture with petroleum diesel). A standardized formula for SMD of the mixture may be presented as follows:

$$SMD = f(x) \cdot 3.08 v_L^{0.385} (\sigma \rho_L)^{0.737} \rho_G^{0.06} \Delta P_L^{-0.54} \qquad (4)$$

where: ν_L – kinematic viscosity of fuel mixture [m^2/s], ρ_L – density of fuel mixture [kg/m^3], σ – surface tension of fuel mixture [N/m], ρ_G – density in the gas medium to which fuel mixture is injected [kg/m^3], ΔP_L – pressure difference between the fuel and the gas medium [Pa].

The significant matter in the relation above (4) is that it includes all physical parameters of the fuel: surface tension, viscosity, density. It confirms the impact of these parameters on the quality of the atomization process.

5. Method for determining the suitability of synthetic fuels for self-ignition engines by using criterion numbers

Based on the laboratory tests and the literature analysis, the authors wish to propose a methodology that allows specifying additional features that prove the suitability of synthetic fuels for self-ignition engines.

As mentioned above, fuel atomization process is fundamental for the engine working process management. It may be specified qualitatively by the Sauter mean diameter of the atomized fuel droplets. This parameter, sequentially, is dependent on the fuel physical parameters being a part of the criterion equations (4). For the purpose of this paper, Ohnesorge and Reynolds numbers have been selected along

with the Ohnesorge diagram in order to present visually the usefulness of synthetic fuel for self-ignition engines.

At the first stage of the analysis, the methodology provides that the following physical parameters of the tested fuel are specified: fuel dynamic or kinematic viscosity, η_F or υ_F accordingly, fuel density ρ_F and surface tension σ.

The second stage is related to the determination of the structural parameters of the engine that are directly part of the criterion equations: atomization holes' diameter d_o, fuel injection pressure p_F, rotational speed n, engine compression ratio ε or pressure p_A at the end of the compression stroke. If the parameters are not available in the engine technical documentation, they may be calculated based on the literature sources [21].

The next stage is to calculate the criterion numbers' values (Oh and Re) as follows:

$$\mathrm{Oh} = \frac{\eta_F}{\sqrt{\varrho_F \sigma d_o}}, \qquad \mathrm{Re} = \frac{0{,}6\sqrt{2\frac{p_F - p_A}{\varrho_F}}d_o \varrho_F}{\eta_F} \tag{12}$$

where: η_F – fuel dynamic viscosity $\eta_F = \upsilon_F \varrho_F$ [Pa], υ_F – fuel kinematic viscosity, ρ_F – fuel density [kg/m^3], σ – surface tension [N/m], d_o – atomization hole diameter [m], p_F – fuel pressure [Pa], p_A – air pressure [Pa].

The calculation results shall be plotted on the Ohnesorge diagram. If the values are within the diagram field that corresponds to the specific atomization, the tested fuel upon its injection to the combustion chamber will undergo a specific atomization process. It proves its suitability for self-ignition engines.

An example of how to apply the methodology for the petroleum-based fuel mixed with synthetic polymer fuel is presented in Fig. 5.

The intersection point of Oh and Re numbers on the Ohnesorge diagram for a mixture of diesel oil and 7% additives of synthetic polymer fuel is located in the area of atomization. This entitles to determine the suitability of the tested fuel for self-ignition engines.

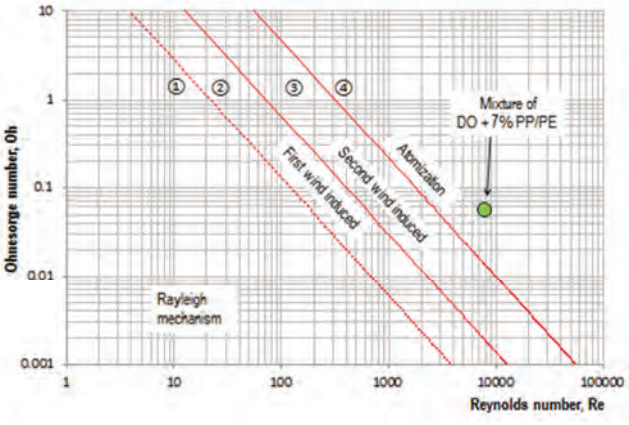

Fig. 5. Graphical presentation of the suitability of the tested fuel in the Ohnesorge diagram

Conclusions

The conducted analysis of knowledge base, analytical studies and laboratory tests entitle to form and present the following conclusions:

– Plastic waste is a serious problem as it has an adverse impact on the environment and ecosystem. However, the concept of a circular economy, where the environment is affected by the products produced through the selection of raw materials at the minimum level as well as by their respective products, provides for a minimization of the number of resources used and the volume of waste. The variety of polymer materials, their properties and areas of application make it necessary to analyze the methodologies and technologies of their processing and the production of synthetic liquid fuels,

– The most standard and low-cost method for synthetic polymer fuels is a technology where the catalytic depolymerization process is applied;

– The initial stage of feeding the fuel to the combustion chamber involving the atomization of fuel is the key one for further processes such as preparation of fuel and air mixture, its ignition and combustion. At that stage, the fuel disintegrates into droplets, the size of which (and the total surface area resulting from it), with specific parameters of fuel condition and geometrical parameters of the atomizer nozzle, depend on the viscosity and surface tension of the liquid. Atomization process may be presented qualitatively by applying the mean diameter (SMD) parameter of the droplet determined by equations containing primarily the physical parameters of the fuel, which are the components of criterion equations,

– The relation of the Oh and Re numbers in the Ohnesorge diagram specifies the jet break-up surface areas where one refers to the atomization. The Oh and Re values, obtained upon having the actual physical parameters of the fuel applied, are presented as a point on the Ohnesorge diagram. The location of the coordinates of this point in the area of atomization indicates the suitability of the fuel.

– The laboratory tests have shown that almost every physical parameter of both the mixture of synthetic fuel and petroleum-based oils and 100% synthetic fuel meet the standards for fuels for self-ignition engines. The exception is the ignition temperature of a mixture of petroleum oils and synthetic fuels, which exceeds the ignition temperature allowed by PN. However, it applies to a mixture with more than 7% synthetic fuel content. The obtained results for ignition temperature corresponding to the 7% synthetic fuel is in line with the permissible content of additives for petroleum-based fuels as per PN-EN590.

– The obtained results of SMD measurement on a laboratory bench using the laser diffraction method have been compared with SMD values calculated according to the formulas known from the literature of the research subject. The result closest to the outcome of the measurement resulted in the analytical determination of SMD by the application of the Elkobt equation, which may be modified by the use of a polynomial equation.

– A methodology to determine the suitability of tested fuel in self-ignition engines has been developed. The methodology includes the determination of physical fuel parameters, engine structural parameters, calculation of Oh and Re criterion values based on the data obtained at the first and second stage of the methodology and introduction of the coordinates of the criterion numbers on the Ohnesorge diagram. The coordinates in the Ohnesorge diagram

illustrate the point where the presence in the area of atomization proves the suitability of the tested fuel for self-ignition engines. The used mixture of petroleum oil and the 7% addition of synthetic fuel meets this condition.

Acknowledgements

This research outcome has been achieved under the research project No 1/S/IESO/2014 financed from a subsidy of the Ministry of Science and Higher Education for statutory activities.

Bibliography

[1] AMBROZIK, A. Wybrane zagadnienia procesów cieplnych w tłokowych silnikach spalinowych, *Wydawnictwo Politechniki Świętokrzyskiej*. Kielce 2003.
[2] BACZEWSKI, K., KAŁDOŃSKI, T. Paliwa do silników o zapłonie samoczynnym. *Wydawnictwa Komunikacji i Łączności*. Warszawa 2008.
[3] BALAWENDER, K., JAKUBOWSKI, M., KUSZEWSKI, H. Parametry fizykochemiczne paliwa syntetycznego przeznaczonego do zasilania silników o ZS. Вісник Націо-нального транспортного університету. 2014, **30**(1).
[4] CHEN, P-C., WANG, W-C., ROBERTS, W.L., FANG, T. Spray and atomization of diesel fuel and its alternatives from a single-hole injector using a common rail fuel injection system. *Fuel*. 2013, **103**.
[5] FANG, Z., MARCHETTI, J.M. Biodiesel: blends, properties, and applications. *Nova Science Publishers* 2011.
[6] GRONOWICZ, J. Ochrona środowiska w transporcie lądowym. *Wydawnictwo i Zakład Poligrafii Instytutu Technologii i Eksploatacji*. Poznań–Radom 2003.
[7] HEYWOOD, J.B. Internal combustion engines fundamentals. *McCraw-Hill Book Co*. New York 1988.
[8] HIROYASU, H., Diesel engine combustion and its modeling, diagnostics and modeling of combustion in reciprocating engines. *COMODIA 85. Proceedings of Symposium.* Tokyo 1985.
[9] Instrukcja obsługi analizatora wielkości cząstek Spraytec, Tłumaczenie AP Instruments, wersja 3.0., 2007.
[10] KLYUS, O., ZAMIATINA, N. Residual fuel atomization proces simulation. *Combustion Engines*. 2017, **169**(2).
[11] KOWALEWICZ, A. Podstawy procesów spalania. *Wydawnictwa Naukowo-Techniczne PWN-WNT*. Warszawa 2000.
[12] KRAUSE, P. Assessment criteria for ignition properties of diesel engine fuels. *Problems of Mechanics*. 2014, **3**(56).
[13] LEFEBVRE, A.H. Atomization and Sprays. *Hemisphere Publishing Corporation* 1989.
[14] LIU, H. Science and Engineering of Droplets – Fundamentals and Applications, Noyes Publications, Park Ridge, New Jersey, U.S., *William Andrew Publishing*. LLC Norwich, New York 2000.
[15] LOTKO, W. Studium zastosowań paliw alternatywnych do silników z zapłonem samoczynnym. *Politechnika Radomska*. Radom 2000.
[16] LUBOWICZ, J. Węglowodory z odpadowych tworzyw sztucznych i biomasy. *Nafta-Gaz*. 2009, **65**, 9.
[17] MACEIRAS, R., Diesel fuel from plastic waste. *Pharmaceutical Analytical Chemistry*. 2016, **2**.
[18] MĄCZKA, T. Technologia plazmowego zgazowania biomasy i odpadów organicznych dla wytwarzania paliw płynnych. *Wydawnictwo Książkowe Instytutu Elektrotechniki*. Warszawa 2014.
[19] ORZECHOWSKI, Z., PRYWER, J. Rozpylanie cieczy w urządzeniach energetycznych. *Wydawnictwa Naukowo-Techniczne*. Warszawa 1994.
[20] SKARBEK-ŻABKIN, A. Analiza przydatności paliw syntetycznych polimerowych do zasilania silników o zapłonie samoczynnym. *Rozprawa doktorska*. Szczecin, 2019.
[21] WAJAND, J.A., WAJAND, J.T. Tłokowe silniki spalinowe, *WNT*. Warszawa 2005.
[22] WIELGOSIŃSKI, G. Przegląd technologii termicznego przekształcania odpadów. *Nowa Energia*. 2011, **1**.
[23] ZABŁOCKI, M. Wtrysk i spalanie paliwa w silnikach wysokoprężnych. *WKiŁ*. Warszawa 1976.
[24] ZWIERZYCKI, W. Paliwa silnikowe i oleje opałowe. *Rafineria Nafty „Glimar"*. 1997.
[25] ВОИНОВ, А.Н. Процессы сгорания в быстроходных поршневых двигателях. *М., Машгиз*, 1980.
[26] КУЛЕШОВ, А.С. Программа расчета и оптимизации двигателей внутреннего сгорания ДИЗЕЛЬ-РК. Описание математических моделей, решение оптимизационных задач. *МГТУим. Н.Э.Баумана*. 2004.
[27] СВИРИДОВ, Ю.Б. Топливо и топливоподача автотракторных дизелей. *Л, Машиностроение*. 1979.
[28] www.handerek-technologies.com 03.2018.

Prof. Oleh Klyus, DSc., DEng., D.h.c. – Faculty of Mechanical Engineering, Maritime University of Szczecin.
e-mail: *olegklus@o2.pl*

Paweł Krause, DEng. – Faculty of Mechanical Engineering, Maritime University of Szczecin.
e-mail: *p.krause@am.szczecin.pl*

Prof. Vladimir A. Markov, DSc., DEng. – Department of Piston Engines, Bauman Moscow State Technical University, Russian Federation.
e-mail: *vladimir.markov58@yandex.ru*

Anna Skarbek-Żabkin, DEng. – Warsaw Motor Transport Institute.
e-mail: *anna.skarbek@its.waw.pl*

Bowen SA, MEng. – Department of Piston Engines. Bauman Moscow State Technical University, Russian Federation.
e-mail: *bowensa@yandex.ru*

Article citation info:
SITNIK, L.J. Emissions of e-mobility. *Combustion Engines*. 2019, **178**(3), 135-139. DOI: 10.19206/CE-2019-323

Lech J. SITNIK

CE-2019-323

Emissions of e-mobility

E-mobility is treated as emission-free. Generally, this sentence can only be true in a very small range. Namely, about selected parameters and in a very limited area. An example of this is the measurement of CO_2 emissions in the immediate vicinity of BEV (battery electric vehicle) . The situation can change dramatically if you take into account the emissions in the energy production necessary for car traffic. This work presents this issue taking into account the energy mix in the various countries of the European Union. Simulation research shows that there are already countries in the EU where the operation of electric vehicles makes sense. Especially when it concerns CO_2 emissions. Emissions below the standards for 2025 can be obtained there. Unfortunately, in most EU countries, the operation of BEV is associated with increased (in relation to present-day) CO_2 emissions. Without changing the energy policy, and in particular the energy mix, introducing e-mobility is problematic.

Key words: *e-mobility, emissions*

1. Introduction

E-mobility is treated as emission-free. Generally, this sentence can only be true in a very small range. Namely, about selected parameters and in a very limited using area. An example of this is the measurement of CO_2 emissions in the immediate vicinity of BEV (battery electric vehicle) . The situation can change dramatically if you take into account the emissions in the energy production necessary for car traffic. This work presents this issue taking into account the energy mix in the various countries of the European Union. In Figure 1 is the energy by sources in EU countries given.

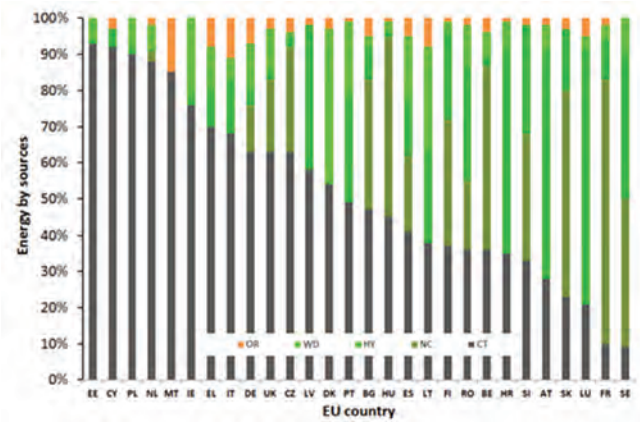

Fig. 1. Energy by sources in some countries in Europe. (CT – conventional thermal, NC – nuclear, HY – hydro, WD – wind, OR- other resources, based on [1])

As can be seen in the European Union there is a strong diversification of sources of electricity. In some countries the dominant role is played by conventional sources, while in others the acquisition of electricity from renewable resources is definitely more important.

But nowhere has such a state of affairs been achieved that all electricity comes from renewable resources.

Today's electricity production covers today's needs. E-mobility is "new" in energy demand. Hence the question arises from which energy sources e-mobility will be powered, and in particular how it will affect emissions.

When discussing emissions, the most common issues are global emissions such as CO_2 emissions. However, from the point of view of people, also important are the emissions of PM – solid particles (e.g. from grated tires or roadways), NO_x – nitrogen oxides, SO_x – sulfur oxides or HC – hydrocarbons.

Generally, emissions are also divided into so-called low emissions (smog) and high emissions.

Such a division may perhaps make sense, but each emission has a negative impact on people and the environment, and unfortunately there is no exception.

The problem of emission assessment is therefore multifaceted. This work is devoted to the global approach to emission issues by assessing CO_2 emissions during the operation of electric vehicles. It goes without saying that with the emission of CO_2, the emission of the above compounds will follow. These emissions are not linearly correlated. This will have to be subjected to a deeper analysis, for which it is also necessary to develop appropriate methods, and this publication is also devoted this issue to .

The issue of emissions from e-mobility can be considered in static terms (thus analyzing what is happening at a given moment) or in dynamic terms, thus as a function of time (for example including the increase in the number of electric vehicles).

In this work the issue was treated statically. But even in this case there are issues that cannot be omitted.

Such issue is, for example, the issue of energy import and export between countries. In one country, more "pure" energy can be produced and this energy is exported to a country that produces "dirty" energy. Then, in the importing country, "more pure" energy is used. Of course, the opposite is also possible. This undoubtedly affects energy LCA in individual countries.

An important factor affecting energy LCA is also the use of electricity, by BEVs, in individual countries. The issue here is a way of assessing the use of electricity during the natural exploitation of vehicles.

These issues are (somewhat) more accurately presented in this publication.

2. Well-to-Wheels methodology

The methodology presented here as chapter 2, 3 and 4 are on basis of [2] The methodology considered in this article is Well-To-Wheel (WTW) detailed in version 4a of the [3]

This approach allows quantifying the amount of energy required for greenhouse gas emissions resulting from the production, transport and distribution of conventional and alternative fuels for road transport (Well-To-Tank, WTT), as well as for quantifying the performance of various drive units (Tank- To-Wheels, TTW).

Compared to the Comprehensive Attribution Life Cycle Assessment (LCA) approach, WTW considers part of the LCA impact category "energy consumption" and "greenhouse gas emissions".

In the WTW approach, emissions related to the construction of equipment, maintenance and decommissioning of fuel and vehicle production plants, including material cycles, are not taken into account. Water pollution requirements or emissions are not taken into account if they do not affect GHG emissions. GHG included is carbon dioxide, methane and dinitrogen monoxide. The WTW methodology can be seen as a simplified LCA, designed to assess only energy consumption and greenhouse gas emissions from the use of road transport fuels.

3. CI – Carbon intensity of electricity

Carbon intensity of electricity can be defined as the GHG emitted for producing or using a certain amount of electricity as shown in equation (1):

$$\text{CI} = \text{GHG emissions/electricity amount} \tag{1}$$

Since GHG emissions are expressed in grams [g] of CO_2 equivalent and the electricity (e.g. produced or using) is expressed in [kWh] the consequent carbon intensity (CI) is usually expressed in [gCO_2eq/kWh].

In this paper it will be report the carbon intensities for all the following stages of the electricity pathway: gross production, net production, electricity traded, supply post-trade, consumed at high voltage after transmission, consumed at medium voltage after distribution and consumed (by the most of users) at low voltage.

The JEC WTW analysis considers GHG emissions occurring in two main steps, that is: combustion emissions occurring when fuels are burnt and upstream emissions.

The upstream emissions are caused by the extraction, refining and transport of the fuels to the power plants. For other fuels and renewables such as peat, municipal and industrial wastes, hydropower, geothermal, solar, wind and tidal power the upstream emission factors were considered equal to zero.

For nuclear power plants the approach in use by main international statistical bodies (IEA, EUROSTAT, IAEA) has been adopted. Converting the electric energy produced from nuclear or renewables into an equivalent primary energy have a average thermal efficiency (e.g. IAEA, 2007) equal 33%.

4. Electricity trade and carbon intensity

The carbon intensity of the electricity consumed in a country depends also on the CI and amount of electricity traded with other countries. Logically, electricity imported in a country embeds also the GHG necessary for its production, so a WTW (or LCA) calculation aiming at realistically representing the carbon intensity of electricity consumed, should also consider the trade aspect, especially for countries having high electricity imports.

The electricity supplied (ElS) to a national network, considering the trade, is defined by the IEA with the equation (2):

$$\text{ElS} = \text{El}_{\text{net production}} - \text{El}_{\text{Pumping}} + \text{EL}_{\text{Imports}} - \text{El}_{\text{Exports}} \tag{2}$$

For all these terms presented in equation (2) it can be used the IEA statistical data.

In order to calculate the CI of the electricity supplied (post trade) in a country it is possible to use equation (1), considering in the denominator the result of equation (2), and in the numerator the value of total GHG emissions embedded in the electricity supplied, calculated according to equation (3):

$$\text{GHG}_{\text{Total}} = \text{GHG}_{\text{Combustion}} + \text{GHG}_{\text{Upstream}} - \text{GHG}_{\text{Exported}} + \text{GHG}_{\text{Imported}} \tag{3}$$

Combustion and upstream GHG emissions are the same values used to calculate the CI of electricity produced in each country, the exported GHG is simply the product between the CI of electricity traded multiplied by the Upstream and combustion emissions

Imported GHG emissions can be treated as

$$\text{GHG}_{\text{Import}} = \text{S}(\text{GHG}_{\text{Imoirt from i-th Country}} \text{ x } \text{CI}_{\text{Elproduction in i-th Counttry}}) \tag{4}$$

where for each country it is necessary to consider the sum-product of all the amount of electricity traded (El. Import from Country “i”) and the respective Carbon Intensities (CI El traded Country “i”).

Table 1 shows the results of calculations for the different values of carbon intensity, calculated for each EU country (for the year 2013).

Table 1 Carbon intensity (CI) in EU countries in several steps of production trading and supplied

Country	CI of gross electricity Production (combustion only [g/kWh]	CI of gross electricity production (with upstream) [g/kWh]	CI of net electricity production with upstream emissions) [g/kWh]	CI of electricity traded (with upstream) [g/kWh]	CI of electricity supplied (with upstream) [g/kWh]	Variation of CI after trade [%]	CI of electricity consumed at HV (with upstream) [g/kWh]	CI of electricity consumed at MV (with upstream) [g/kWh]	CI of electricity consumed at LV (combustion only) [g/kWh]	CI of electricity consumed at LV (with upstream) [g/kWh]
Austria	133	151	156	170	315	0.85	322	325	305	334
Belgium	188	224	233	239	257	0.08	261	262	224	267
Bulgaria	507	532	585	601	589	-0.02	618	628	636	669
Croatia	231	273	282	285	465	0.63	487	494	463	524
Cyprus	646	737	773	773	773	0.00	787	792	710	810
Czech Republic	518	545	587	596	640	0.07	657	663	643	685
Denmark	316	368	386	386	356	-0.08	364	367	328	377
Estonia	1020	1022	1152	1152	840	-0.27	878	891	931	944
Finland	171	200	209	209	204	-0.02	207	207	181	211
France	66	88	92	93	97	0.04	100	101	80	105
Germany	485	534	567	574	588	0.02	599	602	558	615
Greece	655	695	753	757	712	-0.06	732	739	723	767
Hungary	310	340	368	368	369	0.00	383	388	365	407
Ireland	459	533	555	568	570	0.00	588	594	530	617
Italy	358	427	444	448	402	-0.10	413	417	362	431
Latvia	134	173	185	185	1075	4.82	1110	1122	1140	1168
Lithuania	204	246	262	315	358	0.14	370	374	331	390
Luxembourg	236	283	283	585	505	-0.14	508	509	467	513
Malta	731	831	868	868	910	0.05	954	970	908	1032
Netherlands	479	559	582	582	547	-0.06	555	558	494	569
Poland	770	847	929	934	911	-0.03	937	946	890	980
Portugal	295	346	355	365	357	-0.02	372	378	340	400
Romania	356	379	413	416	425	0.02	449	457	460	492
Slovakia	173	199	211	215	407	0.90	412	414	388	420
Slovenia	315	329	351	361	302	-0.16	309	312	291	321
Spain	248	295	305	312	309	-0.01	321	325	287	341
Sweden	16	24	25	25	44	0.74	45	46	36	47
United Kingdom	469	555	584	591	576	-0.03	593	599	526	623
EU 28 average	340	387	407	413	417	0.01	428	432	393	447

The order of the countries listed in Table 1 is the same as shown in Fig. 1. Countries were presented according to the decreasing share of non-renewable sources in the generation of electricity.

Interesting are the results presented in Fig. 2. The results from Table 1 have been added to the results presented

in Fig. 1. The percentage of electricity from combustion processes (in individual EU countries) are compared as well with the CO_2 mass emissions (per kilowatt-hour) by electricity production and its use (together with import) in every country.

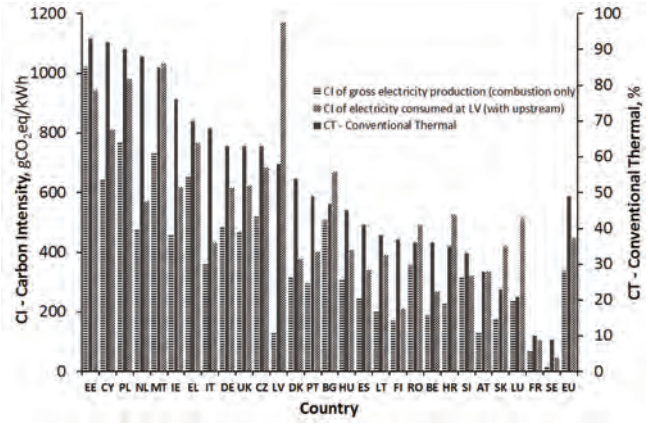

Fig. 2. Carbon intensity by production and use of electricity in EU countries

The data primarily indicate that centralized electricity generation and distribution systems cause large losses in energy transmission – which means a significant increase in specific CO_2 emissions (in g_{eq}/kWh).

Electricity imports (especially if this energy is produced in the exporter's country from non-renewable resources), can lead to a significant increase in CO_2 emissions "in the country that imports" electricity.

5. Electricity use by BEV's operation

For the correct emission assessment related to the production and use of energy in e-mobility, it is necessary to know the electricity demand of electric vehicles (BEVs)

Based on the assumption that the emission related to the supply of electricity to the vehicle's charging point is known (Table 1), it is necessary to assess how much of this energy must be used to drive at a particular section of road.

The necessary data can be obtained from the appropriate tests (in the EU previously NEDC test and currently WLTP [4]) but it is known that the test results do not coincide with the data from natural exploitation [11]

Therefore, it is crucial to assess the operational energy "consumption" in the natural exploitation of vehicles (energy cannot be consumed – possible is the change of its form only – but as parallel to the historical term "fuel consumption" in following will be the term "energy consumption" used).

It seems that for assessing the energy consumption in natural exploitation of BEVs in particular is the theory of cumulative energy consumption useful.

The theory of cumulative energy consumption was originally developed (as author work) to assess the cumulative consumption of fuel in the natural exploitation of ICE vehicles [5].

The usefulness of the theory has been repeatedly confirmed, also when powering the engines with various fuels [6–9]. The main applications of the theory have been found in assessing the fuel consumption of urban bus fleets. Special software has been created for proper data collection (for obvious reasons, it will not be described here).

The energy consumption of a car in its natural exploitation is a random process. Energy is consumed in the "quantum" model. Energy quanta have a random size. Also, the time between the quantum of energy consumed is random.

Total amount of quanta of energy supplied to the car engine in the its operating period is called as cumulative energy consumption.

Energy quantum summation leads to determining the cumulative energy consumption. Energy consumption caused by the time *t* of the engine work. can be designated as

$$\mathrm{CFC_c}(t_d) = \sum_{i=1}^{n(t_d)} q_i = n(t_d) \cdot \bar{q}(t_d) \tag{5}$$

where: $\mathrm{CFC_c}(t_d)$ – the cumulative energy consumption to the mileage t_d, t_d – mileage
q_i – i-th quantum of energy, $\bar{q}(t_d)$ – the average size of the quantum of energy used to the mileage t_d, $n(t_d)$ – number of the energy quantum used to the mileage t_d.

To know the cumulative energy consumption to the mileage t_d should be familiar with the average size of the quants and the number of quantum of consumed energy to that mileage.

The way to reach these values has been presented in [5].

These publications also provide a way to obtain a mathematical model describing the cumulative energy consumption as a function of the vehicle's mileage.

The model has a form

$$\mathrm{CFC_c}(t_d) = \sum_{i=1}^{n(t_d)} q_i = n(t_d) \cdot \bar{q}(t_d) = c t_d^{(a+1)} \tag{6}$$

The intensity of energy consumption is a mathematical derivative from equation (6), so it has a form

$$\mathrm{CFC'c} = \mathrm{ICFCc}(t_d) = \frac{\mathrm{dCFC_c}}{dt} = c(a+1)t_d^a \tag{7}$$

where: $\mathrm{ICFCc}(t_d)$ – the intensity of cumulative energy consumption to the mileage t_d, c, a – coefficients.

Constants "c" and "a" equations (6) can be derived from data obtained from the use of vehicles in natural operation. Such data are collected by various institutions and individuals. One of a good database is from the website spritmonitor.de [11]. The advantage of this database is not only the large amount of data collected there. but also their widespread (and easy) availability. Data from this database will be used in further consideration.

Figure 3 presents operation data of the SMART Fortwo car No 641784. To determine the coefficients "c" and "a", data from the operation are necessary and sufficient.
After calculations, the following results are obtained

$$c = 0.131752,\ a = 0.004568 \tag{8}$$

and accordingly

$$\mathrm{CFC_c}(t_d) = c t_d^{(a+1)} = 0.131752 t_d^{1.004568} \tag{9}$$

and

$$\mathrm{ICFCc} = c(a+1)t_d^a = 0.132354 t_d^{0.004568} \tag{10}$$

Six decimal places of coefficient values look a bit shocking. They were, however, deliberately entered. The author's experience shows that the more accurately the value of coefficients is given, the mathematical model is more adequate. On the other hand, in today's computing calculations, the accuracy of calculations results from the use of values with a much larger number of decimal places. These values are stored in the computer's memory and it does not matter how they are displayed on the screen.

Similarly, the results of the analysis but in the case of a TESLA S car (No. 829324) lead to data

$$c = 0.193178 \text{ and } a = 0.004073 \qquad (11)$$

The models adequacy assessment (6) was carried out using the analysis of variance. The results are as follows (Table 2).

Table 2. Results of the analysis of variance to determine the adequacy of the model (6).

	SMART Fortwo	TESLA S
Multiple R	0.999620	0.999943
Rsquare	0.999241	0.999885
Matched Rsquare	0.999221	0.999883
Standard error	0.024617	0.000314
Observations	40	104

The observations number is in this case the same as the charging number.

The results are amazingly good. It was not expected that the correlation coefficients will be so high (it is worth recalling here that the maximum theoretical value of, for example, the R square (R^2) coefficient is $R^2 = 1$.

It is hardly surprising that the correlation coefficient has such a high value since the "measuring" points lie almost perfectly on the curve of the model.

A graphic illustration of the results obtained is shown in Figures 4 and 5. In this form presented results can be treated as a kind of energy footprint of the defined vehicle.

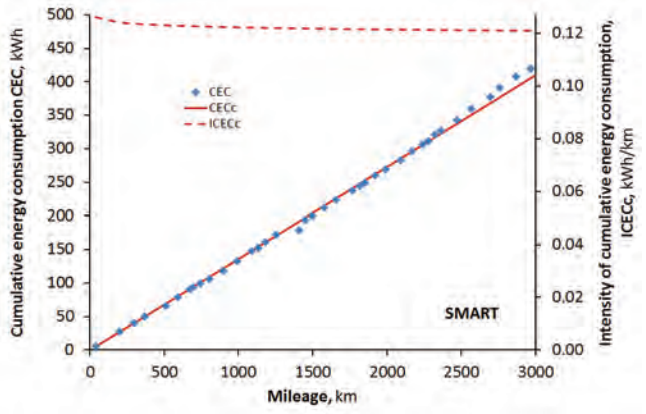

Fig. 3. Energy footprint of SMART Fortwo car No. 641784

Both curves (CFCc and ICFCc) give the impression that they are straight lines. However, when analyzing values of coefficients, it must be clearly stated that they are curves, and only in some cases (as presented here) quasi straight-lines.

Both drawings show that the average intensity of cumulated electricity consumption can be reported relative to one kilometer of the car's mileage.

The intensity of cumulative energy consumption for both car are in Table 3 given.

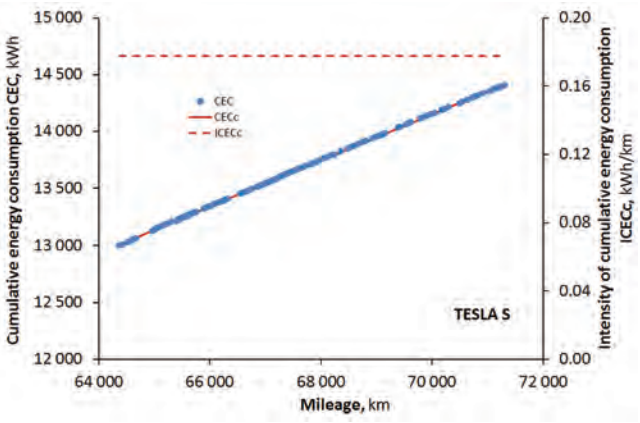

Fig. 4. Energy footprint of TESLA S car No. 829324

Table 3. Intensity of cumulative energy consumption data for analyzed car

Car	Car No.	ICEC [kWh/km]
SMART Fortwo	641784	0.1420
TESLA S	829324	0.2019

If the data on the ICECc for more cars are known, then can be achieve the values for a given type of car. The relevant data are shown in Table 4.

Table 4 Intensity of cumulative energy consumption statistical parameters for analyzed cars types

Statistical parameters	SMART Fortwo	TESLA S
Average	**0.1647**	**0.2083**
Standard error	0.0039	0.0039
Median	0.1624	0.2093
Dominant	0.1554	0.2111
Standard deviation	0.0233	0.0315
The variance of the sample	0.0005	0.0010
Kurtosis	0.7362	3.1771
Slant	0.8955	0.4176
Range	0.1023	0.2177
Minimum	0.1250	0.1109
Maximum	0.2273	0.3286
Sum	5.9294	13.5366
Counter	36	65
Confidence level for the average (95.0%)	0.0079	0.0078

Table 4 shows that 36 SMART Fortwo cars and 65 TESLA S cars were analyzed. Obviously, average cumulative energy intensity values are different than those for only two cars. It is interesting that the confidence interval for the average is relatively wide but almost the same for both types of cars. However, the standard deviations for both types of vehicles differ significantly.

The analysis of kurtosis and skewness indicates that the potential statistical distributions for describing both sets of data will differ significantly. It is likely to use the normal distribution for describing the SMART Fortwo data, but the TESLA S car data will have to be described in a different statistical distribution.

With the data from Tables 1 and 4 is possible to achieve of CO_2 emission in each country of EU. The calculations results are here in the Fig. 5 given.

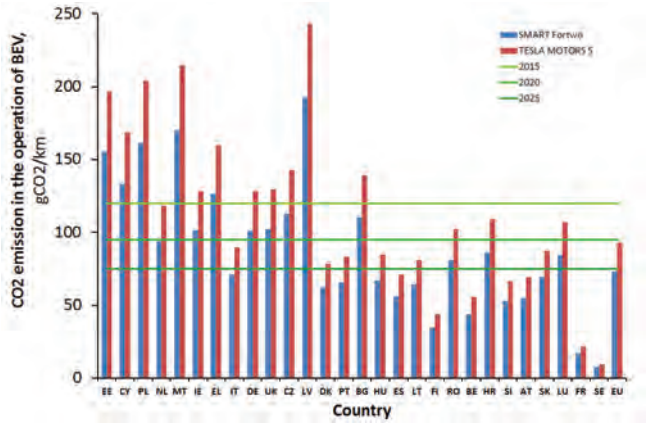

Fig. 5. CO_2 emission in the operation of BEV's in countries of EU and also average for EU

For the comparison in Figure 5 are the maximum emission of CO_2 for car fleets in EU for next year's showing. These values are correct for NEDC but for the WLTP test they are only slightly lower.

The results of the calculations proved to be in line with expectations. On average, in the European Union it is already worthwhile to use electro vehicles (BEV's) because CO_2 emissions are within the limits of the adopted standards for 2020. The use of small BEV's already allows to meet the standards for 2025 today.

If the average is good it means that in some states of the union is better (much) than in others where in terms of emissions there is still a lot to do.

Figure 5 shows that in some countries, in order to get closer to the standards for 2020, it would be necessary to reduce CO_2 emissions by at least a half. This means that although any action is aimed at reducing energy consumption of vehicles have a sense, then the main burden of change should concern the change in energy production and distribution.

6. Conclusions

This paper presents two important methods for assessing the emission of electric vehicles

– an emission assessment method for generating and supplying electricity to battery charging points,
– a method of assessing energy consumption in the natural use of vehicles.

Both methods are shown in a static application – although there are no contraindications to use them together in dynamic applications, including emission forecasting.

The method of using both methods is presented on the example of CO_2 emission assessment resulting from the operation of battery electric vehicles.

Simulation research shows that there are already countries in the EU where the operation of electric vehicles makes sense. Especially when it concerns CO_2 emissions. Emissions below the standards for 2025 can be obtained there. Unfortunately, in many EU countries, the operation of BEV is associated with increased (in relation to present-day) CO_2 emissions.

Because the high emission, in the first place, corresponds to the use of energy coming from non-renewable resources, together with excessive CO_2 emissions probably occur excessive emissions of nitrogen and sulfur oxides and a number of others, as well as heavy and radioactive metals. Even if the plants are equipped with appropriate exhaust gas treatment systems, there are no systems operating with 100% efficiency - therefore emissions cannot be avoided.

Without changing the energy policy, and in particular the energy mix, introducing e-mobility is problematic.

The methods to the assessment of the political solutions are available and are here now presented.

.

Bibliography

[1] 2018. Eurostat data base http://ec.europa.eu/eurostat/data/database

[2] MORO, A., LONZA, L. Electricity carbon intensity in European Member States: Impacts on GHG emissions of electric vehicles, European Commission, Joint Research Centre (JRC), Via Enrico Fermi 2749, 21027 Ispra (VA), Italy. https://www.sciencedirect.com/science/article/pii/S1361920916307933

[3] JEC WTW report (JEC, 2014a, b) https://ec.europa.eu/jrc/en/jec

[4] WLTP for electric cars – what does the new test procedure mean? https://www.mobilityhouse.com/int_en/magazine/e-mobility/wltp-for-electric-car-new-test-procedure.html

[5] SITNIK, L. Skumulowane zużycie paliwa. *Archiwum Motoryzacji*. 2004, **7**(3), 227-254.

[6] SITNIK, L. Skumulowane zużycie LPG zasilającego silniki samochodów. *Journal of KONES*. 2009, **16**(4), 429-434.

[7] SITNIK, L. Teoria skumulowanego zużycia paliwa i jej aplikacja. *Transport Przemysłowy i Maszyny Robocze*. 2014, **2**, 116-121.

[8] SITNIK, L. Theory of cumulative fuel consumption and example for its application. *Trans & MOTAUTO' 14: XXII international scientific-technical conference: proceedings*. Varna, 23-24.06.2014.

[9] SITNIK, L. Theory of cumulative fuel consumption by LPG powered cars. *Journal of KONES*. 2015, 22(4), 275-280.

[10] Spritmonitor.de https://www.spritmonitor.de/de/detailansicht/628759.html

[11] TIETGE, U., DÍAZ, S., MOCK, P. et al. From laboratory to road. A 2016 update of official and 'real-world' fuel consumption and CO_2 values for passenger cars in Europe. WHITE PAPER November 2016, www.theicct.org

Prof. Lech J. Sitnik, DSc., DEng. – Faculty of Mechanical Engineering, Wroclaw University of Science and Technology.
e-mail: *lech.sitnik@pwr.edu.pl*

Article citation info:
BRZEZANSKI, M., RODAK, L. Investigation of a new concept of hydrogen supply for a spark ignition engine. *Combustion Engines*. 2019, **178**(3), 140-143. DOI: 10.19206/CE-2019-324

Marek BRZEŻAŃSKI
Łukasz RODAK

CE-2019-324

Investigation of a new concept of hydrogen supply for a spark-ignition engine

The article presents the results of conceptual and research works of an internal combustion engine adapted for hydrogen supply. The engine was equipped with a direct injection of hydrogen into the combustion chamber, allowing the control of the heat release rate. The developed concept of the power supply system and the fuel injection strategy were presented. Initial results of bench tests were also presented.

Key words: *hydrogen, combustion engine, direct injection*

1. Introduction

The rationalization of energy use requires searching for new carriers that in the future may be widely available, and their use will not cause environmental changes. Hydrogen is predicted to be hydrogen in the near future. The most rational use of this fuel in the application to vehicle engines is considered as fuel cells in which the efficiency of energy conversion exceeds 50%. Currently however, there are serious technological limitations, as well as economic conditions that require solutions before the widespread implementation of this type of power units for transport. However, it is possible to use hydrogen as a fuel for piston combustion engines, which has a valid practical justification. On the one hand, the existing potential of the piston engine industry and the service facilities of this type of drive units will be used, and on the other hand, it will be a period in which users will be prepared to use a new type of energy carrier. For this reason, research centers for hydrogen supply systems for piston combustion engines are being carried out in many research centers, and in some cases advanced operational tests of such types of drive sources are being carried out. In connection with the above, the undertaking of scientific research and development works on the development of hydrogen supply systems is justified in every case.

2. Hydrogen fuel systems for internal combustion engines

In currently used hydrogen fuel systems for internal combustion engines, hydrogen is supplied in a gaseous form by dosing to the inlet channel or directly to the cylinder. The method of creating a hydrogen-air mixture in the inlet channel of the engine is currently the most common method of feeding piston engines. It should be noted that this method of hydrogen supply is also used when application of hydrogen as an additional fuel in spark and compression ignition engines takes place. With this method, an increase in the repeatability of ignition can be achieved for the low load range of spark ignition engines. In the case of supplying hydrogen to the inlet channel, this is accomplished via a mixer or a metering valve that is mechanically or electrically controlled. This way of feeding the motor causes a low density of energy supplied to the cylinder. This is due to the high volume fraction of hydrogen in the mixture, relative to the mixture formed with liquid fuels. The stoichiometric constant for hydrogen is 2.38 [Nm^3/Nm^3], from which it follows that in the stoichiometric mixture the volume of hydrogen is about 30% of the volume of the total charge delivered to the cylinder. This results in a significant reduction in the unit power of the hydrogen-powered engine compared to the supply of hydrocarbon fuels. In addition, when the engine is powered with a stoichiometric hydrogen-air mixture there is a high risk of self-ignition of the mixture in the inlet channel. Such a situation may for example, occur in the case of uncontrolled backflow of the flame from the combustion chamber during the co-opening of inlet and outlet valves. The mixture formed in the inlet channel heats up from the valves and from the cylinder walls during the filling process, then is compressed and is subject to a strong swirl. These phenomena lead to increased internal and kinetic energy of the hydrogen-air mixture, which promotes uncontrolled self-ignition. Then, the pre-ignition reactions intensity growing with the load, increase the risk of self-ignition or anomalies in the combustion process.

The hydrogen direct delivery systems into the combustion chamber just after the filling process are also known. This method of feeding motors with hydrogen shows an analogy to the direct injection of liquid hydrocarbon fuels. This is accomplished by a mechanically or electrically controlled valve. Hydrogen is supplied to the injectors at a pressure of (5–10) MPa. Such a high fuel pressure before the injector results from the necessity of delivering the right dose of hydrogen in a short time, and also because the hydrogen injection takes place at variable pressure in the engine working space. The direct injection of hydrogen into the cylinder also increases the weight of the load in the working space, which results in a significant increase in the unit power of the engine. In addition, such a method of hydrogen delivering to the cylinder effectively eliminates the problems of hydrogen self-ignition in the intake channels and reduces the problems of the combustion anomalies. The problem, however, is the course of the hydrogen-air mixture combustion process in the working space of the reciprocating internal combustion engine, because in the case of engine feeding with a stoichiometric hydrogen-air mixture, the self-ignition phenomenon may occur before the flame is initiated from the electric discharge. The problem is also the high value of the pressure increase $dP/d\alpha$, especially for a hydrogen-air mixture with a stoichiometric composition.

3. The concept of a hydrogen combustion system in internal combustion engine

At Cracow University of Technology a power system was developed, in which the main hydrogen dose is delivered directly to the engine's working space during the combustion process. This new hydrogen and air mixture creation and combustion system may be a reason to avoid problems associated with the self-ignition of the combustion mixture or anomalies. Using the wide range of flammability of the hydrogen-air mixture it will be possible to both qualitative and quantitative control of the engine power. The concept shows that in the initial phase of the process, during the filling process, a lean mixture will be created with a composition that allows it to be ignited from the electric discharge on the spark plug. The composition of the mixture should be selected so that the engine can work in the entire speed range without load, overcoming only internal resistance. The role of this first part of the fuel dose is only the initiation of the combustion process, while the remaining main part of the dose is being delivered along the process. Due to the high combustion rate of the hydrogen-air mixture, the supply of hydrogen already during the combustion process must be such that the $dP/d\alpha$ value must not exceed about (0.3–0.7) MPa/°C.A. It should be noted that the assumed pressure increase of 0.3 MPa/°C.A. is usually the maximum value found in spark ignition engines, while the value 0.7 MPa/°C.A. corresponds to the pressure increase for the normal combustion process in self-ignition engines.

The proposed concept of hydrogen injection during the combustion process may allow the use of both qualitative and quantitative power control. The choice of regulation will depend on the pressure rise values obtained for a given engine load value, taking into account the criterion of the highest overall efficiency of the engine.

4. Research object and test bench

The object of experimental tests was a single-cylinder, self-ignition engine Kipor 186F, whose technical data is presented in Table 1.

Table 1. Technical data of a test engine adapted for hydrogen supply

Model		Kipor 186F
Item	Unit	
Type of engine		Single-cylinder, vertical 4-stroke air-cooled diesel
Cooling system		Forced air cooling by flywheel fan
Combustion system		Direct injection system
Bore x Stroke	mm	86 × 70
Displacement	dm^3	0.406
Compression ratio	–	19.3
Power output	kW	Continuous 6.6 , Maximum 7.4
Speed	rpm	3600

The engine has been adapted for spark ignition and hydrogen supply, directly to the combustion chamber. For this purpose, an additional hole for screwing in the spark plug was made in the cylinder head and a hole for screwing in the pressure sensor. Design changes of the cylinder head are shown in Fig. 1.

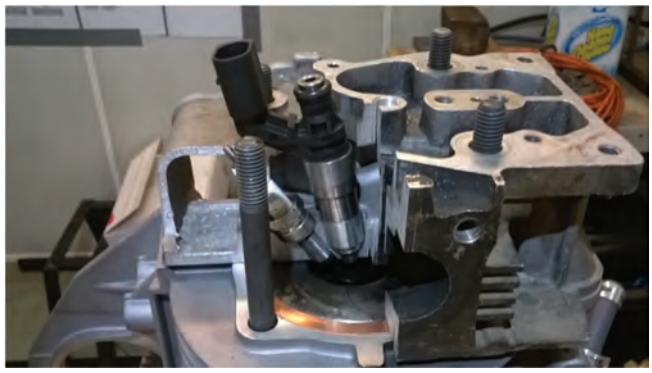

Fig. 1. The scope of structural changes of the engine head adapted for spark ignition and direct hydrogen injection

In the engine being the subject of tests, the combustion chamber, typical for the compression ignition engine, is located in the piston. It has been changed and enlarged, thanks to which the shape similar to so-called Heron chamber has been obtain and the compression ratio decreased from 19.3 to 15.1. These changes were necessary due to the need to ensure a strong turbulence of the load and due to the protection of the combustion system against anomalies. The design changes of the combustion chamber in the piston are shown in Fig. 2.

Fig. 2. Piston with a standard (left) and enlarged combustion chamber (right)

The engine has been equipped with throttle, wideband lambda sensor, sensors measuring the intake air and exhaust gas temperatures. Exhaust gas sampling probes for analysis are placed in the exhaust system. The stand has been equipped with a hydrogen consumption measurement system, ignition timing adjustment system and hydrogen injection time control system, as well as a system that allows changing the angle of hydrogen dosage. The computer program written in the LabView environment was responsible for managing changes in the engine's regulation parameters as well as for acquiring measurement data.

The engine was placed on a test bench equipped with an eddy current brake from firm Schenk type W70. Figure 3 presents the tested engine, equipped with control and measurement equipment, placed on the test bench.

The computer control program, developed in the LabView environment, allowed not only for the archiving of measured physical quantities, but also for their current preview. This was very beneficial, especially during the initial measurements, when the range of variation of individual parameters was determined and disturbances were identified. Figure 4 shows the window of the program con-

trolling the cylinder's indication of the engine being tested. This type of preview allowed for the current identification of combustion anomalies.

Fig. 3. Investigated engine on the test bench

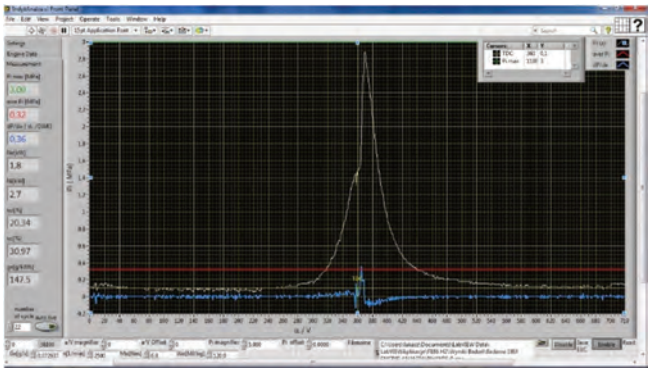

Fig. 4. Window of the current preview of cylinder indication

The remaining measured parameters were presented in the form of a digital record in determined ranges of values, where the exceeding of a given range was signaled by a change in color. Figure 5 shows the window of the preview of measured parameters.

Fig. 5. Windows of the control program controlling the parameters of the eddy current engine break and the tested engine

5. Research methodology

Hydrogen-powered engine tests were carried out at a constant rotational speed of n = 2500 rpm. For reference purposes, preliminary tests were carried out with indirect hydrogen injection into the intake duct during the filling process. The basic research was carried out while supplying the engine with direct injection into the working space of the cylinder during the process of compression and subsequent combustion. The essence of the research was to create regulatory characteristics of the hydrogen-air mixture composition for different engine load values. The change of the load of the motor was made by changing the degree of throttle opening, while the composition of the mixture was regulated by the change of the injector opening time, with constant hydrogen supply pressure. In the reference tests, when the engine was fed to the inlet channel, the angle of the injection beginning was constant. In the basic tests during direct injection feeding, the value of the injection advance angle was individually selected based on the criterion of the highest value of torque, taking into account the knock combustion limit. A similar criterion was adopted when selecting the ignition advance angle value at each engine work point. The hydrogen injection started during the compression process, while the main part of the hydrogen injection was injected after the spark ignition during the combustion process.

6. Investigation results

The results of the initial reference tests of investigated engine equipped with the hydrogen injection system for the intake duct, prepared for three selected throttle opening degrees of 12.5%, 25% and 50% respectively, are shown in Fig. 6. When working with a small load, the engine could work properly, without knocking effects, while feeding a mixture with a composition of λ = 1.4. There was then a reduced efficiency of the engine, due to the fuel bit and the increased share of mechanical losses in relation to the value of the torque developed. During operation with 50% load, the correct engine operation was possible while feeding the mixture with the composition of λ = 1.85, at which point the lowest value of unit fuel consumption was obtained.

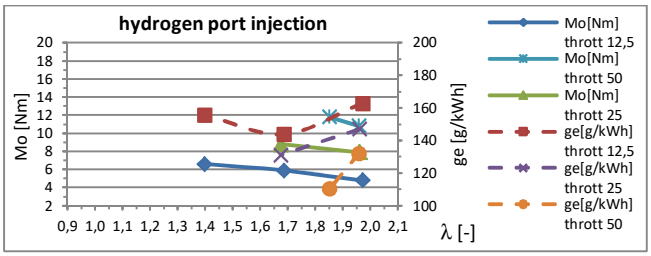

Fig. 6. Regulation characteristics of the mixture composition for selected engine loads (hydrogen injection into the intake pipe)

The use of direct hydrogen injection into the cylinder resulted in a significant extension of the scope of correct engine operation, without occurrence of knock combustion in the richer mixture. For the three selected load states, it was possible to operate the engine properly without knocking effects when feeding with the hydrogen-air mixture close to the stoichiometric composition. This resulted in a significant increase in torque. Direct injection of hydrogen into the cylinder which also lasts after the occurrence of spark discharge, significantly reduces the duration of pre-flame phenomena, when there is a strong charge ionization and thermal dissociation of hydrogen molecules.

Therefore, the influence of load to any combustion anomalies is less visible and the process of heat release occurs more slowly than during the combustion of homogeneous charge prepared in the filling process.

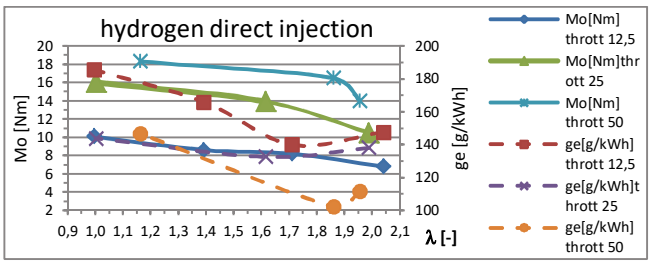

Fig. 7. Regulation characteristics of the mixture composition for selected engine loads (direct injection of hydrogen into the cylinder)

Positive effects of using direct hydrogen injection into the cylinder are confirmed by indicator diagrams. Due to the high rate of hydrogen combustion, both during injection into the intake duct and during direct injection, ignition of the mixture occurred near the TDC position of the piston, which was the most advantageous from the point of view of engine operating parameters. Fig. 8 presents the results of cylinder pressure measurements for different hydrogen supply methods prepared for a throttle opening of 12.5% and a constant value of the air excess number of $\lambda = 1.4$.

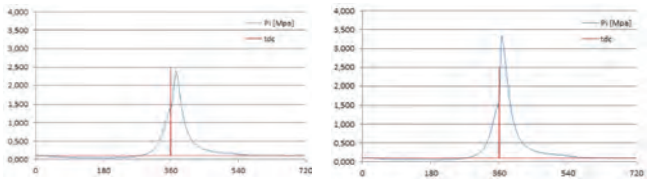

Fig.8. Indicated engine pressure graph with hydrogen injection to the inlet pipe (left) and direct injection (right) (throttle opening 12.5%, air excess number $\lambda = 1.4$)

When the engine was fuelled by direct injection, the maximum combustion pressure of the mixture was clearly higher (about 3.5 MPa) as well as the higher rate of pressure increase (up to 0.4 MPa/°C.A.). During hydrogen injection to the inlet channel, where the maximum pressure value was approx. 2.5 MPa and the rate of pressure increase was less than 0.15 MPa/°C.A. In both cases, the criterion of absence of knocking effects was retained. A similar relationship was obtained during measurements for throttle opening of 25% (Fig. 9). In this case, when the engine was supplied with direct hydrogen injection, the maximum cylinder pressure of almost 4 MPa was obtained, and the pressure rise rate was 0.45 MPa/°C.A. Hydrogen injection into the intake duct allowed for a maximum pressure of approx. 3 MPa, and the rate of pressure increase was approx. 0.16 MPa/°C.A.

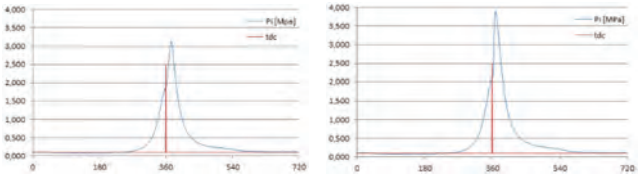

Fig.9. Indicated engine pressure graph with hydrogen injection to the inlet channel (left) and direct injection (right) (throttle opening 25%, air excess number $\lambda = 1.6$)

6. Conclusions

The use of direct hydrogen injection, in relation to the injection of hydrogen into the inlet channel, significantly widens the range of correct engine operation, without knocking occurrence. Adoption of an appropriate direct injection strategy allows the combustion of a load with a smaller value of the excess air coefficient, approaching the stoichiometric composition. As a result, a higher value of the maximum cylinder pressure and significantly better operating parameters of the engine are achieved. The significantly higher cylinder pressure increments occurring at the same time do not lead to knocking effects. The applied strategy of direct injection of hydrogen into the piston engine cylinder during the compression process and the combustion process allows the use of hydrogen as a full-value fuel, which can replace standard hydrocarbon fuels.

Bibliography

[1] BRZEŻAŃSKI, M., CISEK, J., MAREK, W., PAPUGA, T. Investigation of the combustion engine fuelled with hydrogen. *V Congress on Combustion Engines*. PTNSS-2013-SC-192, Bielsko-Biała 2013.

[2] BRZEŻAŃSKI, M., CISEK, J., MAREK, W. et al. Investigation of the combustion engine fueled with hydrogen and mixed n-butanol with iso-butanol. *V Congress on Combustion Engines*. PTNSS-2013-SC-194, Bielsko-Biała 2013.

[3] BRZEŻAŃSKI, M., MARECZEK, M., MAREK, W., PAPUGA, T. Determination of operating parameters of industrial engine fuelled with post processing gases with high hydrogen content. *IOP Conference Series: Scientific Conference on Automotive Vehicles and Combustion Engines*. 2016.

[4] BRZEŻAŃSKI, M., PAPUGA, T., RODAK, Ł. Analysis of creation and combustion process of hydrogen-air mixtures by optical method in isochoric chamber. *Combustion Engines*. 2017, **170**(3).

Marek Brzezanski, DSc., DEng. – Faculty of Mechanical Engineering, Cracow University of Technology.

e-mail: *mbrzez@pk.edu.pl*

Łukasz Rodak, MEng. – Faculty of Mechanical Engineering, Cracow University of Technology

e-mail*: lrodak@pk.edu.pl*

Article citation info:
GIS, W., MERKISZ, J. The development status of electric (BEV) and hydrogen (FCEV) passenger cars park in the world and new research possibilities of these cars in real traffic conditions. *Combustion Engines*. 2019, **178**(3), 144-149. DOI: 10.19206/CE-2019-325

Wojciech GIS
Jerzy MERKISZ

CE-2019-325

The development status of electric (BEV) and hydrogen (FCEV) passenger cars park in the world and new research possibilities of these cars in real traffic conditions

Major markets across the European Union (EU) are concentrated on rapid development of electromobility. This policy is demonstrated – among others – by recent sales of electric cars: within the past 3 quarters of 2018 – 24.7 thousand electric cars have been registered in Germany, 20.3 thousand in France, 15.3 thousand in the Netherlands and 31.4 thousand in Norway. Unfortunately, only 867 EVs have been registered in Hungary, 469 in the Czech Republic, 468 in Romania, 411 in Poland and 348 in Slovenia.

Unit energy consumption of electric cars was often defined in NEDC cycle. In real conditions of road traffic, it may differ from values recorded in a drive cycle. The article presents results of a study on energy consumption of electric cars in Poland along RDE (Real Driving Emissions) testing route in terms of vehicle energy consumption per drive unit (km, 100 km). The use of fuel cells in cars may bring a change in the type of used vehicles in the long run. Both globally and in the EU wide-ranging actions are undertaken to implement fuel cell technology. Also, the infrastructure of hydrogen filling stations is developed. At present the most rapidly developing country in this area is Japan. The article addresses the issue of energy consumption per drive unit by cars equipped with fuel cells as both type of vehicles, i.e. EV and FCV use electric motors. The article also discusses infrastructure development in the EU and Poland, charging and fuelling of the said vehicles, respectively.

Key words: *energy, electric cars, RDE, consumption, fuel cell*

1. Introduction

Since September 1st of this year certification of new type (Euro 6) passenger cars and light trucks in the EU includes the exhaust emissions testing of these vehicles, i.e. the Real Driving Emissions (RDE) procedure [1–7, 18, 19].

Road test specifications cannot be optional. The route must include a drive-in urban area, rural and on a highway. Duration of the trip must be between 90 and 120 minutes. Setting the route for an RDE drive for the purpose of exhaust emission testing from light vehicles requires the fulfilment of numerous requirements, including those relating to ambient temperature, topographic height of the test, driving style (dynamic specifications of the trip), trip's duration, length of specific sections of the test (urban, rural, highway) etc. Setting such route for the purpose of research work by the author of this article was the primary challenge facilitating future certification testing related to the assessment of noxious substances in the exhaust emitted by light vehicles, but also in the development work relating to, for example, the estimation of energy consumption by electric and hybrid vehicles or those equipped with fuel cells in light of the development of electromobility and hydrogenization of vehicle transport.

2. Development of electromobility – battery electric vehicles (BEVs)

In 2010 there had been just 16 thousand BEVs registered worldwide (Table 1), of which 6 thousand were registered that year (Table 2). The registration of newly purchased electric passenger cars began to grow rapidly from that moment to come to 39 thousand in 2011, 58 thousand in 2012, 112 thousand in 2013, 191 thousand in 2014, 325 thousand in 2015, 466 thousand in 2016 and 759 thousand in 2017 [8, 9].

The increased sales had been generated mostly by China with a production of more than 60% of BEVs manufactured globally. The world fleet of such vehicles was respectively 16 thousand vehicles in 2010, 55 thousand in 2011, 113 thousand in 2012, 227 thousand in 2013, 420 thousand in 2014, 740 thousand in 2015 and over 1.2 million in 2016, of which 255 thousand in Europe (including approx. 160 thousand vehicles in the EU).

The largest fleet of BEV passenger cars was noted in China (over 480 thousand vehicles), the US (almost 300 thousand vehicles), Japan (86 thousand vehicles), Norway (100 thousand vehicles), France (67 thousand vehicles) and Germany (approx. 41 thousand vehicles). Poland with its fleet of several hundred BEVs has been outpaced significantly by countries such as Italy or Portugal (in 2018 about 1,3 thousand vehicles) [10].

Despite an over 70-fold increase of the world fleet of BEVs in years 2016-2017 electric passenger cars still account for just 0.1% of the total number of passenger cars registered in the world.

Table 1. Newly registered electric passenger cars (BEV) in years 2010-2017, in thousands [8]

Description	2010	2011	2012	2013	2014	2015	2016	2017
Poland	–	0	0	0	0.1	0.2	0.1	0.4
EU28	0.5	7.9	12.4	22.1	35.2	54.2	63.5	97.5
Norway	0.4	1.8	4.2	8.2	18.1	27.8	29.5	44.9
Switzerland	–	–	1.0	1.0	1.0	3.3	3.3	4.8
Europe	0.9	9.9	17.4	31.0	54.2	85.3	96.3	147.2
Canada	–	0,2	0,6	1,6	2,8	4,4	5,2	14,9
China	1.0	4.7	9.6	14.6	48.9	146.7	257.0	468.0
Japan	2.4	12.6	13.5	14.8	16.1	10.5	15.5	24.5
USA	1.2	9.7	14.6	47.7	63.4	71.0	86.7	104.5
In total	6.4	38.5	57.8	112.1	190.8	325.4	466.4	759.1

Electric vehicles (plug-in and battery electric) comprised 1.48% of all new car registrations in EU-28 in 2017 [11]. There is a significant variation across the EU countries for example, in Sweden electric vehicle registrations

are 5.5% of all new cars [11]. Outside of the EU, Norway is a clear leader with 39.2% of new car registration being electric vehicles [12, 13].

Table 2. Registered fleet of passenger BEVs in years 2010-2016, in thousands [8]

Description	2010	2011	2012	2013	2014	2015	2016
EU28	1.9	9.3	21.2	44.3	74.2	121.8	161.3
Norway	3.3	5.3	9.5	19.7	41.8	72.0	98.9
Europe	2.7	12.1	28.1	59.0	107.0	182.4	251.4
Canada	0	0.2	0.9	2.5	5.3	9.7	14.9
China	1.5	6.3	15.9	30.6	79.5	226.2	483.2
India	0,9	1,3	2,8	2,9	3,3	4,3	4,8
Japan	3.5	16.1	29.6	44.3	60.5	70.9	86.4
South Korea	0	0.3	0.8	1.4	2.8	5.7	10.8
USA	3.8	13.5	28.2	75.9	139.3	210.3	297.0
In total	16.4	55.1	112.9	226.8	420.3	745.6	1208.9

In [9] is suggested that by 2030 battery electric vehicles sales could be between 13% and 21% of total new car sales in climate goal and regulation scenarios. Including range extended electric vehicles increase is 34% and 51%. According to one of the scenarios aims to achieve is 10 g CO_2-eqv/km [9].

If Europe were to move to a zero – emission car fleet the share of new car sales which would have to be zero emission (battery electric and fuel cell) would need to be around 20% in 2030, 40% in 2040 and 50% under a medium forecast [9].

In terms of total vehicles, there could be around 24 million electric cars on the road in Europe in 2030, around 10% of Europe's car fleet. This is based on there being 18 million new cars sold in Europe [14] and assuming a 7% market share of new cars in 2020, a 17% market share in 2030 and linear growth between the years [13].

The majority of life cycle analyses suggest that well-to-well (WTW) GHG emissions per km driven of BEVs in Europe lower than ICEVs and hybrid vehicles. Based on the carbon-intensity of the EU electricity mix in 2015, the WTW emissions of a mid-sized BEV were between 60 and 76 g CO_2eqv/km. This is between 47% and 58% lower than the emissions of an average mid-sized ICEV passenger car in 2015, at 143 g CO_2 eqv/km [13].

The growth of electromobility observed at present is forcing a number of research efforts with respect to electric vehicles. The main ones here are the determination of their range, the power of engines implemented on these vehicles, battery durability or the test of energy use by these vehicles. The latter issue is discussed in this article, which presents examples of the measurements of energy consumption by passenger cars on a route set for the purpose of RDE tests.

3. RDE test and testing energy consumption by an electric passenger car

The trip sequence includes driving in an urban area and then in a rural area and on a highway. The trip component in urban area, rural area and on the highway is conducted in a continuous manner. The use in rural area may be interrupted by brief periods of use in urban areas if these are located along the route path. The use on a highway may be interrupted by brief periods of use in urban or rural areas, for example while driving through toll collection booths or along sections where road construction work is being conducted. If, for practical reasons, another test sequence is justifiable, the sequence of use in urban area, rural area and on a highway may be changed upon permission of the body issuing the certification [15].

The use in urban area is characterized by vehicle speeds not exceeding 60 km per hour, in an rural area vehicle speed ranges from 60 km per hour to 90 km per hour and on a highway above 90 km per hour (Table 3). The trip included approximately 34% use in an urban area, 33% in rural area and 33% on a highway. The term 'approximately' means a range of ±10 percentage points from the above percentage values. However, the use in urban area must account for at least 29% of the total route driven. Vehicle speed will usually not exceed 145 km per hour. The maximum speed may be exceeded by 15 km per hour for no more than 3% of the duration of highway component. Local speed restrictions remain in force during PEMS test regardless of other legal consequences. Exceeding local speed restrictions as such does not nullify the results of PEMS test. Average driving speed (including stop periods) in the urban area should be between 15 km per hour and 30 km per hour. Stop periods, defined as time when vehicle's speed is less than 1 km per hour, should account for at least 10% of the time of use in the urban area. Use in urban area includes several stop periods lasting at least 10 seconds. Avoid situations where a single excessively long stop period would account for over 80% of the total stop period during the use in an urban area. Driving speed on a highway includes range of 90 km per hour to at least 110 km per hour. Vehicle speed must exceed 100 km per hour for at least 5 minutes.

Table 3. Requirements for the drive [15]

Requirements	Unit	Urban	Rural	Highway
Speed	km/h	0–60	60–90	90–130
Distance	%	~34 (±10%)	~33 (±10%)	~33 (±10%)
Minimum distance	km	16	16	16
Share of trip component	%	> 29	–	–

Trip duration must range from 90 to 120 minutes. The difference between the starting and end point of the trip may not exceed 100 meters in altitude above the sea level. Minimum distance during the use in urban area, rural and on the highway must reach at last 16 km (detailed requirements are listed in Table 4) [15].

In the RDE studies, a A passenger car was used (Fig. 1).

Fig. 1. Electric passenger car tested

Table 4. Detailed requirements for RDE tests [15]

Specification	Requirements
Ambient temperature (T_z)	– normal range: $0^oC \leq T_z < 30^oC$
	– lower extended range: $-7^oC \leq T_z < 0^oC$
	– upper extended range: $30^oC < T_z \leq 35^oC$
Topographic test height (h)	– normal: $h \leq 700$ m n.p.m.
	– extended: $700 < h \leq 1300$ m n.p.m.
Assessment of the impact of ambient weather and road specification and driving style	– cumulative altitude gain: below 1200 m/ 100 km
	– relative positive acceleration (RPA): greater than RPA_{min} (for all types of driving conditions)
	– a product of acceleration and speed ($v \cdot a_{pos}$): less than $v \cdot a_{pos\ min}$ (for all types of driving conditions)
Thermal state of the vehicle prior to test	– cold start of the vehicle: coolant below 70^oC, – duration of at least 300 s
	– emission from cold start not included in RDE test
Duration of individual stop	– not to exceed 180 s
Use of exhaust purification systems	– one-time regeneration of solid particle filter may cause a repeat of the RDE test; two regenerations are taken into consideration in RDE fume exhaust test results
Use of driving comfort systems	– normal usage as intended (e.g. use of air conditioning system)
Vehicle load	– vehicle weight: driver (and the passenger) plus test equipment; maximum load at < 90% of the total of passenger weight and vehicle payload
Test requirements	– duration 90–120 min
Requirements for urban test component	– 29–44% of the entire test length
	– distance: more than 16 km
	– vehicle speed (v): $v \leq 60$ km/h
	– average speed: 15–40 km/h
	– duration of stops: 6–30% of the urban component
Requirements for rural test component	– 23–43% of the entire test length
	– distance: more than 16 km
	– vehicle speed (v): 60 km/h $< v \leq 90$ km/h
Requirements for highway test component	– 23–43% of the entire test length
	– distance: more than 16 km
	– vehicle speed (v): $v > 90$ km/h
	– vehicle speed in excess of 100 km/h for at least 5 minutes
	– vehicle speed in excess of 145 km/h for a maximum of 3% of the trip

Designated trip route was shown on Fig. 2. It consists of urban, rural and highway components.

Fig. 2. Course of the designated RDE route

The speed of the car over time is shown on Fig. 3.

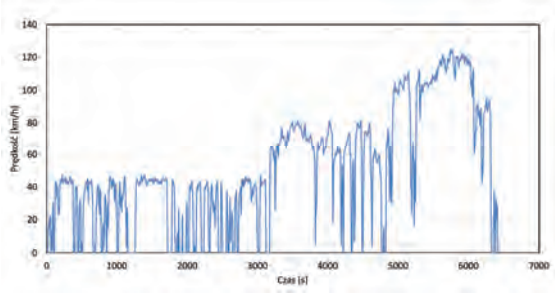

Fig. 3. The speed of the car over time

Energy consumption on this c. 92 km route was tested using Yokogawa 1806E power analyser (which allows the measurement of energy consumption and energy recovery, battery charging efficiency, etc.) and Semtech DS with GPS device (measuring the length of the distance travelled).

Tested electric passenger car had the following basic criteria:

- Overall length x width x height [mm]: 4140 x 1800 x 1593;
- Wheel base [mm]: 2570;
- Curb weight [kg]: (excluding a drivers with 75 kg) 1510;
- Gross weight [kg]: 1800;
- Electric motor (type: Permanent Magnet AC Synchronous Motor), Voltage [V]: 360 V, Max. power [kW/rpm]: 81.4/2730–8000, Max. torque [Nm/rpm]: 285/0–2730;
- Gear reduction unit: final gear ratio (constant): 8.206;
- OBC (On Board Charger): Max. power [kW] 6.6;
- High-Voltage Battery pack: Type: LIPB (Lithium Ion Polymer Battery), Voltage [V]: 360, Capacity [Ah]: 75, Energy [kWh]: 27, Power [kW]: 90, Weight [kg]: 277;
- 12V Battery: Capacity [Ah]: 45.

Test found to be carried out correctly (Table 5). For example:

Table 5. Confirmation the test has been carried out correctly

Test correctness			
Test specification	**Result**	**Requirement**	**Correctness**
Urban component [km]	30.0	> 16	Correct
Rural component [km]	28.6	> 16	Correct
Highway component [km]	33.3	> 16	Correct
Total route length [km]	91.9	> 48	Correct
Urban component [%]	32.7	29-44	Correct
Rural component [%]	31.1	33 ±10	Correct
Highway component [%]	36.2	33 ±10	Correct
Average speed on urban route [km/h]	27.8	15-40	Correct
Duration of stops on urban route [%]	20.8	6-30	Correct
Trip duration at more than 100 km/h [min]	15.8	> 5	Correct
Maximum speed [km/h]	125.1	< 160	Correct
Trip duration at more than 145 km/h during the highway component [%]	0.0	< 3	Correct
Trip duration [min]	106.9	90-120	Correct

Table 5cont.

Cold start (t = 300 s)			
Coolant temperature [°C]	0,0	< 70	Correct
Maximum vehicle speed [km/h]	47.7	< 60	Correct
Duration of vehicle stops [s]	20	< 90	Correct
In neutral after ignition [s]	0	< 15	Correct
RPA			
Urban: data set no. $a_i > 0,1$ m/s^2	964	> 150	Correct
Rural: data set no. $a_i > 0,1$ m/s^2	274	> 150	Correct
Highway: data set no. $a_i > 0,1$ m/s^3	205	> 150	Correct
Urban: average speed [km/h]	28.1		
Rural: average speed [km/h]	72.1		
Highway: average speed [km/h]	109.2		
Urban: 95. percentile $V \cdot a_{pos}$ [m^2/s^3]	14.1	Correct	Correct
Rural: 95. percentile $V \cdot a_{pos}$ [m^2/s^3]	19.5	Correct	Correct
Highway: 95. percentile $V \cdot a_{pos}$ [m^2/s^3]	15.5	Correct	Correct
Urban: RPA [m/s^2]	0.14	Correct	Correct
Rural: RPA [m/s^2]	0.08	Correct	Correct
Highway: RPA [m/s^2]	0.04	Correct	Correct

Results of energy consumption tests by the electric passenger vehicle tested on the route set for the purpose of RDE test was presented in Table 6.

Table 6. Energy consumption by an electric passenger car on a route set for the purpose of an RDE test

Item	Unit	Test 1	Test 2	Average
Energy consumption	kWh/100 km	18.9	20.2	19.6

Results of the tests of electrical energy consumption by the electric passenger car tested show that it is from the upper range of energy consumption at 15–20 kWh/100 km, an energy use range by typical electric city cars. Assuming the cost of electrical energy consumption at, for example PLN 0.6/kWh, operating costs of such vehicle, at PLN 9–12 per 100 km are modest. They can be reduced further using night time electricity rates and the cost of electrical energy of PLN 0.3–0.4/kWh in that case [16]. Larger passenger electric cars use greater amounts of electrical energy (20–25 kWh/100 km), but electrical energy consumption costs are in their case far lower than fuel consumption costs by passenger cars with conventional engines [16].

Electric cars include cars equipped with fuel cells. At present, the development of hydrogenization of vehicle transportation in a number of countries (e.g. Japan, Germany, Sweden) is very dynamic.

4. Development of hydrogenization – cars equipped with fuel cells (FCEV)

Area for practical use of hydrogen as a fuel carrier is transport, including in particular road transport. In recent years 2 motor companies (Hyundai, Toyota) have launched the serial production of fuel cell vehicles (FCEV) and others such as Volkswagen, Mercedes Benz, BMW, General Motors also produce such vehicles. The start of serial production by those companies depends on the availability of expanded hydrogen refuelling network of HRS (Hydrogen Refueling Stations). In 2016 there were only c.a. 200 such stations available in the world. It is expected that by 2020 the number of HRS should come to approx. 1000 and by 2025 – to c.a. 3500 (Table 7).

Table 7. Number of public HRS worldwide in 2016 and their projected number in 2020-2025 [9]

Year	USA	Europe	Asia	Total
2016	60	100	103	263
2020	130	520	340	990
2025	600	2000	830	3430

Source: H2 Mobility, USDOE, Hydrogen Europe, Air Liquid – cited from: How hydrogen empowers the energy transition, Hydrogen Council 2017, p. 9.

This HRS in 2025 should provide service for approx. 2 million hydrogen vehicles. Currently approx. several thousand vehicles fuelled with hydrogen are used in the world, including more than 1000 in the US and 2000 in Japan and several hundred in Western Europe. A dynamic growth of fleets of hydrogen vehicles is planned – for example China expects to have 50 thousand hydrogen vehicles in 2025, to eventually exceed one million in 2030, whereas Japan will have a fleet of 40 thousand hydrogen vehicles in 2020 and approx. 300 thousand in 2030. According to projections of 2014 – the European fleet of hydrogen vehicles is expected to have 350 thousand vehicles in 2020, the fleet in Japan – 100 thousand, in Korea – 50 thousand and in the US – 20 thousand [9].

Also, the fleet of hydrogen-fuelled buses is to be developed – in Europe it will have 1000 buses in 2020, while for instance in South Korea – almost 30 thousand buses by 2030.

In Poland, there are practically no vehicles equipped with fuel cells (for that reason, at present, it is impossible to obtain a vehicle of this type for energy consumption tests, such research will be conducted at a later date). However, it was developed by Motor Transport Institute "Circumstances of the national plan for hydrogenization of road transport in Poland". In the first place taken into account were [17]:

- already existing refuelling opportunities in the neighboring countries,
- the expected future HRS locations in the Baltic countries,
- gradually increasing the area available for hydrogen-powered cars as a result of the subsequent location of new stations at distances up to 300 km from the existing or sequentially from the newly-opened ones [17].

With the above criteria, the order of preliminary proposals to build base HRS in Poland are as follows: 1 – Poznan, 2 – Warsaw, 3 – Bialystok, 4 – Szczecin, 5 – Lodz area, 6 – Tri-City area, 7 – Wroclaw, 8 – Katowice region, 9 – Krakow (Fig. 4, Fig. 5) [17].

Fig. 4. Map of Poland with marked sites of the proposed public hydrogen refuelling station locations [17]

4. Summary

Development of electromobility and hydrogenization of vehicle transport is determined by the development of infrastructure consisting of charging stations for electric vehicles and refuelling stations for cars equipped with fuel cells (HRS). This will generate an increase in the number of vehicles of that type in use. For example, at present in Japan there are 92 HRS stations and approximately 2300 cars equipped with fuel cells are in use.

It will also generate the need to solve a number of technical issues, research related to, for example, determining battery durability or the range of electric vehicles and the associated consumption of electrical energy, which also applies to electric cars equipped with fuel cells. With respect to the latter issue, the article presents a method to evaluate such consumption during an RDE test on a new research route in a real driving condition.

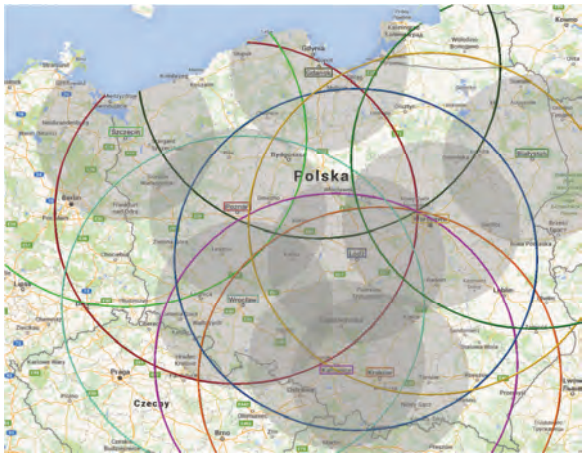

Fig. 5. Penetration area of cars using fuel cells based on 9 hydrogen refuelling stations situated on the national TEN-T road network by the 2030 [3] a) when driving in one direction (diameter of large circles – to approx. 600 km), b) when driving there and back (diameter of small, shaded circles – to approx. 300 km) [17]

Nomenclature

BEV	Battery Electric Vehicle
EV	Electric Vehicle
FCEV	Fuel cell Electric Vehicle
NEDC	New European Driving Cycle
RDE	Real Driving Emissions

Bibliography

[1] COMMISSION REGULATION (EU) 2016/427 of 10 March 2016 amending Regulation (EC) No 692/2008 as regards emissions from light passenger and commercial vehicles (Euro 6)

[2] COMMISSION REGULATION (EU) 2017/1151 of 1 June 2017 supplementing Regulation (EC) No 715/2007 of the European Parliament and of the Council on type-approval of motor vehicles with respect to emissions from light passenger and commercial vehicles (Euro 5 and Euro 6) and on access to vehicle repair and maintenance information, amending Directive 2007/46/EC of the European Parliament and of the Council, Commission Regulation (EC) No 692/2008 and Commission Regulation (EU) No 1230/2012 and repealing Commission Regulation (EC) No 692/2008

[3] COMMISSION REGULATION (EU) 2018/1832 of 5 November 2018 amending Directive 2007/46/EC of the European Parliament and of the Council, Commission Regulation (EC) No 692/2008 and Commission Regulation (EU) 2017/1151 for the purpose of improving the emission type approval tests and procedures for light passenger and commercial vehicles, including those for in-service conformity and real-driving emissions and introducing devices for monitoring the consumption of fuel and electric energy

[4] MERKISZ, J., PIELECHA, J., LIJEWSKI, P. et al. Conference: 21st International Conference on Modelling, Monitoring and Management of Air Pollution. *WIT Transactions on Ecology and the Environment*. 2013, **174**, 27-38.

[5] MERKISZ, J., PIELECHA, J. Comparison of real driving emissions tests. *IOP Conf. Ser.: Mater. Sci. Eng*. 2018, **421**, 042055. DOI: 10.1088/1757-899X/421/4/ 042055

[6] PIELECHA, J., MAGDZIAK, A., BRZEZIŃSKI, L. Nitrogen oxides emission evaluation for Euro 6 category vehicles equipped with combustion engines of different displacement volume. *IOP Conf. Ser.: Earth Environ. Sci*. 2019, **214**, 012010. DOI: 10.1088/1755-1315/214/012010

[7] PIELECHA, I., CIEŚLIK, W., SZAŁEK, A. Energy recovery potential through regenerative braking for a hybrid electric vehicle in a urban conditions. *IOP Conf. Ser.: Earth Environ. Sci*. 2019, **214**, 012013.

[8] GIS, W., MENES, M. The development of the world electric vehicles fleet in years 2010-2017. *KONMOT*. 2018.

[9] GIS, W. Electromobility and hydrogenization of the motor transport in Poland now and in the future. *Journal of KONES Powertrain and Transport*. 2018, **25**(4).

[10] GIS, M., BEDNARSKI, M., ORLINSKI, P. Energy analysis of charging infrastructure for electric vehicles on the TEN-T road network. *11th Conference on Interdisciplinary Problems in Environmental Protection and Engineering. EKODOK*. Polanica Zdrój, 8-10.04.2019.

[11] EEA, 2018a Electric Vehicles as the Proportion of the Total Fleet. (https://www.eea.europa.eu/data-and-maps/indicators/proportion-of-vehicle-fleet meeting-4/assessment-2)
[12] EAFO, 2018, Electric Vehicles Market Share. (https://www.eea.europa.eu/publications/electric-vehicles-ineurope), Accessed 24 May 2018.
[13] HAMPSHIRE, K., GERMAN, R., PRIDMORE, A., FONS, J. Electric vehicles from life cycle and circular economy perspectives. Version 2, 25 June 2018.
[14] ACEA Registration Figures. http://www.acea.be/statistics/tag/category/registrations-and-press-release-calendar. Accessed 23 June 2018.
[15] PIELECHA, J. (ed.). Badania emisji zanieczyszczeń silników spalinowych. *Wydawnictwo Politechniki Poznańskiej*. Poznań 2017.
[16] http://samochodyelektryczne.org (accessed 11/2018).
[17] GIS, W., MENES, E., WAŚKIEWICZ, J. et al. Circumstances of the national plan or hydrogenization of road transport in Poland. *Report prepared as part of the HIT-2-Corridors project*.
[18] MERKISZ, J., GIS, M. The growth in the use of methane fuel for fuelling urban buses. *10th Conference on Interdisciplinary Problems in Environmental Protection and Engineering (EKO-DOK)*. Polanica Zdroj, 16-18.04.2018.
[19] GIS, W., PIELECHA, J., WASKIEWICZ, J. et al. Use of certain alternative fuels in road transport in Poland. *Scientific Conference on Automotive Vehicles and Combustion Engines (KONMOT)*. Krakow, 22-23.09.2016.

Wojciech Gis, DSc., DEng. – Prof. ITS, Motor Transport Institute.
e-mail: *wojciech.gis@its.waw.pl*

Prof. Jerzy Merkisz, DSc., DEng. – Faculty of Transport Engineering, Poznan University of Technology.
e-mail: *jerzy.merkisz@put.poznan.pl*

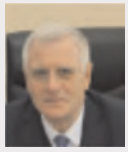

Article citation info:
BEBKIEWICZ, K., CHŁOPEK, Z., LASOCKI, J. et al. Inventory of pollutant emission from motor vehicles in Poland using the COPERT 5 software. *Combustion Engines*. 2019, **178**(3), 150-154. DOI: 10.19206/CE-2019-326

Katarzyna BEBKIEWICZ
Zdzisław CHŁOPEK
Jakub LASOCKI
Krystian SZCZEPAŃSKI
Magdalena ZIMAKOWSKA-LASKOWSKA

CE-2019-326

Inventory of pollutant emission from motor vehicles in Poland using the COPERT 5 software

This article presents results of the inventory of pollutant emission from motor vehicles in Poland. To determine emission from motor vehicles in Poland COPERT 5 software was used for the first time. In addition, a comparison of the national emission from motor vehicles in 2016 and in 2015 was included. Pollutants harmful to health were considered primarily: carbon monoxide, organic compounds, nitrogen oxides and particulate matter. Emission of substances contributing to the intensification of the greenhouse effect were also examined: carbon dioxide, ammonia and nitrous oxide. It was found that the relative increase in volume of emission of carbon monoxide and non-methane volatile organic compounds is less than 10%, and nitrogen oxides and particulate matter less than 15%. The relative increase in carbon dioxide emission is approximately 14%, which corresponds to a relative increase in fuel consumption. The relative increase of volume of heavy metal emission is similar. The assessment of the energy emission factor (emission of pollution related to energy equal to used fuel) proves that – amongst pollutants harmful to health – for carbon monoxide and non-methane volatile organic compounds there is a relative reduction by approximately 5% in 2016, and for nitrogen oxides and particulate matter – increase by approximately (3–4)%.

Key words: *inventory of pollutant emission, motor vehicles*

1. Introduction

Since 2017, a new version of the software – COPERT 5 has been used for the purpose of the inventory of pollutant emission from motor vehicles [4, 5]. The new version differs from the previous one, among others in the structure of motor vehicles – this is primarily due to the differences offered by manufacturers of types of vehicles. There are also some differences in the emission characteristics of individual substances, that are mainly the result of increasing level of knowledge of the ecological properties of motor vehicles considering emission of pollutants under conditions simulating real operation.

Therefore, it is advisable to conduct an inventory of pollutants from motor vehicles using the new version of the software. Such inventory was performed for Poland for the year 2016 as part of pollutant emission reporting. For comparative purposes also pollutant emission from motor vehicles for previous years was inventoried.

Detailed methodology for the selection of COPERT software input data has been described in publications [1–3] – there are no significant differences compared to the COPERT 4 software version [4].

The main differences in the software input data for 2016 in relation to 2015 year result from variations in the number of vehicles in each category and the consumption of different types of fuels.

Figure 1 shows the number of motor vehicles in Poland in 2016 and in 2015 for cumulative vehicle categories:

- passenger cars with gasoline spark ignition engine – PC-G,
- passenger cars with compression ignition engine – PC-D,
- passenger cars with liquefied petroleum gas spark ignition engine PC-LPG,
- light duty vehicles with spark ignition engine – LDV-G,
- light duty vehicles with compression ignition engine – LDV-D,
- heavy duty vehicles – HDV,
- buses with compression ignition engine – B-D,
- NG (natural gas): CNG (compressed natural gas) and LNG (liquefied natural gas) buses – B-CNG[1],
- motorcycles and mopeds – M.

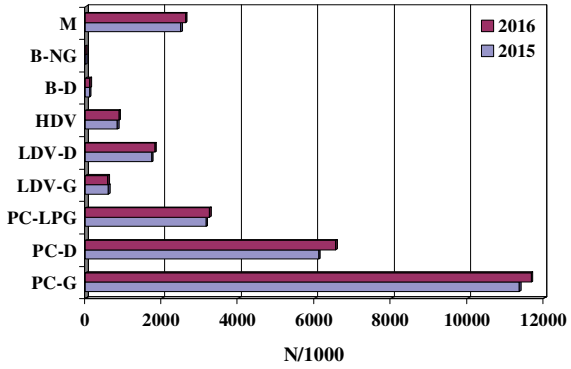

Fig. 1. The number of motor vehicles in Poland in years 2015 and 2016

Differences in the number of vehicles in cumulative categories should be assessed as minor – Fig. 2.

The relative difference in most cases does not exceed 7%. Only in the case of buses equipped with engines powered by natural gas the number of vehicles is noted to increase. In the relative difference reaches 12%. It is also noted the decrease in the number of light duty vehicles with spark ignition engine, which is understandable tendency for economic reasons.

[1] The COPERT software officially encompasses categories of vehicles equipped with CNG-powered natural gas (CNG) engines. In fact, also liquefied natural gas (LNG) is applied. For this reason, a reference NG (natural gas) is used both for natural gas and compressed and liquefied gas.

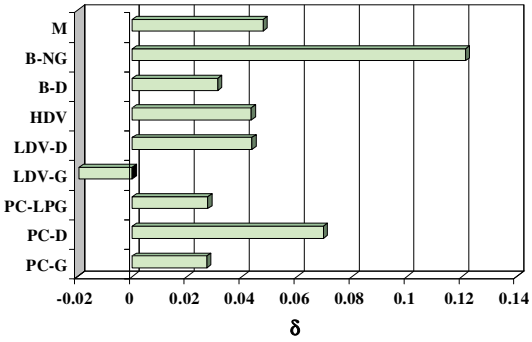

Fig. 2. The relative difference of motor vehicles number in Poland in 2016 year versus 2015 year

Figure 3 shows the consumption of fuels: gasoline – G, diesel – D, liquefied petroleum gas – LPG and natural gas – NG.

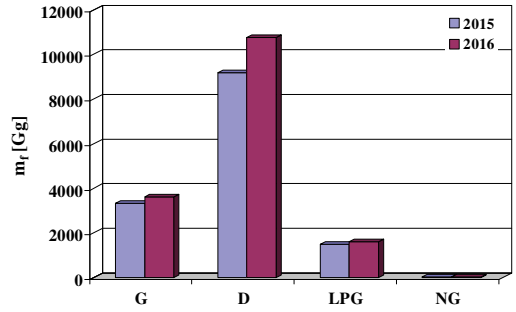

Fig. 3. Fuel consumption from motor vehicles in years 2015 and 2016

There is a significant increase in the consumption of diesel fuel in 2016 comparing to 2015 – a relative difference in consumption of diesel is more than 15%.

The correlation between consumption of different types of fuel, determined as a result of the emission inventory and reported fuel consumption confirms the validity of adopted data for the COPERT software.

2. National annual emission of pollutants from motor vehicles in 2016 comparing to 2015

Figures 4–14 present the national annual emission from motor vehicles in Poland in 2015 and in 2016 of the following substances [6]:

– carbon monoxide – CO,
– non-methane volatile organic compounds – NMVOC,
– methane – CH_4,

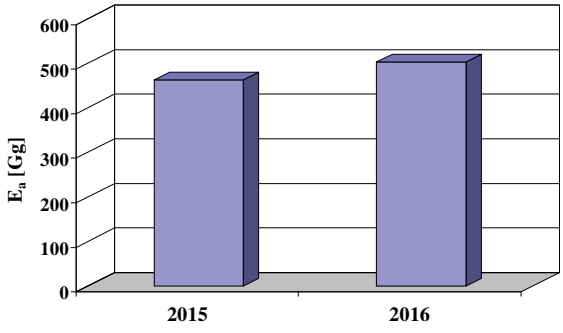

Fig. 4. National annual emission of carbon monoxide from motor vehicles in 2015 and 2016

– nitrogen oxides reduced to nitrogen dioxide – NO_x,
– total suspended particles – TSP,
– particulate matter PM10,
– particulate matter PM2.5,
– BC – black carbon,
– carbon dioxide – CO_2,
– nitrous oxide – N_2O,
– ammonia – NH_3.

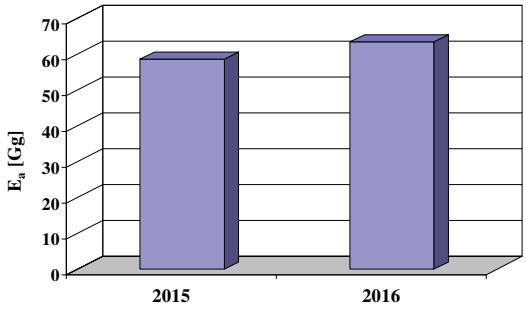

Fig. 5. National annual emission of non-methane volatile organic compounds from motor vehicles in 2015 and 2016

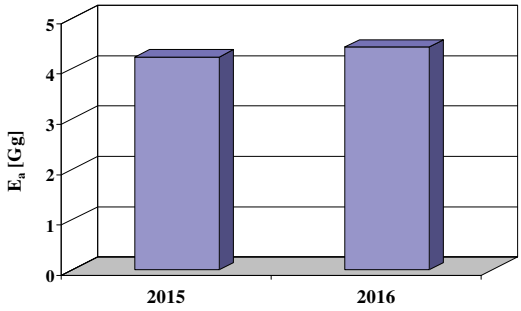

Fig. 6. National annual emission of methane from motor vehicles in 2015 and 2016

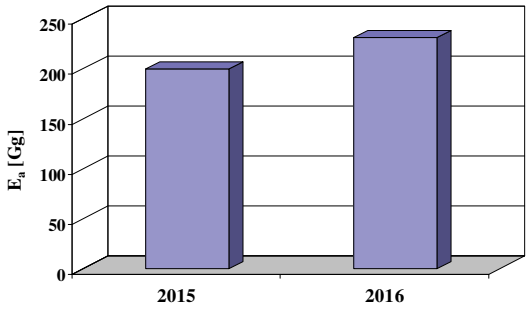

Fig. 7. National annual emission of nitrogen oxides from motor vehicles in 2015 and 2016

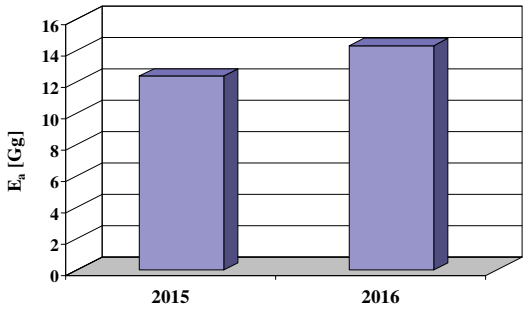

Fig. 8. National annual emission of total suspended particles from motor vehicles in 2015 and 2016

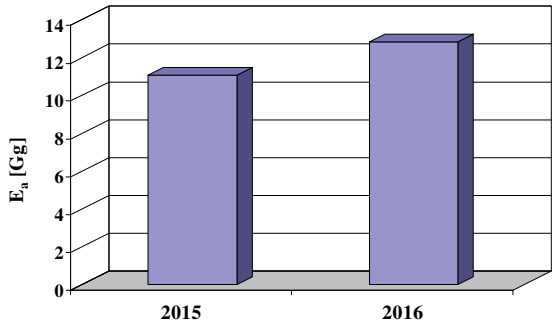

Fig. 9. National annual emission of particulate matter PM10 from motor vehicles in 2015 and 2016

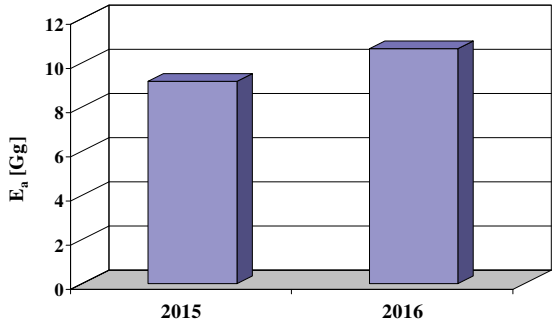

Fig. 10. National annual emission of particulate matter PM2.5 from motor vehicles in 2015 and 2016

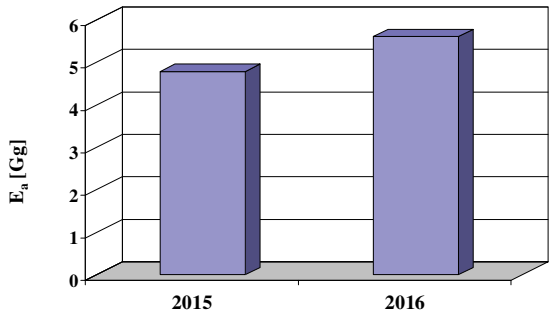

Fig. 11. National annual emission of black carbon from motor vehicles in 2015 and 2016

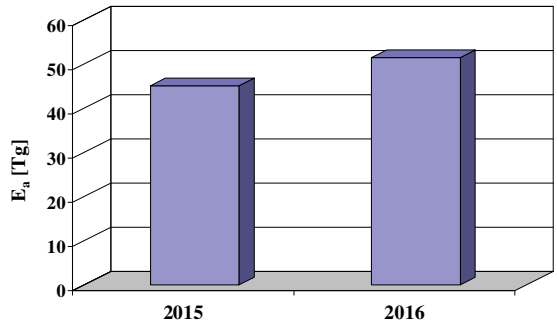

Fig. 12. National annual emission of carbon dioxide from motor vehicles in 2015 and 2016

Differences in values of the national annual emission of pollutants from motor vehicles comparing years 2015 and 2016 are small. In all cases there was an increase in the national annual emission of pollutants, which results mainly from the increase in the number of vehicles in individual cumulated categories (with the exception of light commercial trucks with spark ignition engines) and – as a consequence – from an increase in fuel consumption. The increase of the national annual emission in 2016 as compared to 2015 is various for particular pollutants. Therefore, it was decided to compare the relative change in the national annual emission of all inventoried substances between 2016 and 2015 in relation to the national average annual emission of pollutants for those years. This analysis also includes the results of heavy metal emission – emission is primarily determined by the use of different fuels.

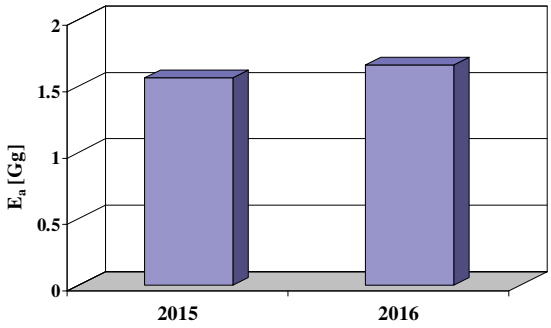

Fig. 13. National annual emission of nitric dioxide from motor vehicles in 2015 and 2016

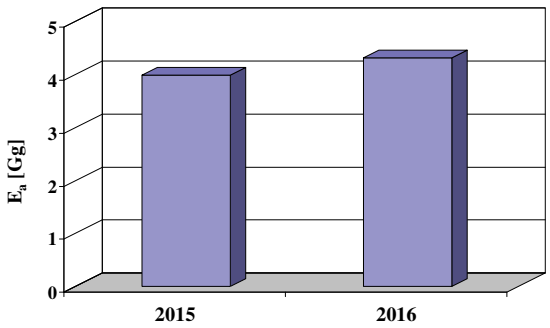

Fig. 14. National annual emission of ammonia from motor vehicles in 2015 and 2016

Figures 15–17 show the relative difference in annual emission of pollutants comparing 2016 to 2015. The relative difference is defined as:

$$\delta = 2 \cdot \frac{x_{2016} - x_{2015}}{x_{2016} + x_{2015}} \tag{1}$$

where: x_{2015}, x_{2016} – the value in 2015and 2015.

The relative difference in annual emission of pollutants comparing 2016 to 2015 is small – it does not exceed 15%. The largest relative difference in national annual emission is noted for particulates, especially for their carbon part. The increase in the annual national emission of carbon dioxide is associated with higher consumption of fossil fuels in 2016, due to a larger number of vehicles. The smallest relative difference in national annual emission is noted for volatile organic compounds, primarily methane, and for nitrous oxide.

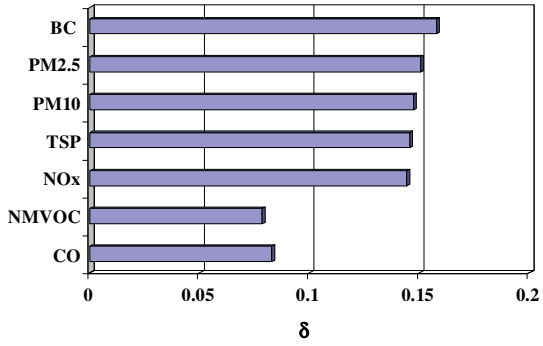

Fig. 15. The relative difference of national annual pollutant emission from motor vehicles in Poland comparing 2015 to 2016

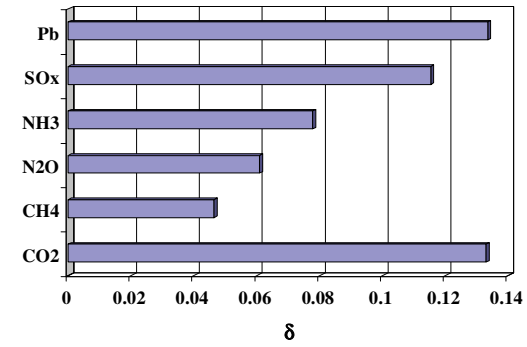

Fig. 16. The relative difference of national annual pollutant emission from motor vehicles in Poland comparing 2016 to 2015

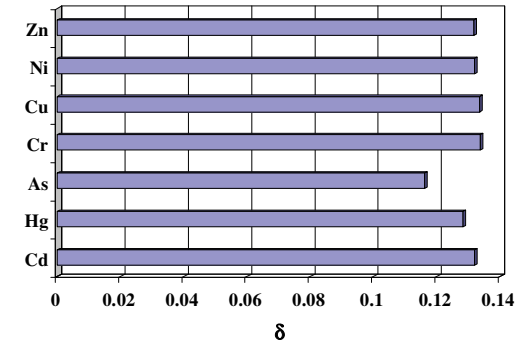

Fig. 17. The relative difference of national annual pollutant emission from motor vehicles in Poland comparing 2016 to 2015

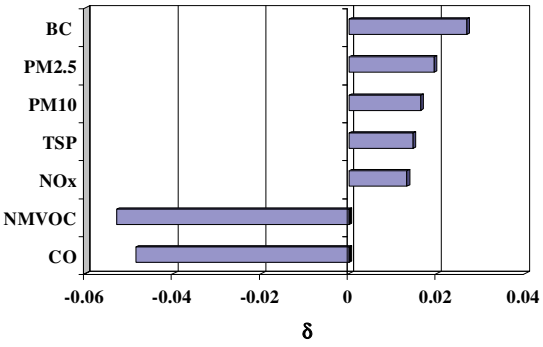

Fig. 18. The relative difference of average energetic index of pollutant emission from motor vehicles in Poland comparing 2015 to 2016

In order to compare the ecological properties of vehicles with regard to the emission of pollutants in 2015 and 2016, the average energy emission factor of these substances was determined for individual substances.

$$WE=\frac{E_a}{R_a} \tag{2}$$

where: R_a – energy equal to the annual consumption of fuels, determined in accordance with their calorific value.

Figures 18–20 show the relative difference in the average energy pollution emission factor from motor vehicles in Poland comparing 2016 to 2015.

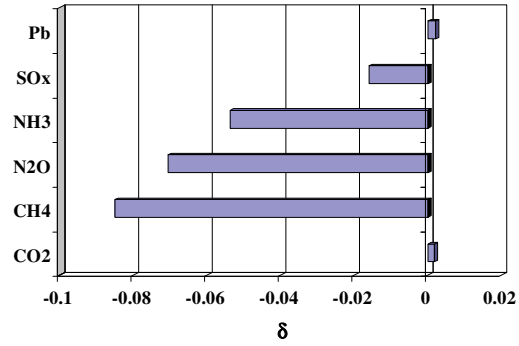

Fig. 19. The relative difference of average energetic index of pollutant emission from motor vehicles in Poland comparing 2015 to 2016

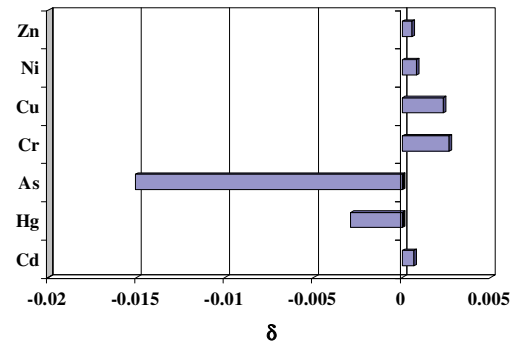

Fig. 20. The relative difference of average energetic index of pollutant emission from motor vehicles in Poland comparing 2015 to 2016

3. Recapitulation

In the summary following conclusions may be drawn from presented research results:

1. Presented results of the total emission of pollutants from motor vehicles are the result of the first use in Poland of COPERT 5 software to official reporting of emission in the framework of cooperation within the European Union.
2. Among the cumulated categories of large-capacity vehicles, the number of passenger cars with compression engines is the category number of which increased the most in 2016.
3. Among fuels consumed by automotive vehicles in 2016, diesel oil consumption increased the most.
4. In 2016, the relative increase in volumes of emission of carbon monoxide and non-methane volatile organic compounds is less than 10%, and nitrogen oxides and particulate matter less than 15%.
5. In 2016, the relative increase in volume of carbon dioxide emission is around 14%, which corresponds to a relative increase in fuel consumption. The relative increase in volume of heavy metal emission is similar.
6. Results of testing the energy emission factor proves that – among contaminants posing a threat to human health –

the energy emission factor for carbon monoxide and non-methane volatile organic compounds shows in 2016 a relative reduction ratio by approximately 5%, and the factor for the nitrogen oxides and particulate matter – increase by approximately (3–4)%. For heavy metals, the relative change in the energy emission factor is small. A light increase also occurs in the case of carbon dioxide, which results from the fact that in subsequent years larger car vehicles are used more often. This is due to the commercial aspects of placing vehicles in the market – contrary to popular publicity concerning the use of smaller cars. This fact is noticeable in both light-duty and heavy-duty vehicles.

Nomenclature

As	arsenic
BC	black carbon
B-D	buses with compression ignition engine
B-NG	NG buses
C	coaches
Cd	cadmium
CH_4	methane
CNG	compressed natural gas
CO	carbon monoxide
CO_2	carbon dioxide
Cr	chromium
E_a	annual emission
HDV	heavy duty vehicles
Hg	mercury
LNG	liquefied natural gas
M	motorcycles and mopeds
N_2O	nitrous oxide
NG	natural gas
NH_3	ammonia
Ni	nickel
NMVOC	non-methane volatile organic compounds
NO_x	nitrogen oxides
Pb	lead
PC-D	passenger cars with compression ignition engine
PC-G	passenger cars with gasoline spark ignition engine
PC-LPG	passenger cars with liquefied petroleum gas spark ignition engine
PM10	particular matter PM10
PM2.5	particular matter PM2.5
SO_2	sulphur oxides
TSP	total suspended particles
Zn	zinc
δ	relative difference

Bibliography

[1] BEBKIEWICZ, K., CHŁOPEK, Z., SZCZEPAŃSKI, K., ZIMAKOWSKA-LASKOWSKA, M. Assessment of results of pollutant emission inventory of the road transport sector in Poland in 2000–2015. *The Archives of Automotive Engineering – Archiwum Motoryzacji*. 2017, **78**(4), 5-25.

[2] BEBKIEWICZ, K., CHŁOPEK, Z., SZCZEPAŃSKI, K., ZIMAKOWSKA-LASKOWSKA, M. Issues of modeling the total pollutant emission from vehicles. *Proceedings of the Institute of Vehicles*. 2017, **1**(110), 103-118.

[3] BEBKIEWICZ, K., CHŁOPEK, Z., SZCZEPAŃSKI, K., ZIMAKOWSKA-LASKOWSKA, M. Results of air emission inventory from road transport in Poland in 2014. *Proceedings of the Institute of Vehicles*. 2017, **1**(110), 77-88.

[4] COPERT Training 5. COPERT 5 vs COPERT 4. European Environment Agency. 2016. http://emisia.com/sites/default/files/COPERT_5_features.pdf. (2019-02-06).

[5] EMEP/EEA air pollutant emission inventory guidebook – 2016. European Environment Agency.

[6] Poland's Informative Inventory Report 2018. Submission under the UN ECE Convention on Long-range Transboundary Air Pollution and the Directive (EU) 2016/2284 Warszawa, National Centre for Emission Management (KOBiZE) at the Institute of Environmental Protection – National Research Institute. February 2018.

Katarzyna Bebkiewicz, MEng. – Institute of Environmental Protection – National Research Institute in Warsaw.
e-mail: *katarzyna.bebkiewicz@kobize.pl*

Jakub Lasocki, DEng. – Faculty of Automotive and Construction Machinery Engineering, Warsaw University of Technology.
e-mail: *jakub.lasocki@pw.edu.pl*

Prof. Zdzisław Chłopek, DSc., DEng. – Professor in the Institute of Environmental Protection – National Research Institute in Warsaw.
e-mail: *zdzislaw.chlopek@kobize.pl*

Krystian Szczepański, DSc., DEng. – Director of the Institute of Environmental Protection – National Research Institute in Warsaw.
e-mail: *krystian.szczepanski@ios.edu.pl*

Magdalena Zimakowska-Laskowska, DSc., DEng. – Institute of Environmental Protection – National Research Institute in Warsaw.
e-mail: *magdalena zimakowska-laskowska @kobize.pl*

Article citation info:
NOWAK, L., TUTAK, W. Combustion stability of dual fuel engine powered by diesel-ethanol fuels. *Combustion Engines*. 2019, **178**(3), 155-161. DOI: 10.19206/CE-2019-327

Łukasz NOWAK
Wojciech TUTAK

CE-2019-327

Combustion stability of dual fuel engine powered by diesel-ethanol fuels

The paper presents result of combustion stability assessment of dual fuel engine. The authors analyzed results of co-combustion of diesel fuel with alcohol in terms of combustion stability. The comparative analysis of both the operational parameters of the engine and the IMEP, as the parameters determining the stability of the combustion process, were carried out. It was analyzed, among others values of the COV_{IMEP} coefficient, the spread of the maximum pressure value, the angle of the position of maximum pressure and the probability density distribution of the IMEP. The experimental investigation was conducted on 1-cylinder air cooled compression ignition engine. The test engine operated with constant rpm equal to 1500 rpm and constant angle of start of diesel fuel injection. The engine was operated with ethanol up to 50% of its energy fraction. The influence of ethanol on ignition delay time spread and end of combustion process was evaluated. It turns out that the share of ethanol does not adversely affect the stability of ignition..

Key words: *combustion stability, heat release, dual fuel, ignition delay, combustion phases*

1. Introduction

Diesel engines are widely used to power engineering devices for its good durability, thermal efficiency and specific power output. On the other hand, these engines are major contributors of air pollutant emission such as carbon monoxide (CO) and nitrogen oxides (NO_x) [1, 2].

Due to stricter emissions standards for diesel engines with regards to NO_x and CO_2 emission and fuel consumption is growing concerns on the applicability of clean energy technologies [3]. Most of investigations showed that using alcohols in diesel engines can reduce emission of hydrocarbon (HC), carbon monoxide (CO) and particulate matter (PM) emissions, but nitrogen oxide (NO_x) emission increases [4–6]. The oxygen content of alcohols structure is an important factor in the NO_x formation, because it causes to high local temperatures due to excess hydrocarbon oxidation. The increased oxygen levels increase the maximum temperature during the combustion, and increase NO_x formation [7–10].

Co-combustion of diesel fuel with alcohol can be made by two different combustion systems. The first one is to prepare a blend of diesel fuel with alcohol and bring the blend to the engine, using a typical supply system for the diesel engine. The main disadvantage of this combustion system is problem with stability of fuels blend and separation of fuels and lack of flexibility on the ratio of diesel/alcohol. The second one is a dual-fuel technology in which alcohol is supplied by injection to intake port of IC engine. Into the engine cylinder is delivered, nearly homogeneous, air–alcohol combustible mixture. The ignition is realized by the injected dose of diesel fuel before TDC. This technology requires the additional injection system, the separate fuel tank, lines and controls system [11, 12].
Ethanol fuel is one of the most interesting fuel among alcoholic fuels due to its relatively high value of LHV, lover value of her of evaporation than methanol and its availability. Ethanol is a biomass based renewable energy source, which can be produced with relatively low cost.

Ethanol can be produced using two methods: from petroleum materials (crude oil, natural gas or coal) using the chemical processes or from plant-based materials through alcohol fermentation of sugars such as glucose contained in biomass. Ethanol can be produced from any plants which contains of sugar or other components which can be converted into sugar, such as starch or cellulose in the fermentation, distillation and dehydration process [13]. Ethanol for a long time was considered as curious engine fuel. At first ethanol was associated with spark-ignition engines. From many years' ethanol is used as a fuel for compression ignition engines [14, 15].

Lee et al. [16] presented effects of varying the ethanol substitution ratio on engine performance and emissions under the dual-fuel combustion condition under various load conditions. The test engine was a heavy-duty single-cylinder diesel engine with two direct injectors. Engine speed was fixed at 1000 rpm and the load condition was varied for an indicated mean effective pressure (IMEP) ranging from 0.2 to 0.8 MPa. The ratio of ethanol to the total input energy was controlled from zero to nearly 50% of the input energy. The NO_x and PM emissions decreased with increasing ethanol substitution and the mean size of the PM emissions decreased. For the mid-load condition (IMEP 0.6 MPa), the substitution was increased to 63%, but for low and high loads, higher ethanol fractions could not be used because of insufficient ignition energy at low loads and sharp increment of the in-cylinder pressure under high loads. Pedrozo et al. [17] presented results of investigation of dual-fuel combustion in CI engine carried out from low to full engine load with the same engine hardware and identical operating conditions to those of the baseline engine. The experiments were executed on a single cylinder heavy-duty diesel engine at a constant speed of 1200 rpm and various steady-state loads between 0.3 and 2.4 MPa net indicated mean effective pressure (IMEP). Ethanol was port fuel injected while diesel was direct injected using a high pressure common rail injection system. The start of diesel injection was optimized for the maximum net indicated efficiency in both combustion modes. Varied ethanol energy fractions and different diesel injection strategies were required to control the in-cylinder pressure rise rate and achieve highly efficient and clean dual-fuel operation. In terms of performance, dual-fuel combustion attained higher net indicated efficiency than the conventional diesel combustion mode from 0.6 to 2.4 MPa IMEP, with a maximum

value of 47.2% at 1.2 MPa IMEP. The comparison also shows the use of ethanol resulted in 26% to 90% lower nitrogen oxides (NO_x) emissions than the conventional diesel combustion operation. At the lowest engine load of 0.3 MPa IMEP, the dual-fuel operation led to simultaneous low NO_x and soot emissions at the expense of a relatively low net indicated efficiency of 38.9%. In particular, the reduction in NO_x emissions introduced by the utilization of ethanol has the potential to decrease the engine running costs via lower consumption of aqueous urea solution in the selective catalyst reduction system. Moreover, the dual-fuel combustion with a low carbon fuel such as ethanol is an effective means of decreasing the use of fossil fuel and associated greenhouse gas emissions. Dong et al. [18] stated that in dual-fuel engines, the fuel stratification produced by direct in-cylinder blending of port injected and direct injected fuels is important for combustion and emission control, while the fuel stratification could be influenced by port fuel proportion, direct injection strategy as well as geometry of direct injector. Authors investigated ethanol/diesel dual-fuel engine. They studied influence in-cylinder fuel stratification as well as auto-ignition and combustion process. The equivalence ratio of premixed ethanol, maximum local equivalence ratio and fuel concentration gradients in radial and circumferential directions of the cylinder were used to evaluate the fuel stratification. Under the tested dual-fuel conditions, the results showed that auto-ignition was more likely to first occur in regions with mixture near stoichiometric ratio, rather than regions with mixtures exhibiting highest fuel reactivity. As a consequence, larger equivalence ratio of premixed ethanol could prolong ignition delay of in-cylinder charge by reducing the fuel reactivity of regions where ignition kernels first occurred. The experimental results showed that with reduced nozzle holes, the peak pressure and heat release rate of dual-fuel operation could be decreased. This was mainly because fewer nozzle holes could result in fuel stratification in both circumferential and radial directions, thus the development of combustion zone was slowed down and consequently the heat release rate was decreased [18]. Rakopoulos et al. [19] studied the impact of using n-butanol or ethanol in blends with diesel fuel (extenders) on combustion, cyclic irregularity, and exhaust emissions trade-off (balance). Experiments were conducted at two speeds and three loads in a fully-instrumented, six-cylinder, four-stroke, heavy-duty direct injection (HDDI), turbocharged, diesel engine. Authors stated that the ignition delay was increased for the n-butanol or ethanol diesel blends compared to the neat diesel cases, more so for the ethanol ones. The HRR traces of the n-butanol or ethanol diesel blends were delayed with respect to the neat diesel ones, more so for the ethanol ones. The cycle-to-cycle variations of the maximum pressure showed that there were small differences among the neat diesel fuel case and its two biofuels blends tested, inside acceptable limits. The little higher values for the ethanol and n-butanol diesel fuel blends signify that this may be due to their higher ignition delay values [19].

There are also works on the evaluation of combustion stability. Yao et al. presented results of investigates on cycle-to-cycle variation of dieseline fueled PPCI engine and introduces a closed-loop control method based on in-cylinder pressure sensor. Experiments were performed on a four-cylinder compression ignition engine. Results showed that p_{max} and θ_{pmax} (crank angle where occurs) cannot be properly identified by the control system. Thus, COV coefficient of variation) of p_{max} and θ_{pmax} cannot reflect the real combustion fluctuation level. COV_{IMEP} can be chosen as the combustion stability indicator to evaluate cycle-to-cycle variation. An et al. [20] investigated the sensitivity of combustion stability to the intake air temperature for partially premixed combustion (PPC). The experiments were carried out in a full view optical engine at low load condition. The results showed that the lower intake temperature could be used for achieving better combustion stability at low load condition along with the retarded CA50, the lower maximum in-cylinder pressure, and the higher IMEP. 70°C was the lower limit of intake temperature to achieve stable PPC operation with the single-injection strategy. The same trend of the combustion characteristics with respect to the start of injection timing was confirmed at various intake temperatures [21]. Zhou et al. studies gasoline compression ignition (GCI) engine as one of the most promising combustion concepts to maintain low pollutant emissions and high efficiency. However, low load combustion stability and firing in cold-start operations are two major challenges for GCI combustion. Strategies including negative valve overlap (NVO), advanced injection strategies, fuel reforming, and intake preheating have been proposed in order to solve these difficulties. The results showed that start of injection (SOI) during the intake stroke yields the best fuel economy, and injection during the compression stroke has the potential to extend the low load limit.

In presented work authors have attempted to assessment of combustion stability of co-combustion process of diesel fuel with ethanol in dual fuel compression ignition engine. The research concerned the analysis of the combustion process and the analysis of non-repeatability for set of subsequent engine operation cycles. The analysis was made for heat release rate, combustion stages and combustion stability.

2. Methods

2.1. Experimental test stand

The researches ware carried out on the compression ignition engine operated with constant rotational speed of 1500 rpm. It was one-cylinder air cooled, naturally aspired, direct injection compression ignition engine. This engine was modernized to work as dual fuel engine. It was equipped with the independent port fuel injection system. Ethanol was injected in the intake manifold at 3 bar pressure and the value of the fuel dose was determined by the time of opening the injector. The injection system was equipped with an electronic control system connected with the signal of the crankshaft position.

Test engine operated with constant angle of beginning of biodiesel fuel injection equal to 23 deg before TDC. The test bed is presented in Fig. 3. The main engine parameters are presented in Table 1.

The experimental studies were carried out on the test stand included elements:

- 1CA90 engine adapted for operating as a dual fuel engine,
- data acquisition system,
- exhaust gas analyzer: THC, CO, CO_2, O_2 – Bosch BEA 350 (THC: range 0–9999 ppm vol. accuracy: 12 ppm vol.; NO_x: range 0–5000 ppm accuracy: 10 ppm.; CO: range 0–10 %vol. accuracy: 0.06 %vol.; CO_2: range 0–18%vol. accuracy: 0.4%vol.; O_2: range 0–22%vol. accuracy: 0.1%vol.; λ: range 0.5–9.999 accuracy: 0.01).

The digital measurement system for data acquisition:

- piezoelectric pressure transducer, Kistler 6061 SN 298131, sensitivity: ±0.5%,
- charge amplifier, Kistler 5011B, the linearity of FS < ±0.05%,
- data acquisition module, Measurement Computing USB-1608HS – 16 bits resolution, sampling frequency 20 kHz,
- the CA encoder, resolution 360 pulses/rev, software for digital recording and analysis of the frequency signals [22].

Table 1. Main engine parameters

Parameter	Value	Unit
Number of cylinders	1	–
Displacement volume	0.573	dm^3
Bore	90	mm
Stroke	90	mm
Compression ratio	17:1	–
Crankshaft rotational speed	1500	rpm
Injection pressure	21	MPa
Injection timing	23	deg bTDC
Maximum rated power	7.4	kW

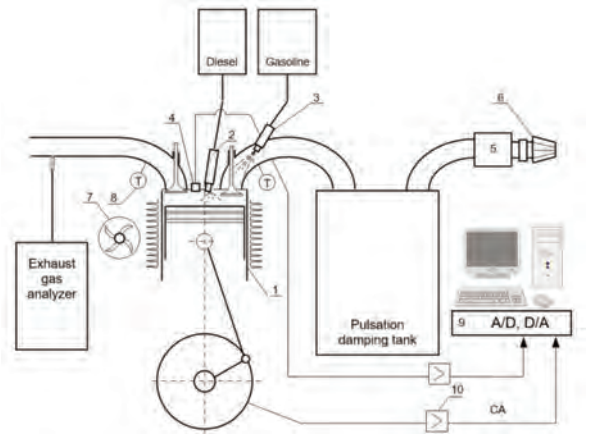

Fig. 1. Diagram of the experimental setup: 1 – engine, 2 – diesel fuel injector, 3 – ethanol fuel injector, 4 – in cylinder pressure sensor, 5 – intake air flowmeter, 6 – air filter, 7 – cooling fan, 8 – exhaust gases temperature sensor, 9 – PC with data acquisition system, 10 – crank angle sensor

In Table 2 are presented fuels properties. The diesel fuel ($C_{14}H_{30}$) was commercial fuel provided by the Polish Refinery and used commonly to feed diesel engines in cars. The fuel is a mixture of liquid hydrocarbons obtained through crude oil distillation. In the case of the diesel fuel, one of the important parameters is cetane number that denotes auto-ignition capabilities of the fuel. Ethanol (C_2H_5OH) is an alcohol with two carbon atoms in its structure. This fuel is obtained through processing of biological matter. Therefore, it can be considered a renewable energy source. This alcohol is numbered among strongly oxygenated alcohols and is characterized by a lower value of the LHV compared to conventional fuels. LHV of ethanol is lower in 40% compared to LHV of diesel's fuel. Therefore, to keep the constant energy dose, comparable to that contained in diesel fuel, bigger ethanol dose, in mass, should be provided. The high heat of vaporization (840 kJ/kg) improves filling coefficient but increases of ignition delay which can cause the "hard" operation of the engine.

Table 2. Fuels properties [4,9,10]

Properties	Diesel	Ethanol
Molecular formula	$C_{14}H_{30}$	C_2H_5OH
Molecular weight	170–198	46
Surface tension (mN/m @ 15°C)	26.9	21.78
Cetane number	51	8
Lower heating value, (MJ/kg)	41.7	26.9
Density at 20°C, kg/m^3	856	789
Viscosity at 25°C, (mPa s)	2.8	1.078
Heat of evaporation, (kJ/kg)	260	918
Stoichiometric air fuel ratio	14.7	9.06
Autoignition temperature, (°C)	300–340	698
Flash point, (°C)	78	16.6
Hydrogen content, wt %	13	13
Carbon content, wt %	87	52.2
Oxygen content, wt %	0	34.8

2.2. Calculation methodology

The analysis of combustion process was conducted on the basis of heat release. The heat release rate was calculated based on the data of in-cylinder pressure regarding crank angle. Analysis was based on the first law of thermodynamics and the equation of state.

The unrepeatability of IMEP (COV_{IMEP}) was used as a parameter determined the cycle-by-cycle variations. The COV_{IMEP} is directly related to the investigated combustion stability. The COV_{IMEP} was calculated based on set of IMEP values from 200 following work cycles of the test engine.

$$COV_{IMEP} = \frac{\sigma_{IMEP}}{(IMEP)_{mean}} \cdot 100 \tag{1}$$

where: σ_{IMEP} – standard deviation of IMEP.

Additionally, there are presented evaluation results of the probability density function of indicated mean effective pressure f(IMEP). This parameter can also be used as an indicator to assess the stability of operation of the internal combustion engine. The probability density of the indicated mean effective pressure:

$$f(IMEP) = \frac{1}{\sigma_{IMEP}\sqrt{2\pi}} \exp\left(\frac{-(IMEP_i - \overline{IMEP})^2}{2\sigma_{IMEP}^2}\right) \tag{2}$$

The paper also presents the results of analysis of combustion stages for both combustion systems. The time of ignition delay and the duration of combustion were determined.

3. Results and discussion

In the paper are presented results of experimental investigation of co-combustion process of ethanol with diesel fuel using dual fuel technology. At each test point, the en-

gine was fully warm up and its parameters were stabilized. The engine was run as long until the engine reached a constant temperature of the exhaust gases and invariable emission. The measurement system allowed for recording of the in-cylinder pressure with resolution of 1 deg CA of 200 engine operating cycles. It was recorded simultaneously: rotational speed of engine, air and fuel consumption, air temperature, fuel temperature, exhaust gas temperature, ambient temperature and pressure.

The examinations were started from indication of the engine fueled with pure diesel as a reference. In the next stage of the research, the engine was powered with ethanol of an energy content: 11.3, 18.5, 24.8, 33 and 55%. The tests were carried out at a constant angle of diesel injection start.

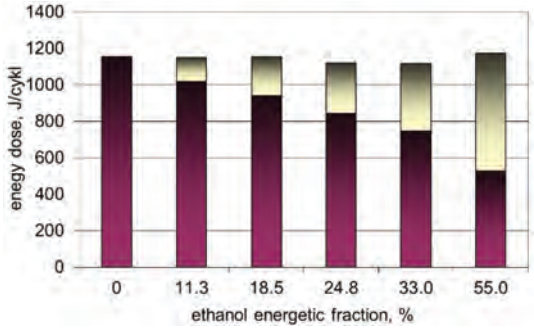

Fig. 2. The composition of the fuel dose

In Figure 2 are presented the fractions of energy dose delivered to the engine per one cycle. There are visible some variations in energy doses. It was due to uncertainty of power system. The variations were in range of 3% of energy content in fuel dose.

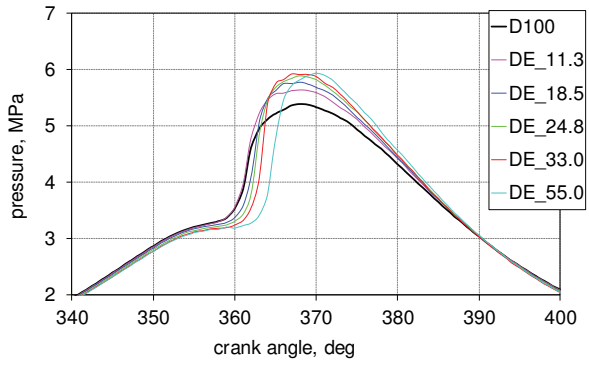

Fig 3. In-cylinder pressure

In Figure 3 are presented pressure changes for analyzed ethanol fractions. It is visible that with the increase in ethanol fraction in combustion process up to 33%, obtained the increase in peak pressure. In addition, this delayed the combustion process. With 55% ethanol fraction, the combustion process has been deteriorated which was accompanied by the increase in SFC. There it is clearly visible cooling effect of evaporation ethanol during compression stroke.

In Figure 4 are presented heat release rate traces for analyzed ethanol fractions. Up to 20% of ethanol fraction noticed increase in peak value of HRR. It was due to an increase in ignition delay. After exceeding this ethanol content, a drop in the maximum value of HRR was observed and the combustion process was significantly extended.

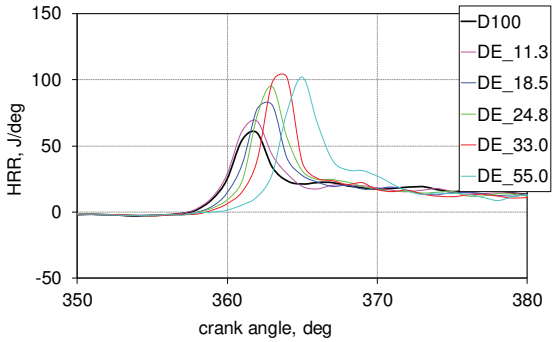

Fig 4. Heat release rate

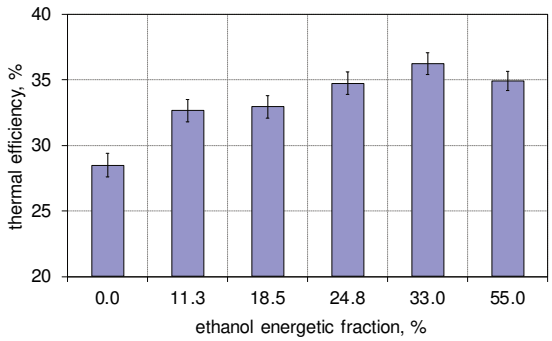

Fig. 5. Thermal efficiency

In Figure 5 are presented thermal efficiency values for analyzed ethanol fraction. It can be stated that with the increase in ethanol content in air-fuel mixture the thermal efficiency increased, it was up to 33% of ethanol fraction.

One of the fundamental problems in combustion engines domain, which has been researched from many years, is non-repeatability of work cycles. Researchers have studied the unrepeatability of engine cycles based on the analysis of combustion pressure [23].

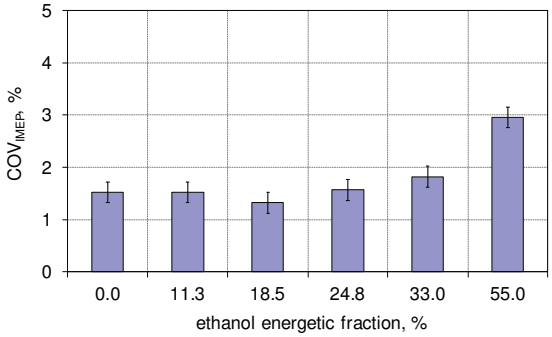

Fig. 6. Coefficient of cycle unrepeatability

In Figure 6 are presented results of cycle-to-cycle variations expressed by COV_{IMEP}. COV_{IMEP} is usually used as the indicator of combustion stability [24]. The threshold value of COV_{IMEP} equal to 5% is considered to provide engine stability [25]. It can be stated that up to 33% of ethanol content in combustion process the cycle-to-cycle

variation were at constant level. For the last ethanol fraction it was observed the increase in COV_{IMEP}. It should be noted that for the entire analyzed range of ethanol fraction the COV_{IMEP} was below 5%.

The combustion process in the internal combustion engine can be divided into two main phases. The first it is ignition delay and second the combustion duration. According to the classic ignition theory by Semenov, compression ignition is characterized by the initial period when the key role is played by chemical reactions before ignition. The physical phenomena which lead to ignition delay in compression ignition engines include decomposition of fuel into separate drops, heating and vaporization of drops and, finally diffusion of fuel vapor into the air. Speed of burning of the liquid fuel is determined by the speed of its vaporization and mixing of the sprayed fuels with air. The ignition delay is defined as the time between the start of diesel fuel injection and the crank angle of 10% heat release. This delay period consists of physical delay and chemical delay which occur simultaneously. In the physical delay takes place atomization, vaporization and mixing of air fuel, and in the chemical delay attributed pre-combustion reactions. Burn duration is calculated as the time from 10 to 90% of heat release.

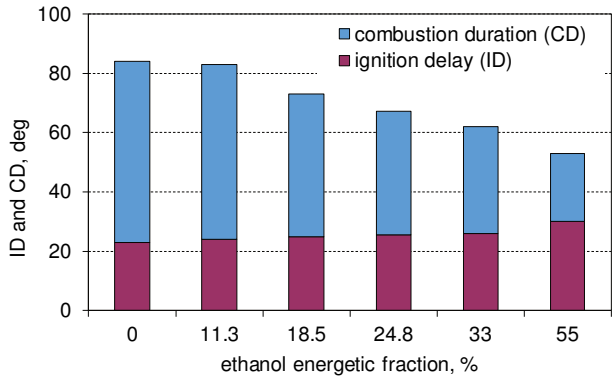

Fig 7. Stages of combustion process

In Figure 7 are presented the combustion stages for diesel/ethanol combustion. It can be stated that with the increase in ethanol content in combustion process the ignition delay increased which also was confirmed by other researchers [26, 27]. However, this increase is not too big. Compared to reference fuel combustion the increase in ID was from 23 to 30 deg. The increase was near to 25%. In case of combustion duration with the increase in ethanol content the combustion time decreased. Compared to reference fuel combustion the increase in ID was from 61 to 23 deg. That the decrease in burning time was over 100%. The study also assessed the uniqueness of the ignition delay and the combustion duration (Fig. 8). The ID and CD values shown in Fig. 8 are determined for the average MFB obtained from 200 consecutive engine cycles.

In Figure 8 is presented set of MFB curves for 55% of ethanol fraction in combustion process. There are indicated intervals of spread of ignition time (SOI) and spread of the end of combustion (SEC). The results of this analysis are presented in Fig. 9.

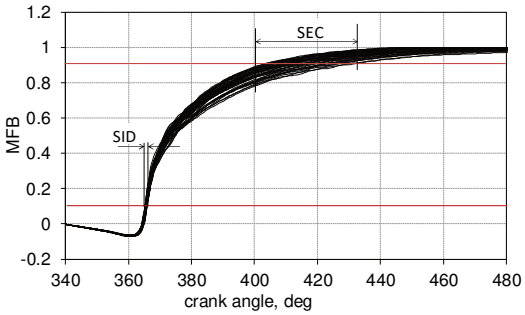

Fig. 8. Mass fraction burned for co-combustion of diesel fuels with ethanol (for 55% of ethanol fraction)

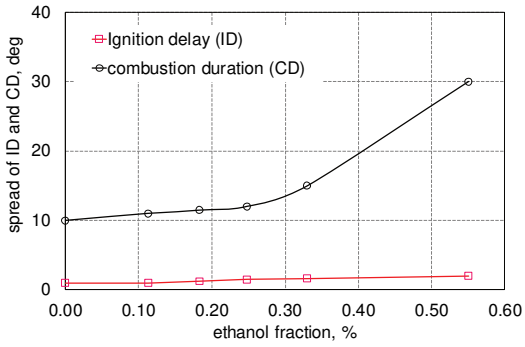

Fig. 9. Spread of ignition delay and combustion duration

In Figure 15 are presented results of spread estimation of MFB. It is directly connected with unrepeatability of combustion process in the IC engine. It can be stated that ethanol participation in combustion of fuels does not affect spread of ignition delay. The distribution of ID was within 2 deg of CA. In case of spread of combustion duration with the increase in ethanol content this indicator was increased. After exceeding the 30% ethanol content noticed significant increase in this parameter. For 0.50 ethanol content noticed 3-times higher value of spread of CD, and it was equal to30 deg of CA.

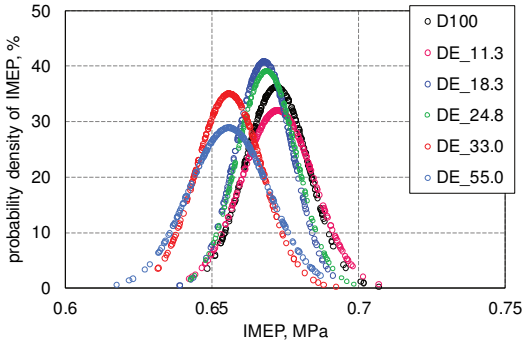

Fig. 10. Probability density of IMEP

In Figure 10 are presented results of assessment of probability density of IMEP. It is visible that for 0.30 ethanol energetic fraction noticed high combustion stability and spread of IMEP was not wider than for reference fuel combustion. After exceeding this ethanol fraction it was visible enlargement of spread of IMEP.

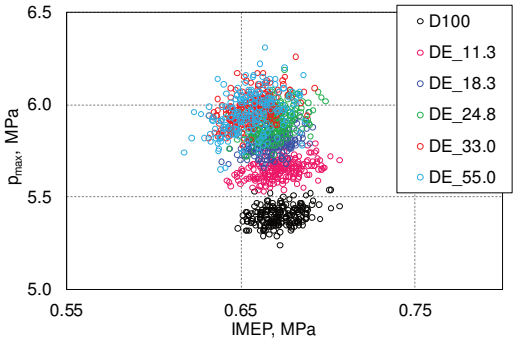

Fig. 11. Relationship of IMEP and p_{max}

In Figure 11 is presented relationship between IMEP and peak pressure value. It presented the correlation between the maximum combustion pressure and the indicated mean effective pressure for an engine powered by pure diesel fuel and a dual fuel engine for co-combustion of diesel with ethanol. It can be stated that with the increase in ethanol energetic fraction the peak pressure values increased. Additionally, with the increase in ethanol content increases the spread of these values.

4. Conclusions

Ethanol used to power IC engines reduce the use of fossil fuels. This study presents experimental results of a CI engine investigation with dual-fuel system, in which co-combustion of diesel with ethanol with energy content up to 55%. The research included the analysis of the combustion process and the analysis of the non-repeatability of the subsequent engine operation cycles. On the basis of results were formed conclusions:

- ethanol used for co-combustion with diesel fuel causes an increase in compression ignition delay and increases the heat release rate and maximum combustion pressure values;
- up to 33% of ethanol content in combustion process the cycle-to-cycle variation were at constant level 1.5–1.8%; for the maximal ethanol fraction it was observed the increase in COV_{IMEP},
- with the increase in ethanol content in combustion process the ignition delay increased but combustion duration decreased;
- on the basis of the function of probability density of the IMEP, it can be stated that the increase in the percentage of ethanol fuel used for co-combustion with diesel does not worse ignition capabilities; the spread of ID was within 2 deg of CA;
- the spread of CD with the increase in ethanol content it was increased. After exceeding the 30% ethanol content noticed significant increase in this parameter. For 0.50 ethanol content noticed 3-times higher value of spread of CD, and it was equal to 30 deg of CA;
- with the increase in ethanol energetic fraction the peak pressure values and the spread of these values increased.

Acknowledgements

Research was financed by the Ministry of Science and Higher Education of Poland from the funds dedicated to scientific research No. BS/PB 1-103-3030/2017/P

Nomenclature

CA	crank angle
CI	compression ignition
CD	combustion duration
ID	ignition delay
IMEP	indicated mean effective pressure
COV	coefficient of variation
LHV	lower heating value
DE	diesel/ethanol
HRR	heat release rate
IC	internal combustion
MFB	mass fraction burned

Bibliography

[1] SZABADOS, G., BERECZKY, Á., AJTAI, T., BOZÓKI, Z. Evaluation analysis of particulate relevant emission of a diesel engine running on fossil diesel and different biofuels. *Energy*. 2018, **161**, 1139-1153. DOI:10.1016/j.energy.2018.07.154

[2] MERKISZ, J., WALIGÓRSKI, M. Strategy of the combustion process diagnosis in direct injection engines. *Procedia Engineering*. 2014, **96**, 294-301. DOI:10.1016/j.proeng.2014.12.141

[3] KUMAR, S., CHO, J.H., PARK, J., MOON, I. Advances in diesel–alcohol blends and their effects on the performance and emissions of diesel engines. *Renewable and Sustainable Energy Reviews*. 2013, **22**, 46-72.

[4] JAMROZIK, A. The effect of the alcohol content in the fuel mixture on the performance and emissions of a direct injection diesel engine fueled with diesel-methanol and diesel-ethanol blends. *Energ Convers Manage*. 2017, **148**, 461-476.

[5] MERKISZ, J., FUĆ, P., LIJEWSKI, P., PIELECHA, J. Actual emissions from urban buses powered with diesel and gas engines. *Transportation Research Procedia*. 2016, **14**, 3070-3078. DOI:10.1016/j.trpro.2016.05.452

[6] FAYYAZBAKHSH, A., PIROUZFAR, V. Comprehensive overview on diesel additives to reduce emissions, enhance fuel properties and improve engine performance. *Renewable and Sustainable Energy Reviews*. 2017, **74**, 891-901. DOI:10.1016/j.rser.2017.03.046

[7] KUMAR, S., CHO, J.H., PARK, J., MOON, I. Advances in diesel–alcohol blends and their effects on the performance and emissions of diesel engines. *Renewable and Sustainable Energy Reviews*. 2013, **22**, 46-72.

[8] TUTAK, W., JAMROZIK, A., GNATOWSKA, R. Combustion of different reactivity fuel mixture in a dual fuel engine. *Therm Sci*. 2018, **22**(3), 1191-1203. DOI:10.2298/TSCI170606299T.

[9] TUTAK, W. Bioethanol E85 as a fuel for dual fuel diesel engine. *Energy Conversion and Management*. 2014, **86**, 39-48. DOI: 10.1016/j.fuel.2017.04.021

[10] TUTAK, W., LUKÁCS, K., SZWAJA, S., BERECZKY, Á. Alcohol–diesel fuel combustion in the compression ignition engine. *Fuel*. 2015, **154**, 196-206.
[11] STELMASIAK, Z., MATYJASIK, M. Simulation of the combustion in a dual fuel engine with a divided pilot dose. *Combustion Engines*. 2012, **151**(4), 43-54.
[12] MIKULSKI, M., BEKDEMIR, C. Understanding the role of low reactivity fuel stratification in a dual fuel RCCI engine – A simulation study. *Applied Energy*. 2017, **191**, 689-708. DOI: 10.1016/j.apenergy.2017.01.080
[13] AYDIN, H., ILKILIÇ, C. Effect of ethanol blending with biodiesel on engine performance and exhaust emissions in a CI engine. *Applied Thermal Engineering*. 2010, **30**, 1199-1204.
[14] STELMASIAK, Z., MATYJASIK, M. Exhaust emissions of dual fuel self-ignition engine with divided initial dose. *Combustion Engines*. 2013, **154**(3), 944-952.
[15] HUNICZ, J., MIKULSKI, M. Investigation of the thermal effects of fuel injection into retained residuals in HCCI engine. *Applied Energy*. 2018, **228**, 1966-1984. DOI:10.1016/j.apenergy.2018.07.075
[16] JEONGWOO LEE, SUNYOUP LEE, SEOKHWAN LEE, Experimental investigation on the performance and emissions characteristics of ethanol/diesel dual-fuel combustion. *Fuel*. 2018, **220**, 72-79.
[17] VINÍCIUS, B. PEDROZO, IAN MAY, WEI GUAN, HUA ZHAO. High efficiency ethanol-diesel dual-fuel combustion: A comparison against conventional diesel combustion from low to full engine load. *Fuel*. 2018, **230**, 440-451.
[18] SHIJUN DONG, ZHAOWEN WANG, CAN YANG et al. Investigations on the effects of fuel stratification on autoignition and combustion process of an ethanol/diesel dual-fuel engine. *Applied Energy*. 2018, **230**, 19-30.
[19] RAKOPOULOS, C.D., RAKOPOULOS, D.C., KOSMADAKIS, G.M. et al. Experimental comparative assessment of butanol or ethanol diesel-fuel extenders impact on combustion features, cyclic irregularity, and regulated emissions balance in heavy-duty diesel engine. *Energy*. 2019, **174**, 1145-1157.
[20] YANZHAO AN, VALLINAYAGAM RAMAN, QINGLONG TANG et al. Combustion stability study of partially premixed combustion with low-octane fuel at low engine load conditions. *Applied Energy*. 2019, **235**, 56-67.
[21] LEI ZHOU, JIANXIONG HUA, HAIQIAO WEI, YIYONG HAN. An experimental investigation on low load combustion stability and cold-firing capacity of a gasoline compression ignition engine. *Engineering*. 2019, **5**. DOI: 10.1016/j.eng.2018.12.010
[22] GRUCA, M. Software for acquisition of internal combustion engine data. *Journal of Kones*. 2004, **11**, 205-211.
[23] TUTAK, W., JAMROZIK, A., Characteristics of the flow field in the combustion chamber of the internal combustion test engine. *Chemical and Process Engineering*. 2011, **32**(3), 203-214. DOI:10.2478/v10176-011-0016-4
[24] CHANGSHENG, YAO, YAODONG, HU, TIANYUAN, ZHOU et al. Combustion stability control of dieseline PPCI based on in-cylinder pressure signals. *IFAC-PapersOnLine*. 2016, **49-11**, 333-339.
[25] Heywood J.B. Internal Combustion Engine Fundamentals. *Mc Graw Hill*, 2018.
[26] KUSZEWSKI, H. Experimental investigation of the autoignition properties of ethanol–biodiesel fuel blends. *Fuel*. 2019, 235, 1301-1308. DOI:10.1016/j.fuel.2018.08.146.
[27] KUSZEWSKI, H., JAWORSKI, A., USTRZYCKI, A. et al. Use of the constant volume combustion chamber to examine the properties of autoignition and derived cetane number of mixtures of diesel fuel and ethanol. *Fuel*. 2017, **200**, 564-575.

Łukasz Nowak, DEng. – Faculty of Mechanical Engineering and Computer Science, Czestochowa University of Technology.
e-mail: *luknowak@imc.pcz.pl*

Wojciech Tutak, DSc., DEng. – Faculty of Mechanical Engineering and Computer Science, Czestochowa University of Technology.
e-mail: *tutak@imc.pcz.pl*

Article citation info:
GIS, W., WAŚKIEWICZ, J., MENES, M. Experts forecasts on the demand for energy carriers in motor vehicle transport in Poland up to year 2035. *Combustion Engines*. 2019, **178**(3), 162-165. DOI: 10.19206/CE-2019-328

Wojciech GIS
Jerzy WAŚKIEWICZ
Maciej MENES

CE-2019-328

Experts forecasts on the demand for energy carriers in motor vehicle transport in Poland up to year 2035

Presentation of the number of passenger cars, vehicles other than passenger cars with GVM up to 3.5 tons and above 3.5 tons (trucks, buses and special vehicles), registered in Poland as at the end of 2015, with types of energy carriers. Forecasts of transport performance of the vehicle fleet and the forecast of the fleet volume in Poland by year 2035. Expert forecasts of energy carriers consumption (petrol, diesel oil, LPG, CNG, electric power, hydrogen) up to year 2035.

Key words: *energy, forecast, vehicle, transport, passenger cars*

1. Introduction

Forecasts of the demand for energy carriers (activities) by motor transport basically arise from the draft Ordinance of the Council of Ministers of 23 December 2011 regarding the scope of information to be included in forecasts of changes in activity in respective sectors of industry. As a result, the Ministry of Infrastructure – among others – is required to submit a forecast to fulfil the authorisation laid down in Art. 9 (3) of the Act on the management of greenhouse and other substances emissions of 17 July 2009 (Journal of Laws of 2017, item 2.8.6).

Exhibit no. 17 to the draft ordinance relating to the scope of the 20-year forecast of the activity of road transport as volumes characterising the said activity lists the following:

- consumption of fuels by passenger cars, including:
  - petrol [Mg], diesel oil [Mg], liquified gas (LPG) [Mg], biodiesel [Mg],
  - bioethanol [Mg], natural gas (LNG) [Mg], electrical energy [MWh], hydrogen [Mg],
- consumption of fuels by vehicles other than passenger cars with mass up to 3.5 tons, including:
  - petrol [Mg], diesel oil [Mg], liquified gas (LPG) [Mg], biodiesel [Mg],
  - bioethanol [Mg], natural gas (LNG) [Mg], electric energy [MWh], hydrogen [Mg],
- consumption of fuels by vehicles with mass above 3.5 tons, including: diesel oil, biodiesel.

The scope of forecasts relates to every group of vehicles separately (as listed in Exhibit no. 17 to the draft Ordinance), i.e.:

- passenger cars,
- vehicles other than passenger cars with mass up to 3.5 tons,
- vehicles with mass above 3.5 tons.

This publication focuses on experts' forecasts of the demand for energy carriers by the Polish vehicle fleet [1] up to year 2035.

The specified group of "vehicles other than passenger cars with mass up to 3.5 tons" includes the following subgroups:

- trucks with GVM up to 3.5 tons,
- special vehicles with GVM up to 3.5 tons,
- buses with GVM up to 3.5 tons,
- "Vehicles with mass above 3.5 tons" includes the following sub-groups:
  - trucks with GVM above 3.5 tons, including trucks with trailers,
  - buses with GVM above 3.5 tons (country, city, tourist),
  - special vehicles with GVM above 3.5 tons (with a different usage range).

The forecasts of the consumption of energy carriers was prepared based on the methodology proposed by MTI and adopted by the Department of the Transport Policy & International Affairs of the Ministry of Transport, Construction and Marine Economy in 2011 [2, 8].

The applied method of predicting the demand for energy carriers by the Polish vehicle fleet in relevant years of the forecast must consider three primary factors determining the volume of the demand and relating to specified subgroups of vehicles, i.e. forecasts of the number of vehicles, forecasts of average annual mileage of vehicles, forecasts of average consumption of energy carriers per 100 km of mileage.

This publication uses the results of the forecasts of demand for transport services in Poland by year 2030 made at the Gdańsk University in 2017. Anticipating the development of the sector's activity in 2035, the trends for years 2015-2030 were used expertly, those trends quantified in the cited forecast paper. The aforementioned forecast comprises numbers of registered vehicles in Poland as at the end of 2015 quoted by official statistical sources – the Main Statistical Office [GUS]. Those data have been determined based on the data of the Central Vehicles Register (CEP). When balancing the fuels (petrol, diesel oil and LPG) consumed by motor transport in 2015, the balance values provided by KOBiZE [The National Centre for Emissions Management] have been used [3].

2. Forecast of the number of vehicles by types of energy carriers

2.1. Passenger cars

Considering – among others – the general predicted data regarding passenger cars ("pessimistic variant of the prog-

nosis of the Gdańsk University of 2017) and considering the conditions and assumptions adopted by the experts as regards the development of the fleet of passenger cars in Poland in terms of number in a breakdown into types of energy carriers up to year 2035, the forecast numbers of passenger cars was presented (Fig. 1).

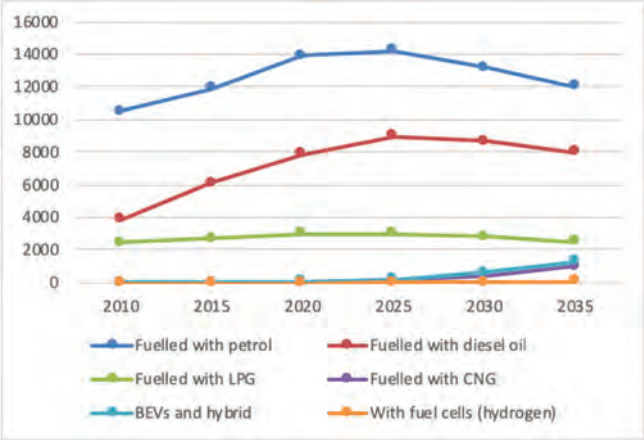

Fig. 1. Forecasted number of passenger cars in Poland up to year 2035 by types of energy carriers [in thousands]

According to the forecasts within the period of the forecast passenger cars equipped with petrol engines and cars fuelled with diesel oil would continue to dominate in Poland, however their share in the structure of the total passenger cars fleet is expected to drop. It is also expected that passenger cars equipped with engines fuelled with natural gas will develop. Similarly, the share of electrical vehicles and hybrids is expected to grow, with PHEV (plug-in) among hybrid vehicles in the 2035 perspective.

2.2. Vehicles other than passenger cars according to GVM groups

The number of vehicles other than passenger cars with GVM up to 3.5 tons in forecasts up to year 2035 according to types of energy carriers is shown in graph 2 below.

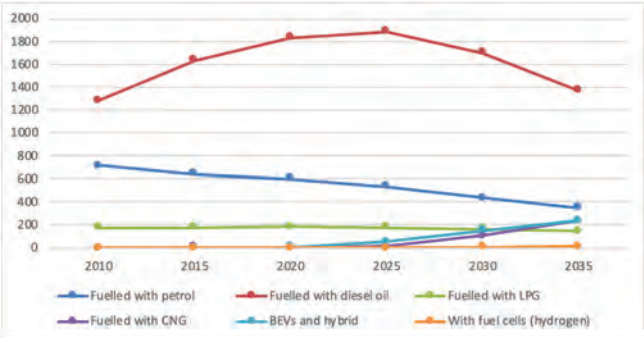

Fig. 2. Forecasts of number of vehicles other than passenger cars with GVM up to 3.5 tons by types of energy carriers in Poland up to year 2035

The number of trucks and buses in the forecasts up to year 2035 was determined based on the volume of the predicted transport performance [4] of those vehicles and the predicted average transport efficiency of statistical vehicles.

In 2015 the motor truck fleet with GVM up to 3.5 tons accounted for approx. 71% of the overall number of trucks registered in Poland. The forecast assumes that the share of vehicles with petrol-fuelled engines in the structure of trucks with 3.5-ton GVM is expected to continue falling as well as that of vehicles with bi-fuel engines.

The expected development of the natural gas distribution network will allow for increasing the use of that fuel in motor transport, including also trucks with up to 3.5 tons GVM.

It is expected that within the period of the forecast the use of electrical and hybrid (combustion-electrical) vehicles [5, 9] should to some extent increase in the fleet of trucks with GVM up to 3.5 tons. Those vehicles will be used mainly as delivery vehicles in areas inaccessible (due to administrative decisions) to diesel-fuelled vehicles.

The 2035 forecast also assumes a minor share of trucks with GVM up to 3.5 ton with fuel cells powered with hydrogen.

The share of trucks with GVM up to 3.5 tons fuelled with diesel oil is expected to dominate but will tend to drop.

From 2025 onwards, considering the forecasted increase in the demand for bus transport services in country transport and the statutory obligation of local authorities to provide public transport in towns presently devoid of public transport, the number of buses with GVM up to 3.5 tons is expected to increase to a certain extent.

As regards buses with GVM up to 3.5 tons, the number of petrol-fuelled buses and buses equipped with bi-fuel engines (LPG) will definitely decrease in the structure of the registered buses fleet. The said fuelling system will be replaced gradually by natural gas fuelling (CNG and LNG). The relatively dynamic development of buses with GVM up to 3.5 tons fuelled with natural gas and electrical and hybrid (combustion – electric) buses stems mainly from the administrative requirements shaped by environmental factors, i.e. limited access to chosen zones for vehicles with conventional combustion engines.

In 2015 among special vehicles with GVM up to 3.5 tons, vehicles with petrol-fuelled engines accounted for 2/2 in the fuel structure of the vehicle fleet. In the period of the forecast the share of vehicles with engines fuelled with natural gas (CNG and LNG) and BEVs or hybrid vehicles (with combustion – electric engines) is assumed to increase.

As regards trucks with GVM above 3.5 tons it is expected that this category of vehicles will be equipped – within the period of the forecast – mostly with diesel-fuelled engines with a minor share of natural gas and electric energy (2–3%).

As regards buses wit GVM above 3.5 tons, considering the EU policy aimed at achieving high environmental standards, over the period of the forecast among energy carriers the importance of natural gas (CNG and LNG) and electric energy is expected to grow. Except that natural gas (also biomethane) – besides diesel oil – will be used in city and country bus transport, whereas electric energy will be used mainly in city transport (BEV and hybrid buses) owing to efforts to limit combustion emissions in the area of – e.g. city centres. However, it should be noted that in the general balance of exhaust gases emission the use of vehicles with electric engines when electrical energy is and will be produced in Poland chiefly from coal, is not favourable for the environment.

Buses fuelled with natural gas characterise with very good combustion emission parameters and moreover – are much more cost-effective compared to the presently promoted electrical buses [6]. Art. 64 (4) of the draft Act on Electromobility stipulates that in 2028 every third bus in city transport should be an electric bus. Electric vehicles – according to the provisions of the draft act – also include hybrid vehicles (with combustion & electric engines).

Because of the safety issue, i.e. the reliability of the city bus transport – in the opinion of city transport specialists' electrical buses in the bus fleet should not be expected to account for more than 1/3. This matter relates to BEV buses.

Apart from the aforementioned energy carriers the use of which most likely will grow in the forthcoming decades, attention should be given to hydrogen. Hydrogen is a fuel used – among others – in city bus transport to power fuel cells producing electric energy used by electric engines, in this case – buses. According to Polish expert opinions as many as 100 buses with fuel cells may be used in 2030 in Poland [7].

In 2015 among a total number of 134.3 thousand special vehicles registered in Poland with GVM above 3.5 tons, just 0.1% was fuelled with methane (CNG). By 2035 the use of that fuel is expected to increase considerably in special vehicles with GVM above 3.5 tons, i.e. up to 15% of the said fleet.

The number of vehicles other than passenger cars with GVM above 3.5 tons according to forecasts up to year 2035 by types of energy carriers is shown in Fig. 3.

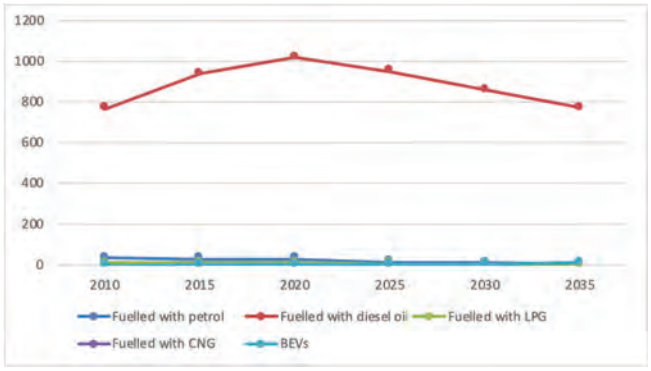

Fig. 3. Number of vehicles other than passenger cars with GVM above 3.5 tons by types of energy carriers in Poland in 2010 and 1015 and in the forecast up to year 2035

3. Forecasts regarding the need for energy carriers

A summary of the results of the estimated energy carrier's consumption by the Polish vehicle fleet in 2015 and experts' forecasts in this respect up to year 2035 are presented in Table 1.

4. Conclusions

Conclusions following the experts forecast of the demand for energy carriers of the Polish vehicle fleet in 2035 in view of the accepted assumptions are as follows:

– the demand for petrol is expected to come to approx. 3835 Gg and show a falling tendency,
– the demand for diesel oil is expected to amount to c.a. 10780 Gg and will also show a falling tendency,
– the demand for liquified petroleum gas (LPG) is expected to come to approx. 1360 Gg and show a falling tendency,
– the demand for natural gas in 2035 is estimated at roughly 1780 Gg and will be greater than the demand for LPG,
– the demand for hydrogen to power fuel cells in EVs equipped with such cells may account for as much as 37 Gg,
– the demand for electric energy to charge batteries in BEVs is expected to be equal to approx. 4806 GWh in 2035.

The mass of bio-components of fuels, i.e. esters of plant oils (biodiesel and bioethanol) – estimated and presented in Table 1 – is included respectively in the demanded mass of diesel oil and petrol to fuel motor engines estimated for 2015 and forecasted up to year 2035.

Table 1. Summary of the results of estimates regarding the consumption of energy carriers by the Polish vehicle fleet in the year 2035

Characteristics feature			Unit	2015	Forecast		
					2025	2030	2035
Transport services		Trucks	mln tkm	273107	328000	329000	329000
		Buses	mln pas km	51500	42600	51700	57800
		Passenger cars	mln pas km	221000	307000	313000	340000
Consumption of energy carriers	Passenger cars	Petrol	Gg	3196	3887	3789	3741
		Diesel oil	Gg	3413	4942	4797	4430
		LPG	Gg	1261	1391	1317	1182
		Biodiesel	Gg	341	692	768	797
		Bioethanol	Gg	160	544	644	748
		Natural gas	Gg	4	101	271	681
		Electric energy	GWh	11	341	1189	3175
		Hydrogen	Gg	0	0.3	4.5	30
	Vehicles other than passenger cars with mass up to 3.5 tons	Petrol	Gg	179	135	112	93
		Diesel oil	Gg	1546	2280	2281	2025
		LPG	Gg	210	227	210	183
		Biodiesel	Gg	155	308	342	334
		Bioethanol	Gg	9	19	19	19
		Natural gas	Gg	3	26	211	535
		Electric energy	GWh	1.3	193	701	1306
		Hydrogen	Gg	0.00	0.02	0.27	2.70
	Vehicles with mass above 3.5 tons	Diesel oil	Gg	4325	4653	4585	4323
		Biodiesel	Gg	432	628	688	713
		Natural gas	Gg	9	60	241	561
		Hydrogen	Gg	0	0	1.3	4.1
		Electric energy	GWh	15	73.1	185.3	325.8
Consumption of energy carriers by the vehicle fleet in total		Petrol	Gg	3375	4023	3901	3835
		Diesel oil	Gg	9284	11875	11663	10778
		LPG	Gg	1471	1617	1527	1364
		Biodiesel	Gg	928	1603	1749	1778
		Bioethanol	Gg	169	563	663	767
		Natural gas	Gg	16	187	722	1777
		Electric energy	GWh	27	607	2075	4806
		Hydrogen	Gg	0	0.32	6.0	36.8

Nomenclature

BEV	Battery Electric Vehicle
CEP	Central Vehicles Register
CNG	Compressed Natural Gas
EV	Electric Vehicle
GUS	the Main Statistical Office
GVM	Gross Vehicle Weight
LPG	Liquefied Petroleum Gas

Bibliography

[1] The "Polish vehicle fleet" is understood as vehicles registered in Poland, owned by individuals and business entities.

[2] WAŚKIEWICZ, J., RADZIMIRSKI, S., TAUBERT, S. Opracowanie metodologii prognozowania zmian aktywności sektora transportu drogowego (w kontekście ustawy o systemie zarządzania emisjami gazów cieplarnianych i innych substancji. *Study of MTI* no. 7101/ZBE, November 2011. Study performed for MTBiGM pursuant to contract no. 0270/2011 of 29 July 2011.

[3] TAUBERT, S. Bilans paliw z transportu drogowego w 2015 r. *Study of MTS* no. 11610/COŚ; Warsaw, July 2017.

[4] The „minimum" variant of the transport performance of trucks and the „maximum" variant as regards far-distance bus transport and the „optimistic" variant as regards city bus transport in the forecast of the Gdańsk University of 2017.

[5] The official statistics (Main Statistical Office – GUS) do not distinguish BEVs and hybrid (combustion & electric) vehicles.

[6] According to Adam Karolak, President of the Economic Chamber of Urban Transport [IGKM]; www.infor.pl.

[7] GIS, W., MENES, E., WAŚKIEWICZ, J. et al. Przesłanki narodowego planu wodoryzacji transportu samochodowego w Polsce [Prerequisites of the national plan of hydrogenisation of motor transport in Poland] Report prepared within the framework HIT-2 Corridors project implemented by an international consortium; Project co-financed under EU funds within the scope of TEN-T; Study financed from the funds for science in 2015 granted for an international project co-financed by the Ministry of Science and Higher Education; Paper of the Motor Transport Institute no. 5502/ITS, Warsaw, November 2015.

[8] MERKISZ, J., GIS, M. The growth in the use of methane fuel for fuelling urban buses. *10th Conference on Interdisciplinary Problems in Environmental Protection and Engineering (EKO-DOK)*. Polanica Zdroj, Poland, 16-18 April 2018.

[9] GIS, W., PIELECHA, J., WASKIEWICZ, J. et al. Use of certain alternative fuels in road transport in Poland. *Scientific Conference on Automotive Vehicles and Combustion Engines (KONMOT)*. Krakow, 22-23 September 2016.

Wojciech Gis, DSc., DEng. – Prof. ITS, Motor Transport Institute.
e-mail: *wojciech.gis@its.waw.pl*

Jerzy Waśkiewicz, DSc., DEng. – Motor Transport Institute.
e-mail: *jerzy.waskiewicz@its.waw.pl*

Maciej Menes, MSc. – Motor Transport Institute.
e-mail: *maciej.menes@its.waw.pl*

Article citation info:
ŚLIWIŃSKI, K., MAREK, W. The use of glycerin as motor fuel. *Combustion Engines*. 2019, **178**(3), 166-172.
DOI: 10.19206/CE-2019-329

Krzysztof ŚLIWIŃSKI
Wojciech MAREK

CE-2019-329

The use of glycerine as motor fuel

Glycerine as waste from production accounts for about 10% of the obtained amount of biodiesel. It is a very attractive substance for the industry, however, currently the industry is not able to absorb such a large amount of glycerine produced during the production of fuel. Therefore, one should look for other ways of disposing of glycerol with simultaneous benefit in the form of energy yield or useful products / semi-finished products. The development of glycerine is necessary due to the continuous development of the biofuel market. In the near future, surplus glycerine may pose serious problems in the growth of biodiesel production. The publication presents the results of scientific research on the use of liquid technical glycerine and its processing products in the gasification process, as engine fuel.

Key words: *internal combustion engines, glycerol, reforming processes, syngas, waste energy.*

1. Glycerine as an environmental problem

Glycerine (glycerol) is one of the simplest trihydric alcohols. In pure form, it appears as a colorless, odorless, dense, hygroscopic liquid with a boiling point of 290°C. It is well soluble in water and alcohols.

Glycerine is used in the pharmaceutical, cosmetics, food and chemical industries as a raw material for the production of plastics, cooling liquids and explosives.

In the modern world of motoring, where an ever stronger emphasis is placed on ecology, the share of fuels from renewable sources increases in place of existing fossil fuels. During the production of methyl or ethyl esters of fatty acids, constituting 3–20% of the biofuel additive, per ton of product is 90 to 110 kg of waste glycerine. Production of glycerine in 2005 reached 3.18 million tons. By 2020, biofuels are to constitute 20% of EU fuel fuels. In the US, diesel oil consumption is about 61 billion gallons annually, which assuming a 3% addition of biocomponents to biodiesel results in production of 810 thousand. t glycerol annually [5]. With the economy's demand for glycerine of approx. 224,000 tons per year means a 4-fold surplus of production.

The crude glycerol obtained in the production of biodiesel, before the traditional process of utilization in a sewage treatment plant, must be subjected to purification, which results in additional costs included in the price of fuel production. In addition, the glycerine must be diluted so that it does not poison the biological deposit in the sewage treatment plant by increasing its volume.

If it is intended for the food or pharmaceutical industry, it must be subjected to additional purification processes consisting in the removal of acrolein-insoluble impurities and dehydration in order to meet the relevant standards. Cleansing glycerol from acrolein is not a problem, because it has high volatility.

Acrylic acid is already produced from acrolein. Acrylic acid is used for the production of polymers. A significant part is used for the production of absorbents for diapers and sanitary napkins. Ethylene glycol is used in fluids as a non-freezing factor in engine cooling systems as well as cooling and heating systems. It is also used for the production of polyester resins, synthetic fibers, solvents, plasticizers and explosives. Nevertheless, this relationship is toxic and dangerous to life. It is withdrawn and replaced by propylene glycol, which is not toxic. At present, the methods for producing propylene glycol are based on the production of propylene oxide. In the years 2003-2006, a team of scientists from the USA improved the method of producing propylene glycol from glycerine making it much cheaper and safer.

The process of purification of glycerine obtained as waste from the production of biodiesel is highly energy-consuming, increasing the cost of its production. Table 1 illustrates the use of glycerine in the purified state.

Table 1. Share of glycerine applications in the market [5]

Application	Percentage on the market
pharmaceutical and cosmetics	26
esters	17
resins	12
polymerisation component	12
food	10
chemistry	10
cellulose processing	5
nitroglycerine	4
other	4

All these elements intensify the research on the development of glycerol.

The need arose for the new use of glycerol, especially in the unhydrated, raw state, which will reduce the costs of biodiesel production.

One of the ways of utilization can be to use it as a motor fuel or as an ingredient added to the fuel.

2. Methods of using glycerine for energy purposes

2.1. Motor power supply with glycerine

Glycerine is not a good motor fuel because of its parameters:

- calorific value of 1662 kJ/mol, 18047 kJ/kg
- dynamic viscosity at 20°C is 1.5 Pa·s
- kinematic viscosity at 25°C, 450–750 cSt
- heating value LHV 16 MJ/kg
- density 1.260–11.261 kg/dm^3
- cetane number CN 0–10

The low calorific value, and in addition a high water content causes a reduction in the combustion temperature through the evaporation process. During this process, very

toxic acrolein is formed. These features affect the big difficulties in using it as an independent motor fuel. Despite these unfavorable properties, attempts are made at various research centers to use it as an independent motor fuel to power internal combustion engines.

Initial research on the compression ignition engine power supply was carried out at the Czestochowa University of Technology [39] using the CRU chamber. It is a fixed combustion chamber with adjustable pressure and temperature parameters. Fuel was delivered to the combustion chamber using an electromagnetic injector. In the first tests glycerol was injected into the chamber without a pilot dose at various parameters of pressure and temperature prevailing inside the chamber. In the next stage, the process of burning glycerol with the pilot dose of diesel oil was observed.

The conclusions of these studies were:

- no possibility of burning pure glycerol in the CRU chamber due to its low cetane number,
- much slower course of glycerol combustion, especially in the final phase in relation to light diesel oil
- it is possible to burn glycerol with a pilot dose of diesel, but in this configuration its stability is very low
- the increase in glycerol injection time does not significantly affect the end of the combustion process and shows no correlation with the increase of injection pressure.

At the University of Warmia and Mazury in Olsztyn PhD Arkadiusz Rychlik and MSc Łukasz Kibalczyc [6] carried out research involving the feeding of a high-powered diesel engine with technical glycerine. The tests were carried out on the engine of the MTU V652 generator set.

To obtain favorable conditions for the combustion of glycerine in a compression-ignition engine, the following conditions should be adapted individually or possibly in combination:

- increasing the compression ratio
- increasing the cylinder fill ratio
- increasing the supply air temperature

The supply air was redirected through the heat exchanger, which increased the air temperature to 190–200°C from the initial 140°C. The effect was to reduce the recharge pressure from 1.5 bar to 1.3 bar. Table 2 presents a part of the measurement results for powering the engine with diesel oil and glycerine. The engine was started and stopped using diesel. While working on glycerine, when the engine was thermally stabilized, an attempt was made to shut down and restart the engine. We managed to stop and restart the engine without any irregularities.

Table 2. Selected results of the glycerine burning tests in the ZS engine [6]

Measurement	Fuel temp [°C]	Power [kW]	CO [%]	CO_2 [%]	HC [ppm]	O_2 [%]	NOx [ppm]	Exhaust temp. [°C]	Fuel type
1	70	470	0.06	1.7	16	18.1	180	420	ON
2	70	960	0.00	5.8	2	12.07	528	480	ON
3	70	1200	0.00	4.4	5	14.2	528	525	ON
4	100	1200	0.00	5.1	8	14.5	100	485	Glic.
5	100	1200	0.01	5.2	10	15	120	480	Glic.
6	100	1200	0.01	4.9	12	16	95	485	Glic.

The conclusions and observations from the conducted tests are as follows:

- The use of technical glycerine as a fuel for the ZS engine enabled the proper functioning of the engine without disturbance for the duration of the tests.
- The combustion of technical glycerine in the ZS engine reduces NO_x emissions. Studies have shown more than five times less emissions for diesel. The CO emission is lower when feeding with technical glycerine.
- The authors of the research indicate the guilt of operating the engine as the reason for the increased amount of HC emissions. During the tests, the permissible engine temperature was exceeded, which caused the lubricating oil to enter the combustion chamber.
- The consumption of technical glycerine as a fuel with 1200 kW load was about 14.25 dm^3/min.

Taking into account the catalog diesel consumption, for this engine and the consumption of measured glycerine, the ratio of glycerine to diesel consumption is approximately 2.2: 1.

2.2. Supplying the SI engine with liquid fuel with the addition of glycerine

The use of glycerol as an additive to conventional liquid fuels due to its hydrophilicity causes difficulty in creating a homogeneous mixture, and hygroscopicity, that there is a need to add a solvent compatible with the base fuels.

Professor Stelmasiak and dr Pietras from the University of Technology and Humanities in Bielsko-Biała conducted research [7] on the combustion of methanol mixtures with the addition of glycerine in an internal combustion engine. The test engine is a Fiat 1100 MPI spark ignition engine. Five different fuel mixtures were burned in the engine, whose composition and properties are shown in Table 3.

Table 3. Properties of fuels used in research [7]

Fuel	E95	Metanol	Metanol +10%	Metanol +20%	Metanol +30%
Density [kg/dm^3]	0.74	0.796	0.842	0.889	0.935
Calorific value [MJ/kg]	42.5	19.5	15.9	16.2	16.6
Octane number	95	115	–	–	–

The diagrams in Figure 1 show the efficiency of the fueled engine from Table 3 during three trials at different engine speeds. The graphs were prepared as a function of the engine torque. The first trial at a speed of 2000 rpm, the second at 2500 rpm, the third at 3000 rpm. The highest efficiency index was characterized by a methanol mixture with a 10% addition of glycerol.

The tests also included an assessment of the content of toxic exhaust components. The analysis was based on commercial supply of unleaded petrol 95, methanol and methanol with 10% addition of glycerol. Figure 2 presents graphs of the content of individual toxic components of exhaust gases as a function of engine torque.

Conclusions from the conducted studies concerning the addition of glycerol indicate that when using alcohol to power a spark-ignition engine, it resulted in increased efficiency and reduced emission of toxic exhaust components. The addition of small amounts of glycerol may lead, in the

area of medium and high engine loads, to increased NO_x emissions compared to pure methanol feed. The addition of glycerine as a fuel intended for spark-ignition engines should not exceed 10% of mixtures with methanol and ethanol.

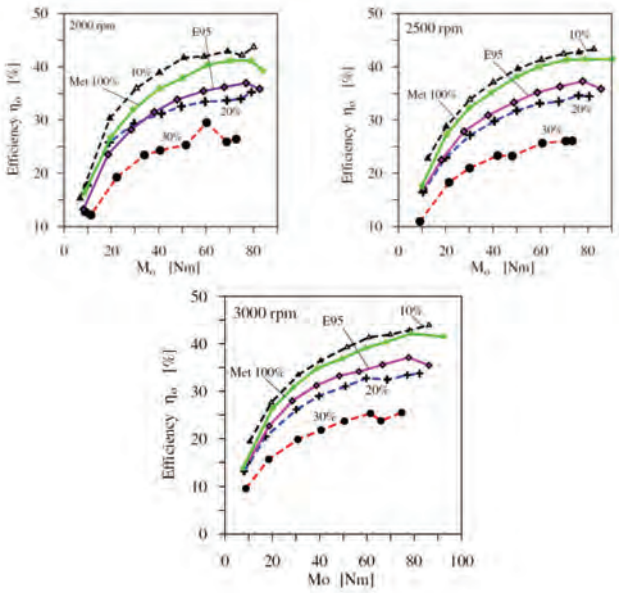

Fig. 1. Efficiency of the engine as a function of torque when fed with different fuel mixtures [7]

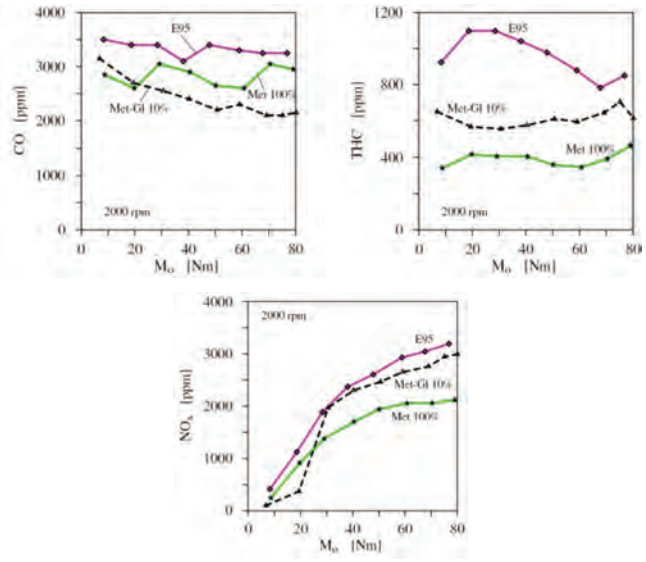

Fig. 2. Content of toxic components of flue gas resulting from the combustion of various fuel mixtures [7]

2.3. Supplying the SI engine with synthesis gas from glycerine

Synthesis gas has long been used as fuel for the combustion engines. Syngas is a mixture of carbon monoxide, carbon dioxide, methane and hydrogen. The content of individual components is variable and results from the selection of process parameters and the type of raw material used for production. The synthesis gas can be obtained from gaseous and liquid hydrocarbons, alcohols and carbohydrates. One of the compounds that can be used to obtain it is glycerol.

The research [13] of Dereck Kyle Pickett from 2013 at Univesity of Kansas consisted in powering a spark-ignition gas engine produced from glycerol and propane for comparison purposes. We successfully managed to power the engine using gas synthesized from glycerine. The author of the project defines three states of the reactor, in which it obtains different proportions of the syngas components. It defines them: No Load, One Load and Two Loads. Table 4 shows the individual proportions of the components of the gas obtained.

Table 4. Definition of the proportion of syngas components [13]

	Component	Volume [µl]
No Load	Hydrogen	18.017
	Methane	0.477
	CO	18.431
	CO_2	8.680
	Ethylene	4.105
	Ethane	2.284
One Load	Hydrogen	20.629
	Methane	0.599
	CO	14.935
	CO_2	5.984
	Ethylene	3.789
	Ethane	2.103
Two Loads	Hydrogen	26.548
	Methane	4.322
	CO	13.608
	CO_2	5.388
	Ethylene	3.628
	Ethane	1.960

Figures 3–5 illustrate the course of the cylinder pressure relative to the angle of rotation of the crankshaft for the individual three compositions of the synthesis gas obtained and for the propane feed. The engine on which the tests were carried out is a General Motors V8 engine with a cubic increment of 350 cubic inches.

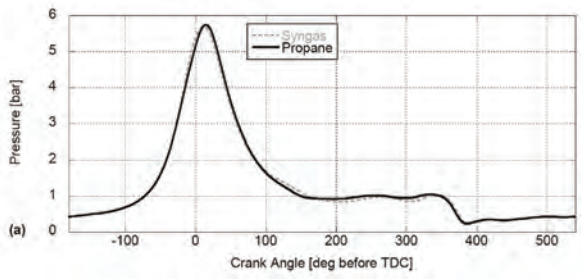

Fig. 3. Pressure course in the combustion chamber as a function of the angle of rotation of the crankshaft for "No Load" [13]

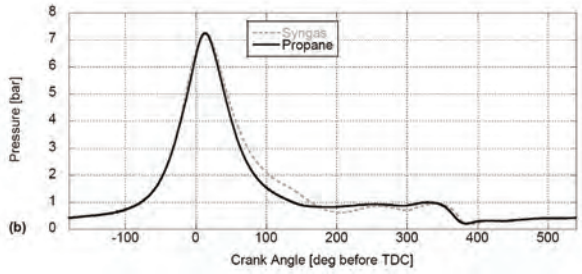

Fig. 4. The pressure course in the combustion chamber as a function of the crankshaft rotation angle for "One Load" [13]

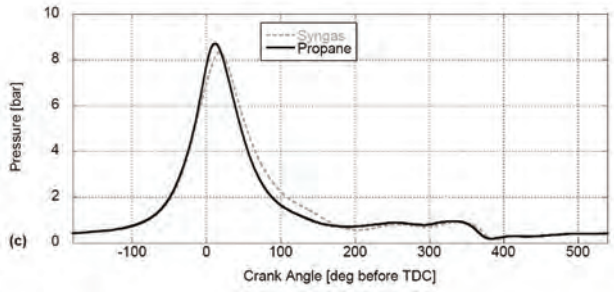

Fig. 5. The course of pressure in the combustion chamber as a function of the angle of rotation of the crankshaft for "Two Loads" [13]

The author draws attention to the mistake made during the test consisting in the lack of regulation of valves supplying the engine with gas. Also the ignition advance angle was the same in the case of propane and synthesis gas supply. This influenced the operation of the engine on the synthesis gas on a richer mixture, which resulted in incomplete and incomplete combustion, which was reflected in emissions, CO, CO_2 and HC residues. During the syngas feed the EGR system was additionally switched on. The difference in the course of curves visible at higher loads in Fig. 4 and 5 is due to the fact that due to the lower calorific value of syngas compared to propane, a larger gas mass was introduced into the charge and exhaust gas recirculation was used, which resulted in a longer combustion time. The analysis of the research presented in the above works concerning the combustion of glycerol and synthesis gas originating from glycerine provided important conclusions. Combustion of unprocessed glycerine is very difficult. In a spark-ignition engine, the main problem is the supply of glycerol by injectors due to its high viscosity, which affects its spraying and, consequently, the stable and efficient operation of the engine. Detailed studies on the burning of glycerol in a laminar manner, and the study of its physical properties are contained in the article [19].

Attempts to feed spark ignition engines using glycerine as an additive to other fuels, in particular alcohols such as methanol or ethanol, have shown a significantly improved fuel combustion efficiency. The question is whether additions of glycerine to traditional commercial gasoline can increase the efficiency of the engine.

Powering the SI engine using synthesis gas made of glycerine is an interesting alternative. The full so-called analysis of environmental impacts of toxic substances accompanying the production of such a fuel. An additional issue concerning the future of supplying engines with syngas is the method of fuel storage. Should it be done as shown in the history from the beginning of the 20th century where the gas generator was in the car or whether to produce syngas in stationary generators.

2. Methods for gasification of glycerine

As it has already been pointed out, the production and use of glycerine is on the one hand related to the scale of biodiesel production, and on the other hand to the development of new processes and technologies of its utilization. Among all possible and technically and physically available methods, the conversion of glycerol to valuable gases – such as hydrogen and synthesis gas used as a valuable energy carrier – is one of the most attractive ways of aggregating glycerol values [4].

The reforming processes used for the production of hydrogen and synthesis gas from glycerine cover a number of processes and technologies, and in the literature there are many articles on this subject. These articles mainly characterize the "catalytic behavior" of the applied systems. The following methods for reforming glycerol may be mentioned:

- steam reforming (SR) [20–26],
- partial oxidation (or oxidative reform) (PO) [27–29],
- autothermal reforming (ATR) [27, 29] and supercritical water gasification (SCWG) [30–34],
- dry reforming (or CO_2 reforming) (DR) [36, 37],
- autothermal dry (and also a combination of dry, oxidation and steam reforming) [37] and pyrolysis [38].

3. Selection of the method due to the possibility of using waste heat from the engine

The use of glycerine for energy purposes brings with it the so-called pro-ecological effect in the form of lower emission of carbon dioxide in relation to the unit weight of fuel. The measurable value of this effect depends on the degree of purity of the glycerine used. For obvious reasons in the utilization processes, the most desirable option is to use the least processed waste – we are interested in the so-called 80% of the technical glycerine remained after the production of biodiesel, table 7. Therefore, in the case of the utilization of this glycerine, one should look for a method that forms part of this postulate. The most rational seems to be here, the use of the so-called waste heat from thermodynamic processes carried out in a piston combustion engine. We mean the energy stream discharged into the atmosphere in the exhaust. In connection with the above, we proposed the use of a modified method of reforming steam glycerine on a catalytic bed. The project included the construction of a dedicated reactor, in which superheated steam of a glycerol water solution under a slight overpressure of 120 kPa, at a temperature of approximately 330°C, reacted on a ceramic catalytic bed. The process diagram is shown in Fig. 6, and the view of the reactor during tests is shown in Fig. 7.

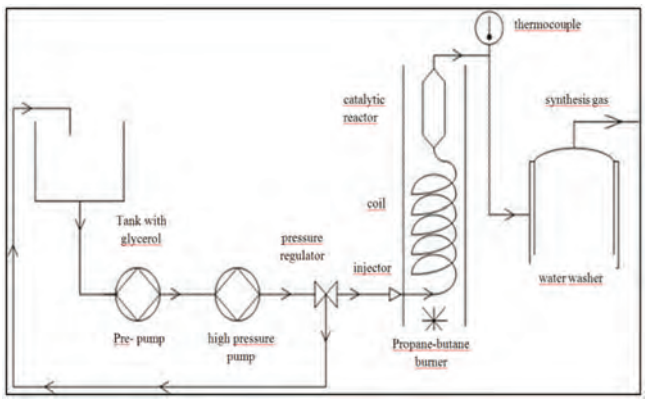

Fig. 6. Diagram of the installation for the production of syngas

During the attempts to obtain syngas, both pure glycerine with a concentration of 99.5% was used. and technical

at 80% concentration. For production, the above-mentioned a reactor in which the glycerine and its vapors were heated by flowing hot flue gases. Glycerine was injected into a unilaterally closed coil, and then as a result of pressure increase, the vapor passed to a catalytic reactor in which the synthesis gas was produced.

Fig. 7. A reactor for the production of synthesis gas

4. Results of production of syngas

The tables below contain the numerical values of volume constituents of gaseous components, so-called synthesis gas, produced using different varieties of glycerol, for different values of thermodynamic parameters of the reforming process, including reforming of steam glycerine on a catalytic bed.

Table 5 presents the chemical composition of synthesis gas obtained in the 99.5% glycerine reforming process. The table also contains information about the gas temperature at the outlet of the catalytic converter. Three gas samples obtained at different temperatures of the catalytic converter were analyzed.

Table 5. Composition of synthesis gas obtained from glycerol at a concentration of 99.5%

Sample number	Temperature [°C]	H_2 [%]	O_2 [%]	N_2 [%]	CO_2 [%]	CH_4 [%]
1	250	19.94	6.37	24.42	2.74	23.62
2	270	23.96	2.16	8.59	3.80	29.32
3	300	24.31	0.69	2.53	5.50	30.40

Table 6 presents the chemical composition of the syngas, which was also produced in the above-mentioned in a reactor, if 20% water is added to pure glycerine. The reaction taking place inside the catalytic reactor was carried out at a higher temperature than before.

Table 6. Composition of synthesis gas obtained from glycerol at a concentration of 99.5% with the addition of 20% water

Sample number	Temperature [°C]	H_2 [%]	O_2 [%]	N_2 [%]	CO_2 [%]	CH_4 [%]
1	316	28.66	1.41	5.53	9.63	24.60
2	350	28.03	1.97	7.30	13.87	21.53
3	389	30.46	2.03	7.80	17.50	19.20

Table 8 contains the results of the analysis of the chemical composition of syngas, which was produced as a result of the use of the technical glycerine composition shown in Table 7.

Table 7. The composition of technical glycerine

Component	content %
Glycerine	72.5
Water	15
Ash	7
MONG (organic compounds except glycerol)	5
Methanol	0.5

Table 8. Composition of synthesis gas obtained from technical glycerine

Temperature [°C]	H_2 [%]	O_2 [%]	N_2 [%]	CO_2 [%]	CH_4 [%]
350	36.53	0.3	1.14	6.89	34.10

Synthesis gas obtained from technical glycerine at a temperature of 350°C is characterized by the highest content of combustible components in its volume. The experiment was to show whether it is possible to obtain valuable synthesis gas in terms of using it to power SI engines with the possibility of using the energy of exhaust gases coming from the engine to conduct the reaction. The content of combustible components of synthesis gas was reached at the level of 70% of the gas volume. The synthesis gas obtained in accordance with the conditions of the above test was used to power the SI engine.

6. Supplying the SI engine with synthesis gas from glycerine

The tests were carried out on a two-cylinder, four-stroke SI engine with a displacement of 0.65 dm^3, with a constant crankshaft speed of 2500 1/min. During the tests, the engine was powered by two fuels through a mixer installation. Comparative measurements were made on LPG fuel. Due to the initial character of motor tests, the engine operation indicators were registered only in two points of the field of work on the regulatory characteristics of the mixture composition. During engine operation, measurements of such quantities as:

- torque
- exhaust gas temperature of individual cylinders
- lambda value
- concentrations of exhaust components: CO, CO_2, HC, NO_x

Table 9 presents comparative data during operation of the engine powered by LPG.

Table 9. Measurement data of the operation of the engine powered by LPG

M [Nm]	N [kW]	T_{S1} [°C]	T_{S2} [°C]	λ	CO [%]	CO_2 [%]	HC [ppm]	NO_X [ppm]
18.05	4.87	699	711	1.55	0.09	8.6	67	499
23.64	6.38	652	655	1.01	4.74	8.4	252	338

Table 10 shows the data during the operation of the engine powered by synthesis gas.

With unchanged throttle position adjustment settings and ignition timing values, a drop in the torque value was noted when feeding the synthesis gas during the enrichment

of the mixture. This is related to the lower value of the synthesis gas energy parameters. At the same time, a drop in CO_2 concentration was observed with this gas. Due to the simplified methodology of motor measurements, further investigation will be devoted to this issue. Despite a very fragmentary research program, in the case of engine operation on the above synthesis gas, a typical for this fuel was found a very stable course of the formation of a combustible mixture, using a simple power supply system.

Table 10. Measurement data of the engine operation when fed with synthesis gas

M [Nm]	N [kW]	T_{S1} [°C]	T_{S2} [°C]	λ	CO [%]	CO_2 [%]	HC [ppm]	NO_x [ppm]
18.15	4.89	630	629	1.4	0.17	4.7	45	814
19.12	5.16	630	623	1.02	0.17	6.2	45	912

6. Analysis of results

Attempts were made to produce syngas in variants allowing gas analysis to be used to power the SI motor. In the first case glycerine with a concentration of 99.5% was used. A gas was obtained which is a mixture of combustible components in a gas volume of about 45-50%. The process temperature did not exceed 300°C. It is noticeable that the percentage of combustible components in the gas volume increases with increasing process temperature.

The addition of 20% water to pure glycerine maintains the proportion of combustible parts in the gas composition of about 50%. With the increase of the temperature of the process, a reduction in the proportion of CH_4 in the volume is noticeable. The volume of CO_2 is almost doubled, and the increase in the share of H_2 is insignificant. In the first case, as the temperature increased, it was possible to observe an increase in the proportion of combustible components in the volume. In the second case, the share stays on a more or less stable level, but it can be seen that the addition of water causes a change in the proportion of CH_4 and CO_2 shares with small changes in the other components. The use of technical glycerine in the third case resulted in the highest share of combustible components in the volume. Water and other technical glycerine components had a beneficial effect on the production process of synthesis gas. The graph shown in Figure 8 illustrates the contribution to the volume of individual components of the synthesis gas, which was used to power the engine in the further part of the study.

For the production of syngas, an average of 100 g glycerine was consumed during every 15 minutes of the reactor operation. The obtained amount of synthesis gas from 100 g glycerine is on average 40.6 l when producing a total of 1000 l of syngas.

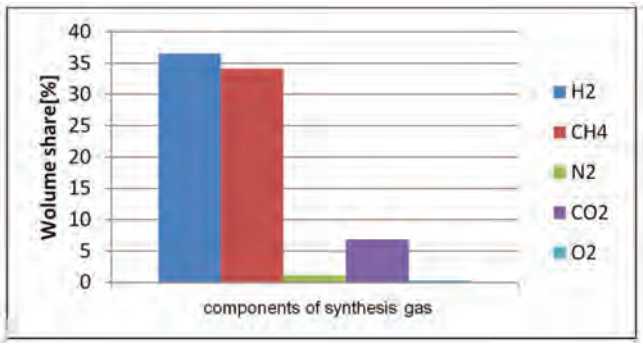

Fig. 8. Volume fraction of syngas components

Each average of approximately 4.17 kWh of energy was used to process each 100 g glycerol. A total of 1 m^3 of syngas was produced for engine tests. About 2.5 kg of glycerine was used to produce this volume of synthesis gas.

Comparison of the operation of the engine powered by LPG and synthesis gas shows the fundamental difference in fuel consumption. The consumption of synthesis gas is several times greater than the consumption of LPG. This is due to the significantly lower heating value of synthesis gas and the heating value of the syngas and air mixture. There is also a difference in the temperature of the exhaust gas. The temperature of exhaust gases in the case of synthesis gas combustion is lower by several dozen degrees. The reason for the lower exhaust gas temperature for synthesis gas is the different heat recovery process. The content of toxic exhaust components is as follows. An almost two-fold increase in the CO share in the exhaust composition is visible, but it does not exceed 0.2%. For comparison, vehicles homologated until June 1995 must meet the CO emission standard in Poland up to 3.5%. CO_2 emissions are at a comparable level. There are discrepancies, but with a small number of comparative measuring points, they are negligible. There is a clear drop in hydrocarbon emission. There has been an almost two-fold reduction in the emission of this toxic exhaust component, which is due to the fact that synthesis gas consists of much simpler molecules than LPG. Comparison of NO_x emissions is impossible due to the large discrepancy between measurement data when the engine is running on LPG. A small amount of measurement data does not allow to clearly determine the difference or similarity in the amount of NO_x particles emitted when burning both fuels.

Bibliography

[1] BOROWIECKI, T., RYCZKOWSKI, J. Procesy i Katalizatory pozyskiwania gazu syntezowego. Uniwersytet Chemii w Lublinie, *Instytut Nawozów Sztucznych w Puławach*.

[2] PAŃCZYK, M., BOROWIECKI, T. Otrzymywanie i zastosowanie gazu syntezowego. Zakład technologii chemicznej, *Wydział Chemii Uniwersytetu w Lublinie.*

[3] CHMIELNIAK, T., STELMACH, S. Współczesne technologie zgazowania węgla. *Problemy Ekologii*. 2009, **2**.

[4] PIETRZKIEWICZ, L. I co z węglem? *Chemia przemysłowa*. 2011, **1**.

[5] KIJEŃSKI, J., KRAWCZYK, Z. Perspektywy rynku gliceryny. *Przemysł chemiczny*. 2007, **4**.

[6] RYCHLIK, A., KIBALCZYC, Ł. Application of glycerine for powering piston diesel engines of large power. *Combustion Engines*. 2015, **162**.

[7] STELMASIAK, Z., PIETRAS, D. Utilization of waste glycerine to fuelling of spark ignition engines. *Materials Science and Engineering*. 2016, **148**.

[8] CHMIELNIAK, T., POPOWICZ, J. Fluidalne zgazowanie węgla przy użyciu CO_2 dla produkcji gazu syntezowego. *Chemik*. 2013, **67**.
[9] DĄBROWSKI, W., BEDNARSKI, W. Ekologiczne aspekty produkcji oraz stosowania biodiesla. *Nauki inżynierskie i technologie*. 2013, **10**.
[10] ZASTĘPOWSKI, M., KASZKOWIAK, J., BOROWSKI, S. et al. pływ zastosowania paliwa z dodatkiem alkoholu na efektywność pracy silników spalinowych. *Logistyka*. 2012, **6**.
[11] IGLIŃSKI, B., KUJAWSKI, W., BUCZKOWSKI, R., IGLIŃSKA, A. Ekologiczne efekty stosowania biopaliw. Wydział Ochrony Środowiska, *Uniwersytet Toruński*.
[12] KUBALA, A. Efekty termiczne przy odwadnianiu etanolu w cyklicznym procesie adsorpcyjno-desorbcyjnym zmiennociśnieniowym. *PK Wydział Inżynierii i Technologii Chemicznej*.
[13] PICKETT, D.K. Design and operation of the synthesis gas generator system for reformed propane and glycerine combustion. *University of Kansas*. 2013.
[14] PALARSKI, J. Pozyskiwanie metodami niekonwencjonalnymi energii z pozabilansowych pokładów węgla z uwzględnieniem ograniczenia emisji CO_2. *Górnictwo i Geologia*. 2010, **5**(1).
[15] STRUGAŁA, A., CZERSKI, G. Badania nad technologiami zgazowania węgla w Polsce. *Przemysł Chemiczny*. 2012.
[16] BEDNARCZYK, J. Rozwój technologii podziemnego zgazowania węgla i perspektywy jej przemysłowego wdrożenia. *Górnictwo i Geoinżynieria*. 2007.
[17] SARBAK, Z. Gaz syntezowy i jego przemiany. LAB 2018, **6**.
[18] SILVEY, L.G. Hydrogen and syngas production from derived crude glycerol. *Univesity of Kansas*. 2011.
[19] JACH, A., CIEŚLAK, I., TEODORCZYK, A. Investigation of glicerol doping on ignition delay times and laminar burning velocites of gasoline and diesel fuel. *Combustion Engines*. 2017, **169**.
[20] ZHANG, B., TANG, X., LI, Y. et al. Hydrogen production from steam reforming of ethanol and glycerol over ceria supported metal catalysts. *International Journal of Hydrogen Energy*. 2007, **32**, 2367-2373.
[21] BUFFONI, I.N., POMPEO, F., SANTORI, G.F., NICHIO, N.N. Nickel catalysts applied in steam reforming of glycerol for hydrogen production. *Catalysis communications*. 2009, **10**, 1656-1660.
[22] ADHIKARI, S., FERNANDO, S.D., HARYANTO, A. Hydrogen production from glicerin by steam reforming over nickel catalysts. *Renewable Energy*. 2008, **33**, 1097-1100.
[23] THYSSEN, V.V., MAIA, T.A., ASSAF, E.M. Ni supported on La_2O_3-SiO_2 used to catalyze glycerol steam reforming. *Fuel*. 2013, **105**, 358-363.
[24] IRIONDO, A., BARRIO, V.L., CAMBRA, J.F. et al. Glycerol steam reforming over Ni catalysts supported on ceria and ceria promoted alumina. *International Journal of Hydrogen Energy*. 2010, **35**, 11622-11633.
[25] POMPEO, F., SANTORI, G.F., NICHIO, N.N. Hydrogen production by glycerol steam reforming with Pt/SiO_2 and Ni/SiO_2 catalysts. *Catalysis Today*. 2011, **172**, 183-188.
[26] POMPEO, F., SANTORI, G.F., NICHIO, N.N. Hydrogen and/or syngas from steam reforming of glycerol. Study of platinum catalysts. *International Journal of Hydrogen Energy*. 2010, **35**, 8912-8920.
[27] WANG, H., WANG, X., LI, M. et al. Thermodynamic analysis of hydrogen production from glycerol autothermal reforming. *International Journal of Hydrogen Energy*. 2009, **34**, 5683-5690.
[28] WANG, W. Thermodynamic analysis of glycerol partial oxidation for hydrogen production. *Fuel Processing Technology*. 2010, **91**, 1401-1408.
[29] YANG, G., YU, H., PENG, F. et al. . Thermodynamic analysis of hydrogen generation via oxidative steam reforming of glycerol. *Renewable Energy*. 2011, **36**, 2120-2127.
[30] BYRD, A.J., PANT, K.K., GUPTA, R.B. Hydrogen production from glycerol by reforming in supercritical water over Ru/Al_2O_3 catalyst. *Fuel*. 2008, **87**, 2956-2960.
[31] CHAKINALA, A.G., BRILMAN, D.W.F, VAN SWAAIJ, W.P.M., KERSTEN, S.R.A. Catalytic and non catalytic supercritical water gasification of microalgae and glycerol. *Industral & Engineering Chemistry Research*. 2009, **49**, 1113-1122.
[32] GUO, S., GUO, L., CAO, C. et al. Hydrogen production from glycerol by supercritical water gasification in a continuos flow tubular reactor. *International Journal of Hydrogen Energy*. 2012, **37**, 5559-5568.
[33] VAN BENNEKON, J.G., VENDERBOSCH, R.H., ASSINK, D., HEERES, H.J. Reforming of methanol and glycerol in supercritical water. *The Journal of Supercritical Fluids*. 2011, **58**, 99-113.
[34] VOLL, F.A.P., ROSSI, C.C.R.S., SILVA, C. et al. Thermodynamic analysis of supercritical water gasification of methanol, ethanol, glycerol, glucose and cellulose. *International Journal of Hydrogen Energy*. 2009, **34**, 9737-9744.
[35] WANG, X., LI, M., WANG, M. et al. Thermodynamic analysis of glycerol dry reforming for hydrogen and synthesis gas production. *Fuel*. 2009, **88**, 2148-2153.
[36] FERNÁNDEZ, Y., ARENNILAS, A., BERMÚDEZ, J.M., MENÉNDEZ, J.A. Comparative study of conventional and microwave assisted pyrolysis, steam and dry reforming of glycerol for syngas production, using a carbonaceous catalyst. *Journal of Analytical and Applied Pyrolysis*. 2010, **88**, 155-159.
[37] KALE, G.R., KULKARNI, B.D. Thermodynamic analysis of dry autothermal reforming of glycerol. *Fuel Processing Technology*. 2010, **91**, 520-530.
[38] VALLIYAPPAN, T., BAKHSHI, N.N., DALAI, A.K. Pyrolysis of glycerol for the production of hydrogen or syngas. *Bioresource Technology*. 2008, **99**, 4476-4483.
[39] Grab-Rogaliński K., Szwaja S. The possibililty of use a waste product of biofules production – glycerol as a fuel to the compression ignition engine. *Journal of KONES*. 2016, **23**(3).

Krzysztof Śliwiński, DSc., DEng. – Faculty of Mechanical Engineering, Cracow University of Technology.
e-mail: *ksliwin@pk.edu.pl*

Wojciech Marek, DSc., DEng. – Professor in the Faculty of Mechanical Engineering, Cracow University of Technology.
e-mail*: wmarek@pk.edu.pl*

Article citation info:
LASOCKI, J., CHŁOPEK, Z., GODLEWSKI, T. Driving style analysis based on information from the vehicle's OBD system. *Combustion Engines*. 2019, **178**(3), 173-181. DOI: 10.19206/CE-2019-330

Jakub LASOCKI
Zdzisław CHŁOPEK
Tomasz GODLEWSKI

CE-2019-330

Driving style analysis based on information from the vehicle's OBD system

The purpose of this study was to analyse the possibility of using information from the On Board Diagnostics (OBD) system of the vehicle to determine the characteristics of the driver's driving style. Available data from the OBD system were considered and the most useful ones were selected for further investigation. Selected zero-dimensional characteristics of vehicle velocity as well as characteristics of relative position of the accelerator pedal were proposed as criteria for the assessment of driving style. The tests were carried out in conditions of real road traffic using a passenger car with a spark-ignition engine. The car was equipped with a device for recording signals from the OBD system. The tests included two drivers traveling on routes in the urban and rural areas. The obtained results were used to analyse the driving style of both drivers separately in the considered traffic conditions. On this basis, conclusions on the suitability of information from the OBD system for the assessment of the driver's driving style were formulated.

Key words: *driving style, driving pattern, OBD, On Board Diagnostics, road tests*

1. Introduction

Driving style refers to the way a driver chooses to drive a vehicle. Driving style differs across individuals or between groups of individuals. It tends to be habitual and relatively permanent, including both automatized skills and more consciously controlled behavior, but at the same time it is determined by the actual driving conditions which create opportunities or constraints for driver's actions [13].

The study on driving style is of a great importance in various fields related to road transport. It is useful for the research on road safety, plays an important role in the construction of road infrastructure and can be applied to the optimization of driver assistance systems, so they adapt to the particular driver. In the case of vehicles with combustion engines, the most important is the influence of the driving style on fuel consumption and emission of pollutants.

Several studies have proved the relationship between driving style, vehicle fuel or energy consumption and pollutant emission [7–9, 12]. According to Gonder et al. [9], efficient driving behavior results in the reduction of fuel consumption by 5% to 10%, compared to moderate driving style, and up to 20%, compared to aggressive driving style. This is confirmed by the findings of Fonseca et al. [7], whose conclusions are that eco-driving contributes to 14% decrease in fuel consumption and carbon dioxide emission, while aggressive driving – 40% increase. The effect of the driving style is not so clear in relation to the emission of toxic substances. The aforementioned study [7] revealed that although aggressive driving brings an increase in nitrogen oxides emission by more than 40%, carbon dioxide and hydrocarbon emission show different trends, in general being increased for eco-driving. Similar conclusions have been drawn by investigators conducting vehicle tests in real driving conditions, with the use of mobile exhaust gas analyzers [8, 12].

The analysis of driving style in order to examine its impact on pollutant emission and fuel consumption requires adoption of appropriate assessment criteria. Most of previous research works focus on the statistical metrics of driving data obtain in road tests, e.g. average value, maximum value, median, standard deviation of vehicle velocity, acceleration, brake pressure and throttle position [7, 9, 15, 16]. In some papers, e.g. [1, 3, 10, 11], it was proposed to use the On Board Diagnostics (OBD) system of the vehicle to obtain necessary driving data.

Current study follows this direction, aiming at investigation whether and what signals acquired from the OBD system may be relevant for characterizing a driving style. It includes some descriptive statistical analysis of the results of experiment, in which two drivers were compared, operating the same vehicle in urban and extra-urban traffic conditions.

2. OBD parameters relevant to driving style

The OBD system, which was originally intended by its creators to facilitate vehicle monitoring and diagnostics, gives access to various information from the Engine Control Unit (ECU), sensors integrated with parts of the vehicle chassis, vehicle body and accessory devices. A complete list of standard parameters available from the current version of the system, i.e. OBD-II/EOBD, through the connection port called Data Link Connector (DLC) is defined in SAE J1979. Vehicle manufacturers can also implement their own parameters that provide extended information. Some of these additional parameters would be highly desirable to assess the impact of driving style on fuel consumption and pollutant emissions. However, most manufacturers are unwilling to reveal additional data.

By assumption, the investigation presented in this paper was limited to the standard parameters that can be obtained from the OBD system using widely available diagnostic devices. With a reference to previous research works [1, 3, 10, 11, 15] and taking into account the abovementioned limitations, the following parameters were selected as relevant to driving style:

– vehicle velocity,
– engine rotational speed,
– relative accelerator pedal position,
– relative throttle valve position,
– relative engine torque,
– intake manifold pressure.

Among them, the velocity of the vehicle and the relative position of the accelerator pedal were found to be particularly useful and effective in practice for assessing the impact of driving style on vehicle fuel consumption and pollutant emission. Therefore further investigation consisted in the analysis of OBD signals corresponding to these two parameters, recorded during vehicle road tests.

3. Experimental procedures

3.1. General approach

The empirical part of the research took place under real traffic conditions. The vehicle was driven by two drivers, marked A and B. The drivers were aware of the tests, but instructed not to adapt their driving style due to participation in the experiment. The tests were conducted in urban traffic conditions (Warsaw) and in extra-urban traffic conditions (Mazowieckie Voivodeship). While driving a vehicle, signals from the OBD system were recorded.

3.2. Test vehicle

The vehicle used for road tests was Nissan Juke, presented in Fig. 1. Its technical specifications are given in Table 1.

Fig. 1. Vehicle subject to road tests

Table 1. Technical specifications of the vehicle tested

Parameter	Data
Manufacturer	Nissan
Model	Juke
Manufacturing date	2011
Body type	5-door crossover
Number of seats	5
Curb weight	1172 kg
Drive axle	Front
Engine type	Spark-ignition
Fuel	Gasoline
Cylinder number and configuration	4, in-line
Engine displacement	1598 cm^3
Gearbox type	Manual, 5 forward gears, 1 reverse gear
Pollutant emission standard	Euro 5
Maximum useful power of the engine	86 kW at 6000 rpm
Maximum engine torque	158 N·m at 4000 rpm
Fuel supply system	Multipoint, indirect injection
Maximum velocity	178 km/h
Acceleration time from stand to 100 km/h	11 s

3.3. Apparatus

Data from vehicle's DLC port was recorded while driving using Texa OBDLog. It is the on-board logging device, which supports all OBD-II/EOBD compliant vehicles, and requires PC with software interface to collect data saved in its internal memory during vehicle testing. The technical specification of Texa OBDLog is presented in Table 2.

Table 2. Technical specifications of the apparatus [14]

Parameter	Data
Manufacturer	TEXA
Name	OBDLog
Vehicle interface	DLC port
OBD protocols supported	All included in J1850-41.6, J1850-10.4, ISO9141-2 K/L, CAN (ISO 11898)
Power supply	12 V (DLC), 5 V (USB)
Processor	ARM 32-bit Cortex-M3
Internal memory	2048 kB
Sampling frequency	1 Hz
Maximum working time	90 h
Dimensions	23 mm × 45.5 mm × 28.2 mm
Weight	19.5 g
PC interface	USB 2.0 cable
Software	OBD Log SW Suite

3.4. Data processing

As a result of road tests, 494 samples of driving data from individual trips of both drivers were obtained. Driver A made 152 trips, while driver B – 352. The data was further processed using MS Office Excel. In the first step, a minimum time limit of 180 s was set, which resulted in the rejection of 37 samples. The remaining samples were assigned to one of the three categories of vehicle traffic: urban, extra-urban and road congestion. The criteria were the average vehicle velocity and an arbitrary assessment of the driving conditions. In extra-urban traffic, the average vehicle velocity was larger than 45 km/h, in urban traffic it was in the range (10 ÷ 45) km/h, and in road congestion – less than 10 km/h. The number of samples in each category was as follows (for driver A and B, respectively): 98 and 243 in urban traffic, 42 and 63 in extra-urban traffic, 1 and 10 in road congestion traffic. For further analysis, samples from road congestion category were rejected because driving in these conditions is largely dependent on external factors, such as road capacity during peak traffic hours, thus it is difficult to conclude about driving style on this basis.

Due to the low sampling frequency (1 Hz), it was necessary to apply the filtering of recorded signals. In the case of the velocity signal, a two-stage moving average from three measuring points was used, while for acceleration – a one-stage moving average from three measuring points. The acceleration itself was calculated based on velocity value.

In the next step, the values of selected zero-dimensional characteristics of vehicle velocity as well as characteristics of relative position of the accelerator pedal were calculated (Table 3). They were examined for their effectiveness as criteria for the assessment of driving style.

4. Results and discussion

Normalized histograms of the values of characteristics listed in Table 3 are presented in Figures 2–31. They allow comparison of the results obtained for drivers A and B.

Table 3. Zero-dimensional characteristics considered as criteria for the assessment of driving style

Type	Name	Symbol	Unit
Related to vehicle velocity	Average velocity	v_{AV}	km/h
	Average velocity excluding stops	v_{DAV}	km/h
	Maximum velocity	v_{MAX}	km/h
	Average acceleration	a^{+}_{AV}	m/s^2
	Maximum acceleration	a^{+}_{MAX}	m/s^2
	Average deceleration	a^{-}_{AV}	m/s^2
	Maximum deceleration	a^{-}_{MAX}	m/s^2
	The average value of the absolute value of the velocity and acceleration product	$\|v \cdot a\|_{AV}$	m^2/s^3
	The average value of the velocity and acceleration product	$v \cdot a^{+}_{AV}$	m^2/s^3
	Relative positive acceleration	RPA	m/s^2
Related to the position of accelerator pedal	Average relative position of accelerator pedal	AP_{AV}	%
	Average relative position of accelerator pedal, excluding vehicle stops	AP_{DAV}	%
	Average relative position of accelerator pedal, excluding zero position	AP_{0AV}	%
	Average relative position of accelerator pedal, excluding stops and zero position	AP_{D0AV}	%
	Average value of the derivative of the relative position of accelerator pedal	AP_{DVAV}	%

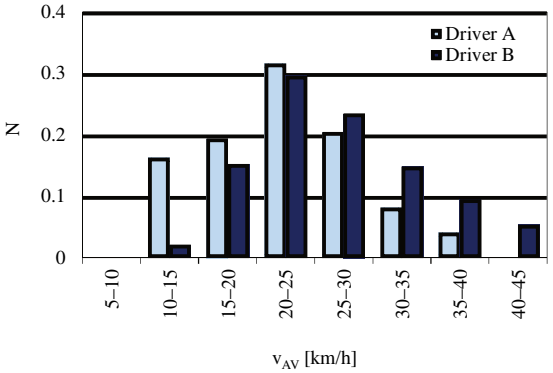

Fig. 2. Average velocity of the vehicle in urban driving conditions

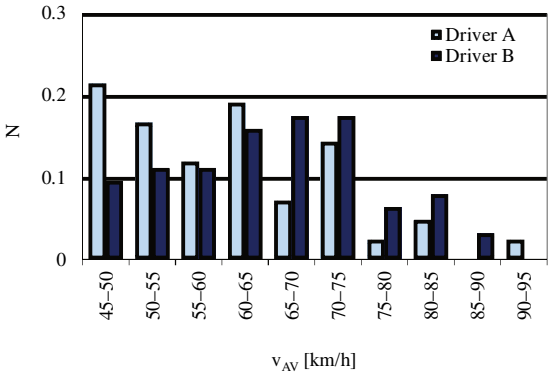

Fig. 3. Average velocity of the vehicle in extra-urban driving conditions

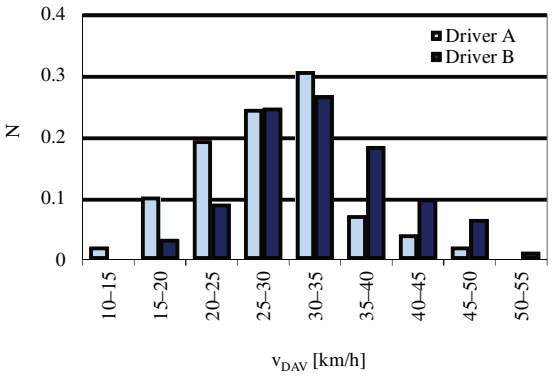

Fig. 4. Average velocity of the vehicle excluding stops in urban driving conditions

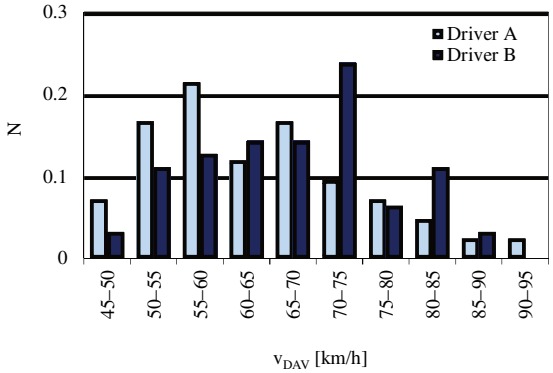

Fig. 5. Average velocity of the vehicle excluding stops in extra-urban driving conditions

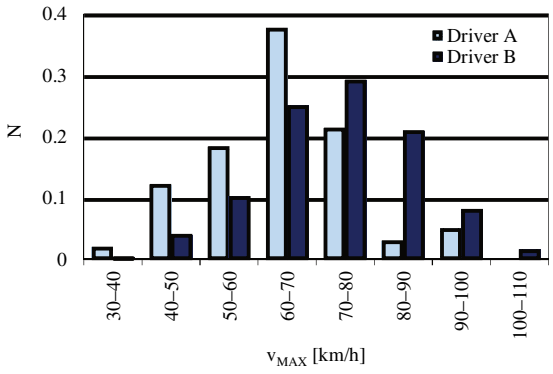

Fig. 6. Maximum velocity of the vehicle in urban driving conditions

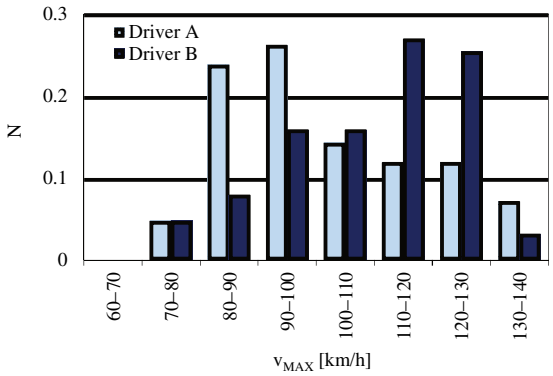

Fig. 7. Maximum velocity of the vehicle in extra-urban driving conditions

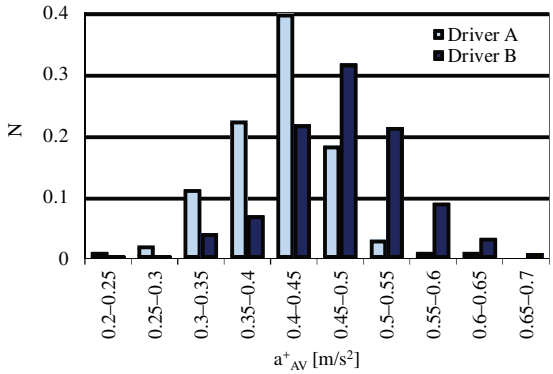

Fig. 8. Average acceleration of the vehicle in urban driving conditions

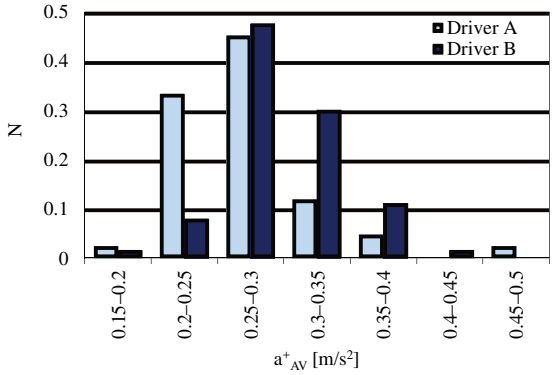

Fig. 9. Average acceleration of the vehicle in extra-urban driving conditions

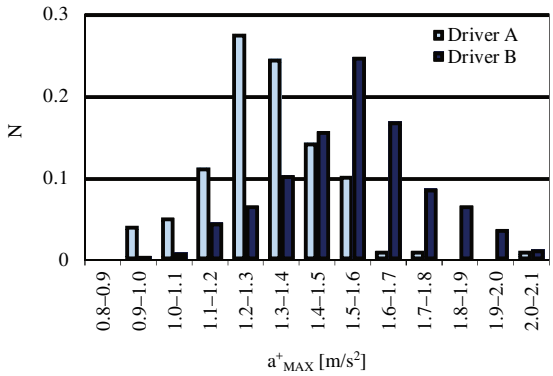

Fig. 10. Maximum acceleration of the vehicle in urban driving conditions

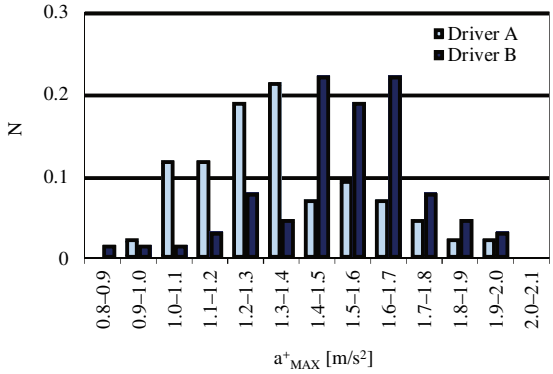

Fig. 11. Maximum acceleration of the vehicle in extra-urban driving conditions

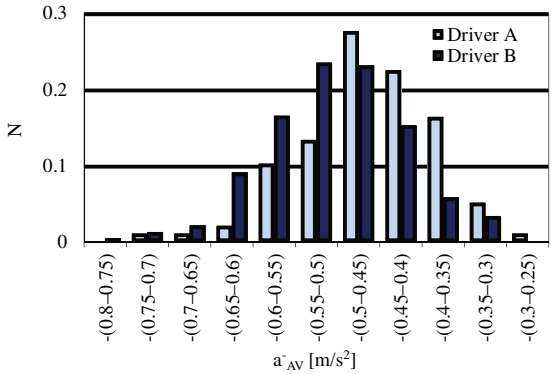

Fig. 12. Average deceleration of the vehicle in urban driving conditions

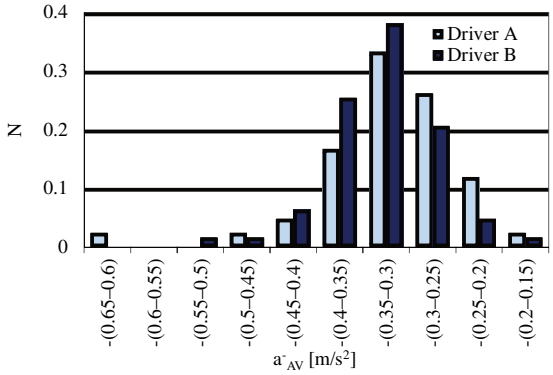

Fig. 13. Average deceleration of the vehicle in extra-urban driving conditions

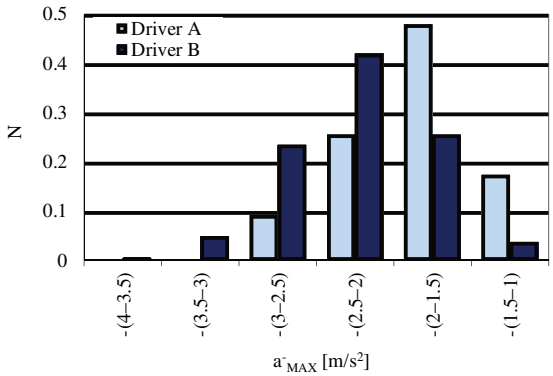

Fig. 14. Maximum deceleration of the vehicle in urban driving conditions

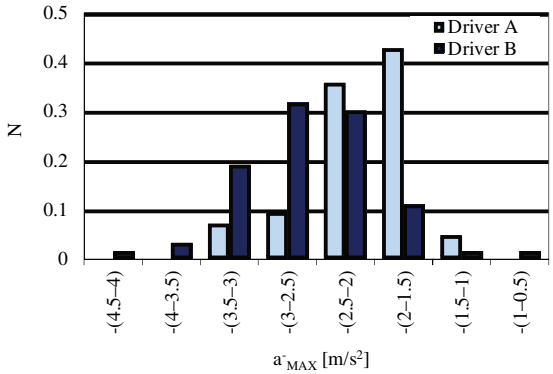

Fig. 15. Maximum deceleration of the vehicle in extra-urban driving conditions

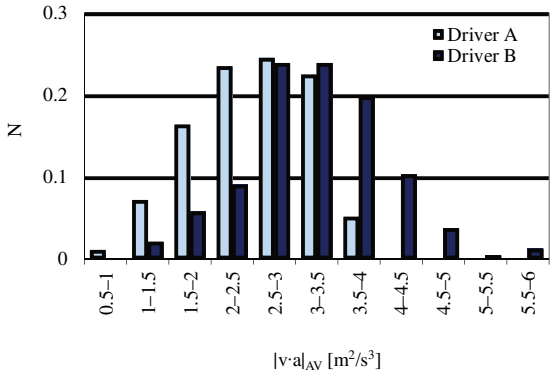

Fig. 16. The average value of the absolute value of the velocity and acceleration product in urban driving conditions

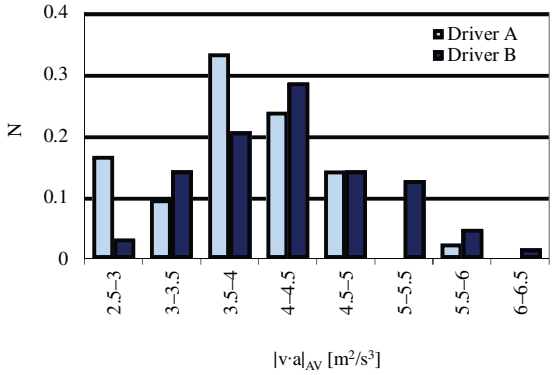

Fig. 17. The average value of the absolute value of the velocity and acceleration product in extra-urban driving conditions

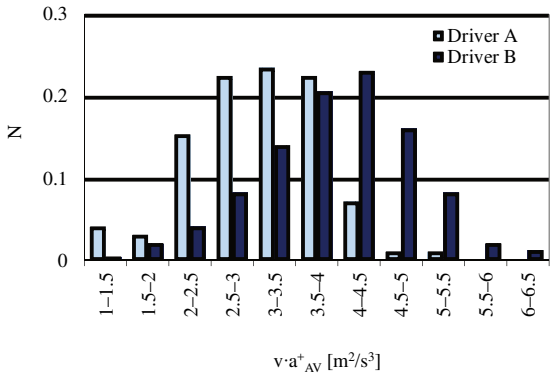

Fig. 18. The average value of the velocity and acceleration product in urban driving conditions

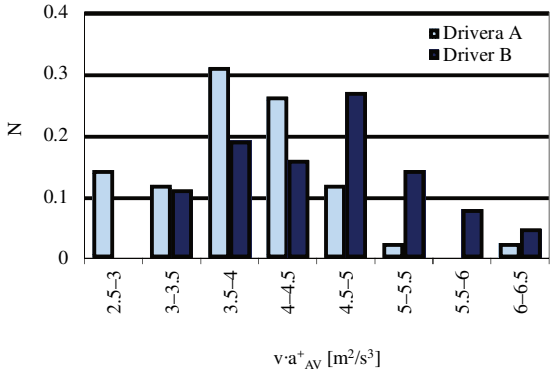

Fig. 19. The average value of the velocity and acceleration product in extra-urban driving conditions

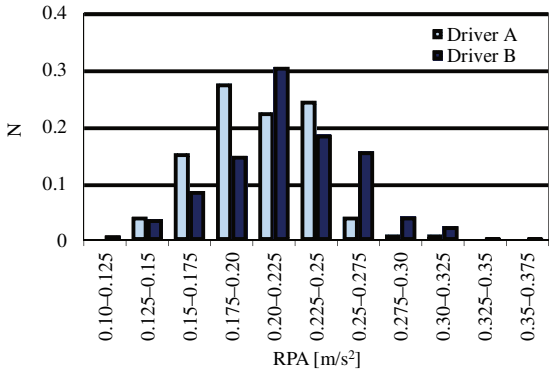

Fig. 20. Relative positive acceleration of the vehicle in urban driving conditions

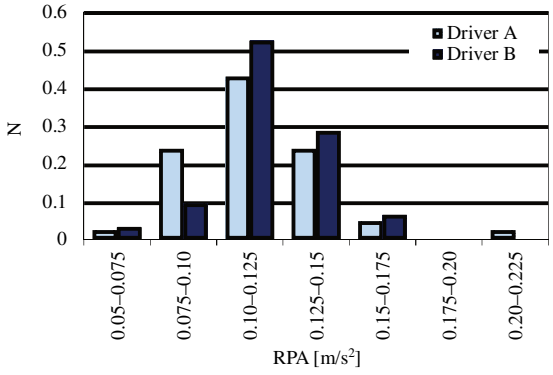

Fig. 21. Relative positive acceleration of the vehicle in extra-urban driving conditions

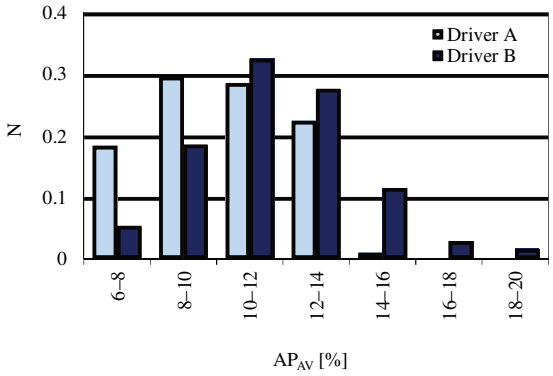

Fig. 22. Average relative position of accelerator pedal in urban driving conditions

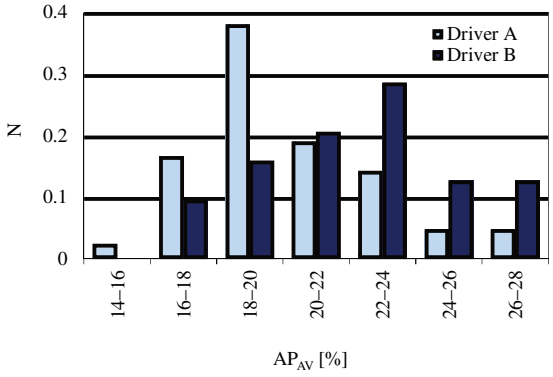

Fig. 23. Average relative position of accelerator pedal in extra-urban driving conditions

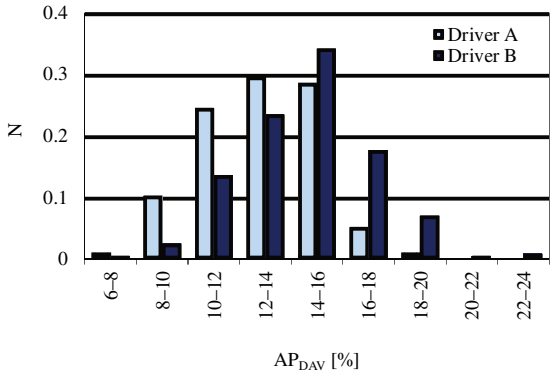

Fig. 24. Average relative position of accelerator pedal, excluding vehicle stops, in urban driving conditions

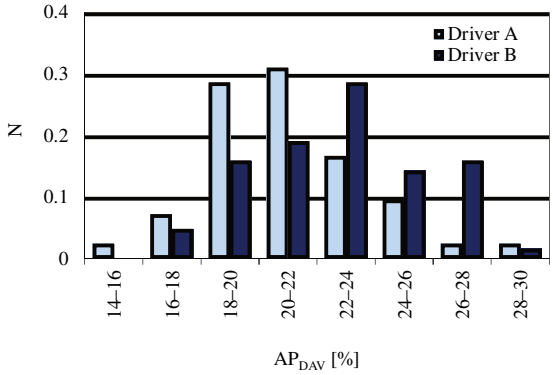

Fig. 25. Average relative position of accelerator pedal, excluding vehicle stops, in extra-urban driving conditions

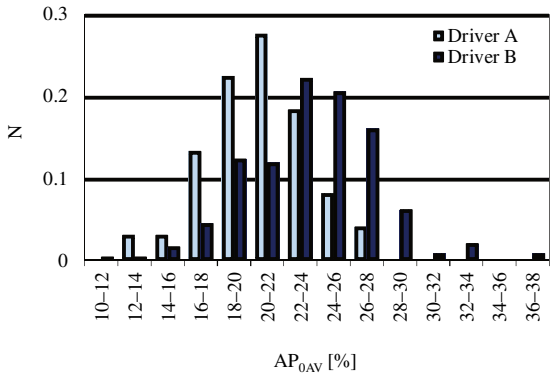

Fig. 26. Average relative position of accelerator pedal, excluding zero position, in urban driving conditions

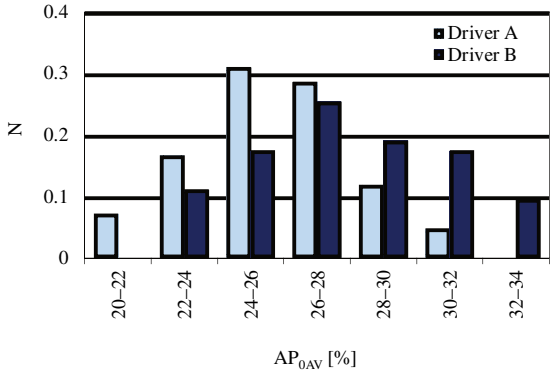

Fig. 27. Average relative position of accelerator pedal, excluding zero position, in extra-urban driving conditions

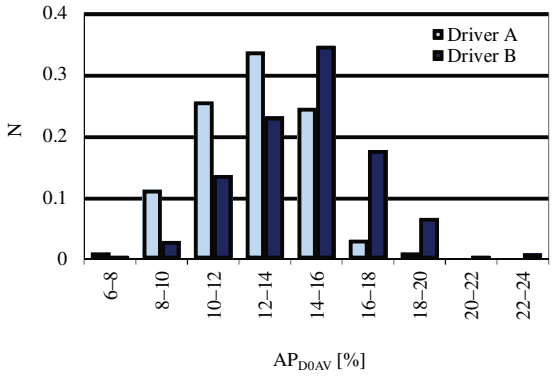

Fig. 28. Average relative position of accelerator pedal, excluding vehicle stops and zero position, in urban driving conditions

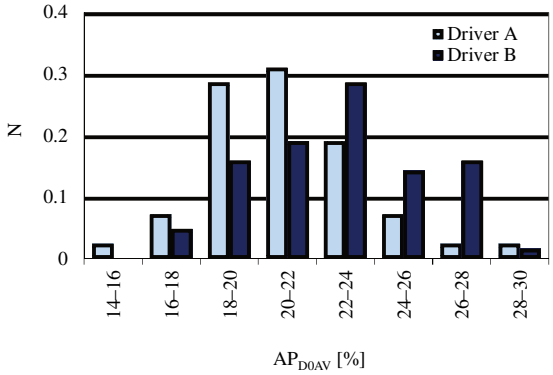

Fig. 29. Average relative position of accelerator pedal, excluding vehicle stops and zero position, in extra-urban driving conditions

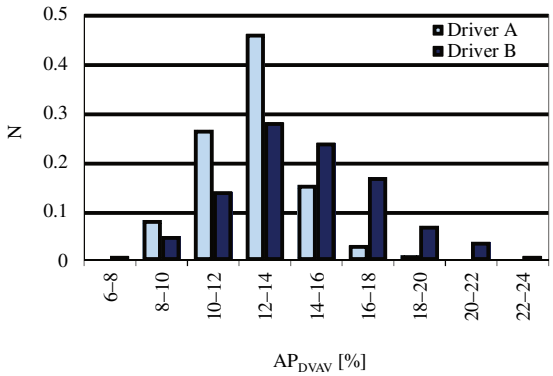

Fig. 30. Average value of the derivative of the relative position of accelerator pedal in urban driving conditions

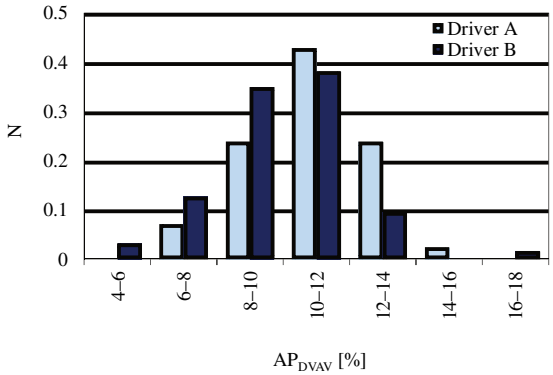

Fig. 31. Average value of the derivative of the relative position of accelerator pedal in extra-urban driving conditions

A detailed analysis of the histograms shown in Figures 2–31 reveals some trends in the obtained results.

In general, most histograms have a regular shape close to normal distribution. The exception are:

– average velocity of the vehicle, both including and excluding stops, in extra-urban driving conditions (Figures 3 and 5) – multimodal distribution;
– maximum velocity of the vehicle in extra-urban driving conditions (Fig. 7) – asymmetric distribution, for driver A moved towards moderate velocity values, and for driver B towards large velocity values;
– maximum deceleration of the vehicle in both urban and extra-urban driving conditions (Figs 14 and 15) – for driver A moved towards lower absolute values;
– the average value of the velocity and acceleration product in both urban and extra-urban driving conditions (Figs 18 and 19) – distribution that can be classified between normal and bimodal, especially for driver A.

The variability of the values of the designated characteristics is quite large, however, in the majority of cases, one clearly dominant range of values can be indicated.

Due to the purpose of this study, it is important to notice that the analysis of the histograms of the values of some characteristics allows the drivers to be distinguished. These include, above all:

– maximum velocity of the vehicle in extra-urban driving conditions (Fig. 7), which suggests that driver B has a clear tendency to drive with larger velocity than driver A;
– maximum acceleration of the vehicle in both urban and extra-urban driving conditions (Figs 10 and 11) – again, driver B has a tendency for more aggressive driving, with greater maximum acceleration;
– the average value of the velocity and acceleration product in both urban and extra-urban driving conditions (Figs 18 and 19) – the least clear difference between drivers, but still noticeable.

The above characteristics can be treated as potentially the best criteria to assess driving style. In fact they are often used to evaluate the dynamic properties vehicle velocity. The average value of absolute value of product of velocity and acceleration can be interpreted as a measure of engine power output per unit mass of the vehicle [2, 4]. The average value of the product of velocity and acceleration also takes into account engine operating conditions with a negative torque.

Characteristics related to the position of the accelerator pedal can also be used to analyze driving style and distinguish drivers. However, they are not as effective as the characteristics related to the velocity and acceleration of the vehicle. In this case, best ones seem to be:

– average relative position of accelerator pedal, especially in extra-urban driving conditions (Fig. 23), which is obviously due to the preference for driving with larger velocity by driver B than driver A;
– average relative position of accelerator pedal excluding zero position (regardless of taking into account vehicle stops), especially in urban driving conditions (Fig. 26), because in extra-urban conditions, when driving at a larger average velocity than in urban conditions, the accelerator pedal position is rarely zero.

The obtained results can be compared with results published previously by other researchers. In principle such a comparison is subject to a certain discrepancy, due to the influence of many factors on the driving style of the driver. In particular, not only the personal factors of the vehicle driver are important, but also vehicle performance, driving conditions, including weather, traffic, road infrastructure, etc. It is therefore difficult to find the results of tests that would have the same scope to current results. However, selected aspects of similar research may be compared.

Paper by Ericsson [6] presents an analysis of data collected in Sweden from five vehicles that were driven by 29 randomly chosen families for two weeks each. Comparing to present investigation, similar distribution of vehicle velocity, acceleration and deceleration can be observed. In Ericsson tests, vehicle velocity most often had a value between 50 km/h and 70 km/h when driven along two arterial roads, which corresponds to the results of current tests for extra-urban driving conditions (Fig. 3). It is also possible to indicate similarity in the case of urban driving (Fig. 2), but with less convergence, as the study of Ericsson took into account speed limits on specific roads, which affected the velocity achieved by the drivers. In the results of Ericsson's research, the most common acceleration and deceleration values were in the ranges (0–0.5) m/s^2 and (–0.5–0) m/s^2, respectively, both for urban and non-urban driving. The same value ranges were found in current study (Figs 8–13), except that under urban conditions driver B accelerated and braked more intensely.

An interesting comparison of average velocity of a vehicle is possible with a paper by Chłopek et al. [4], due to similar driving conditions. In that experimental work over 70 test drives were carried out by a single driver within the area of Mazowieckie and Łódzkie Voivodships, with the urban driving conditions tested in Warsaw. During the tests, driving parameters were recorded from the vehicle OBD system and in parallel from the device equipped with the GPS module. The following traffic conditions were distinguished in results: urban traffic congestions, urban traffic without congestions, extra-urban traffic, high-speed traffic. Under these conditions, the average velocity of the vehicle was: 8.6 km/h, 38.8 km/h, 75.8 km/h, and 123.1 km/h, respectively. In the current paper, only two categories of road conditions were distinguished: urban and extra-urban driving, with the following average vehicle velocity (respectively for the A/B driver): 22.4 km/h/ 26.7 km/h, 61.0 km/h/65.6 km/h.

When interpreting the results presented in this paper, the limitations of the study should be kept in mind. First of all, for the assessment of driving style, identical driving conditions should be created for both drivers, which of course is not possible during real traffic. In the road tests under consideration, drivers reacted to various road situations, used different, randomly selected routes, with different speed limits, and operated the vehicle in different weather and traffic conditions. On the other hand, the randomness of driving conditions has the advantage that, with a large number of samples taken, it reduces the influence of the test methods on the obtained results. Another limitation is the small range of recorded signals from the OBD system and

low sampling frequency. It would be beneficial to conduct similar tests using other signals that can be extracted from the CAN bus. This can be a future direction of development of current work.

5. Conclusions

To sum up the effects of this study, the following conclusions can be drawn:

– Information derived from the OBD vehicle system can be used to characterize and evaluate the driving style.
– The most important signals that are easily accessible from the OBD system and useful for assessing the driving style, are: vehicle velocity, engine rotational speed, relative accelerator pedal position, relative throttle valve position, relative engine torque and intake manifold pressure.
– Among the analyzed zero-dimensional characteristics, it was found that the most effective to assess the driving style are: maximum velocity of the vehicle (in extra-urban driving conditions), maximum acceleration, the average value of the velocity and acceleration product and finally average relative position of accelerator pedal excluding zero position.
– The use of appropriate criteria, based on the analysis of information from the OBD system of the vehicle, allows to distinguish the driving style of two drivers of the same vehicle.
– Driving style is generally easier to evaluate in urban traffic, which is characterized by greater dynamics than extra-urban traffic, although there are exceptions to this rule (e.g. the aforementioned application of maximum vehicle velocity).

Nomenclature

a^+_{AV} Average acceleration
a^-_{AV} Average deceleration
a^+_{MAX} Maximum acceleration
a^-_{MAX} Maximum deceleration
AP_{0AV} Average relative position of accelerator pedal, excluding zero position
AP_{AV} Average relative position of accelerator pedal
AP_{D0AV} Average relative position of accelerator pedal, excluding vehicle stop and zero position
AP_{DAV} Average relative position of accelerator pedal, excluding vehicle stops
AP_{DVAV} Average value of the derivative of the relative position of accelerator pedal
DLC Data Link Connector
ECU Engine Control Unit
OBD On Board Diagnostics
RPA Relative positive acceleration
v_{AV} Average velocity
v_{DAV} Average velocity excluding stops
v_{MAX} Maximum velocity
$v{\cdot}a^+_{AV}$ The average value of the velocity and acceleration product
$|v{\cdot}a|_{AV}$ The average value of the absolute value of the velocity and acceleration product

Bibliography

[1] ANDRIEU, C., PIERRE, G. Using statistical models to characterize eco-driving style with an aggregated indicator. *Proceedings of the IEEE Intelligent Vehicle Symposium (IV 2012)*. 2012, 63-68.

[2] ANDRYCH-ZALEWSKA, M., CHŁOPEK, Z., MERKISZ, J., PIELECHA, J. Evaluation of the test drive cycle conditions impact on exhaust emissions from an internal combustion engine. *Combustion Engines*. 2018, **175**(4), 3-9.

[3] BEUSEN, B., BROEKX, S., DENYS, T. et al. Using on-board logging devices to study the longer-term impact of an eco-driving course. *Transportation research part D: Transport and Environment*. 2009, **14**(7), 514-520.

[4] CHŁOPEK, Z., BIEDRZYCKI, J., LASOCKI, J., WÓJCIK, P. Investigation of the motion of motor vehicles in Polish Conditions. *The Archives of Automotive Engineering – Archiwum Motoryzacji*. 2013, **60**(2), 3-20.

[5] CHŁOPEK, Z., LASOCKI, J., WÓJCIK, P., BADYDA, A.J. Experimental investigation and comparison of energy consumption of electric and conventional vehicles due to the driving pattern. *International Journal of Green Energy*. 2018, **15**(13), 773-779, DOI:10.1080/15435075.2018.1529571

[6] ERICSSON, E. Driving pattern in urban areas – descriptive analysis and initial prediction model.. *Traffic Planning*. Bulletin 185. Lund Institute of Technology, Lund 2000.

[7] FONSECA, N., CASANOVA, J., ESPINOSA F. Influence of driving style on fuel consumption and emissions in diesel-powered passenger car. *Proceedings 18th International Symposium Transport and Air Pollution.* Dübendorf 2010.

[8] FUĆ, P., SIEDLECKI, M., SOKOLNICKA, B., SZYMLET, N. The influence of the driving style on the exhaust emission from a passenger car with a Euro 5 diesel engine. *Journal of Mechanical and Transport Engineering*. 2017, **69**(4), 5-19.

[9] GONDER, J., EARLEYWINE, M., SPARKS, W. Final report on the fuel saving effectiveness of various driver feedback approaches. *Report NREL/MP-5400-50836*. National Renewable Energy Laboratory, Golden 2011.

[10] HADGU, R. Statistical analysis of driver behaviour and eco-driving model based on CAN bus data. Master thesis report. School of Information Science, Computer and Electrical Engineering, *Halmstad University*. 2015.

[11] LEE, M.L., PARK, Y.K., JUNG, K.K., YOO, J.J. Estimation of fuel consumption using in-vehicle parameters. *International journal of u- and e-service, science and technology*. 2011, **4**(4), 37-46.

[12] MERKISZ, J., PIELECHA, J., PIELECHA, I. Influence of behaviour driver on vehicle ecology. *Logistyka.* 2010, **2**, 1911-1920.

[13] SAGBERG, F., SELPI, PICCININI, G.F., J. ENGSTRÖM, J. A review of research on driving styles and road safety. Human Factors, *The Journal of the Human Factors and Ergonomics Society*. 2015, **57**(7), 1248-1275, DOI:10.1177/0018720815591313

[14] TEXA. Promotional materials, www.texa.com.

[15] VAITKUS, V., LENGVENIS, P., ZYLIUS, G. Driving style classification using long-term accelerometer information.

Proceedings of 19th International Conference on Methods and Models in Automation and Robotics (MMAR). IEEE, 2014, 641-644. DOI: 10.1109/MMAR.2014.6957429

[16] WANG, W., XI, J., CHONG, A., LI, L. Driving style classification using a semi-supervised support vector machine. *IEEE Transactions on Human-Machine Systems*, 2017, **47**(5), 1-11. DOI:10.1109/THMS.2017.2736948

Jakub Lasocki, DEng. – Faculty of Automotive and Construction Machinery Engineering, Warsaw University of Technology.
e-mail: *jakub.lasocki@pw.edu.pl*

Prof. Zdzisław Chłopek, DSc., DEng. – Faculty of Automotive and Construction Machinery Engineering, Warsaw University of Technology.
e-mail: *zdzislaw.chlopek@pw.edu.pl*

Tomasz Godlewski, Eng. – Faculty of Automotive and Construction Machinery Engineering, Warsaw University of Technology.
e-mail: *tomus239@wp.pl*

Article citation info:
SROKA, Z.J., DWORACZYŃSKI, M.K. Assessment of thermodynamic cycle of internal combustion engine in terms of rightsizing. *Combustion Engines*. 2019, **178**(3), 182-186. DOI: 10.19206/CE-2019-331

Zbigniew J. SROKA
Maciej K. DWORACZYŃSKI

CE-2019-331

Assessment of thermodynamic cycle of internal combustion engine in terms of rightsizing

The modification of the downsizing trend of internal combustion engines towards rightsizing is a new challenge for constructors. The change in the displacement volume of internal combustion engines accompanying the rightsizing idea may in fact mean a reduction or increase of the defining swept volume change factors and thus may affect the change in the operating characteristics as a result of changes in combustion process parameters - a research problem described in this publication. Incidents of changes in the displacement volume were considered along with the change of the compression space and at the change of the geometric degree of compression. The new form of the mathematical dependence describing the efficiency of the thermodynamic cycle makes it possible to evaluate the operation indicators of the internal combustion engine along with the implementation of the rightsizing idea. The work demonstrated the invariance of cycle efficiency with different forms of rightsizing.

Key words: *internal combustion engine, thermodynamic cycle, rightsizing*

1. Introduction – defining the research problem

Continuous work on improving the efficiency of internal combustion engines results in a variety of development trends. One of them is downsizing, lasting for over ten years, which has recently been modified in the direction of not reducing the displacement volume, but also the proper selection of its size in order to ensure reduction of fuel consumption and carbon dioxide emission to the atmosphere while simultaneously satisfying users' comfort of operation as, for example, the possibility of transporting a certain size of cargo, constituting a sustainable development of means of transport. The new development trend is called rightsizing.

Each change in the geometrical volume of the combustion chamber is accompanied by a change in the conversion of energy contained in the fuel, which in its assumption should burn completely. The change in the swept volume of internal combustion engines accompanying the rightsizing idea may in fact mean a reduction or increase in the coefficients defining the displacement volume and thus may affect the change in the operating characteristics as a result of changes in the combustion process parameters.

The assessment of the impact of changes in the rightsizing index on the efficiency of the thermodynamic cycle of an internal combustion engine is a research problem described in this publication.

2. Rightsizing vs. downsizing

Constructive activities in the field of development works with the use of the rightsizing idea are associated primarily with the increase in unit power as one of the significant engine performance indicators. So these are actions that coincide with earlier ones in the field of downsizing.

In order to preserve or even increase the unit power of the engine, it is necessary to support geometric changes in the displacement volume with systems, among which the most important place is: boosting, direct fuel injection and variable valve timing [6, 10–12].

The boosting of the internal combustion engine, which aims to increase the filling factor, has a different constructional and functional form, the most common of which is turbocharging using the energy of exhaust gases. It can be realized using a single turbo compressor system with fixed operation parameters or with variable settings of the turbine blades. Such systems can be one or two-stage, with or without cooling, etc. Boosting is the simplest system to support structural changes of the displacement volume, both in terms of preventing power losses and creating conditions conducive to burning poor mixtures that occur both in downsizing and rightsizing.

The second of the support systems - direct fuel injection is a system that guarantees the correct atomization of fuel droplets, which together with the possibility of several times their injection during a single cycle ensures full evaporation and combustion. The use of direct injection fits well into the operation of an engine with a reduced displacement volume (downsizing) because it directly replenishes the power losses resulting from changes in geometry. In the case of an increase in the displacement volume (possible rightsizing version), direct fuel injection ensures combustion of poor mixtures.

In turn, the variable valve timing system is characterized by a large range of different constructions, but their general working principle is to ensure that the angles and opening times of valve are adjusted to the current operational situation, i.e. rotational speed and engine load. Variable valve timing ensures proper filling of the combustion chamber, thus ensuring that the efficiency of the internal combustion engine is maintained and even increased and through functional boost and direct injection support conditions of stoichiometric combustion for both downsizing and rightsizing.

An engineering practice can show a number of examples of the development of downsizing ideas. These include engines mounted in Ford vehicles, where the 6.2 dm^3 V8 unit has undergone structural changes to 3.5 dm^3 V6, followed by 1.6 dm^3, to achieve a spectacular 0.999 dm^3 EcoBoost. In turn, the Volkswagen brand engines changing the displacement volume from 2.8 dm^3 or 2.0 dm^3 to 1.8 dm^3 and then to 1.4 dm^3, fulfilled the downsizing assumptions, reaching the 0.90 and 0.64 volume change ratios, to achieve

1.07 when balanced (rightsizing) – when 1,4 dm^3 TSI changed to 1.5 dm^3 TSI.

The mentioned measure, both downsizing and rightsizing, is the degree (index) of changes, which is variously defined [4, 5, 8, 14, 18, 19], but generally informs about the change or the degree of residue after reducing or increasing the displacement volume. Unlike everybody, the authors defined the downsizing index (W_d) based on the degree of changes in the components describing the cylindrical combustion space, which dominates the construction of internal combustion engines [19]. According to this definition, the downsizing index can be described as in formula (1).

$$W_d = 1 - AB^2 \tag{1}$$

$$A = \frac{S_d}{S} \qquad B = \frac{D_d}{D}$$

In practical solutions, a mixed downsizing dominates, i.e. in which a simultaneous change in piston stroke is accompanied by a change in cylinder diameter. From the point of view of engine construction and manufacturing technology, single modifications are also possible. In [18, 19], various types of changes in the displacement volume of internal combustion engine were defined and described, taking them into mathematical and graphic forms.

By implementing the rightsizing idea, it is possible to obtain the same changes in the W_d index at various changes in the value of stroke and diameter, which results from the difference in the values of the coefficients A and B (see Eq.(1)) – Fig.1.

	A																				
	1.60	-0.60	-0.44	-0.30	-0.16	-0.02	0.10	0.22	0.32	0.42											
	1.55	-0.55	-0.40	-0.26	-0.12	0.01	0.13	0.24	0.35	0.44											
	1.47	-0.47	-0.33	-0.19	-0.06	0.06	0.17	0.28	0.38	0.47											
	1.45	-0.45	-0.31	-0.17	-0.05	0.07	0.18	0.29	0.39	0.48											
	1.39	-0.39	-0.25	-0.13	0.00	0.11	0.22	0.32	0.41	0.50											
	1.35	-0.35	-0.22	-0.09	0.02	0.14	0.24	0.34	0.43	0.51											
	1.28	-0.28	-0.16	-0.04	0.08	0.18	0.28	0.37	0.46	0.54											
	1.25	-0.25	-0.13	-0.01	0.10	0.20	0.30	0.39	0.47	0.55											
	1.22	-0.22	-0.10	0.01	0.12	0.22	0.31	0.40	0.48	0.56											
	1.15	-0.15	-0.04	0.07	0.17	0.26	0.35	0.44	0.51	0.59											
	1.08	-0.08	0.03	0.13	0.22	0.31	0.39	0.47	0.54	0.61											
	1.05	-0.05	0.05	0.15	0.24	0.33	0.41	0.49	0.56	0.62											
B	1.60	1.55	1.50	1.45	1.40	1.35	1.30	1.25	1.20	1.15	1.10	1.05	Wd	1.00	0.95	0.90	0.85	0.80	0.75	0.70	0.65	0.60
	-1.56	-1.40	-1.25	-1.10	-0.96	-0.82	-0.69	-0.56	-0.44	-0.32	-0.21	-0.10	1.00	0.00	0.10	0.19	0.28	0.36	0.44	0.51	0.58	0.64
	-1.46	-1.31	-1.16	-1.02	-0.88	-0.75	-0.62	-0.50	-0.38	-0.27	-0.16	-0.06	0.96	0.04	0.13	0.22	0.31	0.39	0.46	0.53	0.59	0.65
	-1.30	-1.16	-1.03	-0.89	-0.76	-0.64	-0.52	-0.41	-0.30	-0.19	-0.09	0.01	0.90	0.10	0.19	0.27	0.35	0.42	0.49	0.56	0.62	0.68
	-1.20	-1.07	-0.94	-0.81	-0.69	-0.57	-0.45	-0.34	-0.24	-0.14	-0.04	0.05	0.86	0.14	0.22	0.30	0.38	0.45	0.52	0.58	0.64	0.69
	-1.05	-0.92	-0.80	-0.68	-0.57	-0.46	-0.35	-0.25	-0.15	-0.06	0.03	0.12	0.80	0.20	0.28	0.35	0.42	0.49	0.55	0.61	0.66	0.71
	-1.00	-0.87	-0.76	-0.64	-0.53	-0.42	-0.32	-0.22	-0.12	-0.03	0.06	0.14	0.78	0.22	0.30	0.37	0.44	0.50	0.56	0.62	0.67	0.72
	-0.82	-0.71	-0.60	-0.49	-0.39	-0.29	-0.20	-0.11	-0.02	0.06	0.14	0.22	0.71	0.29	0.36	0.42	0.49	0.55	0.60	0.65	0.70	0.74
	-0.65	-0.55	-0.45	-0.36	-0.26	-0.18	-0.09	-0.01	0.07	0.15	0.22	0.29	0.65	0.36	0.42	0.48	0.53	0.59	0.64	0.68	0.73	0.77
	-0.51	-0.42	-0.33	-0.24	-0.16	-0.08	0.00	0.08	0.15	0.22	0.29	0.35	0.59	0.41	0.47	0.52	0.57	0.62	0.67	0.71	0.75	0.79
	-0.38	-0.30	-0.22	-0.14	-0.06	0.02	0.09	0.16	0.22	0.29	0.35	0.40	0.54	0.46	0.51	0.56	0.61	0.65	0.70	0.74	0.77	0.81
	-0.28	-0.20	-0.13	-0.05	0.02	0.09	0.16	0.22	0.28	0.34	0.40	0.45	0.50	0.50	0.55	0.60	0.64	0.68	0.72	0.76	0.79	0.82
	-0.13	-0.06	0.01	0.07	0.14	0.20	0.26	0.31	0.37	0.42	0.47	0.51	0.44	0.56	0.60	0.64	0.68	0.72	0.75	0.78	0.81	0.84
	-0.02	0.04	0.10	0.16	0.22	0.27	0.32	0.38	0.42	0.47	0.52	0.56	0.40	0.60	0.64	0.68	0.71	0.74	0.78	0.80	0.83	0.86
	0.09	0.15	0.20	0.25	0.30	0.35	0.40	0.45	0.49	0.53	0.57	0.61	0.36	0.65	0.68	0.71	0.74	0.77	0.80	0.83	0.85	0.87
	0.23	0.28	0.33	0.37	0.41	0.45	0.49	0.53	0.57	0.60	0.64	0.67	0.30	0.70	0.73	0.76	0.78	0.81	0.83	0.85	0.87	0.89

Fig. 1. Matrix of downsizing index W_d with coordinates marked (coefficients A and B) with the same values $W_d = 0.22$

The changes in the W_d included in the matrix in Fig. 1. indicate the possibility of any choice of changes in the A and B coefficients shaping the geometry of the combustion chamber. Positive values show decrease in downsizing volume and negative values declare its increase (upsizing). In this way it is possible for multiple actions to fulfill the idea of mixing according to the mixed rule i.e. with simultaneous change of A and B. The values described in the matrix also indicate changes in the stroke volume realized by reducing one of the coefficients with the simultaneous increase of the second. For an exemplary change of W_d = 0.22 (change in engine volume from 1.8 to 1.4 dm^3), many variants are possible, including changes in coefficients: A from 0.50 to 1.60 and B from 0.70 to 1.25 – Table 1.

Table 1. The matrix of changes of the coefficients A and B for the downsizing index $W_d = 0.22$

No	Coefficient A		Coefficient B		B/A	Remarks
	value	form	value	form		
1.	1.60	upsizing	0.70	downsizing	0.44	
2.	1.39		0.75		0.54	
3.	1.22		0.80		0.66	
4.	1.08		0.85		0.79	Analyze range
5.	0.96	downsizing	0.90		0.94	
6.	0.86		0.95		1.10	
7.	0.78		1.00	neutral	1.28	
8.	0.71		1.05	upsizing	1.48	
9.	0.65		1.10		1.69	
10.	0.59		1.15		1.95	
11.	0.54		1.20		2.22	
12.	0.50		1.25		2.50	

Having knowledge about the design of the internal combustion engine in the area of the combustion chamber and crank system and commonly accepted geometrical relationships between the cylinder diameter and stroke [9, 13, 15], as well as based on real relations of these parameters determined on the basis of engines from the Engine of the Year Competition [19, 20] it was possible to determine the range of variation of the ratio of cylinder diameter to piston stroke, which was evaluated from 1.28 to 0.79. This authorizes to limit further considerations of the research problem to this range i.e. consideration of the influence of volume changes according to the rightsizing rules on cycle efficiency for cases: A = 0.78–1.08 and B = 1.00–0.85 – from Table 1.

The research problem put forward in the introduction, such as the variability of geometric changes demonstrated by the different values of the A and B coefficients, while maintaining the same swept volume change index, affect the operation of the internal combustion engine based on the identification of the generalized thermodynamic cycle.

3. Efficiency of a generalized engine cycle in the aspect of rightsizing - research methodology

In the combustion chamber of a reciprocating internal combustion engine, fuel mixed with air creates a working medium that undergoes thermodynamic changes related to, inter alia, changes in the volume of the combustion space. These changes are repetitive, although their size depends on the current engine operating conditions. The occurring transformations form the engine work cycle, described mathematically in various ways [2, 3, 7, 16, 17]. In the generalized form, corresponding to all known theories of internal combustion engines, the work cycle can be described by the efficiency (ηt) as per formula (2) and expressed graphically as in Fig. 2 [1, 2, 16, 17].

$$\eta_t = 1 - \frac{\frac{\lambda_p \rho_p \varepsilon_s^{\kappa-1}}{\delta^{\kappa-1}} + \kappa(\rho' - 1) - \rho'}{\varepsilon_s^{\kappa-1}\{\lambda_p[\kappa\rho_p - (\kappa-1)(1+\rho_p \ln\rho_T)] - 1\}} \tag{2}$$

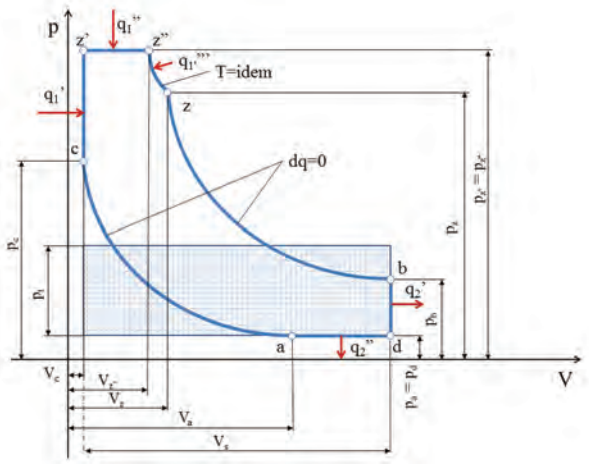

Fig. 2. Generalized thermodynamic cycle of a four-stroke internal combustion engine [2]

If each of the values forming the formula for efficiency are included in the volume change function, it will be possible to use the relationship (2) to describe the changes caused by changes in the engine swept volume (3) [19].

$$\eta_t = 1 - \frac{\frac{\lambda_p\left(\frac{V_z''}{V_c}\right)\left(\frac{V_a}{V_c}\right)^{\kappa-1}}{\left(\frac{V_b}{V_z}\right)^{\kappa-1}} + \kappa\left[\left(\frac{V_b}{V_a}\right)-1\right] - \frac{V_b}{V_a}}{\left(\frac{V_a}{V_c}\right)^{\kappa-1}\left\{\lambda_p\left[\kappa\left(\frac{V_z''}{V_c}\right)-(\kappa-1)\left(1+\left(\frac{V_z''}{V_c}\right)\ln\left(\frac{V_z}{V_z''}\right)\right)\right]-1\right\}} \quad (3)$$

Components λ_p, V_a, V_z, V_z'', κ are resulting from the properties of the fuel used and the logistics of the combustion process, while V_b and V_c are constructional parameters of the combustion engine related to the combustion space and are therefore related to the operation within the rightsizing idea.

When assessing the effectiveness of using the rightsizing idea, three cases can be considered:

1. $V_{sd} \neq V_s$; $V_{cd} = V_c$; $\varepsilon_d \neq \varepsilon$
2. $V_{sd} \neq V_s$; $V_{cd} \neq V_c$; $\varepsilon_d \neq \varepsilon$
3. $V_{sd} \neq V_s$; $V_{cd} \neq V_c$; $\varepsilon_d = \varepsilon$

In the first case, along with the change of the engine volume V_s to V_{sd} (index "d" informs about the change in volume) and while maintaining the volume of compression space ($V_c = V_{cd}$) will change the compression ratio (ε to ε_d).

In the second case, the analysis of changes caused by rightsizing is possible when either the volume of the compression space (V_{cd}) or the geometric compression ratio (ε_d) will be a known input value.

In engineering practice, the known input value is the compression ratio, the value of which defines the correctness of self-ignition in the diesel engine and in the case of spark-ignition engines, it allows combustion of the working medium without knocking. In general, this means that the theoretical efficiency of the work cycle will be independent of the rate of changes in the volume of W_d, i.e. independent of the coefficients A and B.

The third case determines the change in the engine's swept volume (V_s to V_{sd}), which will be accompanied by the change of the compression space volume (V_c to V_{cd}) while maintaining the geometric degree of compression ($\varepsilon = \varepsilon_d$). This case was decided to consider in detail taking into account possible changes in the A and B coefficients described in Table 1.

Formula (3) describing the theoretical efficiency of the combustion engine cycle after rightsizing, in the case under consideration takes the form (4) [19]:

$$\eta_t = 1 - \frac{\frac{\lambda_{pd}\left(\frac{V_z''_d}{V_cAB^2}\right)\left(\frac{V_{ad}}{V_cAB^2}\right)^{\kappa_d-1}}{\left(\frac{V_b}{V_z}\right)^{\kappa-1}} + \kappa_d\left[\left(\frac{(V_s+V_c)AB^2}{V_{ad}}\right)-1\right] - \frac{(V_s+V_c)AB^2}{V_{ad}}}{\left(\frac{V_{ad}}{V_cAB^2}\right)^{\kappa_d-1}\left\{\lambda_{pd}\left[\kappa_d\left(\frac{V_z''_d}{V_cAB^2}\right)-(\kappa_d-1)\left(1+\left(\frac{V_z''_d}{V_cAB^2}\right)\ln\left(\frac{V_{zd}}{V_z''_d}\right)\right)\right]-1\right\}} \quad (4)$$

In the research methodology, successive values of pairs of coefficients A and B from table 1 are introduced, calculating changes in the thermodynamic efficiency of the work cycle. Other data was taken from the research on the 1.4 TSI engine, which is one of the links in the rightsizing engine chain of the Volkswagen brand.

4. Evaluation of work cycle efficiency with variable volume of compression space for maintaining the geometric degree of compression

The theoretical and experimental data from the tests of the VW 1.4 TSI combustion engine carried out in the Department of Automotive Engineering at the Wroclaw University of Science and Technology were used to assess the presented research problem. The tested 1.4 TSI engine is a smaller version of the 1.8 FSI one, which means the value of the change in the displacement volume W_d = 0.22 – Figures 3 and 4.

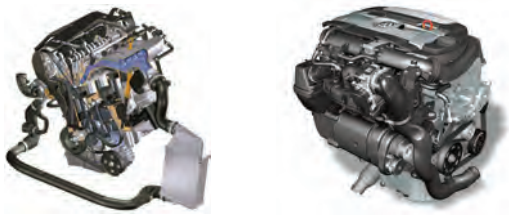

1.8 T (years 1995-2008)
AMB (125 kW; 225 Nm)
CFMA (110 kW; 220 Nm)

1.4 TSI (years 2005-…)
CAVC (125 kW; 240 Nm)
CAVB (103 kW; 220 Nm)

Fig. 3. VW 1.8 and 1.4 dm^3 engines constituting the rightsizing chain [21]

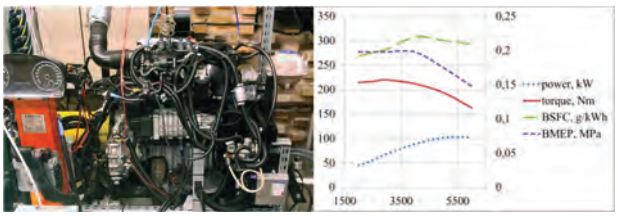

Fig. 4. VW 1.4 dm^3 engine on the test bench and its performance

Four different values (based on Table 1) of coefficients A and B were adopted for the study to obtain the same value of W_d = 0.22. The remaining data filling the form of equation No. 4 was obtained from the mentioned laboratory tests. In this way, it was possible to estimate the efficiency value for the assessment of the impact of rightsizing when changing the compression space, while maintaining the geometric degree of compression – Table 2.

Table 2. Efficiency values of the generalized motor cycle for the W_d ratio = 0.22 at variable values of piston stroke changes (factor A) and cylinder diameter (factor B)

A	B	W_d	η_t
1.08	0.85	0.220	0,502
0.96	0.90	0,222	0,500
0.86	0.95	0,224	0,499
0.78	1.00	0,220	0,502

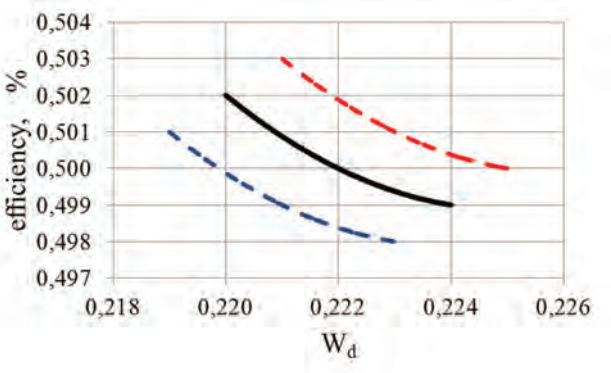

Fig. 5. Determination of significance of efficiency changes

The diagram – Fig. 5. presents changes in the average efficiency of the engine (center line) within the range of permissible deviations (bar lines) indicating the lack of significance of changes. For the case studied, the obtained results together with the evaluation of deviations of their value and thus the lack of statistical significance, indicate the invariance of the generalized cycle of operation of the internal combustion engine for different coefficients of change of parameters A and B shaping the size of geometrical changes of stroke volume while maintaining the index of changes in the displacement volume.

5. Summary

The work discusses the issue of the change in the displacement volume of an internal combustion engine, occurring in the generally realized development trend of rightsizing. The research problem was defined which was the assessment of the impact of different geometric changes in piston stroke and cylinder diameter while maintaining the same value of the index of changes in the displacement volume on the efficiency of the engine's work cycle. The data for the analysis was obtained from laboratory tests and using own software ensuring multiple estimation of indirect values defining the efficiency of the engine.

Assessing the case of the implementation of the rightsizing idea, in which the compression space was changed, while maintaining the geometric degree of compression, the results showed the invariance of the efficiency of the combustion engine cycle independently of the factors A and B, which determine the geometric changes in the swept volume of the engine. The results obtained should be interpreted so that the magnitude of changes in the efficiency of the work cycle depends on the global value of the volume change and not on its partial values.

Nomenclature

A	coefficient of change of piston stroke
B	coefficient of change of cylinder diameter
D	cylinder diameter – input state
D_d	cylinder diameter in the downsized engine
S	stroke of the piston – input state
S_d	stroke of the piston in the downsized engine
W_d	downsizing index
δ	degree of another expansion process
ε	geometric compression ratio
ε_s	effective compression ratio
η_t	theoretical efficiency of the work cycle
κ	isentropic exponent
λ_p	degree of pressure increase during isochoric heat transfer
ρ'	degree of pre-compression when heat is drained at constant pressure
ρ_p	degree of expansion during isobaric heat transfer
ρ_T	degree of expansion during isothermal heat transfer

Bibliography

[1] AMBROZIK, A. Wybrane zagadnienia procesów cieplnych w tłokowych silnikach spalinowych. *Wydawnictwo Politechniki Świętokrzyskiej*. Kielce 2003.

[2] AMBROZIK, A. Analiza cykli pracy czterosuwowych silników spalinowych. *Wydawnictwo Politechniki Świętokrzyskiej*. Kielce 2010

[3] AMBROZIK, A., DANILCZYK, W., KRUCZYŃSKI, S.W. Simulation of on indicato diagram of a diesel engine. Polish Academy of Sciences Branch in Lublin, *Commission of Motorization and Energetics in Agriculture*. 2003, **Vol. III**, 12-17.

[4] BRZEŻAŃSKI, M., ŚLIWIŃSKI, K. Downsizing nowy kierunek rozwoju silników samochodowych. *Silniki Spalinowe*. 2004, **119**(2), 3-11.

[5] FRASER, A.D.J. How low can we go? Challenges and opportunities of engine downsizing to reduce CO_2 emissions. *Seminar Proceedings IMechE*. London, 9 February 2011, 1-9.

[6] FRASER, N., BASSETT, M. Extreme engine downsizing with a single turbochanger – 100 kW/l and 30 bar BMEP. *Seminar Proceedings IMechE*. London, February 2011, 31-45.

[7] GNUTEK, Z., NEMŚ, A., POMORSKI, M. Badania niestechiometrycznego spalania mieszanek wzbogaconych w tlen w silnikach cieplnych o zapłonie iskrowym. Materiały XIV Sympozjum Wymiany Ciepła i Masy. Międzyzdroje, 2010, *Wydawnictwo Uczelniane Zachodniopomorskiego Uniwersytetu Technologicznego*. Szczecin 2010, 217-224.

[8] GNUTEK, Z., KOLASIŃSKI, P.K. Application of volumetric machines in micro steam power plants. *Archiwum Energetyki*. 2010, **40**(1/2), 63-74.

[9] HEYWOOD, J.B., Internal Combustion Engine Fundamentals, *McGraw HiU International Editions.* 1989.
[10] JENTEGES, M., VAN DER WEEM, D. et al. Optimized activation of a downsizing concept with electrical boost. *MTZ.* 2006, **67**(4).
[11] KEMPER, H., BAUMGARTEN, H., HEBERMANN, K. et al. On the road towards consequent downsizing. *MTZ Worldwide.* 2003, **54**(5), 16-18.
[12] KING, J. Application of synergistic technologies to achive high levels of gasoline engine downsizing. *Seminar Proceedings IMechE.* London, 9 February 2011, 59-72.
[13] LUFT, S. Podstawy budowy silników. *WKŁ.* Warszawa 2006.
[14] PIELECHA, I., CIEŚLIK, W., BOROWSKI, P. et al. Reduction of the number of cylinders in internal combustion engines – contemporary trends in downsizing. *Combustion Engines.* 2014, **159**(4), 12-25.
[15] PISCHINGER, S. Verbrennungskraftmaschinen I. Aachen: *RWTH. Aachen* 2011.
[16] POSTRZEDNIK, A., ŻMUDKA, Z. Termodynamiczne oraz ekologiczne uwarunkowania eksploatacji tłokowych silników spalinowych. *Politechnika Śląska.* Gliwice 2007.
[17] RYCHTER, T.J., TEODORCZYK, A. Teoria silników tłokowych. *WKŁ.* Warszawa 2006.
[18] SROKA, Z.J., Some aspects of thermal load and operating indexes after downsizing for internal combustion engine. *Journal of Thermal Analysis and Calorimetry.* 2012, **110**(1), 51-58.
[19] SROKA, Z.J. Wybrane zagadnienia teorii tłokowych silników spalinowych w aspekcie zmian objętości skokowej. *Oficyna Wydawnicza Politechniki Wrocławskiej.* Wrocław 2013.
[20] http://www.ukimediaevents.com/engineoftheyear/
[21] http://www.auto-swiat.pl

Zbigniew J. Sroka, DSc., DEng. – Faculty of Mechanical Engineering, Wroclaw University of Science and Technology.
e-mail: *zbigniew.sroka@pwr.edu.pl*

Maciej K. Dworaczyński, MSc. – Faculty of Mechanical Engineering, Wroclaw University of Science and Technology.
e-mail: *maciej.dworaczynski@pwr.edu.pl*

Article citation info:
STRUŚ, M., POPRAWSKI, W. Improvement of the compression ignition behaviour and combustion efficiency of the second generation biofuel BIOXDIESEL. *Combustion Engines*. 2019, **178**(3), 187-190. DOI: 10.19206/CE-2019-332

Mieczysław STRUŚ
Wojciech POPRAWSKI

CE-2019-332

Improvement of the compression ignition behaviour and combustion efficiency of the second generation biofuel BIOXDIESEL

Biodiesel fuel is covering more and more place in the market. The reason is a limited fossil fuels resources and the need to reduce emission of harmful substances by application of the fuel made of renewable resources. Currently in Poland and in Europe, the Fatty Acid Methyl Esters are used as biocomponent of the biodiesel fuel or it is used as pure biodiesel fuel. This paper presents the research on the biofuel, which contains mainly Fatty Acid Ethyl Esters, (the energetic value of FAEE is higher than FAME) and mineral Diesel fuel is a small addition. This paper presents research on the improvement of the compression ignition behaviour and combustion effectiveness of the second generation biofuel BIOXDIESEL, which contains up to 75% of biocomponents (FAEE with bioethanol) with addition of mineral Diesel fuel. Improvement of the auto-ignition properties is achieved through the multi-component composition of Bioxdiesel fuel and dosing of enriching additives. The quality of the fuel has been evaluated during engine testing and during laboratory measurement of fuel parameters. Whereas satisfactory results show that it is appropriate to supplement the composition of biofuels produced from waste vegetable and animal fats and alcohol with the refining additive.

Key words: *biodiesel, fatty acid ethyl esters, compression ignition engines*

1. Introduction

Modern Diesel engines and increased environmental attention require constant improvement of the physical and chemical properties of the fuel obtained during crude oil processing. This improvement is achieved both on the way of refinery processing and by dosing of various types of additives.

One of the most popular enriching additives are those used in order to increase low temperature behaviour of the Diesel fuel used in cold climate conditions. Some other additives are used to increase storage ability of fuel by improving oxidation stability and the biocydes to eliminate microorganisms, which presence increase biodegradation of fuel are used to increase to lifetime of the fuel. One of the most important group of the additives are those, which are increasing cetane number of the fuel. The value of cetane number is responsible for compression ignition properties of the fuel, which are significantly important during variable load of the engine, ie in non-stationary conditions.

Properties of pure biodiesel fuels, consisting only Fatty Acid Methyl Esters FAME or Fatty Acid Ethyl Esters FAEE, are very similar to the properties of mineral Diesel fuel. Main differences between FAME or FAEE and the fuel standard are related to the flash point, cetane number, low temperature properties – cloud point (CP) and cold filter plugging point (CFPP), kinematic viscocity and density. Comparison of the selected properties of FAEE, FAME and Diesel fuel are presented in Table 1.

Table 1. Selected properties of FAEE, FAME and Diesel fuel

Properties	FAEE	FAME	Diesel Fuel
Flash Point [°C]	135	101	55
Cloud Point [°C]	–8	–6	–10 (grade F)
Cold Filter Plugging Point [°C]	–11	–16	–20 (grade F)
Cetane Number (CN)	49	47	51
Kinematic viscosity at 40°C [mm^2/s]	4.5	3.5	2
Density at 15°C [kg/m^3]	877	860	820–845
Calorific value [MJ/kg]	39	36–38	42.8

Properties, presented in the table above can be adjusted by dosing the right additives. Low temperature properties of Diesel fuel are season depending. The PN-EN 590 standard divides fuel into 6 grades depending on season. For arctic or severe winter climate the CP and CFPP are set to –34°C and –44°C respectively.

The possibilities of cetane number (CN) improvement of Diesel fuel and/or BIODIESEL by use of specially selected additives has been a subject of many research. In [1] authors test various types of CN improvers and test the presence of CN improvers in various fraction of distilled fuel.

In [2] author test the Diesel engine fed with different biodiesel fuel (containing methyl esters) with CN improvers and measure energetic and exergetic behaviour of the engine.

An influence of cetane number improvers on performance of biodiesel fuel containing FAME is also presented in [3], where authors also study influence of CN improvers on coking of the fuel injector nozzles.

2. Preparation of the samples of the BIOXDIESEL fuel

Bioxdiesel fuel is a composition of bio-components containing Fatty Acid Ethyl Esters and/or Fatty Acid Methyl Esters with bioethanol and an addition of mineral Diesel fuel. The BIOXDIESEL fuel has been previously tested during the fleet vehicle testing over long distance [4, 5]. Papers [4, 5] indicate good properties of the three component fuels in application for the Diesel engines. However, some of the properties still require improvement.

The samples of the FAEE used to prepare the BIOXDIESEL fuel were obtained on the way of the transesterification with bioethanol reaction of the waste animal (poultry and pork) fats and waste vegetable fats (frying oil), with small addition of rapeseed oil in the presence of alkali (KOH) catalyst. The reaction has been performed with the use of laboratory scale set up, which contains vacuum evaporator to separate excess of bioethanol (see Fig. 1).

Further, the glycerine is separated from FAME on the way of sedimentation. Fatty acid ethyl esters obtained in above described way are the base of the biofuel BIOXDIESEL (approximately 70%). Further, the standard Diesel fuel, purchased in local fuel station has been added (approx. 25%). The last ingredient was bioethanol (approx. 5%).

Fig. 1. The set up used to perform the transesterification reaction

3. Improvement of the low temperature properties of the BIOXDIESEL fuel

Pure biodiesel fuel, which contains only FAME or FAEE has similar properties as the mineral Diesel fuel. Main differences are related to low temperature behavior of the fuel. The standards (eg. PN-EN 590) are specifying the values of main parameters (CP and CFPP) as climate dependent requirements. So the fuel, which contains only esters can easily be used as a fuel in the regions with mild or warm climate conditions. To use the biodiesel fuel in colder weather condition, it would be necessary to improve the values of the CP and CFPP parameters.

There are various strategies to meet standardized requirements. One of the methods is to prepare the blended fuel, which contains both FAME and/or FAEE as well as mineral Diesel fuel. In such a case, mineral Diesel content would have to be increased. Table 2 presents the results of the low temperature testing of the fuel samples with various FAEE content. It is noticeable, that even for the samples, with maximum 80% of the mineral Diesel content, the lowest values of CP and CFPP does not meet the standard requirements for colder climate conditions.

Table 2. Low temperature properties of the fuel with various FAEE content

Sample	FAEE content [%]	Diesel content [%]	CP [°C]	CFPP [°C]
B20	20	80	–10	–12
B30	30	70	–7	–12
B40	40	60	–5	–9
B50	50	50	–4	–6

The other method would be related with dosing cold flow additives to improve the cold flow properties of the fuel, which contains only FAEE (without addition of mineral fuel). The result of the improvement of the CFPP is shown in Table 3. The CFPP of pure FAEE has been improved significantly by 6°C.

Table 3. Improvement of the FAEE cold flow properties by addition of cold flow improving additives

Sample	Cold flow improver content	Biocyde and oxidation stability additive content	CFPP [°C]
B100-1	0	0	–12
B100-2	4000 ppm	250 ppm	–18

The other strategy of improvement of cold flow properties of the FAEE fuel would be a combination of addition of mineral Diesel fuel and cold flow improving additives.

Table 4. Cold flow properties of the fuel containing FAEE and mineral Diesel fuel with cold flow improving additives

Sample	FAEE content [%]	Diesel content [%]	Cold flow improver content	CFPP [°C]
B50	50	50	4000 ppm	–25
B70	70	30	4000 ppm	–23
B80	80	20	4000 ppm	–21

Table 4 shows result of the cold flow properties improvement on the way of dosing mineral Diesel fuel and cold flow improving additives. It is noticeable, that the fuel, which contains 70% of FAEE and the cold flow improvement additives shows a balance between the FAEE content and low temperature behavior of the fuel.

4. Improvement of compression ignition behaviour of BIOXDIESEL fuel

Selected properties of the FAEE, FAME and Diesel fuel are presented in Table 1. The properties of ethyl and methyl esters are very close to the properties of mineral fuel. The main differences, except cold flow properties, are related to cetane number and calorific values of the fuels. The properties of mineral Diesel fuel are slightly higher than in esters. The differences can be easily equalized on the way of dosing of the cetane number improving additives and blended with small amount of standard Diesel fuel.

Table 5 shows the results of the cetane number improvement of the BIOXDIESEL fuel. The fuel contained 70% of the bio-components (FAEE and bioethanol) and 30% of mineral Diesel. One can notice, that the careful addition of the cetane number improvers enables to meet the requirements given in the standards, describing the properties of Diesel fuel (eg. PN-EN 590).

Table 5. Results of cetane number measurement as a function of cetane number improver content

Sample	FAEE + Bioethanol content [%]	Cetane number improver content [ppm]	Cetane number
Biox 1	70%	0	48.5
Biox 2	70%	1500	49.4
Biox 3	70%	3000	51.1

5. Determination of energy generated by the engine fed with BIOXDIESEL fuel with various content of cetane number improvers

The procedure of engine testing at non-stationary condition is described in details in [4, 6, 7]. The method is based on the accurate recording of the rotational speed of the crankshaft of the tested engine during cyclical acceleration and deceleration, from idling to maximal engine speed and back to idling. The cyclical changes of engine speed is very similar to the one during smoking test of the vehicles during periodical technical inspection of the vehicle.

The engine rotational speed can be either recorded with a use of encoder (in case of the laboratory engines) or in case of the whole vehicles, the engine speed is recorded with the use of the inductive sensor (similar one to the one used to measure crank shaft or cam shaft position in the engine) and a magnet installed on the crank shaft ending and high speed data acquisition device. The recorded signal is being processed in order to calculate the engine crankshaft rotational speed and angular acceleration.

Assuming, that the polar moment of inertia of the moving parts of the engine is constant, the equation (1) shows relation between torque generated by the engine angular acceleration of the engine crank shaft.

$$M = J\frac{d\omega}{dt} = J\varepsilon \tag{1}$$

where M – torque generated by the engine, ω – angular speed of engine's crank shaft, J – polar moment of inertia of the rotary parts, ε – angular acceleration of the engine crank shaft.

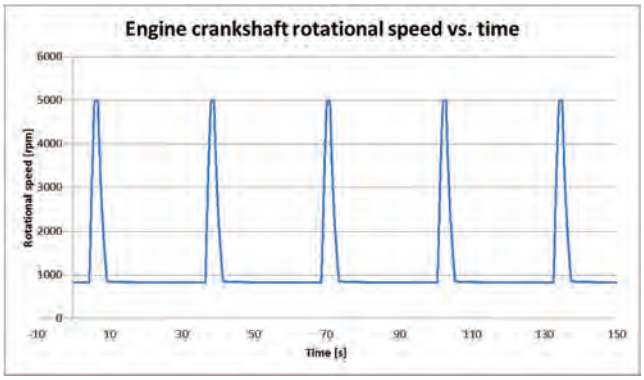

Fig. 2. Example of recorded data (engine crankshaft speed vs. time)

Figure 2 shows cyclical acceleration and deceleration of the engine crankshaft. One can notice, that the acceleration time and deceleration is separated with longer periods with idling speed in order of thermal stabilization of the engine.

The recorded and processed data, drawn on torque vs. engine speed shows loops. It is worth to notice, that the shape of the positive parts of the curves and its area depends on the fuel used for testing. The shape and area of the negative part of the area does not depend on the used fuel.

The value of polar moment of inertia is very difficult to calculate, but this value remains constant for each engine. The testing in non-stationary test can be used for comparison of the engine properties, when the same engine is fed with for example different fuels (see Fig. 3).

The area under the positive part of the curves (Fig. 3) on the torque–engine crankshaft rotational speed plane has the same measures (units) as energy obtained during acceleration of the engine. It is also worth to notice, that the area of the cyclodyne obtained during the test is proportional to the calorific value of the fuel used in the test (see Table 6 and Fig. 3).

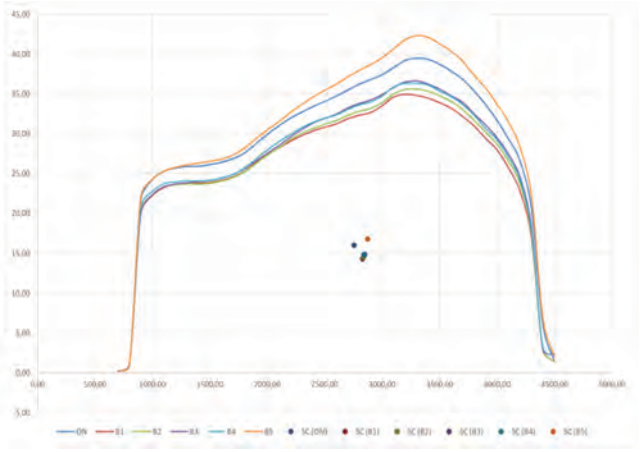

Fig. 3. Example of the positive part of the cyclodynes obtained during the engine test with the fuels with different properties [7] with centres of gravity marked with dots

Table 6. Calorific values of the samples, which testing results are presented in Fig. 3

	Diesel fuel	Biox B1	Biox B2	Biox B3	Biox B4	Biox B5
Calorific value [MJ/kg]	42.8	38.1	38.3	38.4	38.2	42.4

The area under the curve is proportional to the energy generated by the engine during one cycle of acceleration from idling to maximal crankshaft speed. The acceleration time is measured during one cycle of acceleration; it is the time between idling and maximal crankshaft speed.

Figure 4 presents results of engine test for the BIOXDIESEL fuel with different content of cetane number improving additive. The values of the areas of the cyclodynes have been obtained during a series of acceleration and deceleration of the engine. Each point represents an average of 10 acceleration-deceleration cycles. The fuel used for the test contained 70% of FAEE and bioethanol with 30% of mineral Diesel fuel.

The minimal acceleration time and maximal area of the cyclodynes (the positive part of the curves on angular acceleration-engine speed curves) occurs at the same range of cetane number improver content, as the values presented in Table 5. The data presented in Table 5 show the dependence of the cetane number as a function of the cetane number improver content.

It is also worth to notice, that the increase of the cetane number improver content (more than it is recommended either in Table 5 and Fig. 4) is not improving the energy generated by the engine during combustion of the engine.

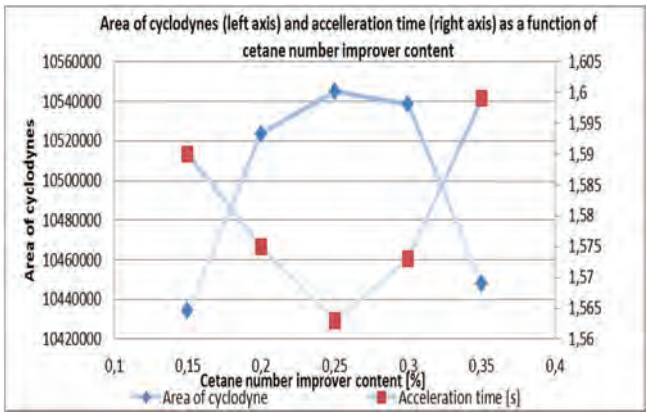

Fig. 4. Area of cyclodyne (left axis) and acceleration time (right axis) as a function of cetane number improver content

6. Conclusions

This paper presents research on improvement of the properties of the BIOXDIESEL fuel, which is a mixture of FAEE and/or FAME, bioethanol with addition of mineral Diesel fuel.

The properties of the BIOXDIESEL fuel are very similar to the properties given in the standards for the fuel of the vehicles with compression ignition engines. The cold flow properties of the BIOXDIESEL fuel can be improved by dosing the additives which are improving low temperature behavior of the fuel. This fuel can with the additives can be used even in winter condition in Poland.

Results of measurement presented in this paper also show, that the selection of cetane number improvers can improve compression ignition behaviour of the BIOXDIESEL fuel, which contains large amount of FAEE with addition of mineral Diesel fuel and bioethanol.

It is also worth to notice accordance of the results of determination of cetane number with results of engine tests in non-stationary condition.

Based on the studies presented above and based on previous experience of the authors one can conclude, that the BIOXDIESEL fuel is very advanced and can be used as an alternative fuel for all Diesel engines.

Nomenclature

FAEE	Fatty Acid Ethyl Esters	CFPP	Cold Filter Plugging Point
FAME	Fatty Acid Methyl Esters	CN	Cetane Number
CP	Cloud Point		

Bibliography

[1] BURGER, J.L., LOVESTEAD, T.M., GOUGH, R.V., BRUNO, T.J. Characterization of the effects of cetane number improvers on diesel fuel volatility by use of the advanced distillation curve method. *Energy & Fuels*. 2014, **28**(4), 2437-2445.

[2] MUSTAFA ERTUNC TAT. Cetane number effect on the energetic and exergetic efficiency of a diesel engine fuelled with biodiesel. *Fuel Processing Technology*. 2011, **92**(7), 1311-1321.

[3] STANIK, W., MAZANEK, A., JAKÓBIEC, J. Study of diesel oil containing 7% (v/v) of FAME and cetane boost additive for the assessment its utility and purity of injectors. *Combustion Engines*. 2015, **162**(3), 933-943.

[4] STRUŚ, M., POPRAWSKI, W., REWOLTE, M., KARDASZ, P. Feeding the engines of fleet vehicles with Bioxdiesel fuel and heavy alcohols. *Journal of KONES Powertrain and Transport*. 2016, **23**(4), 495-504.

[5] STRUŚ, M., POPRAWSKI, W., REWOLTE, M. Testing the fleet of the vehicles with diesel engines fed by BIOXDIESEL fuel. *Combustion Engines*. 2017, **170**(3), 37-41.

[6] STRUŚ, M. Ocena wpływu biopaliw na wybrane właściwości eksploatacyjne silników. *Oficyna Wydawnicza Politechniki Wrocławskiej*. Wrocław 2012.

[7] STRUŚ, M., POPRAWSKI, W., REWOLTE, M. Efficiency of feedstock selection for the second generation BIOXDIESEL biofuel for Diesel engines. *Combustion Engines*. 2015, **3**.

Prof. Mieczysław Struś, DSc., DEng. – Faculty of Mechanical and Power Engineering, Wrocław University of Science and Technology
e-mail: *mieczyslaw.strus@pwr.edu.pl*

Wojciech Poprawski, DEng. – Faculty of Mechanical and Power Engineering, Wrocław University of Science and Technology
e-mail: *wojciech.poprawski@pwr.edu.pl*

Article citation info:
SKRZEK, T. Duel fuel compression ignition engine fuelled with homogeneous mixtures of propane and kerosene-based fuel. *Combustion Engines*. 2019, **178**(3), 191-197. DOI: 10.19206/CE-2019-333

Tomasz SKRZEK

CE-2019-333

Duel fuel compression ignition engine fuelled with homogeneous mixtures of propane and kerosene-based fuel

The paper presents some results of examination of DF CI engine fuelled with kerosene-based fuel (Jet A-1) and propane. The aim was to obtain the maximum engine thermal and overall efficiency and checking the engine emissions for the application of significant share of propane as a main source of energy. The fuel which initiates the ignition was Jet A-1 provided by common rail system during the beginning of compression stroke. Propane was provided to inlet manifold in a gas phase. The method of providing of both fuels to the engine cylinder allowed to create nearly homogeneous mixture and realized HCCI process for dual fueling with Jet A-1 and propane. It was possible to compare two combustion strategies PCCI and HCCI for fuelling of CI engine with single fuel (Jet A-1) and dual fuelling with Jet A-1 and propane. The results of experiment show that the NO_x and soot emissions are much lower than for standard CI or SI engines. The results also show very interesting potential role of propane in control of HCCI dual fuel combustion process which gives the new perspective of dual fuel engine development. The low levels of toxic components in exhaust gases encourage to test and develop this type of fuelling which could radically confine the negative influence on the environment as well as enable to apply an alternative fuels.

Key words: *dual-fuel engine, kerosene-based fuel, propane, HCCI process, low NO_x emission*

1. Introduction

Despite of anti-diesel campaign which is undertaken by some authorities especially municipal authorities from large cities to promote electromobility compression ignition engines are still widely used for transportation and power generation and have rather good perspective. There are many reasons for that:

1. High fuel efficiency – about 20% less fuel consumed than equivalent petrol cars.
2. 15% less CO – emissions/km than equivalent petrol-powered vehicles. Diesel vehicles contribute to reduce CO_2 emissions from road transport and therefore to mitigating climate change.
3. 2021 targets – while petrol and diesel engines will continue to improve efficiency, diesel will continue to be important in meeting EU's 2021 CO_2 fleet average targets and beyond.
4. Heavy duty – diesel engines are suited for use in heavier commercial or long-haul commercial vehicles, which is why they will remain difficult to replace for trucks and vans.
5. Longer range – diesel's high fuel economy ensures a longer range between refuelling stops [8].

However, diesel engines can cause environmental pollution owing to their high NO_x and soot emissions. Emission aftertreatment devices have problems in terms of their cost and durability. Since emission aftertreatment systems such as Diesel Particulate Filters (DPF), Lean NOx Trap (LNT) and Selective Catalytic Reduction (SCR) systems also often increase fuel consumption, in-cylinder technologies for emission reduction have therefore been the focus of intense research [10]. Considerable effort has thus been devoted toward reducing these pollutant emissions as these have adverse effects on the environment and human health [5].

The are some areas for research to make CI engine more environmental friendly as well as more efficient. First of all revolutionary in-cylinder combustion strategies, especially low-temperature combustion, could convert the combustion process to more clean and more effective process. It also can be connected with application of alternative fuels, especially more clean gas fuels. When we add new generation exhaust emission aftertreatment systems which will meet stringent emission regulations the future of CI engine looks right.

The paper presents some results of research on combustion of kerosene-based fuel (Jet A-1) and dual fuel combustion of kerosene-based fuel (Jet A-1) together with propane in CI engine for low loads and constant engine speed.

Depending on the way of fueling two combustion strategies were examined during the tests:

- PCCI (premixed charge compression ignition) – fueling with Jet A-1 only and dual fueling with Jet A-1 and propane for standard injection timing of Jet A-1
- HCCI (homogeneous charge compression ignition) – fueling with Jet A-1 only as well as dual fueling with Jet A-1 and propane.

2. Propane – clean fuel for IC engine

Propane (C_3H_8) has been recognized as a clean fuel for last decades. The reason is that compared to the gasoline or diesel oil used as a automotive fuel, propane fuel gives about 25% fewer greenhouse gases. When the unburned propane is released into the atmosphere it doesn't contribute to the greenhouse effect. However, other clean fuels (such as natural gas) contribute greatly to global warming if released before combustion. For instance unburned methane in natural gas creates 25 times more greenhouse gases than carbon dioxide [11].

Despite declines in oil prices, propane production is expected to continue to grow. This should enable propane to remain competitively priced relative to gasoline and diesel fuel in engine fuel market. It is sold as a clear propane (especially on US market) or as a part of LPG fuel. Although processing has changed in many ways over the years, there are still two main ways that propane is produced today: refining, and natural gas production. Because natural gas production is growing and propane makes up about 5% of

unprocessed natural gas the production of propane is also growing. The same is happening for propane production from crude oil refining (propane is also a natural byproduct in the crude oil refining process). The actual percentage of propane extracted from the crude oil depends on the process and the type of refinery [12]. The additional reason for propane sale growth is that propane could be also produced from 100% renewable raw materials such as waste and residues and sustainably produced vegetable oils. In use, renewable propane is identical to conventional propane and, therefore, can easily be blended with conventional propane and used by all existing appliances suitable for use with propane [13]. As far as transportation infrastructure constraints resulting from the rapid growth in natural gas liquid (LNG) production, propane sales for use in internal combustion engines are projected to grow steadily, as clean propane applications (such as commercial lawn mowers, irrigation pumps, and propane vehicles) become more widespread in the marketplace [14].

In the experiment described in the paper propane was used as a second fuel which modified the combustion process of Jet A-1 fuel in CI AVL experimental engine. So, the engine was dual-fueled with kerosene based fuel Jet A-1 and propane. Chosen physical properties for Jet A-1 vs. propane are described in Table 1.

Table 1. Chosen physical properties for Jet A-1 vs. propane

Parameter	Jet A-1 [10]	Propane
Flash point [°C]	38	−104
Autoignition temperature [°C]	210	470
Max adiabatic burn temperature [°C]	2230	1980 [11]
Density at [15°C]	0.804 kg/l	1.882 kg/m^3
Specific energy [MJ/kg]	42.8	50.34
Distillation	Initial boiling point: 156ºC 10% vol. at 167ºC 20% vol. at 172ºC 50% vol. at 188ºC 90% vol. at 234ºC end point of distillation 258ºC	–
Boiling Point - saturation pressure 760 mm Hg (ºC)	–	–42.2
Lower flammability limit (LFL) in % by volume of air	0.6–0.7	2.1
Upper flammability limit (UFL) in % by volume of air	4.9–5.0	9.5–10.1
Stoichiometric mixture composition (air/fuel)	14.3	15.7

3. JET-A1 fuel

JET-A 1 aviation fuel is dedicated to turboprop engines mainly to drive aircrafts. Jet A-1 is made of components obtained in a specific technological regime in hydrodesulfurization, hydrocracking and distillation processes [15]. Jet Fuel consists of four groups of hydrocarbons:

1. paraffins, isoparaffins, cycloparaffins
2. aromatics
3. naphthalenes
4. olefins

4. Test stand

The test was carried out on an AVL experimental common rail, naturally aspirated CI engine. The test equipment was specified in accordance with the Directive of European Parliament and European Council 1999/96 dated 13 December 1999 as well as Regulation (EC) No 715/2007 of the European Parliament and of the Council dated 20 June 2007 and Commission Regulation (EC) No 692/2008 of 18 July 2008.

Propane port injection system used in the experiment was based on standard components of gas injection system such as a two-stage gas regulator with a water jacket and a gas port fuel injector. The gas injector was synchronized with the crankshaft position so that gas injection timing was optimized to reduce loss of gas occurring during valve overlap. It is particularly important from the point of view of the hydrocarbon emission and engine overall efficiency.

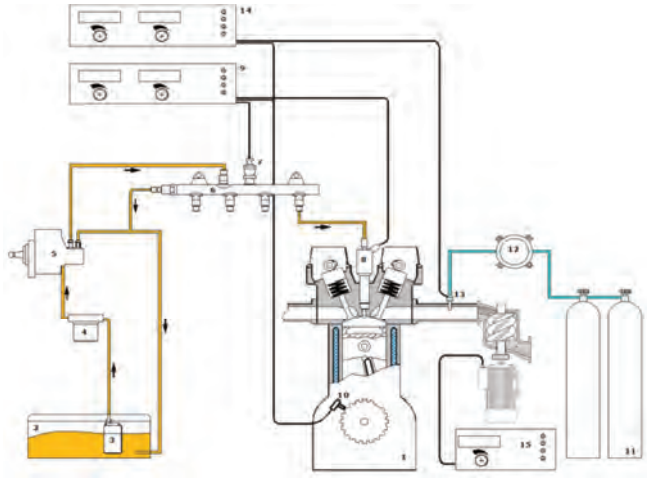

Fig. 1. General layout of dual-fuel system of CI engine supply: 1) engine, 2) Jet A-1 fuel tank, 3) electric fuel pump, 4) fuel filter, 5) high-pressure fuel pump, 6) rail, 7) fuel pressure sensor, 8) Jet A-1 fuel injector, 9) controller of common rail supply system, 10) crank shaft speed sensor, 11) propane container, 12) pressure regulator, 13) propane injector, 14) propane controller supply system,15) engine charging control system

Table 2. Engine characteristics

Model	AVL 5402
Type	direct injection
Number of cylinders	1
Displacement [cm^3]	511
Bore / stroke [mm]	85.01 / 90.00
Cycle	four stroke
Compression ratio	17.5
Maximum power [kW]	ca.16
Maximum speed [rpm]	4200
Valve overlap [deg]	80

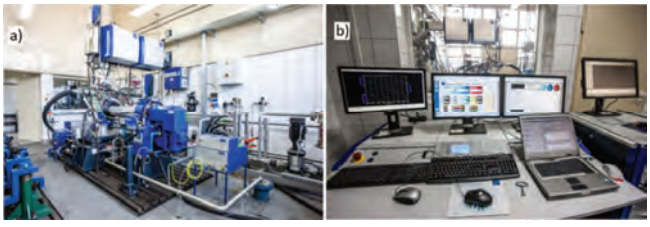

Fig. 2. AVL test bed: (a) general view of the test bed, (b) view of the control room

5. Fueling of CI engine with Jet A-1 fuel only

The first step of the tests was the fuelling of CI engine with Jet A-1 fuel only. There were two options examined:

1. standard injection timing (PCCI)
2. very early injection (HCCI)

5.1. Standard injection timing of Jet A-1 fuel

In order to realize the Premixed Charge Compression Ignition (PCCI) process two doses of Jet A-1 fuel per cycle were applied. The injection timing and the quantity of the first pilot dose have been selected based on the preliminary studies to obtain the highest thermal efficiency and to reduce the maximum engine pressure to confine the possibility of hammering.

Table 3. Engine adjustment parameters for standard injection timing of Jet A-1 fuel

Engine speed [rpm]	1500
Common rail injection pressure [bar]	390–760
Injection timing of the first dose [deg BTDC]	Variable (10.5–14.9)
Injection timing of the second dose [deg BTDC]	Variable (1.1–6.7)

Figure 3 presents the set of cylinder pressure diagrams together with heat release diagrams for different engine load and constant engine speed (1500 rpm). The diagrams are similar to those which are obtained for standard fueling of CI engine with diesel oil only.

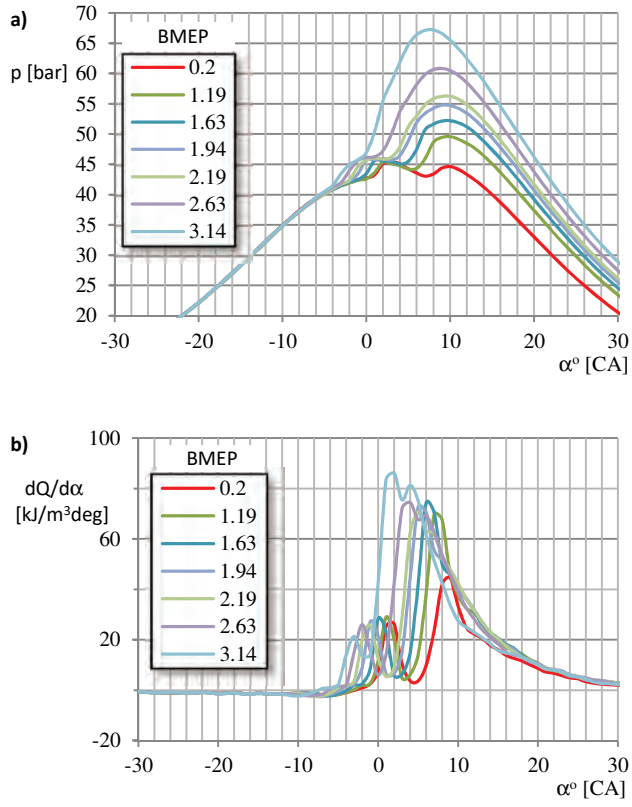

Fig. 3. Pressure diagrams (a) and heat release diagrams (b) for different engine load and constant engine speed (1500 rpm) for fueling with standard injection timing of Jet A-1 fuel

5.2. Very early injection timing of Jet A-1 fuel

The application of very early injection timing of the Jet A-1 dose completely changed the combustion process of the fuel. The process starts with small heat release phase and then the heat is released rapidly in the way resembles SI engine heat release diagram. Fig. 4 presents the set of cylinder pressure diagrams together with heat release diagrams for different engine load and constant engine speed (1500 rpm) for the early injection of Jet A-1.

Table 4. Engine adjustment parameters for very early injection timing of Jet A-1 fuel

Engine speed [rpm]	1500
Common rail injection pressure [bar]	350
Injection timing [deg BTDC]	180

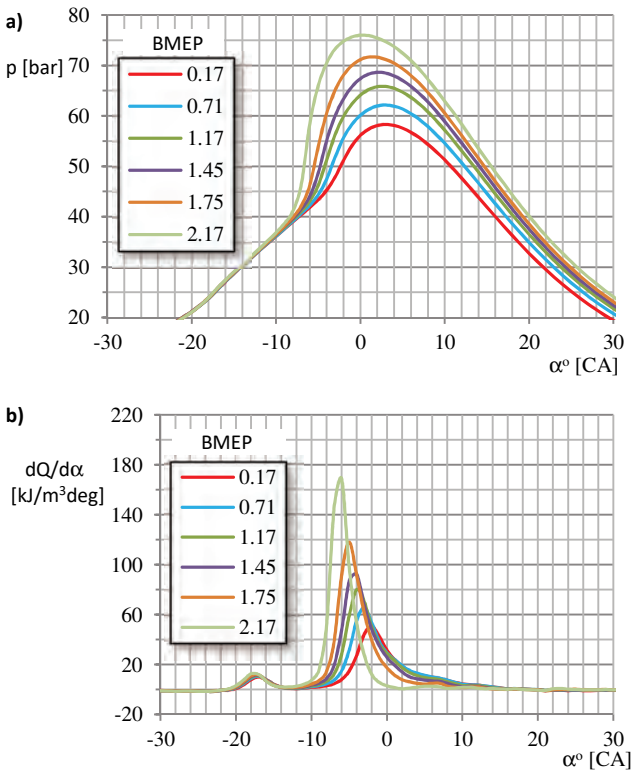

Fig. 4. Pressure diagrams (a) and heat release diagrams (b) for different engine load and constant engine speed (1500 rpm) for fueling with very early injection timing of Jet A-1 fuel

6. Dual fueling of CI engine with Jet A-1 fuel and propane

The main objective of the research was to observe the results of combustion process in dual fuel CI engine fueled with Jet A-1 fuel with the addition of propane.

The first step of engine examination was dual fueling with standard injection parameters of Jet A-1. The experiment enable to observe PCCI combustion. The second step was realization of HCCI process with the use of dual fuel mixture. Thanks to application of two fuels (low reactivity fuel – propane and high reactivity fuel – Jet A-1) and modified injection timing of Jet A-1 (very early injection) as well as modification of injection pressure (low), HCCI (homogeneous charge compression ignition) combustion was possible to observe.

The substitution ratio of propane in the propane/Jet A-1 mixture was defined as:

$$E_P = \frac{Q_P \cdot m_P}{Q_P \cdot m_P + Q_{JA1} \cdot m_{JA1}} \cdot 100 \quad (1)$$

where: Q_P – propane calorific value, m_P – dose of propane, Q_{JA1} – Jet A-1 fuel calorific value, m_{JA1} – dose of Jet A-1 fuel.

The total excess air coefficient defined for dual fuelling as:

$$\lambda = \frac{\dot{m}_a}{L_P \cdot \dot{m}_P + L_{JA1} \cdot \dot{m}_{JA1}} \quad (2)$$

where: m_a – air mass flow, m_P – propane mass flow, m_{JA1} – Jet A-1 mass flow, L_P – theoretical air required for complete combustion of 1 kg of propane, L_{JA1} – theoretical air required for complete combustion of 1 kg of Jet A-1.

6.1. Dual fueling of CI engine with Jet A-1 fuel and propane – PCCI process

In order to realize the Premixed Charge Compression Ignition (PCCI) process two doses of Jet A-1 fuel per cycle were applied. Both, the injection timing and the quantity of the first dose of Jet A-1 have been selected based on the preliminary studies to obtain the highest thermal efficiency and to reduce the maximum engine pressure in order to minimize the possibility of hammering.

The injection parameters were the same as for standard fuelling with diesel oil. The change of load was realized by increasing propane dose and its share in the dual fuel mixture. Figure 5 presents the set of cylinder pressure diagrams together with heat release diagrams for different engine load and constant engine speed (1500 rpm) of dual fueled engine with Jet A-1 and propane. In Fig. 5b the increase of ignition delay together with the increase of propane share in the mixture is clearly visible. It means that it is necessary to change the injection parameters to improve engine thermal efficiency [6].

6.2. Dual fueling of CI engine with Jet A-1 fuel and propane – HCCI process

Dual fueling of CI engine with Jet A-1 fuel and propane with very early injection of Jet A-1 gave an opportunity to observe HCCI process in the combustion chamber of research engine. In comparison with DF with Jet A-1 and propane in PCCI mode the combustion is very fast and regular. Like for Jet A-1 fueling only preliminary heat release phase was observed. It is very interesting that the maximum cylinder pressure is delayed for higher amount of propane.

Table 5. Engine adjustment parameters for dual fueling with Jet A-1 and propane for PCCI mode

Engine speed [rpm]	1500
Common rail injection pressure [bar]	390
Jet A-1 fuel energy provided per cycle [J]	250
Injection timing of the first dose [deg BTDC]	10.5
Injection timing of the second dose [deg BTDC]	1.1

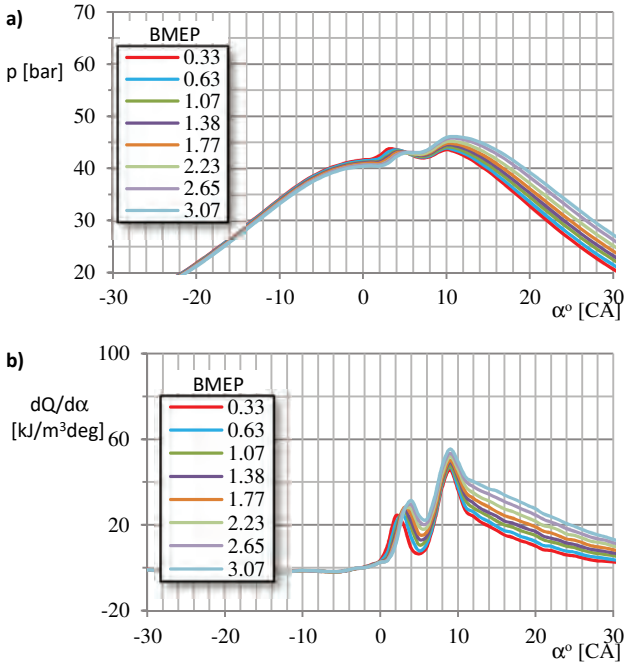

Fig. 5. Pressure diagrams (a) and heat release diagrams (b) for different engine load and constant engine speed (1500 rpm) for dual fueling with Jet A-1 and propane (PCCI mode)

Table 6. Engine adjustment parameters for dual fueling with Jet A-1 and propane for HCCI mode

Engine speed [rpm]	1500
Common rail injection pressure [bar]	360
Jet A-1 fuel energy provided per cycle [J]	525
Injection timing of Jet A-1 [deg BTDC]	180

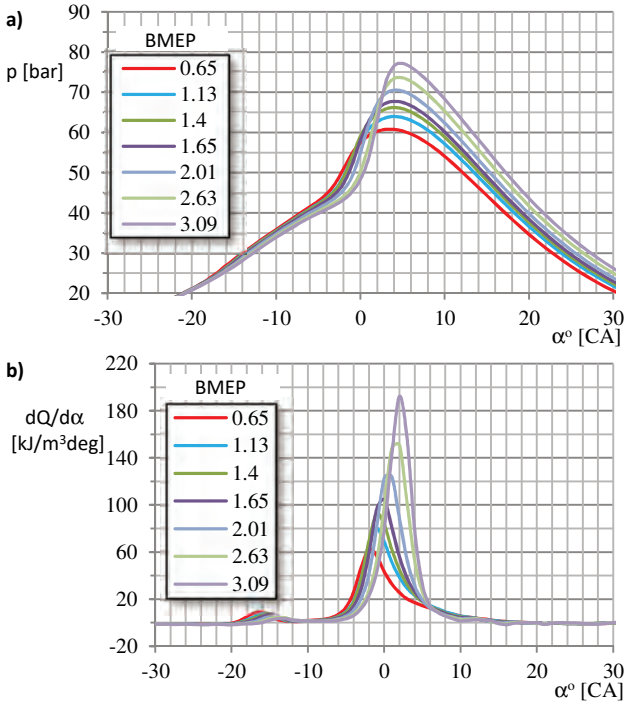

Fig. 6. Pressure diagrams (a) and heat release diagrams (b) for different engine load and constant engine speed (1500 rpm) for dual fueling with very early injected Jet A-1 and propane (HCCI mode)

To get the set engine speed and BMEP = 0.3 bar (nearly idle speed T = 1.5 Nm) the energy consumed by the engine realized HCCI process was twice as much as the engine running according to PCCI process. It means that the fuel could have been deposited on the cylinder wall. it is necessary to further test the engine to find the right proportion of Jet A-1 and propane.

The results obtained for this part of the test gave very promising dual-fuel strategy that yields good results, especially for low and medium loads, allowing greater control over the timing and duration of the heat release. The results resemble RCCI combustion which is a low-temperature combustion strategy that utilizes early injection of high reactivity fuel to create a reactivity gradient leading to a staged auto-ignition, from the highest reactivity region to the lowest [2, 4, 9].

7. Mixture composition and engine emissions

7.1. Excess air coefficient

The conditions for the experiment, especially the way of mixture creation and load control in CI engine resulted in changing of total excess air coefficient λ for the range of the engine load Fig. 7. Excess air coefficient λ varied from about 5 for minimum load to more than 2 for BMEP = 3 bar. It is interesting that in the level of excess air coefficient doesn't affect the mechanism of heat release, especially in case of HCCI process observed in case of fuelling the engine with Jet A-1 and dual fuel mixtures of Jet A-1 and propane.

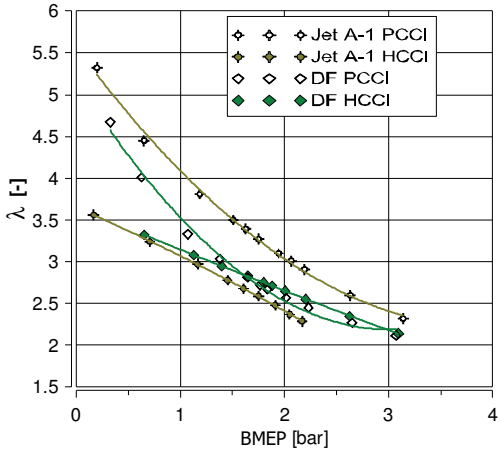

Fig. 7. Total excess air coefficient λ vs. BMEP for four modes of fuelling

7.2. Engine emissions

The results of the emissions measurement, especially NO_x emission confirmed that the early injection of Jet A-1 gave the possibility of realization of low-temperature combustion strategy. In both cases – fuelling with Jet A-1 only and dual fuelling the result is similar – it is very low NO_x emission Fig. 8.

Dual fuel operation usually leads to a higher emission of unburned hydrocarbons mainly due to valve overlap causing a blow of the unburned gas-air mixture out of the cylinder. Usually a relatively high emission of non-methane hydrocarbons (NMHC) appears at low loads because of poor combustion, particularly the phenomenon of flame quenching in a lean mixture caused by its dilution. The measured emission of non-methane hydrocarbons (NMHC) has been presented in Fig. 9. It is very high for HCCI modes of fuelling. It could be discussed if it is a result of flame quenching in a lean mixture ($2 < \lambda < 5$) caused by its dilution or/and the non-controlled turbulence inside combustion chamber. It should be analyzed and explain in the further examination connected with visualization of the combustion process.

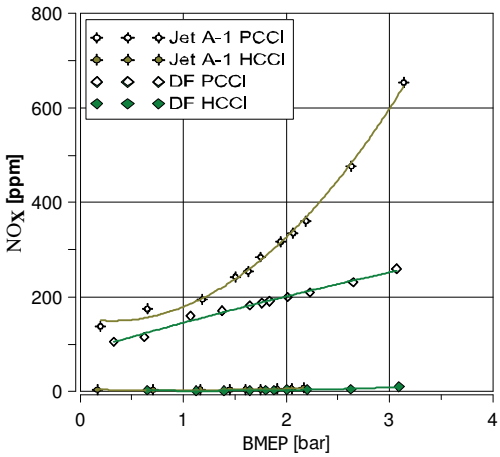

Fig. 8. NO_x emission vs. BMEP for four modes of fuelling

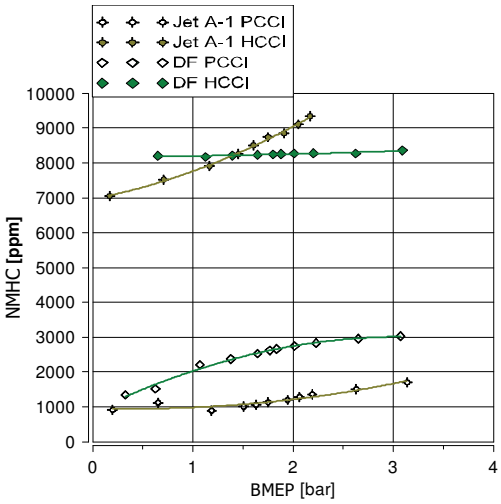

Fig. 9. Emission of non-methane hydrocarbons (NMHC) vs. BMEP for four modes of fuelling

Positive result for HCCI mode of fuelling the engine with Jet A-1 and propane dual fuelling is that the emission of unburned propane is significantly lower for HCCI mode than for standard dual fuelling PCCI – Fig. 10. It was achieve despite of valve overlap. The valve overlap in the experiment was set to 80 deg, typical value of this type of engine.

The soot emission for dual fuelling in both cases (HCCI and PCCI) was lower than for fuelling of the engine with Jet A-1 only. Generally this emission is on the low level but for dual fuelling the rise connected with higher load is slower Fig. 11.

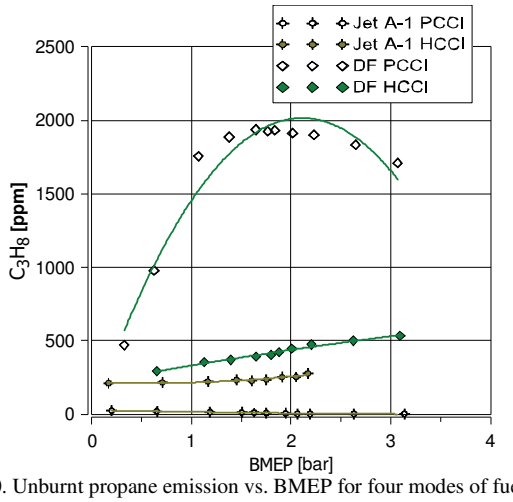

Fig. 10. Unburnt propane emission vs. BMEP for four modes of fuelling

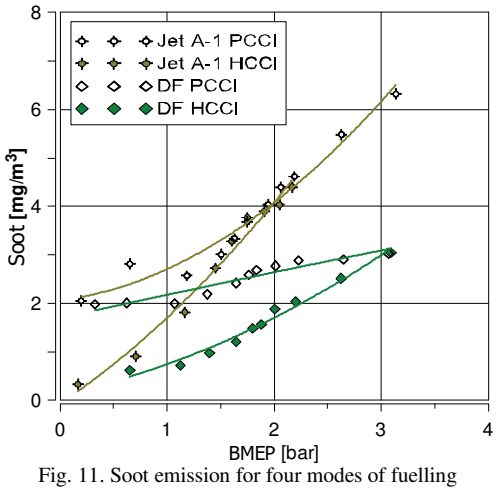

Fig. 11. Soot emission for four modes of fuelling

8. Engine thermal efficiency

The engine thermal efficiency diagrams shows very interesting phenomena. When for PCCI options (Jet A-1 only and dual fuelling with Jet A-1 and propane) the engine thermal efficiency is relatively high for HCCI modes it starts from very low value but steadily and fast rises with higher engine load. The main problem is the combustion control of HCCI process, especially the maximum cylinder pressure location Fig. 4a, 6a.

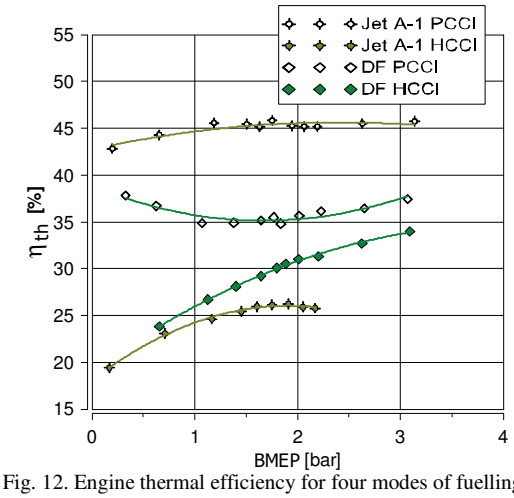

Fig. 12. Engine thermal efficiency for four modes of fuelling

The crank angle position for 50% heat released curves for examined fuelling modes are shown in Fig. 12. Very positive influence of propane is visible in DF HCCI mode. Propane shift the moment of 50% heat released and thanks to this the engine thermal efficiency rises rapidly.

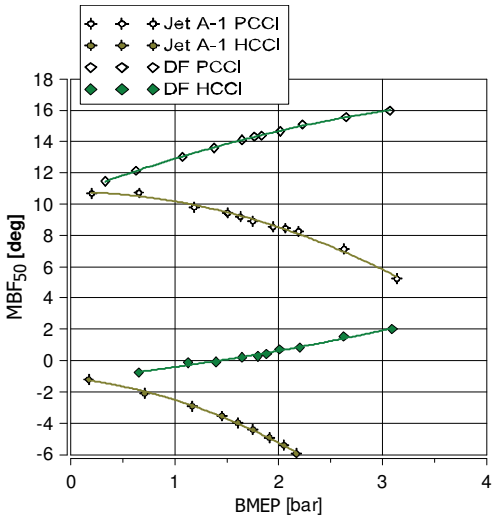

Fig. 13. The crank angle position for 50% heat released for four modes of fuelling

9. Conclusions

The results of the test of utilization of propane as a fuel used together with Jet A-1 for dual fuelling of CI engine are very promising. They show that it is possible to realize HCCI process with the use of alternative fuels combination. The results are very good especially in terms of NO_x and soot emission. Combustion of homogeneous mixtures in CI engine demands more control than PCCI process. The results show very interesting potential role of propane to control of combustion of homogeneous dual fuel charge. Propane could be used to shift the position of maximum cylinder pressure for dual fuel HCCI mode. It is very important from the point of view of efficiency and confining of engine hammering phenomena. For dual fuel (Jet A-1 and propane) mixtures burnt in HCCI process unburned propane emission is much lower despite of high value of excess air coefficient λ measured during experiments.

The results presented in the paper give the perspective of development of DF CI engine and shows vast area for research work which leads to clean, effective CI engine.

Nomenclature

DF CI dual fuel compression ignition
(Jet A-1) kerosene-based fuel
PCCI premixed charge compression ignition
HCCI homogeneous charge compression ignition

Bibliography

[1] JOHNSON, T.V. Review of diesel emissions and control. *International Journal of Engine Research*. 2009. DOI: 10.1243/14680874JER04009

[2] NIEMAN, D.E., DEMPSEY, A.B., REITZ, R.D. Heavy-duty RCCI operation using natural gas and diesel. *SAE Technical Paper* 2012-01-0379, 2012. DOI: 10.4271/2012-01-0379

[3] PAWLAK, G. The concept of a dual fuel highly efficient internal combustion engine. *SAE Technical Paper* 01-1480, 2010. DOI: 10.4271/2010-01-1480

[4] PAYKANI, A., KAKAEE, A.H., RAHNAMA, P., REITZ, R.D. Effects of diesel injection strategy on natural gas/diesel reactivity controlled compression ignition combustion. *Energy*. 2015, **90**, 814-826. DOI: 10.1016/j.energy.2015.07.112

[5] REITZ, R.D., GANESH, D. Review of high efficiency and clean reactivity controlled compression ignition (RCCI) combustion in internal combustion engines. *Progress in Energy and Combustion Science*. 2015, **46**, 12-71. DOI: 10.1016/ j.pecs.2014.05.003

[6] SKRZEK, T. Research on the effect of diesel fuel injection parameters on the combustion process in the charged CI engine fuelled with propane. *Journal of KONES Powertrain and Transport*. 2018, **25**(3). DOI: 10.5604/01.3001.0012.4360

[7] WALKER, N.R., WISSINK, M.L., DEL VESCOVO, D.A., REITZ, R.D. Natural gas for high load dual-fuel reactivity controlled compression ignition in heavy-duty engines. *Journal of Energy Resources Technology*. 2015, **137**(4), 1-7, 042202-1. DOI: 10.1115/1.4030110

[8] YOUSEFI, A., BIROUK, M. An investigation of multi-injection strategies for a dual-fuel pilot diesel ignition engine at low load. J*ournal of Energy Resources Technology*. 2016, **139**(1). DOI: 10.1115/1.4033707

[9] ZHANG, Y., KONG, S.C., REITZ, R.D. Modeling and simulation of a dual fuel (diesel/natural gas) engine with multidimensional CFD. *SAE Transactions, Journal of Fuels and Lubricants*. 2003, **112**(4). DOI: 10.4271/2003-01-0755

[10] www.cleandieseltech.eu/

[11] www.w-erc.com/services/rcci/

[12] www.altogas.com/benefits-of-propane-as-a-clean-fuel

[13] www.smithgas.com/how-propane-is-produced-and-why-it-matters

[14] www.neste.com/companies/products/renewable-fuels/renewable-propane

[15] afdc.energy.gov/files/u/publication/2016_propane_market_outlook.pdf

[16] www.orlen.pl/PL/DlaBiznesu/Paliwa/PaliwaLotnicze/Strony/PaliwoDoTurbinowychSilnikowJetA1.aspx

Skrzek Tomasz, DEng. – Mechanical Engineering Faculty, Radom University of Technology and Humanities.

e-mail: *t.skrzek@uthrad.pl*

Article citation info:
SOKOLNICKA, B., FUĆ, P., SZYMLET, N. et al. Harmful exhaust components and particles mass and number emission during the actual drive of a passenger car in accordance with the RDE procedure. *Combustion Engines*. 2019, **178**(3), 198-202.
DOI: 10.19206/CE-2019-334

Barbara SOKOLNICKA
Paweł FUĆ
Natalia SZYMLET
Maciej SIEDLECKI
Rafał GRZESZCZYK

CE-2019-334

Harmful exhaust components and particles mass and number emission during the actual drive of a passenger car in accordance with the RDE procedure

The article presents toxic exhaust components emission measurement results as well as solid particles mass and number. The test involved a direct gasoline injection engine, in which special attention should be paid to the particulates number emission. Small diameters of nanoparticles make them particularly dangerous to human health. Nowadays, vehicle engines are constantly improved and modernized as a result of the need to meet existing exhaust gas emission standards. One of the few ways to determine the actual content of toxic and harmful compounds in the exhaust gases is the RDE (Real Driving Emissions) procedure, the requirements of which apply from 2016 for new vehicles, and from 2019 will apply to all registered passenger cars. The RDE procedure does not replace the WLTP (World Light-Duty Vehicle Test Procedure), but complements it. The tests on the dynamometer are separated from external conditions such as traffic volume or congestion and are not a sufficient indicator of emissions in real traffic conditions.

Key words: *RDE procedure, particulate mass, particulate number, exhaust emission, direct injection*

1. Introduction

Nowadays, vehicle engines are constantly improved and modernized as a result of the need to meet existing exhaust gas emission standards. One of the few ways to determine the actual content of toxic and harmful compounds in the exhaust gases is the RDE (Real Driving Emissions) procedure, the requirements of which apply from 2016 for new vehicles, and from 2019 refer to all registered passenger cars. Increasing the popularity of engines powered by direct gasoline injection system on the global market resulted in amplified emission of particles with small diameters to the atmosphere [1]. This is directly related to the risk to human health, as it is impossible or very difficult for the organism to remove particles with a diameter of less than 100 nm [5].The issue of particulate filters is standard for compression-ignition engines, but for gasoline engines it is still an area to be analyzed. The tests on the engine test bench are separated from external conditions such as traffic or congestion and are not a sufficient indicator of emissions in real traffic conditions. The RDE procedure does not replace the WLTP test (World Light-Duty Vehicle Test Procedure), but is a supplement to it. The results of hydrocarbons and carbon oxides emission during the discussed studies were published in a separate article [2]. This publication, in addition to data on particle mass and number emission, presents the results of gaseous exhaust components in the form of nitrogen oxides and carbon dioxide emission measurements.

2. Research object

The examined object was a vehicle from the LDV group, equipped with a spark-ignition engine with direct fuel injection of a displacement of 1197 cm^3 produced in 2015 (Fig. 1). The basic technical data of the engine is shown in table 1. The tested vehicle had highline equipment, which could have an impact on fuel consumption, due to the increased weight compared to the basic equipment, mainly caused by additional comfort systems, which affects the vehicle's air resistance.

Table 1. Basic engine technical data

Engine type	spark-ignition
Displacement [cm^3]	1197
Number of cylinders/valves	4/16 (straight)
Injection type	direct
Power [kW]	77
Maximum torque [Nm]	160
Gearbox	automatic/DSG

Fig. 1. Research object

3. Research methodology

3.1. Measuring equipment

The equipment from the PEMS group was used for the tests, which contained a number of analyzers for the harmful compounds measurement such as: carbon dioxide (CO_2), carbon monoxide (CO), hydrocarbons (HC), solid particulates in mass (PM) and number (PN) range (Fig. 2) [3]. The apparatus before the test was calibrated with standard gases according to the procedure provided by the manufacturer. Moreover, just before the vehicle left for the route, the equipment was zeroed in the ambient air, so as to make the obtained results independent of the background contamination.

a)

b)

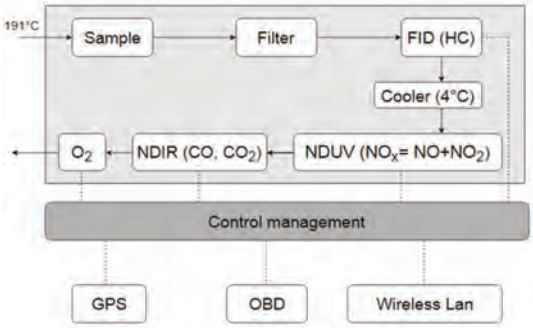

Fig. 2. SEMTECH DS analyzer: a) device view, b) operation diagram

Particulate measurements are particularly important for modern vehicles with spark-ignition engines and direct fuel injection. Research on their impact on human health led to the introduction of limits, at the beginning of the mass, and then the number of particulates for compression-ignition engines. From September 2017, the limit of particle numbers also applies to vehicles with SI DI engines. For this reason, it is required to use two analyzers – one used to determine the mass and the other to the number (Fig. 3).

a) b)

Fig. 3. Equipment used for measuring particulates in the range of: a) number and dimensional distribution – EEPS TSI 3090, b) concentrations – AVL MSS [3]

3.2. RDE route

The requirements for the RDE route are strictly defined. It consists of three driving cycles: urban, extra-urban and highway (Fig. 4).

The share of the traveled distance of individual stages in the whole test is about 33% (Table 2). The ride took place in the afternoon, which allowed to avoid excessive traffic congestion.

Fig. 4. The research route in accordance with the procedure RDE

Table 2. RDE cycles data

	Urban	Extra-urban	Motorway
Average speed [km/h]	25.62	73.83	112.99
Drive duration [s]	4812	949	812
Distance [km]	34.25	19.48	25.52

4. Research results

4.1. Urban cycle

During the 80-minute drive in the urban cycle, nitrogen oxide emission values were obtained in accordance with the emission standards, according to which the tested vehicle was homologated (Fig. 5a). Fuel consumption was regular throughout the entire cycle (Fig. 5b). Driving in urban areas limits the possibility of CO_2 emissions reducing due to congestion and obtaining average speeds of 25 km/h, as in the case of the test run (Table 2).

a)

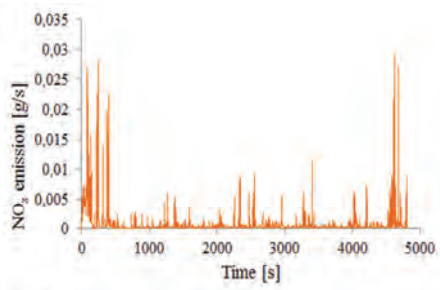

b)

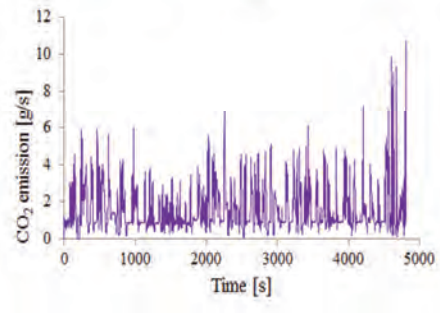

Fig. 5. Measured compounds emission per second: a) NO_x, b) CO_2

The increased emission of particulates mass in the urban cycle could be caused by the cold start of the engine at the beginning of the tests (Fig. 6b). Despite the largest value of all the test stages, the result is still below the limits in the approval standard (Table 2). The increased number of solid particles with small diameters results from direct fuel injection, which promotes their formation (Fig. 6a).

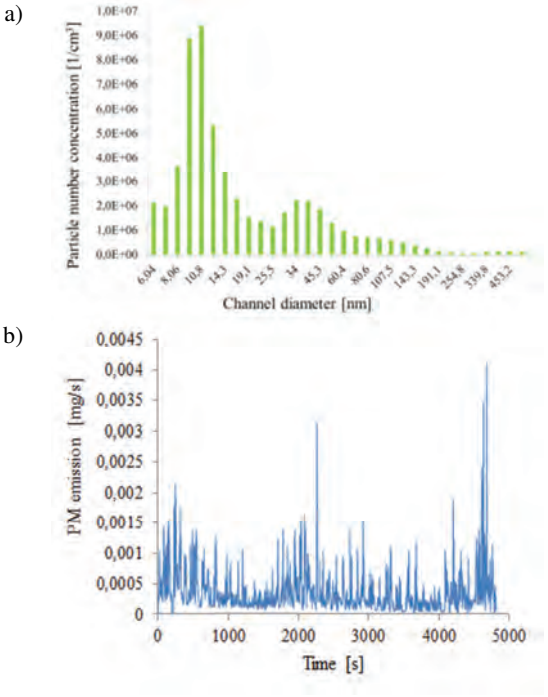

Fig. 6. Solid components of exhaust gases: a) particle number concentration, b) particle mass

With reference to the homologation standard of the tested vehicle, the admissible value was not exceeded for the compounds in the exhaust gases (Table 3).

Table 3. Specific distance emissions results during an urban cycle

Specific distance emission during an urban cycle		Euro 6b standard
NO_x [g/km]	0.12	0.06
CO_2 [g/km]	226.74	–
PM [mg/km]	0.000952	0.0045
PN [1/km]	5e10	6e11

4.2. Extra-urban cycle

The shortest stage of the research was the extra-urban cycle. During the cycle, the driver drove a distance of 19 km. In the initial phase of the test, lower speeds were maintained, which reflects the lower emission of nitrogen oxides, the formation of which is promoted by rapid acceleration. In the final stage of the cycle, the driver moved from the extra-urban area towards the motorway, which allowed to achieve higher speeds, thus increasing NO_x emissions (Fig. 7a). The same trend can be observed in the case of CO_2, which is directly connected to fuel consumption (Fig. 7b).

A three-fold reduction in solid particles mass emission in relation to the urban cycle was observed (Fig. 8b). At this stage of the research, the engine warmed up, which improves the fuel combustion conditions. As a result of the engine's achievement of an appropriate operating temperature, the time needed to evaporate the fuel has been shortened, due to which the emitted particulates number has been increased (Fig. 8a).

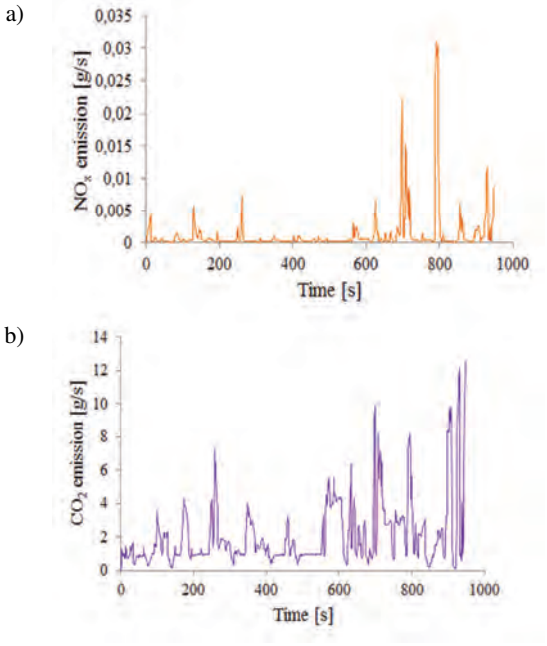

Fig. 7. Measured compounds emission per second: a) NO_x, b) CO_2

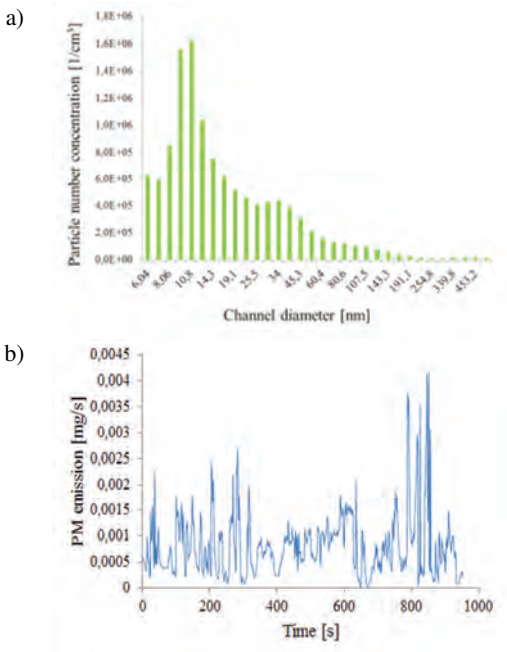

Fig. 8. Solid components of exhaust gases: a) particle number concentration, b) particle mass

The emission of nitrogen oxides reached a value similar to that determined in the Euro 6b homologation standard (Table 4). The number of particles in relation to the distance was the smallest relative to the other parts of the RDE test.

Table 4. Specific distance emissions results during an extra-urban cycle

Specific distance emission during an extra-urban cycle		Euro 6b standard
NO_x [g/km]	0.057	0.06
CO_2 [g/km]	134.6	–
PM [mg/km]	0.000396	0.0045
PN [1/km]	3e9	6e11

4.3. Motorway cycle

Due to the speed characterizing the motorway crossing, its duration was the shortest. The initial stage of the cycle was characterized by higher speeds. At some moments, the vehicle has reached a speed of 130 km/h. This caused a rise in temperature in the combustion chamber, and consequently an increase in the emission of nitrogen oxides (Fig. 9a). Fuel consumption was uniform, increased compared to the extra-urban cycle, adequate to the need to achieve higher speeds and increased air resistance(Fig. 9b).

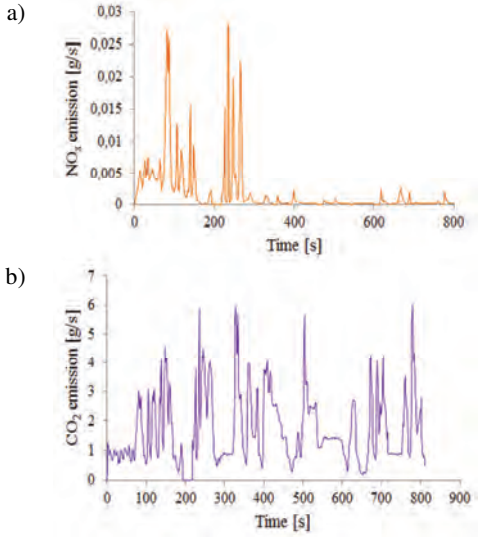

Fig. 9. Measured compounds emission per second: a) NO_x, b) CO_2

Despite warming up the engine and reaching the right operating temperature, the emission of particulate mass is greater than during extra-urban drive, because the vehicle uses more fuel to maintain the set speed (Fig. 10b). The increase in fuel consumption is associated with an increase in the particulate number emission and has an impact on their dimensional distribution (Fig. 10a). Compared to the other stages, an increase in particle diameter was noted.

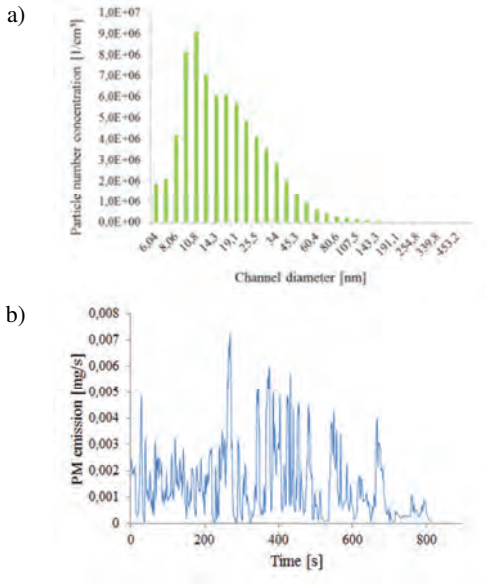

Fig. 10. Solid components of exhaust gases: a) particle number concentration, b) particle mass

The effect of increased fuel consumption can be noticed for the specific distance emission of the particulates number, which significantly approached the limit value of the Euro 6b standard (Table 5). Increasing the average speed to 113 km/h caused an increase in temperature in the combustion chambers and exceeding the limit value of nitrogen oxides emission.

Table 5. Specific distance emissions results during an extra-urban cycle

Specific emission during a motorway cycle		Euro 6b standard
NO_x [g/km]	0.057	0.06
CO_2 [g/km]	134.6	–
PM [mg/km]	0.000396	0.0045
PN [1/km]	3e9	6e11

4.4. Total RDE test

During the total RDE test, fuel consumption reaches the highest values at the end of the stage, which mostly corresponds to the motorway's movement (Fig. 11b). The emission of nitrogen oxides in the initial and final phase of the test corresponds to the specificity of moving in urban and motorway conditions, which was confirmed during the discussion of individual stages of the test (Fig. 11a).

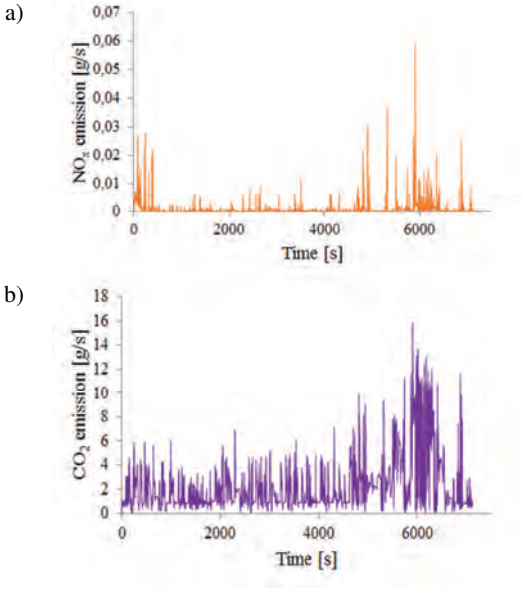

Fig. 11. Measured compounds emission per second: a) NO_x, b) CO_2

The dominance of small diameter particles throughout the test confirms the low impact of the conditions in which the vehicle moves (Fig. 128a). The formation of this type of particles is mainly caused by the type of fuel injection in a given engine type. Emission of particulate mass is associated with increased fuel consumption in the final test phase (Fig. 12b).

Along with the RDE test procedure, the conformity factor (CF) was introduced, amounting to 2. After taking the factor into account, the permissible value of nitrogen oxides emission for the entire test was exceeded (Table 6). No exceeded value for other compounds.

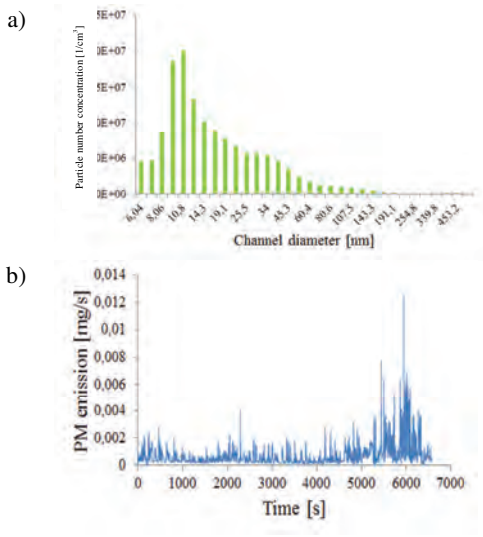

Fig. 12. Solid components of exhaust gases: a) particle number concentration, b) particle mass

Table 6. Specific distance emissions results during an extra-urban cycle

Specific distance emission during a motorway cycle		Euro 6b standard
NO_x [g/km]	0.09	0.06
CO_2 [g/km]	188.12	–
PM [mg/km]	0.000521	0.0045
PN [–/km]	1.6e11	6e11

6. Summary

Current legal regulations force vehicle manufacturers to apply exhaust aftertreatment systems. The tested vehicle was not equipped with a particulate filter, which resulted in increased emission of small particle sizes. They pose a special threat in urban areas because they have a negative impact on human life and health. The introduction of a limit of the number of particulates was necessary, which is confirmed by the results of tests in which the mass emission of solid particles is several times lower than the permissible value, while their number reaches a similar order of magnitude to the limit specified in the Euro 6b standard. Nitrogen oxide emission was exceeded during motorway cycle, which was probably caused by the increased temperature in the combustion chamber due to the need to maintain high vehicle speed. Fuel consumption was adequate to the conditions specific to a given cycle. The highest values of carbon dioxide emissions have been registered for urban cycle, in which the use of methods to reduce fuel consumption is the most difficult due to the occurrence of congestion and increased frequency of acceleration and deceleration of the vehicle. The large number of particles with small diameters is a phenomenon characteristic of this type of engines, therefore it is necessary to improve the exhaust gas aftertreatment systems and adapt them to the manufactured vehicles. Research in real traffic conditions is currently the best method to verify the operation of exhaust aftertreatment systems and to determine the actual emission of harmful and toxic exhaust components.

Bibliography

[1] AIKAWA, K., JETTER, J.J. Impact of gasoline composition on particulate matter emissions from a direct-injection gasoline engine. Applicability of the particulate matter index. *Int. J. Engine Res.* 2014, **15**, 298-306.

[2] FUĆ, P., SOKOLNICKA, B., SZYMLET, N., SIEDLECKI, M. Analiza emisji węglowodorów z pojazdu z bezpośrednim wtryskiem benzyny w rzeczywistych warunkach ruchu. *Bezpieczeństwo i ekologia, Autobusy.* 2017, **12**.

[3] MERKISZ, J., PIELECHA, J., LIJEWSKI, P. et al. Exhaust emissions from vehicles in real traffic conditions in the Poznan agglomeration. *WIT Transactions on Ecology and the Environment.* 2013, **174**, 27-38.

[4] MERKISZ, J., PIELECHA, J., NOWAK, M. Emisja zanieczyszczeń z pojazdów w rzeczywistych warunkach ruchu na przykładzie aglomeracji poznańskiej. *Postępy Nauki i Techniki.* 2012, **15**.

[5] MUÑOZ, M., HAAG, R., HONEGGER, P. et al. Co-formation and co-release of genotoxic PAHs, alkyl-PAHs and soot nanoparticles from gasoline direct injection vehicles. *Athmospheric Environment.* 2018, **178**, 242-254.

[6] SIEDLECKI, M., GALANT, M., RYMANIAK, Ł., ZIÓŁKOWSKI, A. Badania emisji zanieczyszczeń pojazdu wyposażonego w silnik z bezpośrednim wtryskiem benzyny w rzeczywistych warunkach eksploatacji. *Bezpieczeństwo i ekologia, Autobusy.* 2017, **12**.

Barbara Sokolnicka, MEng. – Faculty of Transport Engineering, Poznan University of Technology.
e-mail: *barbara.d.sokolnicka@doctorate.put.poznan.pl*

Natalia Szymlet, MEng. – Faculty of Transport Engineering, Poznan University of Technology.
e-mail: *natalia.r.szymlet@doctorate.put.poznan.pl*

Maciej Siedlecki, MEng. – Faculty of Transport Engineering, Poznan University of Technology.
e-mail: *maciej.s.siedlecki@doctorate.put.poznan.pl*

Rafał Grzeszczyk, DEng. – ODIUT Automex sp. z o.o., WSB Gdańsk.
e-mail: *rafal.grzeszczyk@automex.eu*

Paweł Fuć, DSc., DEng. – Faculty of Transport Engineering, Poznan University of Technology.
e-mail: *pawel.fuc@put.poznan.pl*

Article citation info:
KROPIWNICKI, J., FURMANEK, M. Analysis of the regenerative braking process for the urban traffic conditions. *Combustion Engines*. 2019, **178**(3), 203-207. DOI: 10.19206/CE-2019-335

Jacek KROPIWNICKI
Mariusz FURMANEK

CE-2019-335

Analysis of the regenerative braking process for the urban traffic conditions

In a regular drive system, with an internal combustion engine, vehicle braking is connected with the unproductive dissipation of kinetic and potential energy accumulated in the mass of the vehicle into the environment. This energy can constitute up to 70% of the energy used to drive a vehicle under urban conditions. Its recovery and reuse is one of the basic advantages of hybrid and electric vehicles. Modern traffic management systems as well as navigation systems should take into account the possibility of the energy recovery in the process of regenerative braking. For this purpose, a model of a regenerative braking process may be helpful, which on the one hand will enable to provide information on how traffic conditions will affect the amount of energy dissipated (wasted) into the atmosphere, on the other hand will help to optimize the route of vehicles with regenerative braking systems. This work contains an analysis of the process of the regenerative braking for the urban traffic conditions registered in Gdańsk. A model was also presented that allows calculating the amount of energy available from the braking process depending on the proposed variables characterizing the vehicle traffic conditions.

Key words: *regenerative braking, real traffic conditions, hybrid and electric vehicles, energy consumption, route planning*

1. Introduction

The increasing traffic intensity in cities and the rapidly growing population of the large agglomerations causes a continuous increase in CO_2 emissions and harmful compounds from the combustion of conventional fuels [4]. A number of technical solutions [17, 19, 20] and infrastructure solutions are implemented to reduce the impact of the automotive transport on the environment while maintaining or even increasing the flow of traffic [7, 13]. One of the most important factor actively influencing the working conditions of vehicle drive system and indirectly also the emission of toxic compounds, is the proper planning of the journey. Currently, there are a number of mobile applications that are updated basing on the current traffic conditions [6, 18], that enable shortening the travel time at the declared start and end points of the journey. However, it should be noted that while in the case of classic propulsion systems used in urban conditions, minimal traffic congestion problems transverse into high efficiency of the engine [1], in the case of alternative drive systems [15] such a relationship may no longer be unambiguous.

Using hybrid and electric drive systems, it is possible to use regenerative braking energy [3, 5], which means that the fastest route, with a limited number of braking processes, will not always be the most energy-efficient way. The technical solutions developed in recent years, which use the recuperative braking energy, allow the conversion of mechanical energy into electricity with high efficiency, even for very high power [8, 16]. The control strategies for hybrid and electric vehicles in the field of regenerative braking energy are relatively complex and depend strongly on the state of charge of the batteries [2]. However, as a rule, manufacturers of such vehicles are trying to use as much as possible the regenerative braking energy for charging batteries. Tests performed on Toyota C-HR in urban conditions [14] showed that, the share of energy recovery from regenerative braking is over 50% of all energy supplied to the battery while driving.

It is necessary to consider the possibility of regenerative braking when planning the route of such vehicles, which is not implemented with the use of today's car navigations.

For this purpose, a model of a regenerative braking process may be helpful, which on the one hand will enable to provide information on how traffic conditions will affect the amount of energy dissipated (wasted) into the atmosphere, on the other hand will help to optimize the route of vehicles with regenerative braking systems.

This work contains an analysis of the process of the regenerative braking for the urban traffic conditions registered in Gdańsk. A model was also presented that allows calculating the amount of energy available from the braking process depending on the proposed variables characterizing the vehicle traffic conditions. The model is evaluated using mean cycle parameters, which is crucial for storing data from real world traffic.

2. Identification of the vehicle traffic conditions

Vehicle operating conditions are identified in this work with the use of the specific energy consumption (SEC) that takes into account both an influence of external conditions and driver's style of driving [9, 11]. Factors mentioned above affect the amount of mechanical energy transmitted to the drive wheels, which is one of parameters constituting the specific energy consumption. Information on specific energy consumption for the considered road section can be directly used to calculate electricity consumption in the case of battery-powered vehicles. The value of parameter for assumed cycle duration may be calculated using the following equation:

$$\mathrm{SEC} = \frac{\mathrm{E}}{\mathrm{m} \cdot \mathrm{L}} \tag{1}$$

where: SEC – the specific energy consumption, E – the mechanical energy delivered by drive system to the wheels, L – the distance covered by the car, m – the gross vehicle mass.

Mechanical energy transmitted to the drive wheels may be calculated with the use of two methods. The first method

requires measurement of torque of the engine and rotational speed as well as determining power transmission system efficiency:

$$E = \int_{t=0}^{t=t_c} (k_p \cdot M \cdot \omega \cdot \eta_t) dt \quad (2)$$

where: M – engine torque, t_c – time of the cycle, $\omega=2\pi n$ – engine angular velocity, n – engine rotational speed, η_t – power transmission system efficiency, k_p – positive traction force factor:

$$k_p = \begin{cases} 1 & \text{for powered wheels} \\ 0 & \text{for idlling or breaking} \end{cases} \quad (3)$$

In the second method the mechanical energy transmitted to the drive wheels can be calculated using the following equation:

$$E = \int_{t=0}^{t=t_c} (k_p \cdot F_t \cdot V) dt \quad (4)$$

where: F_t – traction force, V – vehicle velocity.

Alternatively for the data recorded at the uniform time step, mechanical energy transmitted to the drive wheels may be calculated using the following equation:

$$E = \Delta t \cdot \sum_{i=1}^{N} (k_{p_i} \cdot F_{t_i} \cdot V_i) \quad (5)$$

where: Δt – time step.

Concerning usage of electric motor supporting conventional drive system the regenerative braking energy must be taken into consideration. The regenerative braking energy for the registered traffic conditions can be calculated using following equation:

$$E_{reg} = \Delta t \cdot \sum_{i=1}^{N} (k_{reg_i} \cdot F_{t_i} \cdot V_i) \quad (6)$$

where: k_{reg} – negative traction force factor:

$$k_{reg} = \begin{cases} -1 & \text{for idlling or breaking} \\ 0 & \text{for powered wheels} \end{cases} \quad (7)$$

Regenerative braking specific energy (RBSE) for the covered distance can be calculated using following equation:

$$RBSE = \frac{E_{reg}}{m \cdot L} \quad (8)$$

Calculation of the absolute electric energy consumed from battery by drive system in pure electrical mode can be made using the following equation:

$$E_{battery} = m \cdot L \cdot \left(SEC \cdot \frac{1}{\eta_{el}} - RBSE \cdot \eta_{reg} \right) \quad (9)$$

where: η_{el} – efficiency of electric drive system including: battery, inverter, motor and transmission. η_{reg} – efficiency of regenerative braking system including: transmission, generator, inverter, battery, or electric energy consumption:

$$EEC = SEC \cdot \frac{1}{\eta_{el}} - RBSE \cdot \eta_{reg} \quad (10)$$

For further analysis purposes it will be also used the share of the regenerative braking specific energy (in relation to the specific energy consumption).

3. The influence of the traffic conditions on the regenerative braking specific energy

To identify the influence of the traffic conditions on the regenerative braking specific energy the road tests in town Gdansk (app. 1 million inhabitants), in normal urban traffic, were performed. In the tests a passenger car (petrol powered engine, mass app. 1350 kg) was used, equipped with GPS (Global Positioning System) system and on-board CAN–Bus (Controller Area Network) registration system for measuring of operating drive system parameters (Fig. 1). The tests comprise drives during working days and were performed at different time intervals throughout the day and night. The height measurements provided by GPS system have been modified using a phenomenological correction [10]. This correction relayed on excluding the height data that gave the road inclination higher than acceptable by the regulations. This method permits eliminate the influence of false measurements coming from signals affected by high buildings and hills. This method is more reliable than commonly used digital filtering, which only waken this influence. The driver style of driving was subordinated to the style of driving randomly selected vehicle [12]. Selected vehicle was "followed" by test vehicle to prevent the influence of individual driving style of testing driver on test results.

In the Fig. 2 evaluated data set has been presented. The results has been calculated using equations (1) and (8), each point corresponds to real world traffic operating condition registered in city traffic or on the suburban ways (highest speed). Covered distances are not equal for each point and range form 2 up to 18 km. It can be observed that lower average speed corresponds to higher share of the regenerative braking specific energy (71%), which comes from typical city center traffic conditions – high number of stops and braking phases. It can be also seen for those conditions that there is a relatively large spread of points for the same speed (32–64%). For the city center traffic conditions the same average speed can result from high maximum speed and long idling, as well as from almost constant low cruising speed. For higher average speed it can be observed stabilization of the share of the regenerative braking specific energy at the level of 8%, which can be explain by the lack of traffic congestion on suburban ways and low number of braking phases.

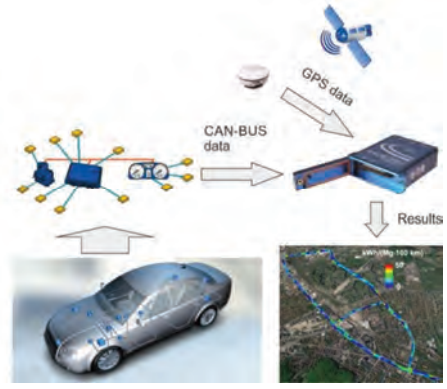

Fig. 1. System used for measurement of car and engine operating parameters

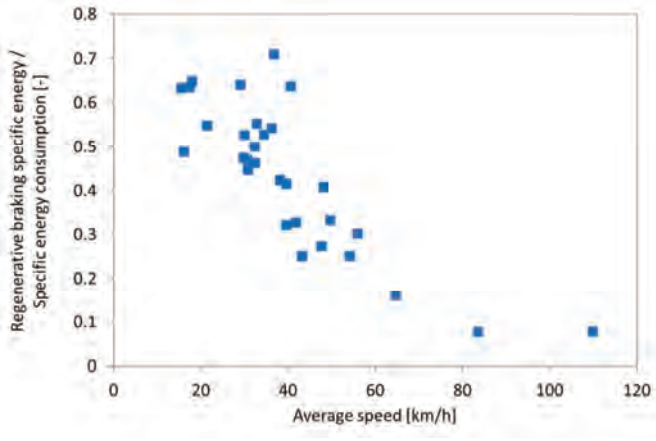

Fig. 2. Traffic conditions registered in urban and suburban area

The share of the regenerative braking specific energy can be evaluated for selected mean operating parameters using speed pattern presented in Fig. 3. It has been assumed that the vehicle movement can be divided into three phases: acceleration, constant speed (cruising) and braking (deceleration).

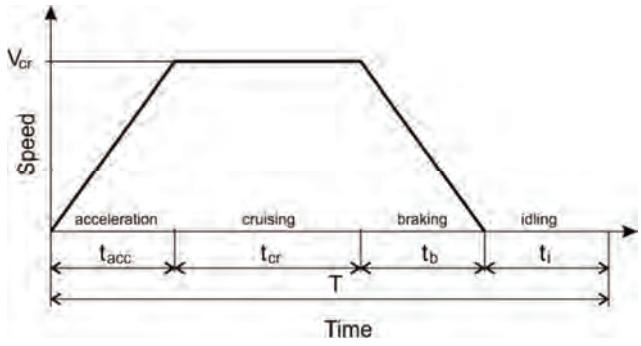

Fig. 3. The speed pattern used for evaluation of the share of the regenerative braking specific energy

Omitting influence of the road gradient the following relation can be made:

$$\frac{\mathrm{RBSE}}{\mathrm{SEC}} = \frac{\left(\frac{m \cdot V_{cr}^2}{2} - f_t \cdot m \cdot g \cdot L_b\right)/(m \cdot L)}{\left(\frac{m \cdot V_{cr}^2}{2} + f_t \cdot m \cdot g \cdot L_p\right)/(m \cdot L)} \tag{11}$$

where: V_{cr} – the cruising speed between acceleration and braking, f_t – the rolling resistance coefficient, g – the gravitational constant, L_b – the braking distance, L_p – the powered distance.

Hence:

$$\frac{\mathrm{RBSE}}{\mathrm{SEC}} = \frac{1 - 2 \cdot f_t \cdot g \cdot \frac{L_b}{V_{cr}^2}}{1 + 2 \cdot f_t \cdot g \cdot \frac{L_p}{V_{cr}^2}} \tag{12}$$

$$\frac{\mathrm{RBSE}}{\mathrm{SEC}} = 1 - \frac{2 \cdot f_t \cdot g \cdot \left[\frac{L_b}{L} + \frac{L_p}{L}\right] / \left(\frac{V_{cr}^2}{L}\right)}{1 + 2 \cdot f_t \cdot g \cdot \left[\frac{L_p}{L}\right] / \left(\frac{V_{cr}^2}{L}\right)} \tag{13}$$

where:

$$\left[\frac{L_b}{L} + \frac{L_p}{L}\right] = 1$$

then equation (13) reduces as:

$$\frac{\mathrm{RBSE}}{\mathrm{SEC}} = 1 - \frac{1}{\frac{1}{2 \cdot f_t \cdot g / \left(\frac{V_{cr}^2}{L}\right)} + \left[\frac{L_p}{L}\right]} \tag{14}$$

Because for the real traffic conditions the cruising speed can not be easy evaluated it has been assumed that there can be formulated relation between this parameter and average speed for the covered distance using pattern presented in Fig. 3:

$$V_{av} = \left[\frac{1}{2} \cdot V_{cr} \cdot t_{acc} + V_{cr} \cdot t_{cr} + \frac{1}{2} \cdot V_{cr} \cdot t_b\right] \cdot \frac{1}{T} \tag{15}$$

where: V_{av} – the average speed of analyzed cycle, t_{acc} – the acceleration phase time, t_b – the braking phase time, T – the analyzed cycle time.

Taking into account that it is much easier for real traffic condition to define braking then accelerating phase, it has been assumed that $t_{acc} = t_b$ and the relation (15) can be simplified:

$$V_{av} = V_{cr} \cdot \left[\frac{t_{acc}}{T} + \frac{t_{cr}}{T}\right] = V_{cr} \cdot \frac{T - (t_b + t_i)}{T} \tag{16}$$

where: t_i – the idling time, hence:

$$V_{cr} = V_{av} \cdot \frac{1}{1 - (t_b + t_i)/T} \tag{17}$$

Finally the relation (14) can be transformed to the equation, which uses relatively easy to evaluate mean cycle parameters:

$$\frac{\mathrm{RBSE}}{\mathrm{SEC}} = 1 - \frac{1}{\frac{1}{2 \cdot f_t \cdot g} \cdot \left(\frac{V_{av}^2}{L}\right) \cdot \left(\frac{1}{1 - \frac{(t_b + t_i)}{T}}\right)^2 + \left[\frac{L_p}{L}\right]} \tag{18}$$

Using equation (18) the real traffic data has been compared to the calculation results (Fig. 4). It can be observed that the correlation between those data is not very good (R^2=0.7011). Hence, a few intuitively established relations have been additionally tested below.

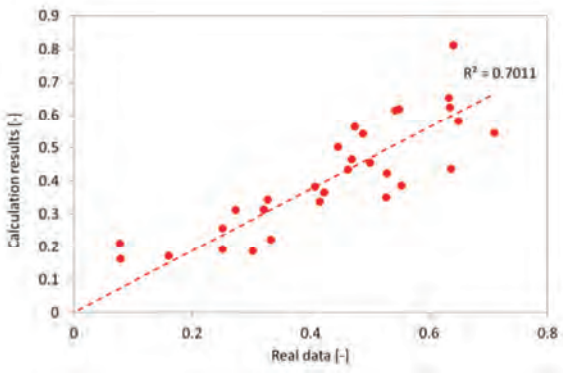

Fig. 4. Result of calculation of the of the share of the regenerative braking specific energy using equation (18) vs. the real traffic data

It can be expected that higher share of the braking distance results in higher share the regenerative braking specific energy. The share of the braking distance for the real traffic data can be calculated using following relation:

$$\frac{L_b}{L} = \frac{1}{L} \cdot \sum_{i=1}^{N} \left(-k_{reg_i} \cdot L_i\right) \tag{19}$$

where: L_b/L – the braking distance share,

$$L = \sum_{i=1}^{N} (L_i)$$

k_{reg_i} – the negative traction force factor defined in equation (7), or it can be defined using powered distance share:

$$\frac{L_b}{L} = 1 - \frac{L_p}{L} = 1 - \frac{1}{L} \cdot \sum_{i=1}^{N} \left(k_{p_i} \cdot L_i\right) \tag{20}$$

where: L_p/L – the powered distance share, k_p – the positive traction force factor defined in equation (3).

It can be observed (Fig. 5) that there is good correlation between braking distance share and the regenerative braking distance share, hence, the general tendency can be confirmed in the following form:

$$\frac{RBSE}{SEC} = a_1 \cdot \frac{L_b}{L} + a_0 \tag{21}$$

where: a_1, a_2 – the function coefficients.

However, there is a relatively large spread of points for the higher braking distance share, which suggests that some additional variables affect the share of the regenerative braking specific energy.

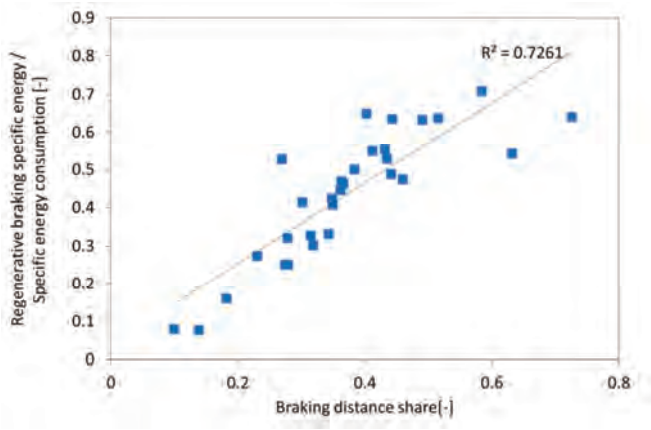

Fig. 5. Relation between the braking distance share and the share of the regenerative braking specific energy

Another two tested relations including: the idling time share and the specific energy consumption have not brought positive results. The idling time share can be defined using following equation:

$$\frac{t_i}{T} = \frac{1}{T} \cdot \sum_{j=1}^{N} \left(t_{i_j}\right) \tag{22}$$

It can be observed that for low values of the idling time share there is large spread of points (Fig. 6) but for higher values concentration of points is much higher, which suggests usage of this relation for limited range.

Using real world data it can be observed that the specific energy consumption and the share of the regenerative braking specific energy are uncorrelated variables (Fig. 7).

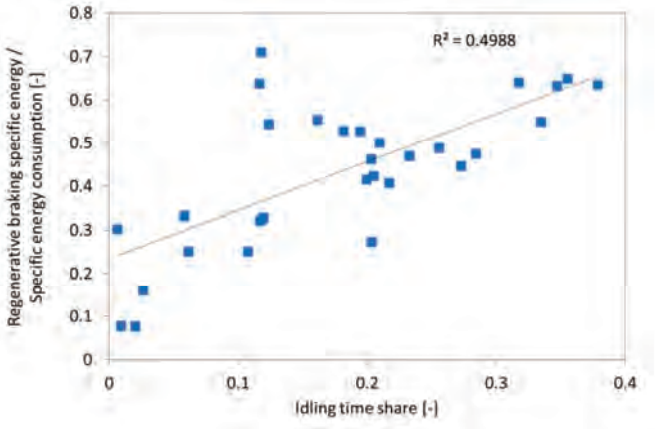

Fig. 6. Relation between the idling time share and the share of the regenerative braking specific energy

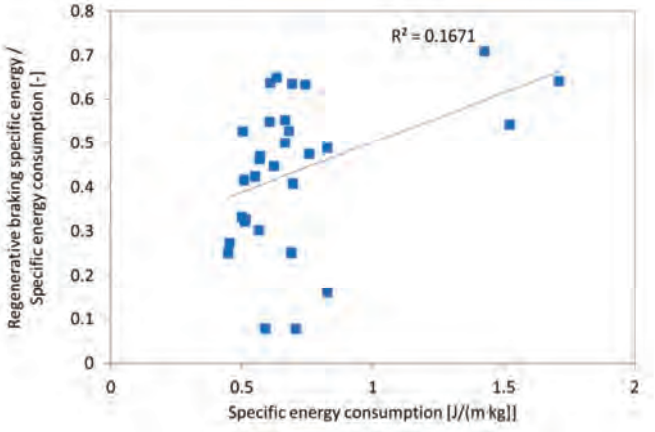

Fig. 7. Relation between the specific energy consumption and the share of the regenerative braking specific energy

4. Conclusions

This work contains an analysis of the process of the regenerative braking for the urban traffic conditions registered in Gdańsk. Information about the achievable regenerative braking energy for selected route should be use, when planning the route of hybrid and electric vehicles. It is expected that this functionality should be implemented in mobile car navigation systems, because continuous updating is necessary to maintain high system efficiency. Observation made in in real traffic in Gdańsk showed that low average speed corresponds to the highest share of the regenerative braking specific energy (71%), which comes from typical city center traffic conditions – high number of stops and braking phases.

Presented in this work analyze of the regenerative braking process has been evaluated for the assumed simple speed pattern. Obtained model (18) enables calculation of the share the regenerative braking specific energy using relatively easy to evaluate mean cycle parameters, which is crucial for storing data from real world traffic. Using the model the real traffic data has been compared to the calculation results. It turned out that the correlation between

those data is not very good (R^2 = 0.7011). Hence, a few intuitively established relations have been additionally tested. The best results have been achieved for tested relation: the braking distance share – the share of the regenerative braking specific energy. Evaluated linear relation (21) gives even better results then phenomenologically evaluated relation (18). Analyzing all tested relations it can be concluded that the share the regenerative braking specific energy is mainly affected by the braking distance share. The influence of other analyzed variables is changing depending on the range of the tested set. That implies, the relation describing the regenerative braking process should be represented by set of equations specific for pointed range of input variables.

Bibliography

[1] BIRRELL, S., et al. Analysis of three independent real-world driving studies: A data driven and expert analysis approach to determining parameters affecting fuel economy. *Transportation Research Part D*. 2014, **33**, 74-86.

[2] CIEŚLIK, W., PIELECHA, I., SZAŁEK, A. Indexes of performance of combustion engines in hybrid vehicles during the UDC test. *Combustion Engines*. 2015, **160**, 11-25.

[3] DAMIANI, L. et al. Improvement of powertrain efficiency through energy breakdown analysis. *Applied Energy*. 2014, **121**, 252-263.

[4] EEA Annual European Union greenhouse gas inventory 1990–2014 and inventory report 2016. Copenhagen 2016.

[5] FIORI, C. et al. Power-based electric vehicle energy consumption model: Model development and validation. *Applied Energy*. 2016, **168**, 257-268.

[6] Goole Maps, https://www.google.com/maps (visited: 28.04.2019).

[7] JEFFREYS, I. et al. Evaluation of eco-driving training for vehicle fuel use and emission reduction: A case study in Australia. *Transportation Research Part D*. 2018, **60**, 85-91.

[8] KALOCIŃSKI, T., RYMANIAK, Ł., FUĆ, P. Powertrain technology transfer between F1 and the Automotive industry based on Mercedes-Benz. *Combustion Engines*. 2018, **172**, 3-13.

[9] KROPIWNICKI, J., KNEBA, Z., ZIÓŁKOWSKI, M. Test for assessing the energy efficiency of vehicles with internal combustion engines. *International Journal of Automotive Technology*. 2013, **14**, 479-487.

[10] KROPIWNICKI, J., KNEBA, Z. Phenomenological correction of height above ground level of vehicle derived from GPS system. *6th International Conference Mechatronic Systems and Materials*. 2010, 1-7.

[11] KROPIWNICKI, J. Identification of real vehicle operating conditions with using of specific energy consumption. *The Archives of Automotive Engineering*. 2010, **3**, 153-166.

[12] KULKARNI, A.V., SAPRE, R.R., SONCHAL, CH.P. GPS-based methodology for drive cycle determination. *SAE Technical Paper* 2005-01-1060, 2005.

[13] MERSKY, A.C., SAMARAS, C. Fuel economy testing of autonomous vehicles. *Transportation Research Part C*. 2016, **65**, 31-48.

[14] PIELECHA, I., CIEŚLIK, W., FLUDER, K. Analysis of energy management strategies for hybrid electric vehicles in urban driving conditions. *Combustion Engines*. 2018, **173**, 14-18.

[15] PIELECHA, I., CIEŚLIK, W., SZAŁEK, A. The use of electric drive in urban driving conditions using a hydrogen powered vehicle –Toyota Mirai. *Combustion Engines*. 2018, **172**, 51-58.

[16] STĘPIEŃ, Z. A new generation of F1 race engines – hybrid power units. *Combustion Engines*. 2016, **167**, 22-37.

[17] TRIANTAFYLLOPOULOS, G. et al. Experimental assessment of the potential to decrease diesel NO_x emissions beyond minimum requirements for Euro 6 Real Drive Emissions (RDE) compliance. *Science of the Total Environment*. 2018, **618**, 1400-1407.

[18] Yanosik, https://yanosik.pl (visited: 28.04.2019).

[19] ZAHABI, S.A.H. et al. Fuel economy of hybrid-electric versus conventional gasoline vehicles in real-world conditions: A case study of cold cities in Quebec, Canada. *Transportation Research Part D*. 2014, **32**, 184-192.

[20] ZHANG, R., YAO, E. Electric vehicles' energy consumption estimation with real driving condition data. *Transportation Research Part D*. 2015, **41**, 177-187.

Jacek Kropiwnicki, DSc., DEng. – Faculty of Mechanical Engineering, Gdańsk University of Technology.
e-mail: *jkropiwn@pg.edu.pl*

Mariusz Furmanek, MEng. – Faculty of Mechanical Engineering, Gdańsk University of Technology.
e-mail: *mfurmanek1@gmail.com*

Article citation info:
DZIDA, J., BRZEŻAŃSKI, M. An analysis of SCR reactor deactivation impact on NO_x emissions from a compression ignition engine. *Combustion Engines*. 2019, **178**(3), 208-212. DOI: 10.19206/CE-2019-336

Jakub DZIDA
Marek BRZEŻAŃSKI

CE-2019-336

An analysis of SCR reactor deactivation impact on NO_x emissions from a compression ignition engine

Catalytic exhaust gas aftertreatment devices fitted to combustion engines are susceptible to partial deactivation as their operating time progresses. This includes selective catalytic reduction (SCR) reactors meant for NO_x emission control. There are several known deactivation mechanisms of SCR reactors already analyzed in detail in the literature. This paper, however, approaches the analysis of reactor deactivation by comparison of exhaust gas characteristics over repeatable cycle for fresh and aged samples of a SCR reactor for non-road mobile machinery. The research aims to outline which parameters describing the SCR reactor's performance are most affected by its ageing. In order to do that, fresh and aged samples of the reactor were tested under the Non Road Steady Cycle. The acquired emission results, including concentration traces of particular compounds were analyzed. The specific NO_x emission of the aged reactor was significantly higher than that of the fresh one. The NO_x conversion efficiency of both reactors was found similar at periods of steady engine operation. It was recognized that during transient conditions the NO_x conversion efficiency of the aged reactor was decreased. It was found that the main factor contributing to that phenomenon is the drop in the ammonia storage capacity of the aged SCR sample.

Key words: *SCR system, SCR deactivation, SCR ageing, nitrogen oxides emission, ammonia emission*

1. Introduction

On a global scale, the impact of internal combustion engine (ICE) operation on the natural environment is significant, as it is the most common vehicular propulsion system worldwide. The ICE exhaust gases contain both harmful and greenhouse gases. The legislation intends to limit both; however, the harmful gases have been regulated for decades while the limitation of greenhouse gases is just becoming more common. To comply with the requested emission limit of a particular harmful compound, effective exhaust aftertreatment system (ATS) is applied [1]. Nowadays, the selective catalytic reduction (SCR) of NO_x by NH_3 is recognized as the most comprehensive solution for NO_x emission control. The system is capable of reaching high overall conversion efficiency – frequently exceeding 90% [2, 3]. It is considered to be the major future deNO_x solution and considerable research is being conducted to maximize its potential [4, 5]. Nevertheless, the SCR system is susceptible to partial deactivation as its operating time progresses. There are several known reversible and irreversible SCR reactor deactivation mechanisms already analysed in detail in the literature [2, 6]. In the case of reversible phenomena, recovery of reactor functionality occurs at elevated exhaust temperature, which allows oxidation of compounds inhibiting catalytic activity. Irreversible deactivation occurs when the porous zeolite structure collapses and materials of higher density, e.g. quartz, are formed. The influence of SCR ageing on the composition of tailpipe exhaust gas is complex, as it affects the emission of NO_x, NH_3 and N_2O. This research aims to characterize which parameters describing the SCR reactor's performance are most affected by its ageing and how it influences the tailpipe emissions. For research purposes an SCR system for non-road mobile machinery applications was considered.

2. Legal requirements regarding NO_x emission

Legal regulations regarding emissions of harmful exhaust gas compounds are becoming more restrictive. The current EU emission limits for non-road mobile machinery engines (STAGE IV) have been in force since 2014. The recent tightening of this limit mainly concerned the reduction of specific NO_x emissions to 0.40 g/kWh (Table 1) [7]. This change forced engine manufacturers to apply an effective method of purifying exhaust gas from nitrogen oxides. This challenge primarily concerned CI engines operating on lean mixtures, where due to the presence of oxygen in the exhaust gas, it is not possible to reduce NO_x by a TWC reactor. In this case, it is assumed that the most efficient method of NO_x emission control is an SCR system. Such systems are now widely used in engines for non-road mobile machinery meeting the STAGE IV limits.

Table 1. STAGE IIIB and STAGE IV emission limits of NO_x [7]

Limit	Power range [kW]	Date of introduction	Brake specific NO_x emission limit [g/kWh]
STAGE IIIB	$130 \le P \le 560$	2011.01	2.00
STAGE IIIB	$56 \le P < 130$	2012.01	3.30
STAGE IV	$130 \le P \le 560$	2014.01	0.40
STAGE IV	$56 \le P < 130$	2014.10	0.40

Table 2. Required period of compliance with the STAGE IV limit for non-road mobile machinery engines [8]

Limit	Power range [kW]	Limit compliance [h]
STAGE IV	< 37	5000
STAGE IV	> 37	8000

The legal provisions specify not only the maximum permissible specific emission of harmful exhaust compounds, but also the period of operation during which the limits will not be exceeded (Table 2). According to these regulations, engines – and in particular their ATS – must not only meet the emission limits in "as new" condition, but also guarantee their fulfilment throughout the required period of engine operation [8]. A key condition to meet this requirement is the lifespan of the ATS. However, such systems, including those incorporating SCR, a characterized by efficiency drops as they age. There are several known mechanisms of

SCR deactivation and they can be classified as follows [1, 3]:

- Hydrothermal deactivation: the exposition of SCR reactor to exhaust gas of temperature exceeding 600°C and humidity above 4% may lead to zeolite structure collapse.
- Hydrocarbon accumulation deactivation: the SCR reactor tends to accumulate HC, especially at exhaust temperatures below the DOC light-off point; under certain conditions the stored HC oxidizes, leading to local spots where the safety temperature of the reactor is exceeded.
- Sulphur poisoning: reduced catalytic site activity caused by the presence of sulphur compounds.
- Chemical deactivation: alkali metals may displace Cu from the exchange sites and thus reduce catalytic activity.
- Ammonia deposits deactivation: reducing catalytic sites activity by UWS-derived compounds.

3. ATS and engine setup

The unit selected for the research was a regular SCR reactor designed for a non-road mobile machinery engines. The active layer of the reactor's substrate was made of Fe-exchanged zeolite. The substrate had a cylindrical shape 18 inches (45.7 cm) long, 10 inches (25.4 cm) in diameter and thus 11.6 dm^3 of volume. The SCR reactor tested was installed in the exhaust aftertreatment system (Fig. 1), the functionality of which ensured compliance with the emission limits of STAGE IV. The system incorporated a DOC reactor, the function of which was to oxidize the CO and HC present in the exhaust gas and to oxidize a fraction of the NO present to NO_2. The right ratio of NO_2 to NO, not exceeding 50:50, ensures optimal performance of the SCR reactor [2]. Subsequently, downstream of the DOC, the UWS injector was installed in the exhaust line. In order to ensure the most uniform UWS distribution in the exhaust stream, in the close proximity of the injector, a mixing element was placed. Behind this element, at a distance of about 80 cm, the tested SCR reactor was installed. The span between the mixing element and the reactor provided time for the evaporate water from UWS and to for the thermolysis and hydrolysis reactions necessary to obtain NH_3 from urea to occur.

In addition to the active components of the ATS system, it also included a control system for the UWS rate introduced into the exhaust stream. The applied UWS dosing system worked in so-called closed loop, where the parameters determining the UWS injection rate were the mass flow of exhaust gas, the engine-out concentration of NO_x and the alpha factor regulating the composition of the obtained mixture of NH_3 and NO_x. This system consisted of an electronic controller with appropriate software and a set of sensors. At the inlet to the ATS, a NO_x concentration sensor was located in the raw engine exhaust. This sensor was of key importance for the operation of the SCR system, as its reading was a parameter directly influencing the calculated value of the UWS dosing rate. Together with the NO_x sensor, a temperature sensor was used, according to which the lower temperature threshold for the start of the UWS dosing functioned. At the end of the exhaust aftertreatment system, downstream of the SCR reactor, there was another set of sensors: an NH_3 concentration sensor, a NO_x concentration sensor and exhaust gas temperature sensor. The NH_3 concentration sensor monitored the NH_3 concentration value after the catalytic converter. Based on its readings, the UWS dosing system could reduce the amount of NH_3 introduced to minimize its emission to the atmosphere. The NO_x sensor monitored the correctness of NO_x conversions in order to diagnose the entire system functionality, e.g. to diagnose a lack of UWS. The temperature sensor could provide feedback causing the engine's performance to be limited, if the safe temperature threshold for the system was exceeded.

The exhaust aftertreatment system incorporating the investigated SCR reactor was built into the exhaust line of the CI internal combustion engine with the following parameters:

- displacement: 4500 cm^3,
- number of cylinders: 4,
- rated power: 103 kW,
- Common Rail fuel injection system,
- turbocharging with a waste gate,
- fuel: B7 Diesel fuel,
- engine application: non-road mobile machinery.

4. Experiment setup and ageing procedure

The engine and exhaust aftertreatment system were installed on the laboratory engine test bench. The bench was capable of executing both the emission measurements and the ageing procedure. Prior to the emission measurements,

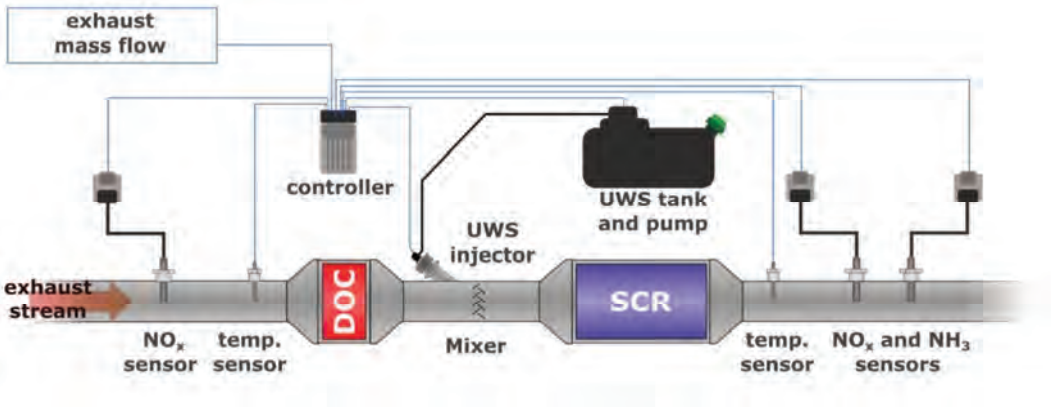

Fig. 1. Exhaust aftertreatment system including SCR reactor under test

the ATS was degreened for 5 h in a controlled manner by exposing it the exhaust stream of 350°C temperature. This operation aimed to stabilize the zeolite structure and remove any potential debris deriving from the production process. Such operation ensured the performance stability of the reactor from the very first measurement cycles.

The prepared test bench installation allowed performance of the experimental activities in the following order:

1. measurement of chosen gaseous exhaust gas compounds downstream of the ATS for the new SCR reactor,
2. controlled ageing of the SCR reactor,
3. measurement of chosen gaseous exhaust gas compounds downstream of the ATS for the aged SCR reactor.

The measurement of gaseous exhaust emissions downstream of the ATS before and after the SCR reactor ageing was done according to the same methodology. As a measurement test, the NRSC RMC (Non Road Steady Cycle Ramped Mode Cycle) stationary cycle was adopted, which is a part of the type approval procedure for engines intended for non-road mobile machinery. For the purpose of the research, the NO_x, NO and NH_3 concentrations were measured.

The test bench automation system was capable of executing the predefined cycle and acquiring measurement results at a rate of 10 Hz. Apart from exhaust gas compound concentrations, a number of channels necessary for specific emissions calculations were acquired. These included the engine speed and torque. The mass flow of air supplying the engine and the fuel consumption were also measured. On the basis of the sum of these two parameters, the mass flow of exhaust gas through the ATS was determined. In addition, the following parameters were measured: temperature and humidity of the engine intake air and atmospheric pressure. Moreover, ATS signals readings and the UWS injection rate were acquired during the test.

The test bench automation system featured data post-processing tools enabling calculation of specific emissions (g/kWh) achieved over the test. The intermediate steps of the emission calculation were the determination of the total emitted mass of each of the measured compounds and mechanical work done by the engine during the whole test.

The procedure of the controlled ageing of the SCR reactor was the following:

1. Engine operation with gradual increase of load and speed from idling up to the rated power point. Duration of the phase: 2 h 10 min, engine run time: 2 h 10 min.
2. Three repetitions of the NRSC cycle. Duration of the phase: 1 h 30 min, engine run time 1 h 30 min.
3. Two repetitions of the NRTC cycle (cold and warm test), including engine conditioning for cold tests. Duration of the phase: 6 h, engine working time 1 h 20 min.

The total duration of a single ageing cycle was 9 h 30 min, including engine operation time of 5 h. The total number of cycle repetitions amounted to 50, reaching 250 h of engine operation along with the ATS undergoing ageing.

5. Test results

Table 3 presents results of measurements of NO_x specific emission and maximum NH_3 concentration obtained in the NRSC RMC test on the fresh and aged SCR reactor. In the case of the fresh rector, the measured NO_x emission was 0.151 g/kWh, and for the measurement of the aged reactor, the obtained NO_x emission was 0.322 g/kWh. This increase in NO_x emissions is 218%, which clearly confirms the partial deactivation of the SCR reactor and the appropriateness of the selected ageing procedure. Despite a more than a twofold increase in post-SCR NO_x emissions, the obtained result of the aged SCR reactor is still below the STAGE IV limit of 0.4 g/kWh. A similar tendency was observed for NO emissions, where the aged sample displayed emissions 224% of the fresh sample's emissions. In line with the NO_x and NO emission trends, the fresh SCR reactor featured a lower maximum NH_3 concentration downstream of the aftertreatment system.

Table 3. Results summary of NRTC RMC test for fresh and aged sample

Reactor condition	Brake specific NO_x emission	Brake specific NO emission	NH_3 maximum concentration
	[g/kWh]	[g/kWh]	[ppm]
Fresh	0.151	0.087	13
Aged	0.329	0.195	19
Increase	218%	224%	146%

Figure 2 presents traces of selected parameters during the NRSC RMC test performed for a fresh and aged SCR reactor. The engine speed and torque lines show the selected operating points. Obtained traces in both tests are almost identical, showing very good repeatability of the test. In the NRSC RMC test, the engine operates at 9 fixed operating points, including two periods of idling: the first and the last test step.

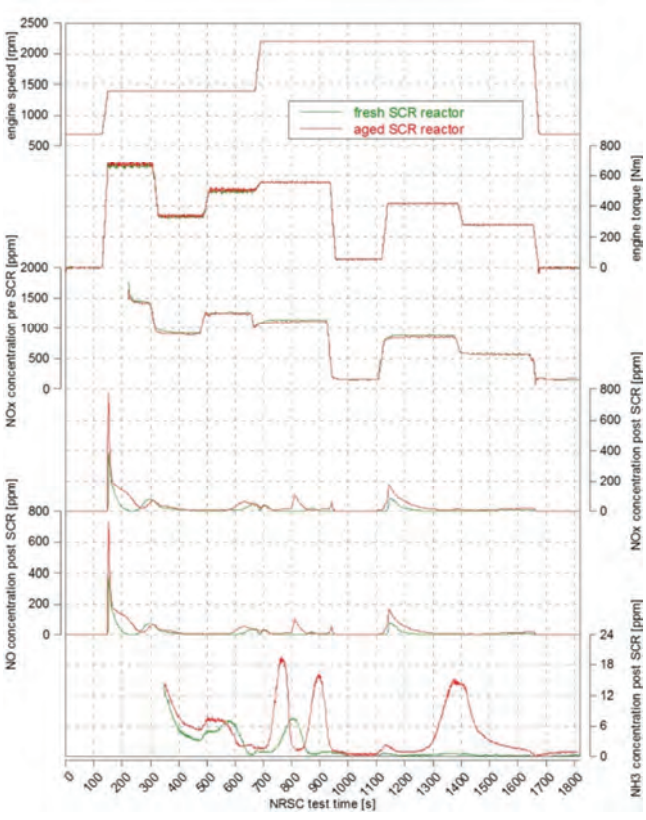

Fig. 2. Traces of chosen parameters over NRTC test

The NRSC RMC test is a hot condition test. Before starting the test, controlled warmup of the engine and exhaust aftertreatment system was performed. The engine was then stopped and immediately restarted to initiate the test without delay. The temperature of the SCR reactor at the start of the test exceeded 200°C and it was found that it was saturated with NH_3 supplied during the warm up phase.

The first step of the test was idling. In this step, lasting 120 s, a small dose of UWS was delivered to the exhaust gas stream, amounting to 0.5 g. The NO_x concentration after the SCR reactor was less than 1 ppm throughout the entire step, both for the fresh and aged reactor. Such low NO_x concentrations were possible due to the NH_3 stored in the SCR reactor and due to the appropriate exhaust temperature (approx. 200°C). A similar phenomenon occurred in the last test step, in which the engine was also idling, and the measured NO_x concentration after the SCR reactor was below 1 ppm.

At the 120th second of the NRSC test, the engine's operating point changed: from idle to the point of maximum torque. This point is characterized by the highest NO_x concentration in the raw exhaust gas, the value of which exceeds 1400 ppm. Despite the immediate response of the UWS dosing system, an increase in the NO_x concentration after the SCR reactor was noted. This tendency occurred both in the case of the fresh and the aged reactor, but the values of the concentrations obtained were different: the maximum NO_x concentration for the fresh reactor was 393 ppm, while in the case of an aged reactor it was 778 ppm. The stabilization time of the SCR system was also different for both reactors. The fresh SCR reactor revealed the minimum NO_x concentration in the analysed step 80 seconds after the beginning of the step (i.e. 145 seconds into the test) and its value was 4 ppm. In case of the aged reactor, the lowest observed NO_x concentration was 21 ppm, occurring 120 seconds after the beginning of the step (i.e. 265 seconds into the test). A significant increase in engine load also occurred at 1100 into the test. In this case, the engine load increased from 10% to 75% of the maximum torque at the engine speed for its rated power value. The SCR system response to an immediate increase in NO_x emissions was similar to that observed in the 120th second test for both the fresh and the aged SCR reactor. The fresh reactor revealed maximum NO_x concentration of 85ppm, while in the case of the aged reactor, a maximum concentration of 178ppm was obtained.

Over the entire test, the NO concentration trace is of similar trend to NO_x. The concentration traces of NH_3 clearly indicate its lower emission downstream of the fresh reactor.

6. Conclusions

An aged SCR reactor is characterized by an increase in total NO_x and NH_3 emissions after the exhaust gas aftertreatment system. The NO_x conversion efficiency of both reactors was found similar at periods of steady engine operation. It was recognized that during transient conditions the NO_x conversion efficiency of the aged reactor was decreased. Different responses of SCR system equipped with fresh and aged SCR reactor for an immediate increase in NO_x emissions of raw exhaust gases resulted from a change in the storage capacity of NH_3. A sudden increase of the NO_x concentration forces the UWS dosing system to proportionally increase the UWS dose delivered to the exhaust stream. However, this response is delayed. Initially, due to the insufficient amount of UWS in the exhaust, nitrogen oxides reacts with NH_3 stored in the SCR reactor. During this period, the amount of NO_x leaving the SCR reactor was inversely proportional to the amount of previously absorbed NH_3. With the ageing of the SCR reactor, the storage capacity of NH_3 decreases; consequently the NO_x emission increases behind the SCR reactor in the states of sudden rise in NO_x emissions of raw exhaust gas.

A reduction of the NH_3 storage capacity of the aged SCR reactor was also noted in the plot of NH_3 concentration downstream of the reactor. For the vast majority of the test duration, the NH_3 concentration behind the aged reactor was greater than in the case of the fresh reactor. Ammonia entering the SCR reactor, which was not used to reduce NO_x, in the case of the aged SCR reactor, was stored to a lesser extent. The NO_x conversion efficiency of both reactors was found to be similar at periods of steady engine operation. The deactivation of the SCR reactor primarily affected its performance under transient conditions, when ammonia storage capacity is the most crucial parameter influencing NO_x conversion efficiency.

Acknowledgements

The researched was conducted in Engine Research Laboratory of BOSMAL Automotive Research and Development Institute.

Nomenclature

ATS	aftertreatment system
CI	compression ignition
CO	carbon monoxide
Cu	copper
$deNO_x$	aftertreatment device meant for nitrogen oxides
DOC	diesel oxidation catalyst
HC	hydrocarbons
ICE	internal combustion engine
N_2O	nitrous oxide
NH_3	ammonia
NO	nitric oxide
NO_2	nitrogen dioxide
NO_x	nitrogen oxides
NRSC	non-road steady cycle
NRTC	non-road transient cycle
RMC	ramped mode cycle
TWC	three-way catalyst
UWS	urea-water solution
SCR	selective catalytic reduction

Bibliography

[1] JONHSON, T.V. Diesel emissions in review. *SAE Int. J. Engines*. 2012, **5**, 216-234; DOI: 10.4271/2012-01-0368

[2] NOVA, I., TRONCONI, E. (Eds.) Urea-SCR technology for $DeNO_x$ after treatment of diesel exhaust; fundamental and applied catalysis. *Springer*. Berlin 2014.

[3] KRÖCHER, O. Selective catalytic reduction of NO_x. *Catalysts*. 2018, **8**, 459. DOI: 10.3390/catal8100459

[4] BRZEŻAŃSKI, M., SALA, R. A study on the indirect urea dosing method in the selective catalytic reduction system. *Scientific Conference on Automotive Vehicles and Combustion Engines (KONMOT 2016), Materials Science and Engineering*. 2016, **148**, 012062 DOI: 10.1088/1757-899X/148/1/012062

[5] SALA, R., KRASOWSKI, J., DZIDA, J. The influence of engine warm up phase on nitrogen oxides emission for heavy-duty Euro VI diesel engine. *MATEC Web of Conferences*. 2017, **118**, 00035, DOI: 10.1051/matecconf/201711800035

[6] MAJEWSKI, W.E. Selective Catalytic Reduction. www.DieselNet.com [access in 03.2019].

[7] Regulation (EU) 2016/1628 of the European Parliament and of the Council.

[8] Annex V of Regulation (EU) 2016/1628 of the European Parliament and of the Council.

Jakub Dzida, MEng. – Aftertreatment System and Engine Control Laboratory, BOSMAL Automotive Research & Development Institute Ltd, Bielsko-Biala, Poland.
e-mail: *jakub.dzida@bosmal.com.pl*

Marek Brzeżanski, DSc., DEng. – Institute of Motor Vehicles and Combustion Engines, Cracow University of Technology.
e-mail: *mbrzez@pk.edu.pl*

Article citation info:
ORKISZ, M., WYGONIK, P., KUŹNIAR, M., KALWARA, M. Comparative analysis of combustion engine and hybrid propulsion unit in aviation application in terms of emission of harmful compounds in the exhausts emitted to the atmosphere. *Combustion Engines*. 2019, **178**(3), 213-217. DOI: 10.19206/CE-2019-337

Marek ORKISZ
Piotr WYGONIK
Michał KUŹNIAR
Maciej KALWARA

CE-2019-337

Comparative analysis of combustion engine and hybrid propulsion unit in aviation application in terms of emission of harmful compounds in the exhausts emitted to the atmosphere

Comparative analysis of combustion and hybrid propulsion unit in aviation application in terms of emission of harmful compounds in the exhausts emitted to the atmosphere. For the propulsion of the AOS 71 motor glider, two types of propulsion were planned as development versions. The first analysed propulsion is based on a combustion engine, but of the Wankel type (LCR 814 engine with the power of 55 kW). The second designed propulsion is an hybrid based on a LCR 407 combustion engine with a power of 28 kW, which is connected in series with an electric generator propelling the engine (Emrax 228 engine), total power of the propulsion is 55 kW. The comparison of emissions of harmful compounds emitted to the atmosphere generated by the combustion and hybrid power unit intended for assembly in the AOS 71 motor glider, assuming various loads and methods of hybrid propulsion control, was made. The tests were conducted in laboratory conditions. Several different programs were designed to simulate different energy management methods in a hybrid system, depending on the predicted mission and load of the motor glider. On the basis of laboratory tests, exhaust emission was determined from both propulsions as a function of rotational speed and load. Then, based on the assumed flight trajectory and collected test data, the emission for both propulsions variants was determined. The values of emission parameters were compared and the results were presented in diagrams and discussed in the conclusions

Key words: *hybrid, combustion engines, motor glider, rotary engine, Wankel engine, hybrid propulsion, emission, exhaust gases*

Introduction

The environmental aspects of aircraft operation are discussed more and more frequently [7, 10, 12]. It has become important to reduce fuel consumption and emissions of harmful and toxic compounds present in the exhausts of aircraft engines [10]. The impact of aviation on the environment refers not only to commercial communication aviation, but also to small, short-distance or amateur aviation using aircraft equipped with reciprocating engines. Attempts to use hybrid propulsion are made, following the solutions used in the automotive industry, which are characterized by lower emission of pollutants and fuel consumption compared to traditional propulsion systems (especially in the range of work under load – acceleration) [7, 12]. A similar analysis relating to the flight of the aircraft on a known flight path can be performed for an aircraft.

The paper presents a comparative analysis of conceptual propulsions intended for use in the AOS 71 motor glider. The "pure" combustion propulsion system based on a rotary piston engine (Wankel) and also a hybrid one with an electric generator (so-called range extender) were investigated.

1. Research object

For the analysis there was taken the airframe of the AOS-71 electric glider (Fig. 1), built as part of the cooperation between the Department of Aircraft and Aircraft Engines of the Rzeszow University of Technology and the Faculty of Power and Aeronautical Engineering of the Warsaw University of Technology.

Table 1 shows the basic data of the airframe, while Figs 2 and 3 present the values of power required for the flight for this airframe and the efficiency of its propeller depending on the flight speed.

Fig. 1. The AOS 71 motor glider

Table 1. Basic data of the AOS 71 motor glider) [8, 9]

Wing area	S [m^2]	15.8
Wing span	R [m]	16.4
Aspect ratio	Λ	17
Maximum take-off mass	M_{max} [kg]	660
Minimum motor glider mass	M_{min} [kg]	500

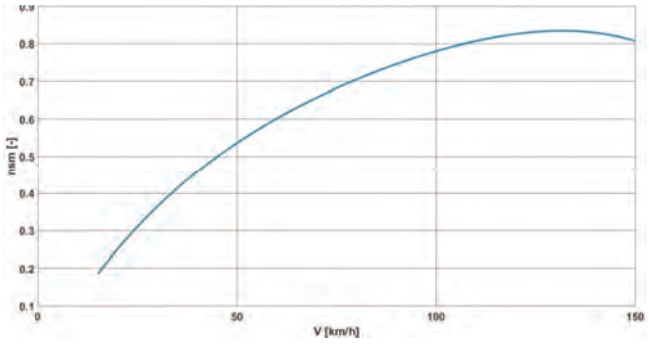

Fig. 2. Efficiency of propeller in the function of flight speed – for the AOS 71 motor glider [6, 7]

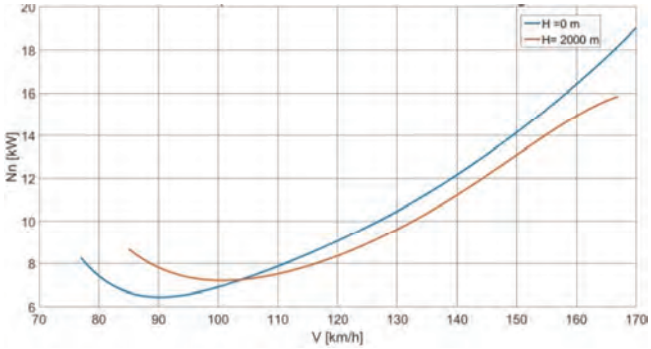

Fig. 3. Power required for flight in the function of flight speed – for the AOS 71 motor glider; M_{max} = 660 kg [6, 7]

For the combustion propulsion, the propeller was driven by a rotary piston 814 TGi. The second propulsion was a hybrid unit, where the batteries located on-board the motor glider deck were supported by an electric generator driven by a 407 TGi combustion engine. Technical data of power units is shown in Table 2.

Fig. 4 and 5 show the indicated rotational characteristics for both engines.

Table 3. Technical data of power unit [8, 9, 13]

Engine		407TGi	814 TGi
Maximum engine power	N_{max} [kW]	31.5	55
Maximum torque	M_{max} [Nm]	51	9
Engine mass	m_s [kg]	20	35
Specific fuel consumption	SFC_{min} [kg/kWh]	0.3	0.3
Battery	-	Li-Pol	-
Capacity	C [Ah]	16	-
Voltage	U_{bat} [V]	355	-
Battery mass	m_{bat} [kg]	50	-

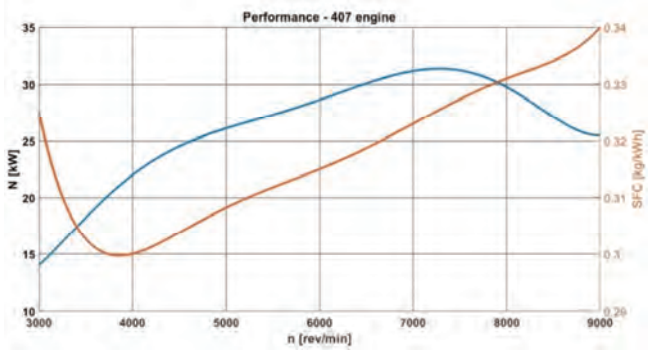

Fig. 4. Rotational characteristics of the 407 engine

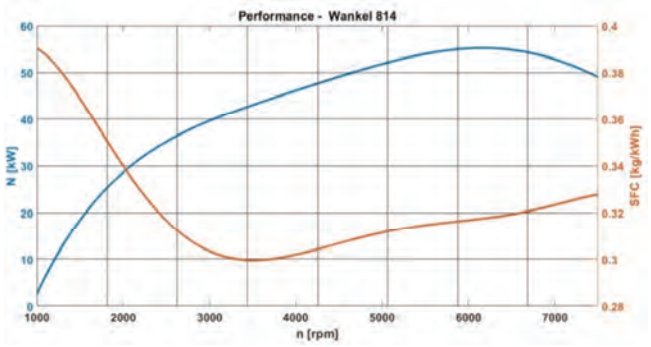

Fig. 5. Rotational characteristics of the 814 engine

2. Research selection of flight mission parameters for analysis

For the parameters of both propulsions were selected for the analysis in such a way that approximately 3 hours of flight duration and 300 km of range is ensured. It was assumed that these parameters will be obtained when the energy resources accumulated on-board the motor glider are completely exhausted. Based on the aerodynamic characteristics of the airframe (Figs 2 and 3) the power required for the flight for a horizontal speed of 100 km/h and a take-off mass of 660 kg was selected. For these parameters, the power required for flight (7 kW) of was determined. Based on the characteristics of the course of specific fuel consumption of the engines, the parameters of their operation were selected to ensure the desired range. As a result of the analysis conducted, the fuel reserve for reaching the range was determined – it was 10 kg for the combustion variant in and 7 kg for the hybrid one. The emission of toxic compounds on a given route depends on the amount of fuel burned and the range of operation of internal combustion engines during the flight. In the case of the 814 TGi engine, the operating parameters for the cruising conditions were 10 kW at revolutions similar the idle speed (1500 rpm). However, for the 407 TGi engine, which worked as an electric generator propulsion, it was 22 kW at the maximum torque value and engine revolutions of 4000 rpm. This range was covered at close to the minimum specific fuel consumption. It was assumed that the propulsions work continuously.

3. Research on emissions of harmful and toxic compounds

In piston engine exhausts there are emitted such compounds as carbon dioxide, carbon monoxide, nitrogen oxides and unburned hydrocarbons [4, 10, 12]. Emission depends on the engine design, the combustion temperature and the pressure in the cylinder. In the case of Wankel engines, which were taken into account in the analysis, a 1:80 oil-fuel mixture was used for feeding, in accordance with the manufacturer's requirements. The emission of harmful compounds was carried out in an experimental way, using Horiba exhaust gas analyser and the test bench for engines located in the Aviation Engine Laboratory of the Department of Aircraft and Aircraft Engines at Rzeszow Technical University.

Figures 6, 7 and 8 show test stands and devices on which engine exhausts measurements were made.

The measurement was made at the ambient temperature of 12°C.

The Horiba apparatus indicated the values of NO_x in [ppm/mol] with reference to the control volume, and CO and CO_2 as a percentage [%/vol] with reference to the control volume.

Based on the obtained measurement results, using Matlab software, the emission profile of pollutants in engine exhausts (CO_2, CO, NO_x) was determined in the function of rotational speed. The results of the tests are presented in Figures 9, 10 and 11.

Fig. 6. Test stand – measurement conducted for the 814 TGi engine

Fig. 7. Test stand – a panel used for reading engine operation parameters

Fig. 8. Test stand – Horiba apparatus display (after switching off the engine)

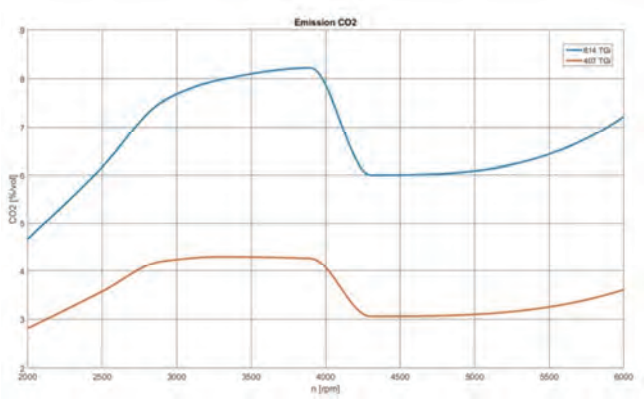

Fig. 9. The CO_2 emission profile for internal combustion engines in the function of rotational speed

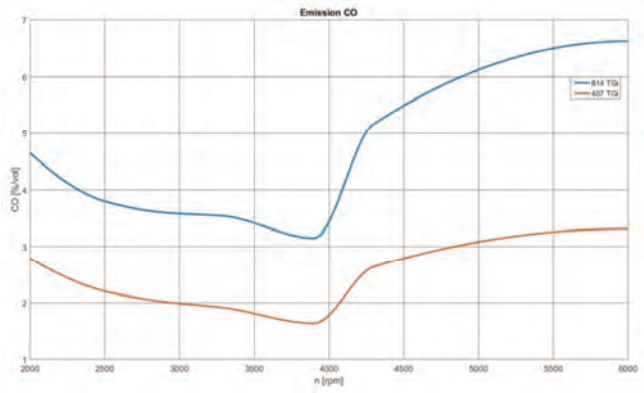

Fig. 10. The CO emission profile for internal combustion engines in the function of rotational speed

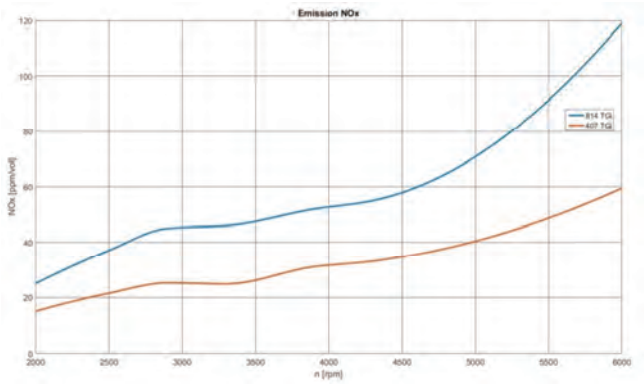

Fig. 11. The NO_x emission profile for internal combustion engines in the function of rotational speed

The analysis of the harts presented in the Figs 9–11, leads to the following conclusions:

1. The CO_2 and CO emissions were the lowest in the vicinity of the maximum torque obtained by the engines (about 4000 rpm), which at the same time was a point close to minimum of specific fuel consumption.
2. The NO_x emission grew continuously in the function of rotational speed, which was associated with the increase in the combustion temperature and the increase in fuel consumption by the engines.

For the assumed mission profile (i.e. start and flight at 600 m, as illustrated in Fig. 12), the emission of particular

compounds generated on a given route in the control volume was determined, assuming:

– the range until the energy source is depleted – about 300 km,
– the flight duration corresponding to the flight range – 3 hours of flight,
– the horizontal flight speed V = 100 km/h, the climb speed W = 2.3 m/s,
– the ambient conditions corresponding to the parameters according to the International Standard Atmosphere at a given altitude and the lack of wind.

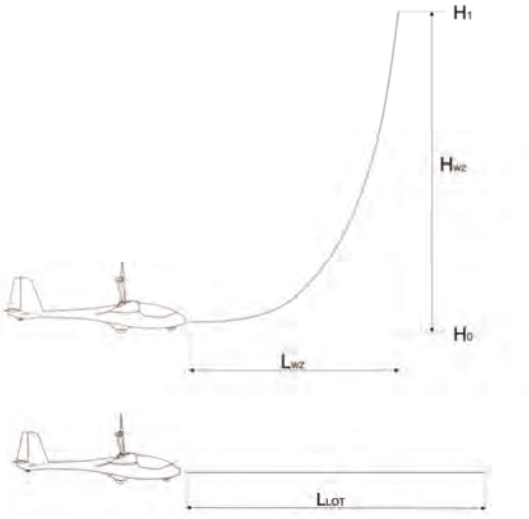

Fig. 12. Flight profile – climb (up) and horizontal flight (down)

4. The analysis results

In the first step, the energy accumulated on-board the motor glider was determined for both propulsions variants.

For the hybrid propulsion, the formula for determining accumulated energy takes the form [1, 11]:

$$E = I \cdot 3600[s] \cdot U_{bat} + \eta_{gen} \cdot (N_s \cdot t_s) \quad (1)$$

where t_s – generator operation time [1]:

$$t_s = \frac{m_{fuel}}{SFC \cdot N_s} \quad (2)$$

The energy generated by the combustion engine accounted for 70% of the energy accumulated on-board, the remaining 30% was accumulated in the battery assembly.

The energy accumulated on-board for the combustion variant is given with the formula [7]:

$$E = W_D \cdot m_{fuel} \quad (3)$$

where: W_D – fuel calorific value, equal to 42 MJ/kg, m_{fuel} – fuel mass, equal to 10 kg.

Figure 13 shows the energy accumulated on-board.

As mentioned, the energy accumulated on-board for both propulsions was selected in such a way that for the same take-off mass and the range of operation of combustion engines for the flight with the speed of 100 km/h, they provide the same range and duration of the flight.

As a result of the conducted analysis, the emission of harmful and toxic compounds was determined for a selected flight trajectory. The obtained data is presented in diagrams (Figs 14–17).

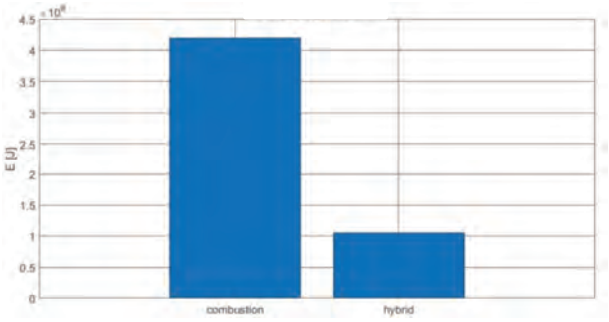

Fig. 13. The energy accumulated on-board

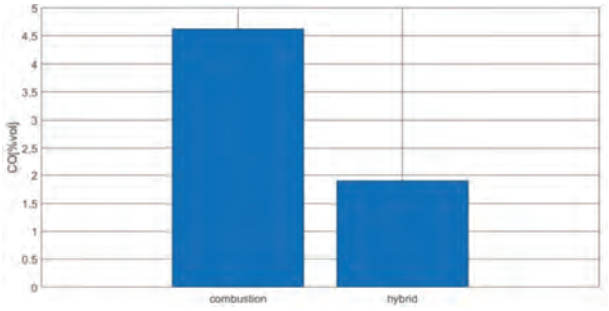

Fig. 14. The CO emission for propulsion units

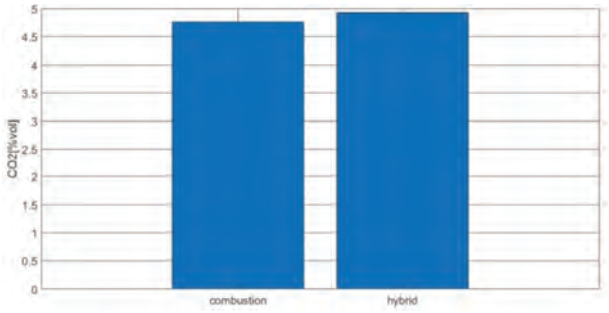

Fig. 15. The CO_2 emission for propulsion units

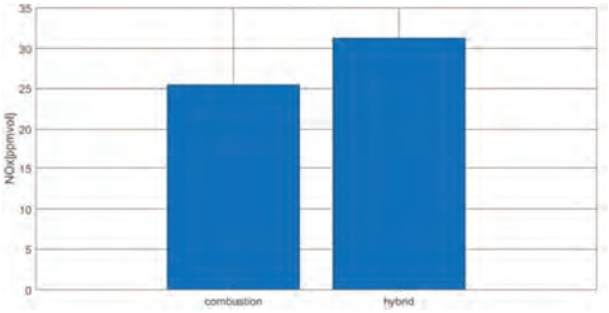

Fig. 16. The NO_x emission for propulsion units

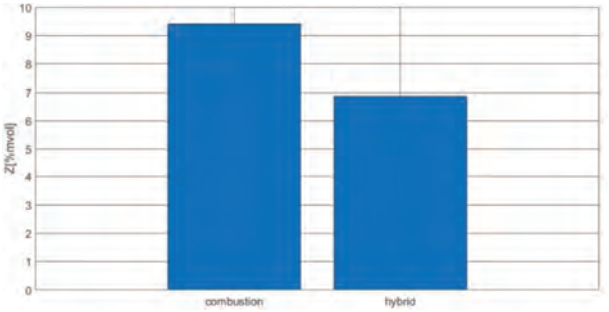

Fig. 17. The total emission for propulsion units

As can be noticed, the hybrid propulsion was characterized by the CO emission lower by almost 60% in comparison to the combustion engine – at the same level of power supplied to the propeller. The CO_2 and NO_x emissions were higher for hybrid propulsion by 3.7% and 22.5% respectively. It was related to the range of work of internal combustion engines. The 814 engine worked at small load, which resulted in low combustion temperature and high fuel consumption. This caused a situation favourable to the formation of excessive amounts of CO as an incomplete combustion product. In the case of the internal combustion engine driving the generator, it operated within its maximum torque, the load was relatively high (22 kW compared to the maximum power of 31.5), which resulted in more favourable exhaust-reheat in the combustion chamber (lower emission of CO, higher emission of CO_2). High NO_x emission was associated with a higher combustion temperature. The total emission of harmful and toxic compounds for the hybrid propulsion was lower by 27% compared to the internal combustion engine. It is worth noting that at the same distance and with the same take-off mass, the hybrid system used 7 kg of fuel in relation to 10 kg by traditional propulsion.

5. Conclusion

The obtained results show that the use of a properly selected and configured hybrid system can bring benefits in the form of a decrease in fuel consumption and total emissions during the flight on a given route. Appropriate matching of the generator operation range to the aerodynamic parameters and mass of the airframe will enable to get even more satisfactory results. Therefore, an interesting research perspective seems to be the optimization of such a propulsion in terms of minimizing fuel consumption while maintaining the same performance parameters of the aircraft (i.e. maintaining the flight duration and range at the same level). However, this requires a systematic approach to the construction of a hybrid propulsion. The tests were conducted on commercial engines. The optimization of the above tested conditions would be possible when the entire propulsion (combustion engine and electric) was designing as systems dedicated for this type of aircraft and the task performed. With unitary production of motor gliders this is uneconomical though. Therefore, attention should be paid to optimization of the selection of individual components in order to minimize emissions while maintaining energy requirements.

Acknowledgements

The research presented in this paper was financed as project PBS3/A6/24/2015 "AOS-H2" of the Applied Research Programme (PBS) of the National Centre for Research and Development (NCBIR), Poland, in the years 2015-19.

Bibliography

[1] ANDERSON, J. Introduction to flight. *McGraw Hill Book Company,* San Francisco 2003.
[2] BOJOI, R., BOGGERO, H. et al. Multiphase drives for hybrid-electric propulsion in light aircrafts: a viable solution. *2018 International Symposium on Power Electronics, Electrical Drives, Automation and Motion (SPEEDAM).* DOI: 10.1109/SPEEDAM.2018.8445241
[3] GEISS, I., VOIT-NITSCHMANN, R. Sizing of fuel-based energy systems for electric aircrafts. *Proceedings of the Institution of Mechanical Engineers Part G-Journal of Aerospace Engineering*. 2017, **231**. DOI: 10.1177/0954410017721254
[4] FAHIM, M. An overview of double-bar single-whee rotary combustion engine. *Advances in Mechanical Engineering*. 2019, **11**(2), 1-13. DOI: 10.1177/1687814019828074
[5] HENDERSON, R.P., MARTINS, J.R.R.A., PEREZ, R.E. Aircraft conceptual design for optimal environmental performance. *The Aeronautical Journal*. 2012, **116**(1175), 1-22.
[6] JAKUBOWSKI, R., ORKISZ, M. A review of selected alternative propulsion systems for UAV applications. *Zeszyty Naukowe/Wyższa Szkoła Oficerska Sił Powietrznych Dęblin.* 2015, **231**. DOI: 10.1177/0954410017721254
[7] KOTLARZ, W. Turbinowe zespoły napędowe źródłem skażeń powietrza na lotniskach wojskowych. *Wyższa Szkoła Oficerska Sił Powietrznych*. Dęblin 2003.
[8] MARIANOWSKI, J., FRĄCZEK, W., CZARNOCKI, F. Założenia podstawowe dla projektu motoszybowca AOS-H2. (not publish)
[9] MARIANOWSKI, J., TOMASIEWICZ, J., CZARNOCKI, F. Analiza masowa motoszybowca AOS-H2. (not publish)
[10] PAWLAK, M. Metoda modelowania emisji szkodliwych i toksycznych składników spalin turbinowych silników odrzutowych samolotów pasażerskich w warunkach przelotowych. Wyd. Uniwersytetu Morskiego. Gdynia 2019.
[11] ROSKAM, J. Airplane aerodynamics and performance. *DARcorporation.* Kansas 2016.
[12] SINGH, V. Perceptions of emission reduction potential in air transport: a structural equation modeling approach, *Environment Systems and Decisions*. 2016, **36**(4), 377-403.
[13] WANKEL AG, Wankel engine manual
[14] www.emrax.com

Prof. Marek Orkisz, DSc., DEng. – Faculty of Mechanical Engineering and Aeronautics, Rzeszow University of Technology.
e-mail: *mareko@prz.edu.pl*

Piotr Wygonik, DEng. – Faculty of Mechanical Engineering and Aeronautics, Rzeszow University of Technology.
e-mail: *piowyg@prz.edu.pl*

Michał Kuźniar, MEng. – Faculty of Mechanical Engineering and Aeronautics, Rzeszow University of Technology.
e-mail: *mkuzniar@prz.edu.pl*

Maciej Kalwara, MEng. – Faculty of Mechanical Engineering and Aeronautics, Rzeszow University of Technology.
e-mail: *kalmac@prz.edu.pl*

Article citation info:
WIRKOWSKI, P., MARKOWSKI, J. The influence of operating conditions of the marine gas turbine engine on the level of emission of pollutants contained in the exhaust. *Combustion Engines*. 2019, **178**(3), 218-223. DOI: 10.19206/CE-2019-338

Paweł WIRKOWSKI
Jarosław MARKOWSKI

CE-2019-338

The influence of operating conditions of the marine gas turbine engine on the level of emission of pollutants contained in the exhaust

Pollution emission tests from turbine engines used for the main propulsion of vessels require measurement of the concentration of harmful compounds in the exhaust and assessment of the exhaust gases mass generated by the engine. The concentration of harmful compounds can be determined in a direct way by measuring it in the stream of exhaust gases. However, due to the large output of exhaust gases, the mass of exhaust gases must be determined indirectly. To do this it is necessary to carry out a series of tests and analyzes that will enable parameterization of operating conditions. The obtained parameters and functional relations between them can be used to assess the mass of generated exhaust gases. The article presents analyzes related to the methodology for assessing the mass of exhaust gases generated by the main propulsion turbine engine of the vessel, and the manner of their use in the assessment of emission of harmful exhaust gases.

Key words: *gasturbine, ship, emission, pollution*

1. Introduction

The assessment of emissions of harmful compounds in the exhaust of turbine engines propulsion systems of vessels is associated with the activity in the field of determining the impact of various types of technical facilities on the human environment. Particular attention is paid to the conditions of exploitation of the objects and the resulting consequences. In the field of means of transport exploitation, power generation of the drive is of great importance in the aspect of the impact on the environment. The combustion engine is responsible for generating energy for the purpose of carrying out the function of destination of the majority of means of transport. It converts chemical energy contained in fuel into mechanical energy using the combustion process to generate heat required for the energy conversion process. The consequence of this is the formation of exhausts containing harmful compounds in their composition [5, 6, 9, 10, 12].

Turbine marine combustion engines, due to their properties, constitute only a few percent share in the entire population of marine combustion engines. Due to economic reasons (relatively high efficiency, low-quality fuel consumption), propulsive compression-ignition internal combustion engines are used in the majority of propulsion and marine power plants of vessels. For the most part, works related to environmental impact analysis of vessels, as well as development works carried out under various projects refer mainly to civil communication vessels, transport vessels and compression-ignition engines, which are used to drive them [2–4, 7, 8, 11]. However, so far only a few research have been taken to assess the emission of pollutants emitted in the exhaust of marine turbine engines with military application, regarding their specific operating conditions [1, 13, 14].

In connection with the above, tests were carried out related to the measurement of carbon dioxide, carbon monoxide, hydrocarbons and nitrogen oxides in the exhaust gas of turbine engines during the cruise of the FFG-7 ship. During the tests, the results of measurements of the concentration of harmful exhaust compounds were recorded while simultaneously recording the values of the operational parameters of the engines and the entire drive system. A comparative analysis of the recorded data was made, which made it possible to assign particular engine performance, propulsion system and ship a proper value of the concentration of harmful exhaust gas compounds. Knowing the concentration values of harmful compounds in relation to particular operational parameters of the objects, an analysis was carried out, from which functional dependences of ecological parameters were obtained in relation to the engine's operational parameters.

2. Research object

The research was carried out with the use of two LM 2500 marine turbine engines from FFG-7 frigate propulsion system (Fig. 1). LM 2500 engines are "milled" turbine combustion engines that are widely used on modern warships and civilian vessels (Fig. 2).

Fig. 1. FFG-7 class ship [16]

The basic structural elements of the engine are:

- 16-stage axial compressor with maximum pressure ratio of 18,
- an annular combustion chamber equipped with 32 injectors,
- 2-stage gas generator turbine with cooled blades,
- 6-stage power turbine.

An integral part in ship constructions is the intermediate shaft transmitting the torque of the drive turbine to the reduction gear.

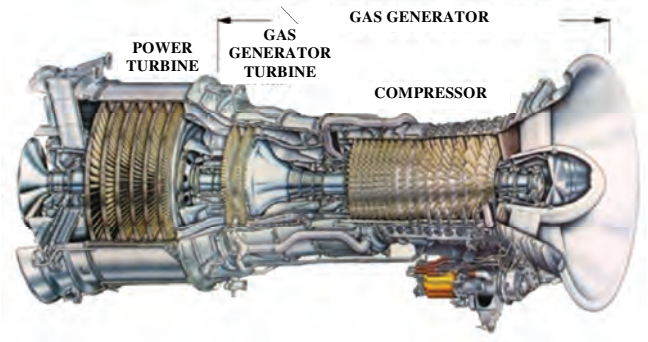

Fig. 2. LM 2500 gas turbine engine [17]

Measurements of the energy parameters of the medium, made in the characteristic control sections of the engine, are an important source of diagnostic information on the state of the constructional structure of its flow part. The presented schematic diagram of the LM 2500 engine (Fig. 3), with the control sections of the flow part marked, makes it possible to display the distribution of measuring points. Measured and determined engine operation parameters with their measuring range, expressed in units valid in the ship's engine room, are shown in Table 1.

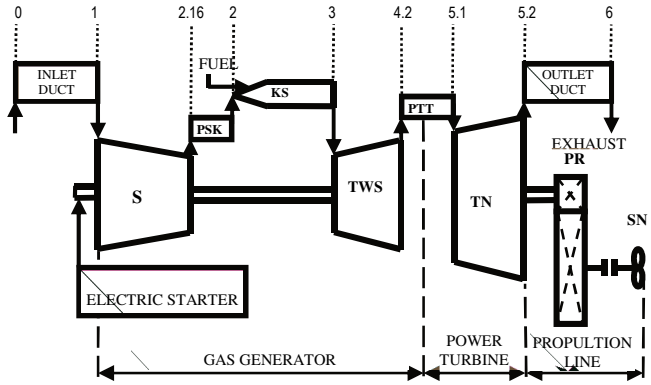

Fig. 3. Schematic diagram of LM 2500 gas turbine engine

The location of the turbine engine in the ship's engine room requires ensuring that its inlet is supplied with a proper stream of air mass and the outlet of gas generated from the exhaust system. For the Oliver Hazard Perry type frigate, equipped with two LM 2500 turbine engines, vertical air intake ducts and vertical exhaust gas channels (Fig. 4) with a length of about 15 m were designed. The air from the inlet channel is mainly directed to the engine inlet. A small part of the air from the intake duct, taken through the side duct, is led into the interior of the container engine body in order to ensure air exchange and proper temperature around the running engine. The air flowing around the external elements of the engine, located in the container housing, ultimately is directed to the outlet channel, where it mixes with the exhaust gases generated by the engine. Depending on the need to ensure proper parameters, the air flowing from outside the engine is properly prepared in terms of obtaining the required temperature using the cooling system and heaters, as well as the required flow speed inside the container housing, controlled with the use of fans. The Semtech-DS exhaust gas analyzer was used for measurements of exhaust components concentration in the exhaust gases, the characteristics of which are presented in Table 2.

Table. 1. Operating parameters LM 2500 engine

Name parameter, designation, unit	Measurment range
Barometric pressure p_o [hPa]	800–1040
Ambient temperature t_o [°C]	–40 – +40
The rotational speed of the gas generator shaft n_{GG} [rpm]	0–12000
The rotational speed of the power turbine shaft n_{PT} [rpm]	0–5000
The inlet air temperature to the engine t_1 [°F]	–40 – +150
The inlet air total pressure to the engine p^*_1 [psig]	0–16
Air pressure on the outlet compressor p_2 [psig]	0–300
The temperature of the exhaust stream before the power turbine $t_{4.2}$ [°F]	0–2000
Total pressure of the exhaust stream before the power turbine $p^*_{4.2}$ [psig]	0–75
Temperature exhaust gas T_6 [°F]	0–1000
The fuel temperature before engine T_f [°F]	0–100
Pressure fuel injectors before p_f [psig]	0–1500
Torque (calculated) on the power turbine shaft M_{PT} [LB FT]	0–50000
Power on the power turbine shaft P_{TN} [KM]	0–25000

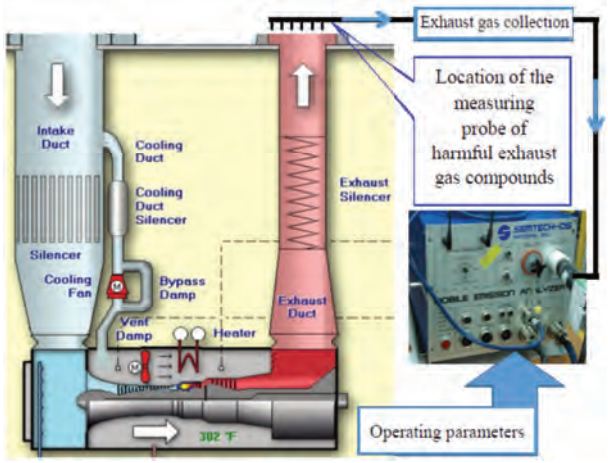

Fig. 4. The air intake system and the exhaust system of the LM 2500 engine installed on the missile frigate with marked sampling point and the Semtech-DS exhaust analyzer view

Table. 2. Characteristics of the Semtech-DS analyzer

Name parameter, designation, unit	Measurment range
The concentration of oxygen c_{O2} [%]	0–20
The concentration of carbon monoxide c_{CO} [%]	0–10
The concentration of hydrocarbons c_{HC} [ppm]	0–10 000
The concentration of nitrogen oxides c_{NOx} [ppm]	0–3 000
The concentration of carbon dioxide c_{CO2} [%]	0–20

3. Emission of harmful compounds from LM 2500 engines in operating conditions during the cruise

Measurements of concentrations of harmful compounds contained in the exhaust gas of the LM 2500 engine were carried out during the ship's departure to the sea. Two engines in the propulsion system of the unit were tested –

each engine was tested separately when only one engine in the drive system was running. The measurements were carried out for the range of engine load from idling to load that could be maximally achieved during tests, with the rotor speed of the flue gas generator (n_{GG}) assumed as the parameter setting the measurement points. This parameter was obtained by appropriate changes of the engine fuel supply stream (m_{pal}). The tests were carried out in such a way that in the first step the defined value of the rotational speed n_{GG} was set. After stabilization of the engine operation parameters, the selected drive system operating parameters (including the engine) were recorded and the parameters of the exhaust gases flowing out of the engine were recorded too. The working time with a predefined fixed engine load was 300 seconds. The measurement time of both the operating parameters of the drive system and exhaust parameters was 20 seconds with a recording frequency of 1 Hz.

Figures 5–8 presents the changes in the parameters of the exhaust gases of the tested LM 2500 1A and 1B engines as a function of the engine load factor expressed by the engine power ratio obtained at the test points to the maximum engine power:

$$W_o = \frac{P}{P_{max}} [-] \quad (1)$$

where: P_{max} – LM 2500 engine maximum power.

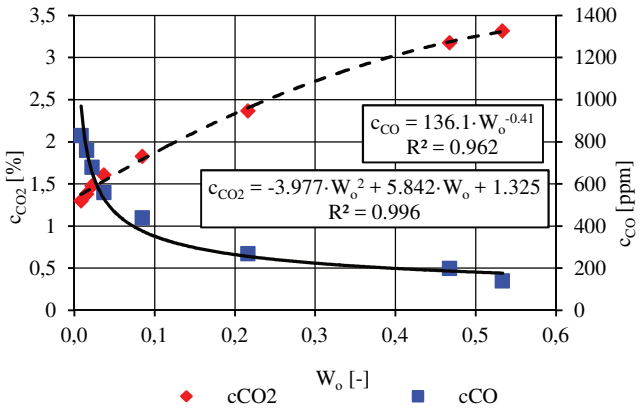

Fig. 5. The concentration of carbon monoxide (c_{CO}) and the concentration of carbon dioxide (c_{CO2}) in the LM 2500 1A engine exhaust as a function of the engine load factor (W_o)

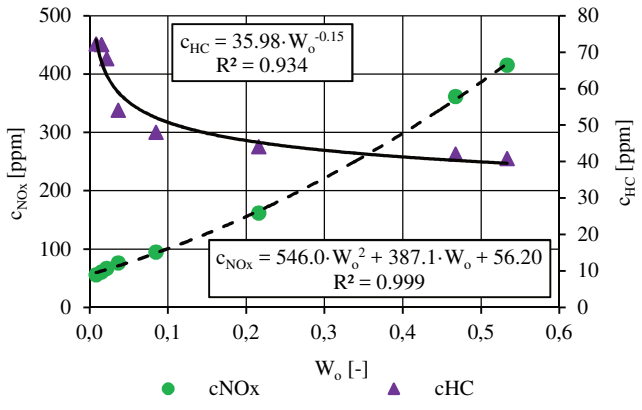

Fig. 6. Concentration of nitrogen oxides (c_{NOx}) and hydrocarbons concentration (c_{HC}) in the LM 2500 1A engine exhaust as a function of the engine load factor (W_o)

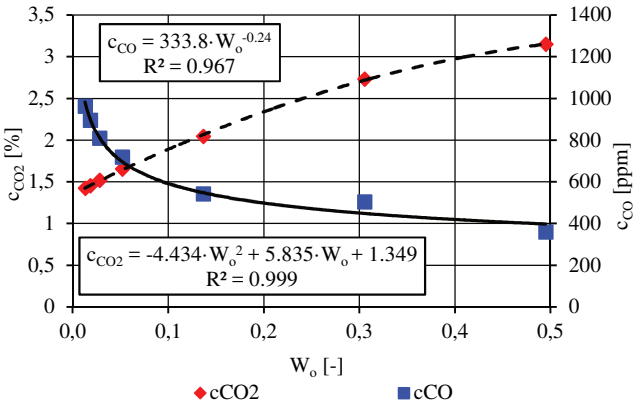

Fig. 7. The concentration of carbon monoxide (c_{CO}) and the concentration of carbon dioxide (c_{CO2}) in the LM 2500 1B engine exhaust as a function of the engine load factor (W_o)

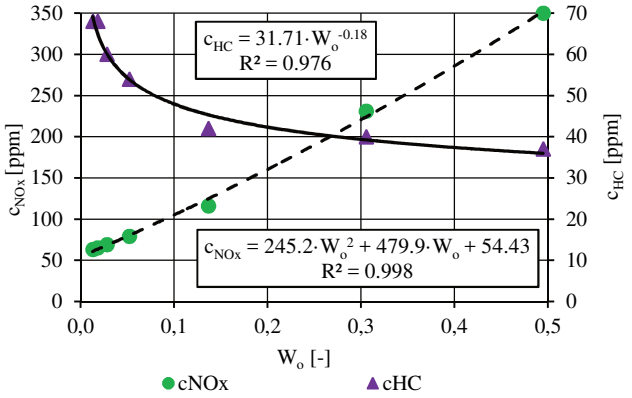

Fig. 8. Concentration of nitrogen oxides (c_{NOx}) and hydrocarbons concentration (c_{HC}) in the LM 2500 1B engine exhaust as a function of the engine load factor (W_o)

With the increase of the load factor of the LM 2500 1A engine from about 0.01 (engine idle load) to the value achieved during tests of about 0.53 (53% of the maximum engine power), the oxygen concentration in the exhaust gas decreases from about 18.3 % to about 15.3%. The excess air coefficient, which, as a rule, the turbine engine operation is characterized by significant values in comparison to other internal combustion engines, with the increase of the engine load factor in the above range decreases from about 10.5 to about 4.4. As the engine load increases, the concentration of carbon monoxide decreases from about 830 ppm to 140 ppm, while the concentration of carbon dioxide increases from about 1.3% to about 3.3%. The concentration of nitrogen oxides during this time increases from about 56 ppm to about 415 ppm, and the concentration of hydrocarbons decreases from about 72 ppm to about 40 ppm.

A similar character of changes in concentrations of registered exhaust components is found in the exhaust gas of the LM 2500 1B engine. With the increase of the engine load factor 1B from about 0.01 to the value achieved during tests of around 0.5 (50% of the maximum engine power), the oxygen concentration in the exhaust gas decreases from about 17.9% to about 15.6%. The excess air coefficient decreases from about 9.6 to about 4.6. As the engine load increases, the concentration of carbon monoxide decreases from about 960 ppm to 360 ppm, while the concentration of

carbon dioxide increases from about 1.4% to about 3.1%. The concentration of nitrogen oxides during this time increases from about 63 ppm to about 350 ppm, and the concentration of hydrocarbons decreases from about 68 ppm to about 37 ppm. Relatively small values of concentrations of particular compounds in the exhaust gases are associated with a large coefficient of excess air in the combustion chamber, which in the case of turbine engines results in a significant dilution of exhaust gases [15].

Using the functional relationships of changes in the concentration of harmful exhaust gas compounds in relation to the engine load factor (W_o), a functional dependence of the mass emission intensity of a given harmful compound ($\dot{E}_{i,j}$) of the tested engines can be proposed as a function of the engine load factor:

$$\dot{E}_{i,j}(W_o) = \dot{m}_{spal\,j}(W_o) \cdot g_{i,j}(W_o) \left[\frac{kg}{s}\right] \quad (2)$$

where: $\dot{m}_{spal\,j}(W_o)$ – exhaust mass stream [kg/s] as a function of the engine load factor for the j-th measurement, $g_{i,j}(W_o)$ – mass share [–] of the i-th exhaust component as a function of the engine load factor for the j-th measurement.

The values of mass emission intensity of the analyzed harmful compounds are presented in Figs 9 and 10.

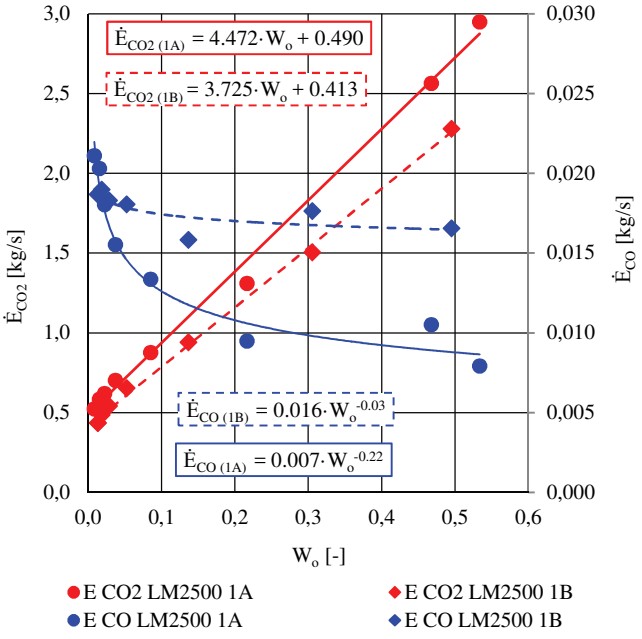

Fig. 9. The mass emission intensity of carbon dioxide ($\dot{E}_{CO2}$) and carbon monoxide ($\dot{E}_{CO}$) in the LM 2500 1A and LM 2500 1B engines exhaust as a function of the engine load factor (W_o)

The next step in the analysis of emissions of harmful exhaust compounds of LM 2500 engines was to determine the unit emission of individual compounds from the dependence:

$$e_{i,j}(W_o) = \frac{\dot{E}_{i,j}(W_o)}{W_{oj} \cdot P_{max}} \left[\frac{kg}{kW \cdot h}\right] \quad (3)$$

where: $\dot{E}_{i,j}(W_o)$ – mass emission intensity [kg/h] of the i-th exhaust component as a function of the engine load coefficient for the j-th measurement, W_{oj} – engine load factor [–] for the j-th measurement, P_{max} – the maximum power of the LM 2500 engine (24 608 kW).

The values of determined unit emissions of individual harmful compounds are presented in Figs 11 and 12.

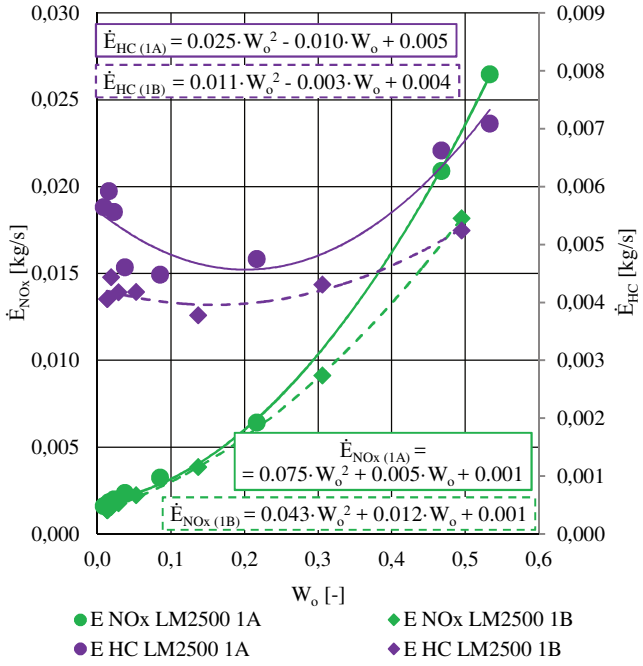

Fig. 10. The mass emission intensity of nitrogen oxides ($\dot{E}_{NOx}$) and hydrocarbons ($\dot{E}_{HC}$) in the LM 2500 1A and LM 2500 1B engines exhaust as a function of the engine load factor (W_o)

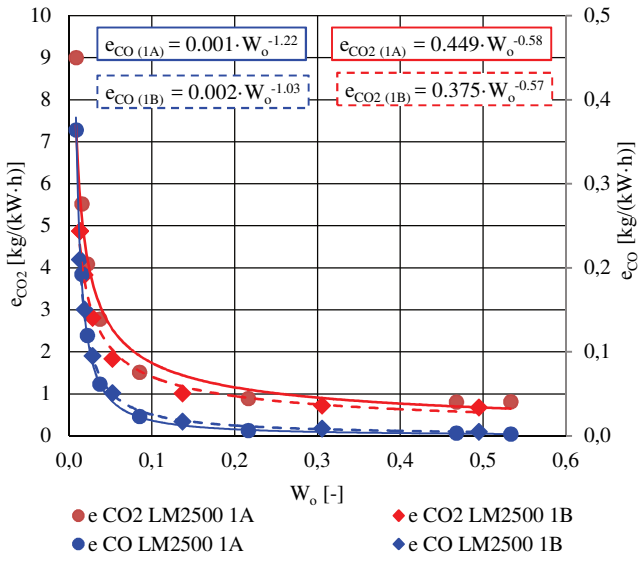

Fig. 11. The unit emission of carbon dioxide (e_{CO2}) and carbon monoxide (e_{CO}) in the LM 2500 1A and LM 2500 1B engines exhaust as a function of the engine load factor (W_o)

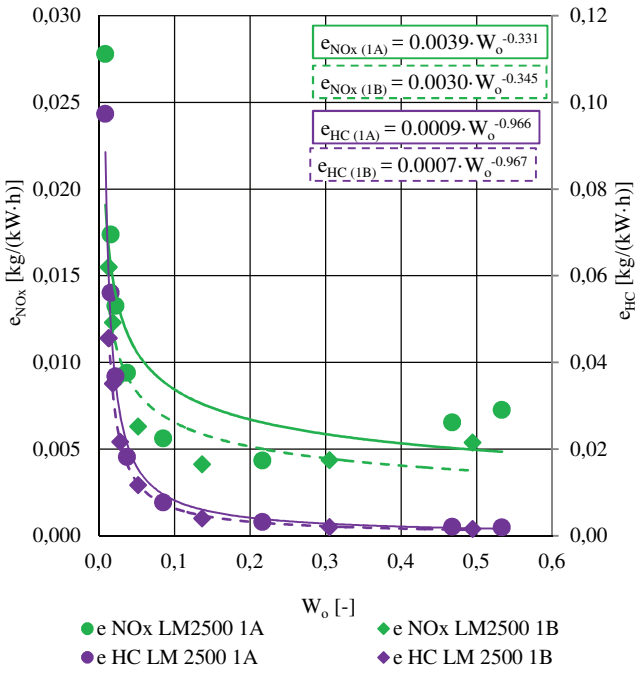

Fig. 12. The unit emission of nitrogen oxides (e_{NOx}) and hydrocarbons (e_{HC}) in the LM 2500 1A and LM 2500 1B engines exhaust as a function of the engine load factor (W_o)

4. Conclusions

On the basis of the conducted research, it can be concluded that the increase in the load on the ship's turbine engine causes a decrease in the concentration of carbon monoxide and an increase in the concentration of carbon dioxide in the exhaust. At the same time, the concentration of nitrogen oxides increases and the concentration of hydrocarbons decreases. The above results from the improvement of the conditions of the combustion process taking place in the combustion chamber of the engine.

Additionally, carried out research and the analysis of the actual working conditions of frigate ships indicate the similarity in the form of the time distribution of engine operation in engine load intervals occurring during the ship's tasks during the cruise. In order to determine the level of emission of harmful compounds contained in the exhaust gas generated by the turbine engines of the main propulsion vessel, an analysis of functional dependence of ecological parameters on the operating parameters were carried out.

The conducted analysis showed the possibility of obtaining mathematical functions describing relations between selected parameters. These functions can be used to assess the mass emission intensity and the unit emission of individual harmful compounds emitted while the engine is running at a given load.

Having the mathematical functions describing the mass emission intensity of the analyzed compounds of harmful exhaust gases of LM 2500 engines and knowing the engine operation time with a given load, there is a possibility to determine the mass of emitted harmful compounds during the operation of the engine with this load.

Nomenclature

c	concentration
CO	carbon monoxide
CO_2	carbon dioxide
e	unit emission
$\dot{E}$	mass emission intensity
FFG	rocket frigate
g	mass share
HC	hydrocarbons
KS	combustor
LM	Lockheed Martin
$\dot{m}$	mass stream
NO_x	nitrogen oxides
P	power
PR	reduction gear
PSK	space between S and KS
PTT	space between TWS and TN
S	compressor
SN	propeller
TN	power turbine
TWS	gas generator turbine
W_o	engine load factor

Indexes

GG	gas generator
i	number of exhaust component
j	number of measurement
max	maximum
pal, f	fuel
PT	power turbine
spal	exhaust

Bibliography

[1] AMMAR, N., FARAG, A. CFD modeling of syngas combustion and emissions for marine gas turbine applications. *Polish Maritime Research*. 2016, **23**, 39-49. DOI: 10.1515/pomr-2016-0030

[2] BIAGIOLI, F., GÜTHE, F. Effect of pressure and fuel–air unmixedness on NO_x emissions from industrial gas turbine burners. *Combustion and Flame*. 2007, **1511-2**, 274-288. DOI: 10.1016/j.combustflame.2007.04.007

[3] COOPER, A. Exhaust emissions from high speed passenger ferries. *Atmospheric Environment*. 2001, **35**, 4189-4200. DOI: 10.1016/S1352-2310(01)00192-3

[4] HERDZIK, J. Emissions from marine engines versus IMO certification and requirements of Tier 3. *Journal of KONES Powertrain and Transport*. 2011, **18**(2), 161-167.

[5] HUNICZ, J., KRZACZEK, P. Detailed speciation of emissions from low-temperature combustion in a gasoline

HCCI engine. *Polish Journal of Environmental Studies*. 2016, **25**, 137-145. DOI: 10.15244/pjoes/60082
[6] HUNICZ, J., MEDINA, A. Experimental study on detailed emissions speciation of an HCCI engine equipped with a three-way catalytic converter. *Energy*. 2016, **117**, 388-397. DOI: 10.1016/j.energy.2016.06.049
[7] KNIAZIEWICZ, T. Process modeling of ship emissions of internal combustion engines for main propulsion under real operating conditions. *Polish Naval Academy Press*. 2013, **193A**.
[8] KOMAR, I., BRANKO, L. Current air quality issues. *Sea Transport Air Pollution InTech Open Science*. 2015, 165-202. DOI: 10.5772/58743
[9] KOWALEWICZ, A. Fundamentals of combustion processes. *Publisher Scientific-Technical*. 2000.
[10] MARKOWSKI, J., OLEJNICZAK, D., WIRKOWSKI, P. Evaluation of turbine microjet engine operating parameters in conditions conducive to inlet freezing. *MATEC Web of Conferences*. 2017, **118**, 1-5, DOI: 10.1051/matecconf/ 201711800031
[11] MERKISZ, J., PIASECZNY, L., KNIAZIEWICZ, T. Issues emissions of marine engines. *Poznan University of Technology Press*. Poznan 2016.
[12] NOWACKI, M., OLEJNICZAK, D. Analysis of Boeing 737 MAX 8 flight in terms of the exhaust emission for selected flight. *Transportation Research Procedia*. 2018, **35**, 158-165. DOI: 10.1016/j.trpro.2018.12.033
[13] WIRKOWSKI, P., KNIAZIEWICZ, T. Evaluation of marine gas turbine engine parameters in terms of issue of emissions of exhaust toxic fumes. *Combustion Engines*. 2017, **171**(4), 87-91. DOI: 10.19206/CE-2017-415
[14] WIRKOWSKI, P., MARKOWSKI, J., KNIAZIEWICZ, T. Initial tests of emissions of harmful compounds in the exhaust of a marine gas turbine engine in operating conditions. *IOP Conference Series: Materials Science and Engineering*. 2018, **421**, 042079, 1-10. DOI: 10.1088/1757-899X/421/4/042079
[15] ZADRĄG, R., KNIAZIEWICZ, T. Ranking of toxic compound concentrations as diagnostic parameters of marine internal combustion engine. *Polish Maritime Research*. 2018, **25**, 234-242. DOI: 10.2478/pomr-2018-0047
[16] https://www.google.pl/search?q=fregata+273
[17] https://www.centerfieldinc.com/lm2500

Paweł Wirkowski, DEng. – Faculty of Mechanical and Electrical Engineering, Polish Naval Academy.
e-mail: *p.wirkowski@amw.gdynia.pl*

Jarosław Markowski, DSc., DEng. – Institute of Internal Combustion Engines and Transport, Poznan University of Technology.
e-mail: *jaroslaw.markowski@put.poznan.pl*

Article citation info:
BRZEZANSKI, M., RODAK, L. Influence of the method of creating a hydrogen-air mixture on the emission of nitrogen oxides in a spark-ignition engine. *Combustion Engines*. 2019, **178**(3), 224-227. DOI: 10.19206/CE-2019-339

Marek BRZEŻAŃSKI
Łukasz RODAK

CE-2019-339

Influence of the method of creating a hydrogen-air mixture on the emission of nitrogen oxides in a spark-ignition engine

The article presents an analysis of phenomena affecting the formation of nitrogen oxides during the combustion of a hydrogen-air mixture in a spark-ignition engine. Studies have been carried out to determine the strategy of creating and burning a hydrogen-air mixture that guarantees a low concentration of nitrogen oxides. This strategy limits the synthesis of nitrogen with atmospheric oxygen during engine operation.

Keywords: *NOx emission, hydrogen, combustion engine, direct injection*

1. Introduction

In the last few years, there has been a discussion about new energy carriers around the world, which in the near future may replace the liquid hydrocarbon fuels currently used to drive all types of vehicles. The problem is very complex, because new fuels should be competitive in every aspect, and additionally they cannot pollute the environment. The fuel that best meets these requirements is hydrogen, which is currently the focus of scientists and practitioners in the energy industry. Intensive works on the development of new sources of vehicle propulsion are also underway. The first results of these works indicate that, ultimately, the basic source of vehicle drive can be a hydrogen-fueled fuel cell, competitive in relation to piston combustion engines. However, at the current development stage, hydrogen-powered fuel cells are still too expensive to produce and troublesome in operation. Therefore, during the transitional period, hydrogen can be successfully used as a fuel for modernly produced piston combustion engines. This will allow, among other things, for the development of a network of filling vehicles with hydrogen, as well as the habituation of users to a new type of fuel.

2. Emission of toxic exhaust components of hydrogen-powered engines

Theoretically, the only product of hydrogen combustion in a reciprocating engine should be water. However, there are small amounts of carbon monoxide and hydrocarbons as well as nitrogen oxides in the exhaust. The first two components come mainly from the lubricating oil of the piston ring seals and the intake valve guides. The concentration of these two components is so small that they can be neglected. A more complex problem is the formation of nitrogen oxides, which strongly depends on the temperature of the combustion process and the availability of oxygen.

In currently used hydrogen fuel systems for internal combustion engines, hydrogen is supplied in a gaseous form by dosing to the inlet channel or directly to the cylinder.

The most common method of feeding piston engines with gaseous fuels is currently the method of creating a combustible mixture in the inlet channel of the engine. In this method, it is possible to obtain a sufficiently homogeneous composition of the mixture, which is conducive to achieving high repeatability of ignitions, while feeding the engines with a lean mixture. This is the preferred feature when supplying the engines with a hydrogen-air mixture, which has a wide range of flammability and allows the use of qualitative power control. It should be emphasized that the formation of a hydrogen-air mixture with a stoichiometric composition in the inlet channel increases the probability of self-ignition. This type of phenomenon can, for example, occur in the event of uncontrolled flame retreat from the combustion chamber during the co-operation of inlet and outlet valves.

The supply of hydrogen to the inlet channel is usually carried out via a mixer or a metering valve, mechanically or electrically controlled. This way of feeding the motor causes a low density of energy supplied to the cylinder. This is due to the high volume fraction of hydrogen in the mixture, relative to the mixture formed with liquid fuels. The stoichiometric constant for hydrogen is 2.38 [Nm^3/Nm^3], from which it follows that in the stoichiometric mixture the volume of hydrogen is about 30% of the volume of the total charge delivered to the cylinder. This results in a significant reduction in the unit power of the hydrogen-powered engine compared to the supply of hydrocarbon fuels. The mixture formed in the inlet channel heats up from the valves and from the cylinder walls during the filling process, then compression and is subject to a strong swirl. These phenomena lead to an increase in the internal and kinetic energy of the hydrogen-air mixture, which promotes the intensification of pre-ignition reactions in the load. This results in increased combustion speed and can also lead to uncontrolled self-ignition. All these phenomena are conducive to the reaction of nitrogen and oxygen synthesis, both in the global and local dimensions, increasing the concentration of nitrogen oxides in the exhaust gas in the entire engine operating range.

Hydrogen injection systems are also directly applied to the combustion chamber just after the completion of the filling process. This method of feeding motors with hydrogen shows an analogy to the direct injection of liquid hydrocarbon fuels. This is accomplished by a mechanically or electrically controlled valve. Hydrogen is supplied to the injectors at a pressure of 5–10 MPa. Such a large amount of fuel pressure before the injector results from the necessity of delivering the right dose of hydrogen in a short time, and also because the hydrogen injection takes place at variable

pressure in the engine working space. The direct injection of hydrogen into the cylinder also increases the weight of the load in the working space, which results in a significant increase in the unit power of the engine. In addition, this method of delivering hydrogen to the cylinder effectively eliminates the problems of hydrogen self-ignition in the intake channels and reduces the problems of the combustion process anomalies. The problem, however, is the course of the combustion process of the hydrogen-air mixture in the working space of the reciprocating internal combustion engine, because there is usually too rapid release of heat leading to knocking combustion. When the engine is powered with a hydrogen-air mixture with a stoichiometric composition, the self-ignition phenomenon may occur before the flame is initiated from the electric discharge. In both cases, this leads to an increased concentration of nitrogen oxides in the exhaust gas, due to the high temperature of the combustion process.

3. The purpose and scope of research

The aim of the conducted research was to create a new method of hydrogen supply of piston combustion engines, enabling control of heat release in the combustion process. The expected results of this work should guarantee both favorable engines operating parameters and low emission of nitrogen oxides. Such a power system, in which the main dose of hydrogen is supplied directly to the working space of the engine during the combustion process, was developed at the Cracow University of Technology. This concept predicts that in the initial phase of the process, during the filling process, a lean mixture will be created with a composition that allows it to be ignited from the electric discharge on the spark plug. The composition of the mixture should be selected so that the engine can work in the entire speed range without load, overcoming only internal resistance. The main role of this part of the fuel dose is only to initiate the combustion process, while the remaining part of the dose is delivered during the main process. This new hydrogen and air mixture creation and combustion system make it possible to control the combustion rate of the mixture, thanks to which it is possible to avoid problems associated with self-ignition of the mixture or combustion anomalies. In addition, it allows predicting the conditions of the combustion process in which there is the greatest tendency for the synthesis of nitrogen and oxygen.

4. Test bench and research methodology

The tests were carried out on a modified Kipor 186F engine (Single-cylinder, displacement 0.406 dm^3) adapted for spark ignition and injection hydrogen supply. To this end, compression ratio increment from $\varepsilon = 19.3$ to $\varepsilon = 15.1$, an additional hole for screwing in the spark plug was made in the head and a hole for screwing the sensor to be used. A new combustion system was developed, with the Heron chamber located in the piston, providing a strong swirled load in the compression process. The engine has been additionally equipped with a throttle, broadband lambda probe, sensors measuring the intake air temperature and flue gas temperatures. The scope of structural changes of the cylinder head and piston are shown in Fig. 1.

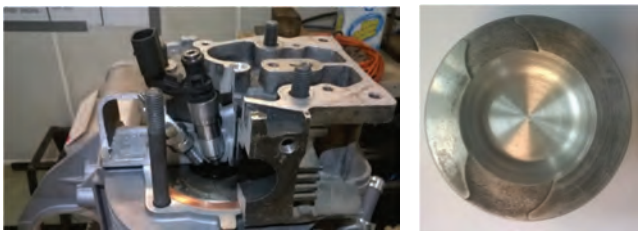

Fig. 1. Structural changes of the cylinder head and combustion chamber in the piston adapted for spark ignition and direct hydrogen injection

Exhaust gas probes are located in the exhaust system. Engine control parameters: the timing of ignition, time and the angle of injection start, throttle opening, was managed by a computer program written in the LabView environment. The engine cooperated with the Schenk type W 70 eddy current brake on the test stand. In addition to engine operating parameters, such as speed, torque value and fuel consumption. The current measurement of the concentration of basic exhaust components such as carbon dioxide CO_2, oxygen O_2, hydrocarbons HC, carbon monoxide CO and nitrogen oxides NO_x was also carried out. At each measuring point, the current value of cylinder pressure was measured using a piezoelectric sensor placed in the combustion chamber. After integrating the pressure values obtained, it was possible to obtain the current values of the pressure increase in the cylinder, useful for analyzing the emission of nitrogen oxides. The adopted test methodology provided for measurements at a constant rotational speed n = 2500 1/min and a constant angle of throttle opening, corresponding to 25% of the full engine load. The dose of fuel supplied was changed to obtain the required value of the excess air factor λ. The beginning of the hydrogen injection into the cylinder was always in the compression phase, and the angle of fuel injection start was selected so that for the determined composition of the mixture, the maximum torque value or the lowest NOx concentration in the exhaust gas can be obtained. In both cases, there was no admission of anomalies in the hydrogen-air mixture combustion process, which was controlled on an ongoing basis based on the analysis of indicator diagrams (Fig. 2).

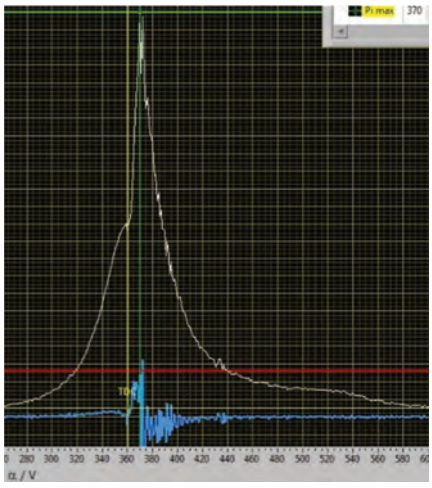

Fig. 2. An exemplary indicator diagram of the engine fed with the hydrogen-air mixture together with the analysis of pressure increments dp/pα index and the calculation of the average pressure of the indicated p_i

5. Results of measurements

A summary chart showing the concentration of nitrogen oxides at selected points of the engine operation is shown in Fig. 3. The engine speed was constant and amounted to n = 2500 1 / min. Measurements of the concentration of nitrogen oxides were carried out while supplying the engine with a hydrogen-air mixture with the following composition: λ = 2.03, λ = 1.55 and λ = 1.05. The given values of the excess air coefficient were obtained by changing the time of hydrogen injection into the cylinder, while the injection took place during the compression process and the combustion process. The ignition advance angle was constant and was 1° C.A. before TDC, because preliminary tests showed that when feeding the engine with hydrogen, changing the ignition timing angle has too rapid impact on the course of the combustion process, preventing the proper regulation of the engine. In connection with the above, the hydrogen injection strategy was chosen as the control parameter of the engine supplied with the hydrogen / air mixture, by implementing it by changing the start and the injection time. In each of the selected engine work points, such adjustment of the start of hydrogen injection into the cylinder was made to obtain the highest value of torque or the lowest value of the concentration of nitrogen oxides.

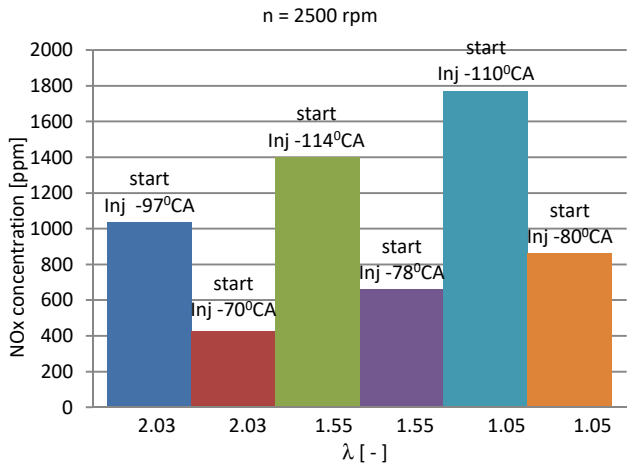

Fig. 3 The concentration of nitrogen oxides at selected engine work points, respectively when working with maximum torque or the minimum concentration of nitrogen oxides

A full analysis of the obtained test results was possible along with the analysis of the hydrogen injection process, including the determination of the start point and the end point of the injection and the analysis of the pressure change graphs in the engine combustion chamber.

Figure 4 shows the operation of the engine when feeding a mixture with an excess air ratio of λ = 2.03. When working with maximum torque, the start of the hydrogen injection was 97°C.A. before TDC, the end of injection 1° C.A. before TDC. In this case, the entire hydrogen dose was injected only in the compression process, before the ignition occurred on the spark plug electrodes. The pressure in the cylinder reached a value of approx. 4 MPa, and the dp/dα index was 0.44 MPa/°C.A. When working with a minimum NO_x concentration, the start of the hydrogen injection was 70°C.A. before TDC, the end of injection 26° C.A. after TDC. The pressure was 3.2 MPa and the dp/dα index was 0.42 MPa/°C.A.

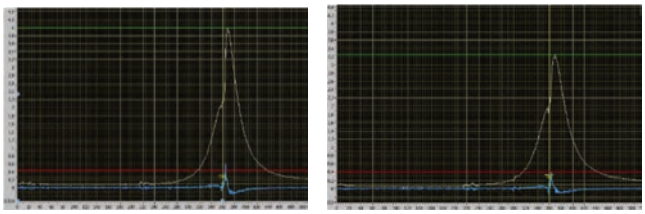

Fig. 4. The course of pressure changes p and dp/dα index during operation with maximum torque (left) and during operation with the minimum concentration of nitrogen oxides (right), λ = 2.03

Figure 5 shows the operation of the engine when feeding a mixture with an excess air ratio of 1.55. When operating at maximum torque, the hydrogen injection start was 114°C.A. before TDC, 6°C.A. injection end after TDC. Cylinder pressure reached a value of 4.23 MPa, and the dp/dα index was 0.57 MPa/°C.A. When working with a minimum NO_x concentration, the start of hydrogen injection was 78°C.A. before TDC, the end of injection 53°C.A. after TDC. The pressure was 3.55 MPa and the dp/dα index was 0.35 MPa/°C.A.

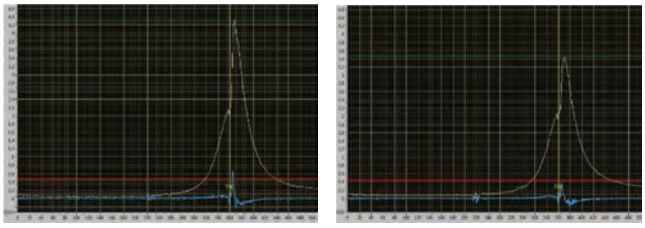

Fig. 5. The course of pressure changes p and dp/dα index during operation with the maximum torque (left) and during operation with the minimum concentration of nitrogen oxides (right), λ = 1.55

Figure 6 shows the operation of the engine while feeding the mixture with an excess air ratio of λ =1.05. When operating at maximum torque, the hydrogen injection start was 110°C.A. before TDC, end of injection 67°C.A. after TDC. Cylinder pressure reached a value of 4.2 MPa, and the dp/dα index was 0.61 MPa/°C.A. In this case, more than 30% of the injected hydrogen was fed into the cylinder during the combustion process. When working with a minimum NO_x concentration the start of the hydrogen injection was 80°C.A. before TDC, the end of injection 97°C.A. after TDC, from which it follows that most of the injected hydrogen was fed to the cylinder during the combustion process. The pressure was 3.47 MPa and the dp/dα index was 0.44MPa/°C.A.

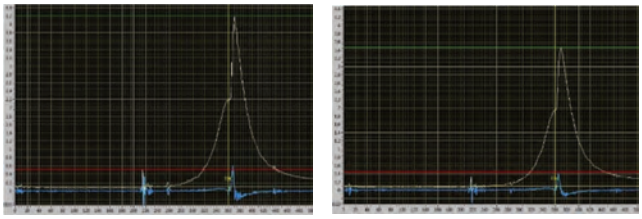

Fig. 6. The course of pressure changes p and dp/dα index during operation with maximum torque (left) and during operation with the minimum concentration of nitrogen oxides (right), λ = 1.05

6. Conclusions

Preliminary studies of the developed strategy of hydrogen injection into the combustion chamber allows the conclusion that are extremely important from the point of view of the use of hydrogen as a fuel for piston combustion engines. The tests have shown that the use of an appropriate injection strategy allows control of the combustion process. In contrast to the hydrogen power systems used so far, this method allows the combustion of a mixture with a stoichiometric composition, without the occurrence of anomalies of combustion or uncontrolled self-ignition. There is also the possibility of controlling the heat release rate and controlling the momentary value of pressure increase in the cylinder. Research has shown that this engine parameter has a significant impact on the quality of the combustion process and the emission of nitrogen oxides. The mentioned properties of the developed power system allow not only to avoid the occurrence of knocking but also to full control of the emission of nitrogen oxides. A good determinant used to evaluate the combustion process and the propensity to form oxides of nitrogen is the average value of the pressure increase. Tests conducted in a wide range of hydrogen-air mixture composition (λ = 2.03–1.05) have shown that the greater pressure on the formation of nitrogen oxides has a temporary increase in pressure in the cylinder, and thus increase the temperature, than the oxygen availability in the mixture.

A strategy for injection of piston engines with hydrogen developed in the Cracow University of Technology which, depending on the engine's operating point, provides for hydrogen injection only during the compression process or during the compression and subsequent combustion process, can significantly affect the operating parameters obtained and the emission of nitrogen oxides throughout the working field engine and may be the basis for its regulation.

Bibliography

[1] BRZEŻAŃSKI, M, CISEK, J., MAREK, W., PAPUGA, T. Investigation of the combustion engine fuelled with hydrogen. *V Congress on Combustion Engines*. PTNSS- 2013-SC-192, Bielsko Biała 2013.

[2] BRZEŻAŃSKI, M, CISEK, J., MAREK, W. et al. Investigation of the combustion engine fueled with hydrogen and mixed n-butanol with iso-butanol. *V Congress on Combustion Engines*. PTNSS- 2013-SC-194, Bielsko Biała 2013.

[3] BRZEŻAŃSKI, M., MAREK, W., MARECZEK, M., PAPUGA, T. Determination of ecological parameters of a stationary internal combustion engine powered by various fuels. *Zeszyty Naukowe Instytutu Pojazdów. Warsaw University of Technology*. 2014, **1**(97).

[4] BRZEŻAŃSKI, M., MARECZEK, M., MAREK, W., PAPUGA, T. Determination of operating parameters of industrial engine fuelled with post processing gases with high hydrogen content. *IOP Conference Series: Scientific Conference on Automotive Vehicles and Combustion Engines*. 2016.

[5] BRZEŻAŃSKI, M., PAPUGA, T., RODAK, Ł. Analysis of creation and combustion process of hydrogen-air mixtures by optical method in isochoric chamber. *Combustion Engines*. 2017, **170**(3).

Marek Brzezanski, DSc., DEng. – Faculty of Mechanical Engineering, Cracow University of Technology.
e-mail: *mbrzez@pk.edu.pl*

Łukasz Rodak, MEng. – Faculty of Mechanical Engineering, Cracow University of Technology.
e-mail*: lrodak@pk.edu.pl*

Article citation info:
GIS, W., GIS, M., WIŚNIOWSKI, P., BEDNARSKI, M. Comparative tests of a passenger car with compression ignition engine on chassis dynamometer during NEDC and WLTC tests and during RDE road test. *Combustion Engines*. 2019, **178**(3), 228-234. DOI: 10.19206/CE-2019-340

Wojciech GIS
Maciej GIS
Piotr WIŚNIOWSKI
Mateusz BEDNARSKI

CE-2019-340

Comparative tests of a passenger car with compression ignition engine on chassis dynamometer during NEDC and WLTC tests and during RDE road test

Air pollution is a challenge for municipal authorities. Increased emission of PM10 and PM 2.5 particles is particularly noticeable in Poland primarily the autumn and winter period. That is due to the start of the heating season. According to the above data, road transport accounted for approximately 5% of the creation of PM_{10} particles, ca. 7% of $PM_{2.5}$ and approximately 32% for NO_x. In Poland, suspended particles (PM_{10} and $PM_{2.5}$) cause deaths of as many as 45,000 people a year. The issue of smog also affects other European cities. Therefore, it is necessary to undertake concrete efforts in order to reduce vehicle exhaust emissions as much as possible. It is therefore justifiable to reduce the emission of exhaust pollution, particularly NO_x, PM, PN by conventional passenger cars powered by compression ignition engines. Emissions by these passenger cars have been reduced systematically. Comparative tests of the above emission of exhaust pollution were conducted on chassis dynamometer of such passenger car in NEDC cycle and in the new WLTC cycle in order to verify the level of emissions from this type of passenger car. Measurements of fuel consumption by that car were also taken. Emission of exhaust pollution and fuel consumption of the this car were also taken in the RDE road test.

Key words: *emissions, pollutant emissions, particle matters, NEDC, WLTP, RDE*

1. Introduction

Air pollution is a challenge for municipal authorities. Increased emission of PM_{10} and $PM_{2.5}$ particles is particularly noticeable in Poland in the autumn and winter period. That is due to the start of the heating season.

According to KOBIZE (The National Centre for Emission Management) data [14], in 2016 the main sources of PM_{10}, $PM_{2.5}$, and PAH (Polycyclic Aromatic Hydrocarbons) emissions were non-industrial combustion processes (45%, 48% and 88% respectively of the total amount of emissions of such substances, estimated at 259,156.3 Mg, 145,506.9 Mg and 146.3 Mg), the predominant share of which came from the combustion of solid fuels by households. In turn, in the case of nitric oxides (NO_x), the industrial sector was the biggest source of emissions (38% of the total amount of emissions of these substances, estimated at 726,431.2 Mg) and road transport (32%). Lack of enough airflow causes the above dust and others to stay suspended above the city, as a result creating smog [1].

According to the above data, road transport accounted for approximately 5% of the creation of PM_{10} particles, ca. 7% of $PM_{2.5}$ and approximately 32% for NO_x. In Poland, suspended particles (PM_{10} and $PM_{2.5}$) cause deaths of as many as 45,000 people a year. The issue of smog also affects other European cities. Therefore, it is necessary to undertake concrete efforts in order to reduce vehicle exhaust emissions as much as possible [2].

In the case of efforts in road transportation sector, several solutions are possible. One is to utilize vehicles with alternative propulsion systems (electric vehicles, vehicles equipped with fuel cells). The use of hybrid vehicles would be justifiable in the meantime. Nonetheless, in 2016 for example, alternative fuel vehicles and those with alternative propulsions accounted for a tiny minority (0.03%) of the vehicles registered.

It is therefore justifiable to reduce the emission of exhaust pollution, particularly NO_X, PM, PN by conventional passenger cars powered by compression ignition engines. Emissions by these passenger cars have been reduced systematically and are tested in laboratory tests (NEDC and WLTP (WLTC)) and also in RDE road cycles [3–9].

2. Methodology

2.1. Test equipment

For the purpose of studies on exhaust emissions in NEDC and WLTP tests the equipment of the Centre for Environmental Protection of the Motor Transport Institute was used. For the purpose of the tests there were used:

- gaseous emissions sampling and analysis system by AVL; during test was used configuration „03 Diluted Bag Particle Diesel" consisting of:
- CFV-CVS exhaust gas sampling system type CVS i60 LD S2 by AVL,
- set of AMA i60 D1-CD LE analysers by AVL equipped with two-range analysers to measure the concentrations of the following gases:
  - carbon dioxide CO_2,
  - nitrogen oxides NO_X,
  - carbon monoxide CO,
  - total sum of hydrocarbons THC,
  - methane CH_4,
- particulate sampling system PSS i60 SD by AVL,
- particle counter AVL489 APC ADVANCED by AVL,
- microbalance MT5 by Mettler Toledo,
- M type thermo-hygro-barometer type LB-701, with a read-out LB-702B display by LABEL,
- Electronic scales PBD655-B120 by Mettler Toledo Company.

For RDE tests mobile analysers were used to measure hazardous RDEs – i.e. Engine Particle Sizer Model 3090 and mobile analyser of exhaust emissions SEMTECH DS

(Fig. 1) of US Sensors Inc. [10]. An exhaust emission sample is taken by a mass exhaust emissions concentration probing device and delivered to the system through a heated path maintaining temperature of 191°C. Exhaust are filtered to remove particle matter (in case of self-ignition engines) and the concentration of hydrocarbons is measured in the Flame Ionization Detector (FID). Next, the sample is cooled to 4°C and Non-dispersion Detector Ultra Violet analyser (NDUV) the concentrations of nitrogen oxide and nitrogen dioxide are measured, while the Non-dispersion Detector Infra-Red (NDIR) measures the concentration of CO and CO_2. The measurement of oxygen is made through an electro-mechanical sensor. The device allows for recording the parameters read from the vehicle's diagnostic system and the geographical location via a GPS module (Table 1) [11].

Table 1. Characteristics of SEMTECH DS mobile exhaust emissions analyser [11]

Parameter	Test method	Accuracy
1. Concentration of CO	NDIR – non-dispersive (infrared), range 0–10%	±3%
THC	FID – flame ionisation, range 0–10,000 ppm	±2.5%
$NO_x = (NO+NO_2)$	NDUV – non-dispersive (ultraviolet), range 0–3000 ppm	±3%
CO_2	NDIR – non-dispersive (infrared), range 0–20%	±3%
O_2	Electrochemical, range 0–20%	±1%
2. Exhaust emissions flow	Mass flow intensity T_{max} do 700°C	±2.5% ±1%
3. Heating time	15 min	-
4. Response time	$T_{90} < 1$ s	-
5. Diagnostic systems operated	SAE J1850/SAE J1979 (LDV) SAE J1708/SAE J1587 (HDV) CAN SAE J1939/J2284 (HDV)	-

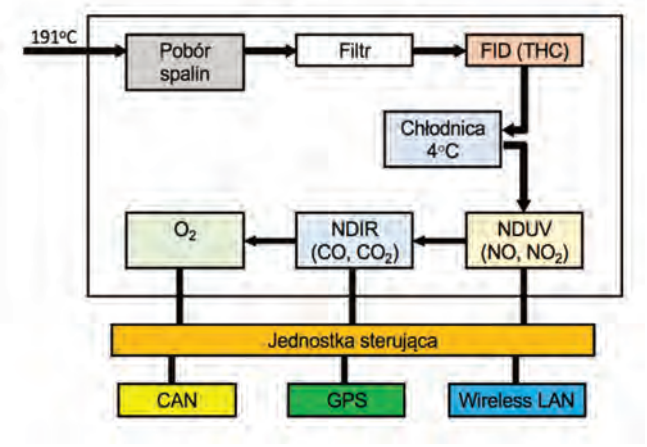

Fig. 1. Operating chart of SEMTECH DS analyser [11]

2.2. Test cycles – NEDC, WLTP

NEDC – The UDC+EUDC test cycle was used to test emissions and fuel consumption of light duty vehicles under EU type-approval [3]. The test is carried out on a chassis dynamometer. The entire cycle includes four ECE segments repeated non-stop, followed by one EUDC segment. Before the test, the vehicle must remain for at least 6 hours at a test temperature of 20–30ºC. Since 2000, the idle period has been eliminated, i.e. the engine starts in 0 s and sampling begins at the same time. This modified cold start procedure is referred to as the New European Driving Cycle (NEDC) [3].

The Extra Urban Driving Cycle (EUDC) segment was added after the fourth ECE cycle to account for more aggressive high-speed driving modes. The maximum EUDC cycle speed is 120 km/h. An alternative EUDC cycle was also determined for vehicles with low energy consumption, with a maximum speed limited to 90 km/h [3].

Emissions are collected during the cycle in accordance with the Constant Volume Sampling technique (CVS), analysed and expressed in g/km for each pollutant. Table 2 summarizes selected parameters for ECE 15, EUDC and NEDC cycles [3].

Table 2. Characteristics of UDC, EUDC and NEDC test [3]

Characteristics	Unit	UDC	EUDC	NEDC[b]
Distance	km	0.9941	6.9549	10.9314
Total time	s	195	400	1180
Idle time	s	57	39	267
Average speed (incl. stops)	km/h	18.35	62.59	33.35
Average driving speed (excl. stops)	km/h	25.93	69.36	43.10
Maximum speed	km/h	50	120	120
Average acceleration[a]	m/s^2	0.599	0.354	0.506
Maximum acceleration[a]	m/s^2	1.042	0.833	1.042

[a] Calculated using central difference method
[b] Four repetitions of UDC followed by one EUDC

WLTC – Under conditions defined by EU law, the Worldwide Harmonised Light Vehicle Test Cycle (WLTC) laboratory test is used to measure fuel consumption and CO_2 emissions from passenger cars, as well as their pollutant emissions [4–5].

WLTC replaces the European procedure based on NEDC for light vehicle type approval tests, with the transition from NEDC to WLTC in 2017-2019 [3–5].

WLTP procedures include several WLTC test cycles applicable to the vehicle category with different power to mass ratio (PMR), Table 3. The PMR parameter is defined as the ratio of rated power (W)/curb mass (kg). Curb mass (or curb weight) means "unloaded mass" as defined in ECE R83. The cycle definitions may also depend on the maximum speed (v_max), which is the maximum vehicle speed declared by the manufacturer (ECE R68) and not the use limitation or safety-related restriction. Cyclical modifications can include steering problems for vehicles with power to mass indicators near boundary lines or at maximum speeds limited to values below the maximum speed required by cycle [4–5].

With the highest power-to-mass ratio, Class 3 is representative of vehicles driven in Europe and Japan. Class 3 vehicles are divided into 2 subclasses according to their maximum speed: Class 3a with v_max < 120 km/h and

Class 3b with v_max ≥ 120 km/h. Selected parameters of the Class 3 cycles are shown in Table 4, and the vehicle speed for Class 3b is shown in Fig. 2 [4–5].

Table 3. Characteristics of ECE15, EUDC and NEDC test [4–5]

Category	PMR [W/kg]	v_max [km/h]	Speed Phase Sequence
Class 3b	PMR > 34	v_max ≥ 120	Low 3 + Medium 3–2 + High 3–2 + Extra High 3
Class 3a		v_max < 120	Low 3 + Medium 3-1 + High 3-1 + Extra High 3
Class 2	34 ≥ PMR > 22	–	Low 2 + Medium 2 + High 2 + Extra High 2
Class 1	PMR ≤ 22	–	Low 1 + Medium 1 + Low 1

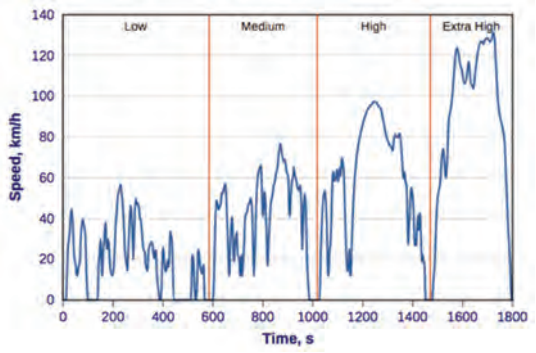

Fig. 2. WLTC cycle for Class 3b vehicles [4–5]

Table 4. WLTC Class 3 cycle: selected parameters [4–5]

Phase	Duration	Stop Duration	Distance	p_stop	v_max	v_ave w/o stops	v_ave w/ stops	a_min	a_max
	s	s	m		km/h	km/h	km/h	m/s²	m/s²
Class 3b (v_max ≥ 120 km/h)									
Low 3	589	156	3095	26.5%	56.5	25.7	18.9	–1.47	1.47
Medium 3-2	433	48	4756	11.1%	76.6	44.5	39.5	–1.49	1.57
High 3-2	455	31	7162	6.8%	97.4	60.8	56.7	–1.49	1.58
Extra-High 3	323	7	8254	2.2%	131.3	94.0	92.0	–1.21	1.03
Total	**1800**	**242**	**23266**						
Class 3a (v_max < 120 km/h)									
Low 3	589	156	3095	26.5%	56.5	25.7	18.9	–1.47	1.47
Medium 3-1	433	48	4721	11.1%	76.6	44.1	39.3	–1.47	1.28
High 3-1	455	31	7124	6.8%	97.4	60.5	56.4	–1.49	1.58
Extra-High 3	323	7	8254	2.2%	131.3	94.0	92.0	–1.21	1.03
Total	**1800**	**242**	**23194**						

The homologation tests carried out in laboratory conditions in the chassis dynamometer are aimed at determining the average exhaust gas emission and fuel consumption in newly produced vehicles. So far, the NEDC cycle has been considered too "easy" to reflect real road conditions. For this reason, works have begun on a new WLTC testing procedure.

Figure 3 shows the most important differences between WLTC and NEDC tests.

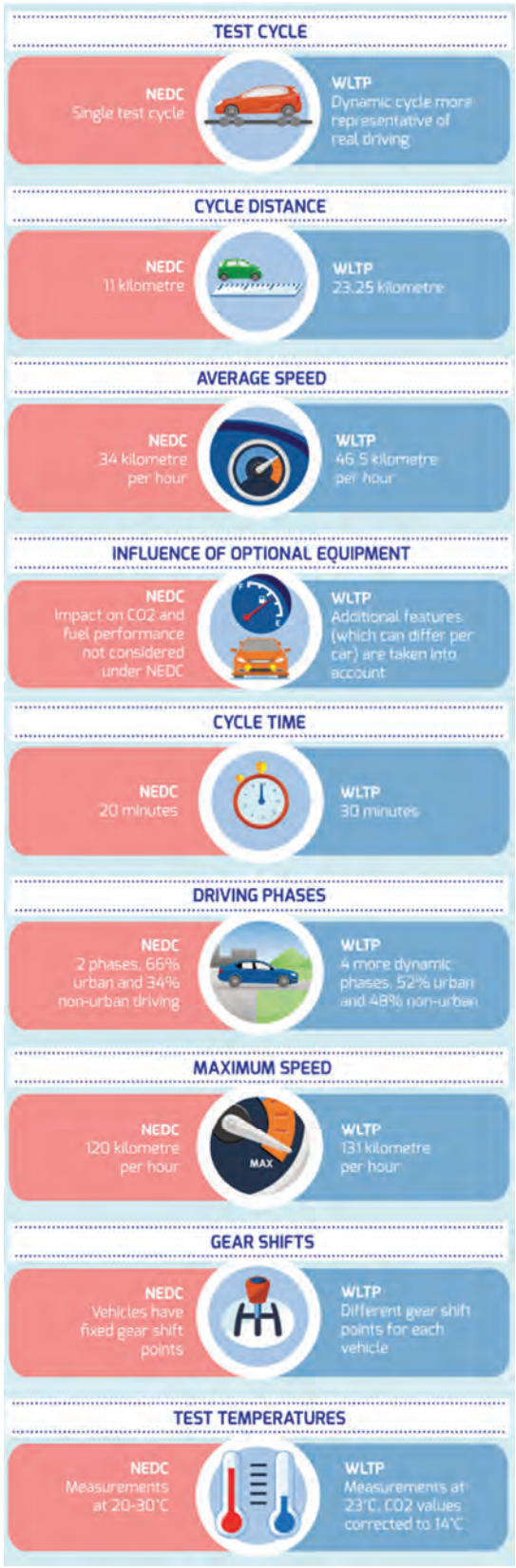

Fig. 3. Differences between NEDC and WLTC [12]

Comparing WLTC with NEDC, you can see that many changes have been made. First, the effect of additional equipment and different engine configuration versions was taken into account, as well as the type of gearbox used in the vehicle (the gearbox change in the case of the manual gearbox is calculated). But it is not everything. The distance and duration of the cycle have been extended. Now, it is extended by 10 minutes (WLTC – 30 minutes, NEDC – 20 minutes) and longer by 12 km (WLTC – 23 km, NEDC – 11 km). The downtime has been shortened. Accurate tests have shown that in real traffic conditions, the vehicle's idle time is shorter than previously assumed. For this reason, it was reduced from 25% in NEDC to 13% in the WLTC cycle [3–5]. An important change is the introduction of differences in the cycle depending on the vehicle's power and the mass ratio in the tested vehicle. Three categories were distinguished. It should be noted, however, that in a larger number of cases, the third category applies to vehicles sold in Europe – above 34 kW/ton [12].

2.2. RDE cycle – real driving emissions

The presented tests are supplemented with real driving emissions (RDE) tests. To perform those tests first the test route had to be specified that would be representative for the tests and fulfil the requirements [6-9]. The requirements set forth by the legislator are presented in the Table 5.

Table 5. Requirements regarding the RDE test route [6–9]

Parameter	Requirements
Ambient temperature (T_z)	normal range: 0 °C ≤ T_z < 30 °C
	lower extended range: –7 °C ≤ T_z < 0 °C
	upper extended range: 30 °C < T_z ≤ 35 °C
Topographic height (h)	normal range: h ≤ 700 m a.s.l
	extended range: 700 < h ≤ 1300 m a.s.l
Impact of external weather and road parameters and the driving style	accumulated height: less than 1200 m/100 km
	(RPA): greater than RPA_{min} (in all driving conditions)
	product of acceleration and speed ($v \cdot a_{pos}$): less than $v \cdot a_{pos\ min}$ (in all driving conditions)
Thermal condition of the vehicle prior to tests	cold start: coolant less than 70 °C, time of at least 300 s,
	emission upon cold start not included in RDE test
Single vehicle stop	no more than 180 s
Exhaust after-treatment system's operation	single regeneration of PM filter can result in RDE test repetition; two regenerations are included in the results of exhaust emissions in RDE test
Driving comfort system operation	used normally according to purpose (e.g. air-conditioning system)
Vehicle load	mass of vehicle: driver (and passenger) and test equipment; max. load < 90% of the sum of weight of passengers and vehicle's usable mass
Test requirement	duration 90–120 min
Requirements for the urban test part	29–44% of the entire test length
	distance more than 16 km
	speed (v): v ≤ 60 km/h
	average speed: 15–40 km/h
	break: 6–30% of the total urban time
Requirements for the rural part	23–43% of the entire test length
	distance: greater than16 km
	vehicle's speed(v): 60 km/h < v ≤ 90 km/h
Requirements for the motorway part	23–43% of the entire test length
	distance: greater than 16 km
	vehicle's speed(v): v > 90 km/h
	driving speed of more than 100 km/h for at least 5 min
	driving speed of more than 145 km/h for at least 3% of the time

The works on outlining the test route were performed by the Motor Transport Institute. To have the test route specified was a priority because of the further possibility of conducting the tests (Fig. 4).

Fig. 4. RDE test route

3. The object of tests

The tests were performed with the use of M1 category vehicle with a self-ignition engine complying with Euro 6 emission level. Key technical parameters of the vehicle are presented in the Table 6 below and the vehicle is shown in Fig. 5.

Table 6. Chosen technical parameters of the vehicle used in the tests

Parameter	Unit	Value
Length	mm	4855
Width	mm	1860
Height	mm	1465
Wheelbase	mm	2805
Engine	–	Combustion, piston, R4 16V, self-ignition
Engine displacement	cm^3	1598
Power	kW/rpm	136/4000
Max. rotational speed	Nm/rpm	320/2000–2250
Compression ratio	–	15.7

Fig. 5. Vehicle used for tests – overview

4. Test results

4.1. NEDC and WLTP cycles

Multiple tests performed on the chassis dynamometer allowed for determining not only the average exhaust emissions but also the concentration of pollutants of exhaust emissions and the number of particle matters.

Figures below (Figs 6–7) present for example results of the number of PM in respective phases for NEDC and WLTC cycles. It can be noticed that the result in NEDC is smaller than in WLTC. The differences are also noticeable in respective phases. In the urban part (UDC – NEDC and Low – WLTC) those differences are considerable. Then in NEDC a much lower emission of particle matters was observed in EUDC – rural part as compared to the rural part in Extra High of WLTC cycle.

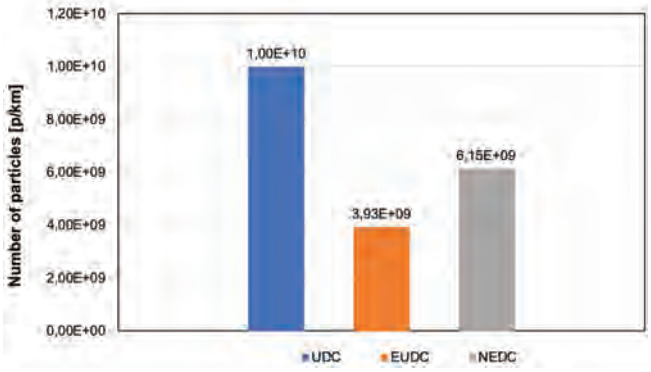

Fig. 6. Particle matters in NEDC and its phases

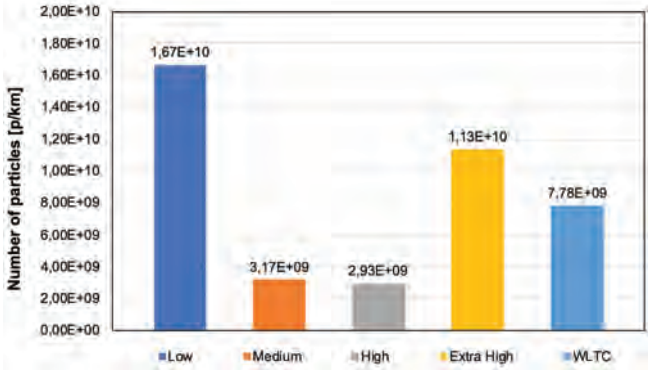

Fig. 7. Particle numbers in WLTP and its phases

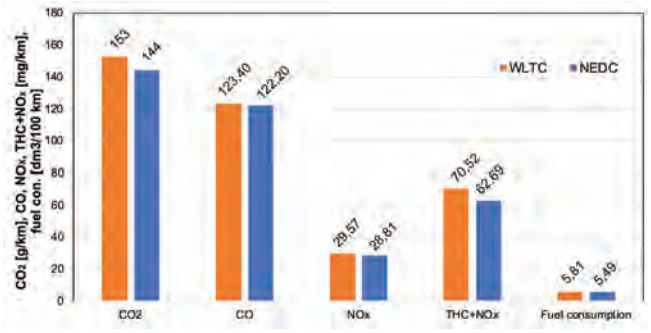

Fig. 8. Comparison of emissions in the tested vehicle in NEDC and WLTC cycles

During the tests of the tested vehicle attention was given to differences in emission of CO, NO_x and THC. It has been observed that in WLTC the tested vehicle characterised with a higher emission of those gases.

As regards carbon oxide the difference was equal to approx. 1% to the disadvantage of NEDC (Fig. 8). As regards nitrogen oxides (NO_x) the difference was 2.6% and was greater in WLTC. As regards hydrocarbons those differences are even greater.

4.2. RDE cycle

The tests performed on the chassis dynamometer were supplemented with RDE tests along a test route outlined in accordance with the requirements. The vehicle was tested in terms of hazardous exhaust emissions. The analyses were made based on window averaging method. The tests focused on the average emissions of CO_2, CO, HC, NO_x, PN and fuel consumption. The analyses allowed for determining the emissions of respective gases in a breakdown into cycle phases and for determining the average emission. As regards CO_2 – its emission in RDE cycle was equal to 187.6 g/km.

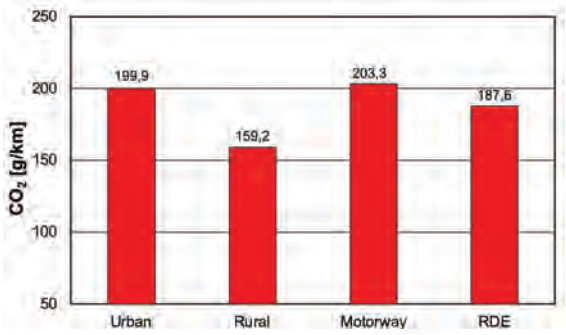

Fig. 9. Emissions of CO_2 in respective phases of RDE cycle and average CO_2 emission in this cycle

The fuel consumption of the tested vehicle remained at a relatively even level (Fig. 10). Only in the rural part the tested vehicle characterised with considerably lower fuel consumption. The average fuel consumption according to the test was equal to 7.05 dm^3 per 100 km.

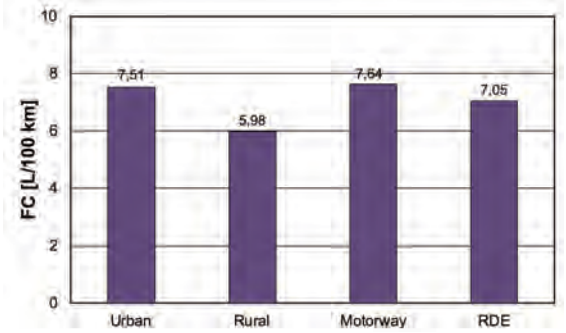

Fig. 10. Fuel consumption in respective RDE cycle phases and average fuel consumption in this cycle

During the RDE cycles of the tested vehicle measured were emissions in respective phases and average emission of CO and hydrocarbons. In the first case the emission levels were almost constant for all cycle phases. Therefore,

also the average value did not differ from those in respective phases. For the purpose of analysing data, a Conformity Factor (CF) was determined for every substance. Based on that it was possible to determine whether this Factor falls within the limit. As regards the tested vehicle this was achieved in case of CO (Fig. 11).

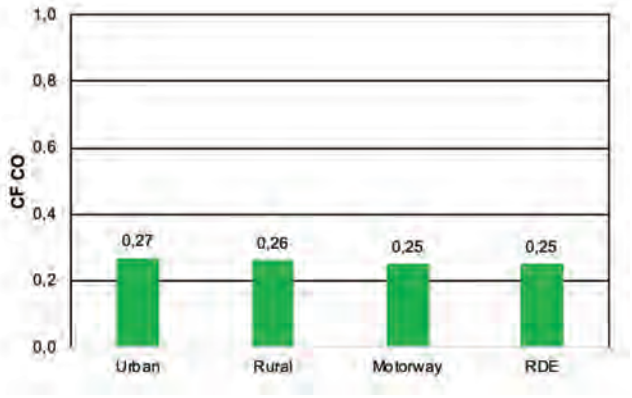

Fig. 11. CF for CO emissions in respective phases of RDE cycle and average CO emission in this cycle

A similar situation related to emission of hydrocarbons. The highest emission of hydrocarbons was recorded in the motorway phase. However, the differences between the phases are minor. This can be seen in Fig. 12 presenting CF for hydrocarbons.

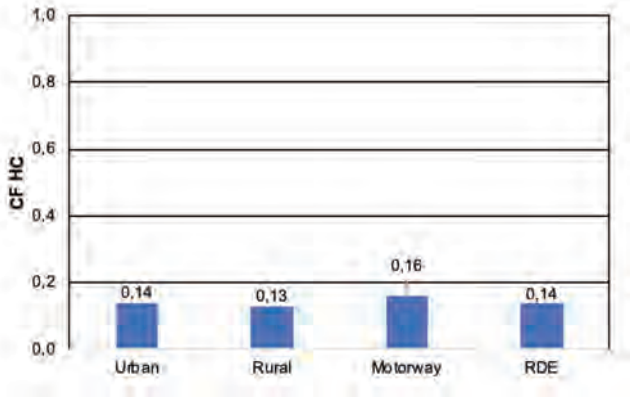

Fig. 12. CF for hydrocarbons in respective phases of RDE cycle and average emission of hydrocarbons in this cycle

The emissions of nitrogen oxides in the tested vehicle fell within the limit CF = 1.5. The result was even significantly lower. The tested vehicle with a self-ignition engine meeting the Euro 6 emission level standard, also fulfilled the requirements of RDE cycle. Moreover, the lowest emission of nitrogen oxides was recorded in the motorway part of RDE cycle (Fig. 13) and the highest – in the rural part. CF for the entire test was 0.39.

Also, it should be noted that the requirements in terms of PN emissions were fulfilled (Fig. 14). Therefore, it can be concluded that modern self-ignition engines do not have problems in fulfilling the exhaust emission standards in relation to PN emissions.

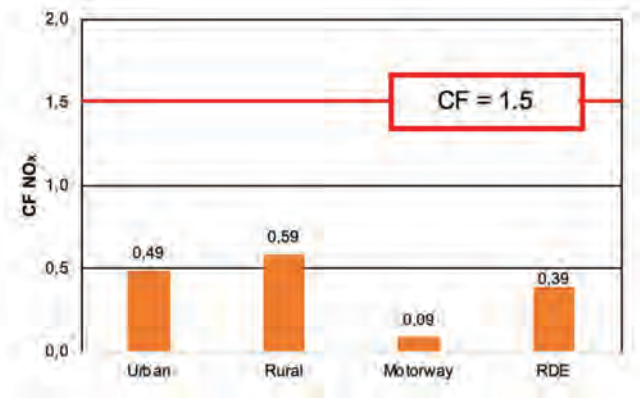

Fig. 13. CF for nitrogen oxides in respective phases of RDE cycle and average emissions of nitrogen oxides in this cycle

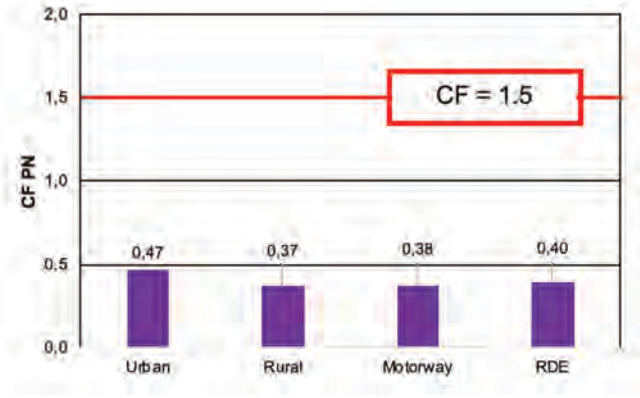

Fig. 14. PN emissions in respective phases of RDE cycle and average PN emissions

On Fig. 15 are given a comparison between the results of road emissions and fuel consumption of the tested vehicle in respective driving cycles.

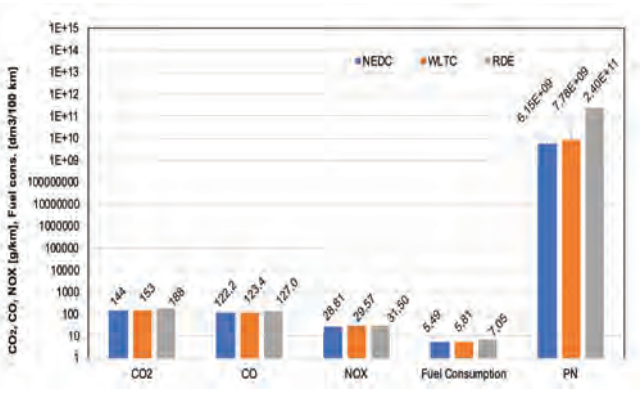

Fig. 15. Comparison of chosen results of road emissions and fuel consumption in the tested vehicle in respective driving cycles.

4. Conclusions

The results of the exhaust emissions in comparative cycles (NEDC, WLTC and RDE cycles) prove that those obtained in RDE cycle – in the case of the tested vehicle with a self-ignition engine – are relatively more unfavourable, though often similar to the results in other test cycles. The tested passenger car fulfils the requirements concerning RDE tests on the tested route for such cycle, and the test route is consistent with the requirements regarding such

routes. Also, the requirements regarding the dynamic of the vehicle's trip along the route have been met. The application of the RDE cycle to verify the results of exhaust emissions tests on a chassis dynamometer is therefore fully justified.

Nomenclature

CAN	Controller Area Network
CF	Conformity Factor
GPS	Global Positioning System
NEDC	New European Driving Cycle
RDE	Real Driving Emissions
WLAN	Wireless Local Area Network
WLTP	Worldwide harmonised Light duty Vehicle Test Procedure

Bibliography

[1] Krajowy bilans emisji SO_2, NO_x, CO, NH_3, NMLZO, pyłów, metali ciężkich i TZO za lata2015-2016 w układzie klasyfikacji SNAP. KOBiZE, styczeń 2018.

[2] NIK. Ochrona powietrza przed zanieczyszczeniami, 2018.

[3] United Nations. Agreement concerning the Adoption of Uniform Technical Prescriptions for Wheeled Vehicles, Equipment and Parts which can be Fitted and/or be Used on Wheeled Vehicles and the Conditions for Reciprocal Recognition of Approvals Granted on the Basis of these Prescriptions. Addendum 82 I Regulation No. 83 Revision 5 Uniform provisions concerning the approval of vehicles with regard to engine fuel requirements. E/ECE/324/Rev.1/Add/82/Rev.5-E/ECE/TRANS/505/Rev.1/Add.82/Rev.5, 4.02.2015.

[4] Global Registry Addendum15: Global technical regulation No. 15. Worldwide harmonized Light Vehicles Test Procedure. ECE/TRANS/180/Add.15.

[5] Proposal for Amendment 4 to UN GTP No 15 (Wordwide harmonized Light vehicles Test Procedures (WLTP). ECE/TRANS/WP.29/2018/71.

[6] Commission Regulation (EU) 2016/427 of 10 March 2016 amending Regulation (EC) No 692/2008 as regards emissions from light passenger and commercial vehicles (Euro 6).

[7] Commission Regulation (EU) 2016/646 of 20 April 2016 amending Regulation (EC) No 692/2008 as regards emissions from light passenger and commercial vehicles (Euro 6).

[8] Commission Regulation (EU) 2017/1154 of 7 June 2017 amending Regulation (EU) 2017/1151 supplementing Regulation (EC) No 715/2007 of the European Parliament and of the Council on type-approval of motor vehicles with respect to emissions from light passenger and commercial vehicles (Euro 5 and Euro 6) and on access to vehicle repair and maintenance information, amending Directive 2007/46/EC of the European Parliament and of the Council, Commission Regulation (EC) No 692/2008 and Commission Regulation (EU) No 1230/2012 and repealing Regulation (EC) No 692/2008 and Directive 2007/46/EC of the European Parliament and of the Council as regards real-driving emissions from light passenger and commercial vehicles (Euro 6).

[9] Commission Regulation (EU) 2018/1832 of 5 November 2018 amending Directive 2007/46/EC of the European Parliament and of the Council, Commission Regulation (EC) No 692/2008 and Commission Regulation (EU) 2017/1151 for the purpose of improving the emission type approval tests and procedures for light passenger and commercial vehicles, including those for in-service conformity and real-driving emissions and introducing devices for monitoring the consumption of fuel and electric energy.

[10] Semtech DS: On Board Vehicle Emissions Analyzer. User Manual.

[11] JAKUBIAK-LASOCKA, J., LASOCKI, J., BADYDA, A.J. The influence of particulate matter on respiratory morbidity and mortality in children and infants. *Advances in Experimental Medicine and Biology*. 2015, **849**, 39-48.

[12] www.wltpfacts.eu

[13] Commission Implementing Regulation (EU) 2018/1002 of 16 July 2018 amending Implementing Regulation (EU) 2017/1153 to clarify and simplify the correlation procedure and to adapt it to changes to Regulation (EU) 2017/1151.

[14] Wdrożenie procedury dotyczącej przejazdu dla realizacji badań emisji zanieczyszczeń spalin (RDE). Praca statutowa 06/18/ITS/008. Instytut Transportu Samochodowego.

Wojciech Gis, DSc., DEng. – Prof. in Motor Transport Institute.
e-mail: *wojciech.gis@its.waw.pl*

Maciej Gis, DEng. – Environment Protection Centre in Motor Transport Institute.
e-mail: *maciej.gis@its.waw.pl*

Piotr Wiśniowski, DEng. – Environment Protection Centre in Motor Transport Institute.
e-mail: *piotr.wisniowski@its.waw.pl*

Mateusz Bednarski, MEng. – Faculty of Automotive and Construction Machinery Engineering, Warsaw University of Technology.
e-mail: *mateusz.bednarski@pw.edu.pl*

Article citation info:
SROKA, Z.J., BUCZMA, K. Adaptation of a gas cogeneration system used in power industry to drive inland waterway transport unit. *Combustion Engines*. 2019, **178**(3), 235-239. DOI: 10.19206/CE-2019-341

Zbigniew J. SROKA
Karolina BUCZMA

CE-2019-341

Adaptation of a gas cogeneration system used in power industry to drive inland waterway transport unit

Cogeneration systems are mainly used in industrial power plants (combined heat and power plants), but based on the analysis carried out in this publication, that suitably adapted and selected devices will be able on board of ships. A number of arguments have been obtained for using the indicated gas engine in a vessel. The cogeneration system guarantees high overall efficiency, as shown in the example of the cogeneration unit under study, for which the value of general efficiency was above 80%. In addition, the use of natural gas as a fuel could ensure a significant reduction in the amount of toxic compounds emitted to the atmosphere, especially nitrogen oxides (2-3 times) and smog (dust with PM10) around 25 times than standard limits. The use of natural gas as a fuel guarantees similar dynamic parameters as with the use of standard fuels.

Key words: *cogeneration, propulsion, natural gas, energy, inland waterway transport*

1. Introduction

The transport sector is one of the key branches of the national economy and plays an increasingly important role in its development every year. It has a stimulating effect on the market and together with a well-developed transport network it creates an integrated system of a smooth flow of people and goods [3, 5, 9].

Emerging road, rail, air and water connections create new opportunities and perspectives, making individual regions of the world better communicated. The efficient flow of goods and services generates, in turn, higher profits, thus creating prospects for further development of this sector. The main factors influencing the evolution and any changes in transport are: globalization, consumerism and striving to improve the comfort of life.

When discussing the transport sector, one should remember about the ecological aspect associated with its functioning, focusing primarily on the attention of designers and manufacturers, as well as users and legislative institutions on the combustion engine, which is the most popular means of transport.

In many countries, in the near future, there will be a boom for the transport industry. New challenges are also being taken in Poland. One of them is the comprehensive revitalization of river infrastructure in order to develop inland waterway transport [13, 15]. This is a signal to undertake a series of activities, among which a significant place is taken up by the intensification of research into the sustainable use of energy. In this group of studies, an important role will be played by research into the combustion propulsion of vessels in the aspect of improving efficiency while using alternative fuels.

Sustainable development in this area may involve the use of useful energy for the drive and part of the energy wasted to supply various devices with electric and thermal energy. In turn, the use of alternative fuels (in the form of CNG and LNG), e.g. natural gas, would be a specific frame improving the environmental efficiency of the drive [1, 6, 9, 12, 14].

Design and research experiences in this field flow directly from other areas of activities, such as energy or mining industry, where high-efficiency cogeneration systems confirm the existence of the possibility of beneficial production and use of mechanical, electrical and thermal energy while reducing the emission of harmful substances. The internal combustion engines tested in these areas can be used as engines for potential means of transport as a source of energy for heating and air-conditioning systems of this unit and as a source of electric energy for own means of transport. The use of a cogeneration system allows for effective use of all the above-described types of energy.

2. Use of cogeneration system in a vessel as a research problem

The research problem described in this publication is the evaluation of the cogeneration system used in power plant industry as an alternative source of propulsion for typical technical solutions currently used in vessels. This activity is the result of investment plans related to the revitalization of river infrastructure. Poland is a country that should develop this type of transport, if only due to the existence of water systems, in the basins of the two largest rivers Vistula and Odra (Fig. 1), extending properly throughout the country. These rivers form combined communication networks with a total length of 3655 km [5, 15].

Fig. 1. One of the views of the Odra river

The development of river infrastructure can largely unload the congested road transport system in Poland. The main advantage of inland transport is low energy consumption. Water transport is useful in the transport of oversized goods, where it does not interfere with other types of rolling stock and does not create restrictions for other users. Water transport is covered by regulations regarding the emission of toxic substances, which imposes an obligation to constantly search for structural solutions that meet the accepted standards.

Water transport is currently the least appreciated and widespread type of transport in our country. This is not a simple undertaking, due to fluctuations in the level of waterways, lack of investment on potential water routes and depleted technical infrastructure used for this type of transport. There are inland water transport modes for passengers and goods. A special case is the transport of goods, during which the barge used for transport does not have its own drive and pushers or tugs are used to overcome distances.

The development of waterways depends on the conditions of natural rivers and water reservoirs. The cost-effectiveness of using waterways depends on their capacity and this is strictly dependent on the speed of vessels, the type of cargo and load capacity of a given ship and the required distance that particular ships would have to keep on a specified water course.

The propulsion system of the watercraft consists mainly of the mechanical energy source, which is usually the diesel internal combustion engine, as well as the transmission that transmits the torque obtained as a result of the propulsion engine operation, which in turn converts the obtained energy into rotation of the propeller, setting the vessel in motion [3, 5]. In figure 2. there is an example of a propulsion system used in a ship and parameters characteristic for a given part of the system.

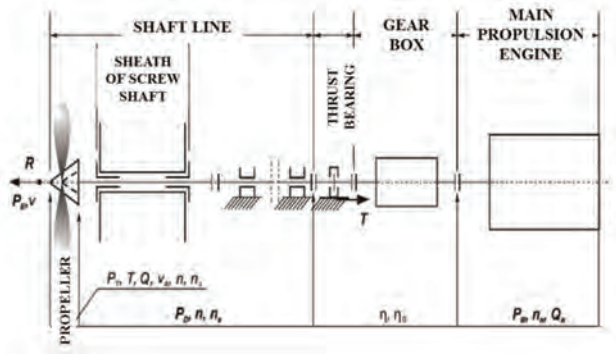

Fig. 2. The propulsion system of a vessel [5]. Main propulsion engine (P_B – power generated, n_n – engine speed, Q_n – heat delivered; Gear (η_P – efficiency of the drive system, η_G – efficiency of the shaft lines); Shaft line (P_D – power delivered to the propeller, n – shaft rotation speed); Propeller (P_T – thrust power, T – thrust, Q – torque on the cone, v_A – speed, n_s – propeller speed, R – towing resistance, P_E – ship towing power)

Due to the fact that transport plays a key role in the modern world, strict requirements are set before it, which define the framework of its functioning and development. This in turn imposes on individual states, their government agencies, state-owned enterprises, private companies, concerns, the obligation to search for new concepts, technologies and solutions in accordance with applicable international arrangements, legal acts, technical and environmental standards. The above-mentioned requirements are to improve the living conditions, reduce the negative impact of transport on the natural environment, increase the level of safety in transport.

All of this focuses on the idea of sustainable transport, which means a balance between mobility, energy resources and pollution emissions. In this way, in terms of transport equivalence, it is reasonable to refer to the problem of low energy efficiency to cogeneration issues. The associated process of generating energy in transport units, via cogeneration systems, will undoubtedly contribute to reducing the emission of toxic compounds [7, 12].

The heat generated in the engine is usually a by-product. Thanks to cogeneration, this heat can be used for heating purposes (e.g. heating of rooms, cabins, decks on a watercraft, providing hot utility water on such a unit), it can be used for air conditioning or cooling purposes of a transport unit, where, e.g. absorption chiller powered with hot water, coming from the engine cooling systems, you can generate the so-called ice water. The mechanical energy generated basically for the unit's propulsion needs can be converted into a synchronic generator coupled with the engine for electricity and used more efficiently than in road transport, e.g. for lighting the premises in a transport unit, supplying measurement systems, etc. [12].

2. Research and results

2.1. Research object

The research object was the CUMMINSgas turbine, which together with the synchronous generator STAMFORD, formed the basis of the energy system at EC Muchobor-Wroclaw City, belonging to the Wroclaw Heat and Power Plant Complex KOGENERACJA S.A. Thanks to courtesy and with the consent of KOGENERACJA S.A., research was carried out and data from the daily reports of the cogeneration aggregate were obtained, which were used for analyzes covered by this publication. The owner of the unit – KOGENERACJA S.A., uses the mentioned unit as a source of electricity and heat for the needs of clients supplied from EC Muchobor. The present research was aimed at recommending this type of engine to drive a floating transport unit.

The tested HE-CG1400-GZ cogeneration gas unit (Fig. 3) consists of:

– CUMMINS four-stroke, turbocharged gas engine with spark ignition, providing electrical power up to 1435 kW at a rotational speed of 1500 rpm;
– STAMFORD synchronous generator with voltage 400/230 V and frequency 50 Hz.

The gas path is connected to the main shut-off valve and other gas flow control elements. The fuel/gas flow and engine speed control system are all with the generator set.

Natural gas was used as a fuel. An important property of most gaseous fuels during the combustion process is the ability to create a homogeneous mixture, which is responsible for the proper course of the process. In addition, gaseous fuels are characterized by wide flammability ranges compared to petrol and diesel. They also have more hydro-

gen than carbon in their composition, which results in a reduced emission of CO_2 to the environment.

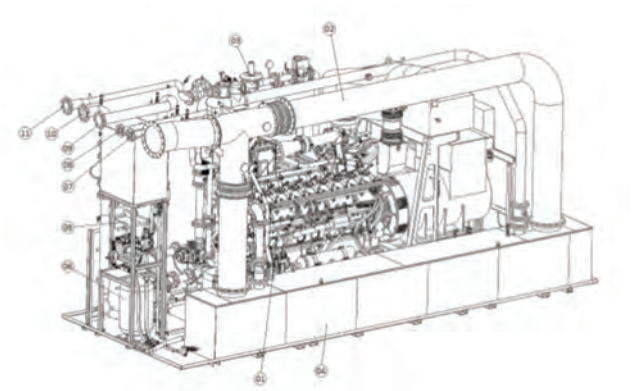

Fig. 3. View of the cogeneration gas system [16]. 01 – HE-EC-1400/1560-CG1400-GZ unit, 02 – Exhaust gas bypass, 03 – Gas path, 04 – Exhaust gas heat exchanger, 05 – Plate heat exchanger, 06 – Collection vessel, 07 – LT circulation outlet LT, 08 – LT circuit inlet, 09 – HT circuit outlet, 10 – HT circuit inlet, 11 – Gas inlet, Motor cooling circuit (HT); The mixture cooling circuit (LT); Coolant temperatures, circuits: HT (engine), LT – (intercooler)

Gaseous fuels are also characterized by a high methane number corresponding to resistance to knocking combustion in the engine. The value in question indicates the percentage share of methane in a given fuel, in turn the higher the share of methane, the more efficient the engine can be. Nevertheless, the methane number does not fully determine the efficiency of the system. Important parameters affecting the usefulness of the mixture in the combustion process are: range of fire limits, burning speed, energy of ignition, chemical composition, air demand, heating value [4, 6, 8].

Because of differ in mentioned properties not every gas will work as an appropriate fuel in a cogeneration system. The given values depend on each other, hence knowing the chemical composition of the gas, the best air demand can be determined, which in turn in connection with the amount of heat release during combustion of the mixture determines the demand for a specific level of calorific value. In order to obtain the expected energy effect, a sufficient volume of the mixture must be supplied to the cylinder, which depends on the composition of the fuel and the amount of air. Often the amount of fuel-air mixture exceeds the engine's construction volume. Then it is necessary to use the recharge of the mixture in order to obtain the required power of the system. The growing interest in this type of fuels results from the reduced emission of pollutants during combustion of the mixture and similar parameters to petroleum products [4, 10, 11]. Fuel for this engine is a depleted gas/air mixture with a coefficient of $\lambda > 1$. Two turbochargers were used to obtain the required mechanical power, one for each side of the engine. The compressed mixture passing through the intercooler, is cooled to the right temperature and then goes to the individual cylinders. The amount of mixture is dosed through the throttle regulator. The mechanical energy of the motor is transmitted to the generator by means of a clutch, whereas the thermal energy can be recovered or dissipated via an external cooler.

2.2. Methodology of research implementation, data and results

The assessment of the cogeneration system consists in the determination of electrical, thermal and total efficiency. In this way, it is possible to assess the suitability of the tested set for use in specific conditions – Table 1.

Table 1. Sources of measurements

Parameter	Method
Electric power of unit	Electricity meter readings
Power factor	
Gas flow	Gas meter readings at the reduction and measuring station
Gas temperature	
Gas pressure	
Calorific value	According to the physicochemical analysis of the gas sample performed on order of unit owner
Coolant temperature – return side	Parameters readings at the operator station
Temperature – coolant supply side	
Heating water flow rate	Parameters readings at the operator station – ultrasonic flow meter on the machine hall
Thermal power	Thermal energy meter readings – temperature and flow

The following relationships were used to calculate the efficiency of a cogeneration unit [2]:

– electrical efficiency of the system η_E [%]

$$\eta_E = \frac{P_E}{E_G} = \frac{P_E}{V_G \times Wd} \times 100\% \quad (1)$$

– thermal efficiency of the system η_c [%]

$$\eta_C = \frac{Q_E}{E_G} = \frac{Q_E}{V_G \times Wd} \times 100\% \quad (2)$$

– overall system efficiency η_o [%]

$$\eta_O = \frac{P_E + Q_E}{E_G} = \frac{P_E + Q_E}{V_G \times Wd} \times 100\% \quad (3)$$

During the tests the following data were recorded – Table 2.

Table 2. Measurement results

Parameter	Unit	Load		
		50%	75%	100%
Gas temperature	°C	6.8	4.2	4.5
Heating water temperature – power supply side	°C	85.2	84.6	85.3
Heating water temperature – return side	°C	63.7	50.7	66,6
Gas pressure	kPa	388	383	387
Gas flow rate	Nm^3/h	190	261	340
Heating water flow rate	m^3/h	37	29	67
Thermal power	kW	926	1156	1459
Electric power	kW	703	1055	1405

However, in the Table 3 the results of calculations of energy effects were included.

Table 3. Calculation results

Parameter	Unit	Load		
		50%	75%	100%
Chemical energy of used fuel	kW	1903	2613	3404
Electric efficiency	%	37	40	41
Thermal efficiency	%	49	44	43
Overall efficiency	%	86	85	84

The above results indicate that cogeneration systems are characterized by high overall efficiency of the system, which means that the thermal energy generated in the gas combustion process has been appropriately used. It was used to heat the heating water and to produce electricity. The increase in the system load has forced the increase of electrical efficiency, which is accompanied by a decrease in thermal and overall energy. In addition, during the tests at 100% load with CNG fueled, environmental measurements were carried out, showing concentration levels: SO_2, NO_x, CO and dust (smog) pollution contained in in the exhaust gas – Table 4.

Table 4. Concentrations of the tested chemical compounds

Tests	Parameter	Unit	Measurement results at 100 % load
Concentrations of substances in exhaust gas under normal conditions	Total dust (smog) including suspended PM10	mg /$m^3{}_U$	1.71
	SO_2	mg/$m^3{}_U$	1.06
	NO_x	mg/$m^3{}_U$	223
	CO	mg/$m^3{}_U$	38.2
Concentrations of substances in exhaust gas converted into a unit of chemical energy contained in the fuel	Total dust (smog) including suspended PM10	g/GJ	0.87
	SO_2	g/GJ	0.505
	NO_x	g/GJ	106
	CO	g/GJ	18.2

From the results presented in the Table 4, it can be concluded that the use of natural gas as fuel for the engine is a pro-ecological solution. Values of concentration of nitrogen oxides (NO_x expressed as the sum of nitric oxide (NO) and nitrogen dioxide (NO_2), carbon monoxide and total dust are within the limits of allowed concentrations of pollutants emitted into the air (NO_x< 300 mg/$m^3{}_u$, CO < 100 mg/$m^3{}_u$ and total dust < 50 mg/$m^3{}_u$) and are definitely below the concentration values for fuels like gasoline or diesel [4, 10].

Similar conclusions can be obtained by analyzing another parameter, i.e. NO_x specific emissions, which is 2.33 kg/h and which is lower than the permissible value of 5.54 kg/h according to the permit of the Chief Inspectorate for Environmental Protection for the introduction of gaseous and particulate matter into the air.

3. Cogeneration system in a vessel

The concept of using the tested engine in a vessel and creating a cogeneration system for such a unit is an alternative to typical technical solutions currently used in the construction of vessels. Such a system would primarily provide the drive for the selected unit, through appropriate translation and coupling with the propeller. In addition, a gas engine coupled with a properly selected generator would provide the unit with power supply for its own needs (lighting, power for on-board devices). Another functionality of the cogeneration system is the use of waste heat coming from the engine cooling system, to heat the deck and to heat utility water.

When using coolant for cooling the engine block, cylinder heads, lubricating oil, intercooler, a certain amount of thermal energy is obtained. In the water-water type exchanger, the coolant gives off heat to drinking water, which circulates in a closed circuit and supplies heat consumers in individual rooms of the vessel. The heating system on the unit will consist of a supply and return piping system, shut-off and regulating fittings, sludge, filters, heat receivers and compensating vessels. The expansion vessels are mainly used for safety reasons, they are to protect the system from pressure increase. Unlike air, water has better thermal and flow properties. With this type of installations it is possible to use smaller cross-sections of pipes, which creates better conditions for heat exchange. Energy obtained in a cogeneration system can also be properly stored and used at a later time. The storage possibility is created, for example, by a buffer exchanger filled with water. By using the buffer it is possible to take in any amount of heat when there is such a need with small losses during the liquid flow. The buffer tank consists of coils, shut-off and regulating fittings and measuring devices that ensure that the set temperature is maintained.

Waste gas is another important source of waste heat. The use of a suitable tube-type or plate-type exhaust gas-air exchanger will make it possible to use the thermal energy contained in the exhaust gases to heat the deck spaces. The exhaust gases leaving the engine cylinders give the heat to the air, which will be used to heat the rooms. The exhaust gases are characterized by high temperature as well as the content of toxic compounds. This requires appropriate materials for the construction of the exchanger, which will ensure its tightness and enable operation in high temperature and acidic environment, which may arise at the moment of condensation of water vapor contained in the exhaust and reaction with sulfur or nitrogen oxides [1, 7, 12].

4. Summary

Cogeneration systems are mainly used in industrial power plants (combined heat and power plants), but based on the analysis carried out in this publication, that suitably adapted and selected devices will prove themselves on board of ships. A number of arguments have been obtained for using the indicated gas engine in a vessel. The cogeneration system guarantees high overall efficiency, as shown in the example of the cogeneration unit under study, for which the value of general efficiency was above 80%. Without waste energy management, the efficiency of the engine alone is only 38%.

The data and parameters collected during the cogeneration system tests were not referred to the actual watercraft with specific dimensions and the expected speed of movement of the unit, as well as no external conditions were identified in which the unit would work (fairway width, river depth, etc.). Nevertheless, the 1435 kW engine with a swept volume of 60 dm^3, powered by natural gas, presented in this paper, seems to be an interesting alternative to currently used engines in vessels. This is supported by favorable emission and toxicological parameters, especially when compared to the parameters of engines fueled by marine fuel. Fuel of this type contains in its composition significant amounts of sulfur, which results in increased emission of sulfur oxides, during its combustion. Therefore, the use of alternative fuels in water transport, such as natural gas, can ensure the maintenance of working conditions in accordance with the applicable emission standards. In addition, the use of natural gas can mean financial benefits while maintaining the current level of the unit price of this fuel.

Nomenclature

CNG	compressed natural gas
E_G	chemical energy of gaseous fuel
HT	engine
LNG	liquefied natural gas
LT	intercooler
n	shaft rotation speed
n_n	engine speed
n_s	propeller speed
PM10	particulate matter (size 10)
P_B	power generated
P_D	power delivered to the propeller
P_E	electric power at the generator terminals
P_T	thrust power
Q	torque on the cone
Q_E	thermal power of the system
Q_n	heat delivered
R	towing resistance
T	thrust
v_A	speed
V_G	gas fuel flow
W_d	calorific value of gas fuel
η_o	overall system efficiency
η_c	thermal efficiency of the system
η_E	electric efficiency of the system
η_e	efficiency of the drive system
η_G	efficiency of the shaft lines

Bibliography

[1] ABRAMEK, K.F., UZDOWSKI, M. Wybrane aspekty eksploatacji pojazdów wykorzystujących paliwa gazowe. *Autobusy. Technika, Eksploatacja, Systemy Transportowe* 2012, **13**(4), 39-42.

[2] GIERNALCZYK, M. Metoda określania zapotrzebowania energii do napędu statku, energii elektrycznej i wydajności kotłów dla nowoczesnych statków pasażerskich przy wykorzystaniu metod statystycznych. *Akademia Morska w Szczecinie, Zeszyty Naukowe*. 2008, **14**(86), 9-13.

[3] KACPERCZYK, R. Środki transportów część 1. *Difin-Edukacja*. Warszawa 2012.

[4] KORDYLEWSKI, W. Spalanie i paliwa – wydanie IV. *Oficyna Wydawnicza Politechniki Wrocławskiej*. Wrocław 2005.

[5] KULCZYK, J. Śródlądowy transport wodny. *Oficyna Wydawnicza Politechniki Wrocławskiej*. Wrocław 2003.

[6] LEJDA, K., JAWORSKI, A. LNG Alternatywne paliwo przyszłościowe dla autobusów miejskich. *Zeszyty Naukowo-Techniczne Oddziału Krakowskiego SITK*. 1999, **31**(70).

[7] MERKISZ, J. Ekologiczne problemy silników spalinowych, *Wydawnictwo Poltechniki Poznańskiej*. Poznań 1998.

[8] MERKISZ, J., PIELECHA, J., RADZIMIRSKI, S. Emisja zanieczyszczeń motoryzacyjnych w świetle nowych przepisów Unii Europejskiej. *WKŁ*. Warszawa 2012.

[9] MIŁASZEWICZ, D., OSTAPOWICZ, B. Warunki zrównoważonego rozwoju transportu w świetle dokumentów w UE. Studia i Prace Wydziału Nauk Ekonomicznych i Zarządzania. *Wydawnictwo Naukowe Uniwersytetu Szczecińskiego*. 2011, **24**.

[10] MYŚKÓW, M. Prognozowanie emisji związków toksycznych w spalinach opalanych pomocniczych kotłów okrętowych. *Zeszyty Naukowe Akademii Morskiej w Szczecinie*. 2005, **5**(77).

[11] PRZYBYŁA, G. Wpływ paliw gazowych na parametry pracy silnika tłokowego silnika spalinowego pracującego w układzie CHP. *Biblioteka Źródłowej Energetyki Prosumenckiej*. 2014.

[12] SKOREK, J. Gazowe układy kogeneracyjne. *WNT*. Warszawa 2005.

[13] WITKOWSKI, K. Problematyka zanieczyszczenia atmosfery przez statki wykorzystywane w transporcie morskim. *Autobusy – Bezpieczeństwo i Ekologia*. 2016, **6**, 468-473.

[14] WOŁOSZYN, R. Gaz ziemny jako paliwo silnikowe. *Autobusy*. 2007, **5,** 18-21.

[15] Ministerstwo Gospodarki Morskiej i Żeglugi Śródlądowej, Założenia do planów rozwoju śródlądowych dróg wodnych w Polsce na lata 2016-2020 z perspektywą do roku 2030, *Dokument przyjęty przez Radę Ministrów* 14 czerwca 2016.

[16] Instrukcja obsługi agregatu kogeneracyjnego CumminsHE-CG1400-GZ.

Zbigniew J. Sroka, DSc., DEng. – Faculty of Mechanical Engineering, Wroclaw University of Science and Technology.
e-mail: *zbigniew.sroka@pwr.edu.pl*

Karolina Buczma, BEng. – Faculty of Mechanical Engineering, Wroclaw University of Science and Technology.
e-mail: *214073@student.pwr.edu.pl*

Article citation info:
KARCZEWSKI, M. Evaluation of the diesel engine feed by unified battlefield fuel F-34/F-35 mixed with biocomponents. *Combustion Engines*. 2019, **178**(3), 240-246. DOI: 10.19206/CE-2019-342

Mirosław KARCZEWSKI

CE-2019-342

Evaluation of the diesel engine feed by unified battlefield fuel F-34/F-35 mixed with biocomponents

The problem of the military vehicles engines fuelling increases with the growth of the amount of vehicles in the armies. At the same time, another problem with fuel supply in modern engines is the use of bio component additives, which changes characteristics (quality) of the used fuels. Therefore, it is important to take actions to adapt engines to powering with fuels coming from renewable sources.

The aim of the research was to evaluate the possibility of feeding the diesel engine (influence on the useful parameters and composition) with mixtures of the unified battlefield fuel F-34/F-35 with biocomponents in the form of anhydrous ethyl alcohol and RME. The tests were conducted during fuelling of the engine with six kinds of fuels: basic fuel (diesel oil), NATO code F-34/F-35 fuel, as well as fuel mixtures: F-34 and RME with different ratio and F-34/F-35 with bioethanol. In the result of the research it was concluded that the parameters of the G9T Renault engine with the common rail fuel system in terms of F-34 and RME consumption (using) decreased in comparison to diesel oil basic fuel. It is not possible to supply the engine with the mixture of ethyl alcohol and F-34 fuel – alcohol precipitation and obliteration of fuel system components

Key words: *diesel engine, fuel supply system, F-34/F-35 fuel, Rapeseed Methyl Esters, bioethanol*

1. Introduction

Liquid fuels are the most important source of energy on modern battlefield. Availability of fuels decides about mobility of the army, effectiveness of weapons or other support equipment and delivery of needed amount of supplies. Realisation of increasing requirements of fighting troops in fuels or lubrication oils is one of the most important problems of logistic supplying of a battlefield. It is calculated, that mean use of fuel and lubrication oil may reach 30 kg per one soldier per day [4, 11]. The delivery of such a big quantity of supplies to the army, in terms of enemy interaction on communication systems and supplying infrastructure is an enormous sophisticated problem. It is why there is a trend to standardize all sorts of fuels in the army.. Fuels known as F-34/35 were introduced. It has the same base components as plane fuel JP8 (JET-A1). It's final quality is the effect of using additive components added to the base fuel before final distribution of fuel to a vehicle's tank.

Nowadays the F-34/35 fuel is taken as unified battlefield fuel for all diesel engines of NATO nations. At the end of 20th century the F-34 fuel was taken under investigation, which focused mainly about elder generation engines completed with in-line and rotation injection pumps [2], without engines with high pressure Common rail systems. From the time of introduction that fuel the injection equipment has changed. In-line injection pumps with plungers and barrels injection units are used very rarely. Common Rail and unit injection systems are used instead. In that system injection pressure reaches 140–200 MPa. It has a significant change on fuel quantity during injection [7, 8, 10, 11, 12]. Terms condition of fuel before injection to combustion chamber are changed relevantly, and temperature is much higher in comparison to classical in-line injection pump.

The Common Rail systems are commonly used in engines of cars, low duty and heavy duty trucks, locomotives and vessels as well as combat vehicles, for instance the MTU engines of MT 880 series. In these engines in-line pumps used in earlier version were replaced by CR systems. Hat systems are widely used in heavy duty trucks, which are in possession of Polish Army (MAN, IVECO, SCANIA).

Using raw F-34 fuel to fuel engine equipped with Common Rail system may cause serious change of work parameters. Own investigation of the G9T engine equipped with CR fuelling system led in Military University of Technology [10, 11] shows important diminish of maximum torque and NO_x in exhaust gases and increasing of specific fuel consumption.

The F-34/35 fuels in compare to diesel oil are characterised by better characteristic in low temperature, less viscosity, less cetan number, less heat value. Technical advantage of unified fuel is: compatibility to aircraft fuel (JET-A1), less sensibility on biological contamination, availability on airports all over the world, better low-temperature characteristic, less possibility of flare/self-ignition in comparison to wide fraction hydrocarbons fuels, less emission of toxic components. Logistic advantages are supplying only one sort of fuel in the whole army, simplification of supply chain and unification of storehouses and storing facilities.

Disadvantages of the unified fuel are increasing needs and demands for fuels based on kerosene and diminish of demands for other fuels. It may cause increasing of a fuel price, diminish of an engine power connected with less heat value of kerosene, needs for modernization of currently used equipment and using fuel additives.

Using of fuels which consist of renewable components such as rapeseed methyl esters (RME) may cause shortening of supply chains. The reason is using local source of a rapeseed from nearby grain elevators which are spread on over the country. The only demand is to introduce an installation for rapeseed oil pressing and for it esterification in the army. Then the vulnerability of the army for fluctuation of supply smoothness in case of a military conflict.

Fuels which consists of RME and bioethanol has a little bit different characteristics then hydrocarbons fuels. It depends on different composition, because in molecule struc-

Table 1. Chosen characteristics of fuels used during investigation [3, 11, 14, 16]

Quantity	Unit	military standard diesel fuel IZ-40	RME fuel	Bioethanol	F-34 fuel
Density in temp. 15°C	g/cm^3	0.831	0.881	0.790	0.804
Heat value	MJ/kg	43.2	38.3	27.2	42.8
Temperature of ignition	°C	66	177	12	57
Temp. of cold filter block	°C	–31	–9		–54
Kinematic viscosity in 40°C	mm^2/s	2.35	4.60	0.90	1.27
Sulphur ratio	mg/kg	350	19	–	3000
Cetane number	–	50	43	8	45

ture apart from a carbon and a hydrogen there is a quite big dose of an oxygen (ca. 12%). An oxygen ratio and unsaturated bindings conduced to auto ignition and complete combustion. An oxygen contained in fuel has more reactivity then an oxygen consisted in the air, it increase of a cetan number of that fuel. Changing of combustion process has positive influence concentration of toxic components and diminishes a smoke emission. Disadvantage of RME is large amount of water and aggressive influence on rubber parts and film-coating lacquer. [6, 9, 12, 15, 16]. That fuel has more density and viscosity, that its addition to standard F-34 fuel should cause the approach of the F-34 fuel attributes to diesel oil characteristic. The most important drawback of ethanol is low calorific value, low cetane number and high hygroscopicity. These features affect negatively the properties of petroleum-based fuel mixtures with bioethanol. These properties are significantly influenced by the injection of fuel into the combustion chamber, mixture formation and combustion process, which in turn affects the engine performance and the emission of toxic exhaust components.

2. Aim and range of work

Current fuel situation in the world and predicted diminishing of natural sources of oil compel to searching for new kinds of fuels. It concerns fuels used to feed of military vehicles as well. Despite that the F-34 fuel was taken by NATO nations as basic fuel, there is very seriously considered the situation that will force to renew this fuel with other, even bio products.

The aim of the research was the empirical assessment of the possibility of feeding the self-ignition engines (influence on the useful parameters and composition) with mixtures of the unified battlefield fuel F-34/ F-35 with biocomponents in the form of anhydrous ethyl alcohol and RME.

3. Object, methodizes and range of investigation

The object of investigation was a four cylinder Renault G9T diesel engine with 95 kW effective power with rotational speed n = 2500 rpm and 280 Nm torque with rotational speed n = 1750 rpm, used in propulsion systems of light duty vehicles (LDV) of different producers. This is an engine with direct injection system equipped with a high-pressure CR injection system. The engine is turbocharged and equipped with charged air-cooling system (intercooler).

The range of investigation consisted of the engine effective parameters, parameters of combustion process and composition of exhaust gases measure. The investigation was led for all the engine work field (speed characteristic and series of load characteristics in all range of rotational speed of the engine). The investigation of load characteristics was led as a method of passive experiment in steady state of the engine work. The external speed characteristic was done as well in range of 1000–3750 rpm with 250 rpm step.

During investigation effective parameters of the engine, temperature (cooling liquid, lubrication oil, exhaust gases before and after turbocharger), concentration of: carbon dioxide, oxygen, carbon monoxide, hydrocarbons, nitrogen oxides, and smoke measured as extinction of radiation absorbed by exhaust gases. Due to the volume of collected research material, article presents only the results obtained during engine operation on external characteristics.

Results of engine parameters measuring were gathered during all experiment. The purpose was current observation of a technical state or reveal of the engine possible malfunction circumstances and observation of next steps of investigation. The results of the engine effective parameters measuring were calculated back to normal atmospheric condition according to PN-ISO 15550:2009 standard.

During the investigation the engine was fuelled with fuels:

- military standard diesel fuel – in the paper it is signed as SDF,
- F-34/F-35 fuel – in the paper it is signed as F-34,
- mixtures of the F-34/35 fuel and RME – in the paper it is signed as B-20, B-40, B-60 and B-80 where the number following letter B stands for a weight ratio of RME in the mixture.
- mixtures of the F-34/35 fuel and bioethanol – in the paper it is signed as E-5, E-10, where the number following letter E stands for a weight ratio of bioethanol in the mixture.

4. Results of investigation

The analysis of investigation results lets to evaluate the different kinds of fuels influence on the engine effective parameters, indicated parameters, concentration of toxic components and smoke in exhaust gases.

Based on the analysis of measured external characteristics of the G9T engine fuelled with different kind of fuels it must be said, that the biggest effective power of the engine is reached when it is fuelled with basic fuel (SDF) –Fig. 1a and 1b. The Usage of the F-34 fuel caused a little diminish of effective power (Ne) ca. (1–2)% . The RME or bioethanol addition to the F-34 fuel caused next diminish of effective power ca. (7–8)%, depending on F-34/RME mixture ratio (Fig 1b). The reason of it is increasing of F-34/RME mixture density and diminishing of a heat value. Differences in effective power increase due to rotated speed of the engine.

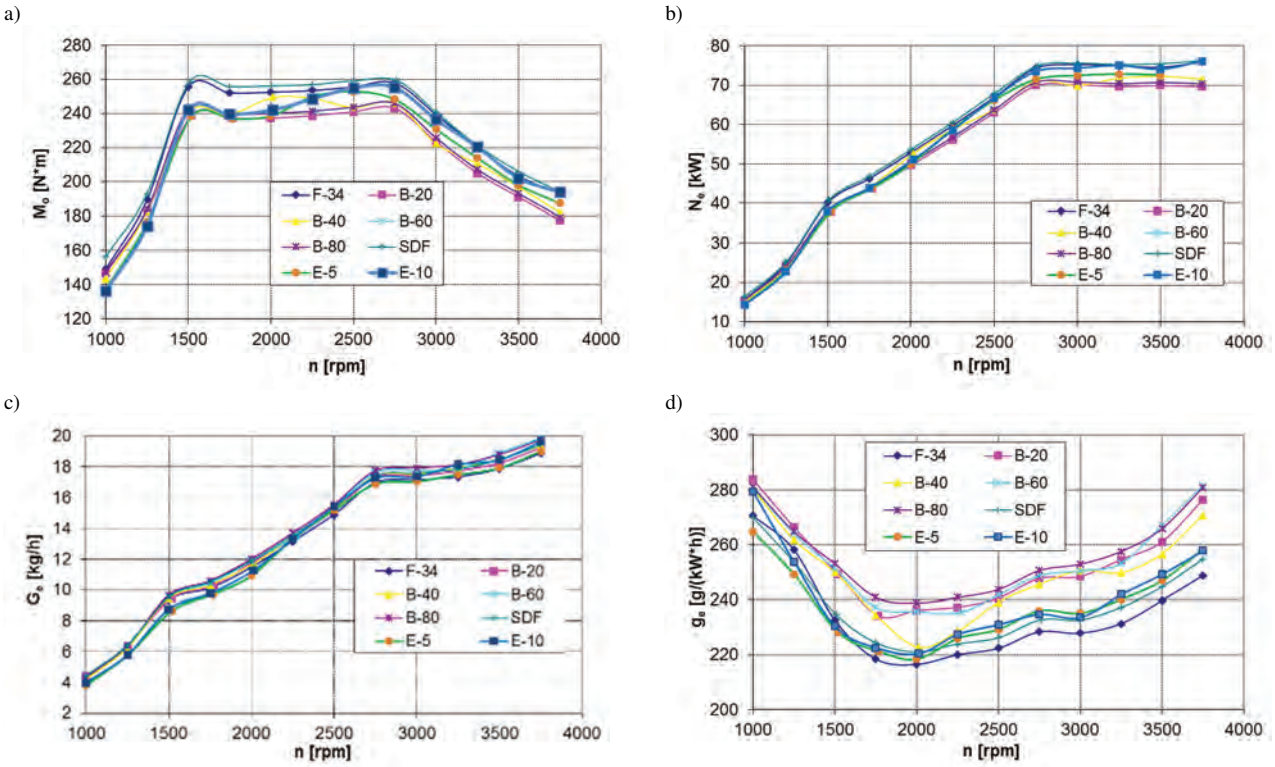

Fig. 1. External characteristic of the engine: a) torque, b) effective power, c) fuel consumption, d) specific fuel consumption

The least fuel consumption is reached for diesel oil (Fig. 1c), which is the basic fuel, although values for F-34 fuel are very similar. Using RME in fuel mixtures caused increasing of fuel consumption (Ge) ca. (3–5)% depending on F-34/RME ratio and rotated speed of the engine. The addition of bioethanol caused a drop in hourly fuel consumption (Ge) by about (6–8)%. depending on the concentration of bioethanol.

It is caused by lesser heat value of the mixture and necessity of delivering more fuel to the cylinder to reach the same effective power. In order to eliminate such impaired phenomena, it is necessary to modify the controller software in order to optimize the time and injection angle to a specific fuel mixture.

The least specific fuel consumption value was observed for the F-34 fuel (similar values for SDF) – Fig. 1d, 2d, which are 233 g/(kW·h) and 236 g/(kW·h) respectively with rotational speed n = 1500 rpm. Higher specific fuel consumption is caused by smaller heat value and bigger viscosity of RME. Bigger viscosity influenced on worse spraying and bigger heterogeneity of fuel stream. It caused incomplete combustion of air/fuel mixture. Changing the viscosity of fuel in order to the optimized results for engine control system was programmed, cause change injectors opening time, which negatively affects the process of creating a combustible mixture and its combustion.

The positive effect of F-34/RME mixtures' influence on emission of smoke was observed – Fig. 2f, 3a. The biggest amount of smoke was observed when the engine was fuelled with F-34 (similar values was for SDF), although with mixtures with of increased ratio of esters smoke is almost 2…3 times lesser for B-100. This trend is observed in whole range of the engine rotational speed. A littlelater beginning of injection caused strong growth of smoke emission when the engine is fuelled with diesel oil. Diminish of smoke emission is caused by lesser effective power as well. Impaired effect of F-34 fuel mixtures with bioethanol on the smokiness of fumes was observed – Fig. 2f, 3a. Increased, almost 5 times, in smoke opacity was noted for rotational speeds above n = 2500 rpm, which indicates the adverse impact of bioethanol on the process of feeding and burning. These changes are accompanied by an increase in the exhaust gas temperature.

Temperature of exhaust gases on outlet tube is the highest when the engine is fuelled with SDF and reaches 620°C with n = 1500 rpm – Fig. 3b. The lowest temperature ca. 592°C of exhaust gases was observed with mixture B-80 with n = 1500 rpm, it can be observed diminish of temperature of more than 45°C. There is observed that with increasing RME ratio in fuel mixture temperature of exhaust is lower. The addition of bio-ethanol to the F-34 fuel caused a significant increase of the exhaust gas temperature above the speed n = 2500 rpm, by about (20–30)°C, depending on the rotational speed. This is related to the extension of the self-ignition delay period and the shift of part of the combustion process to the exhaust stroke. This is a very unfavourable phenomenon due to the decrease in the efficiency of the engine and the possibility of thermal overloading of engine components – specifically turbochargers.

While rotational speed is low big concentration of carbon monoxide is observed. Increasing speed causes significant diminish of carbon monoxide concentration. The biggest concentration is observed during fuelling the engine with F-34. Mixture with RME caused diminish of its concentration in range of high speed of the engine ca. (10–15)% –Fig. 4a. Lower concentration of carbon monoxide in

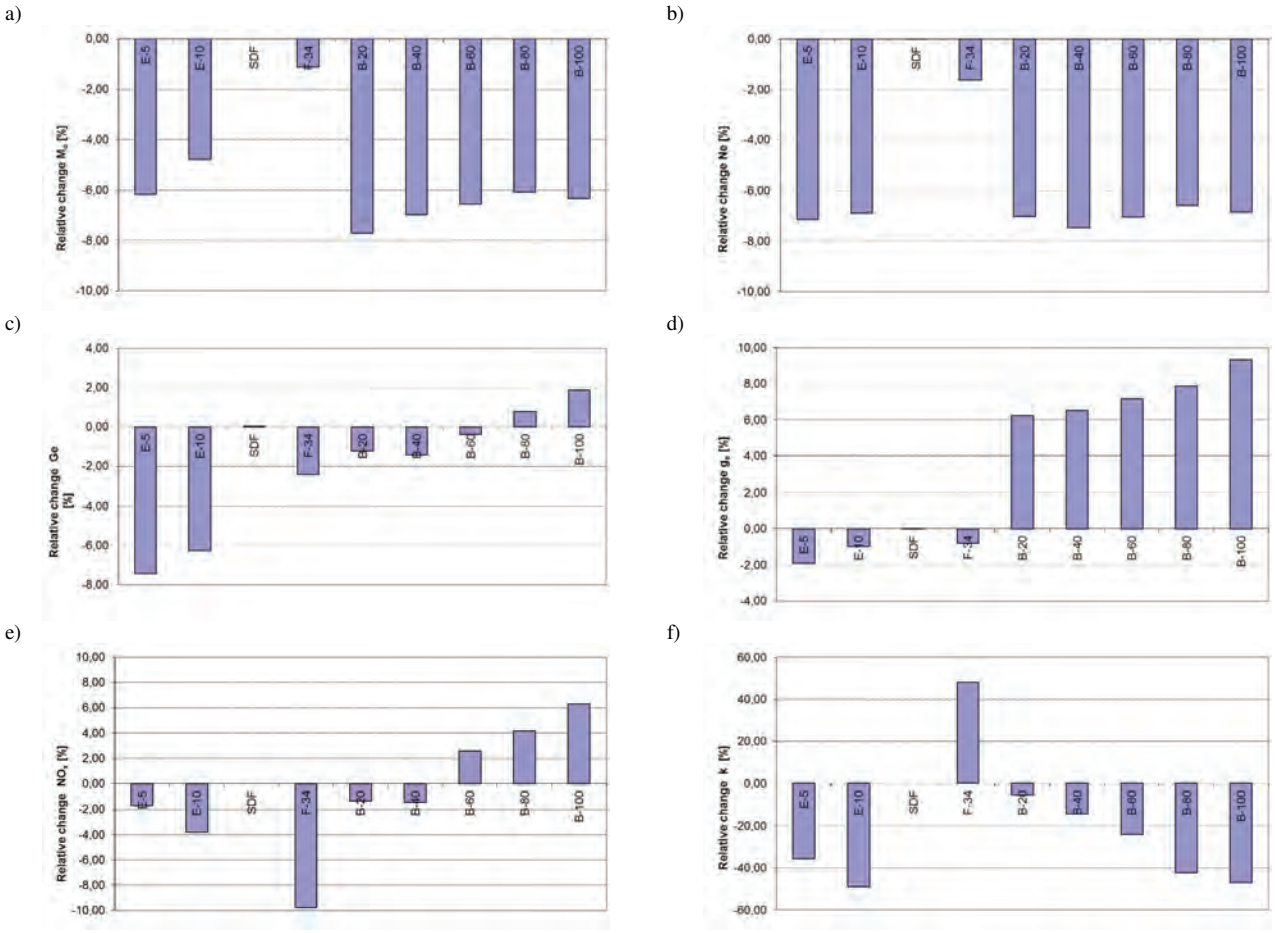

Fig. 2. Relative changes in engine operating parameters for maximum torque – 1500 rpm: a) torque, b) effective power, c) fuel consumption, d) specific fuel, e) concentration of nitrogen oxides in exhaust, f) extinction coefficient of absorbed radiation

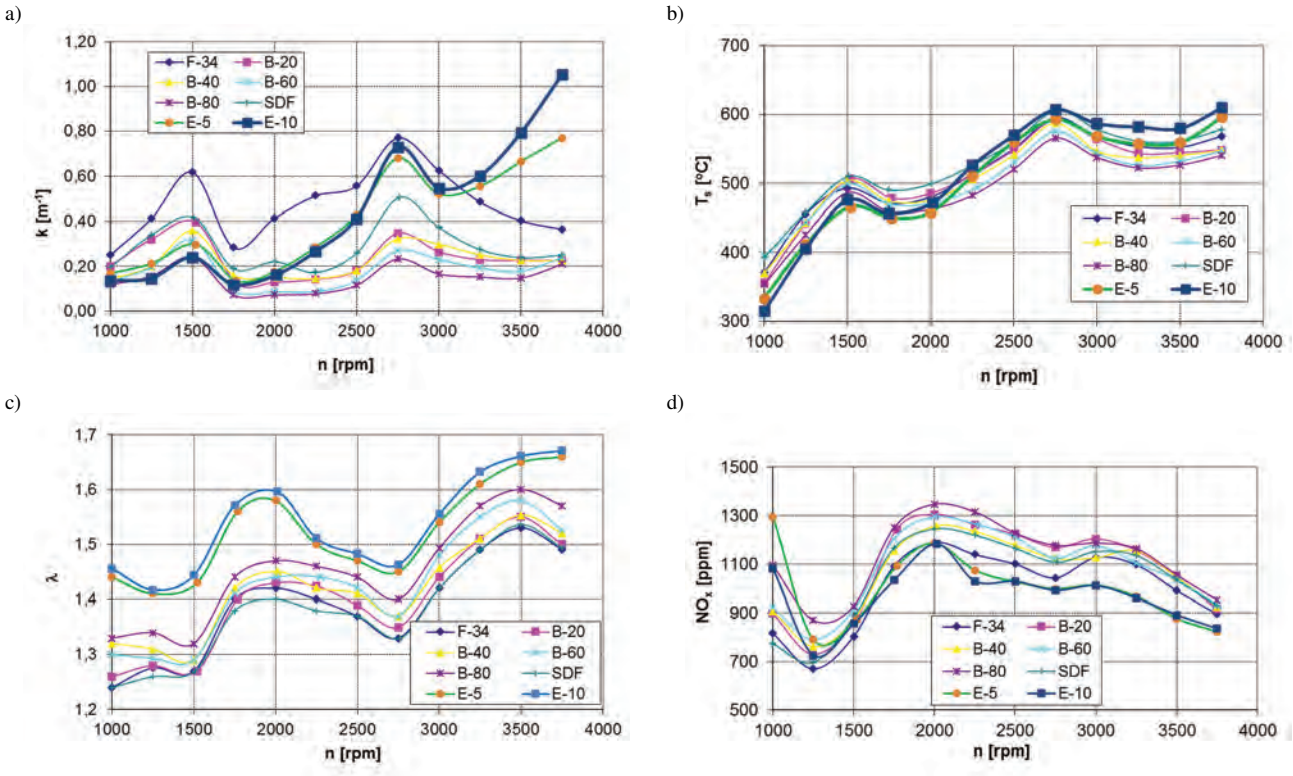

Fig. 3. External characteristic of the engine: a) extinction coefficient of absorbed radiation , b) temperature of exhaust gases, c) air/fuel ratio coefficient, d) concentration of nitrogen oxides in exhaust

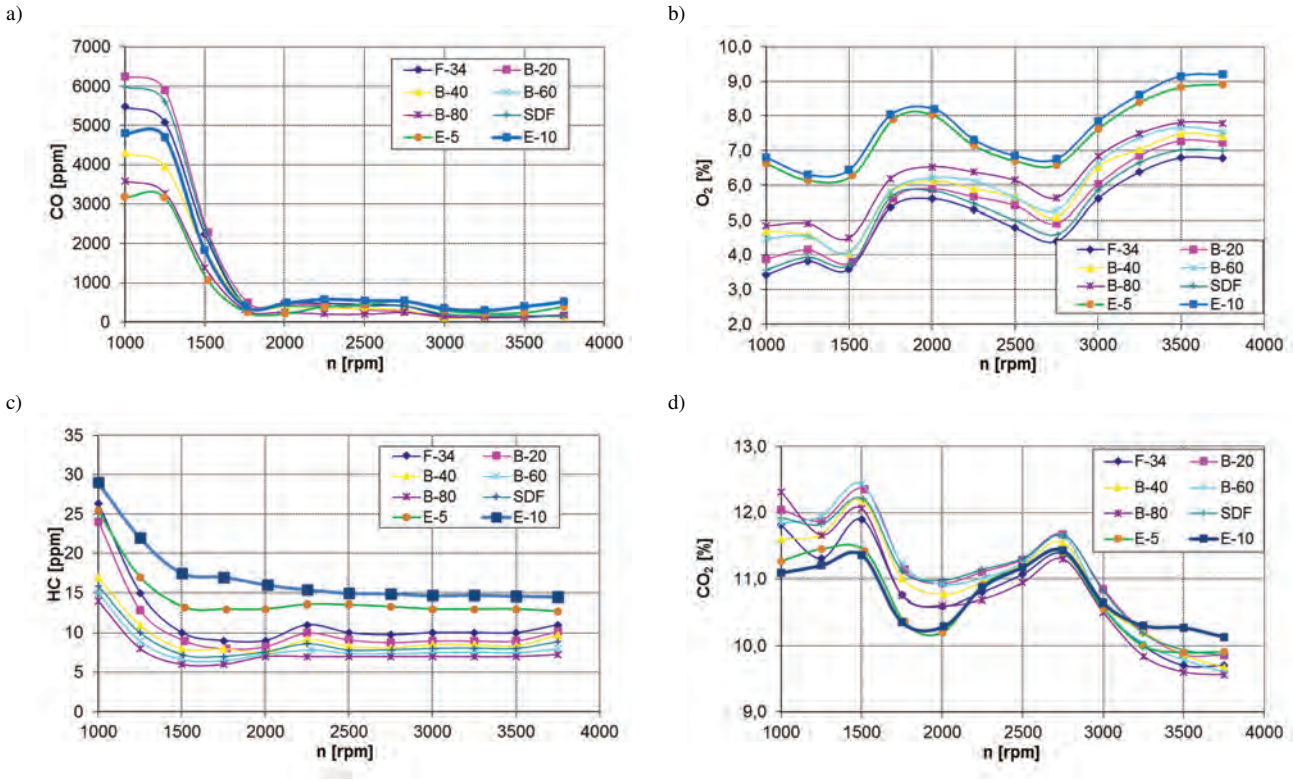

Fig. 4. External characteristic of the engine: a) concentration of carbon monoxide in exhaust, b) concentration of oxygen in exhaust, c) concentration of hydrocarbons in exhaust, d) concentration of carbon dioxide in exhaust

exhaust during fuelling of the engine with F-34/RME mixture testifies about changing of combustion process in compare to pure F-34 and SDF. RME additives positively influenced on carbon monoxide concentration in range of low speed of the engine. When rotational speed is above 1500 rpm it is on the same level, without regard on used kind of fuel.

The lowest value is seen during fuelling with F-34 and SDF. The biggest during fuelling with B-80 – increasing reach ca. (20–25)% – Fig. 4b.

Concentration of hydrocarbons in exhaust gases is about 50% lower when fuelling with B-80 mixture for all range of the engine speed (Fig. 4c). Lower concentration of hydrocarbons in exhaust is a result of higher concentration of oxygen in air/fuel mixture as it was in case of carbon monoxide.. Concentration of carbon dioxide is opposite to oxygen concentration. The lowest value is observed for F-34 fuel and the highest (ca. (6–10)% for F-34/RME mixtures – Fig. 4d).

4.1. Influence of F-34 and RME mixture on working parameters of the engine

Analysis of combustion process in the G9T engine combustion chamber was carried on the basis of the engine working cycles investigation. During investigation several dozen of combustion processes cycles were saved, and next 10 of them were statistically recalculated and characteristic parameters of combustion process were found. the maximum value of pressure and angle of auto-ignition delay are shown on graphs. The angle of auto-ignition delay is appointed as a difference between start of an injector needle lift and start of an active combustion in the engine chamber, which was determined based on the change in the derivative of the pressure course in the engine's combustion chamber

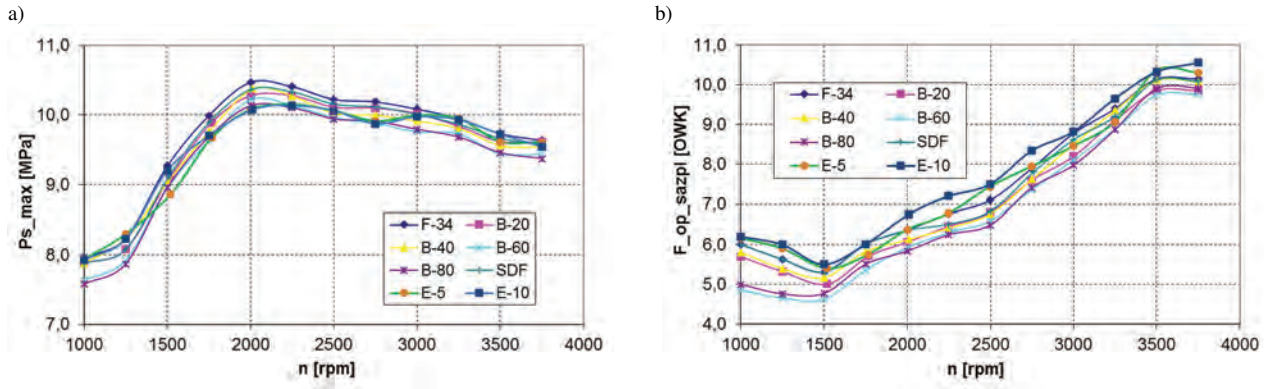

Fig. 5. External characteristic of the engine: a) maximum combustion pressure, b) angle of auto-ignition delay

Significant differences are seen on line of maximum pressure in the combustion chamber. The highest values of pressure were measured on F-34 and SDF fuels. This values are similar but a little bit higher in case of F-34 fuelling. This differences are no higher than 0.1 MPa (Fig. 5a). When mass ratio of RME increasing in a fuel mixture the diminish of maximum pressure value in the chamber is observed. The lowest values were observed for B80 mixture. Differences between maximum value for F-34 and SDF fuels and minimum value for B80 mixture were ca. 0.4 MPa in almost all range of rotational speed of the engine. The reason of such high decrease of pressure value is the lower dose of energy (lower heat value of fuel mixtures) consisted in fuel dose injected to the combustion chamber as well as longer time of injection. It causes slower heat transfer and diminish of peak values of combustion pressure.The addition of bioethanol in the F-34 fuel increases the maximum pressure in the combustion chamber. This is related to the increase of the self-ignition delay angle (decrease in the number of cetane mixture). This phenomenon is disadvantageous due to the increase of mechanical loads of the crank-crank system and the probable increase of noise emission.

After analysing the influence of RME ratio in F-34 fuel on the angle of auto-ignition delay (Fig. 5b) it is seen, that increasing of RME ratio causes shortening of angle of auto-ignition delay. The lowest values of angle of auto-ignition delay were observed for B80 mixture, and the highest were for F-34 fuel. For rotational speed n = 1000 rpm difference is ca. 1^{o} of crank shaft rotation (CSR) and it decreases with the increase of rotational speed. For speed n = 3500 rpm is equal 0.2^{o}CSR. Shortening of angle of auto-ignition delay for B80 fuel mixture is caused by lower temperature of auto-ignition as well as oxygen ratio in RME, which influence on speeding up of fuel oxidation. Observing the influence of the bioethanol content in F-34 fuel on the ignition delay angle (Fig. 5b), it can be noticed that the increase of bioethanol content causes a significant extension of the auto-ignition delay angle by about 1^{o}CSR, which is the result of a very small number of cetane bioethanol.

5. Conclusion

The usage of unconventional fuels for fuelling of military vehicle engines nowadays is a wide disputed problem. The numerous investigations about adaptation of renewable fuels for fuelling of diesel engines are lead. The best matches for fuelling diesel engines are methyl esters of fatty acids. In Poland they are acquired with processing of rapeseed oil (RME).

As the result of investigation it was ascertained that the G9T Renault engine parameters equipped with the Common Rail system fuelled with F-34/biocomponent mixtures changed in comparison to standard F-34 or DF fuels. It is possible to power the engine with the high-pressure common rail supply system with the aviation fuel mixtures F-34/F-35 and RME

On the basis of the research it is to be said that:

- the diminish of the engine effective power reaches 15% (depending of the engine work condition or used fuel mixture), during fuelling with F-34/RME mixtures,
- in comparison to F-34 and DF fuels, lower effective power of the engine is connected with lower heat value of RME,
- specific fuel consumption is 15% higher for F-34/RME mixtures especially in ranges of high speed and load of the engine,
- using RME as additives for F-34 fuel causes the diminish of carbon monoxide concentration up to 15% especially in range of low values of rotational speed and load of the engine,
- increasing of oxygen ratio in exhaust gases of ca. 25% is caused by presence of oxygen in RME molecule,
- hydrocarbons concentration in exhaust gases is lower up to 50% during fuelling the engine F-34/RME mixture.
- The addition of bioethanol adversely affects the engine's operating parameters – smoke and exhaust gas temperature increase. Several hours of engine operation on the E-10 mixture led to damage to the power system – obstruction of one section of the high-pressure pump and the injector.

The investigation about unconventional fuels application contributes to its introduction to mass production. Leading that investigation is crucial because it lets us to evaluate the influence of fuel composition on engine's work in different load and speed condition. The next stages of the researches will be based on the influence of the ternary mixtures (F-34 fuel, RME and bioethanol) on the performances of the diesel engine with Common Rail.

Nomenclature

CSR	crank shaft rotation	DI	direct injection
RME	Rapeseed Methyl Esters	SDF	military standard diesel fuel

Bibliography

[1] AMBROZIK, A., KRUCZYŃSKI, S., JAKUBIEC, J., ORLIŃSKI, S. Wpływ zasilania silnika spalinowego o zapłonie samoczynnym paliwem mineralnym i roślinnym na proces wtrysku oraz rozpad strugi paliwa. *Journal of KONES Powertrain and Transport*. 2006, **3**(13), 21-28.

[2] BACZEWSKI, K., KAŁDOŃSKI, T., WALENTYNOWICZ, J. Sprawozdanie z realizacji pracy naukowo-badawczej. *Opracowanie koncepcji wdrożenia jednolitego paliwa do lotniczych silników turbinowych i silników wysokoprężnych.* Wojskowa Akademia Techniczna, Warszawa 2001.

[3] BACZEWSKI, K., KAŁDOŃSKI, T. Paliwa do silników o zapłonie samoczynnym. *WKŁ*. Warszawa 2004.

[4] BRZOZOWSKI, K., NOWAKOWSKI, J. Toxicity of exhaust gases of compression ignition engine under conditions of variable load for different values of engine control parameters. *Eksploatacja i Niezawodnosc – Maintenance and Reliability*. 2011, **4**(52), 56-62.

[5] CHONG, CH.T., HOCHGREB, S. Spray flame structure of rapeseed biodiesel and Jet-A1 fuel. *Fuel*. 2014, **115**, 551-558.
[6] DAISUKE, K., HAJIME, I., YUICHI, G. et al. Application of biodiesel fuel to modern diesel engine. *SAE Technical Paper*. 2006, 2006-01-0233.
[7] DAGAUT, P., GAÏL, S. Chemical kinetic study of the effect of a biofuel additive on Jet-A1 combustion. *Journal of Physical Chemistry A*. 2007, **111**(19), 3992-4000.
[8] HILEMAN, J.I., DONOHOO PEARL, E., STRATTON, R.W. Energy content and alternative jet fuel viability. *Journal of Propulsion and Power*. 2010, **26**(6), 1184-1196.
[9] HORN, U., EGNELL, R., JOHANSSON, B., ANDERSSON, O. Detailed heat release analyses with regard to combustion of RME and oxygenated fuels in an HSDI diesel engine. *SAE Technical Paper*. 2007, 2007-01-0627.
[10] KARCZEWSKI, M., SZCZĘCH, L. Influence of the F-34 unified battlefield fuel with bio components on usable parameters of the IC engine. *Maintenance and Reliability*. 2016, **18**(3), 358-366. DOI: 10.17531/ein.2016.3.6
[11] KARCZEWSKI, M., WALENTYNOWICZ, J., SZCZĘCH, L. et al. Sprawozdanie z realizacji pracy naukowo-badawczej. Określenie wpływu jednolitego paliwa F34/35 z biokomponentami na pracę wysokociśnieniowego układu zasilania typu „Common Rail". *Wojskowa Akademia Techniczna*. Warszawa 2010.
[12] MAYER, A., CZERWIŃSKI, J., WYSER, M. et al. Impact of RME/diesel blends on particle formation, particle filtration and PAH emissions. *SAE Technical Paper*. 2005, 2005-01-1728.
[13] SZLACHTA, Z. Zasilanie silników wysokoprężnych paliwami rzepakowymi. *WKŁ*. Warszawa 2002.
[14] PAŁUCHOWSKA, M., DANEK, B. Specyfikacje jakościowe bioetanolu i biopaliw do silników o zapłonie iskrowym. *NAFTA-GAZ*. 2009, **2**.
[15] SZABADOSA, G., BERECZKYB, A., AJTAIC, T., BOZÓKIC, Y. Evaluation analysis of particulate relevant emission of a diesel engine running on fossil diesel and different biofuels. *Energy*. 2018, **161**, DOI: 10.1016/j.energy.2018.07.154
[16] SZABADOSA, G., BERECZKYB, A. Experimental investigation of physicochemical properties of diesel, biodiesel and TBK-biodiesel fuels and combustion and emission analysis in CI internal combustion engine. *Renewable Energy*. 2018, **121**. DOI: 10.1016/j.renene.2018.01.048

Mirosław Karczewski, DEng. – Faculty of Mechanical Engineering, Military Academy of Technology.
e-mail: *miroslaw.karczewski@wat.edu.pl*

Article citation info:
BOGDANOWICZ, A., ZADRĄG, R. Identification of emission indicators harmful compounds for assessment of dynamic state of a marine diesel engine. *Combustion Engines*. 2019, **178**(3), 247-251. DOI: 10.19206/CE-2019-343

Artur BOGDANOWICZ
Ryszard ZADRĄG

CE-2019-343

Identification of emission indicators harmful compounds for assessment of dynamic state of a marine diesel engine

The operation of a ship's propulsion system is a variable process in time, which is described in both static and dynamic states. The mutual proportions between them depend primarily on a type of ship and tasks to which it was designed. In a case of special units of particular use (e.g. warships) and ships, which operate on narrow waters such as canals or port basins, participation of dynamic states is increasing significantly. Hence a necessity to analyze the dynamic states of marine diesel engines, among others in terms of their increased harmful compounds emission. The paper presents a methodology of engine dynamic state analysis, emission indicators that can be used to assess the dynamic state of a ship have been proposed. As an example of application, the analysis of harmful compounds emissions during dynamic states while a real cruise of navy ship has been carried out. It has been also proposed to use simple dynamics indicators such as single-base and chain indexes to describe the change in concentrations of harmful compounds in dynamic states.

Key words: *dynamic states, emission, marine diesel engine*

1. Introduction

The operation of a ship's propulsion system is a variable reaction in time, which is described in both static and dynamic states. The mutual proportions between them depend primarily on a type of ship and tasks to which it was designed. In the case of vessels carrying out passage between ports, dynamic states will account for a small share in an entire operational approach [8, 9, 12]. However, when we consider port areas and vessels operating in maneuvering a share of dynamic states of vessel is already a significant part of an operating time and should therefore be subject to separate considerations [6]. There are at least two reasons for this.

First of all, dynamic states are operating states of a marine diesel engine, forced by dynamic working conditions caused mainly by a changing moment of resistance [1]. This is when dynamic properties of processes occurring in marine diesel engines are clearly visible. An increasing load is accompanied by increasing dose of fuel, which clearly determines changes in a pollutant emission intensity. Emission intensity from an engine in its dynamic working states are strongly correlated with each other and depend primarily on a value of extortions that these states cause. The biggest extortion, both as to a value and a number of implemented extortions take place mainly in a port areas, which are close to human agglomerations, thus adversely affect on residents of these areas mainly healthily [5].

Secondly, with an additional converting mechanism, which should take into account, is a technical condition of an engine. During an implementation of a work process engine, its structure parameters change. It does not affect its performance, described by a set of output parameters. The relationship between structure parameters and output parameters of an engine allows, under certain conditions, to treat output parameters as symptoms of engine's technical condition, measured without dismantling it, because physicochemical processes occurring during working process and quantities describing them can generally be observed and measured from outside. These values include, among others, emission intensity of exhaust components [7].

The correct combustion process in an engine cylinder depends to a large extent on a properly operating intake system, which is ensure above all repeatability of a fuel injection process. Due to this repetition, it is not only important a beginning and end of injection, but also its course. The correctness of the first criteria (start and end of injection), in classic power systems, to a large extent, protects a high pressure fuel pump through such control parameters as: fuel dose and injection advance angle, which in first place should be treated as a basic parameter determining correctness of combustion process in diesel engines. In fact, even its slight deviations result in significant changes in a main engine performance indicators, including emission indicators[13].

Unless, as previously mentioned, the fuel pump corresponds to the beginning and the end of injection, the injector is responsible for its course, and more precisely parameters that describe its operation. The most important control parameter, determining a shape of injection, its correctness, and above all repeatability, is opening pressure of the injector. This parameter, compared to previously mentioned, undergoes the most frequent changes during exploatation of engine, and although its effect on combustion process is incomparably smaller than, for example, the angle of advance of fuel injection and it must be taken into account when analyzing combustion process. This parameter determines quality of fuel atomization, and thus preparation of a homogeneous combustible mixture in cylinder, which is particularly important in dynamic states forced by dynamic operating conditions. It is forced mainly by variable moment of resistance, when extortions regarding power supply are particularly important. The remaining parameter, on injector side, affecting injection process, concentrate on parameters describing geometric parameters of atomizer, which it is known, also undergoes changes during use. It could be a result of erosive fuel interaction for example.

Taking above into account, the analysis of engine dynamic states aimed primarily at their comparison, including their high variability, should focus on unambiguous determination of both the beginning and end of dynamic state and its course. In this case, it is desirable to use criteria that

would help in the objective assessment of comparative concentration or emissions from dynamic states. The use of assessment indicators is one of commonly used methods in such cases.

2. Evaluation indicators of dynamic states.

Besides static states where emission level is relatively constant, dynamic states are also present. The nature of these changes depends on various extortions. These extortions can generally be divided into controllable ones, which are related to a way of controlling a ship and external extortion – dependent on atmospheric conditions.

The following relationship can be used to evaluate the dynamic state [13]:

$$W_i = a_i \int_o^t C_{j,i}(t)dt \tag{1}$$

where: W_i – emission rating indicator, $C_{j,i}(t)$ – concentration of any toxic compound at time t [ppm], a_i – factor characteristic for a given compound j: a_{CO} = 0.000966, a_{HC} = 0.000478, a_{NOx} = 0.001587, t – time duration of transient state [s].

By integrating an area under a curve obtained from experiment or model, an integration curve is determined which describes a direction of changes in dynamic state. On the other hand, this indicator still does not describe a nature of changes. As is known from observation, depending on a value of extortion, a course of transient can significantly differ. These differences usually depend on an intensity course of individual phases in a transient state. Usually, two phases can be specified in course of a typical transient. The first one, characterized by the greatest dynamics of changes, which is accompanied by a sharp increase in harmful compounds concentration, as a rule, many exceeding the steady-state concentration. The second phase of transient state is characterized by a much less rapid course, it is monotonic in character and asymptotically approaches values of concentrations from steady states.

The following relationship can be used to identify the beginning and end of a dynamic state:

$$S_i = \frac{dC_{j,i}}{dt} \tag{2}$$

where: S_i – indicator of the beginning and end of the dynamic state, $C_{j,i}(t)$ – concentration of any toxic compound at time t [ppm], t – time duration of transient state [s].

In order to correctly identify dynamic states, analysis of concentration selected harmful compounds registered during a 30 minute cruise of navy ship was carried out. The concentration changes are shown in Fig. 1. The measurements were carried out using the portable TESTO 350 analyzer (Fig. 2). The analyzer data are presented in the Table 1.

The first step in analyzing recorded concentrations (Fig. 1) was identification of static and dynamic states. For this purpose, histograms were built that grouped concentration values of individual compounds in characteristic classes. A graphical example of this analysis is the histogram of nitrogen oxides concentration (Fig. 3).

To make a histogram it is necessary to determine size of data set (measurements), then determine data range and

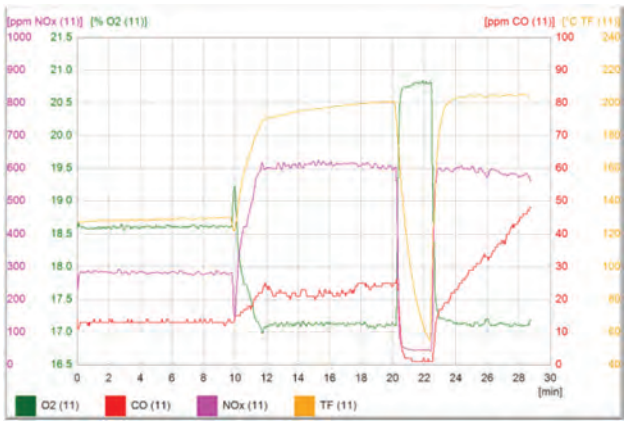

Fig. 1. Concentrations of harmful compounds during ship's operating

Fig. 2. Portable TESTO 350 analyzer [11]

Table 1. Parameters and measuring ranges of the TESTO 350 analyzer [11]

Parameter	Measuring range	Tolerance
ºC (exhaust gas)	from -40 to + 1000ºC	max. ±5 K
O_2	from 0 to 25 %	According to MARPOL, Annex VI or NOx Technical Code
CO	from 0 to 3000 ppm	
NO	from 0 to 3000 ppm	
NO_2	from 0 to 500 ppm	
SO_2	from 0 to 3000 ppm	
CO_2 (IR)	from 0 to 40 %	
P_{abs}	from 600 to 1150 hPa	±5 hPa in 22ºC ±10 hPa from –5 to +45ºC

specify number of intervals. Due to the relatively large data set (registration time 30 min, sampling frequency of the analyzer 1 s), the so-called Smirnov pattern [4]:

$$m = 1 + 3.322 \ln N \tag{3}$$

where: m – number of intervals (classes), N – number of observations (measurements).

Then width of compartment is determined according to relationship:

$$\Delta x = \frac{x_{max} - x_{min}}{m} \tag{4}$$

where: x_{min} – minimum value of data, x_{max} – maximum value of data, m –number of intervals.

Let χ_i represents the output data variable x then:

$$\chi_i = x_{min} + 0.5 \cdot \Delta x + i \cdot \Delta x \quad (3)$$

for i = 0, 1,…, m – 1.

Defining i-th interval, which is to be a range of values from to, but is not including:

$$\Delta_i \in (\chi_i - 0.5 \cdot \Delta x, \chi_i + 0.5 \cdot \Delta x,) \quad (6)$$

for i = 0,1,…,m-1.

The function defined will have the form:

$$y_i(x) = \begin{cases} 1, & \text{when } x \in \Delta_i \\ 0, & \text{elsewhere} \end{cases} \quad (7)$$

Finally, the histogram sequence is evaluated: for i = 0, 1,…, m – 1

$$h_i = \sum_{j=0}^{n-1} y_i(x_j) \quad (8)$$

where: n – number of input elements of the histogram.

The histogram analysis of nitrogen oxide concentrations shows that during the cruise there were three static states in which concentrations reached the following values: 0–50 ppm, 250–300 ppm and 550–600 ppm. The ship lasted the longest in a state where it reached 550–600 ppm, while the shortest was in the state in which concentrations reached value of up to 50 ppm. During this time, main engine of the ship was running idle. Other histogram values are assumed as dynamic states (Fig. 3).

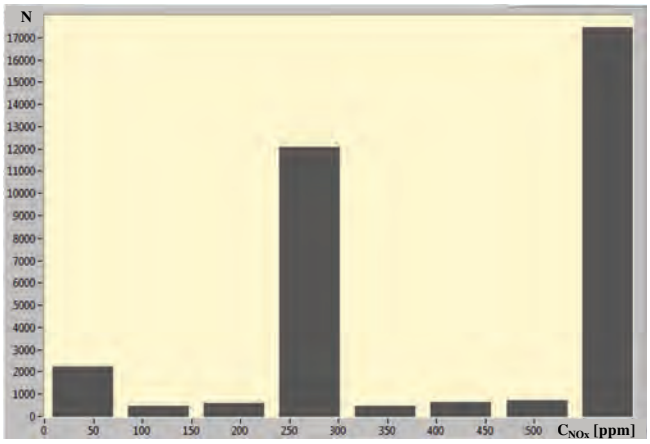

Fig. 3. Histogram of nitrogen oxide concentrations in static states

In order to carry out a correct concentration analysis of harmful compounds during dynamic states, it is necessary to perform filtration of individual time transitions and subject them to further processing eliminating accidental errors and errors related to measurements. For this purpose, a low-pass Butterworth filter has been used. This filter, in relation to other filters, is characterized by the fact that it has a flat course of the amplitude characteristic in a bandwidth. Dynamic state analysis was performed based on the LabVIEW development environment [2].

Figure 4 shows course of nitrogen oxides concentration after filtration.

By identifying the beginning and end of dynamic state, nitrogen oxides concentration in time course was differentiated to obtain waveform shown in Figure 5.

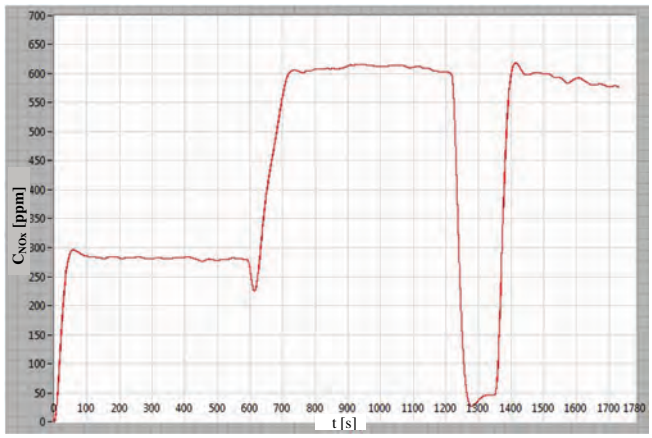

Fig. 4. Filtered course of nitrogen oxides concentration

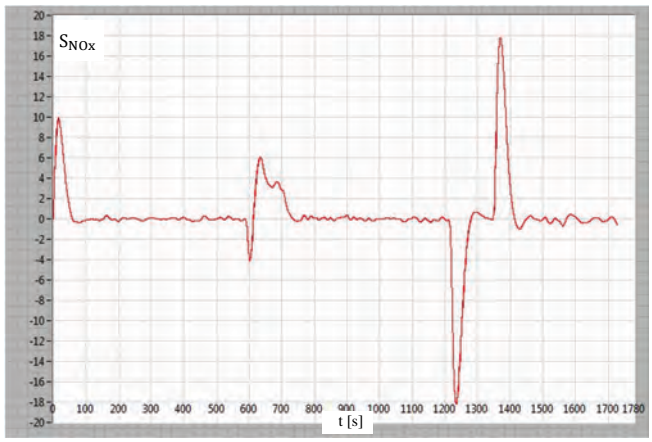

Fig. 5. Derivative course of nitrogen oxides concentration

Figure 6 shows integrated time course of nitrogen oxi-des concentration. In order to carry out a more thorough analysis, integrating defined ranges of transient states should be performed, however, according to goal set by authors, determine the beginning, end and direction of changes in dynamic state, course of obtained curve is sufficient.

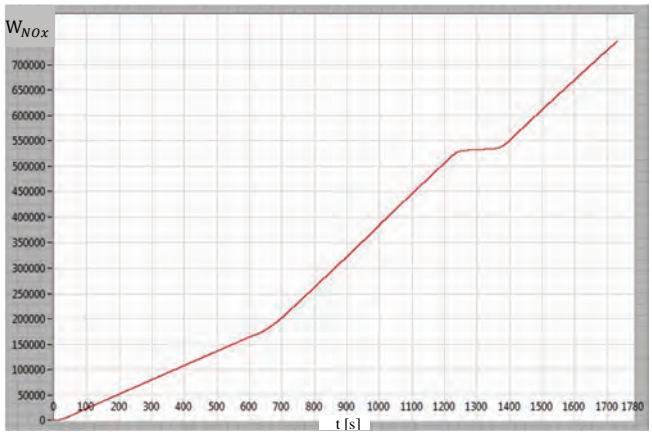

Fig. 6. The integrated course of nitrogen oxides concentration

From presented runs, it is possible to define time intervals in which dynamic states occurred during ship's cruise. In first minutes of the cruise there is a transitory state which will not be taken into consideration due to the lack of initial data. The values of differentials show speed of changes in

harmful compounds emission. They also show direction of changes in dynamic state. The obtained data presented, at time t = 600 s acceleration of the ship, which ended after time t = 200 s. Subsequent changes in the ship's movement occurred between t_p = 1200 s i t_k = 1300 s. At that time, the ship stopped, then accelerated (from t_p = 1350 s to t_k = 1450 s) and then carried out next stages of ship's task.

In Figure 7, integrated and differentiated waveforms were placed with indication of dynamic states during the cruise of navy ship.

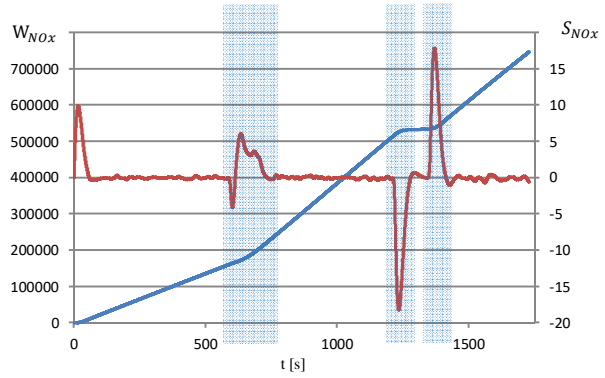

Fig. 7. Dynamic changes in the concentration of nitrogen oxides

Simple dynamics indicators may be used to describe dynamics of harmful compounds concentrations in which a given time series can be analyzed. These include single-base and string indexes. These indexes are widely used, for example in econometrics, but can be successfully used and in other applications.

Dynamics indexes are defined as follows [10]:

$$I = \frac{x_n}{x_0} \text{ or } I = \frac{x_n}{x_0} \cdot 100\% \tag{9}$$

where: x_n – a level of phenomenon during tested period, x_0 – a level of phenomenon during reference period.

These indexes are characterized by the following properties:

- indexes are non-negative numbers ($i \geq 0$),
- indexes are non-dimensional numbers,
- if a level of phenomenon is equal, they are equal to one ($x_n = x_0$),
- in the case of reducing a value by 100%, we get information about percentage of level of phenomenon in n-th period being higher or lower than in an initial period.

Analyzing a given time series of harmful compounds concentrations in a form $C_{j,1}$, $C_{j,2}$,…, $C_{j,n}$ could be used single-base index or chain index strings.

The one-base indexes represent changes that occurred in level of phenomenon in subsequent periods in relation to period assumed as basic (base time). With regard to analysis of harmful compounds concentrations, single-base index is as follows [10]:

$$I_{n/0} = \frac{C_{j,n}}{C_{j,0}} \cdot 100\% \tag{10}$$

where: $C_{j,n}$ – harmful compound concentration during tested period, $C_{j,0}$ – harmful compound concentration during reference period.

Chain indexes inform what changes occurred in period considered in relation to previous period. For analysis of harmful compounds concentrations, chain index is as follows [10]:

$$I_{n/n-1} = \frac{C_{j,n}}{C_{j,n-1}} \cdot 100\% \tag{11}$$

where: $C_{j,n}$ – harmful compound concentration during tested period, $C_{j,n-1}$ – harmful compound concentration in previous period.

Figures 8–10 present changes in nitrogen oxides and carbon dioxide concentration during dynamic states. One-base indexes were used for analysis, while relative values of dynamics index were left. The first state refers to the time interval from t_p = 500 s do t_k = 800 s cruise mode depicted in Fig. 2. During this time the ship carried out a maneuver of increasing velocity. The presented characteristics in Fig. 8 show that during maneuver, a course of changing nitrogen oxide index is larger than the carbon dioxide index. The concentration of nitrogen oxides index has more than doubled and the carbon dioxide index more than 1.5 times compared to initial state. This may indicate that during the maneuver, thermal load of engine increased due to increase of fuel dose, whereas carbon dioxide concentration (which is closely related to fuel consumption) gently stabilized at set level.

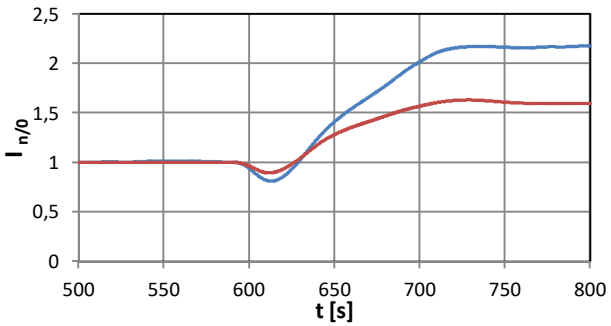

Fig. 8. One-base indexes of nitrogen oxides and carbon dioxide concentrations during acceleration maneuver. Blue line – $I_{n/0\ NOx}$, red line – $I_{n/0\ CO2}$

Figure 9 shows maneuver reducing velocity of the ship. This maneuver was carried out from t_p = 1150 s to t_k = 1350 s. The indexes of both concentrations overlap in entire analyzed range and set at a new level at the end of maneuver.

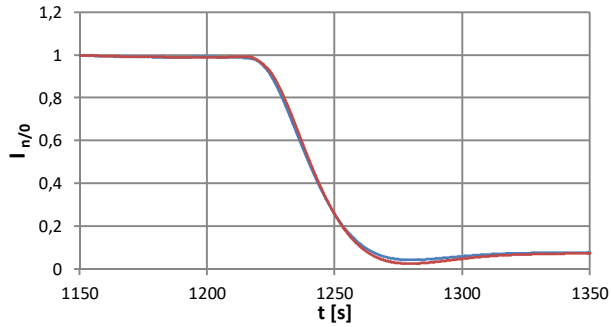

Fig. 9. One-base indexes nitrogen oxides and carbon dioxide concentrations during slowing down velocity. Blue line – $I_{n/0\ NOx}$, red line – $I_{n/0\ CO2}$

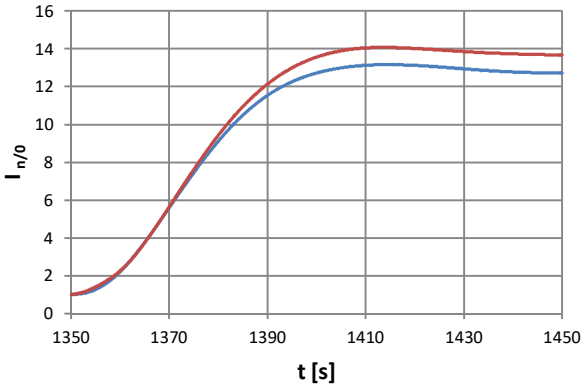

Fig. 10. One-base indexes of nitrogen oxides and carbon dioxide concentrations during acceleration maneuver from a place. Blue line – $I_{n/0\ NOx}$, red line – $I_{n/0\ CO2}$

The last maneuver during ship's cruise was acceleration from a place. This maneuver took place from t_p = 1350 s to t_k = 1450 s. In the first phase of maneuver to time t = 1370 s indexes overlap and then there were discrepancies. The curve of nitrogen oxides index is lower than carbon dioxide index (Fig. 10). In comparison with acceleration realized in time from t_p = 500 s do t_k = 800 s, this maneuver is characterized by a much more rapid course. The carbon dioxide concentration index was even fourteen times higher than initial value, while the nitrogen oxide index increased thirteen times compared to entry value of maneuver. In general, it is assumed an increase in concentration indexes in this range from eleven to fourteen times greater than initial value.

3. Summary

The paper presents the methodology for identification of dynamic states of toxic compounds concentrations. The use of simple indexes of dynamics as a tool that can describe time courses during transient processes of a marine diesel engine gives great possibilities of identification and then analysis of dynamic states. The application of chain indexes to describe changes in dynamic states emissions is only presented in the paper. Future studies should also include the analysis of measurement data using these indexes.

Due to the important role of extortion values as well as dynamics of their changes in future research, it would also be necessary to consider dynamic states related to changing an engine load and perform a comparative analysis with harmful compounds emission in synchronized time intervals of measuring instruments (e.g. sensor connected to the load indicator of governor with a device for measuring harmful compounds emissions). The obtained data should be subjected to filtration process and then, using tools presented in the paper, carry out a comparative analysis of harmful compounds concentration together with recorded load characteristics.

Further analysis of dynamic states should be focused on:

- carry out searching for indicators of engine's dynamic states, e.g. determining intensity of dynamic states by studying a slant of distributions,
- using neural networks to more accurately analyze dynamic states,
- conducting tests for typical ship engine damage and more accurate analysis of time courses using presented description methods.

Bibliography

[1] CARLTON, J. Marine Propellers and Propulsion. *MPG Books Ltd.*

[2] CHRUŚCIEL, M. Labview w praktyce. *Wydawnictwo BTC*. Legionowo 2008.

[3] GATNAR, E. Podejście wielomodelowe w zagadnieniach dyskryminacji i regresji. *Wydawnictwo PWM*. Warszawa 2008.

[4] GATNAR, E., WALESIAK, M. Statystyczna analiza danych z wykorzystaniem programu R. *Wydawnictwo PWM*. Warszawa 2008.

[5] KNIAZIEWICZ, T. Modelowanie procesów emisji spalin okrętowych tłokowych silników spalinowych napędu głównego w rzeczywistych warunkach eksploatacji. *Zeszyty Naukowe AMW*. Gdynia 2013.

[6] MARIN, *Sea shipping emission 2014. Final report*. Bilthoven Netherlands 2016.

[7] MERKISZ, J., PIASECZNY, L., KNIAZIEWICZ, T. Zagadnienia emisji spalin silników okrętowych. *Wydawnictwo Politechniki Poznańskiej*. Poznań 2016.

[8] PIASECZNY, L. Metody wyznaczania statycznych i dynamicznych charakterystyk emisji związków toksycznych z silników spalinowych statków morskich. *Sprawozdanie z projektu badawczego* N509 572 839. AMW Gdynia 2013.

[9] SCHULTEN, P. The interaction between diesel engines, ship and propellers during manoeuvring. DUP science is an imprint of *Delft University Press*. Delft 2005.

[10] STARZYŃSKA, W. Statystyka praktyczna. *Wydawnictwo PWM*. Warszawa 2012.

[11] TESTO 350 MARITIME, *Instruction manual*. Lenzkirch 2010.

[12] WOJNOWSKI, W. Okrętowe siłownie spalinowe. *AMW*. Gdynia 1998.

[13] ZADRĄG, R., ZELLMA, M. Modelowanie emisji związków toksycznych okrętowego silnika spalinowego podczas stanów nieustalonych przy zmiennym kącie wyprzedzenia wtrysku paliwa. *Journal of Polish Cimac*. 2014, **8**(1).

Ryszard Zadrąg, DEng. – Faculty of Mechanical and Electrical Engineering, Polish Naval Academy.
e-mail: *r.zadrag@amw.gdynia.pl*

Artur Bogdanowicz, MEng. – Faculty of Mechanical and Electrical Engineering, Polish Naval Academy.
e-mail: *a.bogdanowicz@amw.gdynia.pl*

Article citation info:
GALANT, M., FUĆ, P., KARDACH, M. Analysis of the ecological effectiveness of passenger transport by jets of various sizes. *Combustion Engines*. 2019, **178**(3), 252-256. DOI: 10.19206/CE-2019-344

Monika KARDACH
Marta GALANT
Paweł FUĆ

CE-2019-344

Analysis of the ecological effectivness of passenger transport by jets of various sizes

The article's aim was to compare an ecological effectiveness of a common jetliner with 189 passenger capacity flying on two CFM engines and a very light jet business aircraft designed to carry up to 8 people on board. The carried-out analysis showed that the NO_x emission per passenger in Very Light Jet (VLJ) is three times higher than in common jet airliner, furthermore there is 15 times difference in CO emission. Based on the results of the analysis, it can be stated that it is appropriate to extend the certification of engines to smaller units, as well as to adjust the LTO test beyond laboratory conditions.

Keywords: *LTO cycle, jet aircraft, air transport emission*

1. Introduction

Aircrafts and airports air pollutant emissions has had the increase of interest since the growth in commercial turbojet traffic in the 1970s. The whole transport branch including air transport is a cause of environment degradation. Pollutions, as well as, noise effective badly on human health. Aircraft Emissions influence climate change by [1]:

– greenhouse gases emissions (CO_2 mainly),
– ozone precursors emission,
– particular matter emission,
– clouds making.

In 2016 aviation was accountable for 3.6% of the total greenhouse gas emission and for 13.4% of the emissions from transport. Emission standards are established for the control of pollutants emitted from aircrafts. Most airports also set the limits on carbon dioxide emissions, which are directly related to the payment of airport charges [2, 11].

Regarding to emission factors for harmful compounds in the exhaust gas of aircraft engines, CO_2 emissions increased from 88 to 156 million tonnes (by 77%) between 1990 and 2005, but by only 5% between 2005 and 2014 [10]. The increase in emissions is not so significant compared to the increase in the number of passengers in the same period of time (2005-2014), which is due to better quality of fuels and the replacement of the old fleet of aircraft with a newer one. During this period, the average amount of fuel consumed per passenger-kilometer in passenger planes (excluding private jets) decreased by 19%. However, it is forecasted that the introduction of new technologies is not able to offset the effects of the growth of air traffic in the future and despite new technological solutions, an increase in CO_2 emissions by 44% is expected (from 144 Mt in 2005 to 207 Mt in 2035).

In the case of NO_x, a significant increase in their emissions can also be noted – by 85% (from 316,000 to 585,000 tonnes) between 1990 and 2005, and by 13% between 2005 and 2014 [10]. As in the case of CO_2 emissions, further increases in NO_x emissions are forecast despite the introduction of new construction solutions (constant introduction of a higher exhaust gas temperature before the high pressure turbine) – it is estimated that in 2035 NO_x emission will reach 920,000 tonnes (what will be an increase of 42% compared to 2005).

In the period 2005-2014, the emission of HC, CO and non-volatile PM particles was noted, but an increase of 7% of volatile particulate matter. However, it is forcasted that the emission of all these compounds will increase over the next 20 years.

The number of flights increased by 8% between 2014 and 2017, and grows by 42% from 2017 to 2040 in the most likely forecast. However, there is a growing trend of Passenger Load Factor (PLF). That trend means that the commercial airplanes are full in more than 80% (Fig. 1) and that affects on lowering the fuel consumption per passenger.

Fig. 1. Passenger Load Factor in commercial aircrafts worldwide since 2005 [13]

Although, the trend is positive, it can be noticed, that there is still some room for improvements.

There are number of emissions sources at the airports. They can be grouped in four categories:

– aircraft emission,
– aircraft handling emission,
– infrastructure or stationary- related sources,
– vehicle traffic sources.

In the article aircraft's main engine emission is taking into consideration [3–10].

2. Landing and Take-Off cycle

The emission of harmful exhaust gas compounds from combustion engines depends on operating conditions. The development of tests, aiming to assess pollutant emissions from various means of transport, is the key to minimize the human impact on the environment. An example of the test is LTO cycle mentioned in ICAO (International Civil Aviation Organization) Annex 16 about aircrafts' emission and noise. The LTO procedure was created to assess emission of harmful exhaust compounds from civil aircraft engines. The measurement is performed in stationary conditions. The flight of the aircraft is mapped by four phases: take-off – 100% Fc max (maximum thrust), climb – 85% of Fc max, approach – 30% of Fc max, taxiing – 7% of Fc max. Each of them has a different duration and power setting (Table 1). The whole test lasts about 30 minutes [12].

Fig 2. LTO cycle phases [14]

The durations of individual phase are proportional to the one in real conditions. The emission in LTO cycle is defined as mass of the harmful compound per mass of used fuel. Emission from one of aircraft's engines is a function of two parameters [9]: time-in-mode (TIM) – is the period that the aircraft engine actually spends at the specific power settings, main engine emissions indicate (EI) – the mass of pollutant emitted per unit mass of fuel burned for a specified engine. The EI for certified engines is provided by ICAO Engine Emissions Data Bank (EEDB) and fuel flow:

$$\mathrm{EPC} = (\mathrm{TIM} \cdot 60) \cdot \mathrm{FFR} \cdot \mathrm{EF} \cdot \mathrm{NE}$$

where: EPC – emissions per cycle for a particular mode [g⁄phase], TIM – Time in Mode [s⁄phase], FFR – fuel flow rate [kg⁄s], EF – emission factor [g⁄kg], NE – number of enigines on aircraft [-].

The LTO cycle is used for aircrafts over 27.6 kN of thrust and does not includes cruising phase above 3000 ft (915 m) above ground level (AGL). Certification procedures are carried out on a single engine in a test cell, referenced to static sea level and International Standard Atmosphere (ISA) conditions. It is widely recognized that the ICAO standards used in certification vary from actual aircraft emissions that occur in specific locations and operational situations. With the development of aviation, the LTO test started to be carried out more often, but not for its' original purpose. A new aim was an assessment impact of aircraft movement on environment in airports area. The cycle consists of four model phases representing: taxiing, approaching, taking-off and climbing (Table 1).

Table 1. List of parameters in the LTO cycle

Phase	Duration [min]	Power setting [%]
Approach	4	30
Take-Off	0.7	100
Climb	2.3	85
Taxiing	26 (7 in, 19 out)	7

Although, the LTO emission is an artificial model, created to certificate engines and the results are slightly different from real conditions, the test can be successfully used as a reference cycle to certify and demonstrate compliance with emission standards. Emission standards are covering CO, HC, NO_x and smoke emission of subsonic, supersonic aircrafts with turbofan and turbojet engines greater than or equal to 26.7 kN of thrust. Turboprop, piston, turboshaft engines and general aviation's aircrafts are excluded from standards due to its' small fuel usage compared to commercial het aircrafts. The certification data for CO, HC and NO_x all along with fuel flow rates are reported according to four different power settings (Table 1). However, smoke emissions are to be reported only as a maximum value of smoke density, reported as a smoke number for each engine. There are three possible approaches to the LTO cycle. The simple approach is the most elementary and requires publicly available data but provides the highest level of uncertainty which may results in overestimating the emission. The advanced approach takes into account specific information about the specific airport. Data needed are still publicly available but can be difficult to get. The most sophisticated approach is the best to obtain actual aircraft emission. It requires maximum amount of data available mainly to the aircraft user and wide analysis. It was notified, that the LTO cycle test results can vary with different operating times, power settings, airports, day-to-day, or even single day conditions for exactly the same type of aircraft. However, fixed conditions of LTO cycle provides a clear reference point from which differences in aircrafts emissions performance can be compared. Moreover, engine manufacturers always design their products for peak efficiency at delivery, as aircraft enter revenue service some performance degradation may be experienced over time due to the harsh environments aircraft and engines will operate in. Erosion, seal degradation and dirt build-up on finely-tuned rotating hardware and airframes over long periods of time can lead to performance loss. If left unchecked, the deterioration can result in noticeable fuel consumption increases over time. Fuel consumption increases are an unnecessary cost increase to the carriers, and as a result they will normally perform maintenance on their products to keep the level of performance loss at acceptable levels.

3. Analysis of jet aircrafts emission

The model airplanes selected for the analysis are:

1. Medium-range, mid-size, narrow-body, twin-engine jetliner, constructed mostly of composite materials with CFM56-7B24 engines,
2. Small business jet with a maximum take-off weight of or under 5000 kg and approved for single-pilot operations.

The aircrafts chose for the analysis are model ones, which means the calculations are suitable for a group of aircrafts, not a single one. For better understanding of the topic, examples have been used (Table 2).

Table 2. The comparison of two sample aircrafts [15, 16]

Aircraft type	Jetliner	VLJ
Aircraft sample model	Boeing 737 	Honda HA-420 
Unit cost	US$ 100.5 million	US$ 4.9 million
Wingspan	35.8 m	12.1 m
Range	7408 km	2234 km
Cruise speed	946 km/h	682 km/h
Max. take-off weight	78,245 kg	4808 kg
Engines	CFM56	GE Honda HF 120
Fuel capacity	20,924 kg	1290 kg

The exhaust gas of turbine engines includes: nitrogen oxides (NO_x), sulfur oxides (SO_x), carbon dioxide (CO_2), carbon monoxide (CO), unburned hydrocarbons (UHC) and particulate matter (PM). These compounds, as a result of further photochemical reactions occurring in the atmosphere, cause a number of adverse phenomena (acid rain, photochemical smog, increased tropospheric ozone, etc.). For the purpose of analysis, CO and NOx were chosen. The emission factor and Fuel Flow Rate necessary to make calculations come from ICAO emission databank. The results of the calculations carried out are presented in the form of diagrams to show the dependencies. As it results from the calculations made, the NOx jetliner emission per passenger is about three times smaller, than VLJ emission, assuming that both model planes were full. Furthermore, the CO emission is nearly 15 times less (Fig. 2). The amount of passenger seats available in jetliner is 189 and in VLJ – 8 [11].

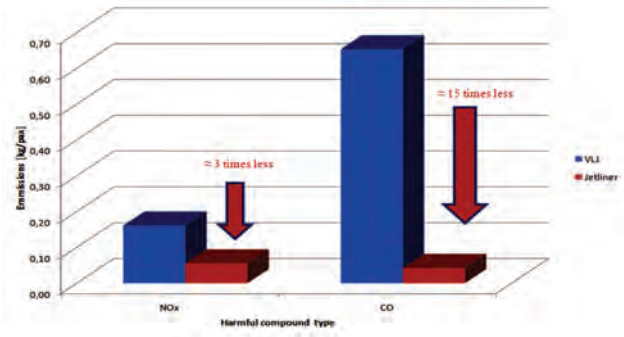

Fig. 3. Comparison between VLJ and jetliner's CO and NOx emission per passenger

Considering CO emission, it is ecologically advisable only to do VLJ flight up to 8 passengers. If there are more than 8 passengers, it is better to engage jetliner, because 2 VLJs emit more CO mass, than one jetliner (Fig. 4). It is optimistic from commercial airlines point of view. If the legislation is tightened, it is possible, that in the future businessmen will be forced to change into commercial aircraft.

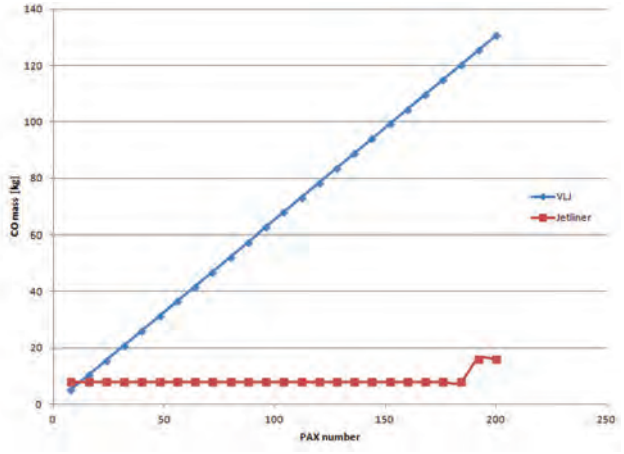

Fig. 4. Comparison between VLJ and jetliner's CO total emission per number of passengers

Analyzing the results considering NO_x emission, as it can be noticed (Fig. 5) according to NO_x emission it is better for ecological reasons to fly 8 VLJ with 8 people each than one jetliner with the same number of people on board. Even two jetliners capable of transporting 378 passengers are more ecologically efficient than 24 VLJs.

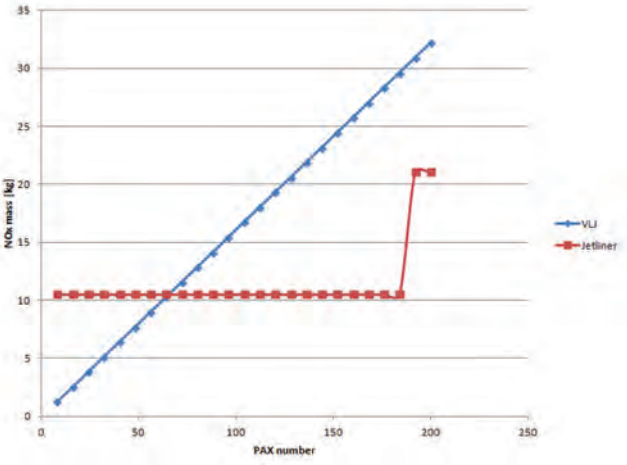

Fig. 5. Comparison between VLJ and jetliner's NOx total emission per number of passengers

Taking into consideration, that about 80% of aircrafts registered in USA are general aviation (for non-commercial purposes) it is advisable to extend the ICAO certification process and consider VLJ's engines in emission standards. Some of the airports around the world, especially big ones are charging aircraft carriers for their airplane's emission and noise. For example, at the Charles-de-Gaulle airport there are five emission classes and six acoustics groups of aircrafts (Fig. 6).

Paris - Orly et Paris Charles-de-Gaulle		
Acoustic group	Day and evening (06h00 - 22h00)	Night (22h00 - 06h00)
Group 1	1.300	1.950
Group 2	1.200	1.800
Group 3	1.150	1.725
Group 4	1.000	1.500
Group 5a	0.850	1.275
Group 5b	0.700	1.050

Fig. 6. Acoustic groups and charges for Paris Charles de Gaulle airport [17]

Due to ecological and social reasons, airport managers impose obligations on air operators to renew the fleet. Older, less effective, consuming more fuel airplanes are more expensive to operate. Bombardier DH8-Q400, ATR 42 I 72, Canadair Regional Jet CRJ-900 are among others in 1 class, which is the most expensive group. In 5th class there is only one airplane Airbus A380. Thus, it can be stated that exploiting the fleet consist of new aircrafts is not only advisable because of lower fuel consumption (A380 has a fuel consumption less than three liters per passenger per 100 kilometers) but also savings resulting from lower airport charges. Another way to reduce the adverse impact of airplanes on the natural environment is the appropriate shaping of flight routes, minimizing the emission of harmful compounds. This requires proper flight planning, taking into account the limitations resulting from the organization of the airspace and the rules in force there and current weather conditions. The weather is one of the most important factors affecting the amount of fuel used, time and cost of the flight. Also, from weather and altitude point of view it is better to fly higher, which effects in more stabilized weather conditions and less fuel consumption, further from the ground.

5. Conclusions

One of the solutions, which could have a positive impact for minimizing the fuel consumption rate per passenger is creating last minute first or business class option for businessmen. To encourage them to fulfill "empty legs", lower ticket prices and special, quick security control would be available for those who decides to exchange private jet for first or business class seat. Furthermore, it should be noted that the change in the time of individual phases of the LTO cycle has a significant impact on the volume of emissions from particular types of aircraft. For testing emission in airports areas, the adjustment should be done. Individual parameters should be special for each airport to get results much closer to the actual local emission. The differences are clearly visible for medium sized airports and for big ones they are significant. The two biggest programs established to limit the negative impact on the environment of air transport and cooperating industry are: SESAR 2020 and Clean Sky 2. First of them is to create new air traffic management solutions (what will diminish air transport impact on environment at about 10%), the second program concentrates on state-of-the-art technological solutions (new airplanes, propulsions, avionics).

It should be remembered that emissions from airport-related surface transportation can constitute a significant portion of the total emissions associated with airport activities. The stationary emission sources such as generators or heating plants emitting from fixed locations can not be forgotten either. There are more and more sophisticated ways to assess the air transport emission from the whole branch including the aircraft's engines on the construction stage, engines in use, stationary and movable equipment at the airport, as well as, airport's users and suppliers. There are special models possible to create in 3D technique, which enables the airport manager to asses and control the emission level during the airport opening hours. It is recommended to manage a comprehensive approach to the problem, so that the emission could be mitigated at every stage from aircraft designing and manufacturing, through ticket booking, to passengers' cars parking.

Nomenclature

AGL	Above Ground Level
CO	carbon monoxide
CO_2	carbon dioxide
EEDB	Engines Emissions Data Bank
EU	European Union
ICAO	International Civil Aviation Organization
ISA	International Standard Atmosphere
LTO	Landing and Take Off cycle
NO_x	nitrogen oxides
PLF	Passenger Load Factor
PM	particulate matter
TIM	time in mode
VLJ	Very Light Jet

Bibliography

[1] International Civil Aviation Organization (ICAO). International Standards and Recommended Practices. Annex 16 to the Convention on International Civil Aviation – Environmental Protection. *Aircraft Engine Emissions*. 3rd edition. 2008, **2**.

[2] MERKISZ, J., MARKOWSKI, J., ŚLUSARZ, G. et al. Comparative analysis of exhaust emission tests for a turbine engine. *Combust. Engines*. 2015, **162**(3), 449-455.

[3] PAWLAK, M., MAJKA, A., KUŹNIAR, M., PAWLUCZY, J. Emission of selected exhaust compounds in jet engines of a jet aircraft in cruise phase. *Combustion Engines*. 2018, **57**(2), 67-72.

[4] International Civil Aviation Organization (ICAO). Operational opportunities to minimize fuel use and reduce emissions Cir 303/AN176. 2003.

[5] MAJKA, A. Ekologiczne aspekty wspomagania startu samolotu systemem wykorzystującym zjawisko magnetycznej lewitacji. *Logistyka.* 2015, **4**, 593-602.

[6] International Civil Aviation Organization (ICAO). Environmental Branch, ICAO Environmental Report 2016, aviation and climate change. 2016.

[7] EEA, EASA and Eurocontrol. European Aviation Environ-

mental Report 2019. 2019.
[8] International Civil Aviation Organization (ICAO). Guidance on Aircraft Emissions Charges Related to Local Air Quality, Doc 9884. 2007.
[9] International Civil Aviation Organization (ICAO), Airport air quality manual. 2011.
[10] PAWLAK, M., KUŹNIAR, M. Problematyka emisji toksycznych składników splain silników lotniczych. *Autobusy*. 2017, **12**, 338-344.
[11] NOWAK, M., JASIŃSKI, R., GALANT, M. Implementation of the LTO cycle in flight conditions using FNPT II MCC simulator. *IOP Conference Series: Materials Science and Engineering*. 2018, **421**, 10.
[12] MERKISZ, J., GALANT, M., KARIŃSKI, D., KUBIAK, K. Evaluation of possibility to use the LTO cycle for emission test on example of the model turbine engine GTM-120. *J. Mech. Transp. Eng.* 2014, **66**(2), 25-33.
[13] www.statista.com
[14] www.easa.europa.eu
[15] www.boeing.com
[16] www.hondajet.com
[17] www.parisaeroport.fr

Monika Kardach, MEng. – Faculty of Transport Engineering, Poznan University of Technology.
e-mail: *monika.t.kardach@doctorate.put.poznan.pl*

Marta Galant, DEng. – Faculty of Transport Engineering, Poznan University of Technology.
e-mail: *marta.galant@put.poznan.pl*

Paweł Fuc, DSc., DEng. – Faculty of Machines and Transport at Poznan University of Technology.
e-mail: *pawel.fuc@put.poznan.pl*

Article citation info:
WOLFF, A. Influence of piston ring profiles and oil temperature distribution on cylinder liner lubrication of a marine two-stroke engine. *Combustion Engines*. 2019, **178**(3), 257-263. DOI: 10.19206/CE-2019-345

Andrzej WOLFF

CE-2019-345

Influence of piston ring profiles and oil temperature distribution on cylinder liner lubrication of a marine two-stroke engine

In the paper a comprehensive model of a piston-ring-cylinder (PRC) system has been presented. The local thickness of the oil film can be compared to height of the combined surface roughness of a cylinder liner and piston rings. Equations describing the mixed lubrication problem based on the empirical mathematical model formulated in works of Patir, Cheng and Greenwood, Tripp have been applied. The main parts of the model have been experimentally verified abroad by the author at the marine engine designing centre.

In contrast to the previous papers of the author concerning the PRC system of combustion engines, new calculation results for a marine two-stroke engine have been presented. Firstly the right selection of barrel-shaped sliding surface of piston rings has been analysed. Secondly the influence of oil temperature distribution along the cylinder liner on the lubrication of the PRC system has been assessed. The developed model and software can be useful for optimization of the PRC system design.

Key words: *marine engines, piston rings, gasdynamics, hydrodynamic lubrication, mixed friction*

1. Introduction

Piston rings are important part of internal combustion engines. Commonly a set of piston rings is used to form a dynamic gas seal between the piston and cylinder wall [5, 6, 13]. The sliding motion of the piston forms a thin oil film between the ring land and cylinder wall, which lubricates the sliding components [2, 4, 11]. The hydrodynamic force generated by this thin oil film is opposed by a combination of the gas pressure acting on the back side of each ring and the ring stiffness. Due to the dynamic nature of these forces, each individual ring is periodically compressed and extended as the piston runs through its cycle. The problem of studying this interaction is further complicated by the high temperatures involved, as these result in low oil viscosity and subsequently very low oil film thickness. The oil film is typically thick enough to expect the existence of mixed lubrication, so this phenomenon should also be taken into account [2, 7, 8, 12, 13]. The use of modern oil of low viscosity, working at a high temperature causes the existence of a very thin oil film thickness comparable to the value of the liner surface roughness. In such conditions, the possibility of direct contact between the ring and cylinder liner surface exists. Therefore the numerical simulation of these processes, which take place in a typical piston ring pack operation, is important from practical point of view.

The purpose of this paper is to present numerical calculations concerning an influence of selected barrel-shaped sliding surfaces of piston rings and oil temperature distribution on cylinder liner lubrication of the PRC system.

2. Modelling of piston ring pack operation

2.1. Developed sub-models

A combined model of piston rings operation has been developed. It consists of two main models: a) model of gas flow through the labyrinth seal piston-rings-cylinder (PRC), b) model of oil flow in the lubrication gap between the ring and cylinder liner. The two aforementioned models are coupled. In addition, sub-models of the following mechanical phenomena have been used: a contact of rough surfaces, an axial movement of rings within piston grooves and an elastic torsional deformation of piston rings (Fig. 1). All the sub-models are described in detail in publications [15–19] of the author. In this paper only the sub-model of mixed lubrication [3, 9, 18] is shortly presented.

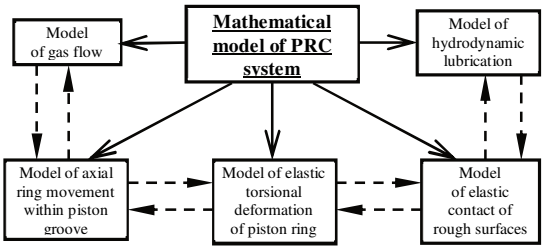

Fig. 1. Developed comprehensive model of the system: piston-ring-cylinder (PRC)

2.2. Model of mixed lubrication

Two main cases of oil flow in the system piston ring – cylinder liner are presented in Fig. 2.

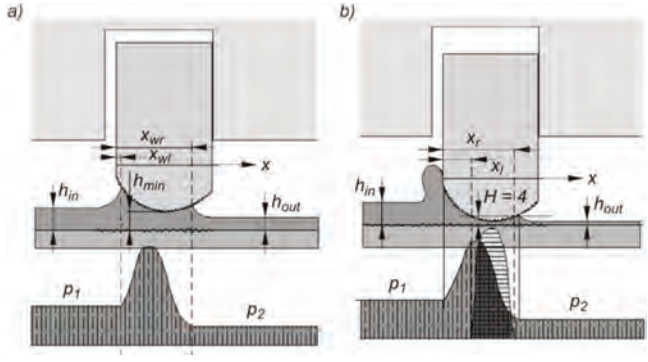

Fig. 2. Scheme of gap between the ring face and cylinder liner in the case of: a) fluid and b) mixed friction

A one dimensional form of the modified Reynolds equation developed by Patir and Cheng [9] has been used to calculate hydrodynamic forces in the case of rough gap surfaces. This equation is applicable to any general roughness structure and takes the following form:

$$\frac{\partial}{\partial x}\left(\phi_x \frac{h^3}{12\mu}\frac{d\bar{p}}{dx}\right) = \frac{U}{2}\frac{d\bar{h}_T}{dx} + \frac{U}{2}\sigma\frac{d\phi_S}{dx} + \frac{d\bar{h}_T}{dt} \qquad (1)$$

where: t – time; x – coordinate along cylinder liner; h – nominal oil film thickness; h_T – average gap (ring-cylinder); p – hydrodynamic pressure; U – axial ring velocity; μ – dynamic oil viscosity; $v = \partial h_T/\partial t$ – radial ring velocity, σ – composite root mean square roughness of sliding surfaces.

The significance and mathematical description of empirical coefficients ϕ_x , ϕ_S and boundary conditions of equation (1) are presented in [9].

The effects of interacting asperities of piston ring and cylinder liner surfaces were modelled using the mathematical model developed by Greenwood and Tripp [3]. In this case the asperity contact force per unit circumference is given by

$$F_C = 16\sqrt{\frac{2}{15}}\pi(\eta\beta\sigma)^2 E'\sqrt{\left(\frac{\sigma}{\beta}\right)}\int_{x_l}^{x_r} F_{5/2}\left(\frac{h}{\sigma}\right)dx \qquad (2)$$

where the integration limits x_l and x_r define a continuous interval, $x_l \le x \le x_r$ in which $h/\sigma \le 4$ and: E' – composite elastic modulus (for cylinder liner and piston ring); η – asperity density; β – asperity radius of curvature; σ – combined root mean square roughness of both sliding surfaces.

The form of function $F_{5/2}$ can be found in article [3]. The model is also described in detail in publication [18] of the author of this article.

2.3. Viscosity as a function of oil temperature

The viscosity of the oil used for lubrication is a key factor influencing oil film thickness. Marine engines have a relatively high temperature of oil film and due to that a relatively low oil viscosity. This explains the very thin oil film left by the periodically moving ring pack. In the analysis presented, it was assumed that the oil film temperature is equal to the liner temperature.

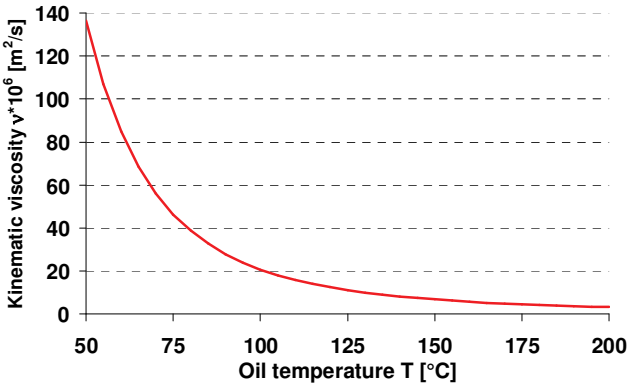

Fig. 3. Oil viscosity versus temperature

The temperature-dependent oil viscosity ν(T) was evaluated by the use of following equation (Fig. 3):

$$\log_{10}[\log_{10}(\nu + 0.8)] = A_\nu - B_\nu \log_{10} T \qquad (3)$$

where parameters: $A_\nu = 8.56$ and $B_\nu = 3.28$.

The assumed oil density $\rho = 940$ kg/m^3 and the lubricating oil feed rate at full engine load $g_{oil} = 1$ g/kWh [18].

2.4. The geometry of the ring lip

The sliding surface of a piston ring shouldn't be treated as an internal cylindrical or conical surface. It is rather a barrel-shaped surface (Fig. 4).

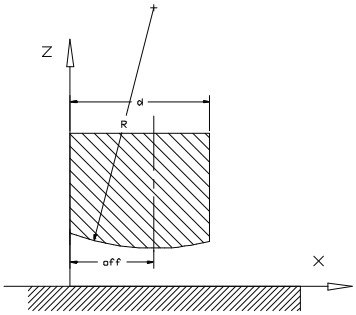

Fig. 4. Piston ring geometry: d – ring axial height, R - radius of the ring surface, O_{ff} – offset of the ring sliding surface

The profile of the sealing ring is described by

$$h(x) = h_{min} + \frac{(x - O_{ff})^2}{2R} \quad \text{for } 0 \le x \le d \qquad (4)$$

where: h_{min} – minimum gap height (Fig. 2); d – ring axial height, R - radius of the ring surface, O_{ff} – offset of the ring sliding surface.

One problem is the definition of the profile geometry of the scraper ring. Initially manufactured as a linear oblique surface with sharp edges, after approximately 600 hours of running it is worn out and its shape can be modelled as a parabolic with very large radius.

3. Experimental verification of developed model

A verification of the simulation model has been done by the author for a two- and four-stroke marine engine [15, 16, 18]. The experimental verification of the model of gas flow through the labyrinth seal of piston rings was carried out using measurements of unsteady gas pressure in the cylinder, between the piston rings and under piston performed by piezoelectric sensors mounted in the piston. A satisfactory qualitative and quantitative compatibility of the analyzed pressure variations has been achieved. The maximal relative differences between measured and calculated pressure values have not exceeded 15% [15, 18]. On the other hand, the experimental verification of the hydrodynamic model of piston rings involved measurement results of scraped oil volumes by a gland-box of a two-stroke marine engine. Unfortunately, similar measurements for piston ring packs of tested engines have not been carried out. Examination of scraped oil volumes by the ring pack (of the gland-box of marine internal combustion engine) proves a satisfactory quantitative agreement between numerical and experimental results. The maximal relative differences between measured and calculated values have not exceeded 10% [15, 18].

4. Calculation results

4.1. Main data of chosen engine

The computer program incorporating the presented model has been used for simulation of two-stroke Diesel engine (Table 1) operating at full load.

Table 1. Main data of the marine engine under consideration [14]

Cylinder bore	960 mm
Piston stroke	2500 mm
Engine rotational speed	102 rpm

The type of ring set considered is common in marine engines. The piston ring pack consists of four rings. The package includes conventional straight ring end gaps.

The surface geometry of the piston ring package, with vertical dimensions magnified by factor of 1000 relative to the horizontal ones, is depicted in Fig. 5.

All the rings have the same asymmetrical barrel shape (Fig. 5, Table 2).

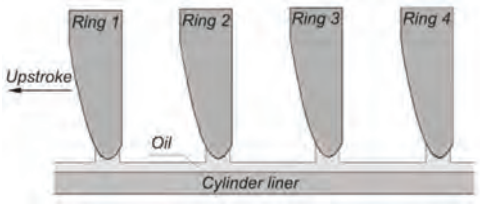

Fig. 5. Ring pack geometry under consideration

In order to ensure very low wear of profiled surfaces, the piston rings are coated (for example the top ring has chromium ceramic coating) [1, 10]. As a consequence, even hydrodynamic conditions during a long period of piston rings operation can be ensured.

Table 2. Basic geometric parameters of piston rings: 1, 2, 3, 4

Axial height of piston ring	H = 20 mm
Radius of parabolic sliding surface	R = 950 mm
Offset of parabolic sliding surface	O_{ff} = 15 mm
Distance between piston rings	L_p = 34 mm

The main parameters of the rough structure of the cylinder liner and sliding surfaces of piston rings are presented in Table 3.

Table 3. Surface roughness parameters

Surface parameters	Cylinder liner	Piston rings
RMS roughness	$\sigma_1 = 0.22$ µm	$\sigma_2 = 0.044$ µm
Elastic modulus	$E_1 = 1.13 \cdot 10^{11}$ N/m^2	$E_2 = 1.5 \cdot 10^{11}$ N/m^2
Poisson's ratio	$\nu_{P1} = 0.26$	$\nu_{P2} = 0.25$
Combined parameters	Cylinder liner and piston rings	
RMS roughness	$\sigma = 0.224 \cdot 10^{-6}$ m	
Asperity density	$\eta = 1.114 \cdot 10^{12}$ m^{-2}	
Asperity radius of curvature	$\beta = 0.2 \cdot 10^{-6}$ m	

The roughness parameters of sliding surfaces of piston rings were determined using mechanical contact measurement method, namely a standard surface roughness tester. The roughness of cylinder liner was non-destructively evaluated and in detail analyzed by the application of new optical measurement methods. It was possible at any stage of the life-time of cylinder liner by the use of rubber compound replicas of the liner surface [10].

4.2. Influence of piston ring profiles

4.2.1. First (top) piston ring

At first two profiles of the 1st (top) piston ring, i.e. with offset of the ring sliding surface O_{ff} = 15 mm and offset O_{ff} = 5 mm (Figs 6, 7) have been analysed in the lubrication aspect of the cylinder liner.

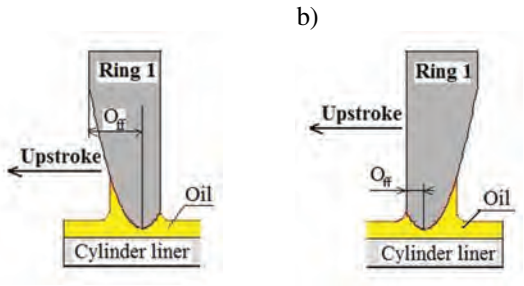

Fig. 6. Analysed profiles of the 1st (top) piston ring: a) offset of the ring sliding surface O_{ff} = 15 mm, b) offset O_{ff} = 5 mm

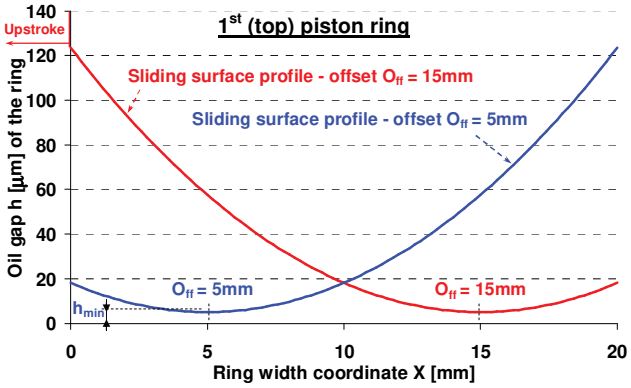

Fig. 7. Comparison of two chosen profiles of the 1st (top) piston ring: chosen offsets of the ring sliding surface O_{ff} = 15 mm and O_{ff} = 5 mm; h_{min} – minimum oil film thickness

The main parameters of the top piston ring and its sliding surface are presented in Table 4.

Table 4. Basic geometric parameters of the 1st (top) piston ring

Parameter	Case 1	Case 2
Axial height of piston ring	H = 20 mm	H = 20 mm
Radius of parabolic sliding surface	R = 950 mm	R = 950 mm
Offset of parabolic sliding surface	O_{ff} = 15 mm	O_{ff} = 5 mm

The motion of the ring pack scraping and distributing oil on the cylinder liner leaves the oil film profile shown in Fig. 8. This profile is formed after a few cycles of operation. An uneven oil film distribution along the cylinder liner can be clearly seen. Low film thickness near TDC and in the other part of cylinder liner at the location of scavenging air ports should be noticed. The minimum oil film thickness at TDC is about 0.2–0.3 µm and is comparable with root mean square (RMS) roughness of the cylinder liner that equals 0.22 µm [18]. The very low local film thickness values near TDC can be explained by occurrence of high gas pressure and high temperature in this area during the compression and working phases of engine operation. Due to high gas forces piston rings are strongly pressed against the cylinder surface. On the other hand, high temperature reduces the oil viscosity.

There are two places of oil supply for the cylinder liner of long-stroke IC engine located below TDC. Two peaks of oil film thickness at these places can be clearly seen in Fig. 8.

In a marine two-stroke engine the location of scavenging air ports is also important for cylinder lubrication. Their presence simply reduces the area of the mating surface between piston rings and cylinder liner. In this area a simplified approach was applied. The oil film thickness was assumed to be reduced at this location reflecting the reduced sliding surface.

Due to low gas pressure and oil temperature the greatest oil film thickness can be seen between scavenging air ports and the bottom dead centre (BDC).

Near the piston top dead centre (TDC) and between two places of oil supply a slightly bigger oil film thickness is noticed in the case of the offset of the ring sliding surface O_{ff} = 15 mm than in the case of the offset O_{ff} = 5 mm. For this reason the lubrication conditions near TDC are better in the first case. In addition less amount of oil scraped to the combustion chamber can be expected.

But from the middle of the cylinder wall to the location of scavenging air ports an opposite situation is observed, i.e. lower oil film thickness is noticed in the case of the offset of the ring sliding surface O_{ff} = 15 mm than in the case of the offset O_{ff} = 5 mm (Fig. 8).

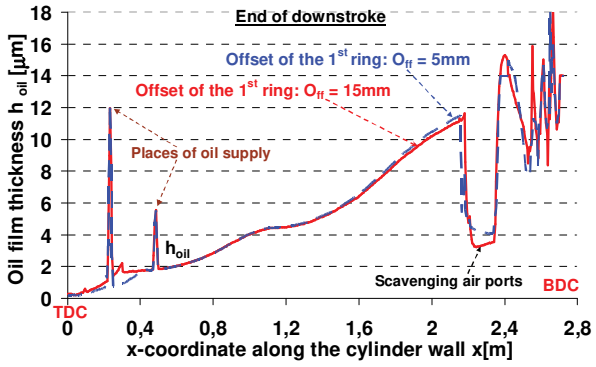

Fig. 8. Comparison of the oil film thickness h_{oil} [µm] left by the piston ring pack along cylinder wall in case of the offset O_{ff} = 5 mm and O_{ff} = 15 mm of the 1st (top) ring

A confirmation of the described results can be noticed in Fig. 9, where the minimum oil film thickness (see Fig. 2) in the gap of the top piston ring versus crank angle is shown. A similar comparison of lubrication conditions concerning the offset of the 1st piston ring (O_{ff} = 15 mm and O_{ff} = 5 mm) can be done.

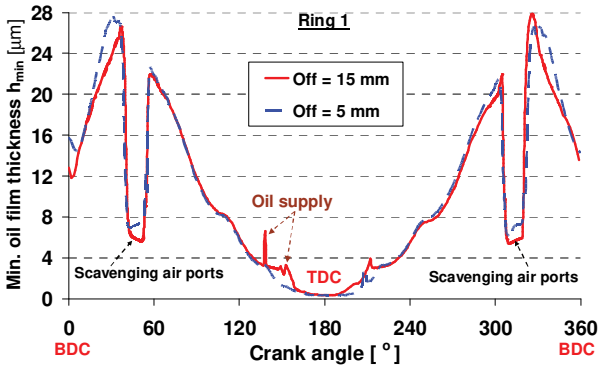

Fig. 9. Comparison of the minimum oil film thickness h_{min} [µm] of the 1st (top) piston ring in case of its offset O_{ff} = 5 mm and O_{ff} = 15 mm

But at first it should be explained that hydrodynamic forces generated in the gap between liner and ring lip are proportional to the ring axial velocity. During a cycle, the axial velocity tends to zero near the turning points (TDC and BDC). In these areas, the oil film thickness is strongly reduced, because the only force acting against the gas and ring stiffness forces is the hydrodynamic force generated by the squeeze velocity. This means that the squeeze velocity should be relatively high.

Near the piston top dead centre (TDC) and between crank angles of oil supply (Fig. 9) a slightly bigger oil film thickness is noticed in the case of the offset of the 1st piston ring O_{ff} = 15 mm than in the case of the offset O_{ff} = 5 mm. In addition less amount of oil scraped to the combustion chamber can be expected.

4.2.2. Asymmetric and symmetric profiles of piston rings: 2, 3 and 4

Two piston ring pack configurations, i.e. asymmetric profiles of all rings and symmetric profiles of rings 2, 3 and 4, have been analysed (Fig. 10 and Tab. 5).

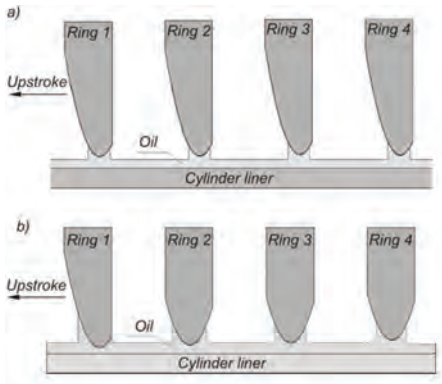

Fig. 10. Piston ring pack geometry under consideration: a) asymmetrical barrel shape of all rings, b) symmetrical barrel shape of rings 2, 3 and 4

The details concerning the considered offset of piston rings are given in Table 5.

Table 5. Chosen geometric parameter of piston rings 2, 3 and 4

Parameter	Asymmetrical barrel shape	Symmetrical barrel shape
Offset of sliding surface	O_{ff} = 15 mm	O_{ff} = 10 mm

The most important calculation results under consideration are depicted in Fig. 11.

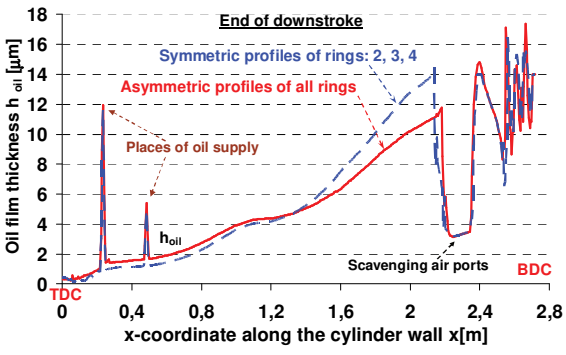

Fig. 11. Comparison of the oil film thickness h_{oil} [µm] left by the piston ring pack along cylinder wall in case of asymmetric profiles of all rings and symmetric profiles of rings 2, 3, 4

Near the piston top dead centre (TDC) and between two places of oil supply a slightly lower oil film thickness is noticed in the case of symmetric profiles of rings 2, 3, 4 than in the case of asymmetric profiles of all rings. For this reason the lubrication conditions near TDC are slightly worse in the first case.

But from the middle of the cylinder wall to the location of scavenging air ports an opposite situation is observed, i.e. much bigger oil film thickness is noticed in the case of symmetric profiles of rings 2, 3, 4 than in the case of asymmetric profiles of all rings (Fig. 11).

A confirmation of the described results can be noticed in Fig. 12, where the minimum oil film thickness (see Fig. 2) in the gap of the top piston ring versus crank angle is shown. A similar comparison of lubrication conditions concerning asymmetric profiles of all rings and symmetric profiles of rings 2, 3 and 4 can be done.

Near the piston top dead centre (TDC) and at crank angles of oil supply a slightly lower oil film thickness is noticed in the case of symmetric profiles of rings 2, 3, 4 than in the case of asymmetric profiles of all rings. But at other crank angles, especially near scavenging air ports, much bigger oil film thickness is noticed in the first than in the second case (Fig. 12).

This is the reason that in new engine types the symmetric barrel shape of piston ring (2, 3 and 4) is used [10].

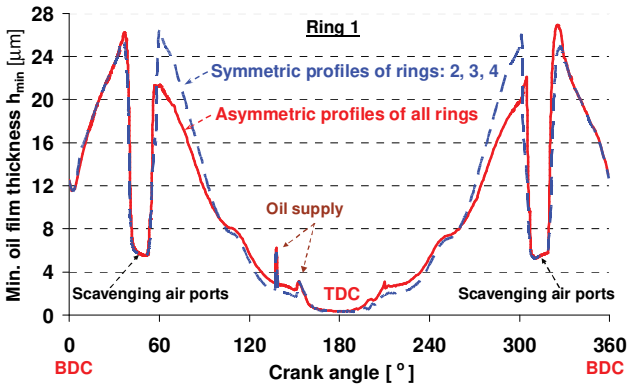

Fig. 12. Comparison of the minimum oil film thickness h_{min} [µm] of the 1st (top) piston ring in case of asymmetric profiles of all rings and symmetric profiles of rings 2, 3, 4

4.3. Influence of oil temperature distribution along the cylinder wall

Finally the influence of oil temperature at the piston TDC on cylinder liner lubrication has been analysed. The appropriate calculations in the case of standard and 30°C lower oil temperature at TDC have been made.

The second case can be technically achieved when more effective cooling system of cylinder liner near TDC is made.

The detailed data concerning thermal state of cylinder liner was proprietary information of the engine development company (see Acknowledgments). Therefore only dimensionless relations could be presented in Fig. 13.

It has been assumed that temperatures of the oil film and cylinder liner are the same.

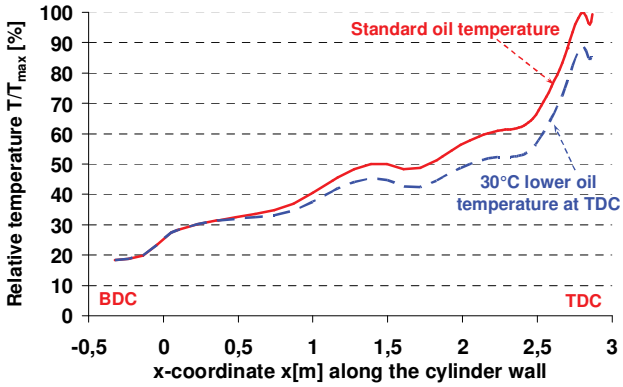

Fig. 13. Relative variations of temperature T/Tmax [%] of cylinder liner at full engine load

From places of oil supply to the location of scavenging air ports considerably bigger oil film thickness is noticed in the case of lower oil temperature than in the case of standard oil temperature. In addition a slightly bigger oil film thickness can be seen near the piston TDC (Fig. 14).

For this reason the lubrication conditions in this area of cylinder liner are much better in the first case. Therefore the lowering of temperature of cylinder liner at the piston TDC is important from practical point of view.

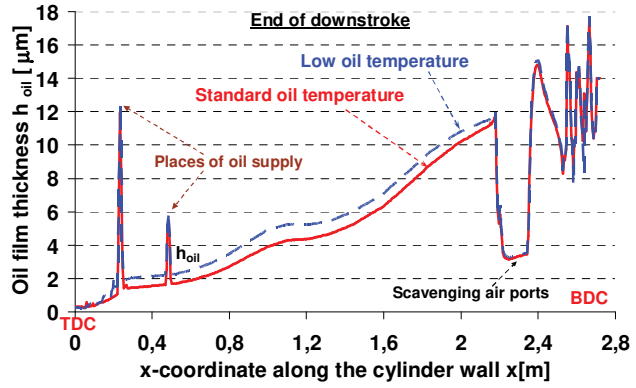

Fig. 14. Comparison of the oil film thickness h_{oil} [µm] left by the piston ring pack along cylinder wall in case of standard oil temperature and lower oil temperature distribution on cylinder liner

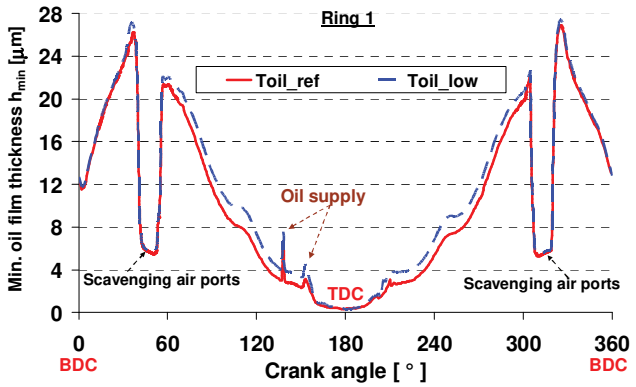

Fig. 15. Comparison of the minimum oil film thickness h_{min} [µm] of the 1st (top) piston ring in case of standard oil temperature and lower oil temperature distribution on cylinder liner

A confirmation of the described results can be seen in Fig. 15, where the minimum oil film thickness (see Fig. 2) in the gap of the top piston ring versus crank angle is shown. A similar comparison of lubrication conditions concerning standard oil temperature and lower oil temperature distribution on cylinder liner can be done.

Significantly bigger oil film thickness is noticed at crank angles from the location of scavenging air ports to oil supply places in the second than in the first case. In addition a slightly bigger oil film thickness can be seen near the piston TDC (Fig. 15). Therefore more effective cooling system of cylinder liner near TDC should be recommended.

5. Conclusions

The major conclusions that may be drawn from the results are as follows:

1. The developed mathematical model and simulation program give a lot of practical information that would be more complicated and expensive to obtain using experimental methods.
2. At first two profiles of the 1st (top) piston ring, i.e. with offset of the ring sliding surface O_{ff} = 15 mm and offset O_{ff} = 5 mm (Figs 6, 7) have been compared in the lubrication aspect of the cylinder liner. In the first case the following main phenomena can be noticed (Figs 8, 9):
   – slightly bigger oil film thickness near the piston top dead centre (TDC) and between two places of oil supply,
   – lower oil film thickness from the middle of the cylinder liner to the location of scavenging air ports,
   – less oil amount scraped to the combustion chamber.
3. Then two piston ring pack configurations, i.e. asymmetric profiles of all rings and symmetric profiles of rings 2, 3 and 4 (Fig. 10), have been analysed. In the second case the following phenomena can be noticed (Figs 11, 12):
   – much bigger oil film thickness from the middle of the cylinder liner to the location of scavenging air ports,
   – slightly lower oil film thickness near the piston top dead centre (TDC) and between two places of oil supply.
4. Finally the influence of oil temperature at the piston TDC (Fig. 13) on cylinder liner lubrication has been analysed. In the case of lower oil temperature than in standard case the following phenomena can be noticed (Figs 14, 15):
   – significantly bigger oil film thickness from the places of oil supply to the location of scavenging air ports,
   – slightly bigger oil film thickness near TDC,
   – therefore more effective cooling system of cylinder liner near TDC should be recommended.
5. The main aim of simulation of piston rings operation is to predict lubrication conditions, define areas of the possible cylinder liner wear and finally determine the gas leakage through the sealing ring set. Further investigation of these phenomena should be recommended.

Acknowledgements

The author expresses his gratitude to Wärtsilä's R&D engine centre (nowadays: Winterthur Gas & Diesel Ltd.) in Winterthur (Switzerland) for having the opportunity to work on projects concerning mathematical modelling and numerical simulation of tribological systems of piston rings during several research periods at this company.

Nomenclature

PRC	piston-ring-cylinder	BDC	bottom dead centre
TDC	top dead centre	RMS	root mean square

Bibliography

[1] DEMMERLE, R., BARROW, S., TERRETTAZ, F., JAQUET, D. New insights into the piston running behaviour of "Sulzer" large bore diesel engines. *CIMAC Congress*. Hamburg 2001.

[2] DOWSON, D. Piston assemblies; background and lubrication analysis, engine tribology. Taylor C.M. (ed.). *Elsevier Science*. 1993, 213-240.

[3] GREENWOOD, J., TRIPP, J.H. The contact of two nominally flat rough surfaces. *Proc Inst. Mech. Eng*. 1971, **185**, 625-633.

[4] ISKRA, A. Parametry filmu olejowego w węzłach mechanizmu tłokowo–korbowego silnika spalinowego. *Wydawnictwo Politechniki Poznańskiej*. Poznań 2001.

[5] KOSZAŁKA, G. Application of the piston-rings-cylinder kit model in the evaluation of operational changes in blowby flow rate. *Eksploatacja i Niezawodność – Maintenance and Reliability*. 2010, **4**, 72-81.

[6] KOSZAŁKA, G., GUZIK, M. Mathematical model of piston ring sealing in combustion engine. *Polish Maritime Research*. 2014, **4**(84), 21, 66-78.

[7] LIVANOS, G.A., KYRTATOS, N.P. Friction model of a marine diesel engine piston assembly. *Tribology International*. 2007, **40**, 1441-1453.

[8] OFFNER, G. Friction power loss simulation of internal combustion engines considering mixed lubricated radial slider, axial slider and piston to liner contacts. *Tribology Transactions*. 2013, **56**(3), 503-515.

[9] PATIR, N., CHENG, H.S. Application of average flow model to lubrication between rough sliding surfaces. *Transactions of ASME*. 1979, **101**.

[10] RÄSS, K., AMOSER, M. Progressive development of two-stroke engine tribology. CIMAC Congress. 2007, **83**.

[11] SERDECKI, W. Badania współpracy elementów układu tłokowo-cylindrowego silnika spalinowego. *Wydawnictwo Politechniki Poznańskiej*, Poznań 2002.

[12] TAMMINEN, J., SANDSTRÖM, C.-E., ANDERSSON, P. Influence of load on the tribological conditions in piston ring and cylinder liner contacts in a medium-speed diesel engine. *Tribology International*. 2006, **39**, 1643-1652.

[13] TIAN, T. Dynamic behaviors of piston rings and their practical impact – part II: oil transport, friction, and wear of ring/liner interface and the effects of piston and ring dynamics. *Proc. I. Mech. E, Part J: Journal of Engineering Tribology*. 2002, **216**, 229-247.

[14] Wärtsilä Technology Review, information materials concerning IC engines designed at Wärtsilä company.

[15] WOLFF, A. Experimental verification of the model of piston ring pack operation of an internal combustion engine. *The Archive of Mechanical Engineering*. 2009, LVI, **1**, 73-90.

[16] WOLFF, A. Numerical analysis of piston ring pack operation of a marine two-stroke engine. *Combustion Engines*. 2011, **146**(3).

[17] WOLFF, A. Influence of engine load on piston ring pack operation of a marine two-stroke engine. *Journal of KONES Powertrain and Transport*. 2012, **19**(2), 557-569.

[18] WOLFF, A. Simulation based study of the system piston-ring-cylinder of a marine two-stroke engine. *Tribology Transactions*. 2014, **57**(4), 653-667.

[19] WOLFF, A. Influence of piston ring pack configuration on blowby and friction losses in a marine two-stroke engine. *Combustion Engines*. 2017, **170**(3), 164-170.

Andrzej Wolff, DSc., DEng. – Faculty of Transport of Warsaw University of Technology.
e-mail: *wolff@wt.pw.edu.pl*

Article citation info:
ORKISZ, M., WYGONIK, P., KUŹNIAR, M., KALWARA, M. Analysis of the possibility of using an engine with a rotating piston as the propulsion of an electric generator in application to a motor glider propulsion. *Combustion Engines*. 2019, **178**(3), 264-268. DOI: 10.19206/CE-2019-346

Marek ORKISZ
Piotr WYGONIK
Michał KUŹNIAR
Maciej KALWARA

CE-2019-346

Analysis of the possibility of using an engine with a rotating piston as the propulsion of an electric generator in application to a motor glider propulsion

Analysis of the possibility of using an engine with a rotating piston as the propulsion of an electric generator in application to a motor glider propulsion The paper presents an analysis of the possibilities of application of a rotating piston engine (Wankel type) as a propulsion for an electric generator in the motor glider propulsion system. This generator would be a part of the propulsion system of a hybrid motor glider using the AOS 71 motor glider airframe. In the research, the rotational characteristics of the LCR 407ti engine were determined experimentally. Driving torque run, power and fuel consumption were determined as a function of engine speed. The obtained results are presented in diagrams. The conceptual diagram of the hybrid drive is presented. The current generator was selected and the effectiveness of the generator and the entire propulsion were assessed from the motor glider's performance point of view. On the basis of the conducted research, conclusions were drawn and there were indicated the objectives and directions of further research on hybrid propulsion with specific aerodynamic and mass limitations of the aircraft

Key words: *hybrid, combustion engines, motor glider, rotary engine, Wankel engine, hybrid propulsion*

1. Introduction – the issue of the application of new types of aircraft propulsion

For many years, the trend of reducing fuel consumption and improvement of ecological indicators has been observed in transport. These processes also do not bypass broadly understood air transport. Aircraft companies and leading research centres are undertaking work on various technical solutions. These may be aircraft equipped with an all-electric propulsion (UAV, Pipistrel Pantera, Airbus E-Fan, AOS-71). The basic disadvantage of electric propulsion systems used in aircraft constructions is their mass. The high mass of batteries with a relatively small capacity, causes a low value of the density of energy stored on the deck – compared, for example, to the density of energy accumulated in hydrocarbon fuel. These features affect the limited range or durability of flight. In addition, these parameters influence the increased demand for power during the manoeuvres, such as start or climb. Therefore, it seems interesting (until the development of an energy source with a sufficient energy density) to develop an aeronautical hybrid propulsion system that would allow to increase the operating parameters of the aircraft.

This paper presents the concept of using a hybrid system (consisting of a combustion engine and electric generator) designed for propulsion of a modified AOS 71 motor glider. A number of simplifying assumptions were adopted for the conceptual computations: no additional mass of electrical installation required for physical connection of the assemblies, nor the mass of additional devices to control the propulsion

2. Description of the research object

The basis for the analysis was the airframe of the electric AOS-71 (Fig. 1), built as part of the cooperation between the Department of Aircraft and Aircraft Engines of the Rzeszow University of Technology and the Faculty of Power and Aeronautical Engineering of the Warsaw University of Technology.

Fig. 1. The AOS 71 motor glider

Table 1 shows the basic data of the airframe, while Figures 2 and 3 present the values of power required for the flight for this airframe and the efficiency of its propeller depending on the flight speed.

Table 1. Basic data of the AOS 71 motor glider [6, 7]

Wing area	S [m^2]	15.8
Wing span	R [m]	16.4
Aspect ratio	Λ	17
Maximum take-off mass	M_{max} [kg]	660
Minimum motor glider mass	M_{min} [kg]	500

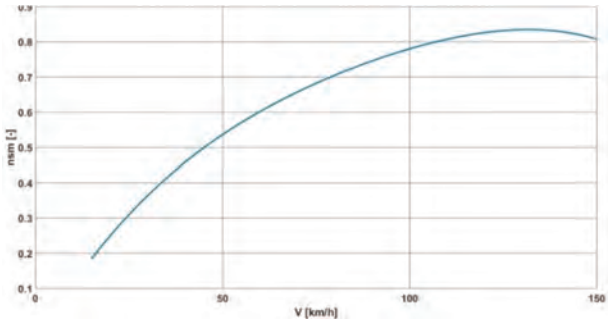

Fig. 2. Efficiency of propeller in the function of flight speed – for the AOS 71 motor glider [6, 7]

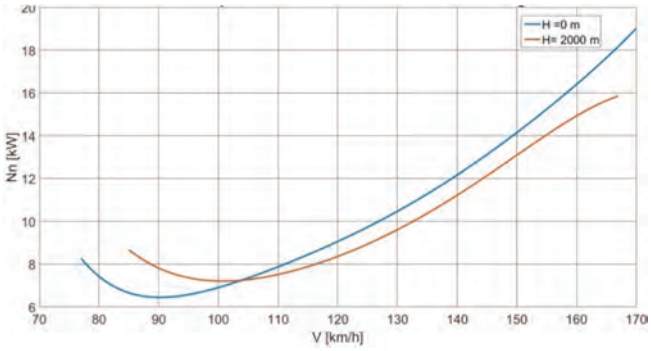

Fig. 3. Power required for flight in the function of flight speed - for the AOS 71 motor glider; M_{max} = 660 kg [6, 7]

The motor glider is powered by the Emrax 228 engine and a battery assembly of the parameters given in Table 2.

Table 2. Technical data of the AOS 71 power unit [6, 7]

Engine	Emrax 228	–
Continuous power	N_{const} [kW]	55
Peak power	N_{max} [kW]	100
Continuous torque	M_{const} [Nm]	120
Engine mass	m_s [kg]	12
Battery type	Li-Pol	–
Capacity	C [Ah]	40
Voltage	U_{bat} [V]	180
Battery mass	m_{bat} [kg]	178

For these data, the energy accumulated on-board is determined from the formula:

$$E = C \cdot U_{bat} = I \cdot 3600[s] \cdot U_{bat} \quad (1)$$

where : E [J] – energy accumulated on-board for battery parameters presented in Table 2; this value was E = 25920 kJ.

For such flight stages as climb or horizontal flight, it is possible to determine the energy required to perform a given manoeuvre and, as a consequence, determine the flight duration and range of the aircraft.

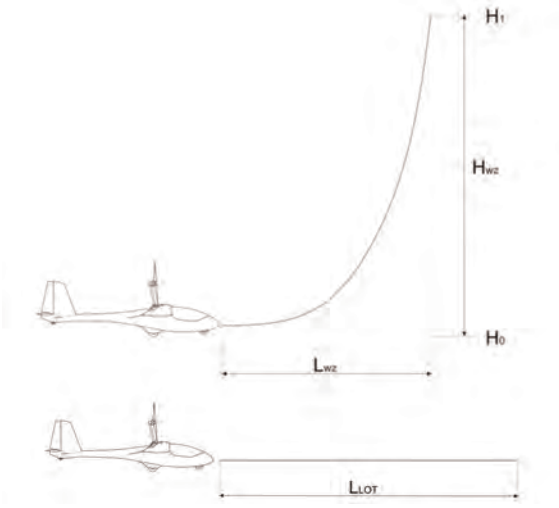

Fig. 4. Flight stages – climb (up) and horizontal flight (down)

The climb time can be determined from the dependence [1, 8]:

$$t_{wz} = \frac{H_1 - H_0}{W} \quad (2)$$

where: H0, H1 – initial and final altitude, W – the climb velocity determined as the product of the flight speed and the trigonometric function of the climb angle [1]:

$$W = V \cdot \sin\theta \quad (3)$$

The energy required to perform the climb is determined from the formula [1]:

$$E_{WZ} = (m \cdot g \cdot W \cdot t_{wz} + N_n \cdot t_{wz}) \div \eta_{sm} \quad (4)$$

where: E_{wz} – total energy of climb, m – aircraft mass (before the manoeuvre), g – gravitational acceleration, N_n – power required for horizontal flight, t_{WZ} – duration of the climb, η_{sm}– propeller efficiency.

The energy required for horizontal flight can be determined from the formula [1]:

$$E_L = (N_n \cdot t_L) \div \eta_{sm} \quad (5)$$

where: t_L – horizontal flight time.

Figure 5 presents the energy required for the flight of the AOS-71 motor glider depending on the flight speed assuming different flight durability.

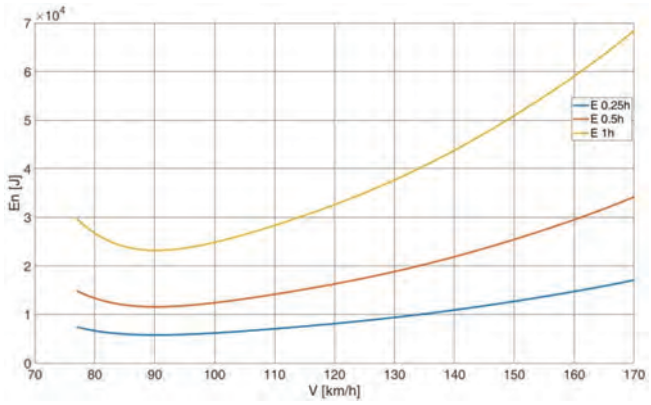

Fig. 5. The course of the change of energy required for the flight as a function of the flight speed

Knowing the energy demand for given flight stages and the value of energy accumulated on board, it is possible to determine the flight range and duration for given flight parameters. These data constituted the starting point for selection of an electric generator and a set of batteries.

3. Selection of an electric generator and performance comparison

A serial hybrid was taken for further analysis in the construction scheme where the combustion engine does not have a kinematic connection with the propeller. It was assumed that the internal combustion engine only recharges the battery or can provide the necessary excess power in the critical stages of the flight (e.g. start, climb).

The Wankel AG 407TGi rotary piston engine was used to build the generator propulsion model. This choice was dictated by the advantages of rotary piston engines, such as low engine mass, low level of vibrations generated by it, and high drive torque compared to reciprocating piston engines. Table 3 presents the comparison of selected data of several internal combustion engines with a similar power range used in general aviation.

Table 3. Technical data of internal combustion engines [9, 10]

Engine		407TGi	Rotax 125	Rotax 28 Max
Maximum engine power	N_{max} [kW]	31.5	25	28
Maximum torque	M_{max} [Nm]	51	22	–
Engine mass	m_s [kg]	20	29	58
Revolutions for M_{max}	n_{Mmax} [rev/min]	4000	10500	–

Table 3 shows that the Wankel engine has a relatively high unit power indicator (power related to the dry engine mass) for the remaining engines. In addition, it has a much higher torque than the 1-cylinder Rotax engine, which is available at low rotational speed. An additional advantage of using this type of engine will be less vibrations generated by a rotary piston engine than a traditional high-speed single-cylinder unit, which will favourably affect the fatigue strength of the engine and airframe structure.

In order to select the generator set properly, the rotational characteristics (power in the function of revolution) of the rotary piston engine (Wankel 407TGi) were measured. Figure 6 shows the view of the test stand with an electro-swirl brake.

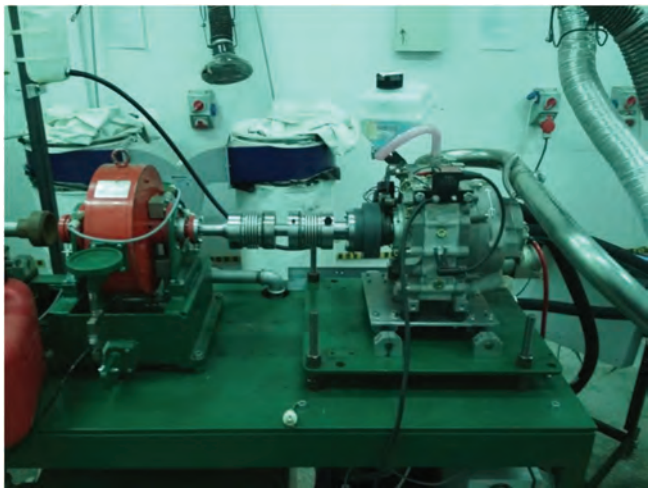

Fig. 6. Stand for testing engine characteristics

Figure 7 shows the dependence of power and drive torque as well as specific fuel consumption in the a function of the rotational speed of the tested engine. Fuel consumption characteristics are not available in the engine manual, hence the need to determine them.

The analysis of the characteristics shows that for the value of maximum torque there is the highest efficiency of the engine and associated with it the lowest specific fuel consumption. The maximum torque is around 4000 rpm, which corresponds to the power of 22 kW and the specific fuel consumption of 0.3 kg/kWh. The analysis was based on the aerodynamic and performance characteristics of the airframe, the horizontal flight velocity V = 100 km/h and the vertical velocity (climb) W = 2.3 m/s.

Giving the formula (3) as follows [1]:

$$W = V \cdot \sin\theta = \frac{N_r - N_n}{m \cdot g} \tag{6}$$

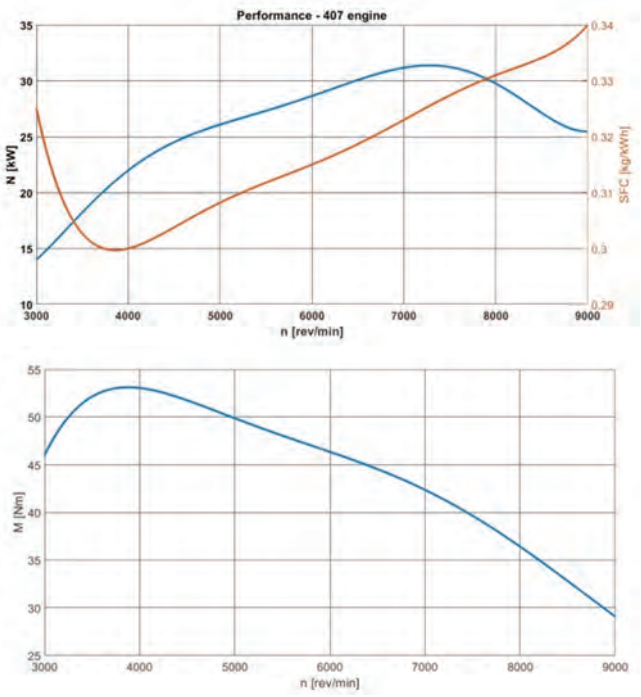

Fig.7. Rotational characteristics of the 407tgi engine (a- power curve, b- torque curve in the function of rotational speed)

there can be determined the power generated by the N_r power unit, which is required to obtain the climb parameters. For the adopted aerodynamic parameters of the motor glider during the climb, the power of N_r is about 20 kW. Taking into account the efficiency of energy transformation in the propulsion system, the calculated power is 22 kW, which is the value that meets the power requirement to perform the climb manoeuvre.

For this power range, the Emrax 188 engine was chosen as the alternator with the following technical data (given in Table 4).

Table 4. Technical data of the Emrax 188 engine[11]

Engine	Emrax 1888	-
Continuous power	N_{const} [kW]	32
Peak power	N_{max} [kW]	50
Continuous torque	M_{const} [Nm]	60
Engine mass	m_s [kg]	6.8

Together with the factory-dedicated control system [lit], this engine is able to operate in generator mode with the efficiency of 98%.

The fuel tank holds 7 kg of oil-gasoline mixture (1:80). The selected generator set works with a set of batteries of the parameters given in Table 5.

Table 5. Specifications of the hybrid battery set

Battery type	Li-Pol	-
Capacity	C [Ah]	16
Voltage	U_{bat} [V]	355
Battery mass	m_{bat} [kg]	60

The energy accumulated on-board can be determined by modifying the dependence (1) to the form[1]:

$$E = I \cdot 3600[s] \cdot U_{bat} + \eta_{gen} \cdot (N_s \cdot t_s) \tag{7}$$

were t_s – generator working time

$$t_s = \frac{m_{pal}}{SFC \cdot N_s} \tag{8}$$

where SFC – specific fuel consumption, N_s – engine power during generator operation mode.

With the above assumptions, the starting mass in relation to the constructed and functioning electric variant of AOS 71 did not change and amounts to 660 kg.

4. Determining the performance of a hybrid power unit

For the propulsion hybrid system, calculations of the performance parameters of the power unit and motor glider were made. The results are presented in the diagrams in Figs 8 and 9.

Figure 8 shows the amount of energy accumulated on-board for the hybrid and electric variants.

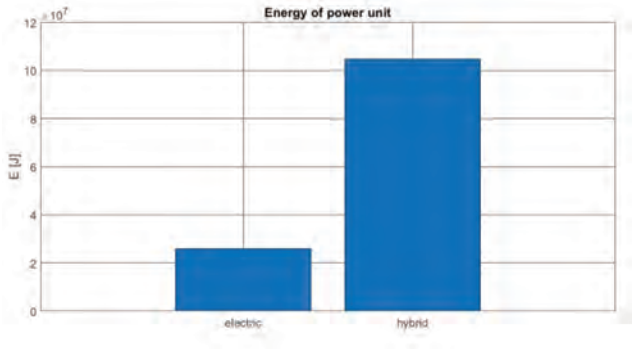

Fig. 8. The amount of energy accumulated on-board

Figure 9 shows the energy density in relation to the take-off mass.

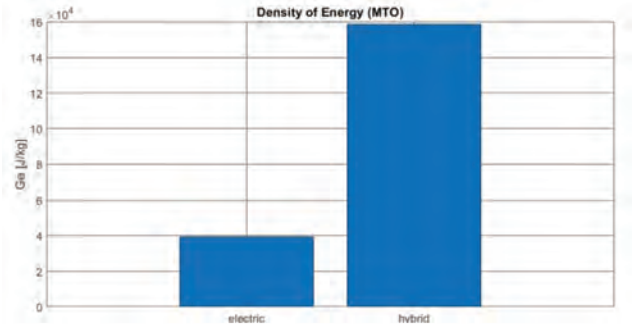

Fig. 9. Comparison of the energy density on-board the motor glider for two propulsion variants, in relation to the take-off mass

Figure 10 shows the range of the motor glide, assuming a flight duration up to depletion of the energy resource, and Figure 11 presents the flight duration corresponding to this assumption.

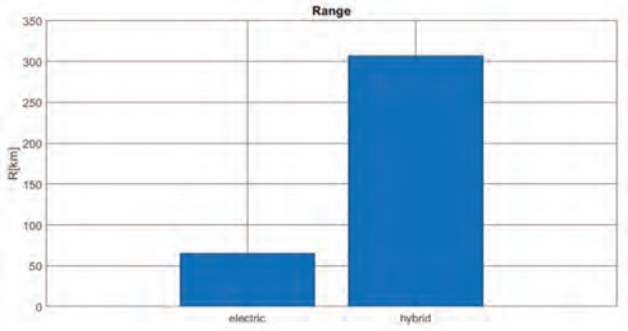

Fig. 10. The range of the motor glide, assuming a flight duration up to depletion of the energy resource

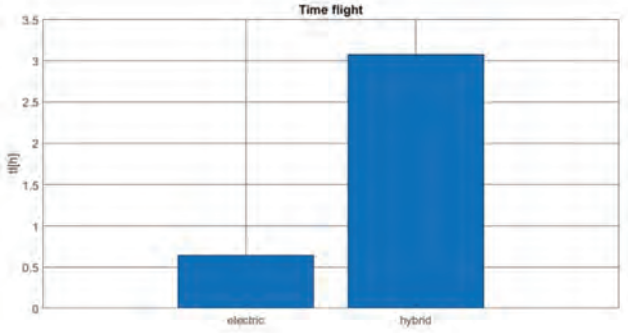

Fig. 11. The flight duration [h], assuming a flight duration up to depletion of the energy resource

5. Results of research conducted and conclusions

The hybrid propulsion provided more than a 5-fold increase in the range and flight time while maintaining the condition of the same take-off mass. It was connected with 4-times more energy accumulated on-board the motor glider. In Fig. 9, showing the energy density related to the take-off mass, the problem of the high mass of the battery in relation to the energy that can be accumulated is shown. The calculations show that the hybrid propulsion variant is an attractive option for the motor glider, both in the mass and economic terms. Despite the extension and complexity of the propulsion in the construction sense, it allows to keep the starting mass unchanged in relation to the electric variant. The high density of hydrocarbon fuel energy allows for a greater (almost 6-fold) range and duration of the flight in relation to the electric drive. In the mass calculations, the increase of mass of the propulsion set due to the necessity of installing electric wires and controllers was not taken into account. Detailed research, taking into account these problems, will be continued.

Acknowledgements

The research presented in this paper was financed as project PBS3/A6/24/2015 "AOS-H2" of the Applied Research Programme (PBS) of the National Centre for Research and Development (NCBIR), Poland, in the years 2015–19.

Bibliography

[1] ANDERSON, J. Introduction to flight. *McGraw Hill Book Company.* San Francisco 2003.

[2] BOJOI, R., BOGGERO, H. et al. Multiphase drives for hybrid-electric propulsion in light aircrafts: a viable solution. *Conference: 2018 International Symposium on Power*

Electronics, Electrical Drives, Automation and Motion (SPEEDAM). DOI: 10.1109/SPEEDAM.2018.8445241
[3] GEISS, I., VOIT-NITSCHMANN, R. Sizing of fuel-based energy systems for electric aircrafts. *Proceedings of the Institution of Mechanical Engineers Part G-Journal of Aerospace Engineering*. 2017, 231. DOI: 10.1177/0954410017721254
[4] FAHIM, M. An overview of double-bar single-wheel rotary combustion engine. *Advances in Mechanical Engineering*. 2019, **11**(2), 1-13. DOI: 10.1177/1687814019828074
[5] JAKUBOWSKI, R., ORKISZ, M. A review of selected alternative propulsion systems for UAV applications. *Zeszyty Naukowe/Wyższa Szkoła Oficerska Sił Powietrznych Dęblin*. 2015. **231**. DOI: 10.1177/0954410017721254
[6] MARIANOWSKI, J., FRĄCZEK, W., CZARNOCKI, F. Założenia podstawowe dla projektu motoszybowca AOS-H2. *(not publish)*
[7] MARIANOWSKI, J., TOMASIEWICZ, J., CZARNOCKI, F. Analiza masowa motoszybowca AOS-H2. *(not publish)*
[8] ROSKAM, J. Airplane aerodynamics and performance. *DARcorporation*. Kansas 2016.
[9] WANKEL AG, Wankel engine manual
[10] www.flyrotax.com
[11] www.emrax.com

Prof. Marek Orkisz, DSc., DEng. – Faculty of Mechanical Engineering and Aeronautics, Rzeszow University of Technology.
e-mail: *mareko@prz.edu.pl*

Piotr Wygonik, DEng. – Faculty of Mechanical Engineering and Aeronautics, Rzeszow University of Technology.
e-mail: *piowyg@prz.edu.pl*

Michał Kuźniar, MEng. – Faculty of Mechanical Engineering and Aeronautics, Rzeszow University of Technology.
e-mail: *mkuzniar@prz.edu.pl*

Maciej Kalwara, MEng. – Faculty of Mechanical Engineering and Aeronautics, Rzeszow University of Technology.
e-mail: *kalmac@prz.edu.pl*

Article citation info:
DASZKIEWICZ, P., RYMANIAK, Ł., KAMIŃSKA, M. Issues of emission evaluation of road-rail vehicles in the aspect of current type approval regulations. *Combustion Engines*. 2019, **178**(3), 269-273. DOI: 10.19206/CE-2019-347

Paweł DASZKIEWICZ
Łukasz RYMANIAK
Michalina KAMIŃSKA

CE-2019-347

Issues of emission evaluation of road-rail vehicles in the aspect of current type approval regulations

One of the ways to reduce exhaust emissions from vehicles is to replace worn-out shunting locomotives with road-rail tractors. The main purpose of this solution is to reduce the negative environmental impact of the vehicle and to reduce the fuel consumption compared to a shunting locomotive performing the same work. The tests on exhaust emissions of rail vehicles are carried out on an engine test bench, making it impossible to determine the environmental performance of these vehicles during real operation. Therefore, it is advisable to carry out measurements in real operating conditions in order to obtain reliable reference results. This enables the verification of vehicles ecological indicators in a wide range of operational work parameters. It is possible to obtain reliable results regarding the impact of the tested vehicle on the natural environment in this way and compare them with the applicable emission standards.

Key words: *engine exhaust emission, road-rail vehicles, fuel consumption, research in real conditions, ecology*

1. Introduction

Rail transport, as compared to other modes of transport, is characterized by a low share in the total emission of harmful compounds in the transport section. Nevertheless, due to the continuous tightening of emission norms, increasingly more emphasis is placed on the exhaust emission of traction vehicles and new methods are being sought to improve their ecological indicators. The tests on rail vehicles exhaust emissions are carried out on the engine test bench, and the results obtained are compared with the permissible limit values included in the relevant legal emission norms [3, 4]. Therefore in order to obtain reliable results for various engine operating states, it is necessary to carry out measurements in real operating conditions, for motor vehicles defined as RDE (Real Driving Emissions). The implementation of such tests makes it possible to verify the ecological indicators of vehicles in the wide operating spectrum of their drive systems. It is hence possible to obtain reliable results regarding their impact on the natural environment in relation to the applicable exhaust emission norms [3, 4, 6, 7, 9].

This article examines the exhausts emission of harmful compounds during real operating conditions of a rail-road tractor that can perform shunting work on the tracks. The vehicle has a 116 kW internal combustion engine and meets the Stage IIIB emission norm according to its technical specifications. Road-rail tractors are increasingly used on the domestic and European market by railway and tramway track managers due to their mobility and design features that facilitate the possibility of installing a set of wheel rollers and pull-buffer devices. The road-rail vehicle also allows performing shunting work on tracks. In the case of a vehicle that is to replace a shunting locomotive, information on its ability to roll over wagons is important. For this purpose, it is necessary to obtain an adequate traction force resulting from friction between the rail head and the vehicle tire. A road-rail tractor, in order to carry 10 wagons, needs adequate pressure to push the tire to the track rails. Higher tire pressure on the rail increases the vehicle wagons transporting capacity. An important parameter is also the permissible gross weight that allows the tractor to move on public roads. The most important issue from the point of view of the conducted research is to reduce the negative environmental impact of the vehicle and to reduce fuel consumption compared to a locomotive performing the same shunting work [1, 2, 5].

The aim of the conducted research was to measure the tractor's ecological indicators during operation on the road without load and on the track with and without load and compare them with the type approval requirements. During the tests, the concentration of gaseous compounds and particulate matter in the exhaust gas was measured. In order to determine the road emission, mass flow rates and signals from the on-board diagnostic system, GPS and METEO were also recorded. Obtained values have been referred to the emission norms for engines with a rated power of 75 kW ≤ P < 130 kW (Table 1), as the test vehicle was classed in this power range.

Table 1. Exhaust emissions limit values according to the Stage I, II and IIIB norms [3, 4]

Norm	P	CO	HC	NO_x	PM
	kW	g/kWh			
Stage I	75 ≤ P < 130	5.0	1.3	9.2	0.7
Stage II	75 ≤ P < 130	5.0	1.0	6.0	0.3
Stage IIIB	75 ≤ P < 130	5.0	0.19	3.3	0.025

2. Issues concerning measurements of the real exhaust emission from non-road vehicles

In the aspect of exhaust emissions, internal combustion engines of off-road vehicles are homologated at stationary brake stations. Based on the research carried out in recent years, it should be noted that qualitative and quantitative measurements of exhaust emissions from internal combustion engines performed in laboratory conditions may significantly differ from the results obtained in field conditions. Continuous development and miniaturization of the measuring equipment belonging to the PEMS mobile analyzers group allows to perform increasingly more accurate studies of vehicle ecological indicators in real operating conditions.

At the same time, the application possibilities of these devices have increased. Thanks to this, it has become possible to take into account the specificity of road/rail traffic for specific groups of machines, including maintaining the size dimensions of the vehicles with the equipment installed within the railway gauge. The apparatus for testing in real traffic conditions requires the use of exhaust gas flow meters. However, due to the engine assembly parameters, this issue is often a problem related to exceeding the permitted dimensions. For this reason, flow characteristics should be determined using information based on: intake manifold air pressure and temperature as well as crankshaft speed. In modern engines it is possible to use data from on-board diagnostic systems.

The assessment of ecological indicators in real operating conditions can be performed in various aspects, most often in relation to the engine operation (specific emission expressed in g/kWh) or to the distance traveled (road emission expressed in g/km). It is also appropriate to make an assessment in the aspect of the vehicle operating parameters variability or the drive system itself. Time density characteristics (TD) have been regularly relied on for several decades in the construction and optimization of internal combustion engines, drive systems and entire vehicles. Using the assumptions, it is possible to determine the combustion engine operation time shares in crankshaft speed and load intervals during tests in a given measurement cycle. They also allow to present the driving characteristics for different speed and acceleration ranges. Therefore, taking into account the operating time, it is possible to characterize the traffic and environmental performance of non-road vehicles by using a discrete function, which will be presented in the time density characteristics.

3. Research method

3.1. Test vehicle

The road-rail tractor is adapted to move both on roads and on tracks, be it railway, tram or metro (Table 2). It is intended mainly for moving wagons on railway sidings and shunting works. The vehicle was built using a road tractor for a base and equipped, among others, with a traction and collision system, a rail chassis (front and rear), a hydraulic system and braking system (installed on the roof) for braking the transit of attached wagons. A compression-ignition engine in a in-line configuration with a rated power of 116 kW and a displacement volume of 6.8 dm^3 was used to drive the tested vehicle [1, 2, 5].

Table 2. List of construction parameters of the tested tractor

Parameter	Value
Max power	116 kW
Max torque	659 Nm
Number of cylinders	6 in-line
Fuel supply system	Common Rail
Exhaust emission norm	Stage IIIB
Specific fuel consumption	211 g/kWh
Max travel speed	40 km/h
Max pulling force on roads	45 kN
Max pulling force on tracks	35 kN
Tractor mass	9000 kg
Max cruising speed on a straight track / road	25 km/h
Max cruising speed on arcs and switches when pulling wagons	5 km/h
Max allowed cruising speed on straight track when pulling wagons with pneumatic brake	10 km/h

3.2. Test route

The tests in vehicle real operation while performing shunting work were performed at the Łukasiewicz Research Network – Rail Vehicles Institute "TABOR". In the case of the second and third test drive, the tests were carried out according to a new method for rail vehicles designed by the authors. For the conducted research tests, the routes included distances amounting to 1.7 km for road travel, 1 km for unladen travel on rail track and 1.3 km for laden rail track travel. The maximum travel speed of research vehicle on the asphalt road was 23 km/h, while in the test made on the track for unladen vehicle it was lower by 3 km/h. The smallest maximum research vehicle speed was obtained when travelling with a load (14 km/h).

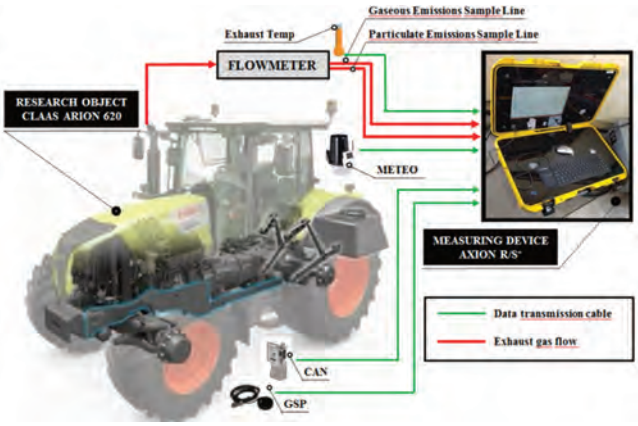

Fig. 1. Road-rail tractor with the PEMS apparatus

3.3. Measuring apparatus

A Micro PEMS (Portable Emission Measurement System) Axion R/S+ mobile analyzer was used for the tests (Fig.1). It made it possible to measure exhaust emissions of various components, such as: carbon dioxide (CO_2), carbon monoxide (CO), hydrocarbons (HC), nitrogen oxides (NO_x) and particulate matter (PM). NDIR (Nondispersive Infrared Sensor) and electrochemical analyzer were used to measure the concentrations of these substances. In the case of PM measurement, a method based on Laser Scatter was used.

The performed tests included the measurements of harmful exhaust emissions in real operating conditions and were divided into three stages. The first of these included an unladen drive on an asphalt road with a vehicle equipped with herringbone tires, increasing traction. In the second (unladen journey) and third (laden) stage the tractor was equipped with a wheel set enabling traveling on rails. The vehicle travelled on the railway tracks owned by Łukasiewicz Research Network – Rail Vehicles Institute "TABOR". Based on the research results, the ecological indicators, exhaust emission were determined in both cases and the specific fuel consumption was determined using the carbon balance method. All measured data was recorded at a frequency of 1 Hz.

4. Results analysis

4.1. Share of operating time

The driving parameters recorded during the tests were used to determine the operating time share characteristics in the speed-acceleration ranges (V–a). Figure 2 shows the operating time share of the road-rail tractor on the road and on the track without load and on the track with the load in open-closed compartments.

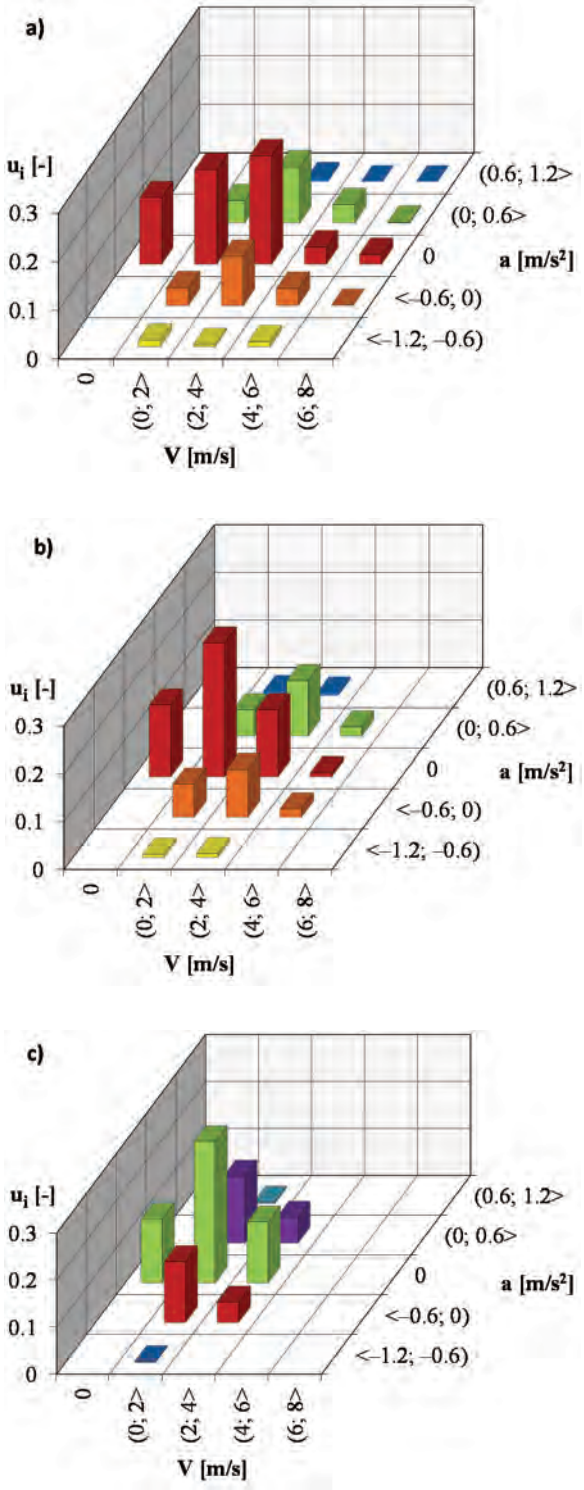

Fig. 2. Operating time share for the road-rail tractor: a) on the road without load, b) on track without load c) on track with load

The distribution of operating parameters includes the range of speed and acceleration values, with the highest values reaching: 22% – the point defined by a single interval described by values (2 m/s; 4 m/s⟩ and 0 m/s^2 (on road), 28% – the point defined by the interval (0 m/s; 2 m/s⟩ for acceleration of 0 m/s^2 (unladen on track) and 35% – single measurement window determined in the speed range (0 m/s; 2 m/s⟩ and acceleration of 0 m/s^2. For the whole operating range including the velocity and acceleration values between ⟨0 m/s; 6 m/s⟩ and ⟨–0.6 m/s2; 0.6 m/s^2⟩ a very similar distribution of the operating time share characteristics was obtained for all the measured drive tests. During the road tests the vehicle was characterized by a larger range of operating parameters variability than in the other two drives.

4.2. Exhaust emissions

During the tests, the specific exhaust emission values were determined. All results were referenced to the Stage IIIB emission norm for internal combustion engines with a power in the range 75 kW ≤ P < 560 kW (Figs 3–6). Based on this analysis, it can be stated:

– The specific emission of carbon monoxide obtained during the unladen drive on rail track was equal to value 0.76 g/kWh, while the emission value for travel on the road was almost five times higher and amounted to 3.64 g/kWh. When laden and on track of research object, a specific emission of 2.21 g/kWh was obtained. All the obtained values met carbon monoxide limit of the Stage IIIB emission standard which is 5.0 g/kWh.

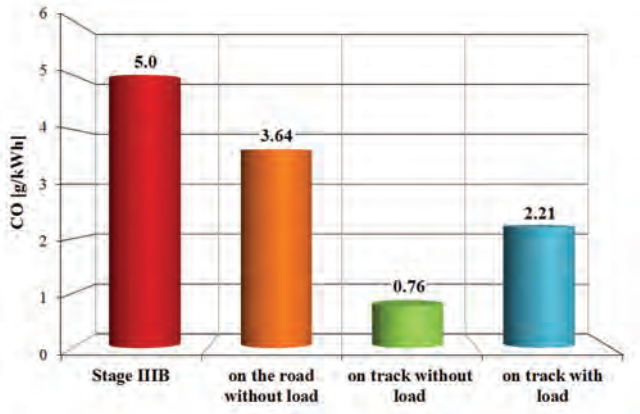

Fig. 3. Specific emission of carbon monoxide for the road-rail tractor traveling on the road and on track without load and on track with load

– With respect to the specific hydrocarbon emission, a lower value of 0.2 g/kWh was obtained during the unladen drive. When travelling on the track when laden resulted in emission of 0.94 g/kWh. The highest HC emission value of 1.39 g/kWh was obtained when travelling on the road. All of the completed trips exceeded the hydrocarbons emission limit value defined in Stage IIIB standard, defined as 0.19 g/kWh. The results obtained for track driving of research object are included in the limits introduced by the Stage II norm, while those obtained during road tests only meet the Stage I norm.

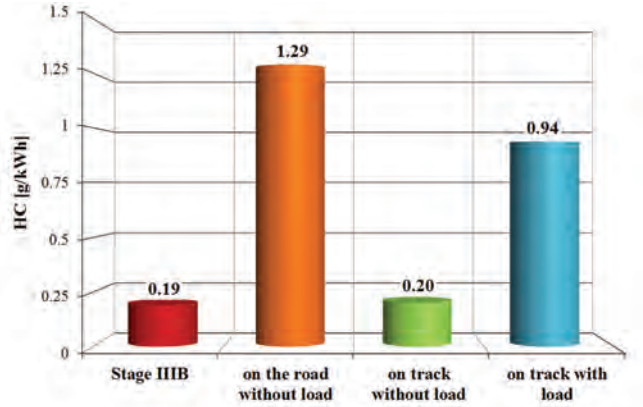

Fig. 4. Specific hydrocarbons emission for a road-rail tractor travelling on the road and on track without load and on track with load

– During the tests the smallest specific emission value of NO_x (3.71 g/kWh) was obtained for the unloaded drive on the track. Travelling when loaded was characterized by a value of up to 10% higher, while for the drive on the road, the obtained value was 1.3 g/kWh higher and reached 5.0 g/kWh. Neither of the measured drives, on the track with and without load, as well as on the road met the NO_x emission limit of Stage IIIB norm, which is 3.3 g/kWh. However, they did meet the limit by the Stage II (6.0 g/kWh).

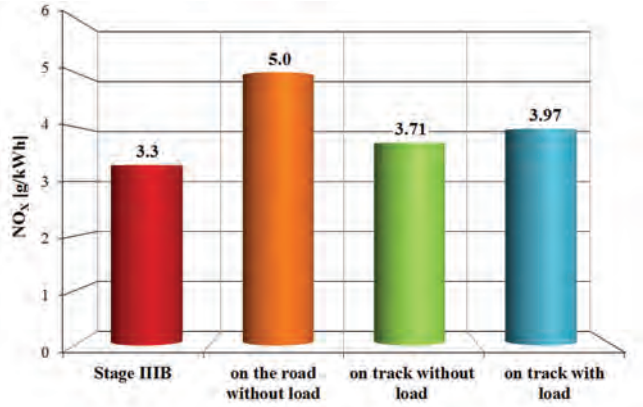

Fig. 5. Specific emission of nitrogen oxides for a road-rail tractor travelling on the road and on track without load and on track with load

– The specific emission of particulate matter obtained for the unladen drive on track was 0.01 g/kWh, while for the road it was 0.003 g/kWh lower and amounted to 0.007 g/kWh. The highest emission value equal to 0.011 g/kWh was obtained for the vehicle travelling on the track with load. All of the measured test drives were in line with the Stage IIIB PM limit of 0.025 g/kWh.

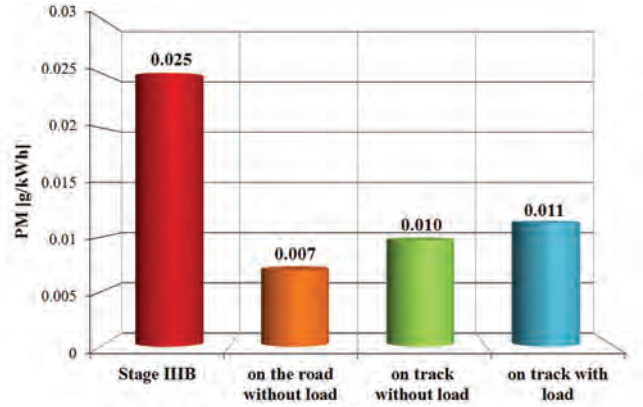

Fig. 6. Specific emission of particulate matter for a road-rail tractor travelling on the road and on track without load and on track with load

The performed tests and their results were supplemented by determining the specific emission of carbon dioxide and fuel consumption obtained for all the tested drive situations of the road-rail tractor (Figures 7 and 8).

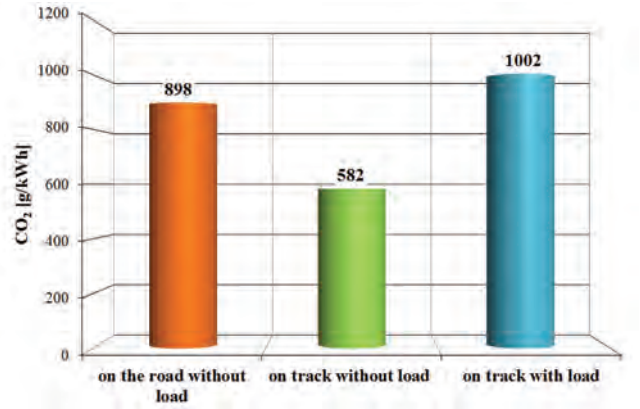

Fig. 7. Specific emission of carbon dioxide for a road-rail tractor travelling on the road and on track without load and on track with load

According to the analysis of the obtained data, the smallest specific emission of CO_2 at the level of 582 g/kWh, and thus the lowest fuel consumption (4.13 kg/h) was observed for the unloaded drive on the track. The values of the specific carbon dioxide emission obtained for road travel were over 150% of that, while the obtained fuel consumption was higher by almost 1 kg/h. The largest CO_2 emission values (1002 g/kWh), as well as the highest fuel consumption (5.47 kg/h) was obtained when travelling on the track and pulling load.

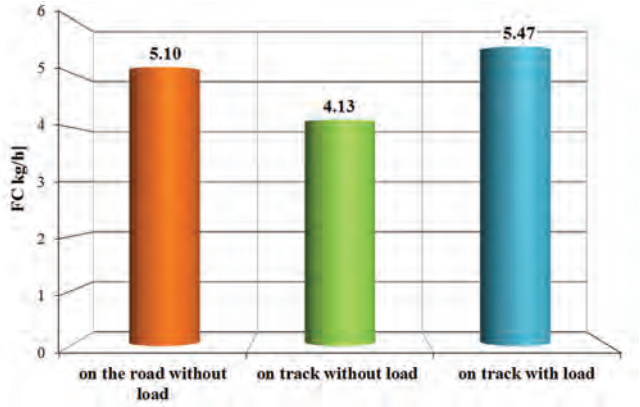

Fig. 8. Fuel consumption for a road-rail tractor travelling on the road and on track without load and on track with load

5. Results analysis

The exhaust emissions measurement from a road-rail vehicle in real operating conditions allowed determining the time density characteristics and the specific emission of engine exhaust components. The fuel consumption was also determined using data on the work done by the drive system. The obtained time density characteristics of the vehicle

in speed-acceleration intervals while travelling on the road and track with and without load have shown similar distribution, which allowed for a comparative analysis. It is related to, among other things, with similar values of average vehicle speed and acceleration.

The unladen drive along the track was characterized by the lowest specific emission value of carbon monoxide and hydrocarbons due to the limited variability of engine operating parameters, and this is associated with more efficient thermodynamic processes. This is mainly related to the characteristics of the engine, at high loads the injected fuel dose is not thoroughly mixed resulting in incomplete combustion. The unladen drive on the track was also characterized by the smallest specific emission value of nitrogen oxides. This is due to the fact that both during the travel on the road and on the track with the load, the vehicle engine was under larger load, even though it is associated with an increase in temperature in the combustion chamber, and a direct impact on the NO_x emission. In the case travel on the road the specific emission of particulate matter yielded the smallest values from all tests. PM emission is greatly affected by variable engine load, which involves the need to bring more fuel to the combustion chamber, which can lead to an increase in local partial and incomplete combustion in the combustion chamber. However, the exhaust aftertreatment system used – the DPF filter effectively limited their emission. The best ecological indicators based on gaseous exhaust emissions were obtained when driving on the track without load. Differences in fuel consumption result from the fact that when traveling on the track with load and on the road the vehicle encountered greater rolling resistance and achieved higher speed values, which translated directly to higher engine load. Emission of carbon dioxide is closely related to fuel consumption, therefore the nature of its value is proportional to the obtained fuel consumption values.

The test results obtained in the subsequent stages of the research can be used to assess the ecological indicators, but only by taking into account the operating conditions, including a larger engine loads, both in road and rail work. In order to improve the assessment of particulate emissions, it will be extremely useful to also measure their dimensional distribution, which is planned for further research.

Nomenclature

a	acceleration
CO	carbon monoxide
CO_2	carbon dioxide
HC	hydrocarbons
NDIR	nondispersive infrared sensor
NO_x	nitrogen oxides
P	power
PEMS	portable emission measurement system
PM	particulate matter
RDE	real driving emissions
u_i	share of working time
V	velocity

Bibliography

[1] BRYK, K., ŁUKASZEWSKI, K., MEDWID, M. Simulation studies of safety against derailment of a road-rail vehicule Class Arion 620. *International Scientific Conference. Transport of the 21th century*. Arłamów 2016.

[2] DASZKIEWICZ, P., ANDRZEJEWSKI, M. Preliminary analyzes in terms of the possibility of reducing energy consumption by the SM42 locomotive used in trackworks. *MATEC Web Conf.* 2017, **118** 00014. DOI: 10.1051/matecconf/201711800014

[3] Directive 97/68/EC of the European Parliament and of the Council of 16 December 1997 on the approximation of the laws of the Member States relating to measures against the emission of gaseous and particulate pollutants from combustion engines to be installed in non-road mobile machinery.

[4] Directive 2004/ 26/EC of the European Parliament and of the Council of 21 April 2004 amending Directive 97/68/EC on the approximation of the laws of the Member States relating to measures against the emission of gaseous and particulate pollutants from internal combustion engines to be installed in non-road mobile machinery.

[5] MEDWID, M., STAWECKI, W., CZERWIŃSKI, J., JAKUSZKO, W. Multi-purpose rail-road tractor of the new generation. *Rail Vehicles*. 2016, **3**.

[6] MARCINIAK, Z., STAWECKI, W., PIELECHA, I., PIELECHA, J. Ecological aspects of diesel rail vehicles exploited on Polish rail lines. *Logistyka*. 2010, **4**.

[7] OŻÓG, M. Requirements for limitation of the diesel exhaust fumes by rolling stock and consequences for railway undertakings. *TTS Technika Transportu Szynowego*. 2008, **5**-**6**.

[8] RYCHLIK, A. Commercial vehicles fuel consumption measurement methods. *Maintenance and Reliability*. 2006, **4**.

[9] STAWECKI, W., MARCINIAK, Z., PIELECHA, I., PIELECHA, J. Ecological aspects of the modernization of diesel locomotives in Poland. *Prace Naukowe Politechniki Warszawskiej. Transport*. 2013, **98**.

Paweł Daszkiewicz, DEng. – Łukasiewicz Research Network – Rail Vehicles Institute "TABOR" in Poznan.
e-mail: *p.daszkiewicz@tabor.com.pl*

Łukasz Rymaniak, DEng. – Faculty of Transport Engineering, Poznan University of Technology.
e-mail: *lukasz.rymaniak@put.poznan.pl*

Michalina Kamińska, Eng. – Łukasiewicz Research Network – Rail Vehicles Institute "TABOR" in Poznan.
e-mail: *m.kaminska@tabor.com.pl*

Article citation info:
PAJDOWSKI, P., WOODBURN, J., BIELACZYC, P., PUCHAŁKA, B. Development of RDE test methodology in light of Euro 6d emissions limits. *Combustion Engines*. 2019, **178**(3), 274-282. DOI: 10.19206/CE-2019-348

Piotr PAJDOWSKI
Joseph WOODBURN
Piotr BIELACZYC
Bartosz PUCHAŁKA

CE-2019-348

Development of RDE/ISC test methodology in light of Euro 6d/VI emissions limits

This paper discusses the fact that vehicle and powertrain test methods have long been guided by type approval requirements – with a focus ot the recent/current example of real driving emissions (RDE) and in-service conformity (ISC) test requirements. The implcations – current and future – of these testing requirement, which force the use of portable emissions measurement system (PEMS) are discussed. In this context, BOSMAL Automotive Research and Development Institute's PEMS systems are presented, and the systems' attributes and versatility are explored. Considerations for testing a very wide range of vehicle, engine and fuel types are mentioned. Non-legislative applications of PEMS systems are briefly explored; finally, it is shown that the emissions laboratory and its chassis dyno remain indispensable when conducting work on light duty exhaust emissions, even in the era of RDE.

Key words: *RDE, Euro 6d, emission limits, high duty, PEMS*

1. EU real driving emissions (RDE) philosophy and introduction

Legal requirements for the measurement and limitation of exhaust emissions have a long history in the EU, as well as in other markets, most notably the USA. Since the year 1990s, maximum permissible exhaust emissions of regulated pollutants in the EU have been updated several times (via the implementation of successive Euro standards), and the test procedure (laboratory test cycle) modified somewhat, but the fundamental means by which vehicles were tested remained unchanged, namely: laboratory tests performed under controlled conditions with the vehicle running on a chassis dyno. During this test, a well-defined and universally-known speed trace was followed by the vehicle and diluted exhaust emissions were measured, with a relatively simple calculation process determining the final results in terms of mass-per-distance (and particles-per-distance for particle number – PN). This approach guided the vast majority of research conducted on light duty vehicles destined for EU markets, as well R&D carried out on their components, engine calibrations, aftertreatment systems, fuel, lubricants, etc. Over the last few years, a new chassis dyno driving cycle and slightly altered test procedure was introduced (the WLTP), but the fundamental approach did not change, as the driving cycle was well-defined and the vehicle was tested on a chassis dyno without the simulation of sloping terrain, variable traffic and weather conditions, etc. While the speed trace of the WLTP attempted to capture the complexity and variability of real-world driving, the speed trace for a given vehicle was the same for every test and defined in advance.

The use of such test procedures created strong pressure for manufacturers to produce vehicles, engines and engine calibrations which performed well under test conditions – that is to say, the laboratory conditions (including the speed trace) known to be the official procedure at the time could be targeted in terms of optimization of exhaust emissions and limiting fuel consumption (which is strongly proportional to CO_2 emissions). Such benefits were not always evident under driving conditions which differed from those occurring during official test procedures. Following a series of widely-reported and discussed concerns that real-world emissions (and fuel consumption) were much higher than during laboratory tests and that laboratory procedures represented something close to a best-case scenario, steps were taken to introduce a test procedure for measuring emissions (but not specifically fuel consumption) from light duty vehicles under normal conditions of use, i.e. when running on public roads. Such testing is possible thanks to PEMS (portable emissions measurement system), a measurement system which can be mounted on/in a vehicle and can travel around with it, measuring exhaust emissions and certain other parameters. The idea of PEMS testing and PEMS hardware itself is not new; it has a long history and was used on a smaller scale for many years by various parties in various contexts [1, 2]. PEMS testing has been – and continues to be – carried out in multiple contexts, ranging from legally mandated official tests to R&D and fundamental emissions research (see, for example [2–6]).

In terms of the implementation of PEMS test as a legal test requirement for light duty vehicles, the situation changed dramatically real driving emissions (RDE) legislation was introduced in the EU [1, 2], as part of updates to the Euro 6 regulation, in four packages:

- The first RDE package was adopted in May 2015 and defines the RDE test procedure, including the measurement of undiluted exhaust gas using PEMS apparatus and the calculation of emissions results.
- The second RDE package was adopted in October 2015 and defines the NO_x Conformity Factors and their dates of entry into force.
- The third package was adopted in December 2016 and adds a Particle Number (PN) Conformity Factor (see Table 1) and inclusion of RDE cold-start emissions (which had previously been measured, but later excluded from the final results)
- The fourth package was adopted in May 2018 and introduces In-Service Conformity RDE testing and market surveillance and lowers the error margin of the 2020 NO_x Conformity Factor from 0.5 to 0.43 (see Table 1).

Table 1. Evolution of light-duty exhaust emissions limits in the EU

	SI – NO_x [mg/km]	CI – NO_x [mg/km]	All engines with direct injection – PN [#/km]
Euro 6 chassis dyno type-approval limits (NEDC/WLTP)	**60**	**80**	**6.0×10^{11}**
Euro 6 (2015) real-world limits	126	168	-
Euro 6 (2016) real-world limits	126	168	9.0×10^{11}
Euro 6 (2018) real-world limits	90	120	9.0×10^{11}
Euro 6 (2020) real-world limits	85.8	114.4	9.0×10^{11}

The differences in the 'chassis dyno' and 'real-word' limits in table 1 result from the use of conformity factors [1, 2]. Throughout the normal life of a vehicle, its emissions determined in accordance with the RDE requirements and emitted during any possible RDE test shall not be higher than the following not-to-exceed (NTE) values:

$$NTE_{pollutant} = CF_{pollutant} \times TF(p\,1,\ldots, pn) \times \text{Euro-6}.$$

As the transfer function (TF) is currently defined as taking a value of 1.0 and as the CF values defined in RDE legislation are all > 1, this means that maximum permisaable emisions of certain compounds measured during an RDE test are be higher than emissions measured under laboraotry conditions on a chassis dyno. Self-evidently, the values of the legal CF factors – and any downwards revisions to those values – are of great concern to vehicle manufaturers and suppliers of components and systems related to emissions control, such as aftertreatment systems [1]. Even components and systems traditionally understood to have little in common with emissions and emissions control can have a part to play in meeting demanding NTE limits: for example, efforts to reduce vehicle mass (lightweighting) and improvements to aerodynamics (streamlining) can aid efforts to reduce regulated exhaust emissions under certain driving conditions. In the current climate of highly demanding exhaust emissions requirements (e.g. Euro 6d) and simultaneous demands to reduce fuel consumption and CO_2 emissions [1, 2], even marginal benefits can add up to significant advantages in meeting goals and ensuring vehicles' legislative compliance in terms of exhaust emissions.

2. EU real driving emissions (RDE) requirements in detail

As mentioned previously, the core idea of PEMS testing is to drive a vehicle in a normal manner on public roads and measure the resulting emissions [1–11]. RDE testing is simply an extension of this idea, which criteria to determine whether the route and its sub-routes were normal and the maximum allowable emissions levels of certain regulated pollutants. The various pieces of RDE legislation ('RDE packages') mentioned in the previous section introduced and refined trip normality criteria, with the aim of ensuring that all RDE tests represented fair and reasonable use of a vehicle, based on time, distance, topography (altitude, gradient), speed, acceleration and measured CO_2 emissions. These validity criteria were much debated and have been developed gradually, with the aim of facilitation quantitative determination of that tests conducted in an unrealistic manner. When identified as such, all the results from a non-normal test are legally deemed non-valid, regardless of the magnitude of the emissions results. Some other, more general and more easily-met requirements apply: RDE trips have to last between 90 and 120 minutes; they have to include specified shares of urban, rural, and motorway driving, which must be conducted in precisely that order.

NTE emissions (resulting from the defined Conformity Factors) then apply to a range of ambient and driving conditions. For example, moderate ambient conditions are temperatures between 0 and 30°C and altitudes up to 700 m; extended ambient conditions are temperatures between |–7 and 0°C and between 30 and 35°C, and altitudes between 700 and 1300 m. Regulated emissions emitted under the extended conditions mentioned above (whether altitude, temperature or both simultaneously) are divided by a fixed value of 1.6 to moderate the emissions results occurring under such conditions. When all calculation steps and corrections have been carried out, the final output emission value has to be below the NTE limit.

A Moving Average Window (MAW)-based methodology (EMROAD, originally developed by the Joint Research Centre – JRC – of the European Commission) is one of the main tools used to check the trip validity. In addition, for a PEMS trip to be valid, the driving cannot be either too aggressive nor too soft; this is checked via the calculation of the 95th percentile of the vehicle speed-positive acceleration product and via the relative positive acceleration value, both assesses for the urban, rural, and motorway phases individually. Another assessment criterion is the positive altitude gain during the PEMS trip, which is limited to 1200 m/100 km, mathematically equivalent to a constant slope of 0.012 radians.

Once the trip validity has been confirmed, PEMS data are post-processed, with a series of correction factors applied to normalize the results. The most important normalization step balances the raw regulated emissions against CO_2 (compared to emissions of CO_2 from the same vehicle undergoing a WLTP test); this way, demanding trips which caused higher emissions (regulated and CO_2) can be considered valid, with the results reduced somewhat by the aforementioned correction. As CO_2 is strongly proportional to the energy supplied by the combustion engine over a given driving cycle, a specific evaluation factor is used in the case of plug-in hybrid vehicles, which compares CO_2 emissions during the RDE test and CO_2 emitted over the WLTP test in Charge Sustaining mode. Ongoing powertrain electrification (hybridization) in the automotive industry will continue to evolve and may create further challenges for RDE legislation to adapt to. Apart from hybridization, the use of alternative engine concepts and even exotic solutions such as the use of dual fuel systems may become more widespread in the future. Thus, despite already having been updated many times, the RDE data evaluation methodology will continue to be reviewed against technological progress and will almost certainly be subject to future updates [1, 2].

3. Other types of legislative testing using PEMS equipment

While it is not the main focus of this paper, legislation on emissions from heavy duty engine engines in fact has a longer history than RDE testing for light duty vehicles. Following similar trends in the USA [1], since 2011 the EU has required in-service conformity (ISC) testing of various types of heavy duty engines. Such testing is carried out by testing a heavy duty vehicle equipped with the concerned engine – for example, a truck or bus. Non-road mobile machinery (NRMM) is now also subject to similar requirements. NRMM is a broad category, containing machinery with very different characteristics, equipped with combustion engines of varying size. In the case of NRMM, there are considerable differences from road vehicles, due to the fact that such machines' primary function is to carry out work (such as excavation or lifting), instead of covering distances of up to several hundred km during a single period of engine operation. Differences in testing details and practicalities are significant, yet nevertheless, the physical basis of ISC testing for heavy duty and NRMM applications has many similarities with RDE testing in terms of its usage of PEMS to sample exhaust gas and limits set by means of the CF mechanism. As will be shown later in this paper, the emissions measurements and result calculation processes are sufficiently similar that in many cases a single PEMS system can be used on a range of vehicles, to perform either RDE or ISC (HD/NRMM) testing.

4. BOSMAL's PEMS hardware and computer software for RDE/ISC testing

Various manufacturers have produced emissions testing equipment and computer software capable of conducted PEMS testing in full accordance with EU RDE and ISC requirements, and often also following US specifications for HDUIT equipment. BOSMAL Automotive Research and Development Institute Ltd possesses two systems which fully meet all RDE/ISC requirements, making them suitable for testing light and heavy duty vehicles, as well as NRMM, in line with all applicable EU legislation. The first system, by AVL was manufactured and commissioned in 2016 (Fig. 1 and Fig. 2). A system from Horiba was manufactured and commissioned in 2018 (Fig. 3 and Fig. 4).

Fig. 1. AVL PEMS system installed on a passenger car. The gas PEMS unit is not visible as it is located inside the vehicle cabin. The PN PEMS, the exhaust flow meter, the sampling line and tubing for re-routing the exhaust are all visible at the rear

Fig. 2. AVL PEMS system installed on the load carrying area of a heavy duty vehicle

Fig. 3. Horiba PEMS system installed in a passenger car

Fig. 4. Horiba PEMS system installed in the passenger seating area of an urban bus. (Note the presence of sandbags serving as ballast surrounding the equipment)

Both systems are equipped with high capacity batteries suitable for powering the equipment, including laptop computer. The capacity of the two systems' batteries is such that an RDE test can easily be performed on battery power.

For HD/NRMM ISC testing, which is longer in duration, both systems can be powered by a portable generator (visible on the right side of Fig. 2).

Both the aforementioned PEMS systems' hardware and software is specifically designed to quantify emissions of regulated gaseous and solid pollutants from vehicles powered by internal combustion engines in full accordance with all relevant requirements formalized in Commission Regulation (EU) No. 2017/1151 with all relevant amendments, as well as applicable legislation for in-service conformity (ISC) testing of heavy duty vehicles (Commission Regulation (EU) No. 2009/595, with multiple updates) and NRMM.

As required by the aforementioned legislation, both systems measure concentrations of CO, NO, NO_2 (or NO_x) and CO_2. While there are some small differences in the two systems' analyzers, in both cases measurement of the aforementioned gaseous species is in full accordance with all applicable legislation. Both systems are also capable of measuring THC – measurement of this compound is not required for RDE testing, but is required for heavy duty ISC testing. In both systems, the measured concentrations are converted into mass emissions vectors using the information from the measured exhaust flow. Both concentration and mass-based results are available following export of the test results, at 1 or 10 Hz.

Following the introduction of PN measurement requirements for both RDE and ISC testing (and upcoming requirements for NRMM), both systems feature their own PN counting module. These two PN modules have different particulate quantification methods (diffusion charger in the case of the AVL system versus condensation particle counter in the Horiba system), but are both in full accordance with all applicable RDE and ISC requirements. PN is counted with a nominal lower cut-off point of 23 nm (the same as for laboratory chassis dyno measurements), with the sample pre-treatment system ensuring that only solid (and not volatile) particles are counted. Both PN modules function as an integrated component of their respective parent systems, but can also be deactivated and even physically removed from the system when not required – thereby reducing system volume, weight and power consumption.

In addition to the aforementioned emissions measurement hardware, each system also features a controlling computer for control of the system and archiving of results during testing. Additionally, both systems are equipped with software for pre- and post-processing of results, data export, as well as various means of data visualization (including map-based presentation of results) and preparation of reports in the rigid format required for submission to type approval authorities (e.g. EMROAD).

Depending on the precise configuration, the weight of each system and all its accessories, batteries, etc. is analogous to the weight of 1–2 adult humans – i.e. a very normal load for even a small passenger car, or negligible load for a heavy duty vehicle. (In the case of NRMM not designed to carry load on the chassis, the weight of the PEMS is normally rather insignificant compared to the weight of the machinery itself.)

As required by all PEMS-based legislation, exhaust gas is sampled raw from a sampling probe connected to the tailpipe of the vehicle or piece of machinery. A heated sampling line is used to transfer the exhaust gas to the PEMS itself. Both BOSMAL's systems can use one of two sampling lines according to the characteristics of the vehicle under test. Where possible, the shorter line is used, for both systems. All sampling lines feature heating circuits with temperature regulation. For legislative testing, the temperature of the sampling line is set to 191°C. The heated line minimizes condensation and related sample loss and the sample line leading to the gas analyzers includes a disposable filter to prevent fouling of the analyzers with particulate.

In addition to high-quality chemical analyzers, a key requirement of all PEMS-based legislation is accurate determination of the exhaust mass flow rate. In line with the legislation, this can be achieved in several ways, but the preferred method is direct measurement via a flowmeter through which the entire exhaust gas flow passes. This direct measurement does not depend on data obtain from the engine's ECU via the OBD port (though it can be cross-correlated with such data) and provides a truly independent measurement. Depending on the vehicle or piece of machinery under test and the type and size of the engine used to power it, the magnitude of this mass flow can vary greatly. In light of this, both BOSMAL's systems feature a range of exhaust flow meters with tubing of different diameters, meeting all the applicable demands of applicable legislation, all of which measure the exhaust flow via the Pitot method. The measurement range depends on the tube connected to the flow meter, with both systems possessing sufficient flow meters and tubes to cover all passenger cars, as well as vans, HD vehicles (including large buses and coaches) and many types of NRMM. Testing of more exotic vehicles and machines, including military vehicles, ships, trains, generators and even aircraft is also possible, as long as physical restrictions regarding the use of the exhaust gas mass flow meter can be overcome. (For certain types of machinery and non-road vehicles, use of the exhaust gas mass flow meter may be impractical or unsafe – in such cases, the flow of exhaust gas reported by the ECU can be used.)

All PEMS systems must feature a weather station measuring ambient temperature and humidity and a GPS receiver – in the case of BOSMAL's systems, all sensors and the GPS units fulfil all relevant requirements the applicable legislation. While ambient temperature, humidity and pressure are monitored and reported (results for the entire test and at 1 Hz), NO_x results are not corrected for ambient humidity by default, in line with legislation (although this option is available and can be used on request).

Since PEMS testing contains a number of steps to be performed on a range of analyzers, an automated control system is required, since human triggering of purging, calibration, data storage (etc.) would be too arduous and error-prone. Thus, a specially-designed automation and acquisition system is a key component of any PEMS.

Both systems' control software includes functions for tasks such as purging and leak checking, which are execut-

ed prior to every test. Similarly, according to BOSMAL procedures, the legislative requirement for analyzer calibration before and after the test is carried out. Zeroing of the exhaust mass flow meter is also carried out before every test. The PN system is leak checked and zeroed before every test. The results of these calibrations are stored and exported as an integral part of the test report, for analysis when reviewing test results. As per the manufacturer's recommendations, at least once every 12 months both units are returned to their respective manufacturer's service department for maintenance – these maintenance procedures are not explicitly mandated by legislation, but ensure sound emissions testing practice in terms of checks of the functioning of heaters, coolers, pumps, fans, transformers, etc. In line with legislative requirements, the linearity of both systems' gaseous analyzers is checked (and if necessary corrected) at least once every three months; the linearity of the both systems' exhaust flow meters and other sensors is checked at least once a year. All calibration gases used are of high quality and meet or exceed all applicable legislative demands. As with chassis dyno CVS-bag testing, the expiry dates of the calibration gases used are stored in a database and hard copies as well as scans of all calibration gas certificates are kept.

Both PEMS systems' control software – and in particular the post-processing functionality – is subject to regular updates by the system manufacturer (note that each RDE package has introduced multiple significant changes requiring modifications to the post-processing, emissions calculation and trip validity determination criteria).

The *sine qua non* of a successful RDE test can be defined as the PEMS equipment (namely its installation, preparation and calibration) and the suitability of test route. The former aspect has been described previously; the latter aspect is expanded upon here, based on the example of one of BOSMAL's RDE-compliant routes in southern Poland. (Note that in discussions of this nature, a "successful" RDE test is not necessarily one where CF values for regulated pollutants are below legal limits; a "successful" RDE test is one which satisfies all applicable RDE requirements, regardless of the emissions results obtained from that test.)

BOSMAL has a range of routes route specially developed with the full requirements of Commission Regulation (EU) No. 2017/1151 in mind are proposed for RDE tests, as well as routes for various types of HD vehicles. These routes have been successfully executed on a range of LD vehicles. In accordance with the demands of Commission Regulation (EU) No. 2017/1151, all routes consist of three sub-routes (called urban, rural and motorway).

For non-legislative testing and R&D purposes, portions of the routes as defined above can be omitted, repeated or performed in a different order, giving many possible combinations to investigate emissions from alternative driving scenarios (examples: cold start followed by motorway operation; urban-only routes). Nearby mountains also provide for multiple possibilities for more demanding driving routes over mountainous terrain at altitudes exceeding 700 m.

Some details and commentary on the sub-routes of the sample route is presented in the remainder of this section.

The urban, rural and motorway sub-routes have been designed with the demands of Commission Regulation (EU) No. 2017/1151 and also with the practicalities of RDE-PEMS testing in mind. Each sub-route covers > 25 km, such that the total distance covered by the three combined is approximately 85 km. Indicative approximate distance shares are: urban – 40%, rural – 30%, motorway – 30%. Continuity of the complete trip (urban-rural-highway) is assured by the fact that the end point of one section is the start point of the following section; the transitions from one section to another are seamless and do not require any unnatural or artificial driving maneuvers.

The urban sub-route is a near-loop (the start and end points are less than 500 metres apart). The urban route's speed profile varies with the traffic conditions (time of day, day of week). The legal speed limits encountered on the urban route is are in the range 40–70 km/h; for the vast majority of the route the legal speed limit is 50 km/h. The urban route features multiple sections where heavy traffic is common, junctions controlled by traffic lights, etc. but is typically not characterised by completely gridlocked traffic, such that the mean speed is typically safely within the 15–40 km/h range and stop events account for 6–30% of the urban travel time. The urban route leads directly into the rural route.

The rural sub-route is a return journey (outwards leg/return leg). The rural route features driving on a dual carriageway with speed limits ranging from 50–100 km/h and including multiple sets of traffic lights, such that a minimum of at least one stop event typically occurs on this sub-route. A controlled U-turn manoeuvre at a junction is used to change the driving direction at the end of the outwards leg. When the return leg is complete, this route leads directly into the motorway route.

The motorway sub-route is a return journey (outwards leg/return leg) this sub-route consists almost entirely of driving on a dual carriageway where the speed limit is 120 km/h and congestion is rare, such that well over 5 minutes' driving occurs at speeds > 100 km/h, as required for a valid RDE trip. However, the route features an "interruption", where vehicle speed is reduced: there is an acute curve in the motorway route where the legal speed limit is progressively reduced from 120 km/h to 60 km/h, returning to 120 km/h immediately after the curve (this situation is the same when travelling in both directions). Including such a feature in the route ensures that speeds in the range 90–110 km/h are always included in the motorway sub-route, since safe and legal negotiation of this curve requires speeds considerably lower than the general speed limit of 120 km/h. In this way, the driver needs to be given no special instructions to drive significantly slower than the speed limit when driving the motorway sub-route. The end of the outwards leg coincides with a junction, where an exit ramp and a roundabout are used to enter the carriageway travelling in the opposite direction. This roundabout-facilitated U-turn manoeuvre requires significantly lower speeds (applicable to rural and urban driving), but is typically achievable without stopping the vehicle. The return leg of the motorway sub-route ends at a junction within 1 km of the start

point of the urban sub-route, such that the entire urban-rural-motorway route is very nearly a closed loop.

Using a route which is a loop or near-loop has evident advantages in terms of reducing travelling time back to base following a test. For RDE testing including the cold start event (according to RDE packages 3 and above), route planning is imperative, because once started, the cold start and warmup cannot be paused or repeated – RDE requirements state that the vehicle must be parked for between 6 and 56 hours before the cold start and start of driving. Following engine startup (cranking) for the cold state, the vehicle must begin to move before 15 seconds elapse (i.e. extended initial idling, even if forced by the prevailing traffic conditions, immediately invalidates a test). There are also additional requirements concerning driving during the cold start period (defined as the coolant reaching a temperate of 70°C for the first time, or 300 seconds elapsing, whichever occurs first). In light of these multiple requirements, which often difficult to fulfil simultaneously, and the strongly anisotropic nature of emissions behaviour following a cold start, route planning for RDE testing according to the 3rd and 4th packages is even more complex than for earlier eras of RDE testing where cold start data was explicitly excluded from the final emissions results.

A further factor which must be considered is terrain: the altitude profile of BOSMAL's RDE route covers frequent yet gentle undulations in the terrain, without large hills. The altitudes of the start and end points differ by < 20 metres (RDE legislation requires < 100 m difference between these points). The mean altitude of the entire route is approximately 350 metres above sea level. When the entire urban-rural-motorway route is performed, the cumulative distance-specific altitude gain is typically approximately 850 m/100 km and is always < 1000 m/100 km. The highest altitudes reached by the vehicle over the full route are all < 430 metres above sea level, thus meaning that no portion of the standard route lies in the altitude range which counts as extended conditions.

Many other RDE routes close to BOSMAL's headquarters in Bielsko-Biala have been defined and validated, for example a route which includes higher altitudes (rural sub-route including altitudes > 700 m) to create a route where a significant portion of the driving occurs in the RDE extended category. BOSMAL also has other RDE-complaint test routes at various locations, including in EU countries other than Poland. Some routes are in southern Europe, meaning the temperature in the winter is significantly higher than in Poland and snowfall is rare.

A variety of variants and changes to the legislative procedure can be made to investigate the impact on the results and thus gain an insight into real-world emissions in scenarios outside RDE boundary conditions. Such modifications can include:

- testing using altered CO_2 input values;
- testing varying the order of the three sub-routes – for example: [cold start]-motorway-rural-urban; [cold start] –rural–motorway–urban;
- testing using an urban traffic jam route with very low mean speed and periods of vehicle standstill (stop time) significantly exceeding the RDE limit for that parameter (30%);
- testing using modified sub-route distance shares – examples: urban 70%, rural 15%, motorway 15%; urban 10%, rural 0%, motorway 90%;
- testing at ambient temperatures below the RDE extended range (i.e. down to the lower limit of the equipment: –10°C):
- post-processing of results to include emissions at idling and speeds < 1 km/h;
- tests performed with heavy electrical load during driving (e.g. high ambient temperature, max. air conditioning power or low ambient temperature, heated seats, cabin heater and all lights on) for assessment of the impact on the emissions (both regulated and CO_2).

Such deviations from the legislative RDE procedure are emphatically not to be employed during legislative RDE tests, but can form an important part of non-legislative, RDE-like PEMS test procedures, with the aim of gaining a deeper understanding of emissions behaviour from vehicles under demanding (yet still realistic) operating conditions outside RDE boundaries. Such insights can be used to provide mathematical input data for real-world emissions inventories and can also assist with efforts to make powertrains, calibrations and aftertreatment systems as future-proof as possible, by testing them under conditions exceeding current type approval requirements.

As a result of favorable assessments of the compliance of its PEMS hardware and software with all applicable requirements, BOSMAL is an accredited laboratory for conducting RDE-PEMS and ISC-PEMS (HD, NRMM) tests in line with all relevant EU legislation (accreditation No. AB 128 according to PN-EN ISO/IEC 17025:2005 – available here: https://www.bosmal.eu/userfiles/file/Certyfikaty/Accreditation_issue_No_17_02_08_2018-EN.pdf).

3. The laboratory (chassis dyno) environment in the era of RDE

The publication of RDE requirements in the EU represented a *revolution* in the automotive industry, in contrast to decades of *evolution* [1, 16]. It is clear that RDE requirements will remain in force in the EU and will become more stringent. A number of other parties and legal jurisdictions are either implementing similar requirements, or will do in the coming years – the global "market" for RDE development will increase further beyond its current level. A process has even begun to harmonize RDE testing internationally [17, 18], though regional emissions limit values will differ somewhat. While RDE requirements are by far the most challenging emissions requirements for the EU market (and other markets with current or planned RDE legislation – i.e. various Asian counties; potentially others), laboratory chassis dyno testing remains a very important element. RDE tests occurring under real-world operating conditions have a very wide range of acceptable parameters and are at the mercy of the prevailing traffic and weather conditions occurring during the test. This leads to RDE and PEMS testing in general being very realistic, but also characterized by low repeatability. For the reason of repeatability, among others, the chassis dyno remains an indispensa-

ble environment for emissions development work at the Euro 6d/RDE level. Use of a chassis dyno in this context includes, but is not limited to, the following activity types:

– verification of the PEMS system installation before (and/or after) an RDE test, as required by RDE legislation (see [15] for a recent detailed discussion);
– determination of WLTP CO_2 emissions values in cases where this information is not available from another reputable source (required for post-processing of RDE results);
– for execution of vehicle preconditioning cycles prior to RDE tests (as an alternative to performing such activities on public roads);
– and – most importantly – for simulation of RDE tests, routes, segments and scenarios and reproduction of given driving conditions on demand.

Concerning the first point in the list above, the aforementioned chassis dyno verification procedure, during which results from the PEMS (including distance travelled) are compared with results from the laboratory is always performed for each individual installation on light duty vehicles. (HD vehicles and NRMM are not testable on a chassis dyno and are subject to their own verification procedures, not discussed here.) BOSMAL's emissions laboratories' systems (including the chassis dynos) are maintained, checked and calibrated according to procedures which meet the applicable demands of legislation including UNECE Regulation No. 83, UNECE GTR No. 15 and Commission Regulation (EU) No. 2017/1151.

Concerning the last point in the list above (simulation of RDE conditions on the chassis dyno – see Fig. 5), there are several important aspects worth mentioning. Firstly, the creation of a pre-programmed speed trace, together with the display of customized gearshifts is easily implemented in a modern chassis dyno emissions laboratory (such as those at BOSMAL). This allows virtually any recorded speed trace and gearshift pattern to be programmed as a test cycle. The speed trace and gearshifts could come from virtually an source – as examples, from a previous RDE test, from recorded real-world vehicle usage, from a simulation study, or from creation a scenario suspected to be challenging in terms of emissions control. Secondly, modern chassis dynos are capable of simulating inclines (slopes) during vehicle running, via mathematical modification of simulated running resistance [13]. In BOSMAL's exhaust emissions laboratories, a slope profile can be loaded alongside speed and gearshift profiles to create a reproduction of the load experienced by the powertrain while driving a given route. Finally, ambient conditions have a considerable impact on exhaust emissions, fuel consumption – and even drivability, NVH, etc. – and so chassis dyno test facilities with climate control (such as BOSMAL's facilities) possess a distinct advantage in terms of full replication of test conditions for chassis dyno RDE simulation. The economic and logistical advantages of the ability to change temperature on demand (rather than waiting for the desired weather conditions to occur) are self-evident.

The legislative method for laboratory measurement of exhaust emissions from light duty vehicles running on chassis dynos (often called the CVS-bag method) is generally of limited use for extended test cycles, due to the finite number and capacity of the sample bags. Furthermore, the CVS-bag measurement gives results of high accuracy, but extremely low resolution: one result per phase (i.e. per sample bag). Thus, a phase (bag-sampling event) lasting say 20 minutes would give one measurement per 1200 sec, i.e. a measurement frequency of ~0.0008 Hz. Non-legislative equipment used for continuous ('modal') analysis of undiluted or diluted exhaust can be used to provide emissions measurement at much higher resolution – up to 10 Hz (see [12–14] for detailed descriptions of BOSMAL's hardware of this type). However, PEMS analyzers themselves can also be used on the chassis dyno, or a combination of laboratory modal analyzers and PEMS can be used (Fig. 5), thereby adding to the breadth and robustness of the emissions results. Such a setup could apply both systems in parallel, to perform two sets of measurements from the same sample point (e.g. the tailpipe), or the different systems could be connected to different sampling points along the powertrain, to assess the effectiveness of various aftertreatment system components (see [13] for a discussion of this technique). Pollutants and compounds of interest not currently measured by standard PEMS equipment (such as NH_3, N_2O and particle size distribution) can be measured in this way, by means of laboratory equipment.

Fig. 5. PEMS system installed on a light duty vehicle undergoing an RDE simulation test on the chassis dyno.

It is also important to note that RDE NTE limits apply to emissions from a vehicle quantified using PEMS equipment (and not laboratory equipment) and calculated using the RDE post-processing procedure. For that reason, using PEMS equipment for RDE-based research has certain advantages in terms of the comparability of the measurement with a genuine RDE test outside the laboratory. While the correlation in emissions results generated by modern, well-maintained and prepared, RDE-compliant legislative PEMS equipment and legislative laboratory CVS-based equipment is generally very good (see [15] for a recent assessment and discussion), certain identifiable differences in results remain. The accuracy requirement of the PN module is the least stringent (±50% of laboratory reference value) [15]. PEMS results which give unexpectedly high emissions (i.e. exceeding, or very close to, the legislative limit) should be

further investigated on the chassis dyno, performing modal emissions measurements in parallel. On the other hand, PEMS equipment is expensive, rather time-consuming to set up and in the current legislative environment, demand for such equipment is very high – and so the use of PEMS for testing on the chassis dyno must be justified, as not every case warrants the use of portable equipment in a stationary (laboratory) environment. In situations where its use is not found to be justified, laboratory equipment for modal analysis is an eminent alternative for use during RDE simulation testing. Some types of somewhat smaller and simpler PEMS equipment exist, often known as SEMS (Smart Emissions Measurement System). Such systems do not fulfill all RDE or ISC requirements, but can be used for R&D purposes, including in the chassis dyno environment, sometimes combined with the laboratory equipment for modal measurement to provide a comprehensive, cost-effective chassis dyno-based emissions measurement approach.

4. Conclusions

The introduction of ISC and RDE requirements in the EU (and, progressively, the introduction of similar requirements in other jurisdictions) is a radical departure from requirements for emissions measurement and control in previous eras. Rugged, flexible PEMS equipment is required to perform the required legislative and R&D testing on the very wide range of vehicles and pieces of machinery subject to this legislation. RDE testing of passenger cars is now the most demanding requirement in terms of emissions control, and this forces the need for very high numbers of tests for development and calibration purposes. However, because of the nature of the open road (real world) and the chassis dyno (controlled laboratory environment), the chassis-dyno based emissions laboratory is in fact more relevant than ever, despite the real world ethos of RDE. As this paper has discussed, equipment of the type BOSMAL has at its disposal (multiple PEMS suitable for light duty vehicles (and HD/NRMM), climate-controlled chassis dyno facilities) are an absolute necessity in the era of RDE. . In addition to BOSMAL fulfilling all legislative RDE/ISC requirements – a fact attested to by the company offering accredited services (Fig. 6) – R&D services relating to RDE/ISC requirements are also provided. The symbiotic advantages provided by the chassis dyno/PEMS/modal analysis combination allows BOSMAL to provide the full range of services relating to the latest emissions type approval requirements for light duty vehicles.

Fig. 6. BOSMAL's accreditation certificate for testing laboratory AB 128 with confirmation of the PN-EN ISO/IEC 17025:2005 standard. The range of accreditation include RDE testing and ISC testing for HD and NRMM

Nomenclature

CO	carbon monoxide
CO_2	carbon dioxide
CI	compression ignition
FC	fuel consumption
ISC	in-service conformity
N_2O	nitrous oxide
NH_3	ammonia
NO	nitrogen oxide
NO_2	nitrogen dioxide
NO_x	oxides of nitrogen
PEMS	portable emsisions measurement system
RDE	real driving emissions
SEMS	Smart Emissions Measurement System
THC	total hydrocarbons
WLTP	Worldwide Harmonised Light Vehicle Test Procedure

Bibliography

[1] BIELACZYC, P., WOODBURN, J. Trends in automotive emission legislation: impact on LD engine development, fuels, lubricants and test methods: a global view, with a focus on WLTP and RDE regulations. *Emissions Control Science Technology*. 2019, **5**(1), 86-98. DOI: 10.1007/s40825-019-0112-3

[2] BIELACZYC, P., WOODBURN, J. Trends in automotive emissions legislation: impact on LD engine development, fuels and lubricants, and test methods – a global view with a focus on WLTP and RDE regulations – Summary of the 6th International Exhaust Emissions Symposium (IEES), *Combustion Engines*. 2018, **174**(3), 56-65. DOI: 10.19206/CE-2018-306

[3] Bielaczyc, P. WLTP, RDE and CO_2 legislation: a global view and their impacts on engine technologies and testing procedure. *2nd Annual Real Driving Emissions Forum*. 6th-7th March 2018, Amsterdam.

[4] BIELACZYC, P. Global development of emissions reduction strategies from light duty vehicles. 2nd International Conference on the Sustainable Energy and Environmental Development. *IOP Conf. Series: Earth and Environmental Science*. 2019, **214**, 012139. DOI: 10.1088/1755-1315/214/1/012139

[5] BIELACZYC, P. WLTP, RDE and global emissions regulations: Current and future development in Europe and worldwide. *6th International Conference Real Driving Emissions*. 17-18 October 2018, Berlin.

[6] BIELACZYC, P. O badaniach emisji związków szkodliwych spalin z silników samochodowych w warunkach trakcyjnych metodą RDE (PEMS). *Przegląd Techniczny*. 2016, **24**, 56-57.
[7] MERKISZ, J., FUC, P., LIJEWSKI, P., BIELACZYC, P. The comparison of the emissions from light duty vehicle in on-road and NEDC test. *SAE Technical Paper* 2010-01-1298, 2010. DOI: 10.4271/2010-01-1298
[8] MERKISZ, J., PIELECHA, J., BIELACZYC, P., WOODBURN, J. Analysis of emission factors in RDE tests as well as in NEDC and WLTC chassis dynamometer tests. *SAE Technical Paper* 2016-01-0980, 2016. DOI:10.4271/2016-01-0980
[9] MERKISZ, J., BIELACZYC, P., PIELECHA, J., WOODBURN, J. RDE testing of passenger cars: the effect of the cold start on the emissions results. *SAE Technical Paper* 2019-01-0747, 2019. DOI:10.4271/2019-01-0747
[10] BIELACZYC, P., MERKISZ, J., PIELECHA, J., WOODBURN, J. A comparison of gaseous emissions from a hybrid vehicle and a non-hybrid vehicle under real driving conditions. *SAE Technical Paper* 2018-01-1272, 2018, DOI: 10.4271/2018-01-1272
[11] PIELECHA, J. MERKISZ, J., BIELACZYC, P., WOODBURN, J. Gaseous emissions from a hybrid vehicle and a non-hybrid vehicle measured under real driving conditions via PEMS. *FISITA Technical Paper* F2018/F2018-PTE-266.
[12] BIELACZYC, P., SZCZOTKA, A., WOODBURN, J. Development of vehicle exhaust emission testing methods – BOSMAL's new emission testing laboratory. *Combustion Engines*. 2011, **144**, 3-12.
[13] BIELACZYC, P., PAJDOWSKI, P., SZCZOTKA, A., WOODBURN, J. Development of automotive emissions testing equipment and test methods in response to legislative, technical and commercial requirements. *Combustion Engines*. 2013, **1**, 28-41.
[14] BIELACZYC, P., KLIMKIEWICZ, D., WOODBURN, J., SZCZOTKA, A. Exhaust emission testing methods – BOSMAL's legislative and development emission testing laboratories. *Combustion Engines*. 2019, **178**(3), 87-97. DOI: 10.19206/CE-2019-316
[15] VARELLA, R.A., GIECHASKIEL, B., SOUSA, L., DUARTE, G. Comparison of portable emissions measurement systems (PEMS) with laboratory grade equipment. *Appl. Sci.* 2018, **8**, 1633. DOI: 10.3390/app8091633
[16] ENGELJEHRINGER, K. Emission regulation and development – from evolution to a paradigm shift (PTNSS-2017-D17). VII International Congress on Combustion Engines PTNSS, Poznan, 27th-29th June 2017.
[17] Informal document GRPE-77-30, The need for an RDE GTR, 77th GRPE, 6-8 June 2018, https://www.unece.org/fileadmin/DAM/trans/doc/2018/wp29grpe/GRPE-77-30e_-_RDE_at_June_2018_GRPE_session_vs4.pdf
[18] Informal document WP.29-175-32. Request for the authorization to develop a new UN GTR on Global Real Driving Emissions, 175th WP.29, 19-22 June 2018, https://www.unece.org/fileadmin/DAM/trans/doc/2018/wp29/WP29-175-32e.pdf

Piotr Pajdowski, DEng. – Engine Research Department, BOSMAL Automotive Research & Development Institute Ltd in Bielsko-Biała.
e-mail: *piotr.pajdowski@bosmal.com.pl*

Piotr Bielaczyc, DEng. – Head of the Engine Research Department at the BOSMAL Automotive Research & Development Institute Ltd in Bielsko-Biała.
e-mail: *piotr.bielaczyc@bosmal.com.pl*

Joseph Woodburn, MSci – Engine Research Department, BOSMAL Automotive Research & Development Institute Ltd in Bielsko-Biała.
e-mail: *joseph.woodburn@bosmal.com.pl*

Bartosz Puchałka, MEng. – Engine Research Department, BOSMAL Automotive Research & Development Institute Ltd in Bielsko-Biała.
e-mail: *bartosz.puchalka@bosmal.com.pl*

Article citation info:
PIETRAS, D., PRASZKIEWICZ, M., CZARNIECKI, K. Methodology of determining the input data of control algorithms for a compression-ignition engine. *Combustion Engines*. 2019, **178**(3), 283-288. DOI: 10.19206/CE-2019-349

Dariusz PIETRAS
Marek PRASZKIEWICZ
Konrad CZARNIECKI

CE-2019-349

Methodology of determining the input data of control algorithms for a compression-ignition engine

The engine control process is usually carried out based on array control algorithms with a fixed mesh size. Modification of control algorithms based on experimental test data requires the use of programs that make it possible to determine the control algorithm parameters. The article presents the methodology of determining the compression-ignition engine control algorithms. A custom computer program was presented, which was used to determine the control algorithm parameters. These control algorithms values were determined based on the results of experimental engine tests, and using the presented program. The parameters were introduced into the laboratory compression-ignition engine controller. The experimental tests performed on the engine, whose operation was managed by the programmed laboratory controller, confirmed the usefulness of the proposed methodology for determining input data of control algorithms.

Key words: *CI engine, engine control, control algorithms, ECU*

1. Introduction

Standard fuel supply systems, used in modern compression-ignition engines, include common rail injection systems that allow for multi-phase injection. Precise engine control (Fig. 1) allows achieving some positive effects, such as: increased engine power, noise and exhaust emission reduction, uniformity of engine operation, high combustion process quality in the engine [2–6].

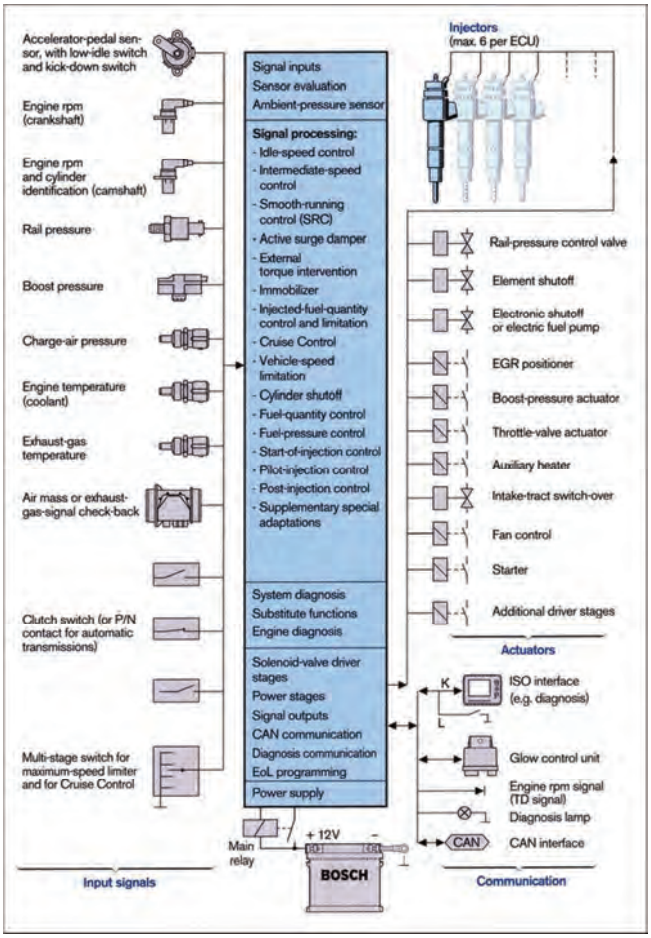

Fig. 1. An example engine control system used in a vehicle [12]

ECU power system controllers are able to adjust the fuel dose for each cylinder and shape the pressure in the combustion chamber by changing the fuel flow rate out of the injectors. Complicated and dependent control algorithms ensure quick and precise control of the engine's operation. Most often, the control algorithms are written in the form of one- or two-dimensional arrays [1, 10] depending on the parameter for which they are responsible. In the case of fuel injection process parameters, the algorithms are built based on two-dimensional arrays, usually presented graphically as so-called "Control maps" (Fig. 2).

The improvement of engine performance, or even the reduction of exhaust emissions are among the often accepted criteria in the research conducted on the selection of engine control parameters. The result of such research works is to obtain "new", "better" input data for the control algorithms, e.g. the fuel injection process in the compression-ignition engine. The implementation of this kind of experimental research is often very difficult when relying on factory engine controllers. Factory controllers, developed for a specific engine model, usually do not allow free modification of the engine operation parameters. Moreover, due to their complex structure, the number of registered and operational parameters reaching up to 3000 parameters and their interdependencies make them impossible to use in scientific research.

Therefore, it is advisable to equip the test bench with a less complicated controller taking into account the dependence of parameters that are important when the engine is mounted into the vehicle [7]. During the research on the selection of control algorithms parameters, it is necessary to have a controller, in which there will be no interdependent changes of some engine operation parameters due to changes being made in other parameters.

From previous experience [8, 9], the controller operating according to the above principles was developed in the Department of Combustion Engines and Vehicles of the University of Bielsko-Biala. The controller, as opposed to the factory controllers, enables the experimental tests to be carried out on the engine test bench taking into account the change of only the selected control parameter. In factory

controllers, forcing a change in one parameter often leads to automatic changes in many other parameters of the engine control.

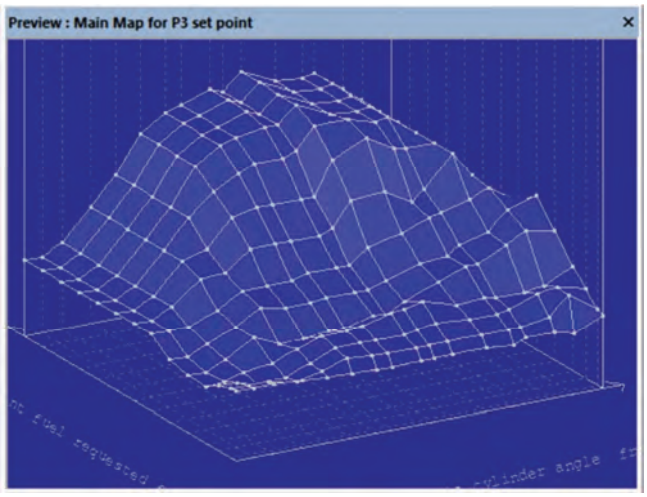

Fig. 2. An example of a „control map" for fuel supply [11]

The specific laboratory programmable controller of diesel engine with the Common Rail system was developed in cooperation with the MiSter company and is characterized by the following parameters:

- MCU controller (MiSter Control Unit) is built-in in a compact housing, input-output signals transferred through the standard engine bundle socket 1.3 SDE, no control buttons and displays on the housing,
- connection between the electronic system and the bundle socket enables modifying the output of individual signals from the controller as well as the input of parameters to individual pins in the socket. This is to ensure the possibility of using the controller for various factory engine bundles,
- the process of setting and monitoring the engine operating parameters is carried out by a PC controller management program (the controller is connected directly to the engine bundle on the test bench,
- MCU software enables monitoring, controlling and archiving defined parameters,
- the controller allows to divide the dose into 5 parts,
- input parameters (sensors and test bench system),
- output parameters (engine control).

2. Program for determining the parameters of control algorithms

As mentioned in the introduction, engine controllers operate based on the data contained in the arrays. These arrays must contain values corresponding to the initially accepted values of the control parameters, e.g. rotational speed and load, mesh division. Such selected engine operating points usually do not correspond to the points obtained during engine tests (Fig. 3). This is the reason behind the appearance of an interpolation problem of the obtained test results, and their extrapolation, where the results of experimental tests do not cover the entire area of the ECU (except the dotted line).

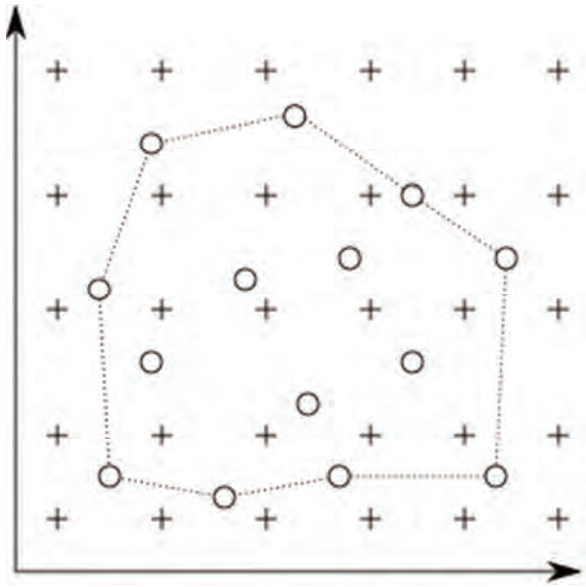

Fig. 3. The distribution of measuring points (circles) in relation to the points contained in the array (+)

The problem of interpolation can be easily solved by creating triangles based on measuring points. This makes it possible to easily determine the interpolated value inside the triangle. Unfortunately, there are many ways to create triangles based on the same set of points. Changing the triangle arrangement results in different interpolation results. In some cases, it is not possible to determine which result is correct and the differences can be very large. Figure 4 shows two ways of combining triangles giving different interpolated values a and b.

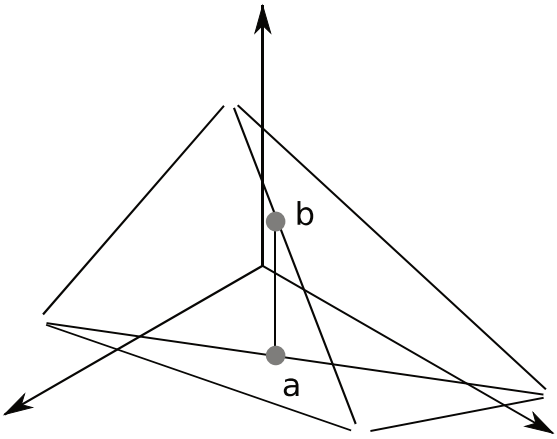

Fig. 4. Two different interpolation results dependent on the method of choosing the triangles

The problem becomes even more significant when extrapolated, because the triangles created may have different inclinations, which sometimes leads to results that make no physical sense.

For this reason, software has been created that does not require division into triangles. The method of determining points is based on interpolation of all measurement data on a plane (or a quadratic function). This plane is calculated independently for each determined point, where the meas-

uring points are taken into account with different weights depending on the distance from the determined point. The weights of the measuring points decrease with the distance thanks to the bell curve (Fig. 5). This allows to uniquely determine the tangent plane to the designated map at any selected point, and using its equation also the location of the interpolated (or extrapolated) point. The only parameter influencing the obtained results is the width of the bell curve. It allows the adjustment of the degree to which the received map is smoothed out.

The presented method is quite complex computationally, however, due to the small number of points determined, the computation time does not exceed one second. Using the program, it becomes possible to quickly transform the experimental results into an array suitable for transfer into the ECU.

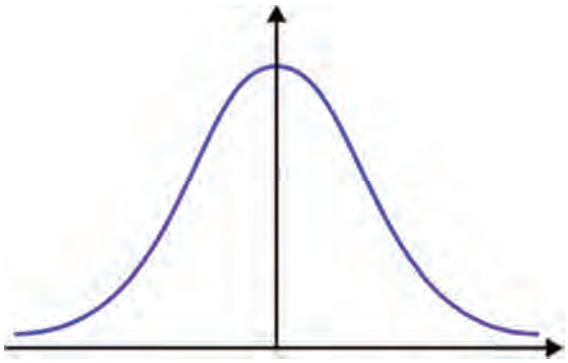

Fig. 5. Function defining the weights of the measuring points

Determining the input data of the control algorithms based on the developed program consists of loading the data file from experimental tests, specifying the desired mesh values and starting the calculation process. It is also possible to choose the type of isoline smoothing, as well as the Line/Square plot type.

Additionally, using the cursor, the values in individual points plotted on the graph presented in the program window can be read. The determined algorithm data can be saved by clicking the File tab, and Save.

3. Base experimental tests

3.1. Research aim and shedule

The aim of the basic research was to obtain the largest possible amount of information for the "factory" engine control, with particular emphasis on fuel dose distribution, dose size, injection timing for individual doses and injection pressure.

The obtained research material is the basis for the development of engine control algorithm parameters that will be used in the programming process of the laboratory controller.

The following engine tests on the engine test bench were performed for the base research:

- engine maximum power characteristic,
- engine idling characteristic,
- engine load characteristics.

The engine power characteristics were made in the range of 1000–4500 rpm every 250 rpm. The torque values used for the characteristic were used to select the engine load values when measuring the load characteristics.

The idling characteristics were made similarly to the engine power characteristics in the range of 1000–4500 rpm every 250 rpm, for the smallest possible load guaranteeing stable engine operation on the engine test bench. The idle characteristics together with the power characteristics determine the so-called range of engine operating parameters.

The engine load characteristics were determined in the engine speed range of 1000–4500 rpm every 500 rpm, 8–10 different load values for each of the rotational speeds. The loads were selected based on the power curve measured when the power characteristics were performed, in such a way that their values were alternated for neighboring rotational speeds.

3.2. Test engine and the test bench station

The test engine was a 1.3 SDE compression-ignition engine. The engine was equipped with an electronically controlled Common Rail system with a Multijet system that allows for fuel dose division in each working cycle. The engine's technical data is shown in Table 1. In basic tests, the engine control was carried out by the factory-provided MJD 6JX controller from Bosch.

Table 1. Technical data of the Fiat 1.3 MJT engine [19]

Engine type	1.3 MJT
Bore × stroke	69.6 × 82 mm
Displacement	1248 cm^3
Number of cylinder	4
Cylinder arrangement	straight
Compression ratio	18
Maximum power	51 kW at 4000 rpm
Maximum torque	180 Nm at 1750 rpm
Injection system	Common Rail
Number of valve per cylinder	4
Timing system	DOHC
Exhaust gas recirculation	Electric EGR valve

The basic research was carried out on the test bench (Fig. 6) in the laboratory of the Department of Combustion Engines and Vehicles at the University Bielsko-Biala [2]. Dynamometer control as well as monitoring and acquisition of test data was done by a fully automated test bench management system. The interface shown in Fig. 7 can be used to read parameters from the engine controller.

4. Determining the control algorithm parameters

Base results obtained in experimental research were recorded in tables in accordance with the requirements for preparing input data for the calculation program. In the calculations, a 20x20 array of algorithms was chosen. The rotational speed was selected in the range from 750 to 5500 rpm and accelerator handle signal in the range of 5 to 100%. Numerical calculations were carried out, selecting the type of isoline smoothing several times, as well as the type of the graph to be used. The data obtained from the calculations were saved in the form of tables in the excel format.

Fig. 6. The engine mounted on the dynamometer stand and the test bench management system monitors [7]

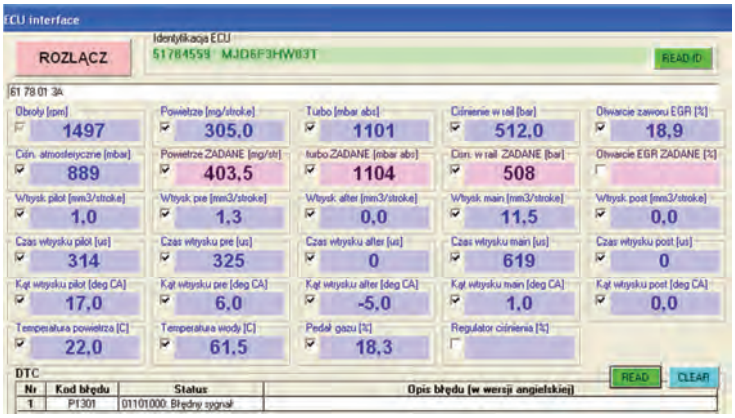

Fig. 7. Screenshot of the parameter monitoring interface window for the 1.3 SDE engine control [7]

Figures 8–11 present a graphical interpretation of the control algorithms obtained for the selected parameters: fuel pressure in the rail, Pilot dose advance angle, Pre dose advance angle and Main dose advance angle. These parameters are presented in relation to the engine speed and the signal from the accelerator. The accelerator position is a parameter representing the given engine load.

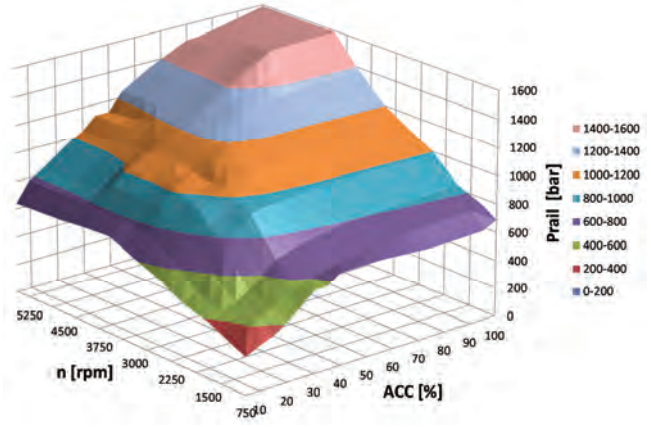

Fig. 8. Fuel pressure in the rail

Figure 8 shows the algorithm for determining the fuel pressure in the tank depending on the signal produced by the accelerator and the engine speed. The graph presents a relation in which the fuel pressure in the reservoir increases with the increase of the rotational speed and engine load. Fuel pressure increase is highest for low engine speeds and loads, as evidenced by the slope of the graph. Further on, the pressure increases in a more steady way (the plane flattens). The minimum fuel pressure in the manifold is 263 bar for minimum engine speed and load. Fuel pressure at the collector reaches a maximum value of 1590 bar for the engine speed value of 4000 rpm and an accelerator position at 75%. Despite the increase of the engine speed and the position of the accelerator, the fuel pressure value remains unchanged.

Figure 9 shows the algorithm for determining the injection advance angle for the Pilot dose depending on the load and rotational speed of the engine. The pilot dose is only used until the engine reaches 1750 rpm. The graph shows the interval in which the injection timing for the pilot dose changes. A decision was made to make the chart more transparent. Injection advance angle for the pilot dose increases as the load increases. As a function of engine speed, the advance angle increases initially, and in the range of 1500–1750 rpm it decreases. The maximum injection advance angle for the pilot dose occurs for the maximum load and the rotation speed of about 1500 rpm.

Figure 10 shows the algorithm for determining the injection advance angle for the Pre dose as a function of the accelerator and engine speed. The Pre dose only occurs until the engine reaches a speed of 4250 rpm. The algorithm

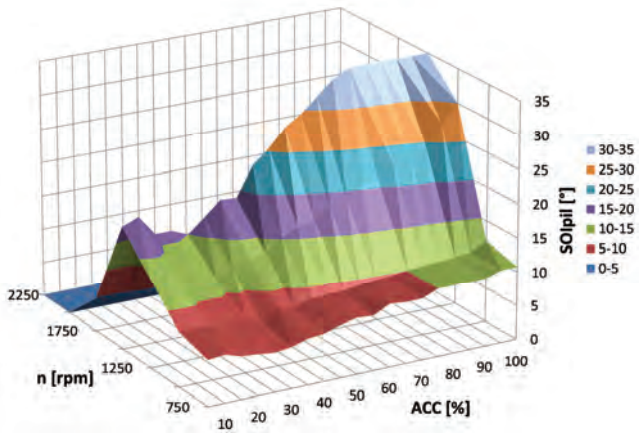

Fig. 9. Visual representation of the advance angle control algorithm for the Pilot dose

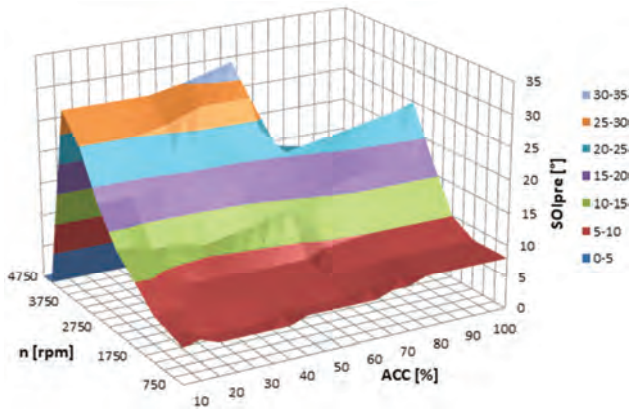

Fig. 10. Visual representation of the injection advance angle control algorithm for the Pre dose

has two main parts. This is due to the absence of a Pre dose for a load greater than 70%, starting at the engine rotational speed of 3500 rpm. The maximum injection advance angle for the Pre dose is 32° on the crankshaft for a load of 55% and an engine speed of 4000 rpm.

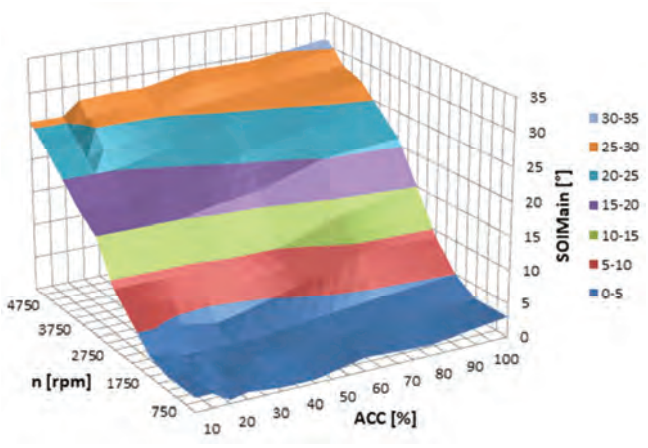

Fig. 11. Visual representation of the injection advance angle control algorithm for the Main dose

Figure 11 shows the algorithm for determining the injection advance angle for the Main dose depending on the signal of the accelerator and the engine speed. The Main dose, in contrast to the previous ones, is used for all values of engine load and speed. Analyzing the parameters of the determined algorithm, it can be noted that as the engine speed and load increase, the injection advance angle for the Main fuel dose also increases. For low engine speed values, the injection advance angle of the Main dose increases more slowly. In the central part of the graph, the plane has a higher incline, which is a result of a faster increase in the Main dose injection advance angle value. For speeds above 3750 rpm, the increase in the injection advance angle of the Main dose is losing its momentum. The minimum injection advance angle for the Main fuel dose is 1° on the crankshaft at the minimum engine load and speed, while the maximum value of 31° on the crankshaft occurs at maximum engine load and speed.

9. Conclusion

The result of the described research was the development of input data of selected engine control algorithms for a compression-ignition equipped with Common Rail fuel supply system in the entire engine operation range and acquiring a significant amount of engineering knowledge in relation to the electronic control of the modern compression-ignition engines. The developed computer program very quickly performs calculations, so it can carry out a wide range of calculations by changing the interpolation parameters. The proposed method of interpolation and extrapolation ensures a very high mapping accuracy of calculated data in relation to the input data. The designated data does not contain random errors, as was the case with the use of the triangles method in the initial versions of the program. The quality of calculations is confirmed by the smooth change of parameters as can be seen on the visual representation charts. None of the calculated algorithms have produced significant local increases or decreases in value, which would not make physical sense in relation to the changing control parameters.

The developed algorithms correlate with the algorithms of the factory engine controller. It can be expected that running the engine with a laboratory controller with programmed algorithms would enable the engine to operate in the entire range of its possible parameters. It should be kept in mind that the number of experimental input data and the distribution of these data against the background of the engine's range of operation have a decisive impact on the calculation quality of the control algorithm parameters.

The methodology for calculating algorithm parameters of the laboratory controller presented in the article is universal and can be used for programming the factory provided engine controllers as well.

Nomenclature

ACC	accelerator
ECU	engine control unit
Main	main fuel dose
n	engine speed
Pilot	pilot fuel dose
Prail	fuel pressure
Pre	preceding fuel dose
SOIpil	advance angle of the pilot injection
SOIpre	advance angle of the pre injection
SOImain	advance angle of the main injection

Bibliography

[1] BOGUTA, A. Elektroniczna modyfikacja parametrów pracy silnika samochodowego o zapłonie samoczynnym. *Motrol*. 2011, **13**, 21–27.

[2] CZAJKA, J., WISŁOCKI, K., PIELECHA, I., BOROWSKI, P. Examination of the influence of multi-injection strategy on thermodynamic indexes of engine cycle and on the emission of toxic compounds. *Combustion Engines*. 2014, **157**(2), 45-59.

[3] HENNEK, K., PRAŻNOWSKI, K., BIENIEK, A. Wpływ modyfikacji map sterowania silnikiem na wybrane wskaźniki jego pracy. *TTS Technika Transportu Szynowego*. 2015, **12**, 631-635.

[4] HETMAŃCZYK, I., HEPNER, W., HALICKI, R. Modyfikacja charakterystyki zewnętrznej silnika o zapłonie samoczynnym poprzez zmianę parametrów wtrysku paliwa. *Inżynieria rolnicza*. 2013, **2**(143), 79-89.

[5] NOWAKOWSKI, J. Wpływ parametrów regulacyjnych silnika ZS na wybrane wskaźniki pracy. *Combustion Engines*. 2011, **146**(3), 1-6.

[6] PIELECHA, I., BOROWSKI, P., CIESLIK, W. Investigations into high-pressure diesel spray-wall interaction on reduction of exhaust emission from DI diesel engine. *SAE Technical Paper*. 2014, 2014-01-1250. DOI: 10.4271/2014-01-1250

[7] PIETRAS, D. Studium sterowania wieloczęściowym wtryskiem paliwa w silniku o zapłonie samoczynnym w aspekcie parametrów pracy silnika. *Wydawnictwo Naukowe Akademii Techniczno-Humanistycznej w Bielsku-Białej*. Bielsko-Biała 2019.
[8] STELMASIAK, Z., KNEFEL, T., LARISCH, J. Sterowniki do badań silników z systemem wtrysku Common Rail. *Pomiary, Automatyka, Kontrola*. 2010, **56**(3), 217-220.
[9] STELMASIAK, Z., LARISCH, J., PIETRAS, D. Selection of an algorithms controlling operation of supercharged compression ignition engine with additional fueling with CNG gas. *Combustion Engines*. 2017, **170**(3), 42-48. DOI: 10.19206/CE-2017-307
[10] STYŁA, S. Komputerowy model dydaktyczny elektronicznego układu sterowania silnikiem o zapłonie samoczynnym. *Autobusy*. 2018, **12**. DOI: 10.24136/atest.2018.474
[11] http://www.vtechpomorze.pl/aktualnosci.html?page_a17=8
[12] http://www.autospeed.com/cms/article.html?&title=Common-Rail-Diesel-Engine-Management-Part-2&A=108105

Dariusz Pietras, DEng. – Faculty of Mechanical Engineering and Computer Science, University of Bielsko-Biala.
e-mail: *pietras@ath.bielsko.pl*

Marek Praszkiewicz, DEng. – Faculty of Mechanical Engineering and Computer Science, University of Bielsko-Biala.
e-mail: *mpraszkiewicz@ath.bielsko.pl*

Konrad Czarniecki, MEng. – BOSMAL Automotive Research and Development Institute Ltd., Bielsko-Biala.
e-mail: *konrad.czarniecki@bosmal.com.pl*

Article citation info:
KOZAK, M. A comparison of thermogravimetric characteristics of fresh and used engine oils. *Combustion Engines*. 2019, **178**(3), 289-292. DOI: 10.19206/CE-2019-350

Miłosław KOZAK

CE-2019-350

A comparison of thermogravimetric characteristics of fresh and used engine oils

The requirements set for engine oils are nowadays very high, varied, often contradictory and significantly go beyond the classic functions of engine oils. Also for the testing of engine oils, many different and advanced research methods are currently used. This article describes tests of fresh and used oil from a diesel engine using thermogravimetric analysis. This method was also used to determine the soot content of the used oil. The tests showed that the thermograms of fresh and used oil are similar, however in the oil used in the diesel engine the soot content increases.

Key words: *engine oil, thermogravimetric analysis, TGA, soot content*

1. Introduction

The constant development of the construction of internal combustion engines is associated with an increase in their efficiency. Modern engines are therefore exposed to increasing thermal and mechanical loads. The proper and reliable operation of an internal combustion engine depends on many factors. The most important such factors include the use of engine oil with appropriate parameters and quality. Despite the increasing pressures and temperatures of combustion in modern engines, it is expected to reduce oil consumption and extended periods of its change. The requirements set for modern engine oils are therefore very high, varied, often contradictory and significantly go beyond the classic functions of oil, such as: reduction of friction, sealing, cooling, cleaning, corrosion protection, vibration damping.

For modern engine oils it is also expected [6]:
- low toxicity of oil combustion products,
- small changes in viscosity as a function of temperature,
- simultaneously low viscosity and volatility,
- low temperature fluidity,
- keeping the engine elements clean,
- resistance to sludge and sediment formation,
- no impact on the engine seals,
- no impact on exhaust gas aftertreatment.

The very wide and varied requirements imposed on engine oils are connected with the necessity of using various methods of testing. This article describes tests of fresh and used engine oils using thermogravimetric analysis. This method was also used to determine the soot content of the used oil.

2. Soot in engine oil

The mechanism of soot formation in the internal combustion engines has not been fully understood. The author of this article discusses the current views on the creation of soot in diesel engines in his work [5]. There is no doubt that the process of creating soot in the engine is very short and complex. The fuel particles generally contain from 12 to 22 carbon atoms and approximately twice as many hydrogen atoms. Within a few milliseconds, soot particles containing thousands of carbon atoms and about ten times less hydrogen atoms are produced. A more detailed analysis of this process indicates that it takes place in several stages. Pyrolytic reactions lead to the breakdown of fuel particles and the formation of soot precursors, which participate in the nucleation process of the first visible particles (nuclei) with a diameter below 3 nm. Next, the process of growth occurs, connected with the attachment of carbon atoms and the removal of hydrogen atoms. As a result, spherules with a diameter of 20–50 nm are formed. At the same time, growth and agglomeration of spherules occurs, which leads to formation of particle aggregations. Another of the processes, i.e. oxidation, gives the opposite effects to the above-mentioned ones, namely removing soot at each of its development phases: precursors, nuclei, spherules and agglomerates.

The smallest possible to be observed under the electron microscope soot particles have a diameter of about 1.5 nm (molecular weight about 1600 amu). The reference [2] presents the opinion that the first distinguishable soot particles that pass from the gas phase and the molecular system have masses of the order of 650–700 amu (e.g. $C_{54}H_{30}$). According to these assumptions, soot nuclei are about 1 nm in diameter.

The soot nuclei formed begin to grow. The increase in the surface of the particles leads to the formation of spherules, which are the primary element (monomer) of the subsequently formed carbon agglomerates. This process is also responsible for the spherulite layered microstructure. Distant regions have an ordered crystallite structure, while the central region created by the nucleation process is amorphous (it also contains more hydrogen).

The growth process does not only apply to individual particles, but also runs in parallel with their agglomeration. Deposition of successive carbon layers on the surface of the agglomerates causes the individual spherules to merge together and become more and more difficult to distinguish within the framework of the structure. Agglomeration of particles is a mainly physical process, the number of particles decreases, and their total mass remains unchanged. The rate of agglomeration depends to a large extent on the number and size of the particles. Polydisperse particles agglomerate faster than monodisperse particles. Young particles are easier to combine with a more sticky surface.

Most of the soot produced in the combustion chamber of the engine escapes with the exhaust, but some of it passes through the piston rings and then mixes with the engine oil. The presence of soot in oil causes a number of adverse phenomena. It deteriorates, for example, the dispersing

properties of the oil. High level of soot content in oil leads to a higher lubricant viscosity impeding oil flow and to carbon deposition in the piston ring. It will also affect anti-wear lubricant additives resulting in increased engine wear and premature engine failures.

The tests described by Mruk [7] showed a significant negative effect of soot in engine oil on the tribological properties of this lubricant. For two different types of friction nodes: with a concentrated point contact of four balls and with a spread contact for the matching pair roller-block, it was found that in comparison to lubrication with neat oil, the increase of frictional forces and wear of elements increases with increasing soot in oil. This increase is already very clear for the soot content of 5%.

3. Test apparatus and procedures

The studies described in the paper include determination of thermogravimetric characteristics of fresh and used engine oil of the same type. The test oil was 5W-30, API SN/CF, ACEA C3 class oil (Table 1). The sample of used oil came from a passenger car with a six-cylinder turbocharged common rail diesel engine with a capacity of 3.0 dm^3. The oil was used during the mileage of the car of 16000 km.

Table 1. Typical characteristics of the tested fresh engine oil [3]

Name	Method	Units	Value
Density @15°C	ASTM D4052	g/ml	0.8524
Kinematic viscosity @100°C	ASTM D445	mm²/s	12.1
Viscosity, CCS –30°C (5W)	ASTM D5293	mPa·s	5750
Kinematic viscosity @40°C	ASTM D445	mm²/s	70
Viscosity index	ASTM D2270	–	173
Pour point	ASTM D97	°C	–42
Flash point, PMCC	ASTM D93	°C	204
Ash, sulphated	ASTM D874	% (m/m)	0.8

Fig. 1. PerkinElmer thermogravimetric analyzer TGA 8000

Thermogravimetric characteristics of oils were determined using a PerkinElmer thermogravimetric analyzer TGA 8000. Thermogravimetric analyzer (abbreviation: TGA) measures the change in mass of the sample as it is heated, cooled, or held at a constant temperature in a controlled atmosphere. Table 2 shows the characteristics of TGA 8000 and Figure 1 shows the picture of TGA 8000.

Table 2. Specifications of TGA 8000 thermogravimetric analyzer used in the research [4]

Design		A vertical design with a high sensitivity balance and quick response furnace. The balance is located above the furnace and is thermally isolated from it. A precision hang-down wire is suspended from the balance down into the furnace. At the end of the hang-down wire is the sample pan. The sample pan's position is reproducible.
Balance	Sensitivity	0.1 µg
	Capacity	1300 mg
	Accuracy	better than 0.02%
	Precision	0.01%
Temperature	Furnace	Low mass (< 10 g); Platinum heating element with ceramic protective coating; resistant to inert and oxidative gas over the full temperature range.
	Range	–20°C to 1200°C
	Scan rates	0.1°C/min to 500°C/min
	Precision	±1°C
Cooling	Method	Forced air cooled with an external fan
	Cycle time	1100°C to 50°C < 13 min
Sample Pans		Platinum or ceramic (60 µL)
Atmosphere	Sample environment	Static or dynamic, including nitrogen, argon, helium, carbon dioxide, air, oxygen, or other inert or reactive gases. Analyses done at normal or reduced pressures.
	Gas control	Balance purge (Mass-flow controlled); Sample purge (switch between 2 gases; Mass-flow controlled); Reactive purge.
	Gas mixing	Up to 3 gases
	Vacuum	10^{-5} Torr
Autosampler		48-position

Thermogravimetric characteristics of the tested oils were determined according to the temperature program based on the temperature program described in the ASTM D5967 standard. ASTM D5967 is a test method which covers engine test procedures for evaluating diesel engine performance characteristics including viscosity and soot concentrations. Annex A4 is a recommendation on how to measure soot in engine oils. Details of the thermogravimetric analyzer working conditions during the tests are presented in Table 3. Pyris software version 13.3.1 was used to analyze the obtained results.

Table 3. TGA experimental conditions

Instrument conditions	ASTM D5967 Annex A4 [8]	Conditions applied in this work
Temperature program	1. Hold for 1 min at 50°C 2. Heat from 50°C to 550°C at 100°C/min 3. Hold for 1 min at 550°C 4. Heat from 550°C to 650°C at 100°C/min 5. Heat from 650°C to 750°C at 100°C/min 6. Hold for 5 min at 750°C	1. Hold for 4 min at 50°C 2. Heat from 50°C to 550°C at 50°C/min 3. Hold for 2 min at 550°C 4. Heat from 550°C to 650°C at 10°C/min 5. Heat from 650°C to 750°C at 10°C/min 6. Hold for 15 min at 750°C
Pan type	Platinum	Ceramic
Balance purge	40 ml/min	60 ml/min
Sample purge	N_2, 30 ml/min for step 1 to 4 O_2, 30 ml/min for step 5 and 6	N_2, 40 ml/min for step 1 to 4 Air, 40 ml/min for step 5 and 6
Sample quantity	Around 10 mg	Around 20 mg

4. Test results and discussion

The obtained thermograms for fresh and used oil are presented in Figures 2 and 3 respectively. In both cases the course of the curve is very similar. This allows us to believe that the used oil was of high quality – it was resistant to hard conditions prevailing in the engine and/or was used in not very unfavorable engine operation conditions. It was certainly favored by the large volume of oil in the engine (ca. 7 dm^3) and oil cooler, as well as good technical condition of the engine.

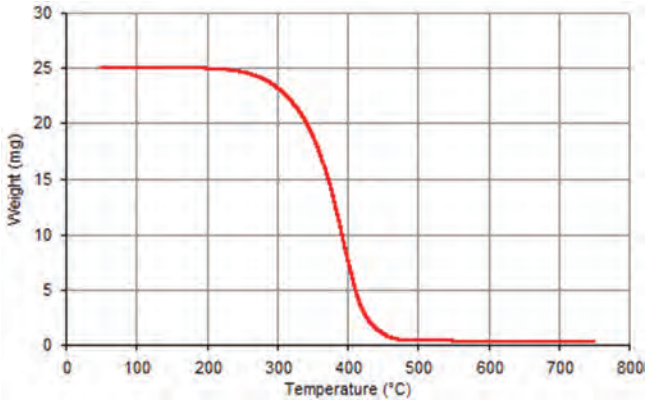

Fig. 2. Thermogram of fresh 5W-30 engine oil obtained during the temperature program presented in the Table 3

As it can be seen in Figure 4, 90% of the mass of the samples of both oils distilled (under conditions of neutral atmosphere – N_2) in the temperature range of: 290–440°C. The characteristic distillation temperatures, i.e. T10, T50 and T90, were very similar for the samples of both oils (temperatures at which 10, 50 and 90% of the samples were evaporated respectively). Strictly speaking, they were by a few degrees Celsius higher for fresh oil, respectively: T10 by 5°C, T50 by 8°C and T90 by 3°C. It proves, among others about the fact that despite the high mileage of used engine oil (16 thousand km), it was only slightly contaminated with fuel.

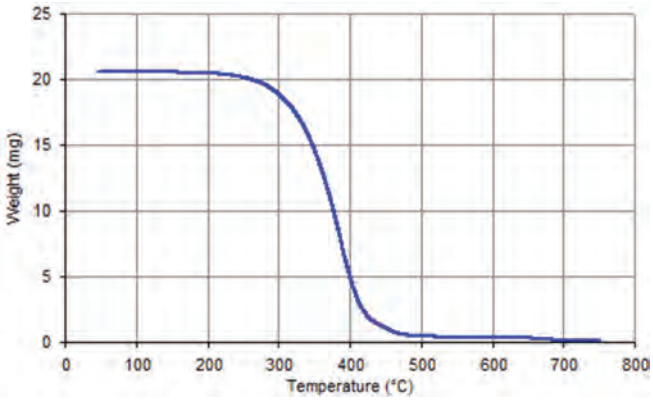

Fig. 3. Thermogram of used 5W-30 engine oil obtained during the temperature program presented in the Table 3

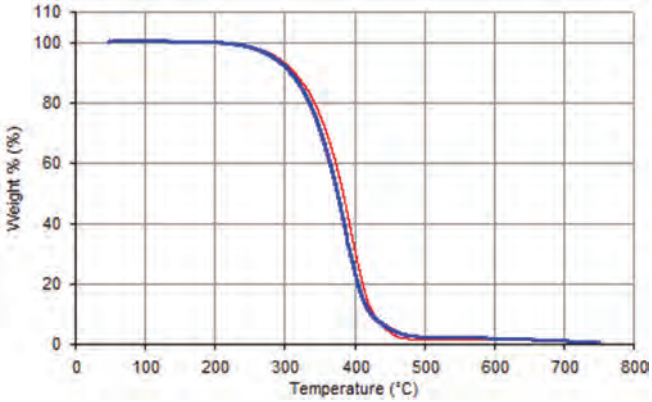

Fig. 4. Comparison of thermograms of fresh (red curve) and used (blue cirve) 5W-30 engine oil obtained during the temperature program presented in the Table 3

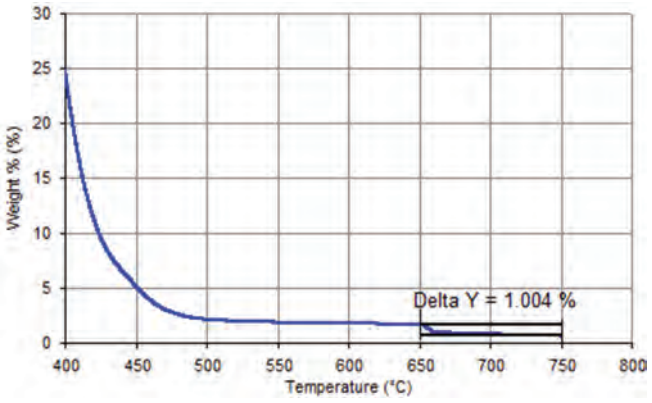

Fig. 5. Thermogram showing percentage soot content in used 5W-30 engine oil sample

The thermogravimetric analysis made also allows determination of the soot content in the engine oil. The first weight loss that occurs as the sample is heated is the evaporative loss of the lubricating oil and any other volatile materials present. All that remains will be soot and other solid residues present in the sample. Switching the purge gas from nitrogen to oxygen or air will remove any soot present in the sample. The calculation of soot content was performed for the weight loss that commences after switching

over the purge gas from nitrogen to oxygen or air at 650°C up to the temperature where constant residue was obtained around 750°C [1].

Figure 5 shows the enlarged part of the thermogram of used oil and the loss of mass of the sample under the conditions of the oxidizing atmosphere. The loss corresponds to the content of soot in the used oil at the level of 1% (m/m). This is a low content considering the mileage of the oil and the fact of its use in the diesel engine.

5. Summary

Thermogravimetric analysis is a modern tool used, among others for testing engine oils, both fresh and used. The advantage of this analysis is the small sample mass necessary to perform the tests (just a few milligrams). In the case of engine oils, thermogravimetric analysis is mainly used to assess the content of soot in oil in accordance with ASTM D5967. High soot content in engine oil is unfavorable and can lead to damage or accelerated engine wear. The level of soot in oil is one of the criteria for considering motor oil to be used up. The analysis of the engine oil thermogram also brings a lot of other information, such as the level of oil contamination (e.g. by fuel) or changes in the oil fractional composition during operation. Volatiles formed from oil during its heating in a thermogravimetric analyzer can then be analyzed, which is a next potential source of important information. Such an analysis can be performed, among others by means of FTIR spectrometer and/or gas chromatograph with mass detector.

Bibliography

[1] DESHMUKH, P. Soot content determination of in-service lubricants of diesel engine as per ASTM D5967 Annex A4. Perkin Elmer application note – thermal analysis. https://www.perkinelmer.com/lab-solutions/resources/docs/APP_Soot_Content_Determination_Diesel_Engine(012934A_01).pdf

[2] GRIFFITHS, J.F., BARNARD, J.A. Flame and combustion. *Blackie Academic and Professional*. London, 1995.

[3] https://msdspds.castrol.com/bpglis/FusionPDS.nsf/Files/FD182837C6D9427B802582D200644540/$File/BPXE-B2WPFG.pdf

[4] https://sim-gmbh.de/images/PDF_Dokumente_neu/GCMS/TGA_8000_Specification_Sheet_012248_01_SPC.pdf

[5] KOZAK, M. Study on the impact of diesel fuel oxygenated compounds on the exhaust emissions from diesel engines. Polish. *Publishing House of Poznan University of Technology*. Poznan 2013.

[6] MERKISZ, J. Ecological problems of internal combustion engines. Polish. *Publishing House of Poznan University of Technology*. Poznan 1999.

[7] MRUK, A. Effects of soot contents in engine oil on its tribological characteristics. *Technical Transactions – Mechanics*. 2008, **7-M**.

[8] SATPUTE, Y. Estimation of soot content in engine oil using Thermo Gravimetric Analysis (TGA) as per ASTM D5967 Method. Perkin Elmer application note – thermal petro. http://www.perkinelmer.com/CMSResources/Images/20130104_6-Estimation%20of%20soot%20content%20in%20engine%20oil.pdf

Miłosław Kozak, DSc., DEng. – Faculty of Transport Engineering, Poznan University of Technology.

e-mail: *miloslaw.kozak@put.poznan.pl*

SAE INTERNATIONAL

Save the Date

Don't miss this valuable opportunity to connect with leading scientists and engineers from around the world to discuss new and emerging technologies.

Abstract Deadline

February 18, 2020

sae.org/pfl

SEPTEMBER 22–24, 2020
KRAKOW, POLAND

Europe Executive Leader: BOSMAL PTNSS

POWERTRAINS, FUELS AND LUBRICANTS

Publisher:

Polish Scientific Society of Combustion Engines

Combustion Engines

Polskie Towarzystwo Naukowe Silników Spalinowych

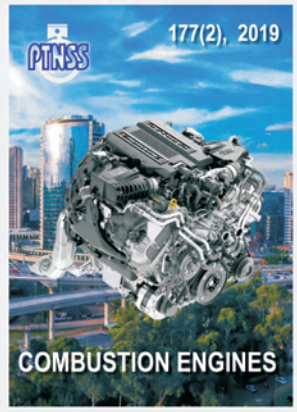

9 772300 989002

ISSN: 2300-9896

www.combustion-engines.eu